Divergent effects of HIV reverse transcriptase inhibitors on pancreatic beta cell function and survival: an interplay between oxidative stress and mitochondrial dysfunction

University of Brighton

Soulef Chahinez Maandi

School of Applied Sciences

University of Brighton

A thesis submitted for the degree of

Doctor of Philosophy

May 2023

Declaration

I declare that the research contained in this thesis, unless otherwise formally indicated within the text, is the original work of the author. The thesis has not been previously submitted to this or any other university for a degree, and does not incorporate any material already submitted for a degree.

Soulef Chahinez Maandi

21/12/2022

Abstract

The advent of antiretroviral therapy (ART) for the management of the human immunodeficiency virus (HIV) was, and to date still is, seminal in reducing the morbidity and mortality associated with HIV infection and subsequent acquired immunodeficiency syndrome (AIDS). Key ART drug classes such as non-nucleoside reverse transcriptase inhibitors (NNRTIs) and nucleoside/tide reverse transcriptase inhibitors (NRTIs) are commonly prescribed in people living with HIV (PLWH), but treatment-related complications include an increased risk of developing type 2 diabetes (T2D). Direct damaging effects on pancreatic beta cell function and survival by NNRTIs or NRTIs may predispose PLWH who are also type 2 diabetic to impaired glycaemic control and loss of beta cell mass, hence increasing the risk of diabetic complications and insulin dependency. The aim of this study was to investigate the direct effects of the NNRTIs efavirenz, rilpivirine and doravirine, and the NRTIs tenofovir, emtricitabine and lamivudine, on beta cell function and survival.

The rat insulinoma INS-1E beta cell line and isolated rat islets of Langerhans were exposed to increasing concentrations of NNRTIs or NRTIs for 24 hours. Beta cell function was assessed by measuring glucose-stimulated insulin secretion (GSIS) from INS-1E cells and isolated rat islets of Langerhans with an ELISA. Beta cell survival was assessed by measuring cell viability using a 3-(4,5-dimethylthiazol-2-yl)-2,5-diphenyltetrazolium bromide (MTT) assay and cell death by flow cytometric analysis following Annexin V and propidium iodide staining. Then, intracellular ROS generation was measured using the 2′,7′-dichlorodihydrofluorescein diacetate probe followed by confocal microscopy. Mitochondrial function was assessed by measuring the activity of mitochondrial complex I by spectrophotometric analysis and cellular ATP levels by luminometry. Flow cytometry was used to assess changes in mitochondrial membrane potential ($\Delta\psi m$) following staining with tetramethylrhodamine ethyl ester, and mitochondrial superoxide generation following MitoSOX staining. mRNA and protein expression of key endoplasmic reticulum (ER) stress markers (CHOP and GRP78) and uncoupling protein 2 (UCP2) were determined by reverse transcription-quantitative polymerase chain reaction and Western blotting or immunocytochemistry, respectively. *In silico* docking studies were carried out using the UCSF Chimera and SwissDock.

Our results show contrasting intraclass and interclass effects. While doravirine had no effect on INS-1E cell function and survival, efavirenz and rilpivirine significantly reduced GSIS from INS-1E cells and isolated rat islets of Langerhans. Efavirenz and rilpivirine also significantly

reduced cell viability and induced apoptosis in INS-1E cells, likely through ER stress as shown by the upregulated expression of CHOP and GRP78. Furthermore, efavirenz and rilpivirine significantly increased intracellular and mitochondrial ROS generation, disrupted $\Delta\psi m$ and decreased cellular ATP levels in INS-1E cells. *In silico* docking studies predict a possible inhibition of the mitochondrial ATP synthase by rilpivirine while efavirenz directly inhibited mitochondrial complex I activity and upregulated the expression of UCP2. On the other hand, the NRTIs had no effect on INS-1E cell function and survival.

This study has identified, for the first time, that the first- and second-generation NNRTIs efavirenz and rilpivirine can impair beta cell function and survival, likely through increased oxidative stress and contrasting mitotoxic effects. Therefore, although these drugs are effective in the management of HIV/AIDS, they potentially increase the risk of impaired glycaemic control and loss of beta cell mass, hence increasing the risk of diabetic complications and insulin dependency in PLWH and T2D.

Table of Contents

List of Figures

Chapter 3

Chapter 4

Chapter 5

Chapter 6

Chapter 7

Chapter 8

Appendix I

Appendix II

Figure 1 Uncropped blot image for CHOP expression in INS-1E cells treated with efavirenz 20 μM (n = 1, n = 2, n = 3) or thapsigargin 1 μM (positive control) for 24 hrs

Figure 2 Uncropped stripped blot image in INS-1E cells treated with efavirenz 20 μM (n = 1, n = 2, n = 3) or thapsigargin 1 μM (positive control) for 24 hrs

Figure 3 Uncropped blot image for GAPDH expression in INS-1E cells treated with efavirenz 20 μM (n = 1, n = 2, n = 3) or thapsigargin 1 μM (positive control) for 24 hrs

Figure 4 Uncropped blot image for CHOP expression in INS-1E cells treated with rilpivirine 10 μM (n = 1, n = 2, n = 3) or thapsigargin 1 μM (positive control) for 24 hrs

Figure 5 Uncropped stripped blot image in INS-1E cells treated with rilpivirine 10 μM (n = 1, n = 2, n = 3) or thapsigargin 1 μM (positive control) for 24 hrs

Figure 6 Uncropped blot image for GAPDH expression in INS-1E cells treated with rilpivirine 10 μM (n = 1, n = 2, n = 3) or thapsigargin 1 μM (positive control) for 24 hrs

Figure 7 Uncropped blot image for CHOP expression in INS-1E cells treated with efavirenz 20 μM (n = 4 and n = 5) or thapsigargin 1 μM (positive control) for 24 hrs

Figure 8 Uncropped stripped blot image in INS-1E cells treated with efavirenz 20 μM (n = 4 and n = 5) or thapsigargin 1 μM (positive control) for 24 hrs

Figure 9 Uncropped blot image for GAPDH expression in INS-1E cells treated with efavirenz 20 μM (n = 4 and n = 5) or thapsigargin 1 μM (positive control) for 24 hrs

Figure 10 Uncropped blot image for CHOP expression in INS-1E cells treated with rilpivirine 10 μM (n = 4 and n = 5) or thapsigargin 1 μM (positive control) for 24 hrs

Figure 11 Uncropped stripped blot image in INS-1E cells treated with rilpivirine 10 μM (n = 4 and n = 5) or thapsigargin 1 μM (positive control) for 24 hrs

Figure 12 Uncropped stripped blot image in INS-1E cells treated with rilpivirine 10 μM (n = 4 and n = 5) or thapsigargin 1 μM (positive control) for 24 hrs

Figure 13 Uncropped blot image for PDX-1 expression in INS-1E cells treated with efavirenz (20 μM) or rilpivirine 10 μM (n = 1, n = 2 and n = 3) for 24 hrs

Figure 14 Uncropped blot image for GAPDH in INS-1E cells treated with efavirenz (20 μM) or rilpivirine 10 μM (n = 1, n = 2 and n = 3) for 24 hrs

Figure 15 Uncropped blot image for GAPDH expression in INS-1E cells treated with rilpivirine 10 μM (n = 1, n = 2 and n = 3) or thapsigargin 1 μM (positive control) for 24 hrs

Figure 16 Uncropped blot image for GRP78 expression in INS-1E cells treated with efavirenz 20 μM (n = 1, n = 2 and n = 3) for 24 hrs

Figure 17 Uncropped stripped blot image in INS-1E cells treated with efavirenz 20 μM (n = 1, n = 2 and n =3) for 24 hrs (GRP78 expression)

Figure 18 Uncropped blot image for GAPDH expression in INS-1E cells treated with efavirenz 20 μM (n = 1, n = 2 and n = 3) for 24 hrs

Figure 19 Uncropped blot image for PDX-1 expression in INS-1E cells treated with efavirenz (20 μM) or rilpivirine 10 μM (n = 1, n = 2 and n = 3) for 24 hrs.

Figure 20 Uncropped blot image for GAPDH in INS-1E cells treated with efavirenz (20 μM) or rilpivirine 10 μM (n = 1, n = 2 and n = 3) for 24 hrs

Figure 21 Uncropped agarose gel electrophoresis for analysis of unlinearised and linearised SUR1 DNA

Figure 22 Uncropped DNA electrophoresis of RNA elutes for Kir6.2 and SUR1

Appendix III

Figure 1 Uncropped cleaved caspase-3 ICC images (control)

Figure 2 Uncropped cleaved caspase-3 ICC images (efavirenz)

Figure 3 Uncropped cleaved caspase-3 ICC images (rilpivirine)

List of tables

Chapter 6

Appendix I

Acknowledgments

I would like to express my deepest appreciation for the support provided by my supervisor Dr. Jon Gunnarsson Mabley. My scientific thinking and writing skills have truly changed for the better. I am grateful for his investment throughout these years to provide me with the support I needed. I am also grateful for my second supervisor, Dr. Wendy Macfarlane for her immense support that made sure my PhD journey ran smoothly. I am extremely grateful for Dr. Rian Manville's support and share of his electrophysiology knowledge. It was a pleasure to work with you all.

I am deeply indebted to the Algerian Government for their support. It has given me the opportunity to pursue my dreams that started when I sat in class as a young pupil.

There is not enough gratitude in this World to thank my parents for their immense support and love that I have received throughout my whole life, let alone these past years. Thank you, to my my father Saad and my mother Nabila, for inspiring me with your great ambition and strive! My parents stressed the importance of education and perseverance, shaping my values and making me the person I am today. As my dad always reminds me: "Success is ten percent inspiration, ninety percent perspiration" and my mum "من جد وجد ، ومن زرع حصد" (The one who sows succeeds and the one who plants reaps). Indeed!

A big thank you to my sister Meriem for her wisdom and never-ending support. I also want to thank my brother Wanis for all his love, making this journey even more pleasant!

I want to dedicate this PhD to all my family and especially to my late grandparents Ameur Maandi, Lounes Chahiani and Yamina Zemoul who sadly passed away during my PhD. You are my true inspiration and I hope I made you proud.

Abbreviations

$\Delta\psi m$	mitochondrial membrane potential
AIDS	acquired immune deficiency syndrome
AGE	advanced glycation end product
ART	antiretroviral therapy
CHOP	C/EBP homologous protein
DCFH-DA	dichloro-dihydro-fluorescein diacetate
DF	disoproxil fumarate
ER	endoplasmic reticulum
ETC	electron transport chain
FFA	free fatty acid
GCK	hexokinase enzyme glucokinase
GRP78	glucose-regulating protein 78
GSIS	glucose-stimulated insulin secretion
HIV	human immunodeficiency virus
IDU	injecting drug users
IKK	inhibitory kappa B kinases
JNK	c-Jun N-terminal kinase
K_{ATP} channel	ATP-sensitive potassium channel
Kir6.2	inward-rectifier K^+ channel subunit
IL-1	interleukin-1
IL-6	interleukin-6
LDH	lactate dehydrogenase
MAPK	mitogen activated protein kinase
MSM	men who have sex with men
mtDNA	mitochondrial DNA
mTOR	mammalian target of rapamycin
MTT	3-(4,5-dimethylthiazol-2-yl)-2,5-diphenyl-2H-tetrazolium bromide
NNRTI	non-nucleoside reverse transcriptase inhibitor
NRTI	nucleoside/tide reverse transcriptase inhibitor
PARP	poly (ADP-ribose) polymerase
PDX-1	pancreatic and duodenal homeobox 1
PI	propidium iodide
PLWH	people living with HIV
PeP	post-exposure prophylaxis
PreP	pre-exposure prophylaxis

ROS	reactive oxygen species
SUR1	sulfonylurea receptor 1
T2D	type 2 diabetes
TCA	tricarboxylic acid
TMRE	tetramethylrhodamine, ethyl ester
TNF-α	tumour necrosis factor alpha
UCP2	uncoupling protein 2

Publications from this thesis

Full papers

Maandi, S. C., Maandi, M. T., Patel, A., Manville, R., & Mabley, J. (2022). Divergent effects of HIV reverse transcriptase inhibitors on pancreatic beta-cell function and survival: potential role of oxidative stress and mitochondrial dysfunction. *Life Sciences*, *294*, 120329. [120329]. https://doi.org/10.1016/j.lfs.2022.120329

Maandi, S.C., Maandi, M.T., & Mabley, J. (2023). Synergistic effects of HIV non-nucleoside reverse transcriptase inhibitors and the saturated free fatty acid palmitate in promoting beta cell dysfunction and death. (In preparation)

Maandi, S. C., Maandi, M. T., Manville, R., & Mabley, J. (2023). Modulation of pancreatic beta cell ATP-sensitive potassium (K_{ATP}) channels by the HIV reverse transcriptase inhibitor rilpivirine. (In preparation)

Abstracts

Maandi, S. C., & Mabley, J. (2020). Enhancement of palmitate-induced lipotoxicity in INS-1E cells by the HIV medications efavirenz and rilpivirine. Abstract from the 58 th EASD Annual Meeting of the European Association for the Study of Diabetes. *Diabetologia, 65, pages1–469*. https://doi.org/10.1007/s00125-020-05221-5

Maandi, S. C., Maandi, M. T., & Mabley, J. (2022). Differential effects of first-and second-generation non-nucleoside reverse transcriptase inhibitors efavirenz and rilpivirine on pancreatic β-cell mitochondria. Abstract from Pharmacology 2022. *British Journal of Pharmacology*. https://doi.org/10.1111/bph.15944

Maandi, S. C., & Mabley, J. (2020). *Damage to pancreatic INS-1E cells through impairment of mitochondrial function by the antiretroviral agents efavirenz and rilpivirine*. Abstract from Pharmacology 2020. https://doi.org/10.1111/bph.15316

Maandi, S. C., & Mabley, J. (2020). *Enhancement of palmitate-induced lipotoxicity in INS-1E cells by the HIV medications efavirenz and rilpivirine*. Abstract from the 56 th EASD Annual Meeting of the European Association for the Study of Diabetes. *Diabetologia, 63,* pages 1–485. https://doi.org/10.1007/s00125-020-05221-5

Maandi, S. C., Patel, A., Alsini, O., & Mabley, J. (2020). Investigation into the effects of HIV pre-exposure prophylaxis (PrEP) agents Truvada® and rilpivirine on INS-1E beta cell function and viability. *Diabetic Medicine*. https://doi.org/10.1111/dme.3_14245

1. General Introduction

1.1 The HIV global epidemic

Defined as a major global public health issue by the World Health Organization, the human immunodeficiency virus (HIV) was identified as the aetiologic cause of the acquired immunodeficiency syndrome (AIDS) in the 1980s. Since the beginning of the HIV epidemic in the early 1980s, it was estimated that 76 million people have been infected with HIV and 40 million people have died of HIV/AIDS so far (World Health Organization, 2022). In 2021 alone, HIV/AIDS has claimed approximately 650,000 lives, making it one the World's deadliest diseases (World Health Organization, 2022).

1.1.1 History and epidemiology of HIV/AIDS

By the 1980s, the HIV epidemic had already been circulating in humans in Central and West Africa, with Kinshasa, in the Democratic Republic of Congo, being the location of origin. It is believed that HIV crossed from non-human primates carrying the Simian Immunodeficiency Virus (SIV) to humans in the 1920s (Wise, 2014). It is speculated that the virus was transmitted through hunting and eating chimpanzee meat carrying SIV, a virus closely related to HIV (Avert, 2018). HIV transmits from human to human through exposure to infected blood or semen, mainly through sexual transmission, unsterilised needle sharing, blood transfusions and perinatal transmission. According to the World Health Organization (2022), it is estimated that more than 38 million people are currently living with HIV globally. The growth of the HIV epidemic is believed to have been facilitated by the social climate in post-colonial Africa.

1.1.2 Global burden of HIV

Different HIV lineages have emerged from multiple independent zoonotic transmissions. HIV-1 (groups M-P) and HIV-2 (groups A-H) (Sharp & Hahn, 2011). HIV-1 has a higher virulence and infectivity compared to HIV-2, which is largely confined to West Africa. The group M of HIV-1 is pandemic, while groups N-P are limited to a small number of individuals and are confined to Central and West Africa. Subtype C of HIV-1 (group M) is by far, associated with

the highest global prevalence. Global trends for HIV are shown in Table 1.1. Sub-Saharan Africa has been heavily affected by the HIV pandemic, as of 2021, approximately 26 million people living with HIV are sub-Saharan African (World Health Organization, 2022). Key populations have been identified as being high-risk for HIV exposure, these include men who have sex with men (MSM), sex workers, clients of sex workers, injection drug users (IDUs) and transgender people. Outside of sub-Saharan Africa, these key populations account for the majority of new infections.

Table 1.1 Global trends for HIV infection in 2020. The global number of people living with HIV was approximately 38 million in 2020. Approximately 1.5 million adults and children were newly infected with HIV illustrating continued HIV transmission on a global level. Sub-Saharan (East, Central, West and South) Africa remains the most severely affected region, with approximately 1 more than 25 million of adults and children living with HIV. (Table retrieved from the Joint United Nations Programme on AIDS, 2021 at https://www.unaids.org/sites/default/files/media_asset/JC3032_AIDS_Data_book_2021_En.pdf. Licence: CC BY-NC-SA 3.0 IGO).

	Adults and children living with HIV	Adults and children newly infected with HIV	Adult and child deaths due to AIDS
Eastern and southern Africa	20.6 million [16.8 million–24.4 million]	670 000 [470 000–930 000]	310 000 [220 000–470 000]
Western and central Africa	4.7 million [3.9 million–5.8 million]	200 000 [130 000–330 000]	150 000 [100 000–210 000]
Middle East and North Africa	230 000 [190 000–310 000]	16 000 [12 000–28 000]	7900 [6000–13 000]
Asia and the Pacific	5.8 million [4.3 million–7.0 million]	240 000 [170 000–310 000]	130 000 [87 000–200 000]
Latin America	2.1 million [1.4 million–2.7 million]	100 000 [66 000–150 000]	31 000 [20 000–46 000]
Caribbean	330 000 [280 000–390 000]	13 000 [8700–18 000]	6000 [4300–8500]
Eastern Europe and central Asia	1.6 million [1.5 million–1.8 million]	140 000 [120 000–160 000]	35 000 [28 000–43 000]
Western and central Europe and North America	2.2 million [1.9 million–2.6 million]	67 000 [53 000–81 000]	13 000 [9200–17 000]
GLOBAL	37.7 million [30.2 million–45.1 million]	1.5 million [1.0 million–2.0 million]	680 000 [480 000–1.0 million]

Note: The ranges around the estimates in this table define the boundaries within which the actual numbers lie, based on the best available information.
Source: UNAIDS epidemiological estimates, 2021 (https://aidsinfo.unaids.org/).

1.1.3 Natural infection of HIV

HIV/AIDS is characterised by a spectrum of conditions caused by infection with HIV. Cells infected with HIV or virions have to cross a mucosal barrier to reach the bloodstream. When in the bloodstream, the virus disseminates throughout the body, resulting in high levels of infected CD4+ T lymphocytes (Sharp & Hahn, 2011). Peak viraemia occurs approximately 30 days post-infection, accompanied by low CD4+ T lymphocyte levels. Additionally, the infected individual starts to experience a HIV-specific immune response, causing an intensive immune response. Subsequently, the HIV-infected individual experiences feverish symptoms. In HIV, virulence is a measurement of the rate at which an HIV-infected patient progresses to AIDS and the transmission potential of the virus. Untreated HIV replication causes progressive CD4+ T-lymphocyte loss and a range of several immunological abnormalities, leading to an increased risk of opportunistic infections, as well as neurological and oncological complications (Deeks *et al.*, 2015; Kramer, 2010). These complications fall under the AIDS condition. Indeed, HIV causes immune compromise subsequent to the gradual decline of CD4+ T cells. HIV inserts its DNA into the genome of the hosts CD4+ T- lymphocytes in order to produce viral proteins and replicate. Active viral replication results in host cell death rendering the patient increasingly immunocompromised. HIV affects almost every system in the body making patients vulnerable to a broad variety of infective and non-infective complications. There is an established link between reduced numbers of CD4+ cells in peripheral blood (CD4+ count) and increased rates of HIV- associated complications and deaths (Lundgren *et al.*, 2015).

However, it should be noted that the number of HIV-related deaths has declined since the advent of antiretroviral therapy in the late 1980s.

1.2 Control of HIV epidemics; the advent of antiretroviral therapy

There is currently no cure for HIV. To prevent transmission, initial efforts to control the spread of HIV relied on intervention approaches such as promotion and provision of condoms, sexual health education, promotion of HIV testing, and counselling and behaviour change interventions targeted at high-risk populations. Unfortunately, none of the interventions had a significant impact in reducing the spread of HIV (Ross, 2010).

Despite several efforts to develop a vaccine against HIV, no vaccine has been successful enough to prevent HIV infection. Strategies in HIV vaccine development involved antibody-induced protection and cell-mediated immune response, both of which were deemed unsuccessful to warrant protection against HIV infection. Out of all the HIV vaccine efficacy trials conducted so far, the HIV-1 RV144 trial conducted in Thailand focusing on canarypox-expressed membrane-anchored gp120 proved to be partially successful, warranting the first and only protection (31.2%). However, this protection diminished with a rapid contraction of a poorly durable antibody response (Robinson, 2018). Hopes for an early breakthrough are not high given that the underlying immunological responses required to provide protective immunity against HIV are currently unknown (Roberts, 2016; Robinson & Gazzard, 2005).

However, advances in modern pharmacotherapy have transformed HIV from a terminal disease to a chronic but manageable condition through the development of antiretroviral therapy (ART). Soon after the availability of antiretroviral agents in the late 1980s, it became evident that ART is an effective management strategy implemented in hopes of reducing progression of disease to AIDS and HIV-related deaths. Many clinical trials and care settings have shown that ART, when adhered to, profoundly improves clinical outcomes in HIV patients by reducing HIV progression to AIDS and HIV-related deaths (Forsythe *et al.*, 2019). These include reduced HIV progression to AIDS, better quality of life, reduced hospitalisation, and death rates (Mannheimer *et al.*, 2006). As shown in Figure 1.1, the number of people newly infected with HIV has declined since 1996. Moreover, the number of deaths related to HIV has decreased since the early 2000s (~2 million deaths), reaching approximately ~750,000 deaths in 2020 (Figure 1.1).

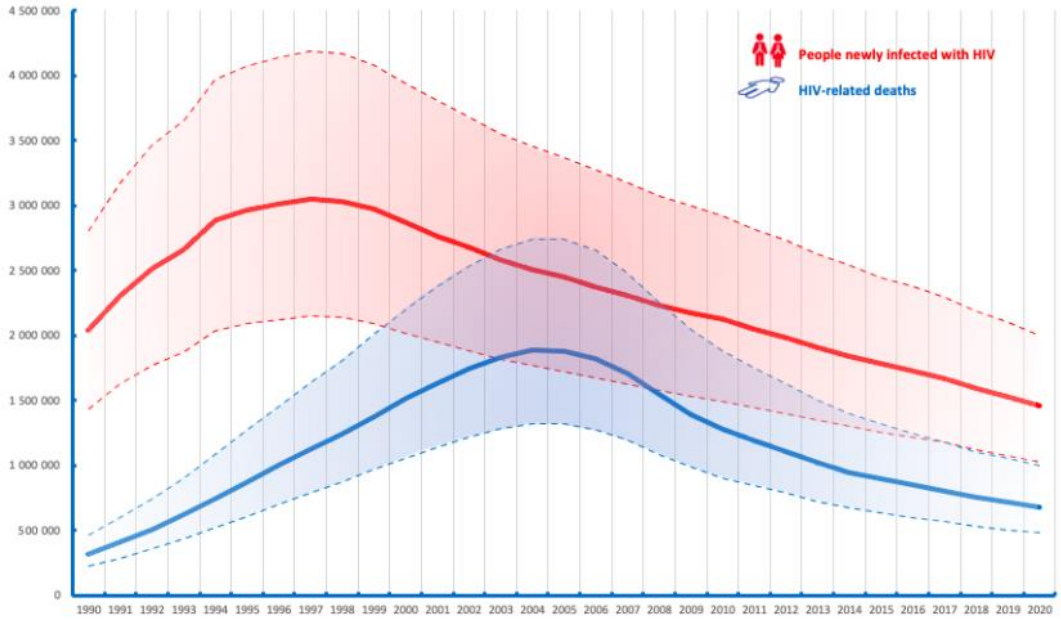

Source: UNAIDS/WHO estimates

Figure 1.1 Decline of HIV incidence and HIV-related deaths globally. Following a peak around 1997, reaching nearly 3 million newly HIV-infected people (red), the number of newly infected people continues to decline since then. In 2020, around 1.5 million were newly infected with HIV, showing a decrease in number of newly infected people by nearly half since the late 1990s. Similarly, HIV-related deaths (blue) continue to decline since reaching a peak of approximately 2 million deaths in 2004-2006. In 2020, the number of HIV-related deaths was approximately 600,000. Figure retrieved from the World Health Organization, (2021a) at https://www.who.int/hiv/data/en/. Licence: CC BY-NC-SA 3.0 IGO.

This decline in HIV-related deaths is strongly linked to the advent of ART (Joint United Nations Programme on HIV/AIDS, 2017). Figure 1.2 shows the number of AIDS-related deaths and the number of people receiving HIV treatment. The increase in the numbers of people receiving HIV treatment coincides with a decline in AIDS-related deaths.

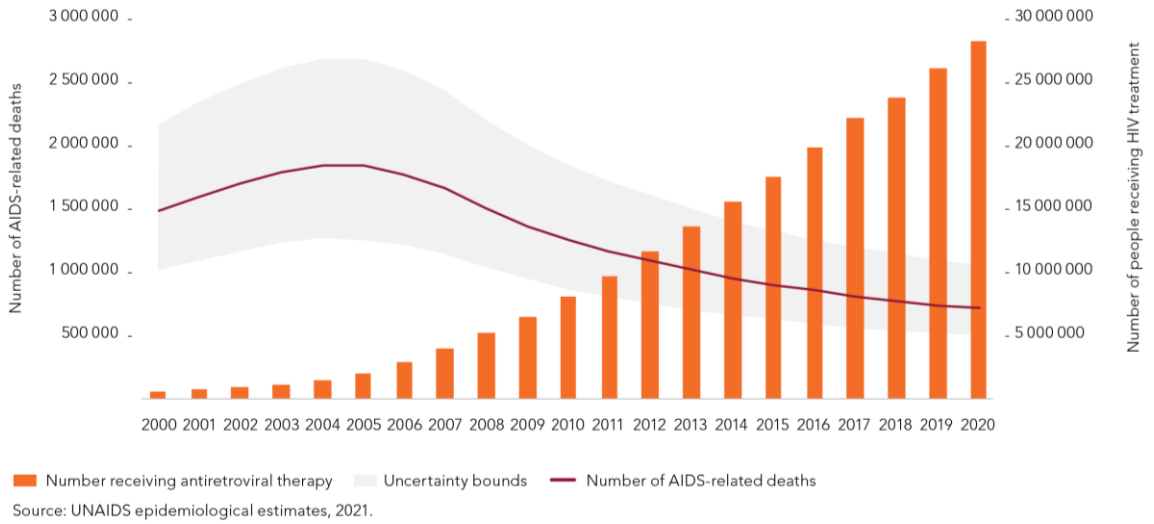

Figure 1.2 Number of global AIDS-related deaths and number of people receiving HIV treatment. Data from 2000 to 2020 show increasing usage of ART coinciding with a radical decline in AIDS-related deaths. In the early 2000s, only approximately 1 million HIV-infected individuals had access to HIV treatment alongside over 1.5 million AIDS-related deaths. In 2020, nearly 30 million people had access to HIV treatment, alongside approximately 750,000 AIDS-related deaths. Figure retrieved from the World Health Organization, (2021a) at https://www.who.int/hiv/data/en/. Licence: CC BY-NC-SA 3.0 IGO.

According to the WHO's 2017 report, ART has been the primary contributor to a 48% decline in AIDS-related deaths on a global level (Joint United Nations Programme on HIV/AIDS, 2017). The WHO guidelines recommend initiation of ART in anyone living with HIV, further to evidence that early intervention with ART was associated with better clinical outcomes in HIV-infected individuals compared to later treatment as per The INSIGHT START Study Group data (2015).

1.2.1 Structure and lifecycle of HIV; Therapeutic targets of ART

HIV is a retrovirus, meaning it is an RNA virus that replicates through reverse transcription and subsequently integrates its viral DNA in the host cell's genome. HIV mainly infects CD4+ T-lymphocytes, as they express a CD4 surface receptor (Lifson & Engleman, 1989). Figure 1.3 summarises the HIV lifecycle and different targets in HIV therapy.

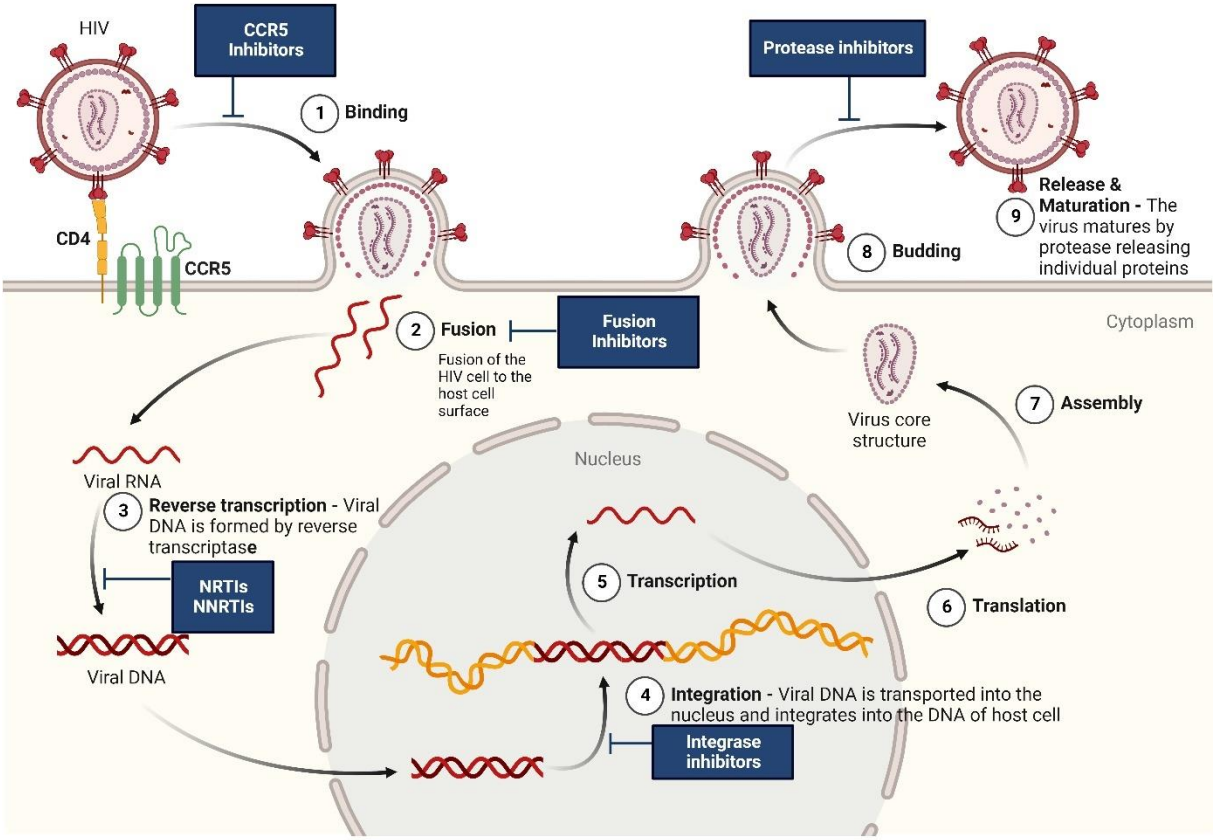

Figure 1.3 Targets of ART in the HIV life cycle. The HIV life cycle undergoes nine steps: binding to the host cell membrane (step 1); fusion, entry of virions, and release of single-stranded RNA into the cytoplasm (step 2); transcription of viral RNA to DNA by reverse transcription (step 3); translocation of DNA to the nucleus and integration to the host DNA (step 4); transcription of mRNA coding for viral proteins (step 5); translation to proteins and post-translational cleavage by HIV protease (step 6, 7 and 8); and viral release and maturation (step 9). Figure adapted from "HIV Replication Cycle", by BioRender.com (2022). Retrieved from https://app.biorender.com/biorender-templates

ART involves a variety of antiretroviral agents that inhibit the replication of HIV at specific steps in its lifecycle. By interrupting the HIV lifecycle, ART reduces viral load and preserves the patients CD4+ T-lymphocytes which helps to maintain an effective immune function. There are currently five classes of antiretroviral agents in clinical use. These include:

(I) Nucleoside/tide reverse transcriptase inhibitors (NRTIs)

NRTIs were the first antiretrovirals to be approved for use in HIV management in the late 1980s (Vella *et al.*, 2012). NRTIs act by disrupting the transcription of viral RNA to DNA (step 3, Figure 1.3) (Atta *et al.*, 2019). They competitively inhibit the viral reverse transcriptase enzyme in the host cell cytoplasm. Subsequently, the conversion of viral single-stranded RNA to double-stranded DNA, also known as viral replication, is prevented. Hence, HIV genetic

material is not incorporated into the host genome. NRTIs mimic nucleoside bases, cytidine, thymidine, guanosine, adenosine, inosine, and uridine, that are needed during the formation of DNA. The nucleoside or nucleotide analogues compete with natural nucleosides/tides and when the HIV reverse transcriptase attempts to incorporate them into the growing DNA chain, the elongation process is halted (Morse, 2015) (Figure 1.4). Older NRTIs include zidovudine, abacavir and stavudine while newer NRTIs, with a better safety and efficacy profile, include tenofovir disoproxil/alafenamide fumarate, emtricitabine and lamivudine. NRTIs are effective against HIV-1 and HIV-2 infection and are also now popular for use as prophylaxis for HIV infection according to the British HIV Association (Reeves *et al.*, 2021).

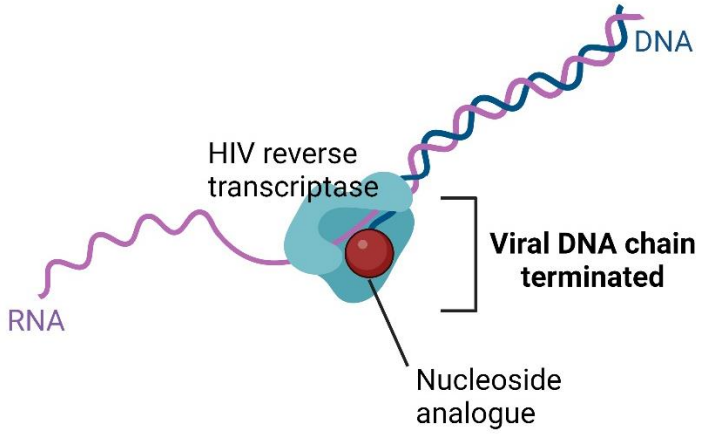

Figure 1.4 The mode of action of NRTIs. Figure created with BioRender.com.

(II) Non-nucleoside reverse transcriptase inhibitors (NNRTIs)

The first NNRTI approved for the management of HIV-1 was nevirapine (1998), now classified as a first-generation NNRTI alongside efavirenz. Second-generation NNRTIs such as etravirine and rilpivirine were approved in hopes of ameliorating first-generation NNRTI efficacy and safety profiles. Only recently, the second-generation NNRTI rilpivirine was considered a promising candidate for the prophylaxis of HIV (Bekker *et al.*, 2020). The most recent NNRTI doravirine, has a better resistance profile against HIV. NNRTIs act by disrupting the transcription of viral RNA to DNA (step 3, Figure 1.3) (Atta *et al.*, 2019). Unlike NRTIs, NNRTIs act by inhibiting HIV-1 reverse transcriptase by non-competitive binding to a hydrophobic pocket found in the enzyme which then causes conformational changes and diminished activity of the HIV reverse transcriptase (Apostolova *et al.*, 2017) (Figure 1.5).

NNRTIs are only effective against the HIV-1 infection, limiting their use in the treatment of HIV-2 infection due to HIV-2 intrinsic resistance profiles.

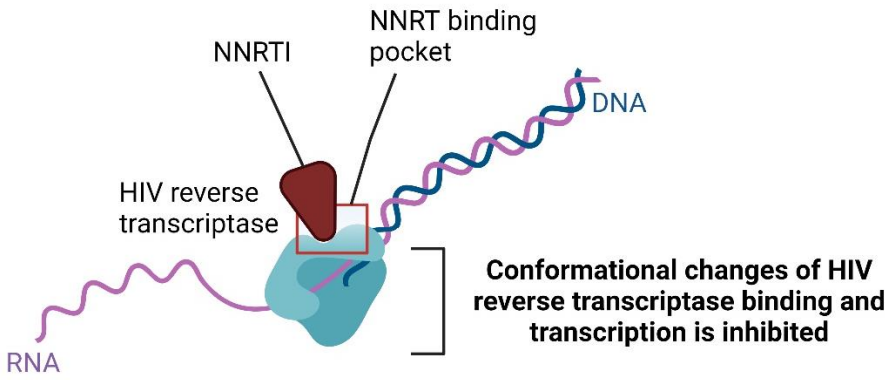

Figure 1.5 The mode of action of NNRTIs. Figure created with BioRender.com.

(III) Protease inhibitors

Soon after the discovery of reverse transcriptase inhibitors, the protease inhibitors were developed in the late 1990s (Vella *et al.*, 2012). Protease inhibitors inhibit the viral protease, a critical enzyme responsible for the synthesis of functional individual viral proteins (step 6, 7 and 8, Figure 1.3) (Atta *et al.*, 2019). Examples of protease inhibitors include nelfinavir, saquinavir, indinavir, darunavir, lopinavir, amprenavir, atazanavir and ritonavir. As part of the improvement of care in HIV patients, ritonavir which was originally developed as a protease inhibitor, is currently exclusively used as a pharmacokinetic booster of other protease inhibitors due to its potent inhibition of the cytochrome CYP 3A4 isoenzyme (Hull & Montaner, 2011). Protease inhibitors are effective against both HIV-1 and HIV-2 infection according to the British HIV Association (Reeves *et al.*, 2021).

(IV) Integrase inhibitors

Integrase inhibitors are relatively new antiretroviral agents, developed in 2007 for the management of HIV-1 and HIV-2 infection (Reeves *et al.*, 2021; Vella *et al.*, 2012). Integrase inhibitors inhibit the viral integrase, hence preventing viral DNA integration into the human genome (step 4, Figure 1.3) (Atta *et al.*, 2019). Examples of integrase inhibitors include: dolutegravir, elvitegravir, cabotegravir and raltegravir.

(V) Fusion and CCR5 inhibitors

The fusion inhibitor, enfuvirtide was developed and approved in the early 2000s (Vella *et al.*, 2012). Enfuvirtide prevents the fusion of the HIV envelope with the host CD4+ cell membrane, which is an essential process for virus replication (step 2, Figure 1.3) (Atta *et al.*, 2019). Another pharmacological approach, consisting of inhibiting HIV co-receptor, was adopted in recent years. Maraviroc, binds to the co-receptor C-C chemokine receptor type 5 (CCR5) which subsequently blocks the entry of HIV into the host cells (step 1, Figure 1.3) (Atta *et al.*, 2019). Fusion and CCR5 inhibitors are effective against both HIV-1 and HIV-2 strains (Reeves *et al.*, 2021).

1.2.2 Clinical use of ART

Confirmation of HIV status using the testing strategy as the original diagnosis must be implemented prior to ART initiation (World Health Organization, 2020). Diagnostic strategies used in HIV are used to detect HIV antigens (*i.e.*, p24) and antibodies specific to HIV. ART is effective at suppressing viral replication; however, it is a life-long treatment that must be taken daily. Over the past years, ART has been improved through the availability of new relatively safer and potent antiretroviral agents. These include the development of newer agents and pharmaceutical formulations.

Zidovudine, the first antiretroviral drug licensed in 1987, paved the way to triple combination ART, also known as highly active antiretroviral therapy (HAART), combination antiretroviral therapy (cART) or simply ART. cART consists of a customised combination of three or more antiretroviral drugs, from different classes, to fit several patient considerations. Triple ART therapy was licensed in 1996 and since then, remains the basis of modern therapy in HIV. This combined pharmacological approach is widely adopted in clinical settings as it has dramatically reduced AIDS-related morbidity and mortality (Sezgin *et al.*, 2018). Furthermore, as opposed to single-drug ART, the combination of three different antiretroviral agents reduces risk of HIV resistance. Current WHO guidelines set in 2019 recommend that initiation of cART should consist of the first-line use of an optimised NRTI backbone which contains two NRTIs and an additional agent, dolutegravir (integrase inhibitor) or efavirenz (NNRTI) for the treatment of HIV-1 in adolescents and adults (World Health Organization, 2021a). In the UK, the current guidelines set by the British HIV association (2016) recommend an NRTI backbone and an

additional NNRTI, ritonavir-boosted protease inhibitor or integrase inhibitor for the treatment of HIV-1. As for the treatment of HIV-2, the British HIV Association suggest the use of two NRTIs plus an integrase inhibitor or a ritonavir-boosted PI, as NNRTIs are not recommended for the treatment of HIV-2 (Reeves *et al.*, 2021).

As drug adherence is of paramount importance in the treatment of HIV, cART has prompted the development of once daily pills to improve patient adherence to ART. The once daily combination pills designed so far include Atripla® (tenofovir DF/emtricitabine/efavirenz), Eviplera® (tenofovir DF/emtricitabine/rilpivirine) and Delstrigo® (tenofovir DF/ lamivudine/doravirine) which contain three antiretroviral drugs and Truvada® (tenofovir DF/emtricitabine) and Kivexa® (abacavir/lamivudine), which contain two NRTIs (Electronic Medicines Compendium, 2018a, 2018b, 2018c, 2019).

In addition to the main use of antiretroviral agents as treatment for HIV infection, antiretroviral agents used as pre-exposure prophylaxis (PreP) and post-exposure prophylaxis (PeP) in HIV are becoming increasingly popular. PreP and PeP represent new opportunities to reduce HIV infection rates in high-risk individuals such as health-care workers, IDUs, sex workers and people engaging in unprotected sex. Since its approval in 2012 by the FDA, Truvada® (tenofovir disoproxil fumarate/emtricitabine) daily has been used to reduce the risk of HIV infection in high-risk adults and has been shown to be effective in doing so in MSM and heterosexual individuals (Grant *et al.*, 2010; Thigpen *et al.*, 2012). As for PeP, according to the UK national guidelines, it is recommended to take a combination of antiretroviral drugs (first-line use of an NRTI backbone) as early as possible and within 72 hours after potential exposure to HIV (National Institute for Health and Care Excellence, 2018). Figure 1.2 shows the ART coverage globally. ART coverage has increased over time since the year 2000. Global ART coverage in 2020 (~28,000,000 HIV-infected individuals on ART) was approximately 28 times higher than that in 2000 (~1,000,000 HIV-infected individuals on ART), reflecting the massive availability of ART coverage throughout the past decades (Figure 1.2). However, the target of providing ART for at least 90% of people diagnosed with HIV, set by the Joint United Nations Programme on HIV/AIDS (UNAIDS) is yet to be achieved globally. This target is part of the UNAIDS 90:90:90 targets agenda for 2020, a major and ambitious treatment target to help eradicate the HIV/AIDS worldwide (Bain *et al.*, 2017). While the target has not yet been achieved on global level, the UK reached the 90:90:90 targets by 2018 and continues to exceed these targets (Public Health England, 2019).

In addition to ART, other treatments are suggested as part of HIV care. These include treatment of HIV-related infections (*i.e.*, antifungals and antibiotics) and non-clinical services used in combination with ART in order to reduce rates of ill health and HIV/AIDS-related deaths among HIV-positive people (Joint United Nations Programme on HIV/AIDS, 2016).

However, despite the undeniable benefits of cART, long-term ART is associated with several adverse effects, some of which are troublesome in some patients.

1.3 ART-associated adverse events

From early on, long-term ART has been associated with adverse effects which continue to cause concern in modern HIV care.

A large list of adverse drug effects is associated with therapeutic doses of antiretrovirals ranging from class-specific adverse events to drug-specific events. Table 1.2 summarises the very common (≥ 1 in 10) and common (≥ 1 in 100 to < 1 in 10) side effects associated NRTIs, NNRTIs, protease inhibitors, integrase inhibitors and fusion/CCR5 inhibitors (Electronic Medicines Compendium, 2018a, 2018b, 2018c, 2019).

Table 1.2 Common adverse events associated with ART classes according to the Electronic Medicines Compendium. The adverse events associated with antiretroviral agents range from gastrointestinal (GI) disorders and lipid abnormalities to psychiatric events.

Drug Class	Adverse reactions
NRTIs	• GI upset (nausea, vomiting and abdominal pain) • Headache • Hyperpigmentation • Rash • Malaise and fatigue • Nasal signs and symptoms • Cough
NNRTIs	• GI upset (abdominal pain, nausea, vomiting and diarrhoea) • Psychiatric events (insomnia, abnormal dreams/nightmares, depression, and anxiety) • Neurological events (dizziness, headache, somnolence, and disturbance in attention) • Rash and pruritis • Dry mouth • Fatigue -Blood tests: decreased white blood cell count, haemoglobin and platelet count • Lab abnormalities Alterations in lipid metabolism: increased total cholesterol, LDL cholesterol and triglycerides Liver tests: increased transaminases and gamma-glutamyltransferase (GGT) Increased pancreatic amylase
Protease inhibitors	• Insomnia • Hyperlipidaemia • Hypocholesteraemia • Diabetes • Headache • Peripheral neuropathy • GI upset • Rash and pruritus • Fatigue
Integrase inhibitors	• Headache • GI upset • Psychiatric events (abnormal dreams, insomnia, depression and anxiety) • Neurological events (headache and dizziness) • Rash and pruritus • Fatigue
Fusion/CCR5 inhibitors	• Anaemia • Anorexia • Psychiatric events (Insomnia and depression) • GI upset • Rash • Lab abnormalities Liver tests: increased transaminases and gamma-glutamyltransferase (GGT)

Despite not being reported in early randomised clinical trials, several other adverse events have been linked to the use of ART as shown in several case reports, observational studies, and *in vitro* and *in vivo* studies. People infected with HIV are now living longer due to the advent of ART and are therefore more likely to acquire additional chronic conditions related to normal ageing, HIV infection itself and ART (Guaraldi *et al.*, 2011; Kalra *et al.*, 2011; Kendall *et al.*, 2014). Several studies were conducted around the World to determine non-infectious comorbidities experienced among the HIV-infected population and the factors associated with the increased incidence of developing these comorbidities in HIV/AIDS infection. According to a retrospective study conducted by Kendall *et al.* (2014) in Canada, the most prevalent comorbidities among the HIV-infected population include diabetes mellitus, hypertension, asthma and chronic obstructive pulmonary disease. In Italy, a 7-year long study showed that diabetes, cardiovascular disease, hypertension, bone fractures and renal failure were the most common non-infectious comorbidities seen in PLWH (De Francesco *et al.*, 2018). The comorbidities experienced in the HIV-infected population are more likely to be a result of the interplay of several factors such as older age, female gender, smoking (which is known to be higher amongst people living with HIV), genetic risk factors, low CD4 count, presence of hepatitis C infection, ART regimens, prolonged ART exposure and HIV severity (Bonfanti *et al.*, 2001; Guaraldi *et al.*, 2011; Kendall *et al.*, 2014; Larson *et al.*, 2006).

Nevertheless, the main comorbidities reported following ART exposure usually fall into the category of metabolic complications such as disorders related to body fat distribution (*i.e.*, lipodystrophy), dyslipidaemia, insulin resistance and diabetes mellitus (Apostolova *et al.*, 2017; De Francesco *et al.*, 2018; Jain *et al.*, 2001; Kendall *et al.*, 2014; Samaras, 2009). Several studies have shown that HIV infection itself causes several metabolic complications such as hypertriglycaemia, hyperlipidaemia, osteoporosis, and hepatic lipogenesis (Brown & Qaqish, 2006; Côté *et al.*, 2002; Jain *et al.*, 2001; Peters *et al.*, 2013).

ART-associated adverse events were extensively investigated by many studies which shed some light into the incidence rates and potential mechanisms underlying the clinical manifestations of these adverse effects. The following section will discuss ART-associated adverse events while giving insight into potential cellular and molecular mechanism(s) behind the adverse events seen in PLWH on ART.

1.3.1 Lipodystrophy and alterations in lipid metabolism in HIV

1.3.1.1 Epidemiology

The main adverse effects reported following long-term ART exposure usually fall into the category of metabolic complications such as changes in body morphology due to fat maldistribution throughout the body (lipodystrophy) and dyslipidaemia (elevated plasma triglycerides and cholesterol) (Apostolova *et al.,* 2017; El Hadri *et al.*, 2004; Jain *et al.*, 2001; Samaras, 2009). The observation that HIV-infected subjects with changes in fat mass or adipocyte dysfunction experienced, in addition to these effects, metabolic dysregulation, prompted several studies to explore abnormal adipose tissue function in this patient population (Hruz, 2010). The findings suggest that NRTIs, NNRTIs, protease inhibitors and integrase inhibitors may play an important role in the development of HIV-associated lipodystrophy syndrome (Pérez-Matute *et al.*, 2013). Lipodystrophy syndrome is characterised by peripheral lipoatrophy and visceral fat redistribution, associated with dyslipidaemia and insulin resistance (Lagathu *et al.*, 2005). HIV infection *per se* can affect adipose tissue as many ART-naïve HIV-infected individuals developed fat alterations (Delpierre *et al.*, 2007 and Koethe *et al*., 2020). While it is appreciated that HIV itself can play a role in impairing adipocyte function in PLWH, ART remains a research area of interest due to its direct role in mediating fat alterations in PLWH.

Early studies have shown that lipodystrophy occurred in patients treated with NRTIs, independent of protease inhibitor therapy (Galli *et al,* 1999; Saint-Marc *et al*. 1999; Boufassa *et al*. 2000; Mallal *et al*. 2000; Molina *et al*. 2000; Jain *et al*. 2001). Later studies suggested that NRTIs, NNRTIs and protease inhibitors act in synergy in causing HIV-associated lipodystrophy syndrome (HALS) (Pérez-Matute *et al.,* 2013). The first-generation NNRTI efavirenz and several protease inhibitors were associated with an increased risk of developing lipodystrophy as per the ACTG 5005 and ACTG 5142 studies (Sension & Deckx, 2015). A recent randomised trial called the Strategic Timing of Antiretroviral Treatment (START) involving a diverse global population of HIV-positive participants with preserved immunity (*i.e*., with high CD4 cell counts) concluded that initiation of the first-generation NNRTI efavirenz was associated with dyslipidaemia, as the data obtained showed increases in total cholesterol, LDL cholesterol and HDL cholesterol (Baker *et al.*, 2017). Besides, one cohort study investigated the lipid profile of dyslipidaemic HIV-positive patients on efavirenz in comparison to their lipid profile after switching to the second-generation NNRTI rilpivirine (Thamrongwonglert *et al.*, 2016).

After the switch to rilpivirine, total cholesterol, LDL cholesterol, HDL cholesterol and triglyceride levels were significantly reduced (Thamrongwonglert *et al.*, 2016). This data prompted the use of rilpivirine instead of efavirenz in these patients for an improved lipid profile. Two recent cohort studies confirmed the improvement of lipid profile after switching to rilpivirine in HIV-positive patients from a PI-boosted or other NNRTI based therapy (Bagella *et al.*, 2018; Gatechompol *et al.*, 2019).

Whether ART or HIV infection itself is responsible for the lipodystrophy and dyslipidaemia observed in PLWH remains a topic of controversy. Therefore, investigation into the role of ART on adipose cells has proven to be useful for initial assessment of the potential of NRTIs, NNRTIS, protease inhibitors and integrase inhibitors to cause a disturbance in lipid metabolism and adipose tissue in PLWH.

1.3.1.2 Mechanisms

Traditionally, adipose tissue is known for its role as a site for fat storage, but it also has an important role in releasing regulatory factors such as adipokines and proinflammatory cytokines that act both locally and on other organs (e.g., pancreas, liver, muscles, heart) to affect overall metabolism (Díaz-Delfín *et al.*, 2011). For example, adipose tissue releases adiponectin, an insulin-sensitising hormone, that affects insulin resistance, as well as the release of inflammatory cytokines including tumour necrosis factor α (TNFα) and interleukin-6 (IL-6) (Díaz-Delfín *et al.*, 2011).

The action of several NNRTIs has been investigated in previous studies, exposing the profound effects of efavirenz on adipocyte function. A study conducted in human preadipocytes showed that efavirenz was cytotoxic and significantly impaired differentiation (Díaz-Delfín *et al.*, 2011). Indeed, efavirenz was associated with inhibition of adipocyte differentiation, and produced an anti-adipogenic and proinflammatory response patterns, effects that could explain the development of lipodystrophy observed in clinical settings (Sension & Deckx, 2015).

The effects of rilpivirine on adipocytes were not investigated until 2013, when Díaz-Delfín *et al.* (2012) compared the effects of the first-generation and second generation NNRTIs, efavirenz and rilpivirine, on adipose cells to further investigate lipodystrophy and changes in lipid metabolism in HIV-1 treated patients (Díaz-Delfín *et al.*, 2012). A 10 μM concentration of both antiretroviral agents revealed that efavirenz was massively cytotoxic to preadipocytes (98% cytotoxicity) in comparison to a moderately cytotoxic rilpivirine (5.1%) (Díaz-Delfín *et*

al., 2012). It was revealed that both efavirenz and rilpivirine caused an impairment in adipocyte differentiation, however, the deleterious effects were more profound following efavirenz exposure. Behl et al's study (2019) found that rilpivirine had no effect on cell viability, however it reduced adiponectin, leptin, and increased resistin levels in adipose cells. Overall, efavirenz can cause deleterious effects in adipocytes, while rilpivirine, at moderate concentrations, did not exert profound damaging effects on adipose cells and endocrine function of adipose cells (Díaz-Delfín *et al.*, 2012). In a study comparing the effects of efavirenz and elvitegravir, an integrase inhibitor, it was shown that elvitegravir altered adipocyte differentiation and function, and promotes induction of proinflammatory cytokines, in a similar way to efavirenz (Moure *et al.*, 2016). Protease inhibitors have also been associated with lipodystrophy and *in vitro* studies support these findings. Protease inhibitors such as ritonavir were shown to induce apoptosis in adipocytes (Grigem *et al.*, 2005).

Mitochondria are complex, unique, dynamic, and semi-autonomous organelles in the centre of a wide range of important cellular physio-pathological roles. These organelles produce large quantities of cellular energy in the form of adenosine triphosphate (ATP), via the electron transport chain (ETC) composed of complexes I through IV. They are also involved in cell growth, signalling, regulation of cell death pathways, ROS generation and oxidative stress. Mitochondria have been implicated in several pathologies such as diabetes, neurodegenerative diseases and cancer, and there is growing evidence that suggests the mitochondria is a targeted organelle in ART-induced toxicities (Apostolova *et al.*, 2011b; Monsalve *et al.*, 2007). These include mitochondrial DNA (mtDNA), mitochondriogenesis, membrane structure and transport (Complex I-IV), matrix metabolism, respiration, and ATP generation (Apostolova *et al.*, 2011b).

Mitochondrial dysfunction is particularly relevant to the aetiology of ART-associated lipodystrophy, which consists of a series of metabolic disturbances caused by changes in adipocyte differentiation, an imbalance between lipogenesis and lipolysis, and induction of apoptosis (Apostolova *et al.*, 2011a; Apostolova *et al.*, 2011b).

Boothby *et al.* (2009) compared subcutaneous fat in HIV-infected individuals before a six-month treatment with the NRTI zidovudine versus the NRTI tenofovir DF and concluded that zidovudine altered several key mitochondrial electron transport genes and subsequently triggered oxidative stress. Older NRTIs such as zidovudine, stavudine and didanosine were also shown to cause mitochondrial dysfunction in adipocytes by depleting mitochondrial DNA

(mtDNA) and reducing mitochondrial proliferation (Chen *et al.*, 1991; Nolan *et al.*, 2003). These depletion in mtDNA were explained by the so-called 'Polymerase γ hypothesis' (Kakuda, 2000). As discussed previously, NRTIs effectively inhibit HIV replication by acting on the viral DNA polymerase, reverse transcriptase. However, they can also, unintentionally, inhibit structurally similar human DNA polymerases such as the mtDNA polymerase γ. The depletion in mtDNA disrupts the production of ETC proteins and comprises mitochondrial function by decreasing mitochondrial membrane potential (Δψm), respiration rate and ATP levels in the mitochondria, while increasing ROS production (Apostolova *et al.*, 2011a). This, in turn, affects the critical metabolic functions of the mitochondria such as oxidative phosphorylation (OXPHOS) and oxidation of fatty acids (Margolis *et al.*, 2014).

Both studies conducted by Díaz-Delfín *et al.* (2011) and (2012) showed that the first-generation NNRTIs efavirenz and nevirapine heavily impaired adipocyte function by affecting decreasing the number of gene transcripts responsible for adipogenic differentiation and of peroxisome-proliferator-activated receptor (PPAR) and CCAAT-enhancer-binding protein alpha (C/EBPα), which are major transcription factors in adipose tissue cells (Díaz-Delfín *et al.*, 2011). In Diaz-Delfin *et al.*'s study (2011), the inhibition of adipocyte differentiation in human preadipocytes exposed to efavirenz occurred in parallel with the induction of proinflammatory pathways (*i.e.*, secretion of proinflammatory cytokines interleukin-6 and -8). Rilpivirine impaired expression of the master transcription factors of adipogenesis and lipid accumulation PPARγ, C/EBPα and sterol regulatory element binding transcription factor 1 (SREBP-1), and their metabolic (LPL) and adipokine (adiponectin) targets (Diaz-Delfin *et al*., 2012). Interestingly, the latter effects were observed at relatively high concentrations of rilpivirine and low concentrations of efavirenz. Additionally, the expression of genes for proinflammatory cytokines such as IL-6 and interleukin-8 (IL-8) were markedly increased in adipocytes exposed to low concentrations of efavirenz (2 and 4 μM) and 10 μM rilpivirine (Diaz-Delfin *et al*., 2012). Similar findings were shown in a recent study were a higher concentration of rilpivirine (10 μM) evoked a significant release of IL-8 in human adipocytes (Behl *et al.*, 2019).

Recently, the integrase inhibitors dolutegravir and raltegravir were shown to directly impact adipocytes and adipose tissue. Indeed, dolutegravir and raltegravir induced adipogenesis, lipogenesis, oxidative stress, mitochondrial toxicity and fibrosis in human/simian adipose tissue and human adipocytes (Gorwood *et al.*, 2020).

Changes in lipid metabolism and lipodystrophy caused by ART may play a role in increasing the risk of further metabolic complications such as insulin resistance and diabetes, due to their blunting role on insulin sensitivity and glucose homeostasis.

Gradually, the accumulation of dysfunctional mitochondria, resulting from mitochondrial toxicity caused by older NRTIs, NNRTIs and integrase inhibitors may manifest in clinical signs and symptoms related to lipodystrophy.

1.3.2 Cardiovascular complications

1.3.2.1 Epidemiology

It is well established that HIV infection *per se* increases the risk for cardiovascular disease (CVD), however, certain antiretroviral agents have been implicated in increasing the risk of cardiovascular disease through their potential in causing alterations of lipid profiles, platelet dysfunction, and/or endothelial dysfunction (Baker *et al.*, 2017; Butt *et al.*, 2011; Freiberg *et al.*, 2013; Sico *et al.*, 2015). HIV-infected patients are at increased risk for early CVD, which is, currently, a major cause of morbidity and mortality. HIV-associated CVD is usually manifested as atherosclerotic disease, which causes coronary heart disease, stroke, heart failure and even sudden cardiac death (Baker *et al.*, 2017; Butt *et al.*, 2011; Freiberg *et al.*, 2013; Sico *et al.*, 2015). HIV-associated atherosclerosis has distinct mechanisms including chronic inflammation and immune activation due to HIV infection but also, due to ART (Hsue & Waters, 2018). A study involving over 24,500 patients infected with HIV showed that exposure to the first-generation NNRTI efavirenz and the NRTIs lamivudine, abacavir and zidovudine, was significantly associated with increased risk of cardiovascular events (Desai *et al.*, 2015).

In summary, certain ART agents increase the risk of cardiovascular disease, mediated, partly, via traditional CVD disease risk factors such as lipodystrophy, dyslipidaemia and insulin resistance (Fiala *et al.*, 2004). However, several NRTIs and NNRTIs were shown to cause endothelial dysfunction, an initiating event in the development of atherosclerosis (Xue *et al.*, 2013).

1.3.2.2 Mechanisms

NRTIs such as zidovudine were found to induce endothelial dysfunction and increase cell death (Hebert *et al.*, 2004; Xue *et al.*, 2013). Furthermore, zidovudine was found to disrupt mitochondrial function and junctions in endothelial cells, which could potentially cause vascular damage (Fiala *et al.*, 2004). Culminating evidence suggests that mitochondrial dysfunction and its subsequent ROS generation are key factors in the pathogenesis of NRTI-induced endothelial dysfunction (Xue *et al.*, 2013). The direct inhibitory effects of NRTIs on the activity of complexes I to IV have been reported and seem to justify the increased ROS production seen in NRTI-induced endothelial dysfunction (Xue *et al.*, 2013).

As for NNRTIs, exposure to efavirenz for 24 hours has been shown to cause a dose-dependent increase in apoptosis and necrosis rates, while reducing cell viability in endothelial cells (Faltz *et al.*, 2017). *In vitro* and *in vivo* evidence points to the ability of efavirenz to cause mitochondrial dysfunction and induce oxidative stress and ER stress in endothelial cells. Jamaluddin *et al.* (2010) concluded that efavirenz increased oxidative stress in human coronary artery endothelial cells, reflected by a rise in superoxide production and a decrease in glutathione. Furthermore, efavirenz has been shown to increase mitogen activated protein kinase (MAPK) and c-Jun N-terminal kinase (JNK) phosphorylation and transcription factor nuclear factor κB (NF-κB) activation in these cells (Jamaluddin *et al.*, 2010). Interestingly, the latter effects observed were believed to be linked to a loss in $\Delta\psi m$ and increases in oxidative stress levels (by promoting superoxide production and reducing GSH levels) in endothelial cells (Apostolova *et al.*, 2011b). Efavirenz was shown to also induce ER stress with a concomitant increase in autophagy in endothelial cells (Weiß *et al.*, 2016b). Faltz *et al.* (2017) study demonstrated that the efavirenz component of Atripla®, but not tenofovir nor emtricitabine, causes cellular dysfunction in endothelial cells. Exposure to efavirenz in male rat aortic rings *ex vivo* resulted in an impaired acetylcholine-mediated relaxant response. Furthermore, the efavirenz-induced endothelial dysfunction observed was mediated by an increased level of oxidative stress and activity of the DNA repair enzyme poly (ADP-ribose) polymerase (PARP). PARP activation has been shown to cause disruption of $\Delta\psi m$ and may lead to the destruction of the mitochondria as demonstrated by broken cristae and swelling (Virág *et al.*, 2013).

In summary, the first-generation NNRTI efavirenz and NRTI zidovudine cause cellular stress and dysfunction in endothelial cells, contributing to the development of cardiovascular complications in PLWH on ART.

1.3.3 Hepatotoxic effects

1.3.3.1 Epidemiology

Since the widespread use of ART, liver diseases represent an important cause of morbidity and mortality in the HIV population, owing to its significance. Data obtained from the Data Collection on Adverse events of Anti-HIV Drugs (D:A:D) concluded that liver-related death was the one of leading causes of non-AIDS-related death in the HIV population (Weber & Sabin, 2006). PLWH who are receiving antiretroviral treatment frequently have mildly abnormal liver test results (Table 1.2) that, to date, have not been linked unambiguously to the toxic effects of several antiretroviral agents. However, several studies found that the incidence of hepatotoxic effects in PLWH was higher in HIV patients on ART than in treatment naïve HIV patients.

Evidence shows that first-generation NNRTIs such as nevirapine and efavirenz have been associated with liver toxicity in several studies (Casado, 2013; van Leth *et al.*, 2004). A large, randomised trial, the 2NN trial, found that the use of efavirenz and nevirapine alone or in combination induced liver toxicity, however the frequency of liver toxicity was higher in subjects treated with nevirapine alone (13.2%) in comparison to subjects treated with efavirenz alone (4.5%) (van Leth *et al.*, 2004). Similar findings were demonstrated in other studies, determining that the incidence of hepatotoxicity in patients on nevirapine (4-18%) was higher than in patients on efavirenz (1-8%) (Casado, 2013; Shubber *et al.*, 2013; Terelius *et al.*, 2016). On the other hand, second-generation NNRTIs show more promising clinical and pathogenic data on hepatotoxicity in the HIV population. As explained by Casado (2013), both the second-generation NNRTIs rilpivirine and etravirine were not linked to liver toxicity, thus suggesting it is safe to use in clinical setting in patients with or without liver abnormalities at baseline.

Protease inhibitors, particularly ritonavir was linked to the highest incidence of hepatotoxicity among other protease inhibitors (nelfinavir, saquinavir and indinavir) and NRTIs (Sulkowski, 2004). Clinical manifestations of NRTI-associated hepatotoxicity have an average of 1.3 patients per 1000-person years (Fortgang *et al.*, 1995). Asymptomatic elevated aminotransferases are noted in PLWH on NRTI-based therapy. However, symptoms of liver damage typically develop gradually over a few days to over several months of ART initiation. Progression of liver damage to fulminant hepatic failure can occur but only infrequently (Casado, 2013). This progressive injury caused by the use of long-term ART, however, may be

of importance in the presence of pre-existing liver disease such as chronic hepatitis co-infection or alcoholic liver disease, and immunodeficiency as reflected by the increased hepatic mortality seen in the HIV population (Antiretroviral Therapy Cohort Collaboration, 2010; Lemoine *et al.*, 2012; Weber & Sabin, 2006). Due to a lack of standardised markers of liver toxicity, there has been a wide variation for the incidence of hepatotoxicity among the HIV population worldwide.

Although several NRTIs and protease inhibitors were associated with hepatotoxic effects, the first-generation NNRTIs efavirenz and nevirapine were found play a key role in ART-associated liver toxicity (Casado, 2013; Ena, 2003; Hernandez *et al.*, 2001).

1.3.3.2 Mechanisms

A number of discrete mechanisms of liver injury in the ART context were identified. These include mitochondrial toxicity, oxidative stress, and ER stress.

The mitochondria are the primary source of useful energy to the hepatocyte. Therefore, any damage to mitochondrial function can lead to hepatic injury. It was reported that the first-generation NNRTI efavirenz, but not the second-generation NNRTI rilpivirine, the integrase inhibitor raltegravir and the protease inhibitor darunavir, was shown to cause mitochondrial toxicity in hepatocytes (Blas-García *et al.*, 2014). Efavirenz triggered mitochondrial dysfunction in hepatocytes, characterised by a loss of $\Delta\psi m$ and reduction of cellular ATP levels (Blas-García *et al.*, 2010; Ganta *et al.*, 2017). These events were linked to efavirenz's direct inhibitory effect on mitochondrial complex I. By inhibiting complex I activity, efavirenz profoundly increased the production of ROS in hepatocytes (Apostolova *et al.*, 2010; Blas-García *et al.*, 2014; Blas-García *et al.*, 2010). Further, efavirenz induced cell apoptosis through the mitochondrial pathway in hepatic cell lines (Apostolova *et al.*, 2017; Apostolova *et al.*, 2011b; Apostolova *et al.*, 2010; Ganta *et al.*, 2017). These findings were replicated in human hepatic cell lines, as efavirenz was shown to activate apoptosis through the intrinsic pathway, confirmed by an observation of several cell death parameters such as phosphatidylserine exposure to the outer cell membrane, chromatin condensation, mitochondrial pro-apoptotic protein translocation and caspase activation (Apostolova *et al.*, 2010; Ganta *et al.*, 2017).

Furthermore, efavirenz but not rilpivirine, caused a significant induction of ER stress in hepatic cells (Blas-García *et al.*, 2014). Indeed, the mRNA and protein expression of ER stress markers such C/EBP homologous protein (CHOP) and glucose-regulating protein 78 (GRP78) was upregulated in hepatocytes exposed to efavirenz (Apostolova *et al.*, 2013). Other signs

suggestive of ER stress, such as morphological changes in the ER and enhanced cystolic Ca^{2+} content, were also observed in efavirenz treated primary human hepatocytes and Hep3B cells (Apostolova *et al.*, 2013).

In all, it is plausible that the deleterious effects caused by older NRTIs and the first-generation NNRTI efavirenz may be relevant to the development of ART-associated hepatotoxicity.

1.3.4 Neuropsychiatric and neurocognitive disorders

1.3.4.1 Epidemiology

Certain antiretroviral agents were reported to mediate neuropsychiatric and neurocognitive disorders. HIV-associated neurocognitive disorders (HAND) encompass a syndrome of progressive deterioration of memory, cognition, behaviour, and motor function induced by HIV infection and fuelled by immune activation. Immune activation plays a central role in neuropathology and neurodegeneration in HAND, by inducing neuronal apoptosis possibly via oxidative stress (Gray & Heart, 2010). Antiretroviral agents with central nervous system penetration effectiveness can be useful in the treatment of HIV-induced neurocognitive disorder. However, there is an important shortcoming: NNRTIs, NRTIs, protease inhibitors and integrase inhibitors are potential contributors to the persistence and evolution of clinical presentation of HAND.

1.3.4.2 Mechanisms

The most researched antiretroviral agent in the context of neurodegeneration in HIV is the first-generation NNRTI efavirenz. Efavirenz has been shown to undermine cellular viability in neurones and astrocytes, as well as induce apoptosis and autophagy in neurones, astrocytes, and glial cells (Apostolova *et al.*, 2017; Apostolova *et al.*, 2015; Stauch *et al.*, 2017). Older NRTIs were also found to induce neuronal apoptosis. More specifically, zalcitabine was shown to increase pro-apoptotic proteins and decrease anti-apoptotic proteins in neuronal cells (Bertrand *et al.*, 2019).

It is widely accepted that mitochondrial dysfunction plays a fundamental role in the pathogenesis of neurodegenerative diseases (Apostolova *et al.*, 2017; Apostolova *et al.*, 2015; Stauch *et al.*, 2017).

Efavirenz has been shown to directly affect mitochondrial function in *in vitro* studies. Signs of mitochondrial dysfunction such as decreased $\Delta\psi m$, increased ROS and reduced cellular ATP

stores were observed in efavirenz-treated SweAPP N2a neurones, striatal nerve terminals, glial cells and astrocytes (Brown *et al.*, 2014). In addition, longer exposure to efavirenz induced nitric oxide synthase (iNOS) expression in cultured glial cells and neurons, which in turn resulted in higher levels of nitric oxide (NO), which is a known mediator of mitochondrial dysfunction in HIV-associated central nervous system symptoms (Apostolova *et al.*, 2015). Efavirenz is believed to cause mitochondrial dysfunction in neurones and glial cells by its established direct inhibitory effect on complex I previously seen hepatocytes (Apostolova *et al.*, 2015). This effect could explain the increased generation of ROS and disruptions in $\Delta\psi m$ seen in efavirenz-treated neurones and glial cells (Apostolova *et al.*, 2015). On the other hand, Streck *et al.* (2011) demonstrated that efavirenz inhibited the activity of mitochondrial complex IV (Streck *et al.*, 2011). Additionally, Jin *et al.* (2016) found that exposure to efavirenz lead to a decrease in the proliferation of neuronal stem cells in both *in vitro* and *in vivo*, ensuing the presence of mitochondrial effects such as a significant drop in $\Delta\psi m$ and ATP levels. In general, oxidative stress has been shown to be a common denominator in the progressive and selective loss of neuronal structure and function seen in neurodegeneration (Apostolova *et al.*, 2017). With this in mind, efavirenz-induced oxidative stress in neurones, glial cells and astrocytes may be of great relevance. As for nevirapine, it was found to cause damaging effects on mitochondrial respiration in the striatal nerve terminals, although these effects were not as significant compared to efavirenz (Stauch *et al.*, 2017).

The toxicity of NRTIs, and particularly the first-generation NNRTI efavirenz in neurones, glial cells, astrocytes and striatal nerve terminals may contribute to the development of neurodegenerative disease in HIV patients on efavirenz-containing regimens.

In summary, several antiretroviral agents, particularly the first-generation NNRTI efavirenz, older NRTIs and protease inhibitors, have been associated with numerous adverse events including lipid metabolism disorders, lipodystrophy, hepatic injury, cardiovascular complications, neurocognitive and neuropsychiatric disorders.

Alterations in lipid metabolism is often accompanied with the development of T2D, another commonly reported adverse event in PLWH. The following section will focus on one of the most commonly reported metabolic disorders in the HIV population: diabetes mellitus.

1.4 HIV and Type 2 Diabetes

An ageing HIV-infected population has augmenting recognition for its unique risk factors for developing metabolic diseases, including T2D. Several studies around the world investigated the rate of incidence of diabetes in PLWH and identified key risk factors for the development of diabetes in the HIV population.

1.4.1 Epidemiology

The Multicenter AIDS Cohort Study conducted across several states in the USA determined a higher incidence of diabetes in HIV-infected men in comparison to non-HIV-infected men (Brown *et al.*, 2005a). The incidence of T2D was reported to be increased by 4-fold in HIV-positive men on HAART in comparison to HIV-seronegative men (Table 1.3). Another 10-year long follow up study conducted in France reported an incidence rate of 14.1 per 1000 person-years of follow-up in HIV-infected patients after ART initiation (Capeau *et al.*, 2012) (Table 1.3). In Taiwan, the incidence rate for developing diabetes was 13.1 cases per 1000 person-years in HIV-infected patients receiving ART (Lo *et al.*, 2009) (Table 1.3). The incidence rate of new-onset diabetes reported in the Data Collection on Adverse Events of Anti-HIV Drugs cohort study (n = 33,389 HIV-infected subjects) conducted in Europe, USA, Argentina, and Australia was 5.72 per 1,000 per-year follow up (Wit *et al.*, 2008). In South Africa, a recent large cohort study which included 56,298 HIV-infected subjects on ART reported an incidence rate of new-onset diabetes of 13.24 per 1000 person-year follow up (Karamchand *et al.*, 2016). In the Asia-Pacific region, the incidence of T2D was reported as 1.08 per 100 person-years (Han *et al.*, 2019).

In sum, the incidence rate of diabetes varied among the global HIV population (5.72 to 47 cases per 1000 person-years), however, it is clear that the incidence of T2D in the HIV-infected population is higher than in the non-HIV population. The differences in incidence rates may be due to several factors. Discrepancies in incidence rates may be due to socio-economic (*i.e.*, diet, lifestyle particularly access to exercising facilities) and socio-demographic (*i.e.*, gender, ethnicity, and age) factors and lack of non-standardised diagnostic criteria of diabetes, as well as differences in research design and length of follow-up time. Also, differences in ART regimens across studies may have played a role in the differences of incidence rates.

1.4.2 Risk factors for diabetes in HIV

While the traditional risk factors for diabetes (older age, specific ethnicities and obesity) are partially responsible for the increased risk of diabetes in the HIV-infected population, numerous studies suggest that long-term chronic inflammation, ART, presence of metabolic syndrome and presence of lipodystrophy contribute to a higher risk of diabetes in the HIV population (Karamchand *et al.*, 2016; Palacios *et al.*, 2003; Peters *et al.*, 2013; Tebas, 2008; Tien *et al.*, 2007; Vigouroux *et al.*, 1999; Wit *et al.*, 2008). According to Capeau *et al.* (2012), older age, being overweight, increased waist-to-hip ratio and lipoatrophy seem to increase the risk of developing diabetes among the HIV population. Similarly, Moyo *et al.* (2013) found that being overweight is associated with the diagnosis of diabetes mellitus in the HIV population in Botswana. More recently, an Ethiopian study reported a link between an increased incidence of diabetes and older age and a high body mass index (BMI) (Getahun *et al.*, 2020). Similar findings were found in a recent study conducted in Thailand, where older age, a high BMI, history of pancreas disease and hyperlipidaemia were identified as risk factors (Paengsai *et al.*, 2019). Another study, conducted by Lo *et al.* (2009), showed that a family history of diabetes was a prominent risk factor for developing diabetes among HIV-infected individuals. In Taiwan, a nationwide cohort study reported that hypertension and hepatitis C virus co-infection increased the risk of diabetes in HIV-infected patients (Lin *et al.*, 2018). In the USA, Tripathi *et al.* (2014) reported that older age, the female gender, non-Caucasian ethnicity, obesity, pre-existing hypertension, dyslipidaemia and hepatitis C infection were linked to a higher risk of diabetes incidence. As for a cohort study conducted in the UK, it was shown that hepatic steatosis, hypertension and HIV infection increased the risk of diabetes in HIV-infected subjects (Duncan *et al.*, 2018).

Despite the fact that some factors may overshadow antiretroviral-mediated effects, specific ART regimens have been directly associated with the development of T2D in PLWH (Brown *et al.*, 2005a; Butt *et al.*, 2009; Karamchand *et al.*, 2016; Lin *et al.*, 2018; Wit *et al.*, 2008). Table 1.3 summarises the main findings of studies focusing on ART use and the risk of diabetes in PLWH.

Since the advent of potent cART in 1996, many HIV-infected patients on ART developed T2D (Carr *et al.*, 1999; Dubé *et al.*, 2005; Jain *et al.*, 2001; Kalra *et al.*, 2011; Vigouroux *et al.*, 1999). Brown *et al*.'s (2005a) large cohort study found that exposure to HAART increased the risk of incident diabetes. Similar findings have been reported in a large cohort study in South

Africa, where exposure to antiretroviral agents increased the risk of incident diabetes, after adjustment of other risk factors such as age and BMI (Karamchand *et al.*, 2016). A study conducted across Europe, the US, Argentina, and Australia reported that exposure to ART increased the risk of diabetes in HIV-infected subjects, ensuing adjustment of other risk factors such as increased lipids and lipodystrophy (Wit *et al.*, 2008). As for the UK, a large cohort study revealed that weight gain following ART initiation increased the risk of diabetes in HIV-infected individuals (Duncan *et al.*, 2018). A nationwide Taiwanese cohort study reported that the HAART cohort had a significantly higher 10-year incidence of diabetes compared to the non-HAART cohort (Lin *et al.*, 2018).

1.4.2.1 Protease inhibitors

According to several studies, most protease inhibitors have been associated with an increased risk of reporting T2D (Capeau *et al.*, 2012; Carr *et al.*, 1999; Justman *et al.*, 2003; Murata *et al.*, 2002; Palacios *et al.*, 2003; Tebas, 2008; Tien *et al.*, 2007) (Table 1.3). The FDA generated labels indicating that protease inhibitors have the potential to cause hyperglycaemia in some HIV-infected patients (Jain *et al.*, 2001). This warning prompted several researchers to conduct studies in order to explore the potential role of protease inhibitors in increasing the risk of developing of T2D. Early studies such as Carr *et al.* (1999) study and Behrens *et al.* (1999) study reported that 7% and 13% of the subjects on protease inhibitors were diagnosed with diabetes mellitus, respectively. Protease inhibitor use was determined as an independent risk factor for diabetes mellitus and was associated with a threefold increase in the risk of reporting incident diabetes (Justman *et al.*, 2003). The Women's Interagency HIV Study showed that the HIV-infected ART-naïve women had a diabetes incidence of 1.53/100 person-years which was lower in comparison to the HIV-infected women on an ART regimen containing a protease inhibitor (2.5/100 person-years) (Tien *et al.*, 2007). According to Lo *et al.* (2009), the use of protease inhibitors was significantly associated with an increased incidence of diabetes mellitus. However, research suggests that not all protease inhibitors have the potential to cause T2D, suggesting a drug-specific effect on the development of T2D (Jain *et al.*, 2001).

1.4.2.2 Reverse transcriptase inhibitors

According to several studies, certain reverse transcriptase inhibitors have also been associated with an increased risk of reporting T2D (Butt *et al.*, 2009; Kalra *et al.*, 2011; Peters *et al.*, 2013) (Table 1.3). The Women's Interagency HIV Study concluded that a NRTI- or NNRTI-containing regimens were associated with a higher diabetes rate (2.89/100 person-years) compared to ART-naïve HIV-infected women (1.53/100 person-years). This study also concluded that longer cumulative exposure to NRTIs (over 3 years exposure) was linked to an increased incidence of diabetes in HIV-infected women (relative hazard 2.64) compared to an exposure of 0 to 3 years (relative hazard 1.81) (Tien *et al.*, 2007). A large cohort study consisting of HIV-infected non-HIV-infected veterans reported that HIV infection itself is not associated with an increased risk of diabetes, however, exposure to an NRTI- or NNRTI-based ART regimens increased the risk of developing diabetes in HIV-infected people (Butt *et al.*, 2009). An increased risk of diabetes in the context of HIV infection was significantly associated with the use of zidovudine (an NRTI), stavudine (an NRTI), and didanosine (an NRTI) (Capeau *et al.*, 2012; Lo *et al.*, 2009; Wit *et al.*, 2008). However, several reverse transcriptase inhibitors such as abacavir (an NRTI) and nevirapine (an NNRTI) were not associated with an increased risk of developing diabetes (Hetherington *et al.*, 2001; Wit *et al.*, 2008).

The first-generation NNRTI efavirenz was also associated with an increased of T2D in HIV-infected individuals (Karamchand *et al.*, 2016; Moyo *et al.*, 2013; Paengsai *et al.*, 2019) (Table 1.3). Regarding nevirapine, a prospective observational study observed that the use of nevirapine was associated with a reduced risk of developing diabetes (Wit *et al.*, 2008). However, to date, no study has attempted to investigate the impact of the use of newer NNRTIs on diabetes in the HIV population. A recent large study conducted across several countries in the Asia-Pacific region observed that NNRTI-based regimens but not NRTI (stavudine and didanosine)-based regimens were associated with incident diabetes mellitus in HIV-infected participants (Han *et al.*, 2019). These findings contradict earlier studies that found an association between stavudine and didanosine use with incident diabetes in HIV.

1.4.2.3 Integrase inhibitors

Limited research focused on the adverse effects of integrase inhibitors; however, integrase inhibitors have recently been shown to cause metabolic effects such as weight gain and new onset diabetes. Following a case report, (Fong *et al.*, 2017) suggested that the use of integrase

inhibitors was associated with diabetes. Recently, a 10-year study with over 22,000 individuals determined that initiating integrase inhibitor- based cART regimens may confer greater risk of diabetes in comparison to NNRTI- based regimens, likely through weight gain (Rebeiro *et al.*, 2021) (Table 1.3).

Table 1.3. Summary of key findings studies investigating T2D incidence in the context of HIV ART

Study details	Study design	Participants	Key findings
Justman *et al*. (2003) USA	Prospective cohort study	HIV-infected women	• PI use was associated with a threefold increase in the risk of reporting incident diabetes
Brown *et al*. (2005b) USA	Cohort study	HIV-infected men and non-HIV-infected men	• The incidence of developing T2D was reported to be increased by 4-fold in HIV-positive men on ART in comparison to HIV-seronegative men • The incidence reported was 4.7 cases per 100 person-years in HIV-positive men on ART vs 1.4 cases per 100 person-years in HIV-seronegative men
Tien *et al*. (2007) USA	Prospective cohort study	HIV-infected women vs non-HIV-infected women	• Cumulative (> 3 years) exposure to NRTIs significantly increased the risk of incident diabetes
Ledergerber *et al*. (2007) Switzerland	Cohort study	HIV-infected adults	• Treatment with NRTI- and PI-containing regimens was associated with the risk of developing T2D • The incidence rate reported was 4.42 cases per 1000 per-year follow up (PYFU)
Wit *et al*. (2008) Europe, USA, Argentina, and Australia	Prospective observational study	HIV-infected men	• The incidence rate of new-onset diabetes was 5.72 per 1,000 PYFU • The NRTIs stavudine and zidovudine were significantly associated with diabetes even after adjustment for potential risk factor for diabetes
Lo *et al*. (2009) Taiwan	Retrospective case-control study	HIV-infected adults	• The incidence rate for developing T2D was 13.1 cases per 1000 person-years in HIV-infected patients receiving ART • Treatment with protease inhibitors or zidovudine (NRTI) increased the risk of incident diabetes
Capeau *et al*. (2012) France	Cohort study	HIV-infected adults	• The incidence rate of developing T2D reported was 14.1 per 1000 person-years of follow-up in HIV-infected patients after ART initiation • Short-term treatment with indinavir (PI), stavudine (NRTI) or didanosine (NRTI) increased the risk of incident diabetes

Moyo *et* al. (2013) Botswana	Retrospective case-control study	HIV-infected adults	• Treatment with efavirenz (NNRTI) or protease inhibitors increased the risk of incident diabetes
Tripathi *et al*. (2014) USA	Cohort study	HIV-infected adults vs non-HIV-infected adults	• Incidence rate of diabetes was higher in the non-HIV-infected group compared with the HIV-infected group (13.60 vs. 11.35 per 1000 person-years) • HIV infection may not be independently associated with increased risk of diabetes • Treatment with protease inhibitors but not NNRTIs significantly increased the risk of incident diabetes in HIV-infected adults
Karamchand *et al*. (2016) South Africa	Cohort study	HIV-infected adults	• The incidence rate of new-onset diabetes in HIV-infected patients on ART reported was 13.24 per 1000 person-year follow up • Treatment with efavirenz (NNRTI), stavudine (NRTI) or zidovudine (NRTI) increased the risk of incident diabetes
Duncan *et al*. (2018) UK	Cohort study	HIV-infected men (several ethnicities)	• T2D prevalence reported was 15.1% in HIV-infected men • ART initiation increased the risk of incident diabetes
Lin *et al*. (2018) Taiwan	Nationwide cohort study	HIV-infected adults	• HAART cohort (7.16%) had significantly higher 10-year incidence of diabetes compared to the non-HAART cohort (2.24%)
Han *et al*. (2019) Cambodia, India, China, Hong Kong, Indonesia, Malaysia, Japan, the Philippines, Singapore, Taiwan, Thailand, Vietnam and South Korea	Cohort study	HIV-infected adults	• The incidence rate of T2D was 1.08 per 100 person-years • No association was found between incident diabetes and NRTI- or PI- based ART regimens • Association was found between incident diabetes and NNRTI-based regimens • T2D in HIV-infected Asians was associated with later years of follow-up, high blood pressure, obesity and older age
Paengsai *et al.* (2019) Thailand	Cohort study	HIV-infected adults	• Regimens containing tenofovir/lamivudine/ritonavir-boosted lopinavir or efavirenz-based regimens were associated with an increased risk of diabetes • The reported incidence of T2D was 11.9 per 1000 PYFU
Fiseha and Belete, 2019 Ethiopia	Cross-sectional study	HIV-infected adults	• Longer duration (>5 years) of ART increased the risk of incident diabetes

Getahun *et al.* (2020) Ethiopia	Cross-sectional study	HIV-infected adults	• Tenofovir (NRTI)-based ART regimens significantly increased the risk of incident diabetes • The prevalence of diabetes reported was 8.6% in HIV-infected adults
Rebeiro et al., (2021) USA and Canada	Cohort study	HIV-infected adults	• The incidence of diabetes reported was 10.7 cases per 1000 persons/year • Initiating first cART regimens with INSTIs or protease inhibitors vs NNRTIs may confer greater risk of diabetes

In summary, conflicting data regarding the incidence of diabetes exists, however, it is apparent that ART is associated with an increased risk of developing T2D in the context of HIV. Certain protease inhibitors, NNRTIs, NRTIs and integrase inhibitors have been associated with an increased incidence of developing diabetes in PLWH. Below, we discuss the iatrogenic effects of these antiretroviral drug classes. In order to explore diabetes in the context of HIV/AIDS, it is necessary to understand the pathophysiology behind T2D, investigate the potential factors linked to an increased rate of incidence of new-onset diabetes in the HIV population and review the current understanding of the molecular basis for diabetes linked to ART.

1.4.3 Pathogenesis of type 2 diabetes in HIV

Due to its complex health and economic sequels, in addition to its steadily increasing prevalence, T2D remains a serious global health problem of our modern day and age. Diabetes has been described as a global burden by the World Health Organization (2016), with an estimated 422 million people living with diabetes worldwide. T2D accounts for more than 90% of all cases of diabetes (Chatterjee *et al.*, 2017). The latest prevalence figures estimate that 3.9 million people in the UK have been diagnosed with T2D during the 2018-2019 period, and 90% of those with T2D. Data obtained from (Diabetes UK, 2018) showcase a frighteningly sharp increase in the number of people diagnosed with T2D, exceeding 100,000 more diagnoses from 2019. At this rate, the number of people living with diabetes is expected to exceed 5 million by 2025 (Diabetes UK, 2018).

T2D has been recognised for its complex pathogenesis and several factors may prevail in individual cases, making it a disease requiring complex personalised care. T2D, previously known as Non-Insulin Dependent Diabetes Mellitus or adult-onset, is a multifactorial disease in which patients suffer from hyperglycaemia ensuing insufficient insulin release, and insulin resistance in target tissues (Chatterjee & Scobie, 2002; Ježek *et al.*, 2019). Hyperglycaemia is followed by hyperinsulinaemia as an over compensatory response of beta cells. This causes a combination of a progressive beta cell dysfunction and loss of beta cell mass, causing further hyperglycaemia (Chatterjee & Scobie, 2002; Ježek *et al.*, 2012). Therefore, the pathogenesis of T2D consists of a vicious cycle between beta cell dysfunction and impaired glucose control. Environmental factors surrounding obesity, which include a sedentary lifestyle and a diet rich in saturated fats, combined with genetic predisposition, contribute to the development of T2D, progressive loss of beta cell function and subsequent beta cell failure (Cnop *et al.*, 2005; Cunha *et al.*, 2008).

The prevalence of T2D in the world is frighteningly increasing and has more than doubled during the past 20 years. Rising obesity rates in both developed and developing countries is partially responsible for this doubling in prevalence (Ciregia *et al.*, 2017; World Health Organization, 2021b). Subjects who are at risk of developing T2D are subject to an initial stage of insulin resistance (IR), defined as 'a subnormal biological response to normal insulin concentrations', followed by beta cell hypersecretion of insulin (hyperinsulinaemia), as a mechanism of compensation (Mantzoros, 2018; Zaccardi *et al.*, 2016). However, beta cells eventually become exhausted and are unable to cope with required insulin secretion. Obese euglycaemic subjects are believed to have reduced insulin sensitivity (approximately -30%) compared to lean euglycaemic subjects. After some time, euglycaemic obese subjects experience further reductions in insulin sensitivity and the subsequent exhausted beta cells are no longer able to secrete enough insulin to normalise blood glucose levels. Therefore, these patients experience hyperglycaemia and hypoinsulinaemia (Zaccardi *et al.*, 2016).

Therefore, T2D is characterized by an interplay between IR and subsequent insufficient insulin secretion (Skelin Klemen *et al.*, 2017). The tissues that are normally involved in glucoregulation such as skeletal muscles, adipose tissue, liver, and pancreas, have been found to be affected by antiretroviral drugs (Hruz, 2010). The relationship between these tissues and their role in glucoregulation should be understood in order to explore the aetiology behind ART-induced metabolic changes seen in PLWH.

1.4.3.1 Insulin Resistance

The susceptibility to T2D is linked to both genetic and acquired factors and its pathogenesis involves the interplay of both IR and beta cell dysfunction (Chatterjee & Scobie, 2002; Skelin Klemen *et al.*, 2017). IR may be defined as an inability of insulin to produce its usual biological effects at circulating concentrations effective in normal subjects. There is failure to stimulate glucose uptake in peripheral insulin-target tissues and to suppress hepatic glucose output (Chatterjee & Scobie, 2002; Garvey, 1992). IR is closely associated with T2D. In considering mechanisms behind IR, it is imperative to summarise the signalling pathway that is triggered by insulin and the downstream metabolic consequences in tissues normally involved in glucoregulation (*i.e.* skeletal muscle, adipose tissue and the liver) (Fazakerley *et al.*, 2018; Ijuin *et al.*, 2015; Summers *et al.*, 2000). Insulin binds to the insulin receptor which in turn stimulates the latter's tyrosine kinase activity, which phosphorylates prototypes of the family of insulin receptor substrate proteins (IRS 1-4) (Ijuin *et al.*, 2015; Summers *et al.*, 2000). This then

activates phosphatidylinositol (PI) 3-kinase and increases phosphatidylinositol 3,4,5-triphosphate (PIP3). PIP3 is responsible for the activation of Akt2 at the plasma membrane, which is essential for the subsequent glucose uptake into the skeletal muscle (Ijuin *et al.*, 2015).

While the role of HIV infection and associated inflammation have been increasingly appreciated, ART remains a key contributing factor in IR in PLWH. Protease inhibitors, NNRTIs, NRTIs and integrase inhibitors have the potential to cause IR, which is considered to be the first step in the development of diabetes in the context of HIV (Gorwood *et al.*, 2020; Larson *et al.*, 2006).

According to Dubé *et al.* (2005), combinations of ART containing zidovudine (an NRTI), lamivudine (an NRTI) and efavirenz (an NNRTI) or didanosine (an NRTI), stavudine (an NRTI) and efavirenz were linked to an increased risk of IR in HIV-infected subjects. Similarly, Wit *et al.* (2008)'s findings suggest that stavudine and zidovudine cause IR. Several studies have come across the deleterious effects of stavudine on glucose metabolism (Dubé *et al.*, 2005; Hadigan *et al.*, 2002; Karamchand *et al.*, 2016; Wit *et al.*, 2008). Stavudine is believed to be a strong positive predictor of IR as shown by insulin response to glucose stimulation, after adjustment of known risk factors of IR (exposure to protease inhibitors, high BMI, older age and high waist-to-hip ratio) in HIV-infected subjects (Hadigan *et al.*, 2002). Additionally, a study conducted by Fleischman *et al.* (2007) observed that insulin sensitivity, evaluated by hyperinsulinaemic euglycaemic clamp significantly decreased after one month of stavudine use in HIV-seronegative subjects. Recently, the integrase inhibitors dolutegravir and raltegravir have shown to induce IR in human and simian adipose tissue and human adipocytes (Gorwood *et al.*, 2020).

As previously discussed, tissues involved in the pathology of IR include skeletal muscle, adipose tissue and the liver. The effects of protease inhibitors, NNRTIs, NRTIs and integrase inhibitors on these tissues are described in the next section.

1.4.3.1.1 Skeletal muscle insulin resistance

Approximately 80% of the insulin-stimulated glucose disposal in the body is found in the skeletal muscles, which reflects the major role of this tissue in the pathogenesis of IR (Phielix & Mensink, 2008). Insulin and contraction stimulate glucose uptake in the skeletal muscles by stimulating the translocation of the glucose transporter type 4 (GLUT4) to the membrane (Hruz,

2010). GLUT4 is vastly abundant in muscle fibres and is responsible for most of the insulin-stimulated glucose transport that occurs in the muscle (Mueckler, 2001). Functional limitation of GLUT4 translocation is believed to predispose individuals to IR. There are two main mechanisms involved in IR in skeletal muscles. These include increased levels of free fatty acids (FFAs) in the plasma and an accumulation of intramyocellular lipid metabolites within the skeletal muscle *i.e.*, long-chain fatty acyl-CoA (LCFA-CoA), diacylglycerol (DAG) and/or ceramide (Phielix & Mensink, 2008). Phielix and Mensink (2008) suggested that increased intramyocellular lipid metabolites are potentially damaging to mitochondrial function, which further exacerbates intramyocellular lipid accumulation.

One of the mechanisms involved in IR induced by ART is the interference with glucose uptake in the skeletal muscle. It is believed that protease inhibitors cause IR by inhibiting the intrinsic activity of the GLUT4 (Noor *et al.*, 2002; Kino *et al.*, 2003; Leow *et al.*, 2003; Murata *et al.*, 2002). According to Ben-Romano *et al.* (2003), the inhibition is rapid, direct, and reversible. According to Nolte *et al.* (2001), indinavir caused a dose-dependent reduction of insulin-stimulated increase in 3-0- methyl-D-glucose transport in rat epitrochlearis muscles, reaching a 58% reduction. Moreover, insulin-stimulated increase in cell-surface GLUT4 was reduced by approximately 70% following exposure to indinavir. These findings suggest that indinavir directly inhibits GLUT4 translocation or intrinsic activity rather than insulin signalling. Interestingly, changes in skeletal muscle glucose uptake caused by the blockade of GLUT4 by lopinavir, ritonavir and amprenavir correlated with reductions in glucose disposal rate as seen *in vitro*. This suggests that protease inhibitor-induced IR is most likely a consequence of a direct mechanistic effect on glucose uptake (Yan & Hruz, 2005).

1.4.3.1.2 Adipose insulin resistance

Adipose tissue plays a critical role in glucoregulation via its role as a storage site for excess energy and endocrine organ (Galic *et al.*, 2010). Beyond its function as a storage site, adipose tissue releases adipocytokines such as adiponectin, leptin and resistin, which have favourable effects on insulin signalling (Hruz, 2010). Research has shown that dysregulation of adipocytokines is an emerging and important mediator by which adipose tissue contributes to systemic IR and metabolic disorders (Waki & Tontonoz, 2007). Changes in adipocytokine secretion by adipose tissue have been observed in the HIV individuals on ART (Hruz, 2010; Jones *et al.*, 2005a; Lagathu *et al.*, 2007). These cytokines, in deficit or excess, are likely

mediators of IR and may contribute to the pathogenesis of diabetes among HIV-infected patients on ART. The protease inhibitors nelfinavir, saquinavir and ritonavir were shown to reduce adiponectin expression in cultured adipocytes (Jones *et al.*, 2005a). Furthermore, studies have reported that several protease inhibitors were associated with altered adipocytokine secretion, which in turn, is linked to the induction of ROS in cultured human adipocytes (Lagathu *et al.*, 2007). NRTIs such as stavudine and zidovudine have also been associated with lower levels of adiponectin (Jones *et al.*, 2005b). Elvitegravir, an integrase inhibitor and the first-generation NNRTI efavirenz, were shown to promote the induction of proinflammatory cytokines and reduce the mRNA expression and release of adiponectin in adipocytes (Moure *et al.*, 2016). Additionally, while elvitegravir had no to little effect on leptin release, efavirenz reduced the release of leptin from adipocytes (Moure *et al.*, 2016).

Obesity, defined as 'increased storage of fatty acids in an expanded adipose tissue mass', is strongly associated with the development of IR in skeletal muscles and the liver (Galic *et al.*, 2010). Previous research has shown that a longer exposure to certain protease inhibitors can lead to disturbance of insulin signalling in adipocytes, which in turn causes an indirect alteration of glucose uptake (Hruz, 2010). Nelfinavir increased intracellular ROS generation and impaired the phosphorylation of protein kinase B in 3T3-L1 adipocytes.

Moreover, protease inhibitors have been shown to interfere with peripheral glucose disposal in *in vitro* studies. Murata *et al.* (2000) observed that indinavir, ritonavir and amprenavir significantly decreased insulin-stimulated glucose uptake in 3T3-L1 adipocytes through a specific and direct inhibition of the activity of the GLUT4 transporter. More specifically, indinavir, at clinically relevant concentrations, seems to selectively inhibit GLUT4 (Murata *et al.*, 2002). Similarly, Yan and Hruz (2005) reported that ritonavir, amprenavir and lopinavir significantly reduced glucose uptake in primary rat adipocytes. However, they also reported that atazanavir had no effect on glucose uptake *in vitro.* These findings are contradicted by a later study conducted by Noor *et al.* (2006). This study concluded that atazanavir alone significantly inhibited glucose uptake by differentiated human adipocytes compared to ritonavir alone (Noor *et al.*, 2006). The mRNA expression of GLUT4, was repressed by the first-generation NNRTI efavirenz and the integrase inhibitor elvitegravir in adipocytes (Moure *et al.*, 2016). By decreasing the levels of adiponectin, rilpivirine may increase the risk of IR (Lihn *et al.*, 2005). Obesity has also been linked to ER stress. The effects of ER stress include activation of JNK or the inhibitory kappa B kinase (IKK) directly or through increased

production of ROS with subsequent serine phosphorylation of IRS-1 (Hruz, 2010).

In summary, NNRTIs, NRTIs, protease inhbitors and integrase inhibitors are associated with IR in muscle and adipose tissue.

1.4.3.1.3 Hepatic insulin resistance

Chronic inflammation associated with visceral obesity induces IR in the liver. Chronic inflammation is linked to the production of abnormal adipokines and cytokines which include TNF-α, IL-1, IL-6, leptin, resistin and FFA. These adipokines and cytokines inhibit insulin signalling in hepatocytes by activating several kinases (*i.e.*, JNK, IKK-β and PKC), protein tyrosine phosphatases and suppressors of cytokine signalling (SOCS) proteins. Subsequently, insulin signalling is impaired at insulin receptor and IRS level. Hepatic IR, in turn, causes impaired hepatic glucose production (HGP) by insulin (Meshkani & Adeli, 2009). These defects in hepatic glucose metabolism are believed to be a consequence of increased plasma FFAs (Buettner & Camacho, 2008; Burcelin *et al.*, 2000; Phielix & Mensink, 2008). Hepatic IR has been observed in individuals following exposure to ART. A study showed that in the absence of HIV infection, a 4-week exposure to indinavir resulted in a worsening of hepatic insulin sensitivity in healthy individuals (Schwarz *et al.*, 2004). Moreover, indinavir impaired insulin signalling in HepG2 hepatocytes (Schütt *et al.*, 2000).

Because the transporter GLUT2 was inhibited after exposure to indinavir in oocytes, this led to the speculation that the blockade of this GLUT2 may be the kinetic mechanism causing these observed effects (Hruz, 2010; Murata *et al.*, 2002).

The cellular and molecular mechanisms of ART-mediated insulin resistance in adipocytes and hepatocytes are outlined in Figure 1.6.

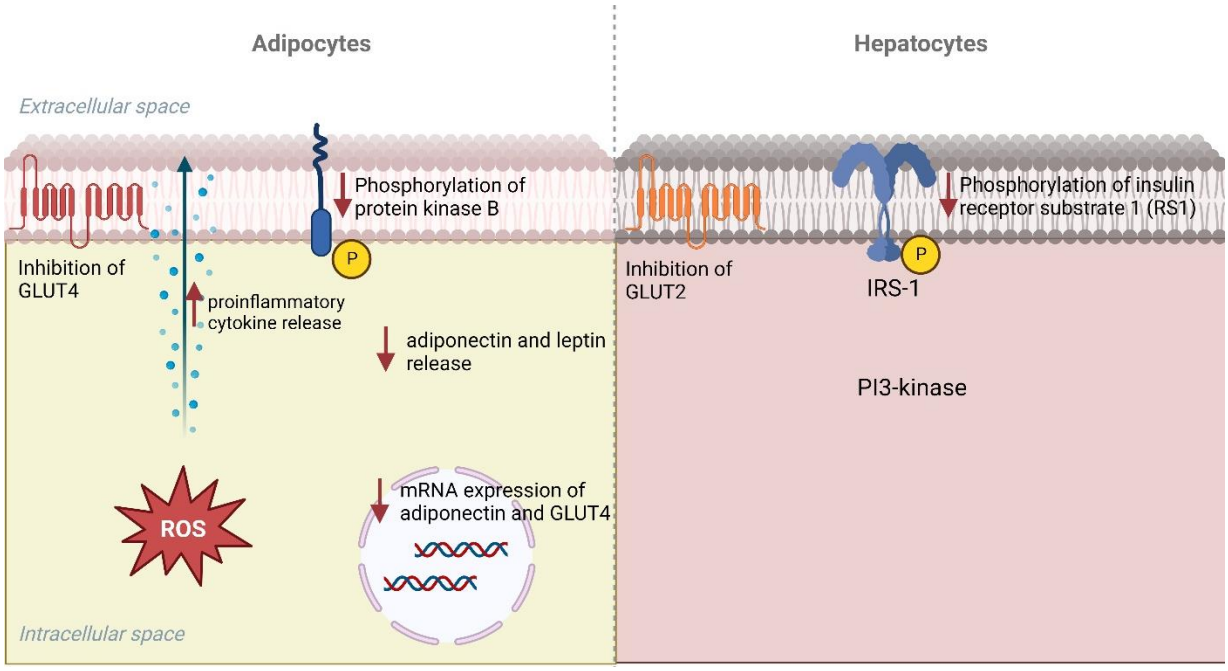

Figure 1.6 Mechanisms of ART-mediated insulin resistance in adipocytes and hepatocytes. Figure adapted from "Cell Membrane Panels Comparison (Layout 3x1)", by BioRender.com (2022). Retrieved from https://app.biorender.com/biorender-templates

It is now widely accepted that when IR develops ensuing environmental factors such as obesity, individuals who are predisposed genetically, fail to effectively compensate for the increased insulin demand, resulting in beta cell failure (Poitout *et al.*, 2010b). However, it is as important to review the role of ART on beta cell dysfunction in the context of diabetes in HIV.

1.4.3.2 Beta cell dysfunction and failure

1.4.3.2.1 Functional identity of beta cells

Pancreatic beta cells are endocrine cells that uniquely synthesise, store and release insulin in a tightly dependent manner (Marchetti *et al.*, 2017). Insulin is an anti-hyperglycaemic hormone that antagonizes the effects of glucagon, glucocorticosteroids, epinephrine, growth hormone and other hyperglycaemic hormones in order to maintain circulating glucose concentration in the physiological range (Marchetti *et al.*, 2017). Beta cells contain approximately 20 pg insulin per cell and constitute around 50 to 80% of all pancreatic islet endocrine cells. In the human pancreas, beta cell mass was reported to be around 0.6 to 2.1 g (DeFronzo *et al.*, 2015). In an adult human being, beta cells release about 30-70 units of insulin per day, mainly depending on body weight (Marchetti *et al.*, 2017). The release of insulin is regulated by a complex network

of several inhibiting, triggering and potentiating signals, which enables the supply of insulin in amount, adaptability, and kinetics to match the minute-by-minute needs of the body (Henquin *et al.*, 2005; Marchetti *et al.*, 2017). Of the secretagogues compounds known to stimulate insulin secretion (e.g., amino acids, FFAs, GLP-1, glucagon, gastrin) glucose is far the most important. Pancreatic beta cells exert their secretory function in a dynamic manner by metabolising glucose, relative to its extracellular concentration by secreting insulin (Joslin & Kahn, 2005; Marchetti *et al.,* 2017). Indeed, intravenous (IV) glucose infusion determines a biphasic insulin response, consisting of an early rapid peak (first phase), followed by a more prolonged and slower increase (second phase) (Marchetti *et al.*, 2017). It is important to maintain an adequate beta cell mass in response to various changes due to the important nature of insulin secretion and overall control of blood glucose levels.

Models of stimulus-insulin coupling are intermingled mechanisms responsible for the exertion of glucose effects on a cellular level. Glucose which is both a trigger and an amplifier of insulin secretion, enters the beta cell via GLUT-1 and -2 (Marchetti *et al.*, 2017). The rapid influx of glucose into the beta cell ensures glucose sensing. This means that the rate of glucose entry is proportional to blood glucose levels. Once in the cell, glucose is rapidly phosphorylated to glucose-6-phosphate (G6P) by the hexokinase enzyme glucokinase (GCK), the molecular glucose sensor that regulates insulin release from beta cells (Skelin Klemen *et al.,* 2017). G6P then undergoes glycolysis in order to produce pyruvate, the three-carbon molecule that enters the mitochondria to be oxidated. In the mitochondria, pyruvate is converted by pyruvate kinase to acetyl-CoA, which in turn reacts with oxalocetate in a reaction catalysed by citrate synthase in order to obtain citrate, a key component of the tricarboxylic acid (TCA) cycle. The TCA cycle leads to the generation of NADH and $FADH_2$, which are used in the production of ATP in the electron chain transport (ETC). Following the ATP production in the mitochondria, ATP is transported to the cytoplasm by the adenine nucleotide translocation (ANT), subsequently triggering the closure of ATP-sensitive potassium (K_{ATP}) channels (Marchetti *et al.*, 2017). Consequently, K^+ efflux is decreased which causes membrane depolarization and subsequent opening of voltage dependent calcium channels, and influx of calcium (Ca^{2+}) ions. This in turn results in increased cytosolic concentrations of Ca^{2+} which allows the fusion of insulin-containing vesicles with the plasma membrane (Skelin Klemen *et al.*, 2017).

Energy in the form of ATP produced by mitochondrial metabolism is the main coupling factor relating glucose metabolism with insulin secretion, whereas other cues amplify and preserve insulin secretion (Marchetti *et al.*, 2017). In T2D, there are several alterations of insulin

secretion (DeFronzo *et al.*, 2015; Marchetti *et al.*, 2017). Reported alterations include absent or blunted first phase insulin release to IV glucose, reduced and/or delayed responses to ingestion of a meal, and progress into decreases in second phase release and secretion to non-glucose stimuli (Marchetti *et al.*, 2017). An early study conducted by Fernandez-Alvarez *et al.* (1994) showed that glucose-stimulated insulin secretion (GSIS) was decreased from T2D isolated human islets. These findings were confirmed in the same setting, where T2D human islets were shown to secrete lower amounts of insulin upon stimulation, while also showing a higher threshold required to trigger insulin release (Deng *et al.*, 2004). Therefore, a key feature of T2D is beta cell dysfunction with subsequent partial or complete lack of insulin release. Several longitudinal studies in type 2 diabetics, including one conducted in the UK, showed that, regardless of the antidiabetic therapy regimen, beta cell function deteriorates during the years following diagnosis with T2D (Kahn *et al.*, 2006a; Poitout *et al.*, 2010a; U.K Prospective Diabetes Study Group, 1995). Insulin insufficiency is present early in the pathogenesis T2D and continues to worsen overtime. It is widely accepted that insufficient insulin secretion by pancreatic beta cells is due to both functional beta cell defects and a loss of beta cell mass by apoptosis (Cunha *et al.*, 2008). In conjunction with IR that develops in peripheral tissues, the impairment of the secretory function of beta cells is a major pathophysiological phenomenon of diabetes resulting in insufficient insulin secretion and chronic hyperglycaemia (Wang & Wang, 2017). Oxidative stress driven by hyperglycaemia results in clinical outcomes: peripheral tissue IR and beta cell dysfunction (Newsholme *et al.*, 2019; Wang & Wang, 2017).

1.4.3.2.2 The role of oxidative stress

Oxygen is responsible for the expansion of life and Earth, however, there are two sides to this molecule: it is crucial for energy production in the mitochondria of cells, but it can be damaging if not fully reduced to water (Newsholme *et al.*, 2019). Where reduction is incomplete (*i.e.*, high -energy electron-transferring chemical reactions), oxygen can be converted to several highly reactive species collectively described as ROS. In mammalian cells, a delicate balance exists between ROS production and the removal of ROS through antioxidants. ROS are generated as products of normal cell metabolism and respiration and are essential for cellular function. In beta cells, basal amounts of ROS regulate islet gene expression, facilitate the regulation of the insulin-secretory function of beta cells and play an important role in apoptosis, immune response, calcium signalling, and kinase activation (Affourtit & Brand, 2008; Keane *et al.*, 2010; Newsholme *et al.*, 2016; Newsholme *et al.*, 2019; Robertson & Harmon, 2007).

However, elevated levels of ROS can negatively affect beta cell function and induce cellular stress and death. Mitochondrial respiration consumes molecular oxygen, the ultimate acceptor of electrons generated by glucose catabolism. During normal oxidative phosphorylation, 4% of all oxygen consumed is converted into the free radical superoxide ($O_2^{\bullet-}$) (Cadenas & Davies, 2000; Newsholme *et al.*, 2019). Superoxide may be converted into other ROS and may react with reactive nitrogen species (RNS) to produce the extremely destructive peroxynitrite molecule (Newsholme *et al.*, 2016). Antioxidants are crucial to neutralise and/or attenuate the damaging effects of ROS and RNS. They can be classified as either enzymatic or nonenzymatic factors. The main enzymatic antioxidants include superoxide dismutase (SOD), catalase (CAT) and glutathione peroxidases (GPx). Superoxide generated are converted into H_2O_2 the antioxidant enzyme SOD. The H_2O_2 is then detoxified to H_2O and O_2 by GPx present in the mitochondria or is detoxified by catalases in peroxisomes (Newsholme *et al.*, 2019). Oxidative stress is a cellular phenomenon generally considered as a physiological imbalance between ROS levels and antioxidant levels, favouring ROS production. Antioxidants, including SOD, CAT and GPx, are believed to be overwhelmed by ROS (Ighodaro & Akinloye, 2018). Furthermore, pancreatic beta cells are vulnerable to oxidative stress as a result of their low content of antioxidant enzymes, which means these cells are rather sensitive to ROS damage when they are exposed to oxidative stress (Ježek *et al.*, 2019; Kajimoto & Kaneto, 2004). Indeed, although these defence mechanisms are present, it has been demonstrated that pancreatic beta cells exhibit a lower expression of CAT and GPx1, suggesting higher susceptibility to ROS damage (Gurgul-Convey *et al.*, 2016; Wang & Wang, 2017). In addition to increasing ROS production, hyperglycaemia and hyperlipidaemia aggravate oxidative stress through reducing antioxidant capability, evidenced by the reduction in reduced oxidised glutathione in hyperglycaemia, and reduced SOD1 and SOD2 expression in hyperlipidaemia in human and rat beta cells (Dai *et al.*, 2016b). ROS is produced via two different ways: enzymatic and non-enzymatic reactions. The enzymatic reactions involved in the generation of ROS include those involved in the mitochondrial respiration (Pham-Huy *et al.*, 2008). The superoxide anion radical ($O_2^{\bullet-}$) is generated via NADPH oxidase, xanthine oxidase and peroxidases. In pancreatic beta cells, there is substantial evidence stating that acute and transient glucose-dependent ROS contributes to normal GSIS. Under pathological conditions, ROS can accumulate in excessive levels for prolonged periods of time, causing oxidative stress and subsequent oxidative damage to cellular lipids, DNA, and proteins through chemical alterations such as nitrosylation, peroxidation and carbonylation (Newsholme *et al.*, 2019; Robertson &

Harmon, 2007). For example, ROS cause amino acid oxidation, lipid peroxidation, degradation of fatty acids of the membranes and damage to purine and pyrimidine bases (Cernea & Dobreanu, 2013). Some of the most common targets of ROS include proteins involved in membrane ion transport, metabolic enzymes, and regulation of gene expression and signal transduction (Gerber, 2017; Newsholme *et al.*, 2019).

Culminating evidence shows that oxidative stress plays a pivotal role in the pathological process of diabetes and diabetic complications, with a potential role in inducing beta cell dysfunction, beta cell apoptosis and decreasing pancreatic beta cell mass (Hou *et al.*, 2008; Kajimoto & Kaneto, 2004; Keane *et al.*, 2010; Newsholme *et al.*, 2019; Newsholme *et al.*, 2012; Robertson *et al.*, 2004). Hyperglycaemia, hyperlipidemia, and inflammation are all potent factors contributing to ROS production in beta cells. It well established that hyperglycaemia induces ROS through mitochondrial respiratory chain enzymes, xanthine oxidases, lipoxygenases, cyclooxygenases, nitric oxide synthases, and peroxidases (Eguchi *et al.*, 2021; Gerber, 2017; Volpe *et al.*, 2018). In hyperglycaemic states, excessive ROS levels are also generated during anaerobic glycolysis and from other pathways when glycolytic capacity is exceeded (Cernea & Dobreanu, 2013; Kajimoto & Kaneto, 2004). These pathways include non-enzymatic glycation, protein kinase C (PKC) activation, glucose auto-oxidation, the hexosamine pathway, the sorbitol pathway and the α-ketoaldheyde pathway (Cernea & Dobreanu, 2013; Kajimoto & Kaneto, 2004).

Under hyperlipidaemic conditions, ROS production is increased through activation of NADPH oxidase (NOX), induction of matrix metalloproteinase 2 (MMP2), and stimulation of macrophage infiltration (Eguchi *et al.*, 2012; Liu *et al.*, 2014; Nemecz *et al.*, 2019). In addition to increasing ROS production, hyperglycaemia and hyperlipidemia aggravate oxidative stress through reductions in antioxidant capacity, evidenced by the reductions in oxidised glutathione in hyperglycaemia, and reduced SOD1 and SOD2 expression in hyperlipidemia in human and rat beta cells (Alnahdi *et al.*, 2019; Dai *et al.*, 2016a; Eguchi *et al.*, 2021). Similarly to hyperlipidemia, inflammatory cytokines increased production of H_2O_2 and other ROS products, which modulated activity of NOX and increased expression of genes that recruit macrophages to beta cells (Gurgul-Convey *et al.*, 2016; Morgan *et al.*, 2007).

Oxidative stress has been shown to alter major pathways important for beta cell function and survival. Oxidative stress causes mammalian target of rapamycin (mTOR) inhibition, JNK and P38 pathway activation in beta cells. Long-term activation of the AMPK pathway by ROS

results in a reduced basal activity of beta cells, insulin release and beta cell proliferation and mass (Richards *et al.*, 2005). ROS can also inhibit the mTOR pathway, a key regulator of apoptosis, hence resulting in beta cell mass loss. The inhibition of mTOR was also shown to decrease insulin secretion and impair mitochondrial function in beta cells (Maedler & Ardestani, 2017). JNK and P38 are members of the complex superfamily of mitogen-activated protein kinase serine/threonine protein kinases (MAPKs), which are activated in response to cellular stress such as oxidative stress. When activated, the JNK pathway increases the expression of proapoptotic genes, thus directly triggering the apoptotic process. The glycation reaction is also believed to be an important mediator in the pathogenesis of diabetic complications because, under hyperglycaemia, the production of reducing sugars *i.e.*, glucose, G6P and fructose is increased through the polyol pathway and glycolysis. These reducing sugars promote the glycation reactions of several proteins (Kajimoto & Kaneto, 2004). More specifically glycated proteins such as glycosylated haemoglobin, albumin, and lens crystalline were produced in diabetic animals via the Maillard reaction (Kajimoto & Kaneto, 2004). Furthermore, the glycation reaction also produces Schiff base, Amadori product, AGEs and ROS (Kajimoto and Kaneto, 2004). ROS overproduction also triggers DNA single-strand breaks which then activates the nuclear poly (ADP-ribose) polymerase-1 (PARP) and subsequently depletes its substrate NAD+. Consequently, this slows the rate of mitochondrial respiration and glycolysis and inhibits the activity of glyceraldehyde 3-phopshate dehydrogenase (GADPH).

The accumulation of cellular oxidative stress and subsequent oxidative damage can trigger the impairment of beta cell function and the activation of pro-apoptotic signals (Figure 1.7).

1.4.3.2.3 The role of mitochondrial dysfunction

The major contributor of ROS production is the mitochondrial ETC, with $O_2^{\bullet-}$ being the most abundant ROS species in cells (Gray & Heart, 2010; Newsholme *et al.*, 2019). The ETC in the mitochondria is considered as an important pathway in the generation of ROS. The most important producers of $O_2^{\bullet-}$ are complexes I and III of the mitochondrial respiratory chain (Bleier & Dröse, 2013). The action of ROS on beta cell is considered a potential mechanism of glucotoxicity seen in diabetes (Robertson *et al.*, 2004). Indeed, under diabetic conditions, hyperglycaemia leads to increased respiration rates in beta cells, which signifies that the electron transport via mitochondrial complexes exceeds their capacity. This process results in

induced electron flux through the ETC to the inside of the mitochondria, with subsequent production of ROS.

Electron leak is a phenomenon that occurs at complex I and III of the ETC, describing electrons derived from NADH or $FADH_2$ that have escaped normal processing with molecular oxygen to form superoxides which are subsequently detoxified by CAT or GPx (Newsholme *et al.*, 2019). This would nullify the toxicity from electron leak. Additionally, beta cells may be subject to chronic exposure to high glucose levels in the diabetic milieu, leading to increased glucose oxidation and glycolytic flux, as well as elevated TCA cycle activity and Ca^{2+} oscillations (Newsholme *et al.*, 2019). Altogether, this may lead to further ROS generation and the potential pathological consequences that may promote beta cell dysfunction and death. It is suggested that mitochondrial overwork, with eventual generation of ROS, is a potential mechanism causing the impairment of first phase GSIS observed in the early stages of T2D (Kajimoto & Kaneto, 2004).

Under hyperglycaemic and hyperlipidemic conditions, expression of glycolytic, oxidative phosphorylation, and TCA related genes is decreased (Chen *et al.*, 2013; Cnop *et al.*, 2014; Eguchi *et al.*, 2021; Haythorne *et al.*, 2019). Furthermore, both hyperglycaemia and hyperlipidemia cause increased respiration, decreased ATP content, lowered mitochondrial membrane potential ($\Delta\psi m$), and increased mitochondrial volume, signs that indicate mitochondrial dysfunction and uncoupling (Carlsson *et al.*, 1999a; Eguchi *et al.*, 2021; Haythorne *et al.*, 2019). Several other mitochondrial pathways are considered to be involved in ROS production in beta cells under hyperglycaemia, which include PKC activation, increased intracellular AGE product formation, hexosamine pathway activation, polyol pathway activation, and oxidative phosphorylation (Eguchi *et al.*, 2021). This, in turn, inhibits mitochondrial ATP generation and GSIS, and results in the accumulation of glycolytic intermediates, hence inducing alternate metabolic pathways such as PKC, polyol and hexosamine. These processes eventually lead to a disruption of cellular function by altering gene expression and the endogenous non-enzymatic glycoxidation of nucleic acids, proteins, and lipids, eventually leading to the formation of AGEs.

Proper mitochondrial function is crucial for insulin secretion from beta cells. The increased metabolism as a result of higher glycolytic flux leads to an increase in cytosolic ATP levels. This rise in cellular ATP causes the closure of K_{ATP} channels, which results in the depolarisation of beta cells and the subsequent opening of Ca^{2+} channels, which is coupled to the exocytosis

of insulin granules (Eguchi *et al.*, 2021; Skelin Klemen *et al.*, 2017). The coupling of glycolysis to mitochondrial ATP production is required for proper beta cell function and insulin exocytosis and defects in mitochondrial function impair this metabolic coupling and ultimately promote beta cell damage (Ciregia *et al.*, 2017).

This signalling cascade is significantly altered in T2D due to defects in mitochondrial metabolism (Anello *et al.*, 2005). Compared to control islets, islets of patients with diabetes show reduced GSIS, which was associated with lower ATP/ADP ratio, decreased $\Delta\psi m$, and downregulation of expression of genes associated with energy metabolism (Anello *et al.*, 2005; Segerstolpe *et al.*, 2016).

In T2D, the activities of the mitochondrial enzymes glycerol phosphate dehydrogenase, pyruvate carboxylase and succinyl-CoA:3-ketoacid-CoA transferase have been reported to be up to 90% lower in diabetic islets vs non-diabetic islets (MacDonald *et al.*, 2009). Additionally, ATP citrate lyase was also decreased by more than 50% (MacDonald *et al.*, 2009). In terms of mitochondrial morphology and size, it is reported that in T2D, beta cell mitochondria appear round shaped with lower density by electron microscopy analysis, and that ATP content was not increased upon acute glucose stimulations (Anello *et al.*, 2005). Therefore, the ATP/ADP ratio was nearly 50% lower in diabetic islets vs non-diabetic islets, while depolarisation of the mitochondrial membrane (*i.e.*, decreased $\Delta\psi m$), as well as increased expression of the mitochondrial uncoupling protein 2 (UCP2) were observed (Anello *et al.*, 2005).

Mitochondrial DNA and some mitochondrial proteins such as UCP2 are vulnerable targets for oxidative damage, further compromising mitochondrial function. In pancreatic beta cells, UCP2 influences mitochondrial oxidative phosphorylation and insulin secretion. Activation of UCP2 by ROS results in proton leak and hence, reduces ATP production and impairs GSIS in beta cells (Affourtit *et al.*, 2011) (Figure 1.7).

Mitochondria also serve an essential role in the control of beta cell mass. Previous data suggest that increased apoptosis underlies the loss of beta cell mass observed in islets from patients with T2D (Butler *et al.*, 2003). Apoptotic pathways converge in the mitochondrion, where a cascade of caspase activation by cytochrome *c*, after being exported from mitochondria, is required for inducing apoptosis (Fex *et al.*, 2018).

1.4.3.2.4 Pancreatic and duodenal homeobox factor 1 (PDX-1)

PDX-1 is a member of the homeodomain-containing transcription factor family that plays a pivotal role in pancreatic development, beta cell function and differentiation (Jonsson *et al.*, 1994; Kajimoto & Kaneto, 2004; Sharma *et al.*, 1999). One of the classical targets of ROS damage includes the pancreatic and duodenal homeobox 1 (PDX-1). In diabetes, hyperglycaemia induces glycation and oxidative stress in beta cells, leading to a marked decrease in the activity and expression of PDX-1 (Kajimoto & Kaneto, 2004). A reduction in PDX-1 activity leads to a decrease in insulin content and glucokinase activity, subsequently reducing insulin release from beta cells (Watada *et al.*, 1996). Further, Kawamori *et al.* (2003) found that oxidative stress alters intracellular distribution of PDX-1 and thereby suppresses its activity in nuclei.

1.4.3.2.5 Endoplasmic reticulum (ER) stress

The endoplasmic reticulum (ER) is a highly dynamic organelle, playing a major role in protein and lipid biosynthesis. Additionally, the ER plays a pivotal role in Ca^{2+} storage and signalling, making it a key component of cellular processes such as apoptosis (Eizirik *et al.*, 2008). The synthesis of protein begins with the translation of proteins by the ribosomes on the cytosolic surface of the ER, then, the unfolded polypeptide chains are translocated into the ER lumen (Eizirik *et al.*, 2008). In the ER lumen, the unfolded polypeptide chains are then folded into secondary and tertiary structures stabilised by disulphide bonds (Eizirik *et al.*, 2008). ER-resident folding factors such as the chaperones GRP94 and Ig heavy chain binding protein (BiP or GRP78), play an essential role in assisting with folding and retaining client proteins in the ER until the maturely folded proteins meet all the quality standards (Eizirik *et al.*, 2008). However, proteins formed in the ER may fail to achieve correct conformation due to Ca^{2+} depletion, a lack of chaperones, a disrupted redox state, proteins mutations and reduced disulphide bonds (Eizirik *et al.*, 2008). ER stress is defined as an imbalance between the protein folding capacity of the ER and the functional demand. This imbalance leads to accumulation of unfolded or misfolded proteins in the ER lumen (Cnop *et al.*, 2017).

The accumulation of misfolded proteins that build-up in the ER lumen causes ER stress and activates the two unfolded protein responses (UPR): Adaptive UPR and apoptotic UPR, which work to promote either insulin biosynthesis and secretion or apoptosis, respectively. This adaptive response aims to increase the functional capacity of the organelle and to decrease the

arrival of newly synthesized proteins (Cnop *et al.*, 2017). The role of the adaptive UPR is to alleviate ER stress and prevent cell death, by triggering coordinated responses such as: 1) increase the levels of ER chaperones; 2) reduce the arrival of new proteins into the ER; 3) induce the extrusion of irreversibly misfolded proteins and lastly; 4) trigger apoptosis in case the former steps fail (apoptotic UPR pathway) (Eizirik *et al.*, 2008). All these steps depend partially on the expression of key genes and proteins ensuing signals from the ER to the nucleus. These signals are mediated by three transmembrane ER proteins also known as UPR inducers: double-stranded RNA activated kinase (PKR)-like ER kinase (PERK), activating transcription factor (ATF) and inositol requiring ER-to-nucleus signal kinase (IRE1). These proteins are activated by BiP dissociation from their luminal side, following the accumulation of unfolded proteins in the ER lumen (Eizirik *et al.*, 2008). Therefore, the UPR attempts to attenuate global protein translation while upregulating ER chaperones. However, in case of UPR failure to solve ER stress, the apoptosis pathway is triggered (Eizirik *et al.*, 2008). The apoptosis pathway is triggered following the recruitment of TNF receptor-associated factor 2 (TRAF2) and activation of the JNK and proapoptotic kinase apoptosis-signal-regulating kinase (ASK1) pathways. The prolonged activation of the protein kinase R-like ER kinase (PERK) pathway can lead to apoptosis via ATF4 overexpression and consequent CHOP and ATF3 activation (Eizirik *et al.*, 2008). In response to ER stress the transcription factor CHOP expression is markedly increased.

Culminating evidence shows that ER stress plays an essential role in the development of T2D by contributing to beta cell loss and IR (Arunagiri *et al.*, 2018; Eizirik *et al.*, 2008). Under physiological conditions, the UPR proves to be beneficial to beta cells, however, under situations of chronic stress, the components of the UPR can cause beta cell dysfunction and death (Eizirik *et al.*, 2008). ER stress is induced by several factors such as glucose, FFAs and islet amyloid polypeptide (IAPP). One of the major conditions that lead to ER stress in beta cells under the presence of hyperglycaemia, is the increased insulin secretory request (Cernea & Dobreanu, 2013). Indeed, the beta cell secretory proteins proinsulin and IAPP are reported to be prone to misfolding. However, there is little data to convince the occurrence of IAPP misfolding in the ER. On the other hand, proinsulin misfolding in the ER has shown to be an important cause of beta cell ER stress (Arunagiri *et al.*, 2018; Sun *et al.*, 2015). Upon ongoing metabolic demand, proinsulin secretion is increased, however, there is an additional proinsulin synthesis if beta cells in islets fail to deliver sufficient signalling from PERK, a major ER sensor (Arunagiri *et al.*, 2018). Even at low glucose levels, PERK function is lost leading to an enhancement in proinsulin synthesis and eventual proinsulin misfolding in the ER.

Accumulation of misfolded proinsulin beyond a certain threshold was found to diminish insulin production and cause hyperglycaemia, while further exacerbating ER stress (Arunagiri *et al.*, 2018). When beta cells are subject to severe, chronic ER stress and strong UPR, they undergo apoptosis through stress kinases and transcription factors (Cernea & Dobreanu, 2013).

Figure 1.7 summarises the mechanisms involved in beta cell dysfunction and death in T2D.

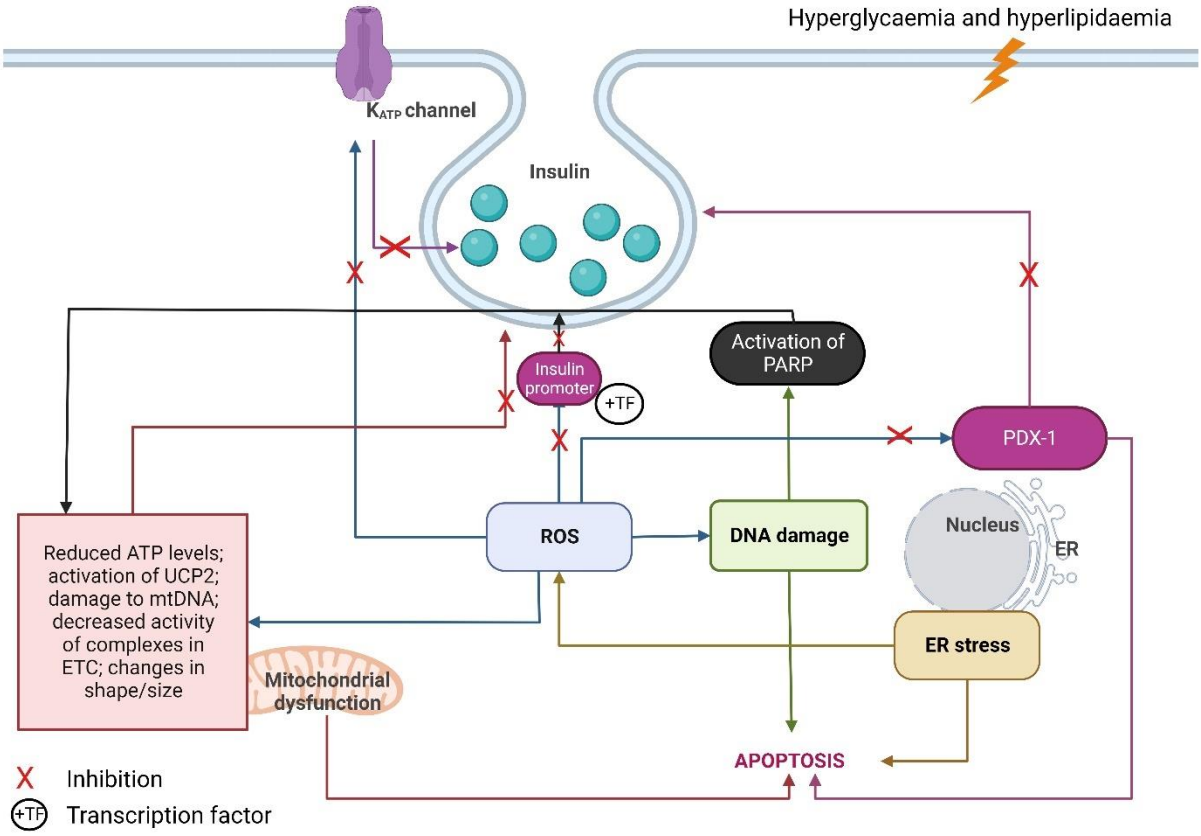

Figure 1.7 Mediators of beta cell dysfunction and death in T2D. UCP2, uncoupling protein 2; ROS, reactive oxygen species; ER, endoplasmic reticulum; mtDNA, mitochondrial DNA; PARP, poly adenosine diphosphate-ribose polymerase. Figure created with BioRender.com.

In summary, specific functional and molecular features characterise pancreatic beta cells and their functional identity as well as their survival properties. Several alterations occur in type 2 diabetic beta cells, playing key roles in this metabolic disease. However, it is difficult to identify single culprits associated with the pathogenesis of T2D due to the pathophysiological interplay between many different mechanisms and pathways. When overwhelmed, the beta cell fails to secrete insulin and can undergo apoptosis, potentially leading to both beta cell dysfunction and a loss of beta cell mass, which constitute the hallmarks of T2D.

1.4.3.3 ART-induced beta cell dysfunction

As previously discussed, certain antiretroviral agents have been associated with an increased risk of T2D in HIV, prompting the need to further investigate the direct effects of protease inhibitors, NNRTIs, NRTIs and integrase inhibitors on beta cell function and survival. However, the only antiretroviral drug class investigated in this context is the protease inhibitor class.

An old study comparing serum proinsulin levels in HIV-infected patients on protease inhibitor-containing regimens vs protease inhibitor-naïve HIV-patients showed that HIV-patients on protease inhibitors had significantly high concentrations of proinsulin, indicating beta cell dysfunction in these patients (Behrens *et al.*, 1999). Yarasheski *et al.* (1999) showed that HIV-infected subjects on indinavir had significantly higher fasting glucose levels compared to non-treated-HIV-seronegative subjects. Woerle *et al.* (2003) concluded that beta cell function, assessed by the HOMA score, decreased by approximately 50% in HIV-infected individuals on protease inhibitor-containing ART regimens compared to baseline levels. Although these studies have employed different measurements to give insight into the effects of protease inhibitors in HIV-infected individuals, it is evident that protease inhibitor-containing regimens contribute to beta cell dysfunction in HIV patients.

The direct effects of HIV protease inhibitors on beta cell function and survival were investigated in several *in vitro* studies. Koster *et al.* (2003) determined that indinavir acutely inhibited insulin release from MIN6 mouse insulinoma cells and rodent islets and impaired beta cell glucose sensitivity in rats. While glucokinase activity was not affected, 2-deoxyglucose uptake and glucose utilisation was impaired in MIN6 cells treated with indinavir (Koster *et al.*, 2003). Schütt *et al.* (2000) showed that the protease inhibitors nelfinavir, ritonavir and saquinavir impaired GSIS from INS-1 cells. Similarly, Yarasheski *et al.* (1999) concluded that indinavir had no significant inhibitory effect on GSIS while also observing that indinavir had no effect on C-peptide secretion from INS-1 cells and rat islets. The different insulin secretory profiles between the MIN6 and INS-1 cell lines may account for the differences in effects observed after treatment with indinavir. Shütt *et al.*'s findings (2000) were replicated in rat pancreatic insulinoma INS-1E cells as both nelfinavir and saquinavir reduced GSIS from INS-1E cells (Chandra *et al.*, 2009). Altogether, these findings suggest that several protease inhibitors impair beta cell function. Additionally, several HIV protease inhibitors reduced beta cell viability and

triggered apoptosis (Zhang *et al.*, 2009). The mechanisms involved in protease inhibitor-induced beta cell secretory dysfunction were also investigated. Figure 1.8 summarises these mechanisms. Chandra *et al.*'s work (2009) suggested that nelfinavir significantly increased ROS production while suppressing cytosolic superoxide dismutase levels. Nelfinavir also reduced ATP levels while increasing UCP2 levels. Additionally, Zhang *et al.* (2009) suggested that protease inhibitors impair the secretory function of beta cells and induce beta cell death through a loss in $\Delta\psi m$, translocation of cytochrome *c*, and activation of mitochondrial-associated caspase-9 in INS-1 cells, suggesting that HIV protease inhibitors can trigger the mitochondria-dependent apoptotic pathway. While the mitochondrion seems to be a key player in protease inhibitor-induced beta cell apoptosis (Figure 1.8), ER stress was not involved in triggering apoptosis in INS-1 cells (Zhang *et al.*, 2009). On the other hand, Koster *et al.* (2003) suggested that indinavir inhibits glucose uptake in MIN6 cells. Schütt *et al.* (2000) concluded that protease inhibitor-induced impairment of insulin secretion involves the reduction of the insulin-stimulated phosphorylation of insulin signalling parameters, particularly IRS-2 (Figure 1.8). Additionally, ritonavir inhibited insulin secretion by lowering intracellular Ca^{2+} concentrations, independent of the opening of K_{ATP} channels or voltage-dependent Ca^{2+} channels in beta cells.

However, it should be noted that there are significant differences between rodent and human pancreatic beta cells. For instance, the expression of glucose transporters in human and rodent beta cells is not identical (De Vos *et al.*, 1995). However, the clinical data support the clinical relevance of the *in vitro* and animal models used in the studies discussed here.

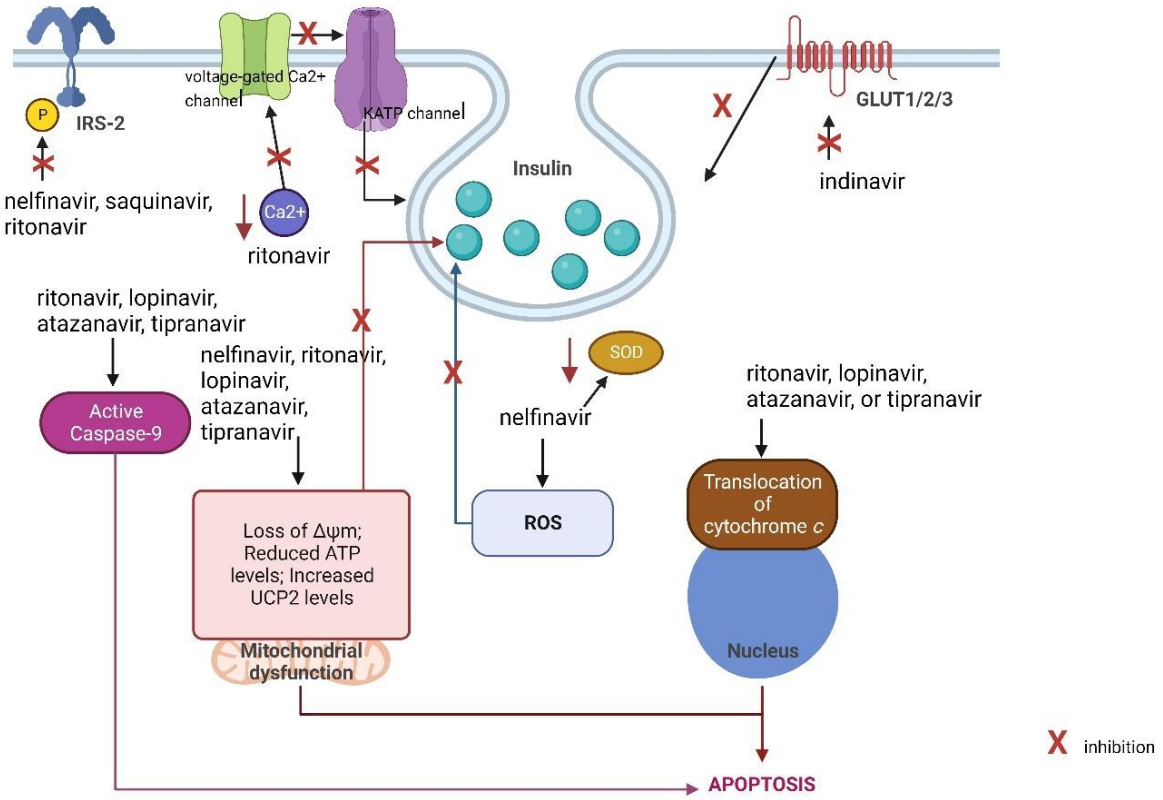

Figure 1.8 Mechanisms in HIV protease inhibitor-induced beta cell dysfunction and death. UCP2, uncoupling protein 2; IRS-2, insulin receptor 2; ROS, reactive oxygen species; Δψm, mitochondrial membrane potential, SOD, superoxide dismutase. Figure created with BioRender.com.

In sum, several NNRTIs, NRTIs, protease inhibitors and integrase inhibitors may contribute to the development of T2D in PLWH through the induction of peripheral IR, and in the case of protease inhibitors, IR is accompanied with the direct impairment of beta cell function and induction of beta cell death. Certain protease inhibitors have been shown to have direct detrimental effects on the secretory function of beta cells possibly through oxidative stress, mitochondrial dysfunction, impaired insulin signalling and/or disturbance in glucose transport in beta cells. ART may potentiate the effects of traditional risk factors (*i.e.*, lipodystrophy and IR) in developing T2D in an ageing HIV population. The investigation into the role of protease inhibitors in beta cells has proven to be useful in clinical settings, as current recommendations suggest avoiding protease inhibitor-based therapy in the PLWH at risk of developing T2D.

1.5 Aims of the study

To conclude, this literature review paints a picture of the reality of ART used in modern HIV care. Despite the benefits of ART, it is safe to say that antiretroviral agents have increasingly caused concern in the HIV population. Researchers investigated these concerns and undeniably found that several ART regimens increase the risk of developing T2D in HIV-infected individuals. Although being the most commonly recommended antiretroviral drug classes for treatment and prophylaxis of HIV infection, no existing study has attempted to establish the effects of NNRTIs and NRTIs on beta cell function and survival, despite the fact that previous studies have found that several NNRTIs and NRTIs cause damage to a variety of cell types mainly via oxidative stress and mitochondrial dysfunction (Apostolova *et al.*, 2011a; Apostolova *et al.*, 2011b; Apostolova *et al.*, 2010; Blas-García *et al.*, 2014; Blas-García *et al.*, 2010; Jamaluddin *et al.*, 2010; Weiß *et al.*, 2016b) (Figure 1.9).

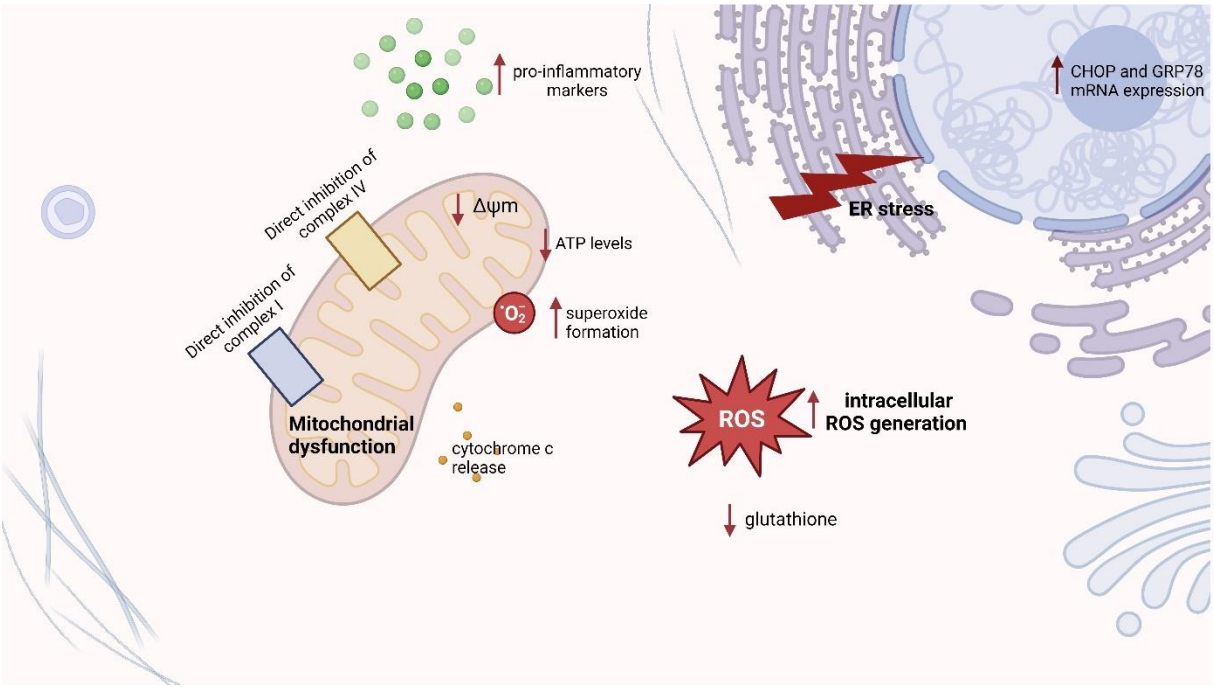

Figure 1.9 Summary of cellular and molecular mechanisms for efavirenz-mediated cellular dysfunction and death. Figure adapted from 'Virtual Background - Inside a Cell' (2022) by BioRender.com (2022). Retrieved from https://app.biorender.com/biorender-templates

Direct damaging effects on beta cell function and survival by either NNRTIs or NRTIs may predispose PLWH who are also type 2 diabetic to impaired glycaemic control and loss of beta cell mass, hence increasing the risk of diabetic complications and insulin dependency. The overall aim of this study was to investigate the direct effects of the NNRTIs efavirenz, rilpivirine and doravirine, and the NRTIs tenofovir DF, emtricitabine and

lamivudine, on beta cell function and survival while giving insight into the potential cellular and molecular mechanism(s) underlying these effects.

2. Materials and Methods

2.1 Materials

The rat insulinoma INS-1E cell line was obtained from Addexbio (Cat#: C0018009, RRID: CVCL_0351). RPMI-1640 media, trypsin-EDTA (0.05%), heat-inactivated fetal calf serum and penicillin-streptomycin (10,000 U ml^{-1}) were purchased from Gibco Thermo Fisher Scientific (Oxford, UK). The drugs efavirenz, rilpivirine, doravirine, tenofovir DF, emtricitabine and lamivudine were obtained from Carbosynth Limited (Compton, UK).

Bradford reagent and Laemmli sample buffer were purchased from Bio-Rad Laboratories Ltd (Hertfordshire, UK). [4,5-dimethylthiazole-2-yl]-2,5-diphenyltetrazolium bromide (MTT), dimethyl sulfoxide (DMSO), bovine serum albumin, phosphate buffered saline, 2-mercaptoethanol, tetramethylrhodamine ethyl ester perchlorate, carbonyl cyanide 3-chlorophenylhydrazone and hydrogen peroxide solution 30% (w/w) were obtained from Sigma-Aldrich (Poole, UK). Annexin V-FITC, propidium iodide and annexin V binding buffer were purchased from BD Pharmingen (Berkshire, UK) and 2′,7′-dichloro-dihydro-fluorescein-diacetate was purchased from Millipore UK Ltd (Hertfordshire, UK). The rat insulin ELISA kit was purchased from Alpco Diagnostics (New Hampshire, USA). The RT-qPCR primers were obtained from Eurofins Genomics (Wolverhampton, UK). Anti-CHOP antibody (Cat#: sc-7351; RRID: AB_627411), anti-UCP2 antibody (Cat#: sc-390189; RRID: AB_2721285), goat anti-rabbit IgG (Cat#: sc-2004; RRID: AB_631746), mouse IgG antibody (Cat#: sc-516102; RRID: AB_2687626) and anti-GAPDH antibody (Cat#: sc-25778; RRID: AB_10167668) were obtained from Santa Cruz Biotechnology (Texas, USA). Anti-PDX-1 antibody (Cat# PA5-78024; RRID: AB_2736337). ECL western blotting detection reagents was obtained from Thermo Fisher Scientific (Oxford, UK). Anti-GRP78 antibody (Cat#: 3216-1; RRID: AB_2279866) was obtained from Epitomics (California, USA).

Protease and phosphatase inhibitors were obtained from Roche (Mannheim, Germany). Cytotox 96® Non-Radioactive Cytotoxicity Assay (Cat #: G1780) was purchased from Promega (Wisconsin, USA). Amersham™ ECL™ Rainbow™ Marker (Cat#: RPN800E) was purchased from Sigma-Aldrich (Poole, UK)

and PageRuler Plus prestained protein ladder (Cat#: 26619) was obtained from Thermo Fisher Scientific (Oxford, UK). Anti-cleaved caspase-3 (Cat#: 9661; RRID: AB_2341188) was obtained from Cell Signalling Technology (New England Biolabs Ltd, Hitchin, UK). Goat anti-rabbit Alexa Fluor™ 488 secondary antibody (Cat#: A-11008; RRID: AB_143165), goat anti-mouse Alexa Fluor™ 488 secondary antibody (Cat#: A32766; RRID: AB_2762823) and SYBR™ Safe DNA Gel Stain were obtained from Invitrogen Thermo Fisher Scientific (Oxford, UK). Sodium palmitate was obtained from Sigma Aldrich (Poole, UK).

All other reagents and cell culture plastics were purchased from Thermo Fisher Scientific (Oxford, UK) and Sigma-Aldrich (Poole, UK).

The buffers and solutions used in this study are listed below in alphabetical order.

0.5 M Tris (Western blot)

0.5 M Tris-HCl

Buffer adjusted to pH = 6.8

1.5 M Tris (Western blot)

1.5 M Tris-HCl

Buffer adjusted to pH = 8.8

100 mM Tris (glucokinase activity)

100 mM Tris-HCl

Buffer was adjusted to pH = 7.4

100 mM Magnesium sulphate (glucokinase activity)

100 mM $MgSO_4 \cdot 7H2O$

Buffer was adjusted to pH = 7.4

Blocking buffer (Western Blot)

5% (w/v) non-fat milk powder in Tris-buffered saline with Tween 20

Blocking Buffer (immunocytochemistry)

1% BSA and 0.1% Triton X-100 in phosphate buffered saline

Gey and Gey Bicarbonate Buffered Salt solution (insulin release measurements)

111 mM NaCl

4.9 mM KCl

27 mM $NaHCO_3$

1 mM $MgCl_2$.6H2O

0.2 mM KH_2PO4

0.3 mM $MgSO_4.7H_2O$

0.7 mM $Na_2HPO_4.2H_2O$

0.1% fatty acid-free BSA

2 mM of glucose

2 mL of 1 M $CaCl_2$ solution

Buffer was adjusted to pH 7.4 by gassing with 95% O2/5% CO2 for 5 mins

Hank's Balanced Salt Solution (mitochondrial superoxide formation)

0.14 M NaCl

0.005 M KCl

0.001 M $CaCl_2$

0.0004 M MgSO4·7H2O

0.0005 M $MgCl_2 \cdot 6H_2O$.

0.0003 M $Na_2HPO4 \cdot 2H_2O$

0.0004 M KH_2PO_4

Buffer was adjusted to pH 7.2

Krebs Ringer Buffer (insulin release measurements)

150 mM NaCl

5 mM KCl

2 mM $CaCl_2$

1 mM $MgSO_4$

2 mM KH_2PO_4

15 mM $NaHCO_3$

1 mM HEPES

0.2% BSA

Radioimmunoprecipitation assay buffer (Western blot)

50 mM Tris-HCL, pH 8.0

150 mM NaCl

1 mM sodium orthovanadate

1 mM NaF

0.5% sodium deoxycholate

0.1% sodium dodecyl sulphate (SDS)

1% Triton X-100

Phosphate buffered saline buffer

137 mM NaCl

2.7 mM KCl

8 mM Na_2HPO_4

2 mM KH_2PO_4

Running buffer (Western blot)

25 mM Tris

190 mM glycine

0.1% SDS

Stripping buffer (Western blot)

0.2 mM glycine

1% SDS

10% Tween 20

Buffer was adjusted to pH 2.2

Tris-buffered saline (TBS) buffer (Western blot)

20 mM Tris

150 mM NaCl

Buffer was adjusted to pH 7.6

Transfer buffer (Western blot)

25 mM Tris

190 mM glycine

20% methanol

0.1% SDS

2.2 Methods

2.2.1 Cell culture

Most experiments in our study involved the use of the rat insulinoma cell line INS-1E, an insulin secreting beta cell derived line. INS-1E cells are widely used as a beta cell surrogate in diabetes mellitus research. They exhibit a secretory response to glucose within physiological range and contain a relatively high insulin amount (Skelin et al., 2010). Additionally, INS-1E cells are proven to be a highly differentiated and glucose-sensitive clone of parental INS-1 cells (Merglen *et al.*, 2004).

INS-1E cells were cultured as an adherent monolayer in 75 cm^2 single-use sterile flasks (Corning, Germany). INS-1E cells were grown in RPMI-1640 medium supplemented with 10% heat-inactivated fetal calf serum (FCS), 5.5 mL of 5,000 U/mL (1%) penicillin-streptomycin and 100 µL of 100 µL/500 mL (50 µM) 2-mercaptoethanol. The cells were incubated in a humidified incubator at constant physiochemical conditions: 37ºC, 95% air and 5% CO_2. The cells were passaged twice a week (every third or fourth day) under aseptic conditions in a class II laminar flow cabinet. Prior cell harvesting, RPMI-1640 medium (supplemented with 10% heat-inactivated FCS, 5.5 mL of 5,000 U/mL (1%) penicillin-streptomycin and 100 µL of 100 µL/500 mL 2-mercaptoethanol) and 0.05% w/v trypsin were warmed up in a water bath at 37ºC. Then, the INS-1E cells were checked under the microscope to ensure the cells were healthy and to estimate confluence (Figure 2.1). Upon confluence (> 80%), the adherent monolayer of INS-1E cells was enzymatically harvested using 3 mL of 0.05% w/v trypsin-EDTA (0.53 mM) before being incubated at 37ºC and 5% CO_2 for 3 mins. After cell detachment, the trypsin was neutralised with 6 mL of RPMI-1640 medium (supplemented with 10% heat-inactivated FCS), 5.5 mL of 5,000 U/mL (1%) penicillin-streptomycin and 100 µL of 100 µl/500 mL 2-mercaptoethanol). Then, the cell suspension was centrifuged for 5 min at 300 x g. After centrifugation, the supernatant was removed, and the cell pellet was resuspended in 12 mL of RPMI-1640 medium supplemented with 10% heat-inactivated FCS. The cell suspension was divided between four single-use sterile 75 cm^2 flasks (2.5 or 3 mL of cell suspension in each flask) in 13 mL of RPMI-1640 medium (supplemented with 10% heat-inactivated FCS), per flask. The cells in the flasks were then incubated for three to four days at 37ºC and 5% CO_2 (Figure 2.1).

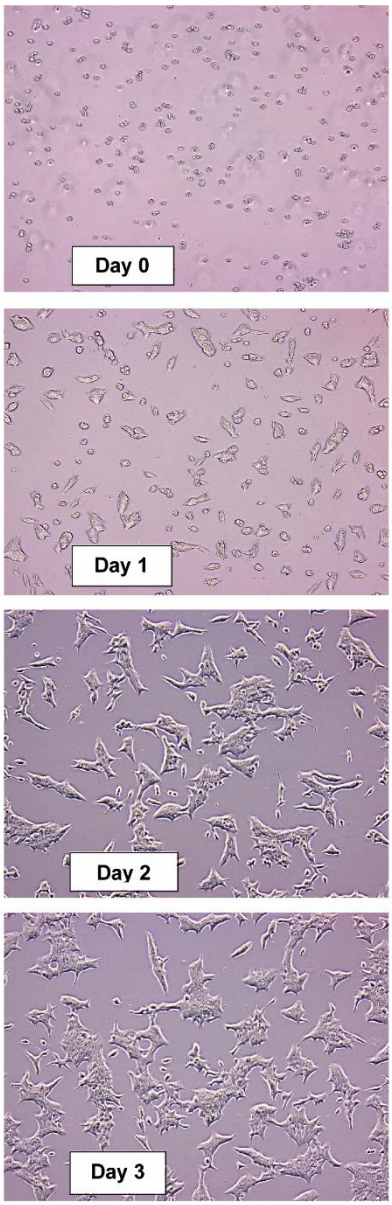

Figure 2.1 Daily microscope images of INS-1E cells in adherent culture on day 0 to day 3 after seeding

In order to prepare the cells for plating, the following protocol has been adopted. Upon confluence (> 80%) INS-1E cells were harvested and centrifuged as described above. Then, the cells were resuspended in RPMI-1640 media (supplemented with 10% heat-inactivated FCS, 5.5 mL of 5,000 U/mL (1%) penicillin-streptomycin and 100 µL of 100 µL/500 mL 2-mercaptoethanol) in order to obtain the appropriate seeding density depending on the application (Table 2.1). Optimal seeding densities of INS-1E cells for the different applications were pre-determined to reach the target number of cells (Table 2.1). In order to obtain the respective seeding density, the number of total cells were counted using a haemocytometer and to confirm, a Countess II FL Automated Cell Counter (Thermo Fisher Scientific). As part of

routine checks, 0.4% trypan blue solution was added to the cells to rapidly assess cell viability using Countess II FL Automated Cell Counter.

After plating, INS-1E cells were incubated at 37°C in a humidified 37ºC incubator with 5% CO_2 for 24 or 48 hrs prior to conducting the treatment protocol (Table 2.1). INS-1E cells from passage 20 to passage 40 were used. The table below summarises the empirically determined cell seeding density, cell culture plate used and incubation time prior treatment protocol respective to each technique used in this study (Table 2.1).

Table 2.1 INS-1E cell plating and incubation conditions for the experiments used in this study. ER, endoplasmic reticulum; GSIS, glucose-stimulated insulin secretion; LDH, lactate dehydrogenase; RT-qPCR, quantitative reverse transcription polymerase chain reaction; ATP, adenosine triphosphate.

Application	Seeding density (in cells/well)	Cell culture plate used	Incubation time prior treatment (in hours)
Insulin measurements (*i.e.*, basal insulin release, GSIS and intracellular insulin content)	2.0×10^5	24-well plate	48
Cell viability (MTT assay)	3.5×10^4	96-well plate	24
Apoptotic histone release measured by ELISA	1.0×10^5	24-well plate	24
Apoptosis and necrosis analysis using Annexin V-FITC and propidium iodide staining	5.0×10^5	6-well plate	48
LDH release assay	1.0×10^4	96-well plate	24
Antioxidant capacity (ABTS assay)	14×10^4	48-well plate for the ABTS assay	24
Intracellular ROS generation (DCFH-DA assay)	2.0×10^5	6-well plate	48
Mitochondrial superoxide generation (MitoSOX™ probing)	5.0×10^5	6-well plate	48
Mitochondrial membrane potential changes (DiOC6 and TMRE probing)	5.0×10^5	6-well plate	48
CHOP measured by ELISA	1.0×10^5	24-well plate	24
Glucokinase activity assay	2.0×10^5	6-well plate	48
Cellular ATP assay	1.0×10^4	White 96-well plate	24
RT-qPCR	0.5×10^6	6-well plate	48
Western Blot	1.0×10^6	10-cm cell culture dish	48
Immunocytochemistry	0.5×10^5	Poly-ornithine-coated coverslips placed in 6-well plates	72

2.2.2 Treatment protocol

The treatment protocol varies depending on the experiment. Each treatment protocol is detailed in each **Results** chapter. Stock solutions of NRTIs (tenofovir disoproxil fumarate, emtricitabine and lamivudine) and NNRTIs (efavirenz, rilpivirine and doravirine) were prepared by dissolving the NNRTI or NRTI in 1 mL of DMSO (all NNRTIs and NRTIs tested in this study are soluble in DMSO as per manufacturer's instructions). The stock solutions were then stored appropriately at room temperature (approximately 25^{o}C). Table 1, **Appendix I** summarises the weight of the drug calculated depending on the final stock concentration required (25 mM) and volume of vehicle used for all NNRTIs and NRTIs.

The different concentrations investigated were prepared by diluting the appropriate volume of stock solution in RPMI-1640 media supplemented with 3% heat-inactivated FCS, 1% penicillin-streptomycin and 50 µM 2-mercaptoethanol. The concentrations used and how to prepare them will be discussed in more detail in each chapter.

Most applications in this study involve the applications mentioned in Table 2.2 unless stated otherwise in the remaining chapters. In summary, following treatment protocol, treated INS-1E cells were incubated at 37°C in a humidified atmosphere of 95% air and 5% CO_2 for different durations depending on the experiment (Table 2.2).

Table 2.2 Treatment exposure time according to experiments used in this study. ER, endoplasmic reticulum; GSIS, glucose-stimulated insulin secretion; LDH, lactate dehydrogenase; RT-qPCR, quantitative reverse transcription polymerase chain reaction; ATP, Adenosine triphosphate.

Application	Treatment exposure time (in hours)
Insulin measurements (*i.e.*, basal insulin release, GSIS and intracellular insulin content)	24
Cell viability (MTT assay)	24
Apoptosis and necrosis analysis using Annexin V-FITC and propidium iodide staining	24
LDH release	24
Apoptotic histone release measured by ELISA	24
Intracellular ROS generation (DCFH-DA assay)	24
Antioxidant capacity (ABTS assay)	24
Mitochondrial superoxide generation (MitoSOX probing)	2, 4, 6 or 24
Mitochondrial membrane potential changes (DiOC6 and TMRE probing)	2, 4, 6 or 24
CHOP measured by ELISA	24
Glucokinase activity assay	24
Cellular ATP assay	24
RT-qPCR	24
Western blot	24
Immunocytochemistry	24

Most of the methods mentioned in Table 2.2 and Table 2.3 are detailed below. The other methods will be detailed in the remaining Chapters.

2.2.3 Insulin measurements

2.2.3.1 Basal insulin release and glucose-stimulated insulin secretion

Principle

Pancreatic beta cells are endocrine cells that uniquely synthesise, store and release insulin in a tightly dependent manner (Marchetti *et al.*, 2017). Beta cells exert their secretory function by secreting insulin through the metabolism of glucose, their most important secretagogue (Malmgren *et al.*, 2009). Therefore, quantification of basal insulin release and glucose-stimulated insulin secretion (GSIS) is necessary to assess the secretory function of INS-1E cells, while intracellular content measurements were determined to assess biosynthesis of insulin. To measure insulin release and intracellular insulin content in INS-1E cells, we used an insulin ELISA kit consisting of a microplate coated with a monoclonal antibody specific for insulin.

Protocol

Following cell growth and treatment protocol, INS-1E cells were incubated for 1 hr in Krebs-Ringer bicarbonate HEPES buffer (KRBH) containing 2 mM glucose and 0.2% bovine serum albumin (BSA) to achieve basal insulin secretion. Then, the cells were incubated for 30 mins with a further KRBH containing 2 mM glucose and 0.2% BSA to assess basal insulin secretion or KRBH containing 20 mM glucose and 0.2% BSA to assess insulin release in response to acute stimulus (GSIS).

Following incubation, the supernatant was centrifuged and collected for quantification using a rat insulin ELISA kit according to the manufacturer's instructions (Alpco, Cat#:80-INSRT-E01, Windham, New Hampshire, United States). In more detail, 350 µL of the supernatant containing the released insulin was collected and centrifuged for 2 mins at 150 x g. After centrifugation, the supernatant was subject to a 1 in 40 dilution in phosphate buffer 0.03 M 1% BSA as per the dilution test. The dilution test consisted of serially diluting a sample in order to select a dilution factor (1:40) that would ensure absorbance values of samples fit within the standard curve. These constitute the samples used for measuring basal insulin release and GSIS. A 10 µL volume of each standard, control, and sample were pipetted into their respective wells in the ELISA plate provided. Then, Working Strength Conjugate (75 µL) was added into each well. The microplate was then incubated for 2 hrs at room temperature (~25^{o}C) at 250 rpm. Following incubation, the solution was thoroughly removed by tapping and the microplate was washed six times with Working Strength Wash Buffer (300 µL) using a multi-channel pipette. Following washing, the wash buffer was completely removed and TMB substrate (100 µL) was added into each well. Then, the microplate was incubated for 15 mins at room temperature, shaking at 350 rpm. Following incubation, 100 µL of Stop Solution was added and absorbance was immediately read at 595 nm with a spectrophotometer (BioTek Synergy HT Microplate Reader, USA).

Data analysis

The average absorbance value for the blank control standards was subtracted from all the absorbance values. The concentration of insulin in the sample was determined by interpolating the blank control subtracted absorbance values against the standard curve. The resulting value was multiplied by the appropriate sample dilution factor, to obtain the concentration of insulin in the sample. Insulin measurements were normalised to total protein content determined by the Bradford assay (see 2.2.4). Data were expressed as % of vehicle (DMSO)-treated cells (control).

2.2.3.2 Intracellular insulin content

Intracellular insulin content in INS-1E cells was measured as described previously (Nakatsu *et al.*, 2015). INS-1E cells were washed twice with 1 mL of cold KRBH. Then, the cells were incubated with 0.1% Triton X-100 (1 mL) that contained a protease and phosphatase inhibitor cocktail at 4^{o}C for 10 mins. The cells were then scraped from the culture plates using a cell scrapper and passed 15 times through a 27-gauge needle. The cell lysates were incubated at 4^{o}C for 30 min and then centrifuged at 20,400 x g for 1 min. Insulin in cell lysates was quantified using a rat insulin ELISA kit according to the manufacturer's instructions (Alpco, Cat#:80-INSRT-E01, Windham, New Hampshire, United States) (see 2.2.3.1). Insulin measurements were normalised to total protein content determined by the Bradford assay.

2.2.4 Bradford protein assay

Principle

The Bradford assay, developed by Marion Bradford, is a colorimetric assay used to determine the total protein concentrations in a sample (Bradford, 1976). The principle the Bradford assay is that the binding of protein molecules such as lysine, histidine and arginine, to the Coomassie dye, resulting in a change of colour from brown to blue. The protein-dye binding represents the various concentrations of proteins.

Protocol

To perform the Bradford protein assay, a standard curve was plotted by using different concentrations of BSA solution (0, 0.0625, 0.125, 0.25, 0.5 and 1 mg/mL) prepared by serially diluting a 1 mg/mL BSA stock solution (30 mg of BSA in 30 mL of distilled H_2O) in distilled H_2O. The standards and samples were assayed in duplicates. The cell lysate for each treatment was obtained by adding 0.2 mL of 0.1 M NaOH to the cells. The cell lysates constitute the samples to be assayed as they contain the proteins extracted from the cells. The standards and samples (10 µL) were pipetted into each well of a 96-well microplate before adding 200 µL of Bradford dye reagent (acidified Coomassie dye) to each well. A spectrophotometer (BioTek Synergy HT Microplate Reader, USA) was used at 595 nm to measure the absorbance of the standards.

Data analysis

The average absorbance value for the blank control standards was subtracted from all the absorbance values. The exact protein concentration of the sample was determined by interpolation from a standard curve of the absorbance of the dilution series of protein standards within the linear response range of the assay.

2.2.5 Cell viability (MTT assay)

Principle

Cell viability was determined by the 3-([4,5-dimethylthiazole-2-yl])-2,5-diphenyltetrazolium bromide (MTT) assay which involves the enzymatic reduction of MTT to MTT-formazan by mitochondrial dehydrogenases, a by-product of mitochondrial respiration (Mosmann, 1983).

Protocol

The following protocol was performed as first described by Mosmann (1983). A fresh MTT solution (0.5 mg of MTT/mL of 3% heat-inactivated FCS RPMI-1640 media) was prepared prior running the MTT assay. Following treatment protocol, the supernatant medium was removed from all the wells before adding 100 µL of freshly prepared MTT solution (0.5 mg/mL) to each well. The cells were then incubated for 30 mins in a humidified 37^{o}C incubator with 5% CO_2. After observing a colouring reaction, the MTT solution was carefully removed from all the wells and 100 µL dimethyl sulfoxide (DMSO) was added to each well in order to solubilise the MTT-formazan purple crystals. The quantity of MTT-formazan was measured using a spectrophotometer (BioTek Synergy HT Microplate Reader, USA) at 540 nm.

Data analysis

The quantity of MTT-formazan measured by changes in absorbance is presumably directly proportional to the number of viable cells. The absorbance measurements of the treated cells were expressed as % of the absorbance observed in vehicle (DMSO)-treated cells (control).

2.2.6 Analysis of cell death

It is important to detect cell death and distinguish between apoptosis and necrosis as an indicator of cellular stress. Whereas apoptosis is a regulated type of cell death that is generally triggered by normal healthy processes, necrosis is the premature death of cells, triggered by external factors or disease. Beta cell death, via apoptosis or necrosis, was detected using three different methods: Cell Death ELISA^{PLUS} kit for preliminary data, flow cytometric analysis to confirm the preliminary data and lactate dehydrogenase release assay to confirm necrosis.

2.2.6.1 Apoptosis measurements by ELISA

Principle

The cell death detection kit ELISA^{PLUS} measures cytoplasmic mono- and oligonucleosomes levels in the cytoplasm of apoptotic cells that rise after apoptosis-associated DNA degradation.

Protocol

The cytoplasmic histone-complexed DNA fragments in INS-1E cells were assayed using the Cell Death Detection ELISA^{PLUS}. Cytoplasmic histone-complexed DNA fragments in cell lysates were quantified according to the manufacturer' instructions (Roche Diagnostics, Mannheim, Germany; Cat#: 11774425001). Following treatment protocol, the supernatant was removed carefully before lysing the cells with the provided lysis buffer (200 µL) for 30 mins at room temperature. The lysate was then centrifuged at 200 x g for 10 mins. Then, 20 µL of the supernatant was transferred into wells of the streptavidin coated microplate. Immunoreagent (80 µL) was added to each well. The microplate was then incubated for 2 hrs at room temperature rpm, shaking at 300 rpm. Following incubation, the solution was thoroughly removed by tapping. Then, each well was rinsed with 300 µL of incubation buffer. Following washing, the solution was removed carefully before adding 100 µL of ABTS solution in each well. The microplate was then incubated for 15 mins at room temperature, shaking at 250 rpm. Following incubation, ABTS Stop Solution (100 µL) was added to each well and absorbance was read immediately at 490 nm using a spectrophotometer (BioTek Synergy HT Microplate Reader, USA).

Data analysis

The average absorbance of the technical replicates was calculated. Then, the background value of the immunoassay was subtracted from each of these averages. The specific enrichment of

mono- and oligo-nucleosomes released into the cytoplasm was calculated from these values using the following formula:

$$enrichment\ factor = \frac{mU\ of\ the\ sample}{mU\ of\ the\ corresponding\ control\ (DMSO\ alone)}$$

mU = absorbance [10^{-3}]

2.2.6.2 Flow cytometric analysis of apoptosis and necrosis

Principle

After preliminarily evaluating cell apoptosis with ELISA, a second method was used to confirm and distinguish apoptotic and necrotic beta cell death. Apoptosis and necrosis levels were detected by Annexin V and propidium iodide (PI) staining followed by flow cytometric analysis. Annexin V is commonly used to probe apoptotic cells, as it recognises phosphatidylserine (PS) externalisation during early apoptosis. It can also stain the PS that remains on the inner face of the membrane of cells undergoing late apoptosis or primary necrosis. PI detects the loss of plasma and nuclear membrane integrity, a classic characterisation of late apoptotic and necrotic cells (Brauchle *et al.*, 2014)

Protocol

This protocol was optimised by testing several parameters (*i.e.*, concentration of PI and harvesting method) after exposure to a positive control, etoposide. Etoposide inhibits DNA synthesis by forming a complex with topoisomerase II, hence induces apoptotic cell death. INS-1E cells were treated with 100 μM of etoposide for 6 hrs to induce apoptosis.

Following treatment protocol, the cells were enzymatically harvested with trypsin/EDTA (0.05%). Then, the cells were centrifuged for 5 mins at 300 x g and washed twice by gently resuspending cells with phosphate buffered saline (PBS) (3 mL) with intermittent centrifugation steps. Cells were then resuspended in Annexin V binding buffer (1 mL) (10 mM HEPES, pH 7.4, 140 mM NaCl, 2.5 mM $CaCl_2$) and 100 μL of cell suspension from each sample (~10^5 cells/mL) was transferred for staining with Annexin V-FITC (5 μL) (BD Pharmingen, Cat#: 556419) and PI (2 μg/mL) (BD Pharmingen, Cat#: 556463) according to the manufacturer's instructions. After a 15-minute staining period at room temperature, the cells were centrifuged for 5 mins at 300 x g and resuspended in 400 μL of Annexin V binding buffer. The cells were then immediately subject to flow cytometric analysis (BD C6 Flow Cytometer;

BD Biosciences; New Jersey, USA). The flow cytometer used was subject to routine maintenance and was calibrated prior each experiment using beads purchased from the manufacturer to ensure accuracy of the data (BD C6 Flow Cytometer; BD Biosciences; Dickinson Co., New Jersey, USA).

Additionally, compensation controls were performed for each experiment. These include:

- Unstained vehicle control (DMSO only)
- Vehicle control stained with Annexin V FITC only
- Vehicle control stained with PI only

These controls were used to analyse the data as described below.

Data analysis

For each flow cytometric analysis, 10,000 events were recorded with the BD CSampler Plus software (BD Biosciences, New Jersey, USA). The recorded events were analysed using the BD Biosciences software and the FlowJo software (Treestar Inc, Ashland, US). A gating strategy was put in place to eliminate cell debris and doublets/clumps of cells using the unstained vehicle-treated (control) cells. To eliminate debris and dead cells, an FSC-A vs SSC-A density plot was drawn up. FSC-A vs SSC-A plots were used for cell population gating and to identify any changes in the scatter properties of the cells. Cell debris and cell clumps tend to have lower forward scatter (FSC) levels and are found at the bottom left corner of an FSC vs SSC density plot, therefore a gate was set up to exclude cell debris (Figure 2.2).

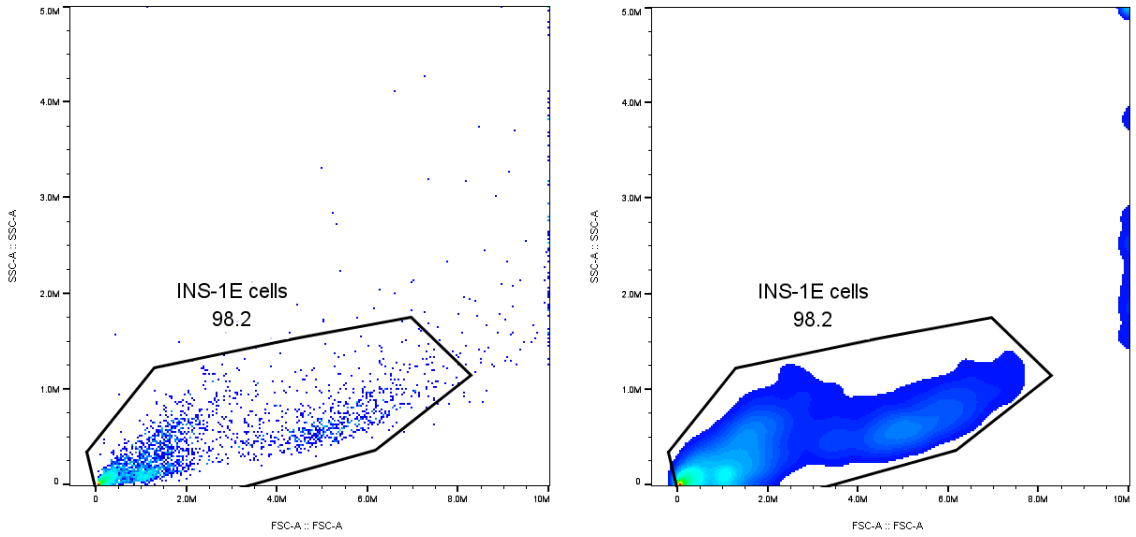

Figure 2.2 Debris exclusion based on scattering parameters. Cell debris and clumps (bottom left) were excluded by drawing up a gate further from the bottom left on a SSC-A vs. FSC-A plot using FlowJo. The gate exclusively includes INS-1E cells without debris.

Then, to obtain singlets (excluding doublets), an FSC-A vs FSC-H plot was created and the INS-1E cells along the densest diagonal were gated (Figure 2.3, A). The same gate was used for the analysis of all the samples to ensure reproducibility. Ultimately, a total of approximately 95-99% of the events were analysed. Then, to set up the quadrants, the unstained control was used. The quadrants were set as to ensure that all the unstained cells were included in the lower left quadrant. An example of the gates and the quadrant set-up is shown below (Figure 2.3, B). The same gate was used for the analysis of all the samples to ensure reproducibility. The full gating strategy used to analyse the samples is shown in an example below (Figure 2.3, B).

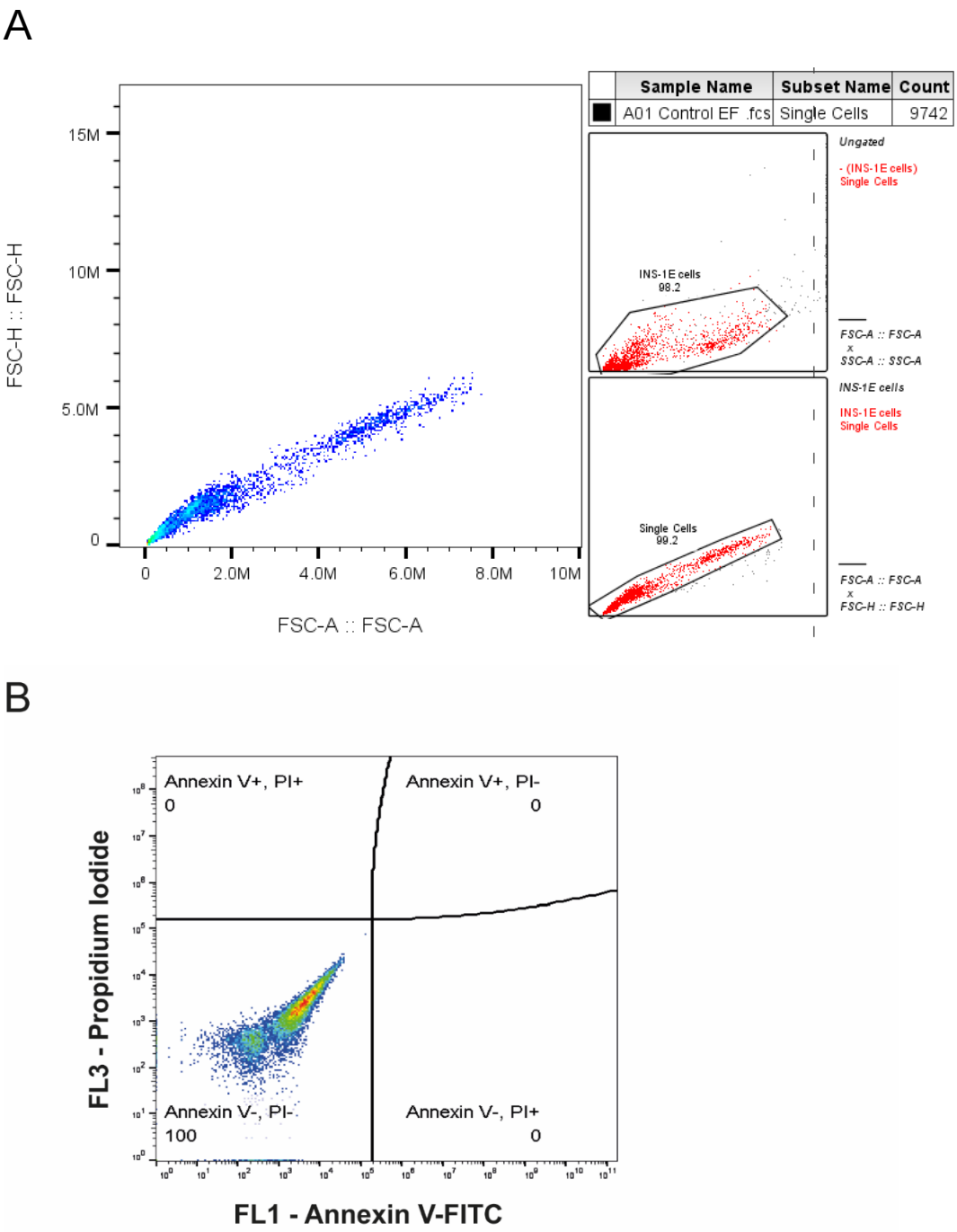

Figure 2.3 Discrimination of singlet INS-1E cells and gating strategy implemented in our study. (A) INS-1E cell population and singlets of a control sample were discriminated based on scatter parameters (FSC-A vs. FSC-H). INS-1E cell population and INS-1E singlet cells were determined and visualised using the back-gating tool. Red dots represent unchanged INS-1E cell population. Multi-coloured dots represent discriminated INS-1E cell to be further analysed. (B) Gating strategy based on unstained control on a FL1 vs. FL3 plot. Each of the four quadrants represent the live cells (Annexin V-, PI- - lower left quadrant), cells undergoing early apoptosis (Annexin V+, PI- - lower right quadrant) or late apoptosis/early necrosis (Annexin V+, PI+ - upper right quadrant) and dead cells (Annexin V-, PI+ - Q1). These plots were created using the FlowJo software. EF, Efavirenz.

The compensation controls were used to reduce the spillover fluorescence in the two channels, using the BD C6 Accuri Software (Figure 2.4). To reduce the spillover fluorescence in the FL1

channel (Annexin V-FITC), the control stained with PI only was used as described in Figure 2.4. Similarly, to reduce the spillover fluorescence in the FL3 channel (PI), control stained with Annexin V- FITC only was used (Figure 2.4).

A

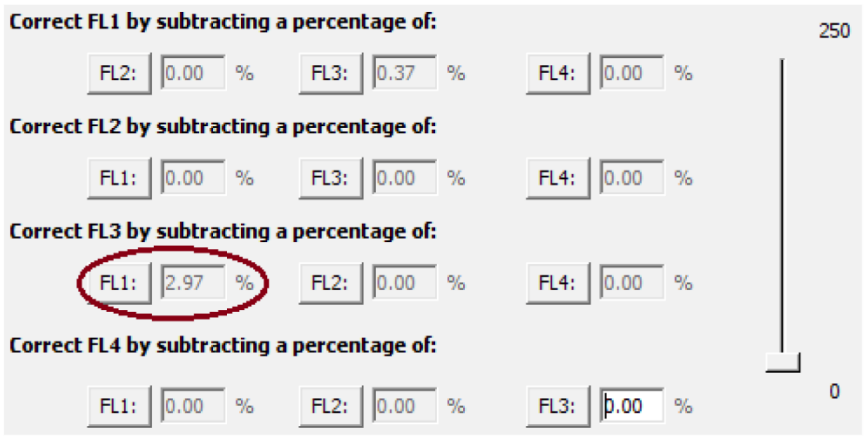

B

Median FL1 - Annexin V FITC-A	Median FL3 - Propidium Iodide-A
100,087.0	279.0
0.0	0.0
0.0	0.0
65,881.0	279.0
421,580.0	280.5

Figure 2.4 Correction of the FL3 (PI) signal with the FL1 (Annexin V-FITC) channel using the BD C6 Accuri Software. A value of the FL1 channel was subtracted from the FL3 channel (A) in order to ensure that the median of the lower right quadrant of the FL3 channel and the lower left quadrant of the FL3 channel were equal (B). Similarly, a value of the FL3 channel was subtracted from the FL1 channel in order to ensure that the median of the upper left quadrant of the FL1 channel and the lower left quadrant of the FL1 channel were equal (not shown).

Then, a plot of the compensated FL1 channel vs. FL3 channel was drawn using the Flow Jo software (Tree Star Inc., USA) to visualise the percentage of viable, early apoptotic, late apoptotic/early necrotic, and dead cells for each sample. Viable cells remained unstained (Annexin V-FITC−/PI−). Early apoptotic cells showed Annexin V-FITC+/PI− staining patterns due to PS externalisation while late apoptotic and primary necrotic cells exhibited Annexin V-FITC+/PI+ staining patterns due to a loss of plasma and nuclear membrane integrity (Brauchle *et al.*, 2014). Cells that stain positive for PI and negative for Annexin V-FITC are considered as dead.

2.2.6.3 Lactate dehydrogenase (LDH) assay

Principle

Plasma membrane leakage from necrotic cells causes the release of intracellular contents into extracellular milieu which include the cytoplasmic enzyme LDH (Chan *et al.*, 2013). Therefore, the release of the enzyme LDH from cells can act as a useful indicator of detection of necrotic cell death. When combined with detection of necrosis by flow cytometry, LDH can be useful in confirming necrosis.

Protocol

LDH release was assayed using the Cytotox 96® Non-Radioactive Cytotoxicity Assay as per manufacturer's instructions (Promega, Cat #: G1780, Madison, Wisconsin, USA). Briefly, aliquots (50 µL) were collected in a fresh 96-well clear bottom plate after centrifuging the 96-well cell culture plate at 400 x g for 4 mins to remove cell debris. Then, 50 µL of CytoTox96® Reagent was added to each sample aliquot before incubating for 30 mins at room temperature, protected from light. Following the 30-minute incubation, 50 µL of stop solution was added to each sample aliquot. LDH release into the medium was measured at 490 nm using a spectrophotometer (BioTek Synergy HT Microplate Reader, USA).

Data analysis

The blank (average of three replicates) was subtracted from all the values. Then, LDH release (% of maximal LDH release) was calculated using the equation below.

$$\%\ of\ maximal\ LDH\ release = 100\ x \frac{experimental\ LDH\ release\ (490\ nm)}{Maximal\ LDH\ release\ (490\ nm)}$$

2.2.7 Detection of oxidative stress

Given the fact that beta cells are extremely susceptible to oxidative stress due to their low antioxidant capacity, reactive oxygen species (ROS) attack is majorly involved in beta cell dysfunction and survival (Drews *et al.*, 2010). Therefore, we measured the generation of intracellular ROS and mitochondrial superoxide, as well as antioxidant capacity.

2.2.7.1 Detection of intracellular ROS; The dichloro-dihydro-fluorescein diacetate (DCFH-DA) assay

Principle

Several fluorescent probes are used to detect intracellular ROS. These include general probes such as dihydro-compounds (*i.e.*, dihydroethidium, dihydrorhodamine 123 and dihydrocalcein) and chloromethyl-2,7-dichlorodihydrofluorescien diacetate. Intracellular formation of ROS was detected using the fluorescent probe 2,7-dichlorodihydrofluorescien diacetate (DCFH-DA). DCFH-DA enters the cell and is hydrolysed by intracellular esterases into dichlorodihydrofluorecein (DCFH), which, upon oxidation by intracellular ROS, turns into fluorescent 2',7'-dichlorofluorescein (DCF) (Eruslanov & Kusmartsev, 2010; Gomes *et al.*, 2005)

Protocol

For method optimisation purposes, a positive control (hydrogen peroxide) was used to empirically determine an optimal DCFH-DA concentration for detecting intracellular ROS generation. This, in addition to extensive literature search, was used to determine the most appropriate conditions for this experiment. The following conditions were tested:

1. Optimal dye-loading concentration of H_2DCFDA (10 or 20 µM)

The concentration of DCFH-DA used differs from study to study depending on several parameters (*i.e.*, cell line used). However, several studies determined that 10 or 20 µM DCFH-DA was sufficient to detect intracellular ROS generation. Therefore, we empirically determined the most appropriate DCFH-DA to detect ROS formation in INS-1E cells by exposing them to 10 or 20 µM DCFH-DA for 30 mins. Figure 2.5 shows that DCFH-DA 10 µM was enough to visualise intracellular ROS formation (green fluorescence) in INS-1E cells exposed to hydrogen peroxide (H_2O_2) for 1 hr, therefore, this concentration was deemed sufficient to use in our study.

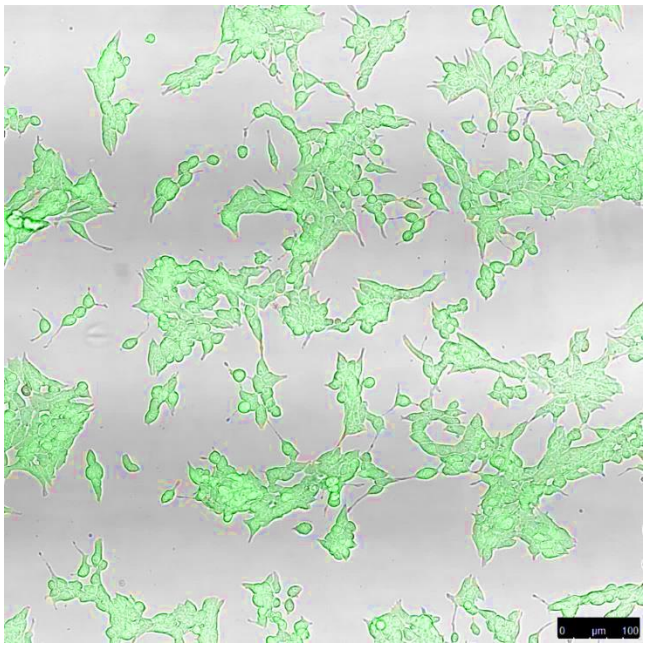

Figure 2.5 Effects of H_2O_2 on intracellular ROS generation on INS-1E cells assessed by the DCFH-DA assay. INS-1E cells were exposed to H2O2 for 1 hr before staining with DCFH-DA (10 μM). The fluorescent with brightfield overlay image of ROS level was obtained by laser scanning confocal microscopy. The green fluorescence represents DCF which was oxidised from DCFH by ROS. (Scale bar, 100 μm).

2. DCFH-DA loading time (30 vs. 60 mins)

Loading time varies from one study to another however, 30 to 60 mins were determined to be sufficient to detect intracellular ROS generation in INS-1E cells. To determine the optimal DCFH-DA loading time, INS-1E cells were stained with 10 μM DCFH-DA for 30 or 60 mins. A 30-minute staining period was enough to visualise DCF fluorescence using confocal microscopy (Figure 2.5).

After determining the optimal conditions for the method, the optimised protocol for intracellular ROS generation measurements with the DCFH-DA probe is as follows.

A 20 mM stock solution of 2′,7′-Dichlorodihydrofluorescein Diacetate (DCFH-DA) (MW = 487.29 g/mol) was prepared by dissolving 1.5 mg of DCFH-DA in 1 mL of DMSO. Several aliquots of DCFH-DA stock solutions were stored at –20°C and thawed when required to measure intracellular ROS generation. A 100 μM H_2O_2 solution was prepared by diluting 0.114 μL of H_2O_2 30% (w/w) in 10 mL of PBS.

After treatment protocol, cells were washed twice with 3 mL of prewarmed (37°C) PBS per well and stained with 1 mL of a 10 μM DCFH-DA working solution which was prepared by diluting 9.76 μL of 20 mM DCFH-DA stock solution in 10 mL of prewarmed PBS. A negative control consisting of unlabeled cells (PBS only) was included for each experiment.

Intracellular ROS generation was observed and photographed using an inverted confocal laser scanning microscope (Leica TCS SP5 Confocal Laser Scanning Microscope, Germany) and the accompanying Confocal LAS AF software or the Zeiss Confocal Laser Scanning Microscope, Germany and the accompanying Zeiss Zen imaging software. The Argon laser at power 0.1-10% was set using the Confocal LAS AF software or Zeiss Zen imaging software (Table 5, **Appendix I**). The imaging parameters were chosen as to ensure a 1024 x 1024 format. Next, the beam path window was set to excite DCFH-DA using the 488 Argon (Blue) laser line (FITC filter settings). Emission light passed through a 20X, 0.5NA objective and was filtered by a bandpass filter of ~500-580 nm. The gain and offset controls were set manually to produce bright and clear images with little noise. The settings were the same for each sample of a biological replicate. Image noise was reduced by rescanning the specimen slice several times using the line average parameter of 2 and a frame average of 3. To avoid biasing, random regions of the well were imaged for each sample.

Data analysis

Images were taken to visualise and quantify intracellular ROS generation using the ImageJ software (Maryland, USA). Intracellular ROS generation was visualised by the resulting green fluorescence. DCF mean fluorescence intensity (MFI) was determined using the imageJ software and used to quantify intracellular ROS generation. DCF fluorescence intensity is directly proportional to the amount of ROS species in the cell. Fluorescence compensation (to avoid autofluorescence measurements) was performed by subtracting the MFI of the DCFH-DA-stained cells by the MFI of unlabelled cells. Additionally, in order to confirm that NNRTIs and NRTIs did not cause an increase the DCF fluorescence in the presence of DCFH-DA, we conducted several experiments to assess DCF fluorescence (no cells) in the presence of 10 µM DCFH-DA. There was no DCF fluorescence detected in these conditions (data not shown).

To confirm our quantitative results for NNRTI treatments, a set of experiments measuring intracellular ROS fluorescence in a 96-well plate.

Following treatment protocol, cells were stained with prewarmed (37^{o}C) PBS containing 10 µM DCFH-DA for 30 mins. Then, stained cells were washed twice with PBS and fluorescence was measured in a microplate fluorometer at 495 nm excitation and 530 nm emission. The values obtained were normalised to cell proliferation by Crystal Violet assay. The crystal violet assay was performed by removing the DCFH-DA solution before adding 50 µL in 0.2% crystal violet in 20% ethanol for 10 mins at room temperature. Then, the cells were washed four times

with 200 µL of distilled H_2O. After complete removal of distilled H_2O, the plates were left to air dry before solubilising the crystal violet with 0.1% SDS in H_2O. A spectrophotometer (BioTek Synergy HT Microplate Reader, USA) was used at 570 nm to measure absorbance. DCF fluorescence was normalised to Crystal violet absorbance.

2.2.7.2 Detection of mitochondrial superoxide formation

Principle

The mammalian mitochondria are the main source of ROS formation in cells. Superoxide is the proximal mitochondrial ROS, and it is therefore important to measure superoxide formation by the mitochondria. Mitochondrial superoxide formation was assessed with the MitoSOX mitochondrial superoxide indicator.

Protocol

A time course experiment was preferred in order to pinpoint the exact occurrence of mitochondrial superoxide production in INS-1E cells. To do so, INS-1E cells were exposed to efavirenz (20 µM) or rilpivirine (10 µM) for 2, 4, 6 or 24 hrs. A 5 mM stock solution of MitoSOX™ Red reagent (MW = 759 g/mol) was prepared by adding 13 µL of DMSO to 50 µg of MitoSOX™ Red reagent. The stock solution was stored at -20°C. Recommendations for experimental protocols provided by the manufacturer were used as a starting point, and optimal labelling conditions were determined empirically.

Following cell growth and treatment protocol, the cells were washed once with 3 mL of prewarmed (37°C) PBS and gently scrapped off the plates with a cell scrapper in 1 mL of prewarmed PBS. Then, the cells were transferred to a 1.5 mL Eppendorf tube and centrifuged for 5 mins at 300 x g. Following centrifugation, the cell pellet was resuspended in 1 mL of prewarmed PBS before equally diving the cell suspension in two 1.5 mL Eppendorf tubes: these account for the unstained vs MitoSOX-stained cells for each sample. The cells were centrifuged once more at 300 x g for 5 mins before resuspending with a freshly prepared 5 µM MitoSOX reagent working solution in Hank's Buffer Salt Solution (HBSS) and incubated in the dark for 10 mins at 37°C. The unlabelled cells were resuspended in 0.5 mL of HBSS and were also incubated for 10 mins at 37°C. Following the 10-minute incubation, cells were centrifuged for 5 mins at 300 x g. After centrifugation, the supernatant was removed, and MitoSOX-stained cells were washed twice by adding 1 mL of prewarmed HBSS with intermediate centrifugation at 300 x g for 5 mins. Then both labelled and unlabelled cells were resuspended in 0.5 mL of prewarmed HBSS. MitoSOX fluorescence intensity was then immediately measured using flow

cytometry (BD C6 Flow Cytometer; BD Biosciences; Becton-Dickinson Co., Franklin Lakes, New Jersey, USA).

Data analysis

The same gating strategy used for flow cytometric analysis of cell death and Δψm changes (see 2.2.5.2) was performed.

A univariate histogram was drawn using the Flow Jo software (Tree Star Inc., USA) to obtain the mean fluorescence intensity (MFI) of MitoSOX fluorescence (excitation/emission 396/610 nm) at the FL2 channel for all the samples. Fluorescence compensation was performed by subtracting the MFI of the stained cells by the MFI of unstained cells. MFI was calculated as % of vehicle treated control cells.

2.2.7.3 Determination of antioxidant capacity; The ABTS 2,2'-azino-bis (3-ethylbenzothiazoline-6-sulphonic acid) assay

Principle

The 2,2'-azino-bis (3-ethylbenzothiazoline-6-sulphonic acid) (ABTS) assay is a colorimetric assay adapted by Re *et al.* (1999). The ABTS assay is commonly used to assess antioxidant activity. The assay is based on the formation of the $ABTS^{\bullet+}$ radical and measures the ability of cells to scavenge the $ABTS^{\bullet+}$ radical. ABTS•+ is decolorised by antioxidants according to their antioxidant capacities (Re *et al*., 1999 and Erel, 2004).

Protocol

An ABTS (MW = 548.68 g/mol)-distilled water solution (8 mg/mL) and a potassium persulfate water solution (1.32 mg/mL) were prepared. Equal volumes (5 mL) of ABTS water solution and potassium persulfate water solution were mixed together to produce an ABTS+ stock solution (7 mM). The ABTS+ stock solution was covered in foil and left in the dark at room temperature for 16 hrs to produce ABTS++ di-cationic radical. This solution is the ABTS stock solution. After the 24-hour incubation period, a volume of 100 µL of ABTS solution was then quickly added to all the prefilled wells on the plate shown above, using a multichannel pipette. The 96-well plate was then immediately placed in the spectrophotometer (BioTek Synergy HT Microplate Reader, USA), to read the absorbance using a kinetic assay mode (total time = 10 mins; interval = 30 secs; absorbance = 405 nm).

Data analysis

The absorbance measurements of the treated cells were expressed as % of the absorbance observed in vehicle (DMSO)-treated cells (control).

2.2.8 Changes in mitochondrial membrane potential

Mitochondrial membrane potential (Δψm) is a strong indicator of mitochondrial function and viability, and overall cellular health. Any sustained changes to the levels of Δψm may be deleterious. Several fluorescent probes have been developed since 1980 to monitor changes in Δψm. These probes can be used to analyse the mitochondria and mitochondrial activities using image analysis and flow cytometry. Examples of these dyes include rhodamine dyes (*i.e.*, tetramethylrhodamine ethyl ester and rhodamine 123), carbocyanine dyes (*i.e.*, $DiOC_6(3)$) and 5,5′,6,6′-tetrachloro-1,1′,3,3′-tetraethylbenzimidazolcarbocyanine (JC-1)) and rosamine dyes (MitoTracker).

In this study, Δψm changes were monitored using two different probes: 3,3′-dihexyloxacarbocyanine iodide ($DiOC_6(3)$) and tetramethylrhodamine ethyl ester (TMRE). Initially, we used $DiOC_6(3)$ as a probe to monitor changes in Δψm. However, we obtained variation in the results (data not shown). Additionally, $DiOC_6(3)$ has previously been shown to be non-specific to the mitochondria, hence this prompted need to evaluate Δψm using another probe. TMRE is a positively charged dye that accumulates in active mitochondria due to their relative negative charge.

Principle

Tetramethylrhodamine ethyl ester (TMRE) and tetramethylrhodamine methyl ester (TMRM) specifically stain polarised mitochondria rather than other intracellular organelles whereas $DiOC_6(3)$ is not specific to mitochondria (Cottet-Rousselle *et al.*, 2011). TMRM and TMRE have been described as non-toxic and highly fluorescent (Cottet-Rousselle *et al.*, 2011; Ehrenberg *et al.*, 1988). Additionally, Cottet-Rousselle *et al.* (2011) explained that TMRE can be used in low concentrations with no quenching effect (non-quenching mode up to 100 nM TMRE). TMRE is a positively charged dye that accumulates in active mitochondria due to their relative negative charge while inactive mitochondria fail to retain TMRE. TMRE fluorescence intensity, relative to the Δψm, can be measured using flow cytometry or microscopy (Cottet-

Rousselle *et al.*, 2011). Hence, TMRE fluorescence was used as a quantitative analytical tool for mitochondrial membrane potential using flow cytometry.

Protocol

For method optimisation purposes, a positive control, carbonyl cyanide m-chlorophenyl hydrazine (CCCP) was used to empirically determine an appropriate technique for monitoring Δψm changes using TMRE in INS-1E cells. CCCP is a mitochondrial oxidative phosphorylation uncoupler and has been used in many studies as a reliable way of evaluating the occurrence of mitochondrial depolarisation (Cottet-Rousselle *et al.*, 2011). Treating INS-1E cells with CCCP is expected to induce depolarization and eliminate Δψm and TMRE staining. A 50 mM stock solution of CCCP (MW = 204.616 g/mol) was prepared by dissolving 10.23 mg of CCCP in 1 mL of DMSO. Several aliquots of CCCP stock solutions were stored at –20^{o}C and thawed when required for Δψm measurements.

When determining optimal TMRE loading time in INS-1E cells (20 vs. 30 mins), the minimal loading time of 20 mins was found to be sufficient to detect Δψm. Then, optimal concentrations of CCCP (10, 30 or 50 µM) and TMRE (50, 100 and 200 nM) were investigated. A 1 mM stock solution of TMRE (MW = 514.95 g/mol) was prepared by dissolving 0.51 mg of tetramethyrhodamine ethyl ester perchlorate in 1 mL of DMSO. Several aliquots of TMRE stock solutions were stored at –20^{o}C and thawed when required for Δψm measurements. This would help determine the lowest concentration of TMRE needed to detect a disruption in mitochondrial membrane potential and the most effective concentration of the positive control to obtain a loss of mitochondrial membrane potential. It was determined that 50 nM TMRE was the most appropriate concentration to use for the determination of Δψm in INS-1E cells as it was sufficient to detect changes in Δψm. A dose-response curve of INS-1E cells exposed to increasing concentrations of CCCP is shown below (Figure 2.6). As expected, the highest concentration of CCCP (50 µM) caused a profound loss of Δψm in INS-1E cells. Therefore, CCCP 50 µM was used a positive control for future experiments (Figure 2.6).

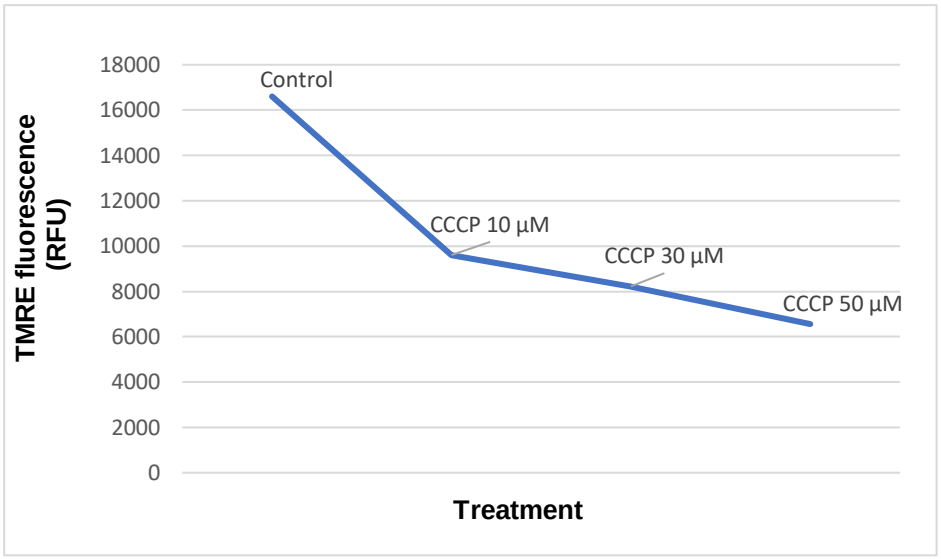

Figure 2.6 Dose-response curve of TMRE fluorescence in INS-1E cells treated with CCCP. INS-1E cells were exposed to vehicle (DMSO) or CCCP (10, 30 or 50 µM) for 20 mins in TMRE (50 nM) working solution. Samples were then subject to flow cytometric analysis.

Mean TMRE fluorescence reduced in CCCP-treated INS-1E cells compared to vehicle-treated cells, confirming that the optimized protocol works (Figure 2.7).

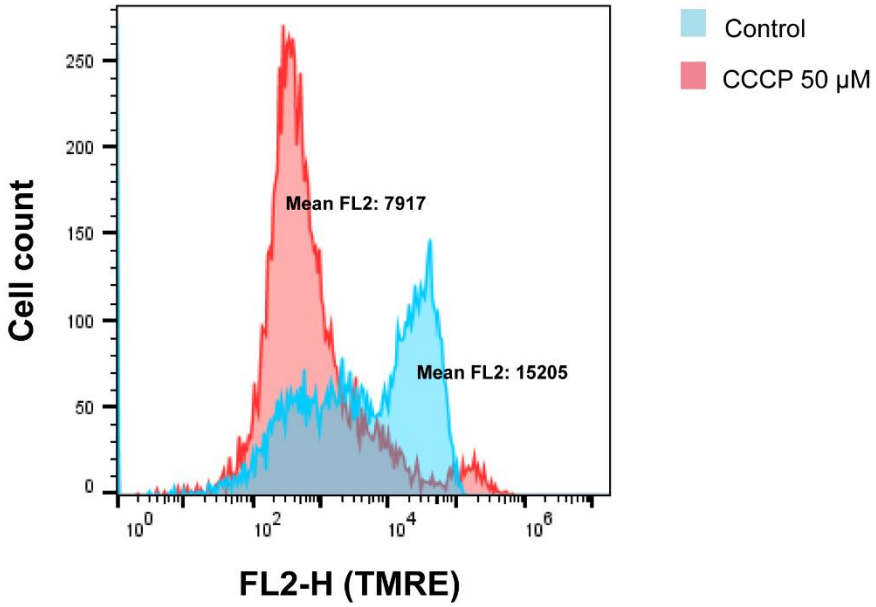

Figure 2.7 Impact of CCCP treatment on TMRE fluorescence in INS-1E cells. INS-1E cells were exposed to DMSO alone or CCCP (50 µM) and stained with TMRE (50 nM) for 20 mins before measuring TMRE fluorescence by flow cytometry. A shift to the left (CCCP treatment) signifies a lower TMRE fluorescence than vehicle-treated cells. A lower TMRE fluorescence signifies a reduced $\Delta\psi m$. FL2 fluorescence and graphs were obtained using FlowJo.

After method optimisation, the following protocol was adopted for the measurements of Δψm in INS-1E cells.

A 50 nM TMRE working solution was freshly prepared prior each experiment by diluting 2.5 µL of the 1 mM TMRE stock solution in 50 mL of prewarmed PBS (37ºC). Following cell growth and treatment protocol, the cells were washed once with 3 mL of prewarmed (37ºC) PBS and gently scrapped off the plates with a cell scrapper in 1 mL of prewarmed PBS. Then, the cells were transferred to a 1.5 mL Eppendorf tube and centrifuged for 5 mins at 300 x g. Following centrifugation, the cell pellet was resuspended in 1 mL of prewarmed PBS before equally diving the cell suspension in two 1.5 mL Eppendorf tubes: these account for the unstained vs TMRE stained cells for each sample. The cells were centrifuged once more at 300 x g for 5 mins before resuspending with a freshly prepared 50 nM TMRE working solution and incubated in the dark at 37ºC for 20 mins; these are the TMRE stained cells. The unstained cells were resuspended in 0.5 mL of prewarmed PBS and incubated at 37ºC for 20 mins to match the conditions of TMRE-stained cells. Cells were also treated with 50 µM CCCP (positive control) by adding 0.5 µL of 50 mM CCCP in 0.5 mL of TMRE working solution. Following staining, cells were centrifuged for 5 mins at 300 x g. After centrifugation, the supernatant was removed, and both stained and unstained cells were resuspended in 0.5 mL of prewarmed (37ºC) PBS. TMRE fluorescence intensity was then immediately measured using flow cytometry (BD C6 Flow Cytometer; BD Biosciences, New Jersey, USA). A vehicle (DMSO)-treated control and positive control (50 µM CCCP) were included in each experiment.

Data analysis

The same gating strategy used for flow cytometric analysis of cell death (see 2.2.6.2) was performed.

A univariate histogram was drawn using the Flow Jo software (Tree Star Inc., Oregon, USA) to obtain the mean fluorescence intensity (MFI) at the FL2 channel for all the samples, including the control and the positive control (50 µM CCCP).

Inactive or depolarised mitochondria have decreased membrane potential and thus fail to retain the TMRE dye and as a result show low fluorescence signal. More polarised mitochondria have increased membrane potential and thus accumulate more TMRE dye and as a result show high fluorescence signal. Fluorescence compensation was performed by subtracting the MFI of the stained cells by the MFI of unstained cells. MFI was calculated as % of vehicle (DMSO)-treated control cells.

2.2.9 Glucokinase activity assay

Principle

Glucokinase is a key enzyme in pancreatic beta cells that phosphorylates glucose into glucose 6-phosphate using ATP as the phosphate group donor. The figure below summarises the principle of this assay (Figure 2.8).

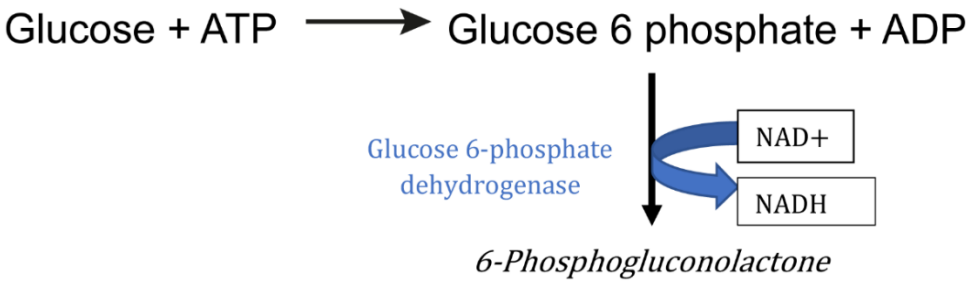

Figure 2.8 Glucokinase activity assay principle. Glucose 6 phosphatase is converted to 6-Phosphogluconolactone by glucose 6-phosphatase dehydrogenase. The formation of glucose 6 phosphate is used to indirectly determine the activity of glucokinase. ADP, Adenosine diphosphate; ATP, Adenosine triphosphate; NAD+, Nicotinamide adenine dinucleotide; NADPH, nicotinamide adenine dinucleotide hydrogen.

The following protocol describes an indirect assay to determine the activity of glucokinase in INS-1E cells. Glucose 6-phosphate formed by glucokinase is measured by the production of NADPH in the presence of glucose 6-phosphate dehydrogenase (Figure 2.8).

Protocol

This protocol was adapted from Pakoskey *et al.* (1965) and was optimised as described below.

Before commencing the procedure, we freshly prepared a 10 mM glucose solution, 20 mM ATP solution and 10 mM NADP solution in distilled H_2O. The spectrophotometer was turned and heated to 37^{o}C.

Following treatment protocol, the cells were washed twice with 3 mL of PBS per well. Cells were then harvested by scraping in 1 mL of PBS per well. Then, the cells were centrifuged for 1 min at 300 x g. The cells were then resuspended in 100 µL of 100 mM Tris buffer. The cells were then subject to freeze-thaw cycles to ensure cell lysis. After the last freeze-thaw cycle, cells were resuspended and centrifuged for 10 mins at 300 x g. The supernatant was used as sample for the glucokinase activity assay.

A mixture of 100 mM Tris buffer (6.275 mL), 100 mM magnesium sulphate buffer (1.15 mL), (0.56 mL) 20 mM ATP solution and (0.56 mL) 10 mM NADP solution was prepared. Then, 13 µL of glucokinase enzyme was added to 2 mL of this mixture, creating a mixture which will be referred as 'glucokinase mixture'.

Each sample was subject to a control (*i.e.*, 10 µL of sample in 40 µL of distilled water) versus an experimental (*i.e.*, 10 µL of sample in 20 µL of 10 mM of glucose solution and 20 µL of distilled water) in 150 µL of glucokinase mixture added to each well of a 96-well plate. The 96-well plate was then immediately placed in the spectrophotometer, to read the absorbance using the kinetic assay mode (total time = 10 mins; interval = 120 secs; absorbance = 340 nm) (BioTek Synergy HT Microplate Reader, USA).

Data analysis

Glucokinase activity was calculated using the following equations **(a)** and **(b).**

(a) $dA/dt(min-1) = [Rate]experimental - [Rate]control = dA/dt$

(b) $Activity = \frac{1000xTVxDxdA/dt}{\varepsilon xVxCF}$

Activity: Volumetric activity (U/L)

TV: Total volume in cuvette (1000 µL)

D: Dilution of the cell extract (50 µL of cell extract was added to 950 µL of deionised water then, D=20)

V: Volume of cell extract used (50 µL)

Ɛ: Molar extinction coefficient for NADPH (6.22 L/mmol for a path length of 1.0 cm)

CF: Concentration Factor of cell extract (if 100 mL sample was concentrated to a 2 mL volume for the French Press, then CF=50

After performing a Bradford protein assay as described above (see 2.2.4), the specific glucokinase activity was calculated using the equation below **(c).**

(c) $Specific\ Activity = \frac{Activity}{Total\ protein\ concentration}$

2.2.10 Detection of ER stress using ELISA

Due to the increased demand for insulin synthesis and secretion under diabetic conditions, beta cell dysfunction and apoptosis are closely associated with ER stress (Eizirik *et al*., 2008; Cnop *et al*., 2017; Egushi *et al*., 2021). ER stress is associated with increased expression of CHOP and ER chaperones such as GRP78.

ER stress was detected using the rat DDTI3/CHOP ELISA kit (LifeSpan Biosciences, Cambridgeshire, UK) in order to obtain preliminary data to determine whether ER stress is involved.

Principle

The DDTI3/CHOP ELISA monitors CHOP expression profile in cells. CHOP is a key marker of ER stress. In this case, the kit can be used for measuring the relative amounts of CHOP in INS-1E cells after exposure to the antiretroviral agents under investigation.

Protocol

Following cell growth and treatment protocol, CHOP expression in INS-1E cells were assayed using rat DDTI3/CHOP ELISA kit, according to the manufacturer' instructions (Cat#: LS-F11285, LifeSpan Biosciences, Cambridgeshire, UK). Briefly, cell lysates were prepared by collecting cells and pelleting the cells by centrifuging at 500 x g for 5 mins. Following centrifugation, the supernatant was removed, and the cells were washed three times with PBS and then resuspended in PBS. The cells were lysed by freezing the cells to -20^{o}C and thawing to room temperature three times. The cells were then centrifuges at 1500 x g for 10 mins at 4^{o}C to remove cellular debris. The supernatant was then collected for assaying. Standards were prepared using the standard stock solution diluted in Sample Diluent. Standards, samples and blanks (100 µL) were added into respective wells of the microplate provided at incubated for 1 hr at 37^{o}C. The solution was then aspirated and 100 µL of Detection Reagent A working solution was added to each well. The microplate was then incubated for 1 hr at 37^{o}C. The solution was then aspirated, and each well was washed three times with 300 µL Wash Buffer using a multichannel pipette. After washing, the Wash Buffer was completely removed, and the microplate was tapped. Then, Detection reagent B (100 µL) was added to each well before incubating for 30 mins at 37^{o}C. After incubation, the solution was removed, and each well was washed five times with Wash Buffer. After the complete removal of the Wash Buffer by tapping, TMB Substrate solution (90 µL) was added to each well and incubated for 15 mins at 37^{o}C. Then, Stop Solution (50 µL) was added to each well before immediately reading

absorbance at 450 nm using a spectrophotometer (BioTek Synergy HT Microplate Reader, Vermont, USA).

Data Analysis

The values obtained were normalised against total cellular protein concentrations determined with the Bradford assay (see 2.2.4) and expressed as % vehicle (DMSO)-treated cells.

2.2.11 Messenger RNA extraction and quantitative reverse transcription polymerase chain reaction (RT-qPCR)

Principle

Quantitative reverse transcription polymerase chain reaction (PCR) is used to analyse the expression of genes of interest. RT-qPCR consists of transcribing the starting material, RNA, into complementary DNA (cDNA) by reverse transcription. The cDNA serves as the template for the qPCR reaction. Here, we analyse the mRNA expression of key markers of ER stress (*i.e.*, *CHOP* and *GRP78*) as well as a key functional gene in beta cells (*i.e.*, *PDX-1*) and mitochondrial uncoupling protein 2 (*UCP2*).

We also assess the mRNA expression of the subunits of the pancreatic beta cell ATP-sensitive potassium channel, the inwardly rectifying potassium channels subfamily 6 and subtype 2 (*Kir6.2)* and sulfonylurea receptor 1 (*SUR1*).

Protocol

Sample preparation

Following cell growth and treatment protocol, INS-1E cells were enzymatically harvested with 1 mL of trypsin/EDTA (0.05%). After trypsinisation for 1 to 2 mins, 2 mL of 1640 RPMI media supplemented with 10% heat-inactivated FCS was added to neutralise the trypsin. Then, 1 mL of cell suspension from each sample was transferred to RNAse-free microfuge tubes (Thermo Fisher Scientific). Cells were then centrifuged at 300 x g for 5 mins. Following centrifugation, the supernatant was completely removed, and the cell pellets were immediately stored at -80^{o}C.

Total RNA extraction

The cell pellets were thawed at room temperature (~25^{o}C). Total RNA was isolated from INS1E cells using the RNeasy Mini Kit (Qiagen, Cat#: 74104, Hilden, Germany) according to the manufacturer's instructions with several alterations as per method optimisation. In summary, INS-1E cells were disrupted in 350 µL buffer RLT and homogenised. Then, 350 µL of 70%

ethanol was added to the lysate, thus creating conditions that promote selective binding of RNA to the RNeasy membrane supplied. Then, 700 µL of the lysate was applied to the RNeasy Mini spin column which was centrifuged at ≥ 8,000 x g for 1 min. Contaminants were washed away, and high-quality RNA was eluted in 40 µL RNAse-free water. Elution was done in two steps: the RNA was firstly eluted in 20 µL of RNAse-free water and centrifuged before adding another 20 µL of RNAse-free water and centrifuged again. RNA was then transcribed into cDNA. The concentration of RNA was determined using a Nanodrop® Lite spectrophotometer (Thermo Fisher, USA), with nuclease-free water as zero absorbance reference. A Nanodrop® Lite spectrophotometer also provides a A260/A280 ratio that allows the assessment of purity. Values close to 2 are generally accepted as 'pure' RNA. Once the purity was deemed acceptable, and the amount of RNA was determined, then reverse transcription was carried out.

Reverse Transcription

Reverse transcription of RNA to cDNA was performed using QuantiTect Reverse Transcription Kit (Qiagen, Cat#: 205311, Hilden, Germany) as per manufacturer's instructions. The genomic DNA (gDNA) elimination reaction was performed by adding the components in Table 2.3 then incubating the gDNA elimination reaction mix for 2 mins at 42°C. The volume of template RNA was calculated depending on the amount of RNA assessed earlier. For example, for 259.3 ng/µL (A260/280: 2), 3.9 µL of template RNA was added to the genomic DNA elimination reaction mix (Table 2.3).

Table 2.3 Genomic DNA elimination reaction components

Component	Volume (in µL) /reaction
gDNA Wipeout Buffer, 7 x	2
Template RNA, up to 1 µg	3.9
RNase-free water	8.1
Total reaction volume	14

Then, the reverse transcription (RT) master mix was prepared by mixing all the components in Table 2.4, except the entire gDNA elimination reaction, in a single 0.2 mL PCR tube. This would reduce the risk of mixing up samples and contaminating one sample with another sample. We also made sure to obtain enough RT mix to add to the entire gDNA elimination reaction. For instance, to prepare five samples, we assumed we had a total of six samples to reduce the risk of pipetting errors. Then, 6 µL of this mixture was added to the entire gDNA elimination reaction (14 µL) obtained earlier. Then, the reverse transcription reaction was incubation for 15

mins at 42ºC to initiate the reverse transcription process, followed by 3 mins at 95ºC to inactivate the Quantiscript Reverse Transcriptase.

Table 2.4 Reverse transcription reaction components

Component	Volume (in µL) /reaction
Quantiscript Reverse Transcriptase	1
Quantiscript RT Buffer, 5x	4
RT Primer Mix	1
Entire gDNA elimination reaction	14
Total reaction volume	20

SYBR green

RT-qPCR analyses were performed on the cDNA preparations to detect the expression of the genes C/EBP homologous protein (*CHOP*), 78-kDa glucose-regulated protein (*GRP78*), pancreatic and duodenal homeobox 1 (*PDX-1*), inwardly rectifying potassium channels subfamily 6 and subtype 2 (*Kir6.2)*, sulfonylurea receptor 1 (*SUR1*) and uncoupling protein 2 (*UCP2*) using SYBR green fluorescence. The previously designed primers for *CHOP, GRP78, PDX-1, UCP2, Kir6.2, SUR1* and *GAPDH* are outlined in Table 2.5 (Azzu *et al.*, 2008; Cardozo *et al.*, 2001; Kharroubi *et al.*, 2004; Zhou *et al.*, 2011). The primers were diluted in EDTA to produce a final stock solution concentration of 100 µM.

Table 2.5 Primer sequences for RT-qPCR

Gene	Sequence	size
***CHOP* (Kharroubi et al., 2004)**	Forward, 5′-CCAGCAGAGGTCACAAGCAC-3′ Reverse, 5′-CGCACTGACCACTCTGTTTC-3′	(125 bp)
***GRP78* (Kharroubi et al., 2004)**	Forward, 5′-CCACCAGGATGCAGACATTG-3′ Reverse, 5′-AGGGCCTCCACTTCCATAGA-3′	(100 bp)
***PDX-1* (Cardozo et al., 2001)**	Forward, 5′-GGTGCCAGAGTTCAGTGCTA-3′ Reverse, 5′-TTATTCTCCTCCGGTTCTGC-3′	(369 bp)
UCP2 (Azzu et al., 2008)	Forward, 5′-GATCTCATCACTTTCCCTCTAGACA-3′ Reverse, 5′-CCCTTGACTCTCTCCTTGG-3’	
Kir6.2 (Zhou et al., 2011)	Forward 5′-CGCATGGTGACAGAGGAATG-3′ Reverse 5′-GTGGAGAGGCACAACTTCGC-3′	(297 bp)
***SUR1* (Zhou et al., 2011)**	Forward, 5′-AGGATGATACGGTTGAGCAGG-3′ Reverse, 5′-TGCCAGCTCTTTGAGCATTGG-3′	(558 bp)
***GAPDH* (house-keeping gene) (Kharroubi et al., 2004)**	Forward, 5′-AGTTCAACGGCACAGTCAAG-3′ Reverse, 5′-TACTCAGCACCAGCATCACC-3′	(118 bp)

The following parameters were checked as part of optimal primer design guidelines:

- Sufficiently long (18-30 nucleotides)
- G and C content between 40-60%
- G or C at the end (GC clamp stabilises primer binding)
- Long sequences of same nucleotide were avoided (e.g., 4 As or Ts)
- Annealing temperature (T_m) - 5^{o}C between forward and reverse primers for one gene

SYBR qPCR amplifications were performed in 25 µL reactions of Rotor-Gene SYBR Green (Qiagen, Cat# 204074, Hilden, Germany), as per manufacturer's protocol. The reactions contained 2x Rotor-Gene SYBR Green PCR Master Mix, forward and reverse primers, and variable volumes of RNAse free water and template DNA, depending on the amount of template DNA present in each sample as each reaction requires ≤ 100 ng/reaction of template cDNA. We empirically determined an appropriate volume of template cDNA (3 µL) which was sufficient to amplify (data not shown). We added all the components of SYBR green master mix shown in Table 2.6, except the template cDNA in a PCR tube. The reaction was made to 25 mL total volume with nuclease-free water. We also made sure to obtain enough SYBR green mix for all samples. For instance, to prepare five samples, we assumed we had a total of six samples to reduce the risk of pipetting errors. Then, 22 µL of the SYBR green master mix (without the template cDNA) was added in individual 0.1 mL PCR strip tubes. Template cDNA was then added to the rest of the SYBR green master mix. The SYBR green reaction mix was then immediately subject to RT-qPCR as explained later.

Table 2.6 Example of reaction setup for RT-qPCR using Rotor-Gene SYBR Green

Component	Volume (in µL) /reaction	Final concentration
2x Rotor-Gene SYBR Green PCR Master Mix	12.5	1x
Primer A (forward)	0.25	1 µM
Primer B (reverse)	0.25	1 µM
RNase-free water	9	------
Template cDNA	3	≤ 100 ng/reaction
Total reaction volume	25 µL	

All samples were subjected to RT-PCR in duplicates or triplicates with the following cycling conditions, as per manufacturer's instructions (Qiagen, Cat# 204074, Hilden, Germany). The cycling conditions used in this study are detailed in Figure 2.9.

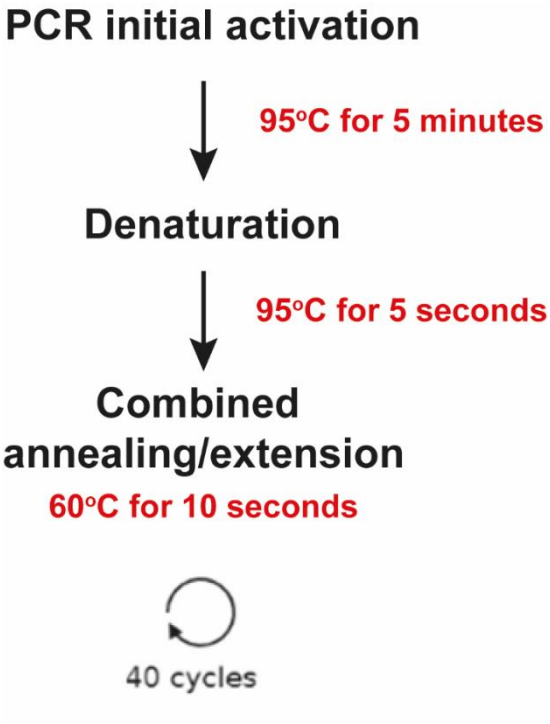

Figure 2.9 Cycling conditions for RT-qPCR. The programme was set to heat the samples to 95°C for 5 mins for the initial denaturation. The second stage was the thermo-cycling phase, which consisted of a further denaturation of 5 secs at 95°C, annealing and extension at 60°C for 10 secs as all primer sets had an annealing temperature (Tm) below 60°C. This was repeated for 40 cycles. Figure created with BioRender.com.

The resulting amplification curves, representing SYBR green fluorescence vs. number of cycles was used to determine a cycle threshold (Ct) value (Figure 2.10). To do so, an amplification

threshold was set using a log SYBR green fluorescence vs number of cycles graph. For accurate quantitation the threshold must be set so that all amplification curves cross this threshold while in the exponential phase. Ct values will be used for further data analysis.

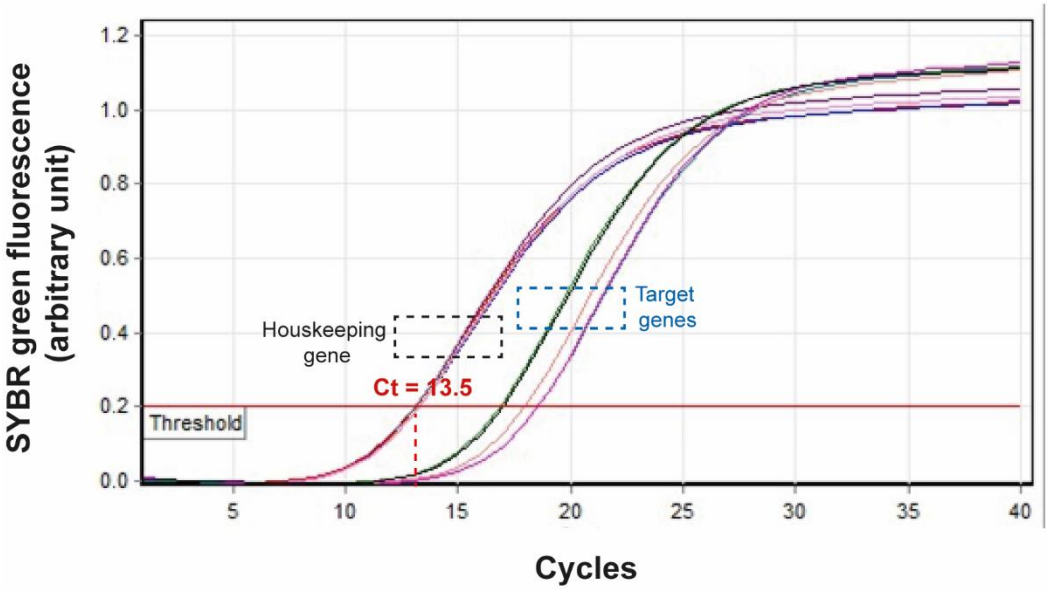

Figure 2.10 Representation amplification plot for RT-qPCR using SYBR green. Amplification curves for housekeeping and target genes from INS-1E cells. A threshold was set to obtain Ct values for housekeeping and target genes

Standard curve and efficiency

We conducted a standard curve to calculate the efficiency of our PCR primers (Figure 2.11). The reason we calculated PCR primer efficiencies is to be able to correctly analyse the results. For the calculation of gene expression, such as the comparative Ct method, it is assumed that the PCR primer efficiencies are comparable for the gene of interest and for the housekeeping gene.

Efficiency was calculated according to the equation below (Figure 2.11):

$$Efficiency\ (\%) = \left(10^{\frac{-1}{Slope\ (i.e.\ -3.3789)}} - 1\right) \times\ 100$$

Therefore, the primer efficiency score was calculated as 98%, which is between the desired 90 -110% range.

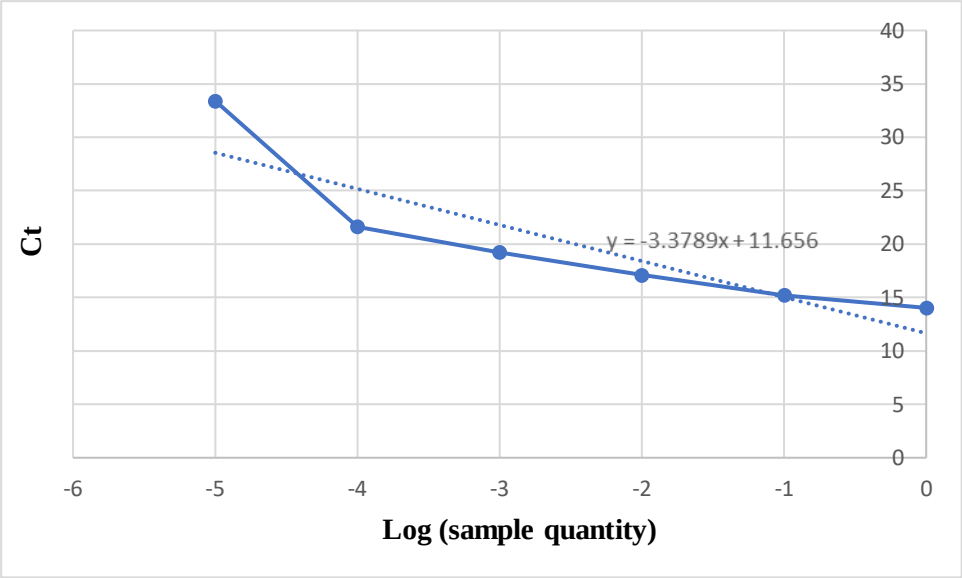

Figure 2.11 Slope of the regression between the log values and the average Ct values for PCR primer efficiency.

Melt curve

Melt curves were performed for each RT-qPCR run to confirm that a single amplicon has been generated by qPCR, confirmed by the presence of a single peak, hence indicating specific amplification (Figure 2.12). Other analysis tools, such as agarose gels can be used in conjunction with melt curves to determine the purity of an amplicon.

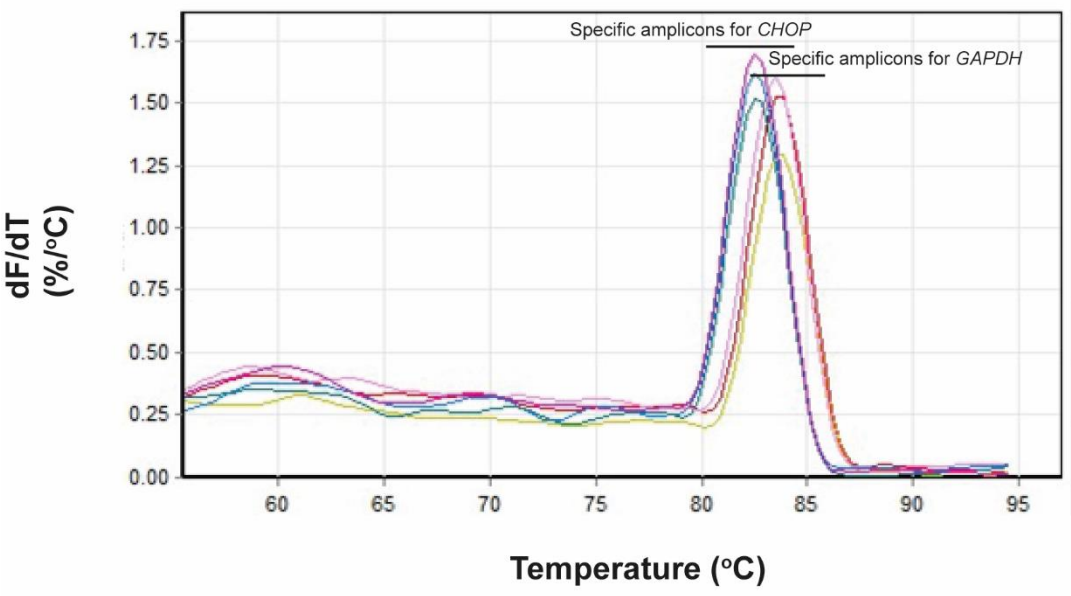

Figure 2.12 Example melt curves for from RT-qPCR. The single peak is observed for an amplicon from *GAPDH* (red, yellow and pink) or from *CHOP* (blue, green and purple), which typically interpreted as a pure, single amplicon.

Agarose gel electrophoresis

PCR products were visualized by agarose gel electrophoresis. The gel (0.8%) was prepared by dissolving agarose powder into 50 mL of 1x TAE buffer and heated until the agarose was dissolved completely. The solution was cooled to ~50°C then 3 µL of SYBR Safe DNA Stain was added before pouring the gel into the gel tray to allow it to set.

The gel tray was fitted into the electrophoresis chamber (Biorad) and submerged in 1x TAE buffer. qPCR products (20 µL) were mixed with 1 µL of 6x TriTrack loading dye (Thermo Fisher, USA) before loading into wells alongside 5 µL of DNA ladder (Sigma-Aldrich). Electrophoresis was carried out at 120 V for 1 hr or until DNA separation was achieved. The product size was determined through visualization of bands under UV light using UV transillumination advanced imaging system (Alpha Innotech Fluorchem HD2). In fact, follow-up analysis by gel electrophoresis revealed that both of these curves (Figure 2.12) generate a single amplicon, verifying a single qPCR product.

Data analysis

The threshold was adjusted accordingly in the exponential phase of amplification, between the initial linear phase of amplification and the plateau in order to minimise background fluorescence (see Figure 2.10). After setting the threshold, the C*t* values were determined and collected using the Rotor-gene Q software (Corbett Research, Australia). Ct values were used to calculate the relative changes of gene expression using the comparative C*t* method. Gene expression values were normalised to the house-keeping gene GAPDH. An example of the calculations required to assess the relative changes of gene expression are shown in Table 3, **Appendix I**.

2.2.12 Measurement of protein levels by Western blot

Principle

Western blot was performed to detect and characterise specific proteins. It is based on the principle of immunochromatography, as proteins are separated into polyacrylamide gel according to their molecular weight. The proteins are then transferred onto nitrocellulose membrane and are detected following incubation with a specific primary and secondary enzyme

(HRP) – labelled antibody. Here, we investigate the expression of the proteins CHOP, GRP78, key ER stress markers in order to confirm the results obtained by ELISA (see 2.2.10). To confirm apoptosis (see 2.2.6), we measured the expression of cleaved caspase-3, an executioner of apoptotic cell death. We also assess the protein expression of PDX-1. GAPDH was used as a loading control.

Protocol

Lysate preparation

Following cell growth and treatment protocol, INS-1E cells were washed twice with cold PBS (10 mL) and scrapped in 10 mL of ice-cold PBS before being transferred to labelled centrifuge tubes placed on ice. The cells were then centrifuged into a pellet for 5 mins at 300 x g. Then, cells were lysed by resuspending the pellet in 200 µL of radioimmunoprecipitation assay (RIPA) buffer with a cocktail of protease and phosphatase inhibitors (0.1%). The samples were then kept on ice for 30 mins prior centrifugation at 20,000 x g for 30 mins at 4^{o}C. The supernatants were then collected and stored at -80^{o}C. To prepare the samples for protein electrophoresis, protein lysates were thawed on ice and a 1:1 protein lysate and 2x Laemmli buffer supplemented with 2-mercaptoethanol (5%) mixture (50 µL the lysate and 50 µL of 2x Laemmli buffer with 2-mercaptoethanol) was prepared in labelled Eppendorfs for each sample. Then, the protein lysates in Laemmli buffer were heated on a heat block. This procedure would allow the denaturation of proteins, facilitating protein electrophoresis strictly by molecular weight. The temperature for denaturation of proteins was determined empirically. A standard 95^{o}C for 5 mins was initially performed, however, CHOP protein was not detected unless the proteins were heated at 70^{o}C for 10 mins. Therefore, protein lysates in Laemmli were heated for 70^{o}C for CHOP expression and 95^{o}C for 5 mins for GRP78 and PDX-1 expression to completely denature the proteins. GAPDH was visible with both conditions.

Protein electrophoresis

Proteins were separated onto polyacrylamide gel by sodium dodecyl sulphate (SDS)-polyacrylamide gel electrophoresis (PAGE).

To do so, a 5% polyacrylamide gel and 10% or 12.5% polyacrylamide gel have been prepared by adding the components in Table 2.7, in descending order. The gel percentage choice depended on the size of protein of interests, with increasing gel percentage for smaller protein sizes. For CHOP (~30 kDa), GRP78 (~72 kDa) and PDX-1 (~38 kDa), a 10% polyacrylamide

gel was used (Table 2.7). For cleaved caspase-3 (~19 kDa) a 12.5% polyacrylamide gel was deemed as appropriate. GAPDH (~37 kDa) was detected in both gel percentages.

Table 2.7 Recipe for 12.5%, 10% and 5% polyacrylamide gels for Western blot. The components were added in descending order. APS, ammonium persulfate; SDS, sodium dodecyl sulfate; TEMED, tetramethylethylenediamine. n.b. 10% w/v SDS was made by adding SDS (MW = 288.38 g/mol) to 1 mL of distilled H_2O. 10% w/v APS was made by adding APS (MW = 228.18 g/mol) to 1 mL of distilled H_2O.

	Polyacrylamide gel (12.5%) (12-70 kDa)	Polyacrylamide gel (10%) (15-100 kDa)	Polyacrylamide gel (5%)
Distilled H_2O	5 mL	4.3 mL	2.8 mL
1.5M Tris	4 mL	2.5 mL	--------
0.5M Tris	-------	--------	1.3
10% w/v SDS	160 µL	100 µL	50 µL
10% w/v APS	160 µL	100 µL	50 µL
TEMED	16 µL	14 µL	7 µL
Acrylamide 30% v/v	6.7 mL	3.3 mL	830 µL

After preparing the 10% or 12.5% polyacrylamide gel, the gel was poured in a gel cassette, leaving space for the 5% polyacrylamide. The 5% polyacrylamide gel was then poured on top of the 10% or 12.5% polyacrylamide gel after it has polymerised. Immediately after pouring the 5% polyacrylamide gel, a gel comb (10- or 15-well gel comb depending on the amount of protein to be loaded) was embedded in the 5% polyacrylamide, on top of the gel cassette. After allowing the 5% polyacrylamide gel to polymerise, the comb was gently removed in order to obtain wells for sample loading.

For each protein of interest, the amount of protein to be loaded was empirically determined by loading different amounts of protein. For instance, to measure PDX-1 protein levels, several concentrations of proteins were tested (10, 20 and 40 µg) to determine the most appropriate concentration of protein to detect PDX-1. The same procedure was done with CHOP and GRP78, showing that an amount of 100 µg of protein was necessary to acquire visible intensity signalling bands by Western blot. Similarly, concentrations of primary and secondary antibodies were empirically determined by starting with the suggested manufacturer's concentration and either increasing or decreasing the concentration depending on the results obtained.

The proteins, quantified using the Bradford assay as described previously, were equally loaded (40 µg for PDX-1 expression and 100 µg for CHOP, cleaved caspase-3 and GRP78 expression) into the wells of 5% polyacrylamide gel. Page Ruler™ Plus molecular weight ladder (5 µL)

(Thermo Fisher, USA) was added to the first well to ensure the identification of proteins. The denatured proteins alongside the molecular weight ladder were separated by SDS-PAGE for approximately 1 hr at 100 V at room temperature (25^{o}C).

Membrane transfer

In this step, the separated proteins were transferred out of the gel and onto a nitrocellulose membrane. The nitrocellulose membrane is popular for its high protein-binding affinity, its ability to immobilise proteins and its compatibility with a variety of detection methods including chemiluminescence. The wet transfer method was adopted and prepared according to Figure 2.13. The 5% polyacrylamide was gently cut off the rest of the gel and the remaining gel with the proteins was submerged in transfer buffer for 10 mins before assembling the wet transfer sandwich (Figure 2.13). The nitrocellulose membrane, filter papers and sponges were also submerged in transfer buffer to ensure a wet transfer. Following the assembly of the wet transfer sandwich, the gel holder cassette was placed in the buffer tank filled with transfer buffer and the proteins were left to transfer for 75 mins at 100 V at room temperature.

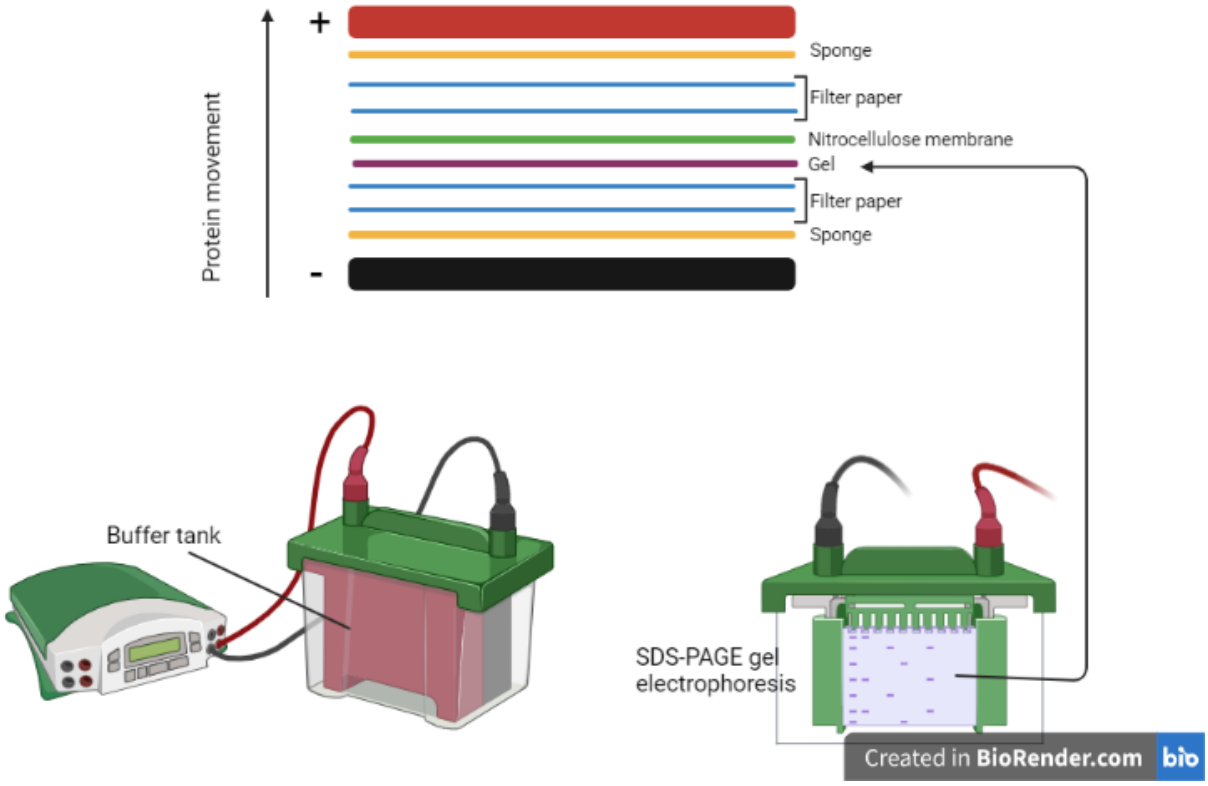

Figure 2.13 Wet transfer sandwich**.** 1) The gel was removed from its cassette and the top portion containing the wells was cut off; 2) The gel, nitrocellulose membrane, filter papers and sponges were equilibrated in transfer buffer; 3) The transfer sandwich was then placed in a gel holder cassette with the order illustrated above. Figure created with BioRender.com.

Fixation (additional step)

After several attempts, it was found that CHOP was not easily detected. Therefore, for CHOP detection, an additional step of fixation of proteins to the nitrocellulose membrane with 0.5% glutaraldehyde v/v in PBS for 5 mins was performed as previously described (Turpin *et al.*, 2020).

Immunoblotting

After the wet transfer of proteins onto the nitrocellulose membrane (or fixation in the case of CHOP protein), the nitrocellulose membrane containing the proteins was blocked with Tris-buffered saline (TBS) containing 0.05% v/v Tween 20 (TBS-T) and 5% non-fat dried milk for 1 hr at room temperature. Then, the protein was immunoblotted with the antibody of interest (dilution in 5% non-fat dried milk in 0.05% TBS-T), the rabbit polyclonal anti-PDX1 IgG antibody (1:1000), the mouse monoclonal anti-CHOP IgG_1 κ antibody (1:200 for efavirenz treatments and 1:500 for rilpivirine treatments), the rabbit polyclonal anti-GRP78 IgG (1:1000) or the rabbit monoclonal anti-cleaved capspase-3 (1:200) overnight at 4^{o}C. The excess primary antibody was washed off by washing the membrane three times with TBS-T for 10 min at 60 rpm and three times for 5 min at 60 rpm. After washing, the membrane was incubated with horseradish peroxidase (HRP)-conjugated goat anti-rabbit-IgG for PDX-1 (1:5000), GRP78 (1:4000) and cleaved caspase-3 (1:500) expression or the HRP-conjugated mouse IgGκ antibody (1:500 for efavirenz treatments and 1:1000 for rilpivirine treatments) for CHOP expression for 1 hr at room temperature. Table 2.8 and 2.9 detail the primary and secondary antibodies used in this study.

Table 2.8 List of primary antibodies used in this study

Primary antibody	**Company**	**Catalogue number**	**RRID**	**Species**
Monoclonal anti-CHOP IgG_1 κ	Santa Cruz Biotechnology	sc-7351	AB_627411	Mouse
Polyclonal anti-GRP78 IgG	Abcam	3216-1	AB_2279866	Rabbit
Polyclonal anti-PDX-1 IgG	Thermo Fisher Scientific	PA5-78024	AB_2736337	Rabbit
polyclonal anti-GAPDH IgG antibody	Santa Cruz Biotechnology	sc-25778	AB_10167668	Rabbit

Polyclonal anti-cleaved caspase 3	Cell Signaling Technology	9661	AB_2341188	Rabbit

Table 2.9 List of secondary antibodies used in this study

Secondary antibody	Company	Catalogue number	RRID
HRP-conjugated mouse IgGκ antibody	Santa Cruz Biotechnology	sc-516102	AB_2687626
HRP -conjugated goat anti-rabbit IgG	Santa Cruz Biotechnology	sc-2004	AB_631746

However, despite optimising all the considerations for protein detection (Figure 2.14), we failed to detect the protein expression of cleaved caspase-3. We opted for a 4-20% gradient gel, while increasing the amount of protein to 100 µg and the concentration of primary and secondary antibodies. We also attempted to fix the proteins with glutaraldehyde and use a PVDF membrane instead. We tested several transfer times (20, 30 and 45 mins) and added an extra PVDF membrane in case the protein was transferred through the first inner membrane. We attempted several times, but the expression of cleaved caspase-3 was not detected using Western blot. Therefore, we attempted to detect cleaved capase-3 by immunocytochemistry (see 2.2.13).

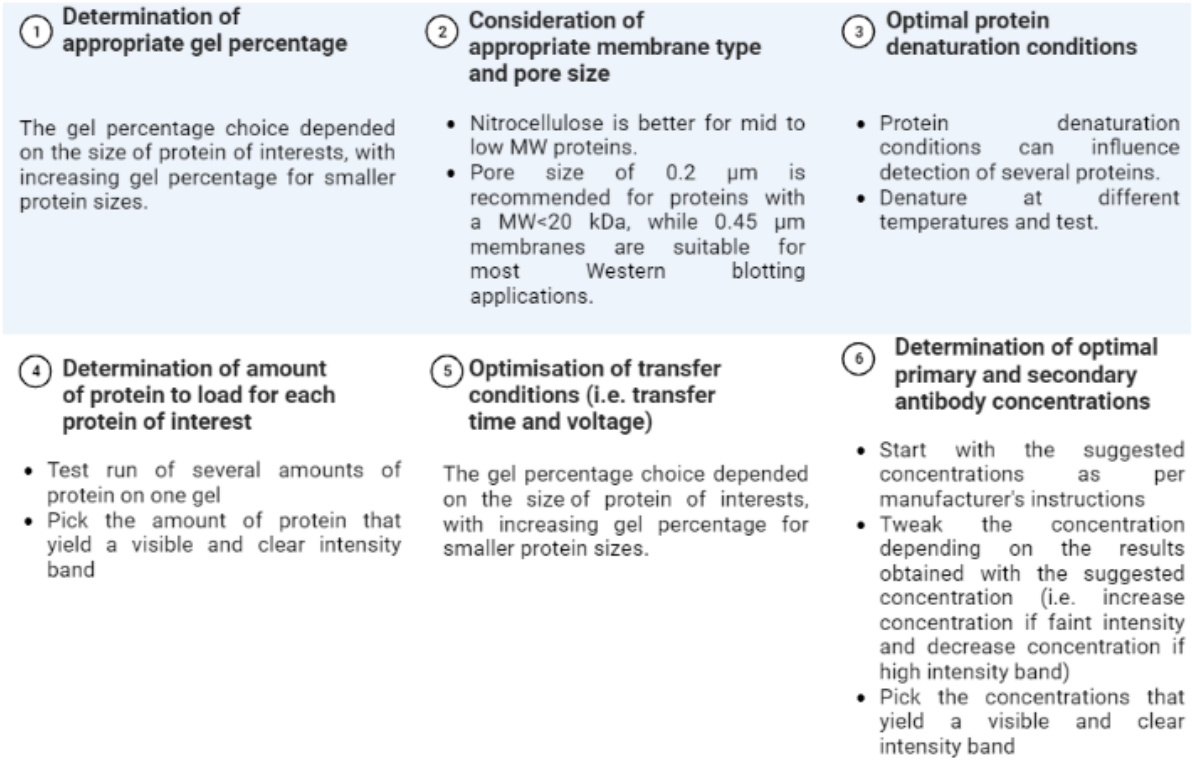

Figure 2.14 Method optimisation for Western blot analysis.

Detection

After washing, the bands were visualised with enhanced chemiluminescence (ECL) western blotting detection reagents and digital images were acquired using C-DiGit (LI-COR Biosciences, Nebraska, USA).

Stripping and reprobing

Following ECL detection, blots were then stripped and reprobed with the house-keeping protein, GAPDH. After stripping the blot twice with stripping buffer for 10 mins on a plate shaker (80 rpm), the blot was washed twice with PBS for 10 mins. Then, the stripped blot was washed twice with 0.1% TBS-T for 5 mins. The blot was then blocked with 5% non-fat milk in 0.1% TBS-T for 1 hr. Following blocking, the blot was incubated with rabbit polyclonal anti-GAPDH IgG antibody (1:1000) for 1 hr at room temperature. Then, the blots were washed 0.1% TBS-T for 45 mins with 10-minute intervals (three times) and 5-minute intervals (three times). Then, the blots were incubated with mouse anti-rabbit antibody (1:5000) for 1 hr at room temperature. The bands were visualised with ECL.

Data analysis

Using the Image Studio 5.0 software (LI-COR Biosciences, Nebraska, USA), the background was subtracted from the bands of interest before measuring densities of proteins of interest. Background-subtracted densities are proportional to protein levels. The results were then normalised to GAPDH protein levels.

2.2.13 Detection and localisation of proteins by immunocytochemistry

Principle

Immunocytochemistry (ICC) was performed to detect and localise specific proteins in INS-1E cells. Here, we detect and localise a key protein involved in mitochondrial function, oxidative stress and GSIS: uncoupling protein 2 (UCP2). We also attempted to detect cleaved caspase-3 by ICC, as we were not able to detect it by Western blot.

Method optimisation

The optimal experimental approaches were empirically determined in our study to ensure the protein of interest is clearly visualised and imaged by confocal microscopy. Therefore, INS-1E

cells were subject to different anti-UCP2 primary antibody and anti-mouse secondary antibody concentrations (Figure 2.15) and different cell culture conditions as detail in Table 2.10.

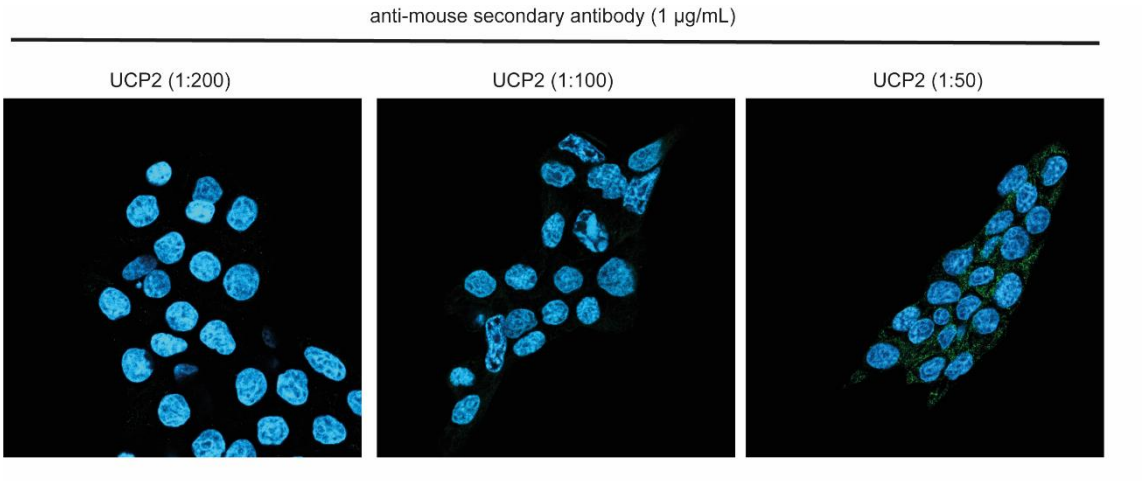

Figure 2.15 Method optimisation for immunocytochemical analysis of UCP2 in INS-1E cells. INS-1E cells were exposed to palmitate 500 µM for 24 hrs before measuring UCP2 protein levels by immunocytochemical analysis. The green fluorescence represents UCP2 protein while blue fluorescence represents DAPI positive nuclei.

After method optimisation as summarised in Table 2.6, the optimal experimental approaches were chosen to ensure the protein of interest is clearly visualised and imaged by confocal microscopy.

Table 2.10 Summary of experimental considerations for ICC method optimisation in INS-1E cells

Experimental consideration	Options considered	Outcome
INS-1E cell seeding density	Seeding density ($0.5x10^5$, $1x10^5$ and $2.5x10^5$ cells/well)	$0.5x10^5$ cells/well used as final seeding density. There were too many cells with higher seeding densities.
Cell culture incubation time	24, 48 or 72 hours	72 hours incubation prior treatment
UCP2 – Unconjugated primary antibody	Concentration (1:50, 1:100, 1:200)	1:50 used as final concentration for UCP2 localisation. UCP2 was not visualised with lower concentrations.
Secondary antibody (anti-mouse)	Concentration (1 µg/mL or 2 µg/mL)	1 µg/mL used as final concentration for localising UCP2 as UCP2 was visualised.

Due to limited amounts of anti-cleaved caspase-3 antibody and to time constraints, we could only run two experiments. Therefore, we were not able to conduct method optimisation for detecting cleaved caspase-3. Hence, we used the suggested anti-cleaved caspase-3 antibody concentration (1:400) and of anti-rabbit antibody (1:500).

Protocol

INS-1E cells were seeded at a seeding density of $0.5x10^5$ cells/well in a 6-well plate and incubated for 72 hrs at 37°C and 5% CO_2. Then, the cells were exposed to efavirenz (20 µM) or rilpivirine (10 µM) for 24 hrs at 37°C and 5% CO_2. Following treatment protocol, the cells were washed twice with PBS and then fixed with 3.7% formaldehyde for 10 mins at room temperature. Then, the cells were washed with 3% BSA in PBS prior permeabilisation with 0.5% Triton® X-100 in PBS for 20 mins at room temperature. The cells were then washed twice with 3% BSA in PBS followed by blocking with 1% BSA and 0.1% Triton® X-100 in PBS for 1 hr at 2-8°C.

Following blocking, the cells on coverslips were transferred into a humid chamber before incubating the cells with monoclonal mouse anti-UCP2 antibody (1:50) (Cat#: sc-390189; Santa Cruz Biotechnology, USA; RRID: AB 2721285) or anti-cleaved caspase-3 (1:400) (Cat#: 9661; Cell Signaling Technology, USA; RRID: AB_2341188) diluted in 1% BSA and 0.1% Triton® X-100 in PBS overnight at 2-8 °C.

After incubation with the primary antibody, the cells were washed 10 times with 3% FBS in PBS. Then, the cells were incubated with goat anti-mouse IgG Alexa Fluor™ 488 (1 µg/mL) (Thermo Fisher Scientific; Cat# A32723, RRID: AB_2633275) for UCP2 detection or with goat anti-rabbit Alexa Fluor™ 488 (1:500) (Thermo Fisher Scientific; Cat#: A-11008; RRID: AB_143165) for cleaved caspase-3 detection for 2 hrs at room temperature. Following incubation with the secondary antibody, the cells were washed 10 times with 3% FBS in PBS and ultimately once with PBS. Then, a coverslip with a drop of mounting medium with DAPI in order to localise the nucleus for localisation and counting purposes. The coverslip was then mounted onto the coverslip with cells facing down on the mounting medium. The cells were then incubated for 15 mins prior analysis with confocal microscopy.

Data analysis

UCP2 expression was measured using ImageJ, a Java-based image processing program (Schneider *et al*., 2012). Mean fluorescence intensity (MFI) of UCP2-labelled cells was measured using ImageJ. Cell numbers were determined by counting the number of DAPI positive cells. MFI was normalised to number of cells per image. A secondary antibody control was performed for each sample by eliminating the primary antibody to ensure that the labelling observed is due to binding of the secondary antibody to the primary antibody. A labelling control (no incubation with primary and secondary antibodies) was also performed for each sample to identify the contribution of endogenous fluorescence, if present.

2.2.14 Chemical structures and *in silico* docking

Chemical structures were plotted using Jmol, an open-source Java viewer for chemical structures in 3D. Unguided docking of efavirenz or rilpivirine to predict binding sites was performed using SwissDock with CHARMM forcefield (Grosdidier et al., 2011). The proteins structures used are explained in more detail in **Chapter 4** and **Chapter 5**. The SwissDock predictions file provided Cluster Rank, Full Fitness scores and estimated Gibbs free energy ΔG. ΔG and the full fitness scores were used to identify favourable poses. A more negative ΔG score signifies a stronger binding affinity of the ligand to the target protein. Sample SwissDock predictions file data for the ligand efavirenz to the ND5 subunit of complex I, is shown in Figure 1, **Appendix I**. A cluster is a predicted binding pocket on the target protein, and the cluster rank represents the different conformations of the ligand in a certain cluster.

2.2.15 Statistical analysis

Data are expressed as the mean ± mean standard deviation (SEM) or standard deviation (SD). The level of statistical significance was set at $p < 0.05$ and was assessed by one-way or two-way ANOVA followed by Bonferroni test or a Student's t-test for parametric analysis. Post hoc tests were only performed if F in ANOVA achieved $p < 0.05$. In case of non-parametric analysis, a Kruskal-Wallis test followed by Dunn's multiple comparison or Friedman's test was performed (Armstrong & Hilton, 2010; Curtis *et al.*, 2018; Daniel & Cross, 2019). We used "fold matched control" and "% of control" to normalise the data obtained in order to avoid unwanted sources and for comparison purposes. All experiments were carried out at least two times, with *n* = number of independent values. In some instances, technical replicates were used

to ensure the reliability of single values. The average of technical replicates per treatment was calculated to obtain an independent value. Statistical analysis was only performed if $n \geq 3$ independent values. Statistical analysis was performed using the Statistical Package for Social Sciences software (SPSS; IBM Corp., New York, USA). Graphs were drawn on GraphPad Prism (GraphPad Software, San Diego, USA).

3. Effects of NNRTIs on beta cell function and survival

3.1 Introduction

Advances in modern medicine have transformed HIV from a terminal disease into a chronic but manageable condition through the development of antiretroviral therapy (ART). Undoubtedly, many clinical trials and clinical care settings have shown that ART, when adhered to, profoundly improved clinical outcomes in HIV patients by reducing HIV progression into AIDS and AIDS-related death rates (Kitahata *et al.*, 2009; Mannheimer *et al.*, 2006; Mocroft *et al.*, 1998). Zidovudine, the first antiretroviral drug licensed in 1987, paved the way to triple combination ART, also known as combination antiretroviral therapy (cART) or simply ART. Inhibition of the HIV reverse transcriptase is highly effective in impairing HIV viral replication, prompting guidelines surrounding standardised regimens for HIV treatment and prophylaxis to include the first line use of reverse transcriptase inhibitors. Reverse transcriptase inhibitors are divided into two classes: the nucleoside/tide reverse transcriptase inhibitors (NRTIs) and the non-nucleoside reverse transcriptase inhibitors (NNRTIs). The NNRTI drug selection includes the commonly used first-generation NNRTI efavirenz and the second-generation NNRTI rilpivirine, approved in hopes of ameliorating the first-generation NNRTI safety and resistance profiles.

The first-generation NNRTI efavirenz is a benzoxamine chemically described as a (S)-6-chloro-4-(cyclopropylethynyl)- 1,4-dihydro-4-(trifluoromethyl)-2H-3,1-benzoxazin-2-one, approved by the FDA in 1998 (Food and Drug Administration, 2006). Considered as an NNRTI *par excellence*, efavirenz forms part of several therapeutic combinations together with lamivudine/zidovudine, abacavir/lamivudine and tenofovir disoproxil fumarate (DF)/emtricitabine (Apostolova *et al.*, 2017). It can also be taken conveniently as part of a once-daily combination pill in combination with tenofovir DF and emtricitabine (Atripla®).

However, the position of efavirenz as an important component of cART regimens has been challenged by the arrival of newer NNRTIs with a higher genetic barrier to resistance development, better tolerability (thus a better patient adherence), yet a similar efficacy in the treatment of HIV-1 infection (Apostolova *et al.*, 2017; Usach *et al.*, 2013). Newer NNRTIs such as the second-generation NNRTI rilpivirine, a diarylpyrimidine compound, were designed with conformational flexibility and positional ability which confers the ability to circumvent resistance mechanisms by altering their shape and position to bind to the NNRTI hydrophobic

pocket of an array of drug resistant reverse transcriptase mutants (Bekker *et al.*, 2020; Yang *et al.*, 2018). Further, rilpivirine shows potent antiviral activity against wild-type HIV-1 strains and several HIV-1 variants harbouring significant resistance mutations to first-generation NNRTIs (Janssen *et al.*, 2005). Following its approval by the FDA in 2011, rilpivirine has been used in three-drug regimens as single-tablet (*i.e.*, Eviplera) or as multiple-tablet regimens, or in the most recent option of two-drug regimens, to treat HIV-1 infection (Cento & Perno, 2020; Sharma & Saravolatz, 2012). More recently, long-acting injectable cART comprising of rilpivirine and an integrase inhibitor cabotegravir, are being trialled and seem to bring promise, so far, of a new mode of delivery in the treatment of HIV-1 (Fernandez & van Halsema, 2019). Long-acting injectable rilpivirine is also a promising candidate for pre-exposure prophylaxis (PreP) in people at risk of contracting HIV-1 infection (McGowan *et al.*, 2016; Ripamonti *et al.*, 2014). In 2011, the ECHO and THRIVE randomised and double-blinded study of 1,368 HIV-1-positive patients, compared the safety profiles of efavirenz and rilpivirine, both in combination with tenofovir DF and emtricitabine. This study concluded that rilpivirine, had fewer neurological and psychiatric adverse events and lower increases in total cholesterol and triglycerides in comparison to efavirenz. Therefore, rilpivirine has a better overall safety and resistance profiles compared to efavirenz. However, some NNRTI resistance-associated mutations can still cause a profound decrease in susceptibility to rilpivirine (Azijn *et al.*, 2010). Therefore, it is crucial to continue to develop newer NNRTIs with improved drug-resistance profiles.

Doravirine, the most recent NNRTI approved in 2018, is a valuable addition that provides much needed variety to the NNRTI class, as it has been associated with less frequent side effects in comparison to older NNRTIs while preserving activity in the presence of common NNRTI resistance mutations (Rock *et al.*, 2020). Doravirine was rationally designed to address limitations regarding common NNRTI resistance-associated mutations in the HIV reverse transcriptase (Martin *et al.*, 2020). Indeed, doravirine had improved potency compared to efavirenz and rilpivirine against viral reverse transcriptase and rilpivirine-specific mutants (Feng *et al.*, 2016). Taken together, these findings suggest that doravirine confers a potentially higher barrier to the development of resistance than both efavirenz and rilpivirine. Furthermore, according to the 96-week DRIVE-AHEAD study, the novel NNRTI doravirine demonstrated non-inferior efficacy and favourable side effects profiles in comparison to efavirenz, as doravirine did not increase LDL-cholesterol and non-HDL-cholesterol as opposed to efavirenz (Orkin *et al.*, 2018).

The 2D and 3D chemical structures of the NNRTIs efavirenz, rilpivirine and doravirine are visualised in Figure 3.1.

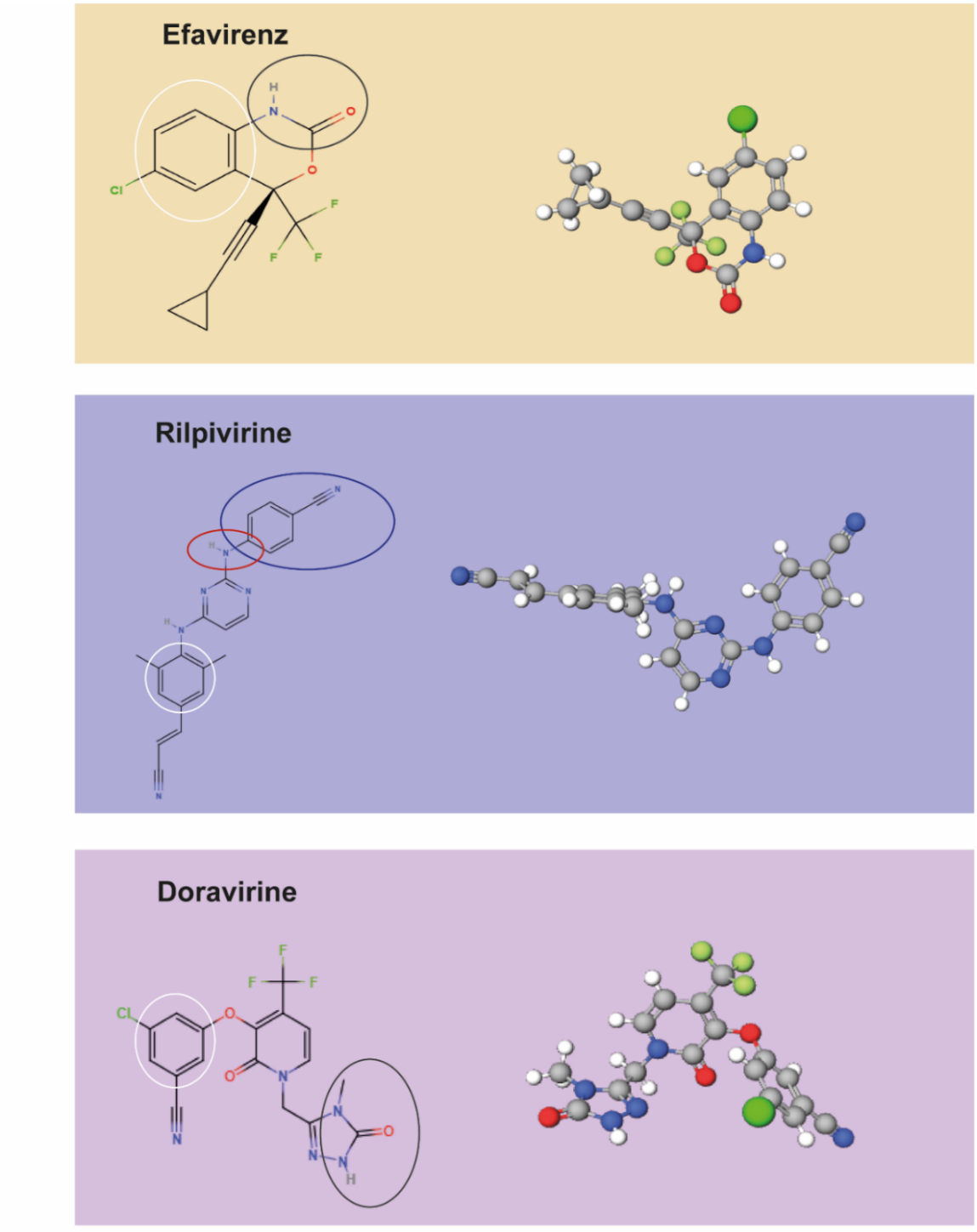

Figure 3.1 2D and 3D chemical structures of the NNRTIs efavirenz, rilpivirine and doravirine visualised by Molview. NNRTIs display a common pharmacophoric model which contain an aromatic ring (white) capable of participating in the π-π stacking interactions, amides or thioamides (black) that can form hydrogen bonds and a conformation that helps the drug to maintain its activity against a range of resistant strains of HIV-1. Rilpivirine has increased activity against HIV-1 strains due to its cyanovinyl moiety (blue). The cyano group potentially interacts with the NNRTI hydrophobic pocket of the HIV reverse transcriptase. Further, a flexible angle between the aniline ring (red) and the cyanovinyl moiety (blue) confers formational flexibility (Janssen et al., 2005; Das *et al*., 2008; Dobson and Luque, 2013).

Despite the undeniable benefits of ART, long-term ART has been implicated in increasing the risk of metabolic disturbances such as insulin resistance and type 2 diabetes (T2D) in HIV-infected patients, with reports of a 4-fold increase of T2D incidence in HIV-positive men on ART compared to HIV-seronegative men (Brown *et al.*, 2005a; Capeau *et al.*, 2012; Dubé *et al.*, 2005; Paengsai *et al.*, 2019; Wit *et al.*, 2008). As detailed in **Chapter 1**, efavirenz was shown to cause mitochondrial dysfunction and induce oxidative stress, ER stress and apoptosis in several cell types (Apostolova *et al.*, 2017). Unsurprisingly, despite the limited studies of the cellular effects of rilpivirine, this second-generation NNRTI was shown not to cause mitochondrial toxicity in neurones and hepatocytes (Blas-García *et al.*, 2014). To date, there are no studies investigating the potential toxicological effects of doravirine in cells, however, it is anticipated to have a better safety profile than rilpivirine.

Although being one of the most commonly used antiretroviral drug classes used for the treatment and prophylaxis of HIV infection, no existing study has attempted to establish the effects of NNRTIs on beta cell function and survival. Direct damaging effects on beta cell function and survival by NNRTIs may predispose PLWH who are also type 2 diabetic to impaired glycaemic control and loss of beta cell mass, hence increasing the risk of diabetic complications and insulin dependency. Therefore, the aim of this study was to investigate the direct effects of the NNRTIs efavirenz, rilpivirine and doravirine on beta cell function and survival while giving insight into potential cellular and molecular mechanism(s) underlying these effects.

3.2 Materials and Methods

3.2.1 Materials

Adult male Sprague-Dawley rats were obtained from Charles River UK Ltd Laboratories (Essex, UK). All other materials were obtained as described in Materials, **Chapter 2** (see 2.1).

3.2.2 Isolation of rat islets of Langerhans and *in vitro* insulin measurements

Although insulin-secreting INS-1E cells, derived from an X-ray-induced rat insulinoma, are deemed to be a reliable beta cell surrogate, we wanted to corroborate our results in a more physiological model by using isolated pancreatic islets, which can be considered as a real endocrine micro-organ (Misler, 2010).

Rat islets have been considered as effective models in the context of diabetes research due to the nature of islets of Langerhans. Islets of Langerhans are small clusters of approximately 1,000 endocrine cells and exocrine tissue found in the pancreas. The healthy human adult pancreas contains approximately 1 million islets, all of which contain 4 types of cells: beta cells (70% of islet mass), alpha cells (10%), polypeptide-producing cells (15%) and delta cells (5%), responsible of producing and secreting insulin, glucagon, pancreatic polypeptide and somatostatin, respectively (Arrington, 2022).

3.2.2.1 Isolation of rat islets of Langerhans

Islet isolation was performed in a manner so as to obtain purified islets that are viable and responsive to glucose stimulation in a manner that reflects their function *in vivo*. To do so, the following protocol has been implemented. Islets of Langerhans were isolated from adult male Sprague-Dawley rats by the collagenase digestion of pancreatic tissue, modification of the method described by Howell and Taylor (Howell & Taylor, 1968).

Adult male Sprague-Dawley rats (180-250 g) were euthanised by carbon dioxide (CO_2) inhalation. The rat was placed in a supine position and its abdomen was sprayed with 75% ethanol followed by dissection of the abdomen to half of the chest cavity. The first loop of the duodenum and the entry of the common bile duct into the lumen was located. A clamp was applied to the duodenum to occlude the common bile duct, but care was taken not to place the clamp on the pancreas. A small incision was made on the surface of the duct (care being taken

not to cut through the duct) near the hepatic end, before carefully inserting a cannula linked to a hypodermic syringe into the opening and held in place using forceps. The hypodermic syringe containing 10 mL of a collagenase (type XI) solution (7 mg/10 mL) was used to slowly inject the collagenase into the common bile duct as to distend the pancreas. By this method, greater accessibility of the collagenase to the acinar tissue was achieved. The inflated pancreas was then excised and transferred into 10 mL of sterile Gey and Gey buffer supplemented with 0.1% fatty acid-free BSA in a Sterilin tube and incubated for 10 mins at 37°C without shaking for digestion. The digestion process ensures digesting the tissues connecting the islets to the exocrine tissue. Following this period, 15-20 mL of Gey and Gey buffer supplemented with 0.1% fatty acid-free BSA was added to the Sterilin tube. Then, the tubes were shaken vigorously for 10 sec by hand to break up the tissue. The collagenase digestion was stopped by placing the disrupted pancreas on ice. The pancreas was then washed three times before the islets were handpicked giving a yield of 150-200 islets per pancreas. Figure 3.2 summarises the islet isolation process.

3.2.2.2 Conditions for islet culture

The isolation and culture of islets was performed in a laminar flow hood and aseptic techniques were used throughout the isolation procedure. Culture was performed as to maintain the viability and function of islets ahead of treatment protocol.

When isolated islets were destined for tissue culture, all glassware and equipment used was autoclaved and non-autoclavable materials were soaked in 75% ethanol. All plastic ware was of tissue culture grade. Buffers and culture medium used in the isolation of islets were filter-sterilised and contained penicillin (50 U/mL) and streptomycin (50 µg/mL). Islets were plated in 100 mm x 20 mm suspension culture dishes with 4 mL of RPMI-1640 supplemented with 10% (v/v) heat-inactivated FCS to promote viability and 1% (v/v) penicillin-streptomycin to reduce contamination. Islets were cultured for 24 hrs in a humidified atmosphere of 95% air and 5% CO_2 at 37°C (Figure 3.2).

3.2.2.3 Treatment protocol

Working solutions of different concentrations (1, 3, 10 or 20 µM) of efavirenz and rilpivirine were freshly prepared by diluting the stock solution (25 mM) in RPMI-1640 media supplemented with 3% heat-inactivated FCS and 5.5 mL of 5,000 U/mL (1%) penicillin-streptomycin as detailed in Table 2 (Appendix I), under aseptic conditions in a class II laminar

flow cabinet. Groups of 30 rat islets were transferred in sterile petri dishes containing 5 mL of efavirenz or rilpivirine working solutions. Vehicle (DMSO)-treated rat islets served as controls. Following treatment, rat islets were incubated at 37°C in a humidified atmosphere of 95% air and 5% CO_2 for 24 hrs (Figure 3.2).

3.2.2.4 Insulin release measurements from rat islets of Langerhans

Following treatment protocol, basal insulin release and glucose-stimulated insulin secretion (GSIS) was assessed. After careful complete removal of RPMI-1640 media, 2 mM glucose in Gey and Gey buffer supplemented with 0.1% fatty acid-free BSA (4 mL) was added to the petri dish containing the rat islets for glucose priming for 1 hr at 37^{o}C, 5% CO_2. Then, 0.6 mL of a 2 mM glucose in Gey and Gey buffer supplemented with 0.1% fatty acid-free BSA was added to 3 wells of a 24-well plate for basal insulin release measurements. Then, 0.6 mL of 20 mM glucose in Gey and Gey buffer supplemented with 0.1% fatty acid-free BSA was added to 3 other wells for GSIS measurements. Three islets from each treatment condition were transferred in one well containing 2 mM or 20 mM glucose in Gey and Gey buffer supplemented with 0.1% fatty acid-free BSA. This was done as to obtain three technical replicates per treatment. The islets were then incubated for 1 hr at 37^{o}C. Then, 0.2 mL of the supernatant was collected and centrifuged at 150 x g for 2 mins. Then, 150 µL of the supernatant was collected and stored at -20^{o}C for quantification.

The amount on insulin was analysed using an ELISA kit, according to manufacturer's instructions (Alpco, Cat#: 80-INSRT-E01, New Hampshire, USA) (see 2.2.3.1).

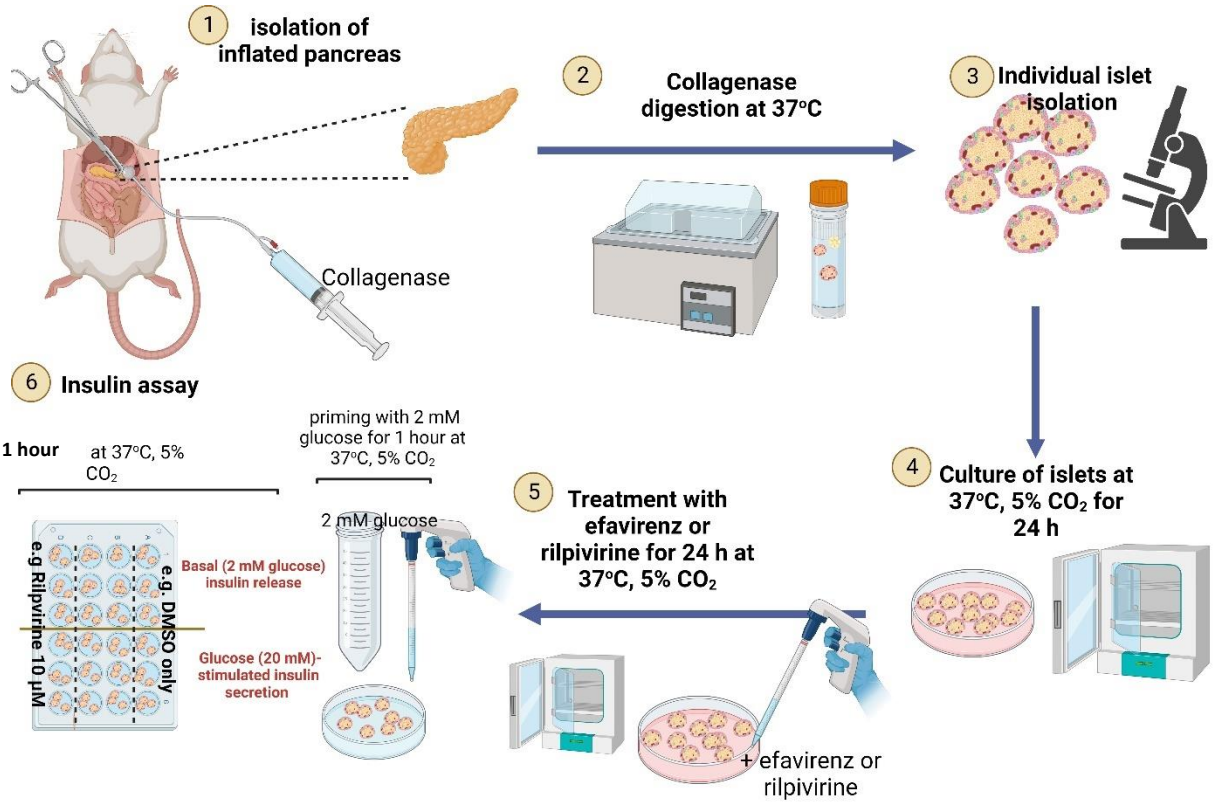

Figure 3.2 Summarised protocol for insulin release studies in isolated rat islets of Langerhans. n.b: islets are not visible to the naked eye and are hence not to scale in the illustration. Figure created with BioRender.com.

3.2.2.5 Data analysis

The average absorbance value for the zero standard was subtracted from all the absorbance values before plotting a standard curve from the standard insulin concentrations. The secreted insulin levels in the samples were determined by interpolating the zero standard subtracted absorbance values against the standard curve. The resulting value was multiplied by the appropriate sample dilution factor (1 in 20), to obtain the concentration of insulin in the sample. Data were expressed as ng mL^{-1}/islet/hour.

3.2.3 Treatment protocol of INS-1E cells

A 25 mM stock solution for each drug was prepared by dissolving each NNRTI in DMSO (Table 1, **Appendix I**). Then, solutions of different concentrations (1, 3, 10, 20 and 30 µM) of NNRTIs were prepared by diluting the stock solution in 5 mL RPMI-1640 media supplemented

with 3% heat-inactivated FCS, 50 µM 2-mercaptoethanol and 1% penicillin-streptomycin (Table 2, **Appendix I**). Controls (DMSO-treated cells) were included in each experiment.

After cell growth in respective conditions as detailed in **Chapter 2** (see 2.2.1), INS-1E cells were treated with increasing concentrations (1, 3, 10, 20 or 30 µM) of the NNRTIs efavirenz, rilpivirine or doravirine.

Following treatment, INS-1E cells were incubated at 37°C in a humidified atmosphere of 95% air and 5% CO_2 for 24 hrs (Table 2.2). After treatment protocol, insulin release (see 2.2.3), cell viability (see 2.2.5), LDH release (see 2.2.6.3), apoptosis and necrosis levels (see 2.2.6) were measured as described in **Chapter 2**. Then, potential cellular and molecular mechanisms were assessed. To do so, intracellular ROS generation (see 2.2.7.1), antioxidant capacity (see 2.2.7.3), $\Delta\psi m$ changes (see 2.2.8), glucokinase activity (see 2.2.9), mRNA (see 2.2.11) and protein expression of CHOP, GRP78 and PDX-1 (see 2.2.13) and cleaved caspase-3 (see 2.2.13) were assessed as described in **Chapter 2**.

3.3 Results

3.3.1 Effects of NNRTIs on insulin secretion from INS-1E cells and isolated rat islets of Langerhans

The primary function of pancreatic beta cells, insulin release, was evaluated in INS-1E cells and isolated rat islets of Langerhans exposed to NNRTIs for 24 hours (Figure 3.3). The first-generation NNRTI efavirenz (20 µM) reduced basal insulin release (Figure 3.3, A) and glucose (20 mM)-stimulated insulin release (GSIS) from INS-1E cells by nearly 40% and 60%, respectively (Figure 3.3, B).

Surprisingly, despite being a second-generation NNRTI, rilpivirine (3, 10 and 20 µM) also reduced both basal insulin release (Figure 3.3, A) and GSIS (Figure 3.3, B) from INS-1E cells and had a more potent inhibitory effect in reducing insulin release as the rilpivirine-mediated inhibition of basal insulin release and GSIS was more potent than efavirenz by 2-fold (Figure 3.2, A) and nearly 7-fold (Figure 3.3, B), respectively.

Strikingly, despite being within the same antiretroviral drug class, the novel NNRTI doravirine significantly doubled basal insulin release (Figure 3.3, A) and GSIS (Figure 3.3, B) from INS-1E cells.

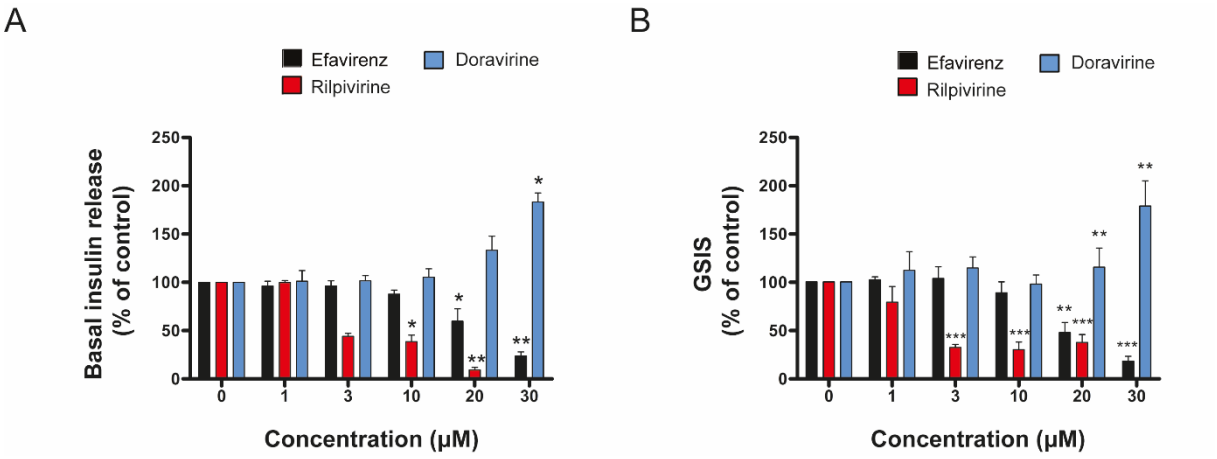

Figure 3.3 Effects of NNRTIs on insulin release from INS-1E cells. Basal (2 mM glucose) (A) and glucose (20 mM)-stimulated insulin secretion (B) was measured in INS-1E cells exposed to DMSO or increasing concentrations of efavirenz, rilpivirine or doravirine for 24 hrs. Efavirenz and rilpivirine markedly reduced basal insulin release and GSIS from INS-1E cells in comparison to vehicle control (2.86±1 ng mg^{-1} of protein for basal insulin secretion and 140.2±35 ng mg^{-1} of protein for GSIS). On the other hand, higher concentrations of doravirine significantly increased basal insulin release and GSIS from INS-1E cells. Data are expressed as mean ± SEM of *n* = 5 independent experiments with 3 technical replicates per treatment. Statistically significant differences were determined using Kruskal-Wallis with Dunn's post hoc test where $p < 0.05$ was considered as significant. * $p < 0.05$, ** $p < 0.01$, *** $p < 0.001$, significantly different from vehicle-treated control cells.

Similarly, efavirenz (20 μM) significantly reduced both basal insulin release (Figure 3.4, A) and GSIS from isolated rat islets of Langerhans by nearly 90% and 50%, respectively (Figure 3.4, B). Efavirenz (10 μM) had an inhibitory effect on GSIS from rat islets of Langerhans, however, statistical significance was not reached (Figure 3.4, B). Similarly, rilpivirine (3 and 10 μM) significantly reduced basal insulin release by nearly 90% from isolated rat islets of Langerhans (Figure 3.4, C). Rilpivirine 3 and 10 μM also reduced GSIS from isolated rat islets of Langerhans by nearly 50% and 90%, respectively (Figure 3.4, D).

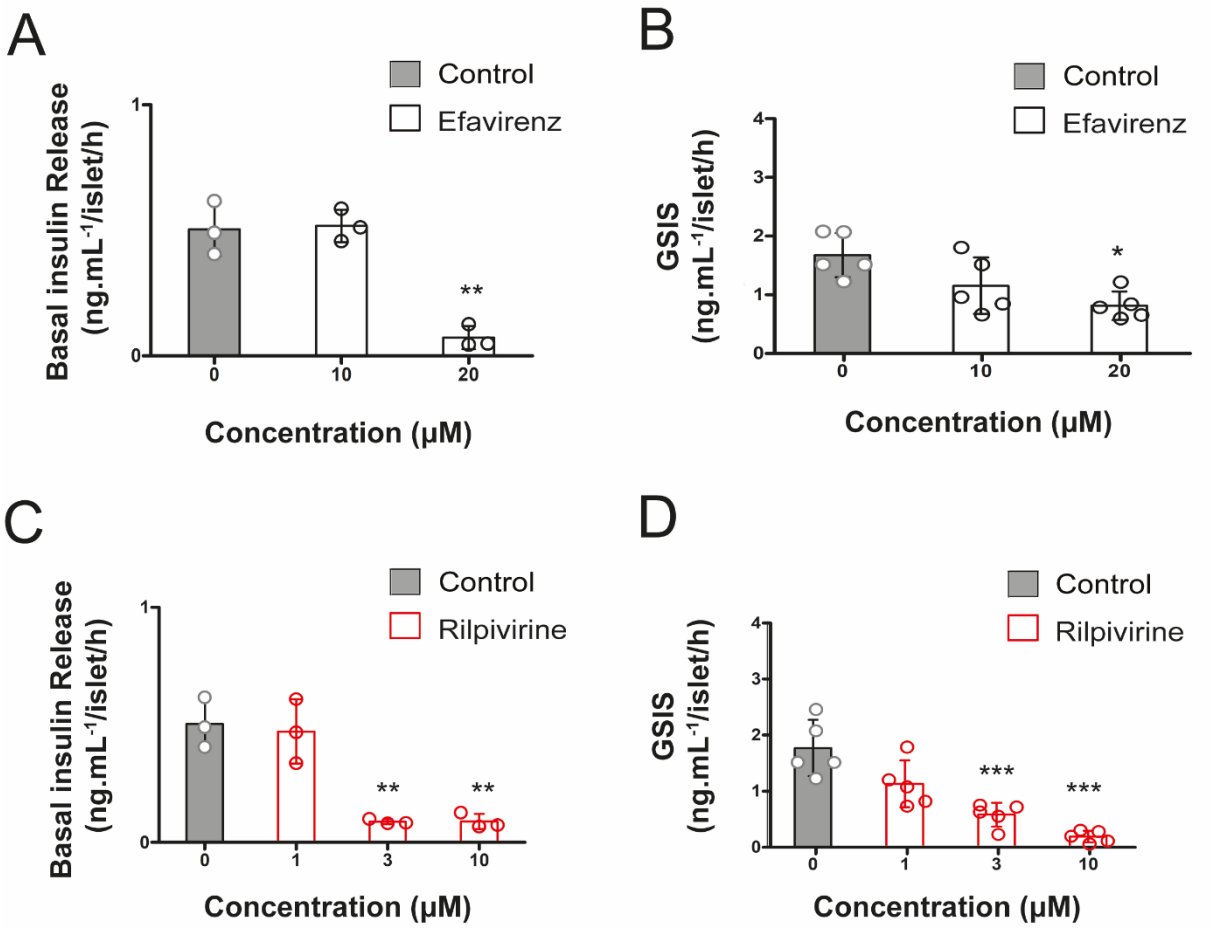

Figure 3.4 Efavirenz and rilpivirine markedly inhibit insulin release from rat islets of Langerhans. Islets were isolated from rats and exposed to DMSO or increasing concentrations of efavirenz or rilpivirine for 24 hrs before assessing basal (2 mM glucose) (A, C) and glucose (20 mM)-stimulated insulin secretion (B, D). Dots represent individual data points from n = 3 - 5 independent experiments (3 technical replicates per treatment) and the histograms represent mean ± SD. Statistically significant differences were determined using one-way ANOVA with Bonferroni post hoc test where $p < 0.05$ was considered as significant. * $p < 0.05$, ** $p < 0.01$, *** $p < 0.001$, significantly different from vehicle-treated control group.

However, both efavirenz and rilpivirine had no effect on intracellular insulin content in INS-1E cells (Table 3.1).

Table 3.1 Effects of efavirenz and rilpivirine on intracellular insulin content in INS-1E cells. Intracellular insulin content was measured in INS-1E cells exposed to DMSO or increasing concentrations of efavirenz or rilpivirine for 24 hrs. Efavirenz and rilpivirine do not affect intracellular insulin content in INS-1E cells. Data are expressed as mean ± SEM of $n = 3$ independent experiments. Statistically significant differences were determined using one-way ANOVA with Bonferroni post hoc test where $p < 0.05$ was considered as significant.

Treatment	Intracellular insulin content ± SEM (ng of insulin/mg of protein)
Control	772 ± 35
Rilpivirine 3 μM	781 ± 41
Rilpivirine 10 μM	792 ± 38
Rilpivirine 20 μM	745 ± 31
Efavirenz 20 μM	748 ± 70
Efavirenz 30 μM	808 ± 40

3.3.2 Effects of NNRTIs on INS-1E cell viability

Next, we investigated the viability of INS-1E cells to determine whether the divergent NNRTI intraclass effects seen with insulin release were also seen in the context of cell viability (Figure 3.5). Indeed, there was a dose-dependent decrease in INS-1E cell viability following a 24-hour treatment with the first-generation NNRTI efavirenz (20 and 30 μM) and second-generation NNRTI rilpivirine (10 and 20 μM) (Figure 3.5). On the other hand, the novel NNRTI doravirine had no effect on INS-1E viability (Figure 3.5).

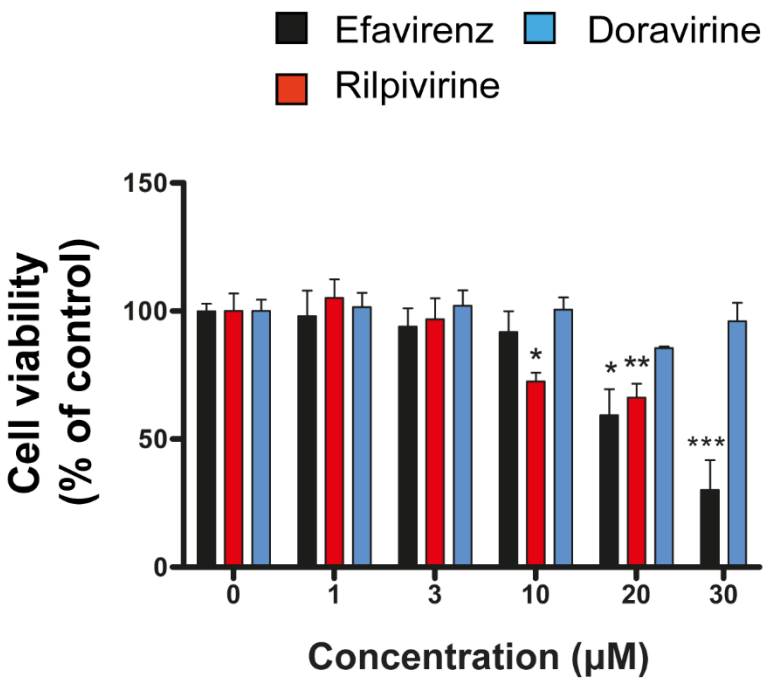

Figure 3.5 Effects of NNRTIs on INS-1E cell viability. INS-1E cell viability was measured following a 24-hour exposure to DMSO or increasing concentrations of efavirenz, rilpivirine or doravirine using an MTT assay. Efavirenz and rilpivirine reduced INS-1E cell viability, while doravirine had no effect on INS-1E cells viability. Data are expressed as mean ± SEM of *n* = 5 independent experiments with 6 technical replicates per treatment. Statistically significant differences were determined using one-way ANOVA with Bonferroni post hoc test where $p < 0.05$ was considered significant. * $p < 0.05$, ** $p < 0.01$, *** $p < 0.001$, significantly different from vehicle-treated control cells.

3.3.3 Effects of NNRTIs on INS-1E cell death

We next sought to determine pancreatic beta cell survival by measuring the levels of apoptosis and necrosis in INS-1E cells exposed to NNRTIs. Measurements of cytosolic histone complexes were used to primarily assess apoptosis (Figure 3.6) while levels of early apoptotic and late necrotic INS-1E cells were confirmed by flow cytometry (Figure 3.7). To further assess the presence of necrotic cell death, we measured release of LDH (Figure 3.8).

3.3.3.1 Apoptosis measurements by cytosolic histone complexes

The histone-complexed DNA fragments in INS-1E cells were assayed using a commercially available ELISA kit (Figure 3.6). Both efavirenz (30 μM) and rilpivirine (10 and 20 μM) induced apoptosis in INS-1E cells (Figure 3.6). However, doravirine had no effect on apoptosis in INS-1E cells (Figure 3.6).

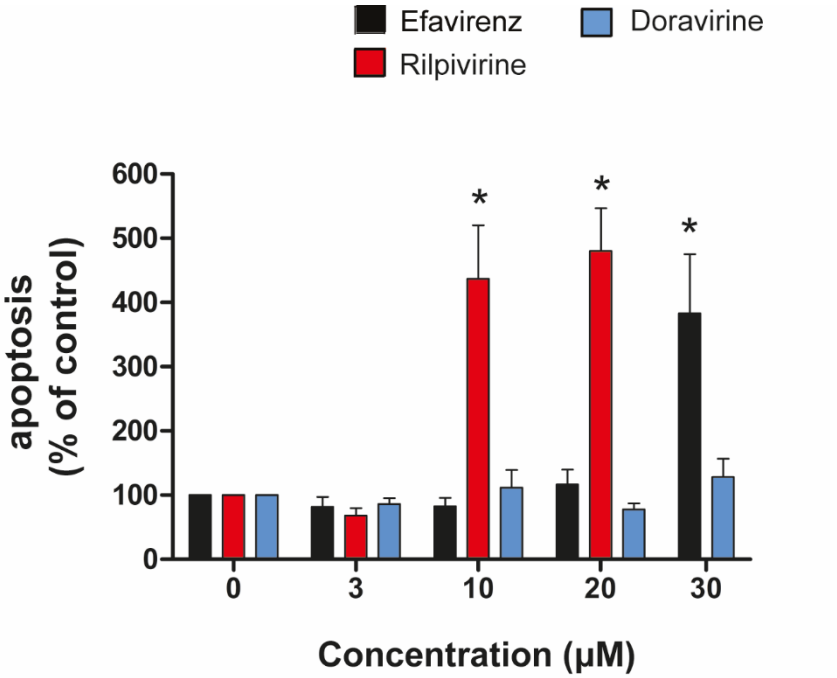

Figure 3.6 Effects of NNRTIs on apoptosis in INS-1E cells. INS-1E cells were exposed to DMSO or increasing concentrations of efavirenz or rilpivirine for 24 hrs before assessing apoptosis via the relative quantification of cytoplasmic histone-complexed DNA fragments. Efavirenz and rilpivirine increased apoptosis in INS-1E cells, while doravirine had no effect on apoptosis. Data are expressed as mean ± SEM from n = 3 independent experiments with 3 technical replicates per treatment. Statistically significant differences were determined using Kruskal-Wallis with Dunn's post hoc test where $p < 0.05$ was considered significant. * $p < 0.05$, significantly different from vehicle-treated control cells.

3.3.3.2 Flow cytometric analysis following Annexin V-FITC and Propidium Iodide staining

We next sought to confirm the results obtained with the cytosolic histone complex measurements (Figure 3.6) by analysing apoptotic and necrotic levels by flow cytometry following Annexin V-FITC and propidium iodide (PI) staining (Figure 3.7).

Efavirenz and rilpivirine, but not doravirine, induced INS-1E cell apoptosis (Figure 3.7). A 24-hour exposure to efavirenz (20 and 30 µM) or rilpivirine (3, 10 and 20 µM) significantly increased early apoptotic cell levels in a dose-dependent manner in INS-1E cells (Figure 3.7, B). The representative plots show an increase in the number of INS-1E cells in the early apoptotic quadrant (Annexin V+/PI-) compared to the control, indicating the induction of early apoptosis in INS-1E cells treated with efavirenz or rilpivirine (Figure 3.7, A).

Efavirenz, rilpivirine and doravirine had no effect on late apoptosis/primary necrosis in INS-1E cells (Figure 3.7, C).

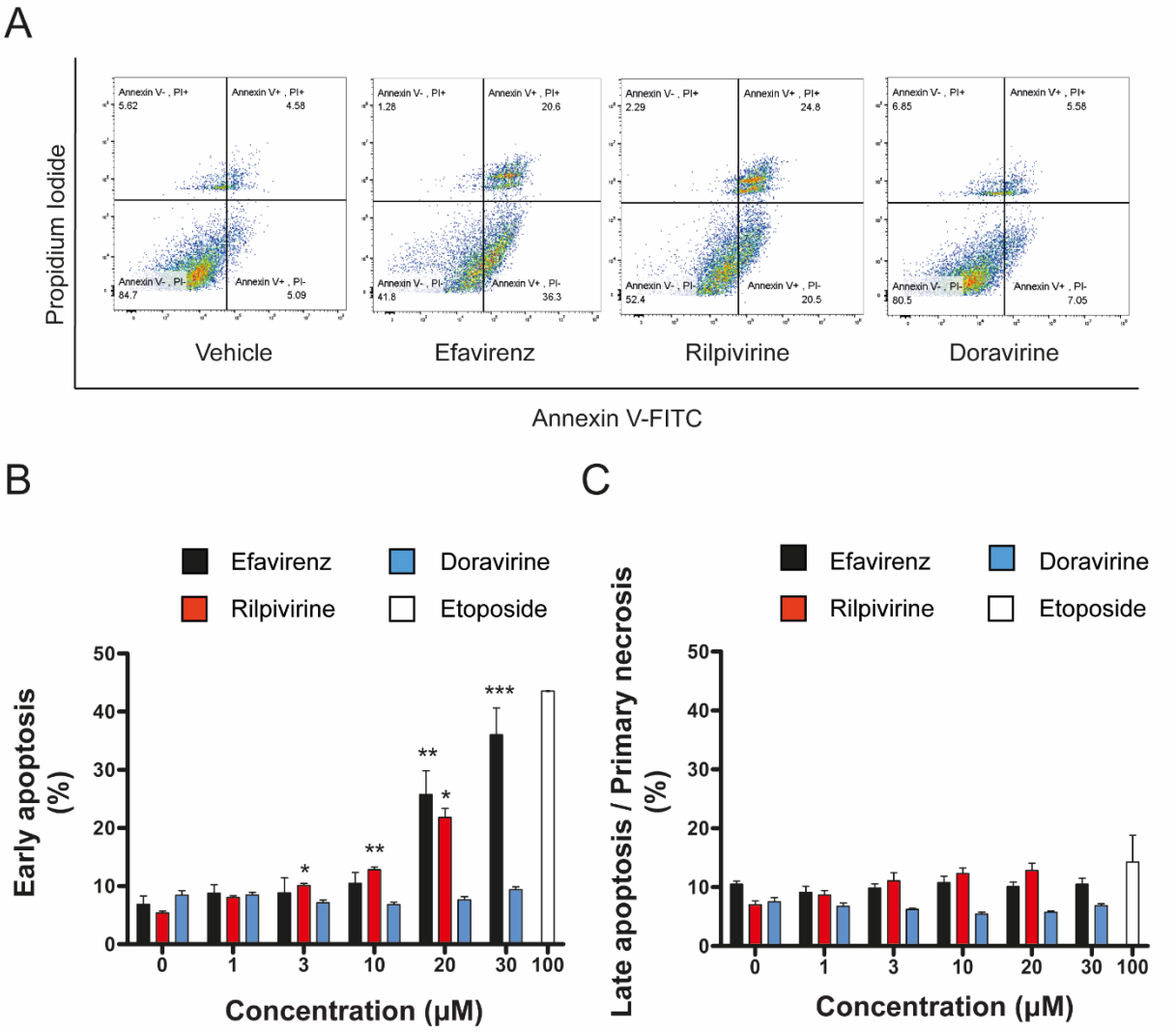

Figure 3.7 Effects of NNRTIs on INS-1E cell apoptosis and necrosis. Representative density plots of INS-1E cells treated with NNRTIs visualised using FlowJo (A). Quantitative representation of early apoptosis in INS-1E cells treated with NNRTIs (B) and late apoptosis/primary necrosis in INS-1E cells treated with NNRTIs (C) for 24 hrs. INS-1E cells were treated with etoposide (100 μM) for 6 hrs to induce apoptosis and serve as a positive control. Data are expressed as mean ± SEM of $n = 5$ independent experiments. Statistically significant differences were determined using one-way ANOVA with Bonferroni post hoc test where $p < 0.05$ was considered significant. * $p < 0.05$, ** $p < 0.01$, *** $p < 0.001$, significantly different from vehicle-treated control groups.

3.3.3.3 Assessment of necrosis using the LDH assay

To further assess necrosis, the release of LDH from INS-1E cells exposed to efavirenz or rilpivirine was measured. Exposure to efavirenz and rilpivirine had no effect on necrotic cell death in INS-1E cells (Figure 3.8).

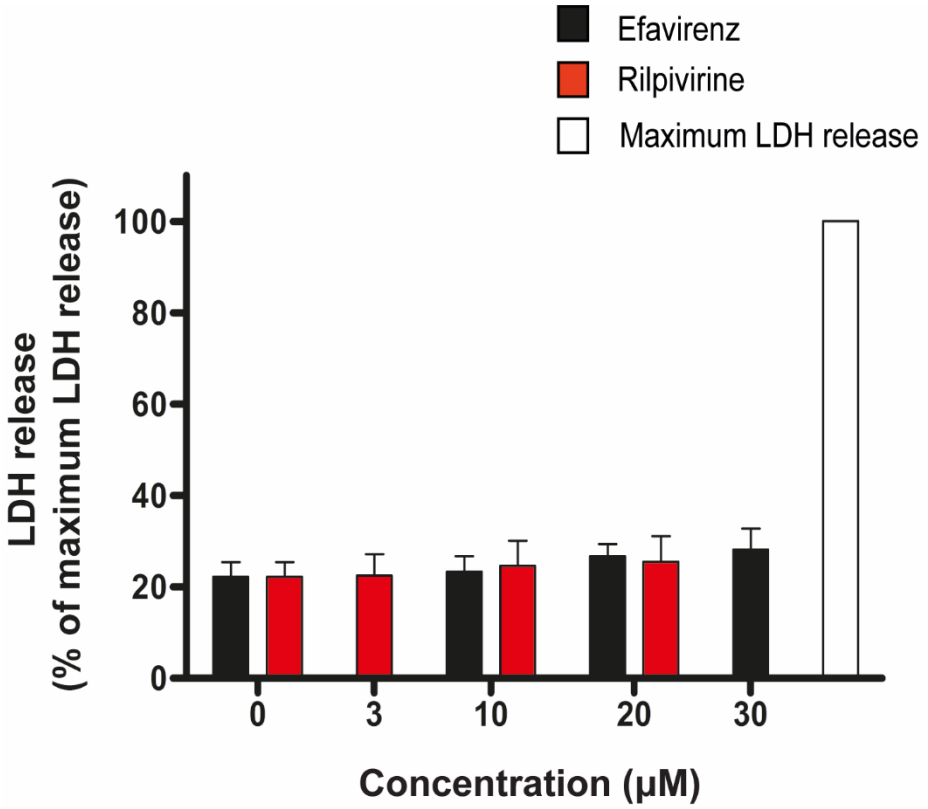

Figure 3.8 Efavirenz and rilpivirine do not affect LDH release in INS-1E cells. LDH release was measured in INS-1E cells exposed to DMSO, efavirenz or rilpivirine for 24 hrs. A maximum LDH release induced by Triton X-100 was included as a positive control. Data are expressed as mean ± SEM of $n = 5$ independent experiments with 3 technical replicates per treatment. Statistically significant differences were determined using one-way ANOVA with Bonferroni post hoc test where $p < 0.05$ was considered significant.

To further confirm apoptosis, the protein expression of cleaved caspase-3 (a critical apoptosis executioner) in INS-1E cells was detected by ICC (Figure 3.9). Only two experiments were conducted, leading to no definite conclusion regarding the expression of cleaved caspase-3. However, there seems to be an increased expression of cleaved caspase-3 in INS-1E cells following exposure to efavirenz and rilpivirine compared to control (Figure 3.9). Uncropped ICC images can be found in **Appendix III**.

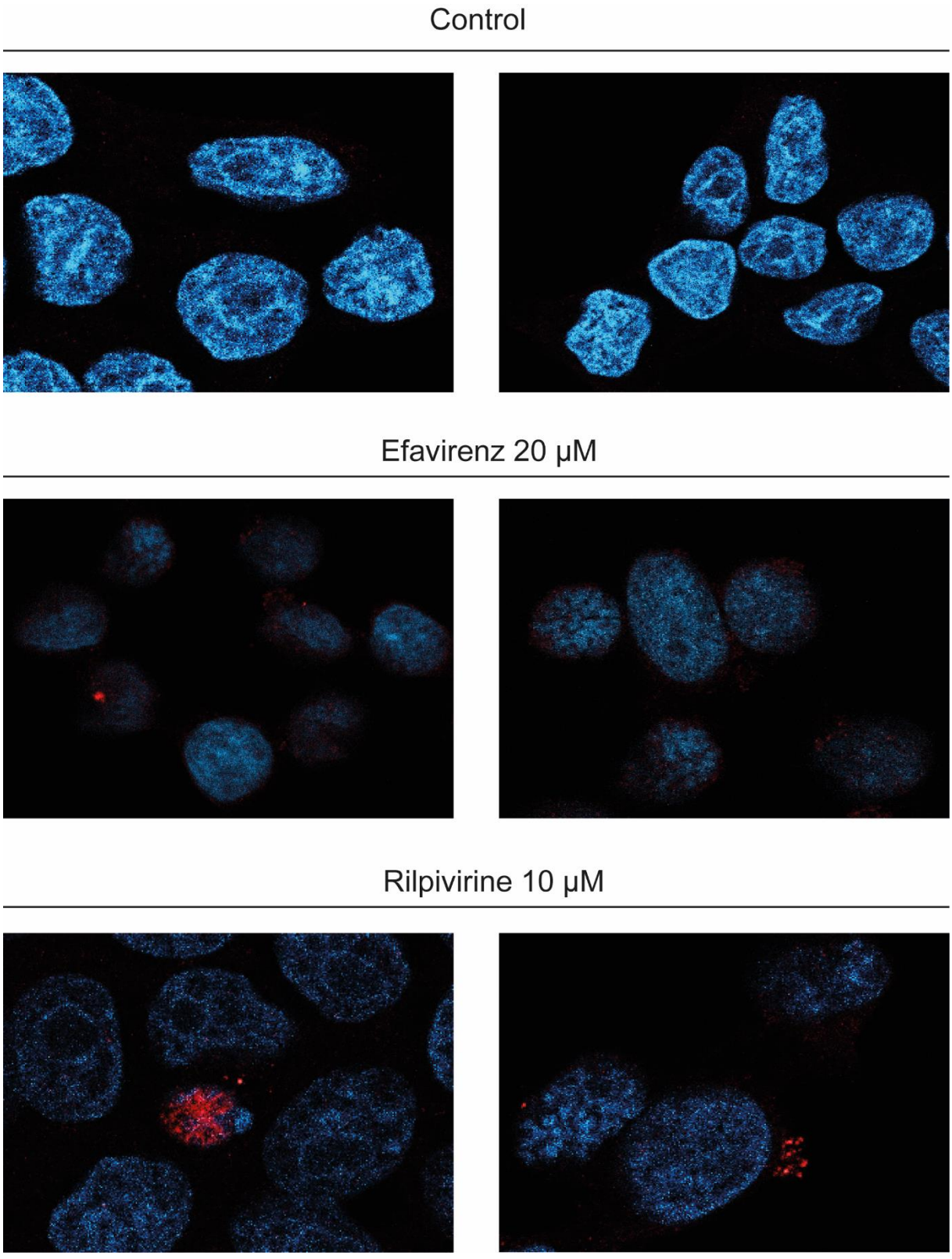

Figure 3.9 Efavirenz and rilpivirine increase caspase-3 cleavage in INS-1E cells. INS-1E cells were exposed to efavirenz (20 µM) or rilpivirine (10 µM) for 24 hrs before visualising cleaved caspase-3 by immunocytochemical analysis. Red fluorescence represents cleaved caspase-3 and blue fluorescence represents DAPI positive nuclei. Close-up overlay immunocytochemical images from one representative ICC experiment. Two independent experiments $n = 2$ were conducted.

3.3.4 Potential Cellular and Molecular Mechanisms

After observing the direct damaging effects of efavirenz and rilpivirine on beta cell function and survival, we focused on identifying possible cellular and molecular mechanism(s) by which efavirenz and rilpivirine contribute to beta cell dysfunction and apoptosis. We assessed potential cellular mechanisms by assessing oxidative stress and Δψm changes.

3.3.4.1 Effects of NNRTIs on oxidative stress

As efavirenz has been shown to induce oxidative stress in other cell types, we suggest that efavirenz may also increase oxidative stress in beta cells (Apostolova *et al.*, 2011b; Blas-García *et al.*, 2014; Blas-García *et al.*, 2010; Jamaluddin *et al.*, 2010; Weiß *et al.*, 2016a). We also hypothesise that rilpivirine may, similarly, cause beta cell dysfunction and death through oxidative stress. Therefore, we examined the potential presence of oxidative stress in INS-1E cells treated with efavirenz or rilpivirine by measuring intracellular ROS generation with a DCFH-DA assay (Figure 3.10) and antioxidant capacity with an ABTS assay (Figure 3.11). For comparative purposes, INS-1E cells were exposed to doravirine. Unsurprisingly, efavirenz caused a dose-dependent increase in intracellular ROS generation in INS-1E cells, with concentrations of 20 and 30 µM significantly inducing intracellular ROS levels (Figure 3.10). Surprisingly, rilpivirine (3 - 20 µM) also increased intracellular ROS levels in INS-1E cells (Figure 3.10). However, doravirine had no effects on intracellular ROS generation in INS-1E cells (Figure 3.10, B and C).

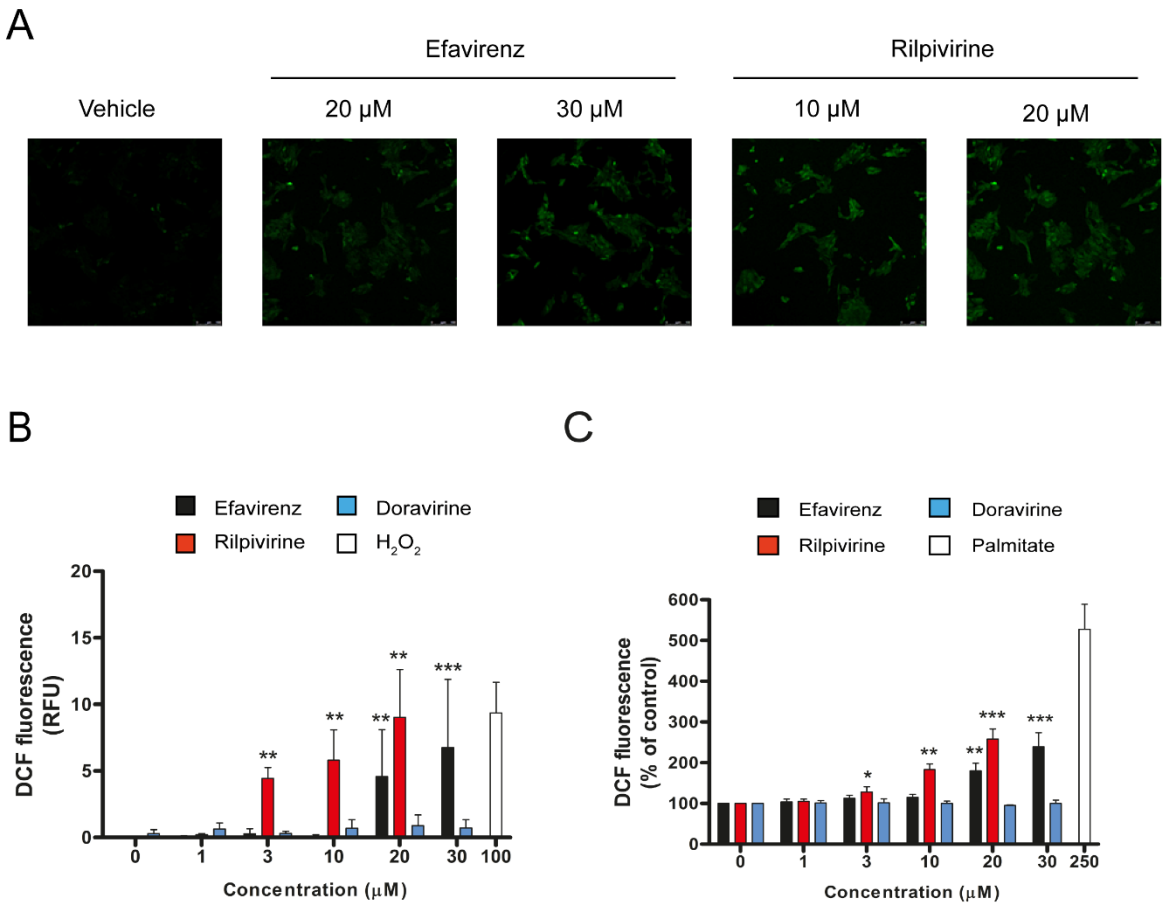

Figure 3.10 Intracellular ROS formation in INS-1E cells exposed to NNRTIs for 24 hours. (A) Confocal images of intracellular ROS levels following NNRTI treatment. The green fluorescence represents DCF which was oxidised from DCFH by ROS. (Scale bar, 100 µm). DCF fluorescence was quantified using two methods. (B) Quantification graphs of intracellular ROS levels in INS-1E cells following exposure to DMSO, efavirenz, rilpivirine or doravirine by analysing DCF mean fluorescence intensity in confocal images using the imageJ software. (C) Quantification of intracellular ROS generation using a 96-well plate, determined by DCF fluorescence normalised to cell proliferation by Crystal Violet assay. DCF fluorescence is proportional to the levels of intracellular ROS. INS-1E cells were incubated with positive controls 250 µM palmitate for 48 hrs (C) or 100 µM H_2O_2 for 1 hr (B) to induce ROS generation. Efavirenz and rilpivirine, but not doravirine, increased intracellular ROS generation in INS-1E cells. Data are expressed as mean ± SEM of $n = 5$ independent experiments (3 technical replicates per treatment in 96-well plate). Statistically significant differences were determined using one-way ANOVA with Bonferroni post hoc test (B) or Kruskal-Wallis with Dunn's post hoc test (C) where $p < 0.05$ was considered as significant. ** $p < 0.01$, *** $p < 0.001$, significantly different from vehicle-treated control groups.

Furthermore, both efavirenz (10, 20 and 30 µM) and rilpivirine (3, 10 and 20 µM) significantly reduced antioxidant capacity in INS-1E cells (Figure 3.11). However, doravirine had no effect on antioxidant capacity in INS-1E cells (Figure 3.11).

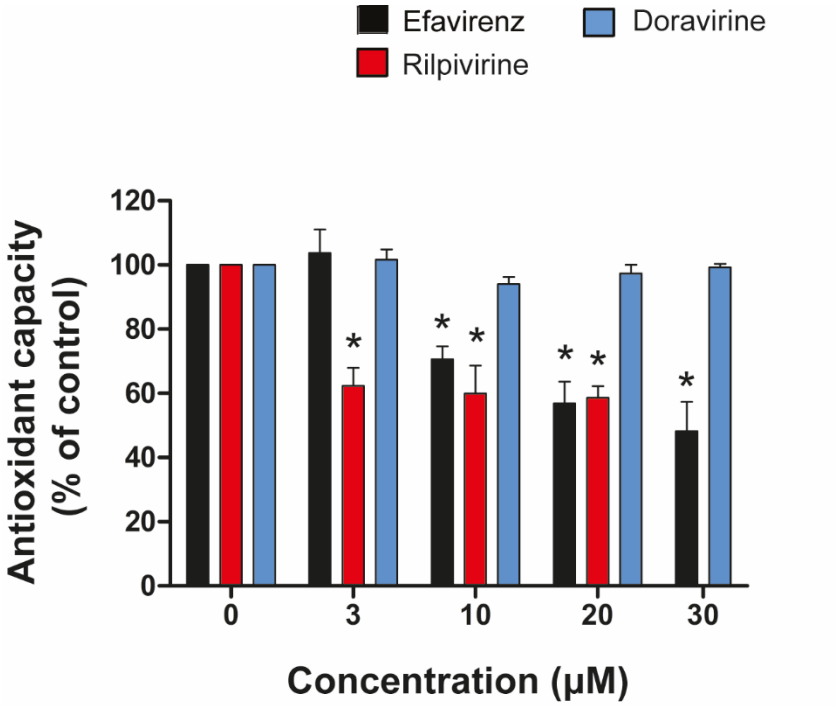

Figure 3.11 Effects of NNRTIs on antioxidant capacity in INS-1E cells. INS-1E cells were exposed to DMSO or increasing concentrations of efavirenz, rilpivirine or doravirine for 24 hrs. Efavirenz and rilpivirine, but not doravirine, reduced antioxidant capacity. Data are expressed as mean ± SEM from *n* = 3 independent experiments with 3 technical replicates per treatment. Statistical analysis was carried out using Kruskal-Wallis with Dunn's post hoc test where $p < 0.05$ was considered significant; * $p < 0.05$ significantly different from vehicle-treated control groups.

3.3.4.2 The effects of NNRTIs on Δψm changes

The mitochondrion is both the main source of ROS and a major target of oxidative stress (Marchi *et al.*, 2012). Therefore, we assessed mitochondrial function by measuring changes in Δψm in INS-1E cells exposed to NNRTIs for 24 hours (Figure 3.12). There was a dose-dependent decrease in Δψm following treatment with efavirenz, reaching an approximate 80% reduction in Δψm (30 μM) (Figure 3.12). Surprisingly, unlike efavirenz, rilpivirine increased Δψm, reaching an approximate 80% increase in Δψm (20 μM) (Figure 3.12). On the other hand, as expected, no changes in Δψm were observed in INS-1E cells treated with doravirine (Figure 3.12).

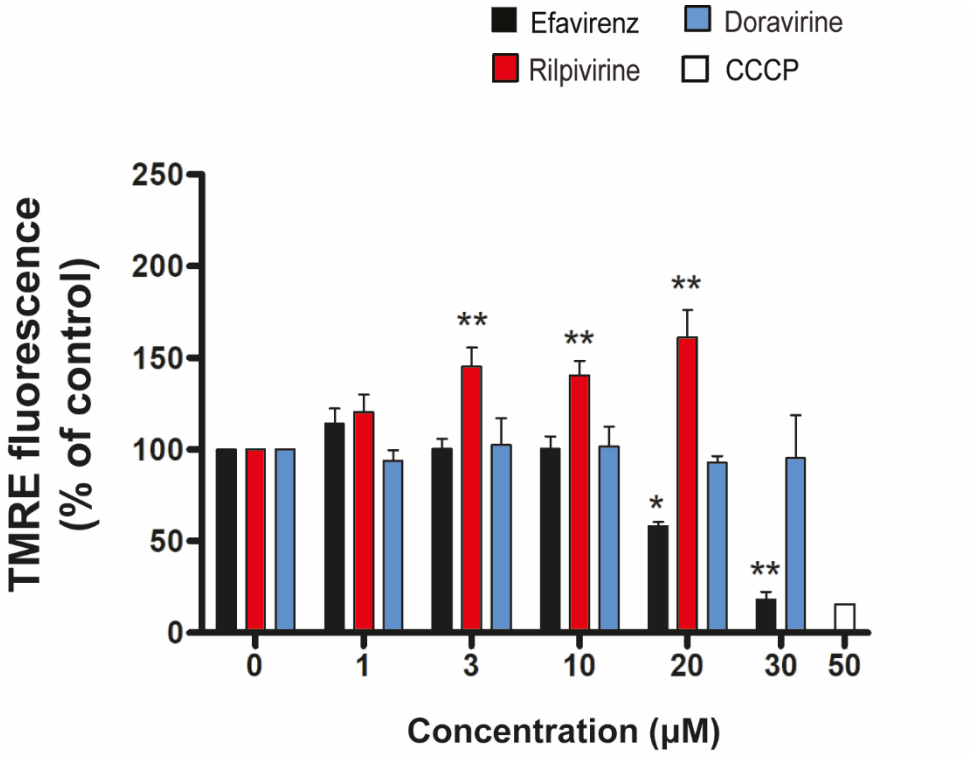

Figure 3.12 Effects of NNRTIs on Δψm changes in INS-1E cells. Changes in Δψm in INS-1E cells exposed to DMSO, efavirenz, rilpivirine or doravirine for 24 hrs were assessed by flow cytometry following staining with TMRE. TMRE fluorescence is proportional to Δψm. A positive control of INS-1E cells treated with 50 μM carbonyl cyanide m-chlorophenyl hydrazine (CCCP) was used to dissipate Δψm. Data are expressed as mean ± SEM of $n = 5$ independent experiments for efavirenz and rilpivirine treatments or $n = 3$ independent experiments for doravirine. Statistically significant differences were determined using Kruskal-Wallis with Dunn's post hoc test where $p < 0.05$ was considered significant. * $p < 0.05$, ** $p < 0.01$, significantly different from vehicle-treated control groups.

3.3.4.3 Molecular mechanisms of efavirenz and rilpivirine

We demonstrate that efavirenz and rilpivirine affect key cellular mechanisms (*i.e.*, oxidative stress and mitochondrial dysfunction) involved in beta cell dysfunction and apoptosis. Here, we focus on the effects of efavirenz and rilpivirine on a molecular level. First, we focus on glucokinase and PDX-1, two important players of insulin synthesis and secretion in beta cells (Figure 3.13).

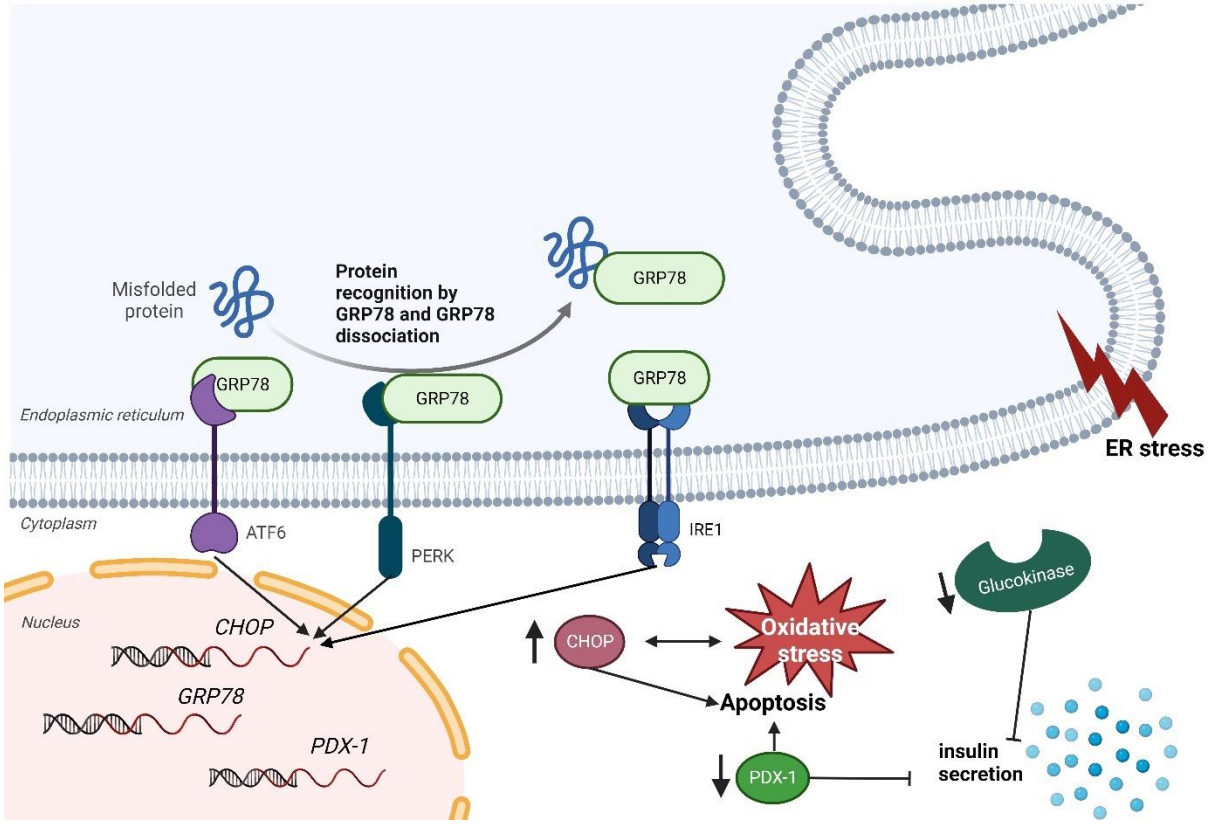

Figure 3.13 Potential molecular mechanisms involved in efavirenz- and rilpivirine-mediated beta cell dysfunction and death. ER chaperone GRP78 under normal conditions binds all the three ER stress sensors (PERK: protein kinase RNA like ER-kinase; IRE1: inositol requiring enzyme 1; ATF6: activating transcription factor 6). ER chaperone GRP78 dissociates from sensors IRE1, PERK and ATF6 under ER stress. This in turn activates the transcriptional induction of CHOP via the following pathways. (i) activation of X-box binding protein (XBP1), p38 mitogen-activated protein kinase (MAPK) and c-Jun N-terminal kinase (JNK) pathway via IRE1. (ii) Activation of ATF4 via PERK. (iii) ATF6 cleavage in the golgi. Glucokinase is a key enzyme in pancreatic beta cells involved in first-hand insulin secretion pathway. Inhibition of this enzyme results in decreased insulin secretion. PDX-1 is a key transcription factor necessary for beta cell function as well as the regulation of beta cell survival. PDX-1 deficiency has been associated with impairment of the GSIS pathway and increased beta cell susceptibility to ER stress and apoptosis. Figure created with BioRender.com.

3.3.4.3.1 Efavirenz and rilpivirine do not affect glucokinase activity

Glucokinase is a key enzyme in pancreatic beta cells and is involved in first-hand insulin secretion pathway (Figure 3.13). Both efavirenz and rilpivirine did not influence glucokinase activity in INS-1E cells (Figure 3.14).

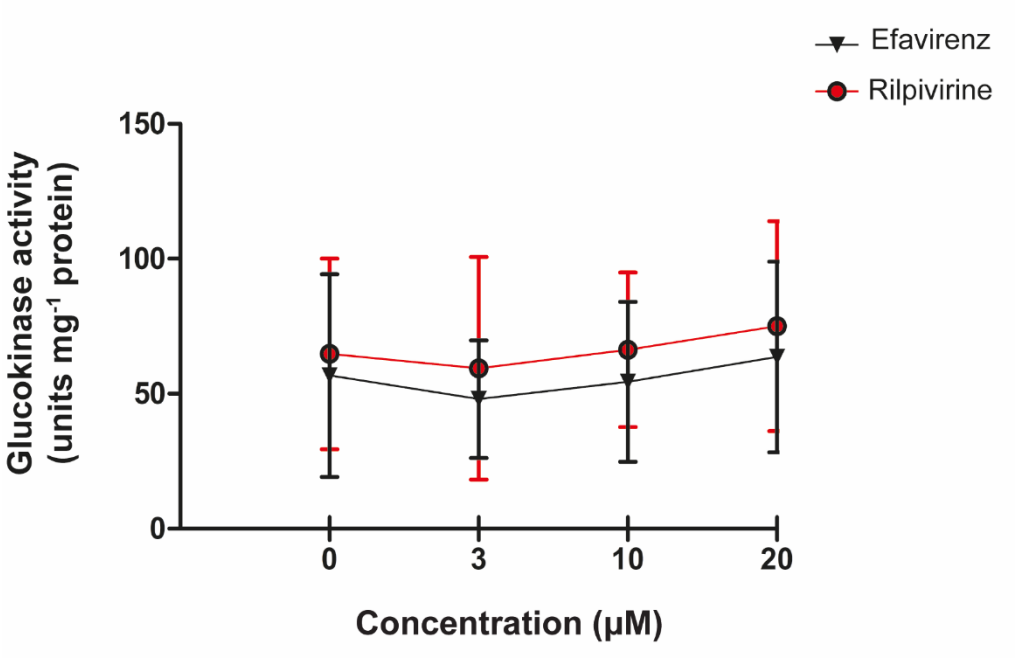

Figure 3.14 Efavirenz and rilpivirine do not affect glucokinase activity in INS-1E cells. INS-1E cells were treated with DMSO or increasing concentrations of efavirenz or rilpivirine for 24 hrs before assessing glucokinase activity using an indirect assay. Specific activity of glucokinase activity was normalised to protein concentrations. Data are expressed as mean ± SEM from *n* = 4 independent experiments with 3 technical replicates per treatment. Statistical analysis was carried out using one-way ANOVA and Bonferroni post hoc test where $p < 0.05$ was considered significant.

3.3.4.3.2 Efavirenz and rilpivirine do not affect PDX-1 expression

PDX-1 is a key transcription factor necessary for beta cell function as well as the regulation of beta cell survival. PDX-1 deficiency has been associated with impairment of the GSIS pathway and increased beta cell susceptibility to ER stress and apoptosis (Brissova *et al.*, 2002; Glavas *et al.*, 2019; Johnson *et al.*, 2003; Sachdeva *et al.*, 2009) (Figure 3.13). Therefore, we investigated the possible involvement of PDX-1 deficiency in efavirenz and rilpivirine-induced beta cell dysfunction and death by assessing whether efavirenz or rilpivirine downregulated the mRNA and protein expression of PDX-1 in INS-1E cells (Figure 3.15). INS-1E cells were exposed to a 24-hour treatment with concentrations of efavirenz (20 µM) and rilpivirine (10 µM) that were shown to induce apoptosis, as well as impair insulin secretion (Figure 3.4, Figure 3.6 and Figure 3.7). Both efavirenz (Figure 3.15, A) and rilpivirine (Figure 3.15, B) had no effect on the mRNA and protein expression of PDX-1 (Figure 3.15, C). Whole uncropped images of the original Western blot that contributed to the quantitative analysis, from which figures have been derived, have been included in **Appendix II**.

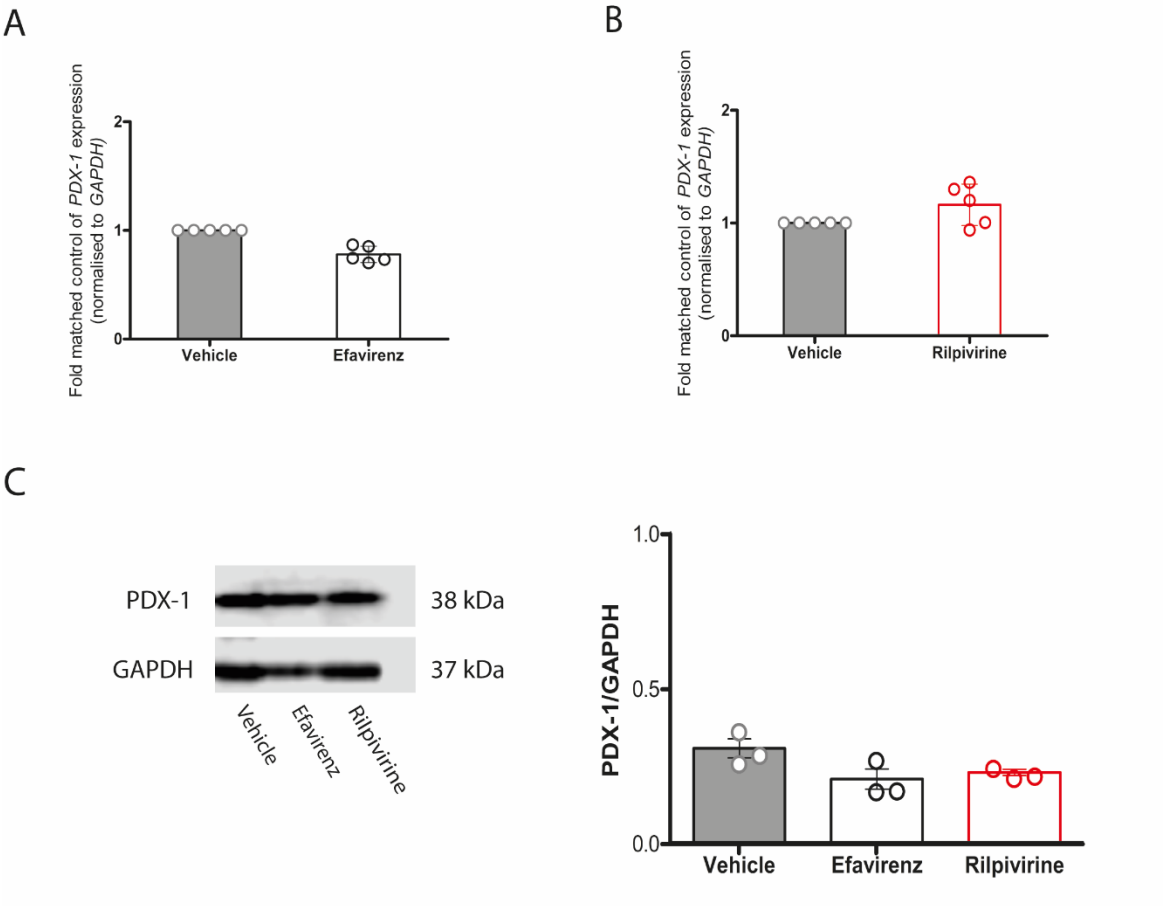

Figure 3.15 A 24-hour exposure to efavirenz and rilpivirine does not affect PDX-1 expression in INS-1E cell. mRNA expression of *PDX-1* after a 24-hour treatment with efavirenz 20 µM (A) or rilpivirine 10 µM (B). (C) Representative western blot of PDX-1 protein expression from one independent experiment (left panel) and results expressed as PDX-1 protein normalised to GAPDH protein (right panel) following a 24-hour exposure to efavirenz 20 µM or rilpivirine 10 µM. Dots represent individual data points from a minimum of n = 3 independent experiments and the histograms represent mean ± SD. Statistically significant differences were determined using Kruskal-Wallis with Dunn's post hoc test for mRNA expression or Student's t-test for protein levels where $p < 0.05$ was considered significant.

3.3.4.3.3 ER stress

Finally, we focus on ER stress, a key regulator of apoptosis in beta cells on a molecular level (Figure 3.13). ER stress has been previously shown to contribute to the pathogenesis of diabetes by inducing pancreatic beta cell loss via apoptosis (Eizirik *et al.*, 2008). Hence, we examined whether ER stress is induced in efavirenz and rilpivirine-treated INS-1E cells by measuring the mRNA and protein expression of CHOP and GRP78, two key ER stress markers.

To preliminarily assess CHOP expression, we conduct an ELISA. We observe that there seems to be a trend in increased protein expression of CHOP following a 24-hour exposure to efavirenz or rilpivirine in INS-1E cells, as determined by ELISA (Figure 3.16). Efavirenz (1, 3, 10 or 20

µM) slightly increased the protein expression of CHOP by approximately 50% compared to control. Similarly, rilpivirine (1, 3, 10 or 20 µM) doubled the protein expression of CHOP compared to control. However, in both cases, statistical significance was not reached (Figure 3.16).

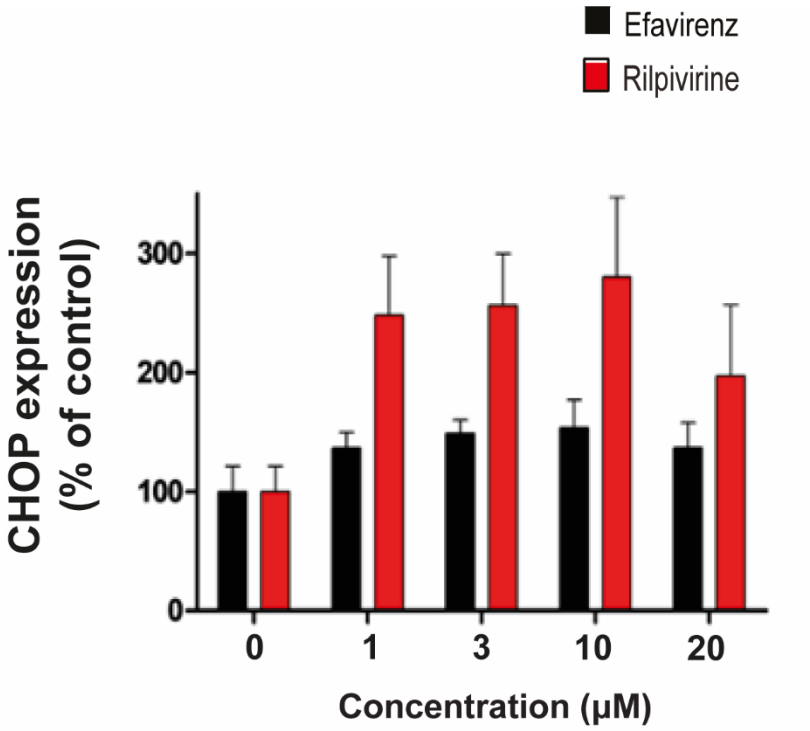

Figure 3.16 Measurements of CHOP protein expression in INS-1E cells following a 24-hour exposure to efavirenz or rilpivirine. INS-1E cells were exposed to DMSO or increasing concentrations of efavirenz or rilpivirine before measuring CHOP protein expression using ELISA. There seems to be a trend in increased CHOP protein expression after exposure to efavirenz or rilpivirine in INS-1E cells. Further investigations were conducted to confirm this. Data are expressed as mean ± SEM from n = 2 independent experiments with 3 technical replicates per treatment.

To confirm the CHOP measurements by ELISA (Figure 3.16), we evaluated the mRNA and protein expression of CHOP, as well as GRP78, an ER chaperone. For this purpose, INS-1E cells were exposed to a 24-hour treatment with concentrations of efavirenz (20 µM) and rilpivirine (10 µM) that were shown to induce apoptosis (Figure 3.6 and Figure 3.7). Efavirenz significantly upregulated *CHOP* (Figure 3.17, A) and *GRP78* (Figure 3.17, C) mRNA expression by approximately threefold in INS-1E cells. Rilpivirine caused a more pronounced upregulation (6-fold) of *CHOP* (Figure 3.17, B) and *GRP78* (Figure 3.17, D) mRNA expression. Additionally, efavirenz resulted in an approximate 1.5-fold increase in CHOP protein expression (Figure 3.17, E) while rilpivirine increased CHOP protein expression by

approximately onefold in INS-1E cells (Figure 3.17, F). Similarly, a 24-hour exposure to efavirenz resulted in an approximate 2-fold increase in GRP78 protein expression (Figure 3.17, G) while rilpivirine increased GRP78 protein expression by nearly fourfold (Figure 3.17, H) in INS-1E cells. Whole uncropped images of the original Western blots that contributed to the quantitative analysis, from which figures have been derived, have been included in **Appendix II**. Thapsigargin (1 μM) was included as a positive control (**Appendix II**).

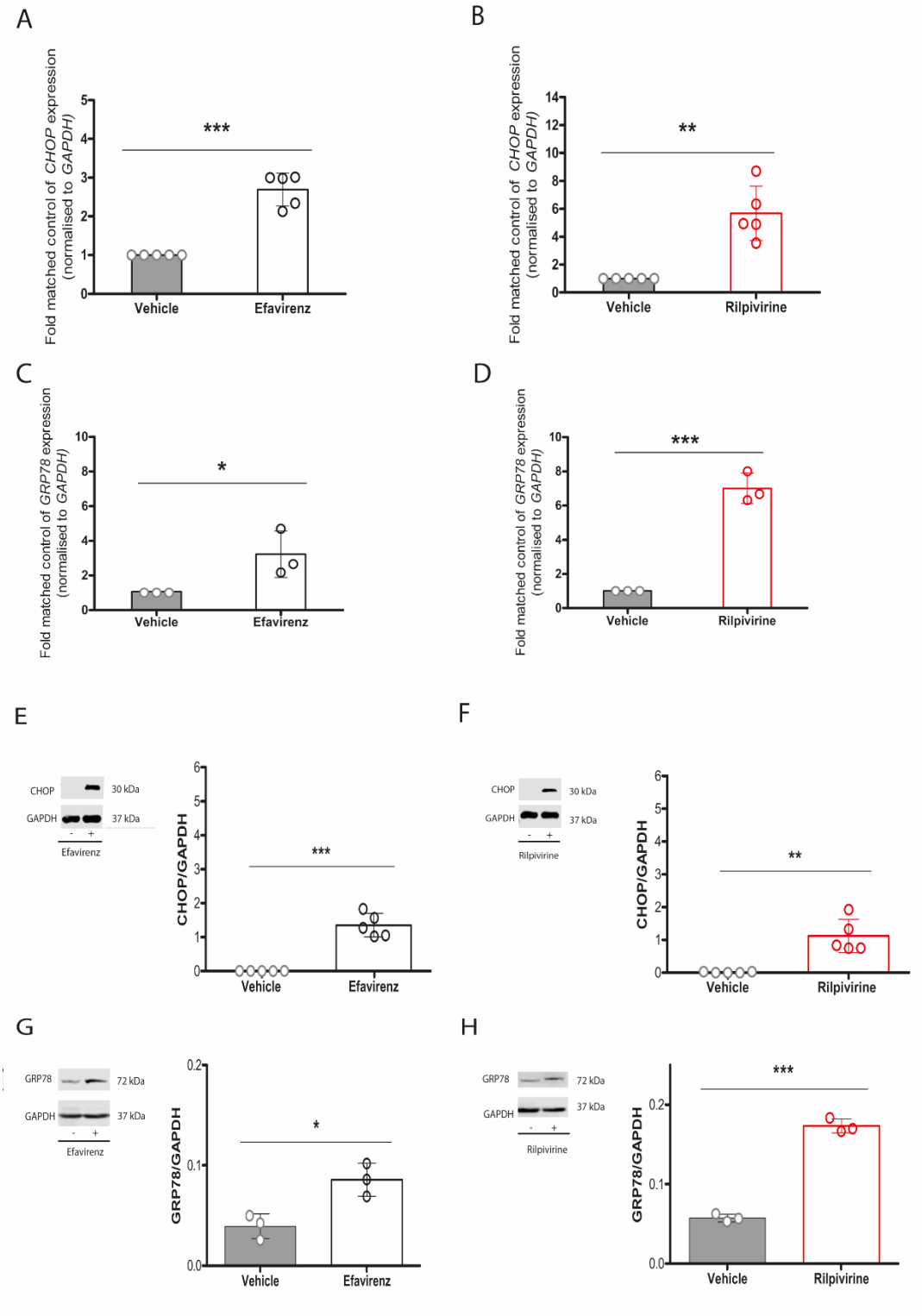

Figure 3.17 A 24-hour exposure to efavirenz and rilpivirine induces CHOP and GRP78 expression in INS-1E cell. mRNA expression of *CHOP* was assessed by RT-qPCR and normalised to GAPDH following a 24-hour treatment with efavirenz 20 µM (A) or rilpivirine 10 µM (B). mRNA expression of *GRP78* was assessed by RT-qPCR and normalised to GAPDH following a 24-hour treatment with efavirenz 20 µM (C) or rilpivirine 10 µM (D). Representative Western blot of CHOP protein expression (left panel) following a 24-hour exposure to efavirenz 20 µM (E) or rilpivirine (F). (E, F) Results are expressed as CHOP protein normalised to GAPDH protein (right panel). Representative western blot of GRP78 protein expression (left panel) following a 24-hour exposure to efavirenz 20 µM (G) or rilpivirine (H). (G, H) Results are expressed as GRP78 protein normalised to GAPDH

protein (right panel). Dots represent individual data points from a minimum of $n = 3$ independent experiments and the histograms represent mean ± SD. Statistically significant differences were determined using Kruskal-Wallis with Dunn's post hoc test for mRNA expression or Student's t-test for protein levels. * $p < 0.05$, ** $p < 0.01$, *** $p < 0.001$, significantly different from vehicle-treated control group.

3.6 Discussion

Although the use of NNRTIs improves clinical outcomes in people living with HIV, there is growing concern about the alarming increase in T2D and insulin resistance in the HIV population on NNRTI-based ART. To the best of our knowledge, this is the first study to demonstrate the direct detrimental effects of the first-generation NNRTI efavirenz and, intriguingly, of the second-generation NNRTI rilpivirine, on pancreatic beta cell function and survival, while suggesting a possible cellular and molecular link between the use of efavirenz and rilpivirine and the potential impairment of glycaemic control and loss of beta cell mass in PLWH and T2D.

The first-generation NNRTI efavirenz has previously been reported to potentiate loss of function and death through mitochondrial toxicity and oxidative stress in adipocytes, hepatocytes, neurones and endothelial cells (Apostolova *et al.*, 2010; Blas-García *et al.*, 2014; Blas-García *et al.*, 2010; Jamaluddin *et al.*, 2010; Weiß *et al.*, 2016b). This study has extended this damage to pancreatic beta cells, as we show that efavirenz significantly decreased basal insulin release and GSIS from INS-1E cells and isolated rat islets of Langerhans. Strikingly, we found that the second-generation NNRTI rilpivirine induces cellular damage in beta cells, a manifestation which has not been previously reported in hepatocytes and neurons (Blas-García *et al.*, 2014). We show that rilpivirine significantly decreased basal insulin release and GSIS from INS-1E cells and isolated rat islets of Langerhans. The use of both models further strengthens the observation of insulin-secretory dysfunction in pancreatic beta cells following exposure to efavirenz and rilpivirine. Interestingly, rilpivirine exhibited a decrease in insulin release in sub-toxic conditions (3 μM), contrary to efavirenz (20 μM), with the latter increasing the rates of apoptosis and decreasing both cell viability as well as insulin release from INS-1E cells.

We also show that efavirenz induces mitochondrial dysfunction in INS-1E cells, as confirmed by a loss of $\Delta\psi m$. In hepatocytes, efavirenz has been shown to inhibit complex I activity of the respiratory chain, resulting in increased ROS levels and depolarisation of the mitochondria

(*i.e.* reduced Δψm) (Blas-García *et al.*, 2010). If the latter mechanism is extended to beta cells, this could suggest that efavirenz may inhibit complex I activity, hence resulting in a potential increase in superoxide generation from the mitochondria, contributing to cellular dysfunction and programmed cell death.

We also demonstrate that rilpivirine, through a rise in Δψm, negatively impacts mitochondrial function in beta cells. Previous evidence has shown that an increase in Δψm may be linked to an inhibition of the mitochondrial ATP synthase (Blas-García *et al.*, 2014). This finding was surprising since, until more recently, *hyperpolarization* of $\Delta\psi_m$ (*i.e.*, increased Δψm) in response to cellular insults had been infrequently reported compared with many more reports of mitochondrial *depolarization* (*i.e.*, decreased Δψm) following cellular stressors. Therefore, we hypothesise that rilpivirine may inhibit the mitochondrial ATP synthase in beta cells, leading to increased oxidative stress and mitochondrial damage in beta cells. Indeed, the rise in Δψm following rilpivirine treatment correlates with elevated intracellular ROS levels, supporting previous evidence that increased Δψm stresses the mitochondrial respiratory chain to become a significant producer of ROS (Zorova *et al.*, 2018).

Indeed, both efavirenz and rilpivirine induced intracellular ROS production in beta cells. Given the fact that beta cells are extremely susceptible to oxidative stress and subsequent oxidative damage due to their low antioxidant capacity, ROS attack is majorly involved in beta cell dysfunction and worsening of beta cell survival (Drews *et al.*, 2010). Particularly, the mitochondrion represents a major target of oxidative damage as elevated levels of ROS can induce mitochondrial DNA damage, lipid peroxidation, protein carbonylation and damage to the mitochondrial respiratory chain components, further aggravating the function of the mitochondria and triggering a cellular energetic catastrophe (Marchi *et al.*, 2012). ROS attack at the mitochondrion level results in the impairment of the function of this organelle, characterised by reduced ATP production (Newsholme *et al.*, 2019). The primary function of pancreatic beta cells is the production and release of insulin to regulate blood glucose levels, which is mainly modulated by mitochondrial metabolism (*i.e.*, ATP production). In parallel to reductions in the insulin-secretory function, we show that there was an increase in intracellular ROS levels in INS-1E cells exposed to efavirenz and rilpivirine, highlighting the potential involvement of oxidative stress in efavirenz and rilpivirine-induced beta cell dysfunction. Due to their low antioxidant ability, a minor oxidative insult in beta cells can severely impair insulin secretion by compromising mitochondrial metabolism, glycolysis, and insulin release through

exocytosis (Drews *et al.*, 2010). Failure of insulin secreting beta cells, a common characteristic of T2D, has been established to arise from various origins including mitochondrial dysfunction secondary to oxidative stress (Li *et al.*, 2009). ROS changes may contribute to important physiological control of cell functions, notably the regulation of insulin secretion in beta cells (Li *et al.*, 2009; Pi *et al.*, 2007a). Oxidative stress agents have been shown to activate the c-Jun N-terminal kinase (JNK), P38 mitogen-activated protein kinase (MAPK) and protein kinase C (PKC) pathways, preceding a decrease in insulin gene expression and biosynthesis, insulin exocytosis and promoting beta cell death (Kaneto *et al.*, 2005; Newsholme *et al.*, 2019; Pi *et al.*, 2007b).

Coupled with intrinsically low antioxidant levels in beta cells, we show that total antioxidant capacity is reduced in INS-1E exposed to efavirenz and rilpivirine. However, we have not investigated the effects of NNRTIs on the activity and expression of key antioxidant enzymes. We can only speculate that efavirenz and rilpivirine might exert their deleterious effects on beta cells by affecting the activity and/or expression of antioxidant enzymes such as superoxide dismutase (SOD), catalase and glutathione peroxidase (GPx). Efavirenz has been shown to decrease the expression of SOD, catalase, GPx as well as glutathione levels in rat liver and decrease SOD activity and glutathione levels in rat midbrain (Adikwu and Bokolo, 2018 and Jenson, 2015). Rilpivirine has also been shown to affect antioxidant enzyme activity in human adipocytes decreasing both SOD, catalase activity, as well as glutathione levels (Behl *et al.*, 2020).

By increasing intracellular ROS generation and reducing antioxidant capacity, efavirenz and rilpivirine potentiate oxidative stress in beta cells, which in turn mediates beta cell dysfunction and death. Through the proposed direct inhibition of complex I or ATP synthase activity, efavirenz and rilpivirine may reduce ATP production in beta cells. However, beta cells have a limited ability to elevate and maintain ATP levels, which may further lead to impaired insulin release (Newsholme *et al.*, 2019). Furthermore, we cannot rule out that efavirenz and rilpivirine may potentially exert their deleterious effects by upregulating the expression of uncoupling protein 2 (UCP2), a phenomenon associated with a reduction in ATP levels (Urbano *et al.*, 2016). UCP2 has been associated with mitochondrial proton leak, reductions in ATP production and attenuations in GSIS in INS-1E cells (Affourtit *et al.*, 2011). Another possible target of ROS includes the beta cell ATP-sensitive potassium (K_{ATP}) channels by which ROS can indirectly modulate K_{ATP} channels through the induction of the mitochondrial uncoupling protein 2 (UCP2) expressed in pancreatic beta cells. The induction of UCP2 causes ATP

depletion which subsequently prevents the closure of K_{ATP} channels and subsequent insulin release from beta cells (Chan & Harper, 2006).

The proposed mechanisms underlying efavirenz- and rilpivirine-induced beta cell dysfunction and death are summarised in Figure 3.18.

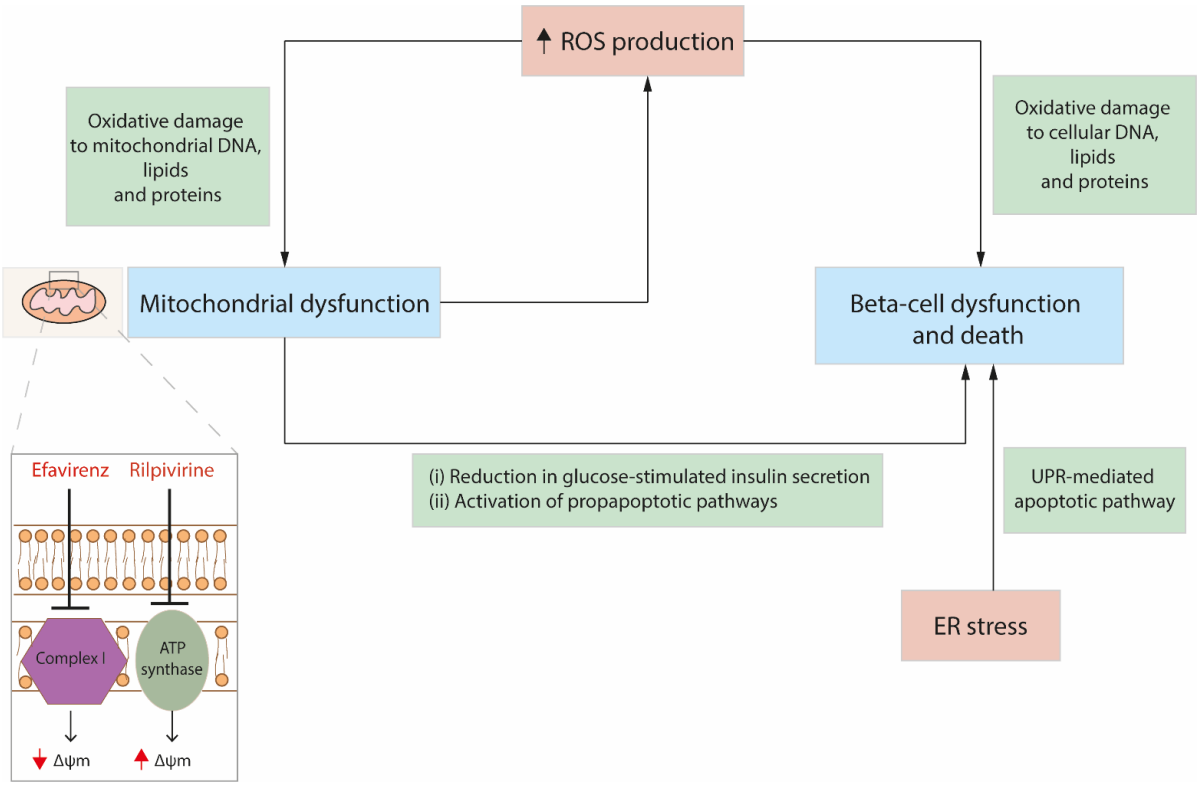

Figure 3.18 Schematic diagram of proposed mechanisms underlying efavirenz- and rilpivirine-induced beta cell dysfunction and death.

While the precise ROS-mediated mechanisms are complex, it has been shown that ROS can alter the function of critical proteins, lipids and DNA through chemical modification including nitrosylation, peroxidation, and carbonylation, thus promoting dysfunction (Gerber & Rutter, 2016; Newsholme *et al.*, 2019). PDX-1 is the beta cell identity gene and plays a major role in maintaining normal beta cell function by controlling key beta cell genes involved in insulin biosynthesis and secretion, and cell survival (Kajimoto & Kaneto, 2004). By reducing the DNA binding activity of PDX-1, ROS can suppress insulin gene expression in beta cells (Gerber & Rutter, 2016; Kajimoto & Kaneto, 2004). ROS can also suppress the mRNA and protein expression of this critical gene (Baumel-Alterzon & Scott, 2022). However, we demonstrate that there were no changes in PDX-1 expression following treatment with efavirenz and rilpivirine, disregarding the involvement of PDX-1 downregulation in efavirenz

and rilpivirine-induced beta cell dysfunction and death. Moreover, efavirenz and rilpivirine did not affect insulin synthesis as confirmed by the lack of intracellular insulin content changes, further implying the non-involvement of PDX-1 in efavirenz and rilpivirine-mediated beta cell dysfunction. These findings strengthen a dysfunction at the insulin-secretory machinery level.

Glucokinase, which phosphorylates glucose to form glucose-6-phosphate, plays a critical role in regulating blood glucose levels by modulating insulin secretion from pancreatic beta cells. Inhibition of glucokinase can negatively impact insulin secretion from beta cells. Efavirenz and rilpivirine had no effect on glucokinase activity in INS-1E cells, disregarding the involvement of glucokinase in efavirenz- and rilpivirine-induced beta cell dysfunction.

We also show that efavirenz and rilpivirine upregulated the mRNA and protein expression of CHOP and GRP78, key markers of ER stress, while also inducing apoptosis in beta cells. ER stress has been previously shown to contribute to the pathogenesis of diabetes by inducing pancreatic beta cell loss via apoptosis (Eizirik *et al.*, 2008). Through the increased formation of intracellular ROS, efavirenz and rilpivirine may cause an accumulation of oxidative damage to proteins which in turn can trigger ER stress and subsequent activation of pro-apoptotic signals, leading to beta cell apoptosis (Ježek *et al.*, 2019; Kajimoto & Kaneto, 2004; Kaufman *et al.*, 2015). Prolonged ER stress can also trigger the unfolded protein response (UPR) mediated apoptotic pathway, through the transcriptional induction of CHOP expression, which is mediated by the ER stress signalling proteins IRE1 (activation of XBP1, c-Jun N-terminal kinase and the P38 pathways), PERK (activation of ATF4) and ATF6 (ATF6 cleavage) (Araki *et al.*, 2003) (Figure 3.18). ER chaperone GRP78 dissociates from sensors IRE1, PERK and ATF6 under ER stress. This in turn permits stress sensors to activate downstream signalling to activate the transcriptional induction of CHOP via the pathways above-mentioned (Bhattarai *et al.*, 2021; Kajimoto & Kaneto, 2004).

Additionally, it is well established that mitochondrial stress plays a major role in inducing apoptotic beta cell death (Szabadkai & Duchen, 2009). Disruptions in $\Delta\psi m$ and ROS accumulation seen following efavirenz and rilpivirine exposure may also induce the mitochondria-mediated pathway of apoptosis. These manifestations may induce apoptosis in beta cells through the release of key proapoptotic players (*i.e.*, BH3-only members of the Bcl-2 family, cytochrome *c*, apoptosis-inducing factor and Smac/DIABLO) and inactivation of antiapoptotic players (*i.e.*, Bcl2 proteins) (Drews *et al.*, 2010; Szabadkai & Duchen, 2009) (Figure 3.18). In an event of cellular stress, proapoptotic BH3-only members of the Bcl-2

family release caspase activators, which in turn activate upstream (caspase-9) and effector caspases (caspase-3) and their downstream pathways, hence triggering apoptosis (Skuratovskaia *et al.*, 2020). We encountered difficulties detecting cleaved caspase-3 by Western blotting, hence we decided to perform ICC instead. Although the ICC data seems promising, there is a lack of both technical and biological replicates, rendering it difficult to make any conclusions. However, it is likely that caspase-3 cleavage, a prerequisite step for the induction of mitochondria-dependent apoptosis, is increased in beta cells exposed to efavirenz or rilpivirine, as per the two experiments conducted, suggesting the potential activation of the mitochondria-dependent apoptotic pathway in efavirenz- and rilpivirine-mediated apoptosis. However, further experiments are warranted to confirm this. Therefore, efavirenz and rilpivirine may induce apoptosis through ER stress and mitochondrial toxicity. Apoptosis plays a detrimental role in beta cell mass formation, contributing to the aetiology of T2D (Donath & Halban, 2004).

However, the damaging effects in beta cells seen with the first- and second-generation NNRTIs were not observed following exposure to the novel NNRTI doravirine. Doravirine did not affect beta cell survival, potentially owing to the absence of mitochondrial dysfunction and oxidative stress in INS-1E cells treated with doravirine. A plausible explanation could be that distinct intraclass structural differences between these three NNRTIs dictate the off-target binding properties of these NNRTIs to key proteins in beta cells, which may explain the presence of oxidative stress, in the case of efavirenz and rilpivirine, or the absence of oxidative stress in the case of doravirine (Figure 3.1). Interestingly, contrary to both efavirenz and rilpivirine, doravirine increased basal insulin release and GSIS. Doravirine may modulate components of the insulin secretory machinery. Further experiments are warranted to understand the mechanism(s) behind this contrasting effect on insulin release.

3.7 Conclusion

Based on the data presented here, we conclude that exposure to the NNRTIs efavirenz and rilpivirine can greatly affect pancreatic beta cell function and survival. These deleterious effects may be, at least partially, mediated by oxidative stress and mitochondrial dysfunction. On the contrary, the novel NNRTI doravirine had no effect on beta cell function and survival.

The next chapter will attempt to uncover the mitochondria-ROS cross talk involved in efavirenz- and rilpivirine-induced beta cell dysfunction and worsening of beta cell survival.

4. Mitochondria-ROS crosstalk in beta cells: the role of efavirenz and rilpivirine

4.1 Introduction

"It is a good thing for the entire enterprise that mitochondria and chloroplasts have remained small, conservative, and stable, since these two organelles are, in a fundamental sense, the most important living things on earth. Between them they produce oxygen and arrange for its use. In effect, they run the place." This description by Lewis Thomas succinctly describes the centrality of mitochondrial function to sustaining life (Thomas, 1971 and Sack, 2006). The pivotal role of the mitochondria is exemplified in pancreatic beta cells as mitochondrial function is closely linked to insulin biosynthesis and secretion, in large part by adenosine triphosphate (ATP) synthesis, mitochondrial oxidative phosphorylation (OXPHOS) and reactive oxygen species (ROS) formation. The characterisation of the role of mitochondria in cellular biology has been extensively studied. Beyond oxygen utilisation and ATP production, mitochondria are now recognised as organelles that orchestrate energy production, reactive oxygen and nitrogen species generation, calcium regulation, apoptosis, and retrograde signalling (Sack, 2006). Oxidative metabolism generates the bulk of ATP from a sequential passage of electrons from high to low redox potentials down the electron transfer chain (ETC). The electrochemical gradient generated across the inner mitochondrial membrane (IMM) facilitates the translocation of protons from the inter-membranous space via the F_o/F_1 ATPase (ATP synthase) back into the mitochondrial matrix (Sack, 2006 and Sha *et al*., 2020). This proton translocation is coupled to the phosphorylation of adenosine diphosphate (ADP) to generate ATP. Altogether, these reactions constitute OXPHOS and the direct synthesis of ATP. The major enzymes part of the ETC include complex I (also known as NADH:ubiquinone oxidoreductase, Type I NADH dehydrogenase), complex II (also known as succinate dehydrogenase), complex III (also known as ubiquonol – cytochrome *c* oxidoreductase), complex IV (cytochrome *c* oxidase) and complex V (also known as ATP synthase) (Sha *et al*., 2020) (Figure 4.1).

Uncoupled oxidative phosphorylation refers to a state in which nutrient fuels are oxidised but the resultant energy is not linked to ATP synthesis but rather is dissipated as heat (Figure 4.1). Uncoupled oxidative phosphorylation can be mediated by specific proteins found in the IMM, called uncoupling proteins. The uncoupling protein family in mammals include uncoupling protein 1 (UCP1) to 4 which are involved in physiological and pathological processes (Chan

and Harper, 2006) (Figure 4.1). Interest in mitochondrial UCP2 in the pathogenesis of type 2 diabetes focuses on the involvement of UCP2, the most abundant UCP isoform in pancreatic beta cells, on the regulation of insulin secretion (Saleh *et al*., 2002). The physiological role of UCP2 in beta cells has not been fully established, however, some researchers believe that UCP2 activity may be important to coordinate the physiological response of beta cells to fluctuating nutrient supply. UCP2 was found to be a negative regulator of insulin synthesis, glucose-stimulated insulin secretion (GSIS) and beta cell mass (Chan *et al*., 2001). A signalling role of UCP2 could be important to restrict insulin secretion when blood glucose levels are low (Affourtit and Brand, 2008).

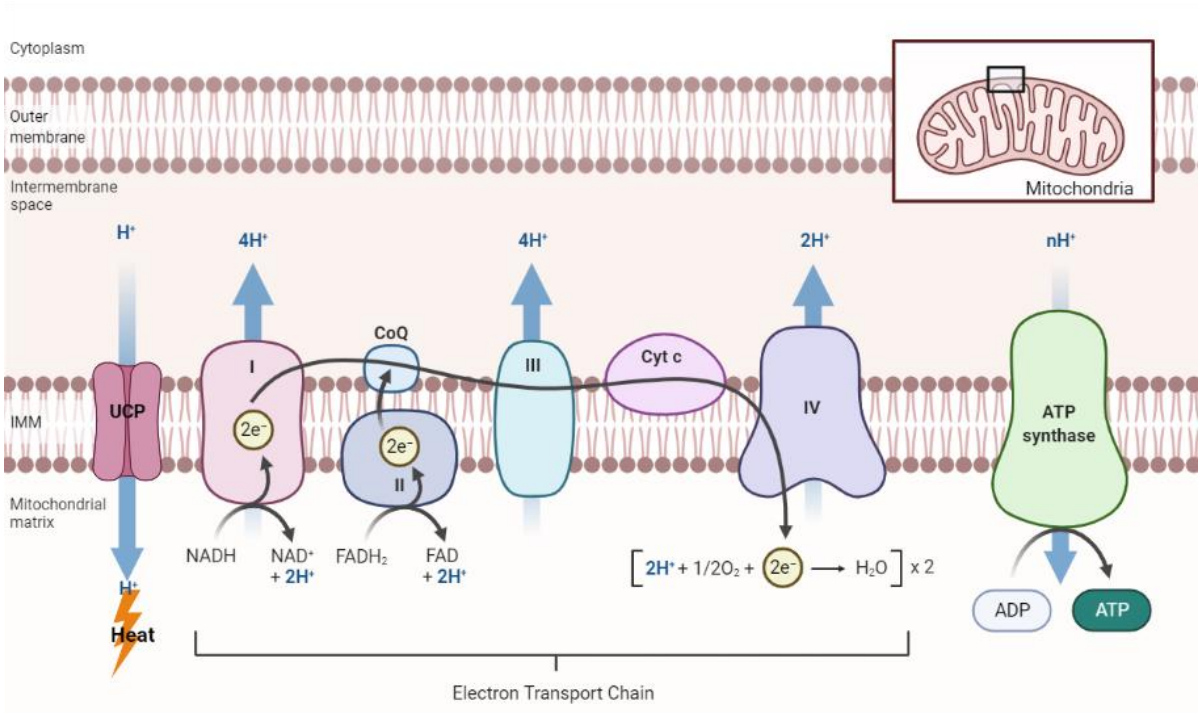

Figure 4.1 The electron transport chain and mitochondrial oxidative phosphorylation. IMM, inner mitochondrial membrane. Complexes I, III and IV pump H^+ ions into the mitochondrial intermembranous space from the mitochondrial matrix to produce a gradient of H^+ ions and subsequently, protons flow back into the mitochondrial matrix via ATP synthase to produce ATP. Uncoupled oxidative phosphorylation occurs via UCP2 which dissipates the mitochondrial protonmotive force as heat. Figure adapted from 'Electron Transport Chain' by BioRender.com (2022). Retrieved from https://app.biorender.com/biorender-templates

The NNRTIs efavirenz and rilpivirine were shown to impair beta cell function and induce beta cell apoptosis, likely through oxidative stress and mitochondrial dysfunction. Mitochondrial function and ROS generation are intertwined, as the mitochondria is the main producer of ROS but also the main target of oxidative stress injury.

We concluded in **Chapter 3** that efavirenz and rilpivirine had differential effects on mitochondrial membrane potential (Δψm), prompting the elucidation of their respective effects on the mitochondrion. While efavirenz has been linked to oxidative stress and mitochondrial toxicity through the inhibition of complex I activity in hepatocytes, the mechanism of rilpivirine-induced mitochondrial stress has not been elucidated (Blas-Garcia et al., 2010). Inhibition of the mitochondrial ATP synthase has been previously linked to an increase in Δψm; therefore, we hypothesise that rilpivirine may directly inhibit the mitochondrial ATP synthase while the complex I inhibition by efavirenz would extend to pancreatic beta cells (Formentini *et al.*, 2012; García-Aguilar & Cuezva, 2018; Sánchez-Cenizo *et al.*, 2010).

Therefore, the aim of this study was to explore the direct and indirect effects of efavirenz and rilpivirine on key regulators and indicators of mitochondrial function such as mitochondrial superoxide production, ATP production, Δψm, UCP2 expression, as well as the activity of mitochondrial complexes.

4.2 Materials and methods

4.2.1 Materials

β-Nicotinamide adenine dinucleotide, reduced dipotassium salt (NADH), fatty acid–free bovine serum albumin (BSA), potassium cyanide (KCN), ubiquinone 1 (Ub_1) were obtained from Sigma-Aldrich (Poole, UK). All other materials were obtained as described in Materials, **Chapter 2** (see 2.1).

The buffers and solutions used in this study are listed below in alphabetical order.

0.1 M Tris/MOPS buffer

0.1 M of Tris in 500 ml

Buffer was adjusted to pH to 7.4 using MOPS

0.1 M EGTA/Tris

0.1 M EGTA/Tris

Buffer was adjusted to pH to 7.4 using Tris

Hypotonic buffer (Tris)

10 mM Tris

Buffer was adjusted to pH 7.6

Mitochondrial isolation buffer

10 ml of 0.1 M Tris/MOPS

1 ml of EGTA/Tris

20 ml of 1 M sucrose.

Buffer was adjusted to a pH to 7.4

0.5 M potassium phosphate buffer

0.5 M potassium phosphate dibasic

0.5 M potassium phosphate monobasic

Buffer was adjusted to a pH of 7.5

4.2.2 Treatment protocol

In our current study, we identified the optimal concentration of efavirenz and rilpivirine to induce INS-1E cell damage, as determined in **Chapter 3**. Following cell culture as described in **Chapter 2** (see 2.2.1), INS-1E cells were exposed to DMSO (control), efavirenz (10 or 20 μM) or rilpivirine (1, 3 or 10 μM) for 2, 4, 6 or 24 hrs before assessing mitochondrial superoxide generation, changes in Δψm, cellular ATP levels and mRNA and protein expression of UCP2. Stock solution (25 mM) of efavirenz and rilpivirine solutions were prepared as per Table 1 (**Appendix I**). Working solution of efavirenz (10 or 20 μM) and rilpivirine (1, 3 or 10 μM) were prepared by diluting the stock solution in RPMI-1640 supplemented with 3% heat-inactivated FCS, as per Table 2, **Appendix II**. For direct complex I activity measurements, isolated mitochondria were exposed to DMSO (control), efavirenz (20 μM) or rilpivirine (10 μM) by adding 0.8 μL of 25 mM stock solution of efavirenz or 0.4 μL of 25 mM stock solution of rilpivirine to 1 mL of complex I activity mixture, respectively.

Following treatment protocol, mitochondrial superoxide generation (see 2.2.7.2), Δψm changes (see 2.2.8) and mRNA (see 2.2.11) and protein (see 2.2.13) expression of UCP2 were assessed as described in **Chapter 2**. Cellular ATP levels, isolation of mitochondria from INS-1E cells and measurements of mitochondrial complex I activity were assessed as follows. *In silico* predictions are also detailed below.

4.2.3 ATP assay

Principle

ATP content is important in assessing overall cellular health and mitochondrial function. We use a bioluminescent ATP assay that takes advantage of the firefly luciferase enzymatic reaction, which uses ATP from viable cells to generate photons of light that are detectable and quantifiable.

Protocol

The following protocol was established as per manufacturer's guidelines (Promega, Wisconsin, US) as well as method optimisation. INS-1E cells were seeded in opaque-walled 96-well plates at a seeding density of 1.0 x10^4 cells/well before incubating for 24 hrs at 37^{o}C and 5% CO_2 (Table 2.1). Then, cells were exposed to efavirenz (10 or 20 µM) or rilpivirine (1, 3 or 10 µM) for 24 hrs at 37^{o}C and 5% CO_2. Control wells containing medium without cells were also prepared to determine background luminescence. Following treatment protocol, the plate and its contents were equilibrated to room temperature for approximately 30 mins. Then, a volume (100 µL) of CellTiter-Glo® 2.0 Reagent (containing the firefly luciferase enzyme and substrate) equal to the volume (100 µL) of cell culture medium was added in each well. The contents were then mixed for 2 mins on an orbital shaker at 300 rpm to induce cell lysis. The plate was incubated at room temperature for 10 mins to stabilise the luminescent signal before recording luminescence with a luminometer with an integration time of 1 sec per well.

Data analysis

The luminescence background measurements were deducted from the luminescence measurements for each treatment condition. The luminescence measurements of the treated cells were expressed as % of the luminescence observed in vehicle-treated cells (control). The average of technical duplicates per treatment condition was calculated to obtain a final value.

4.2.4 *In silico* molecular docking

Chemical structures were plotted using Jmol, an open-source Java viewer for chemical structures in 3D as described in **Chapter 2** (see 2.2.14). For docking, the cryo-EM structure of mitochondrial complex I (PDB: 5LDW) and mitochondrial ATP synthase (PDB: 5FIL) was prepared for docking with UCSF Chimera (Pettersen *et al.*, 2004; Zhou *et al.*, 2015; Zhu *et al.*,

2016). Both proteins were truncated as to obtain key subunits for docking. Unguided docking of efavirenz and rilpivirine to predict binding sites was performed using SwissDock with CHARMM forcefield (Grosdidier *et al.*, 2011).

4.2.5 Assessment of mitochondrial complex I activity

Principle

Mitochondrial complex I (NADH:ubiquinone oxidoreductase) is a key enzyme for OXPHOS, resulting in ATP generation. Inhibition of this enzyme can disturb mitochondrial function and overall cellular health. To assess mitochondrial complexes activities, *in silico* 3D docking predictions were performed before measuring complex I activity in isolated mitochondria of INS-1E cells via spectrophotometric analysis. The protocol for measurements of complex I activity is detailed as follows.

Isolation of mitochondria

In our experience, seeding 1.5 x 10^6 cells per flask 3 days before the experiment results in a good yield of mitochondria (~ 2 mg of mitochondrial protein).

Mitochondria from INS-1E cells were isolated as described by Frezza *et al.*, 2007.

Following treatment protocol, the medium was removed before washing cells once with PBS. The cells were then harvested using a cell scraper in 10 mL of PBS. The INS-1E cell suspension was transferred to a 50 mL polypropylene tube. Then, 10 mL of PBS was added to the flask and the remaining cells were detached using a cell scraper. The cells were then transferred to the same 50 mL polypropylene tube used earlier to collect the cell suspension. The cells were then centrifuged at 600 x g at 4^{o}C for 10 mins. Following centrifugation, the supernatant was discarded, and cells were resuspended cells in 3 mL of ice-cold isolation buffer.

The following steps were performed at 4^{o}C to minimise activation of proteases and phospholipases. Before homogenising the cells, the glassware was precooled in ice for 5 mins before starting the procedure. The cells were homogenised by stroking the cell suspension placed in a glass potter 40 times with a Teflon pestle. The homogenate was transferred to a 50 mL polypropylene tube and centrifuged at 600 x g for 10 mins at 4^{o}C. Following centrifugation, the supernatant was collected and transferred to a 15 mL polypropylene tube and centrifuged at 7,000 x g for 10 mins at 4^{o}C. The supernatant was discarded, and the pellet was washed with 200 µL of ice-cold isolation buffer. Then the pellet was resuspended in 200 µL of ice-cold isolation buffer before transferring the suspension to a 1.5 mL microfuge tube. The homogenate

was centrifuged at 7,000 x g for 10 mins at 4ºC. The supernatant (100 µL) was discarded before resuspending the pellet containing mitochondria in the remaining supernatant using a 200 µL pipettor. The supernatant was visualised by confocal microscopy using TMRE and DAPI staining to observe the presence of nuclei debris and/or mitochondria (Figure 4.2, A). We confirm that the supernatant consisted of only nuclei debris. The mitochondrial suspension was transferred to a microfuge and stored at -80ºC. A sample of isolated mitochondria was visualised by confocal microscopy following staining with TMRE and DAPI to confirm the presence of mitochondria only (Figure 4.2, B). Isolated mitochondria were subjected to three cycles of freeze-thawing in hypotonic buffer before measuring complex I activity in order to maximise the enzymatic rates. The concentration of mitochondria was measured using a Nanodrop® Lite spectrophotometer (Thermo Fisher Scientific), with nuclease-free water as zero absorbance reference.

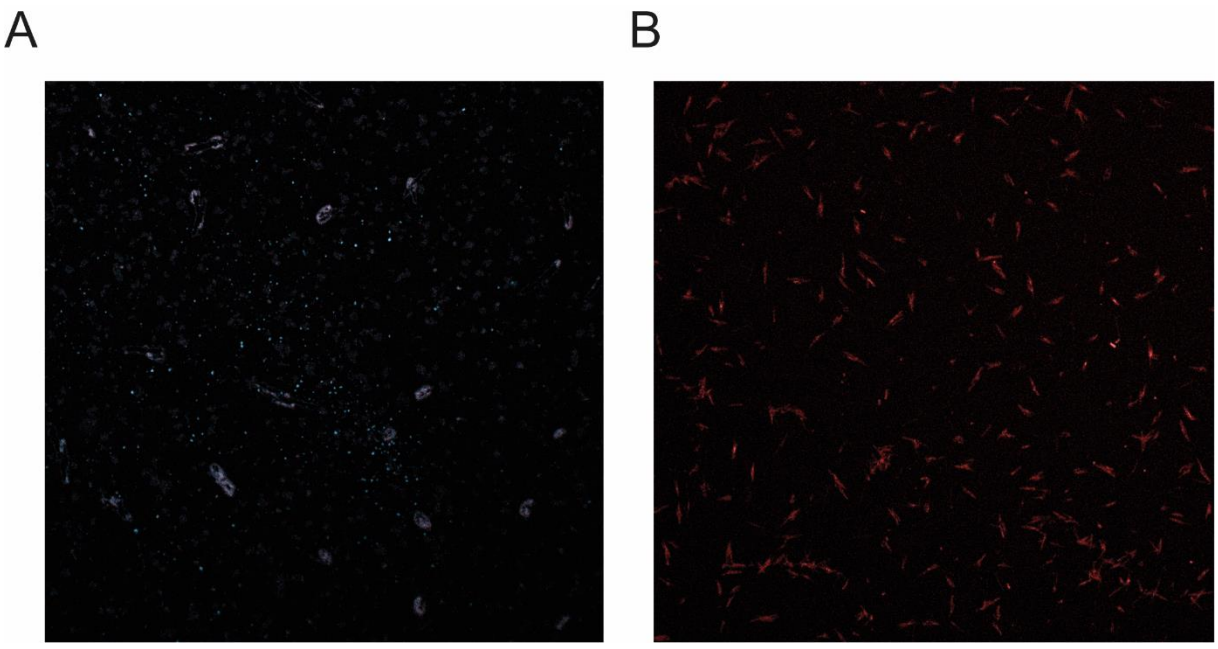

Figure 4.2 Confocal images of supernatant (A) and isolated mitochondria (B) using TMRE and DAPI staining. TMRE (red) stain mitochondria while DAPI (blue) stains nuclei. Supernatant and isolated mitochondria were stained with TMRE (100 nm) and DAPI for 20 min before visualising by confocal microscopy.

Measurements of complex I activity

To measure the direct activity of complex I, Spinazzi *et al.*'s (2012) protocol was used.

To a 1-mL cuvette, 700 µL of distilled water was added before adding 20 µg of mitochondria-enriched fractions from INS-1E cells prepared as described previously. Then 100 µL of

potassium phosphate buffer (0.5 M, pH 7.5), 60 µL of fatty acid–free BSA (50 mg ml^{-1}), 30 µL of KCN (10 mM) and 10 µL of NADH (10 mM) were added to the cuvette. The volume was adjusted to 994 µL with distilled water. This constitutes the complex I activity mixture. In parallel, a separate cuvette containing the same quantity of reagents and sample but with the addition of 10 µL of 1 mM rotenone solution was prepared. Then, the components were mixed by covering the cuvette with Parafilm and the baseline was immediately read at 340 nm for 2 mins. Then, the reaction was started by adding 6 µL of ubiquinone$_1$ (10 mM), mixing the components and then immediately reading the absorbance at 340 nm for 2 mins. The baseline was deducted from the absorbance before calculation complex I activity as nmol min^{-1} mg^{-1} of protein according to the following equation:

$$Complex\ I\ activity\ (nmol\ min-1\ mg-1) = \frac{\Delta\ Absorbance/min \times 1{,}000}{extinction\ coefficient\ (6.2) \times volume\ of\ sample\ used\ in\ mL) \times (sample\ protein\ concentration\ in\ mg\ mL-1)}$$

4.3 Results

4.3.1 Efavirenz and rilpivirine increase mitochondrial superoxide generation throughout a 24-hour time frame

The mitochondrion is an important source of ROS in most mammalian cells including pancreatic beta cells, but it is also a vulnerable target for oxidative stress. Here, we assessed mitochondrial superoxide generation in INS-1E cells exposed to efavirenz or rilpivirine for 2, 4, 6 or 24 hours by flow cytometric analysis. Both efavirenz and rilpivirine significantly increased mitochondrial superoxide generation in INS-1E cells at a 2, 4, 6 and 24-hour time point (Figure 4.3). Both efavirenz and rilpivirine caused a continuous and sustained generation of mitochondrial superoxide during the full 24-hour time course (Figure 4.3). Overall, efavirenz gradually increased mitochondrial superoxide generation, doubling superoxide generation for each time point (Figure 4.3). Rilpivirine profoundly increased mitochondrial superoxide generation in INS-1E cells, as it reached approximately 200-250% at each time point (Figure 4.3).

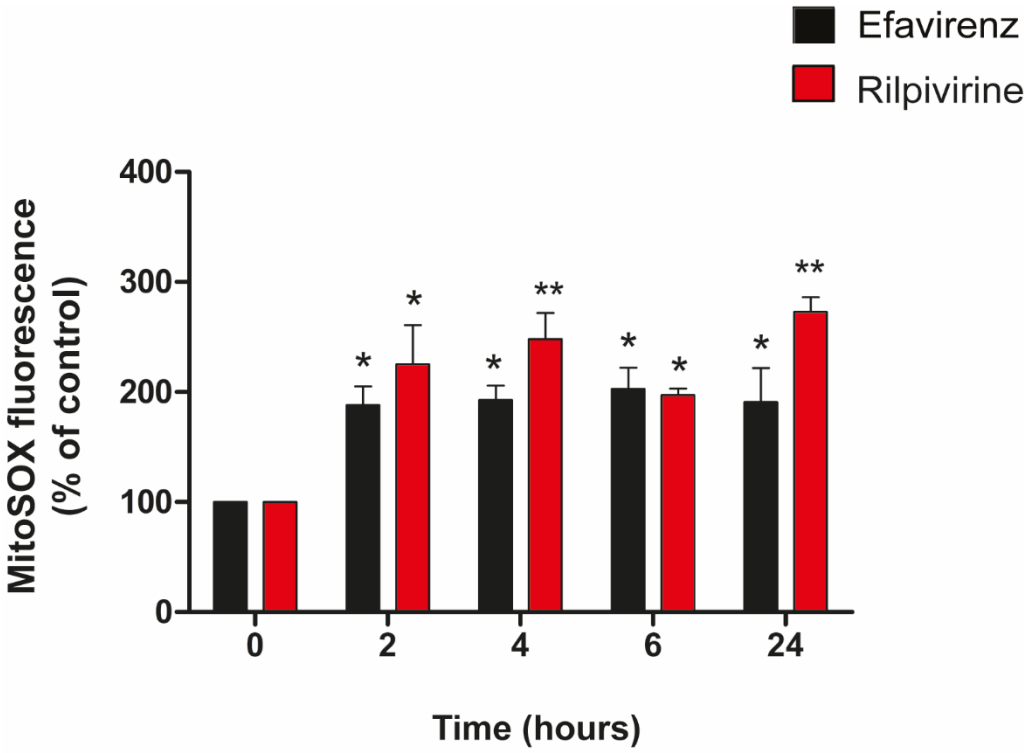

Figure 4.3 Efavirenz and rilpivirine increase mitochondrial superoxide generation in INS-1E cells. INS-1E cells were exposed to efavirenz (20 µM) or rilpivirine (10 µM) for 2, 4, 6 or 24 hrs before quantifying superoxide formation using the MitoSOX probe followed by flow cytometric analysis. MitoSOX fluorescence is proportional to the levels of mitochondrial superoxide. Data are expressed as mean ± SEM from $n = 3$ independent experiments. Statistically significant differences were determined using Kruskal-Wallis with Dunn's post hoc test where $p < 0.05$ was considered as significant. * $p < 0.05$, ** $p < 0.01$ significantly different from vehicle-treated control cells.

4.3.2 Efavirenz and rilpivirine disrupt Δψm throughout a 24-hour time frame

To further understand the efavirenz- and rilpivirine-induced disruptions in Δψm observed in **Chapter 3**, we conducted a time-course experiment to monitor changes in Δψm following exposure to efavirenz or rilpivirine for 2, 4, 6 or 24 hours (Figure 4.4). Interestingly, efavirenz caused a biphasic effect on Δψm changes in INS-1E cells. A short-term (2, 4 and 6 hours) exposure to efavirenz caused a significant increase in mitochondrial TMRE uptake, peaking at 2 hours to 150% before dropping to 60% at 24 hours. Rilpivirine caused a significant increase in Δψm compared to vehicle-treated INS-1E cells throughout the 24-hour time course, reaching a peak at 2 hours (~300%) (Figure 4.4).

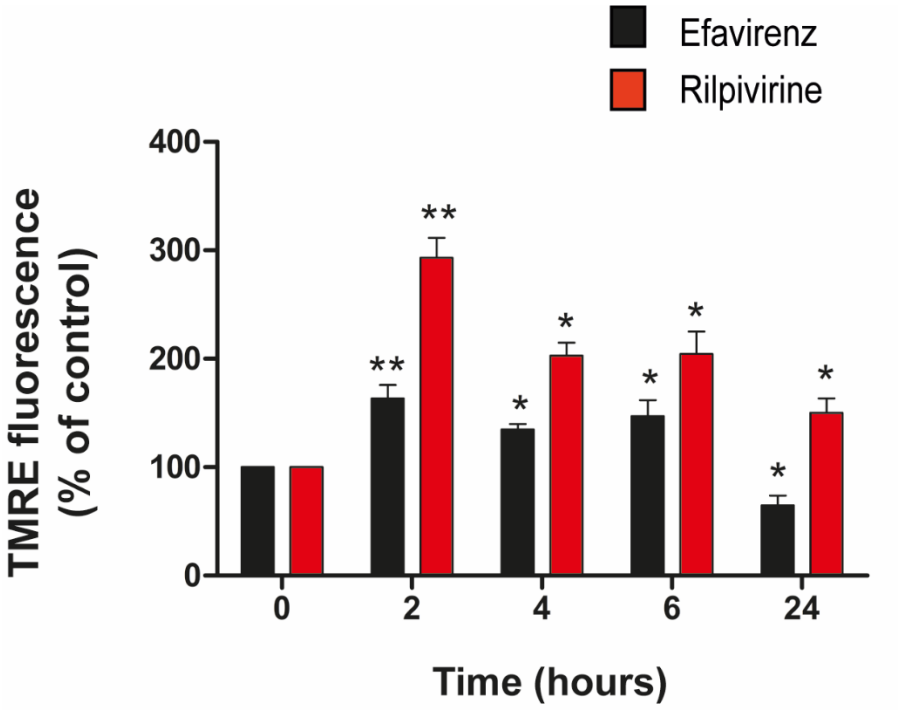

Figure 4.4 Efavirenz causes a biphasic effect on Δψm changes while rilpivirine increases Δψm in INS-1E cells. INS-1E cells were exposed to efavirenz (20 µM) or rilpivirine (10 µM) for 2, 4, 6 or 24 hrs before assessing changes in Δψm using the TMRE probe followed by flow cytometric analysis. TMRE fluorescence is proportional to Δψm. Data are expressed as mean ± SEM from *n* = 3 independent experiments. Statistically significant differences were determined using Kruskal-Wallis with Dunn's post hoc test where $p < 0.05$ was considered as significant. * $p < 0.05$, ** $p < 0.01$ significantly different from vehicle-treated control cells.

4.3.3 Efavirenz and rilpivirine decrease cellular ATP levels

ATP is produced by the ETC in the mitochondria. ATP production is an assessment of mitochondrial function, beta cell function and overall cellular health. Therefore, we measured cellular ATP content in INS-1E cells exposed to efavirenz (10 or 20 µM) or rilpivirine (1, 3 or 10 µM) for 24 hours (Figure 4.5).

Efavirenz (20 µM) and rilpivirine (10 µM) caused a significant drop in cellular ATP levels in INS-1E cells, suggesting that rilpivirine had a more potent effect on reducing cellular ATP levels (Figure 4.5).

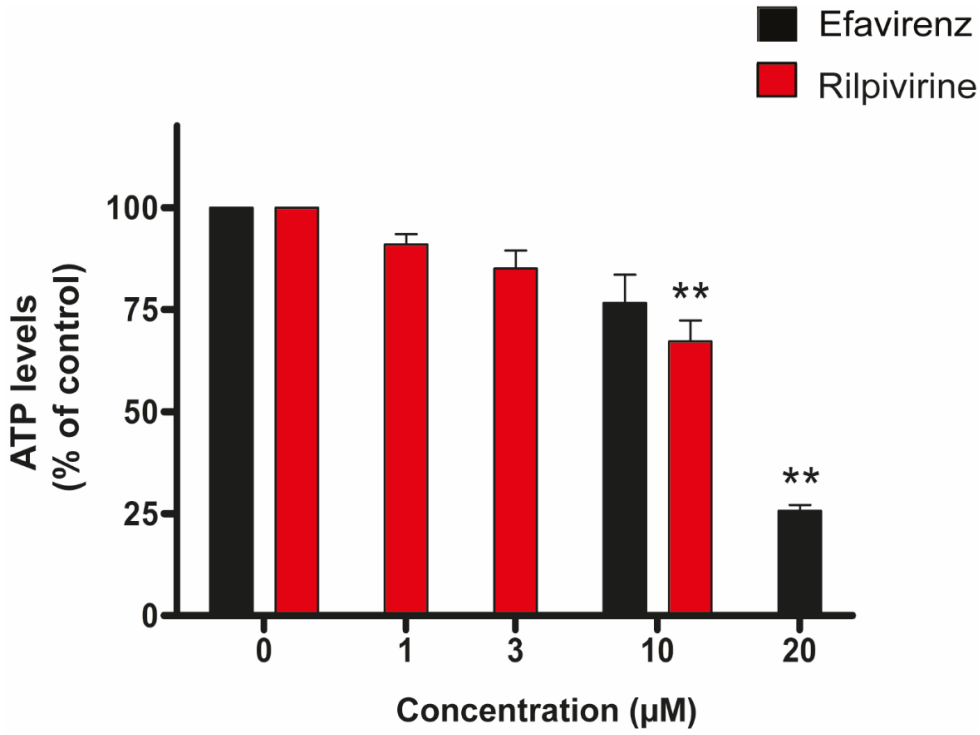

Figure 4.5 Efavirenz and rilpivirine decrease cellular ATP levels in INS-1E cells. INS-1E cells were exposed to efavirenz (10 or 20 μM) or rilpivirine (1, 3 or 10 μM) for 24 hrs before quantifying cellular ATP levels using the luciferase reaction followed by luminometry. Data are expressed as mean ± SEM from *n* = 3 independent experiments. Statistically significant differences were determined using Kruskal-Wallis with Dunn's post hoc test where $p < 0.05$ was considered as significant. ** $p < 0.01$, significantly different from vehicle-treated control cells.

4.3.4 Effects of efavirenz and rilpivirine on mitochondrial complex I and ATP synthase activity

Disturbances in the activity of mitochondrial complexes can collapse the mitochondrial machinery, reflected by disruptions in Δψm, increases in mitochondrial ROS production and reductions in ATP levels. Therefore, we investigated if efavirenz and rilpivirine affect the activity of two key mitochondrial enzymes: complex I (Figure 4.6) and ATP synthase (Figure 4.7).

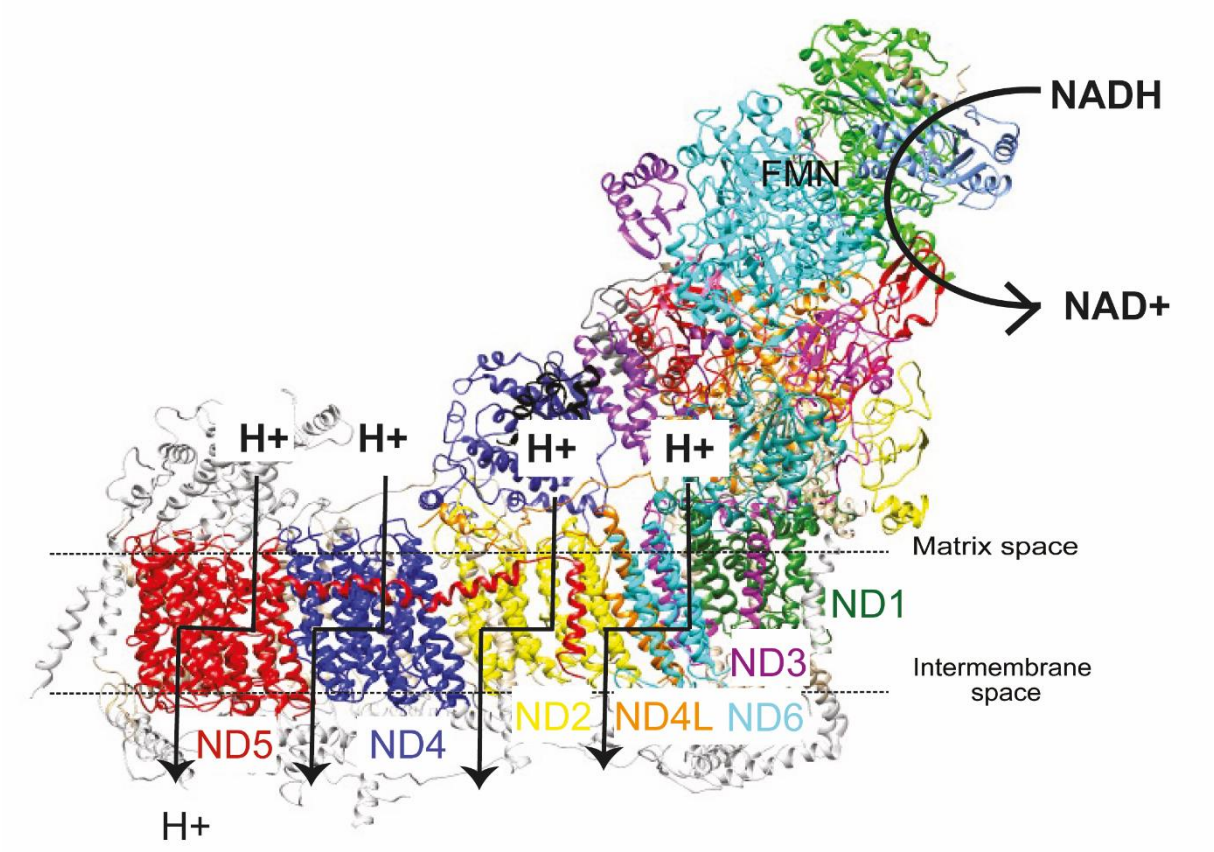

Figure 4.6 Annotated Cryo-EM structure of mitochondrial complex I visualised using UCSF Chimera. Membrane subunits constituting complex I include ND5, ND4, ND2, ND3, ND4L, ND6 and ND1.

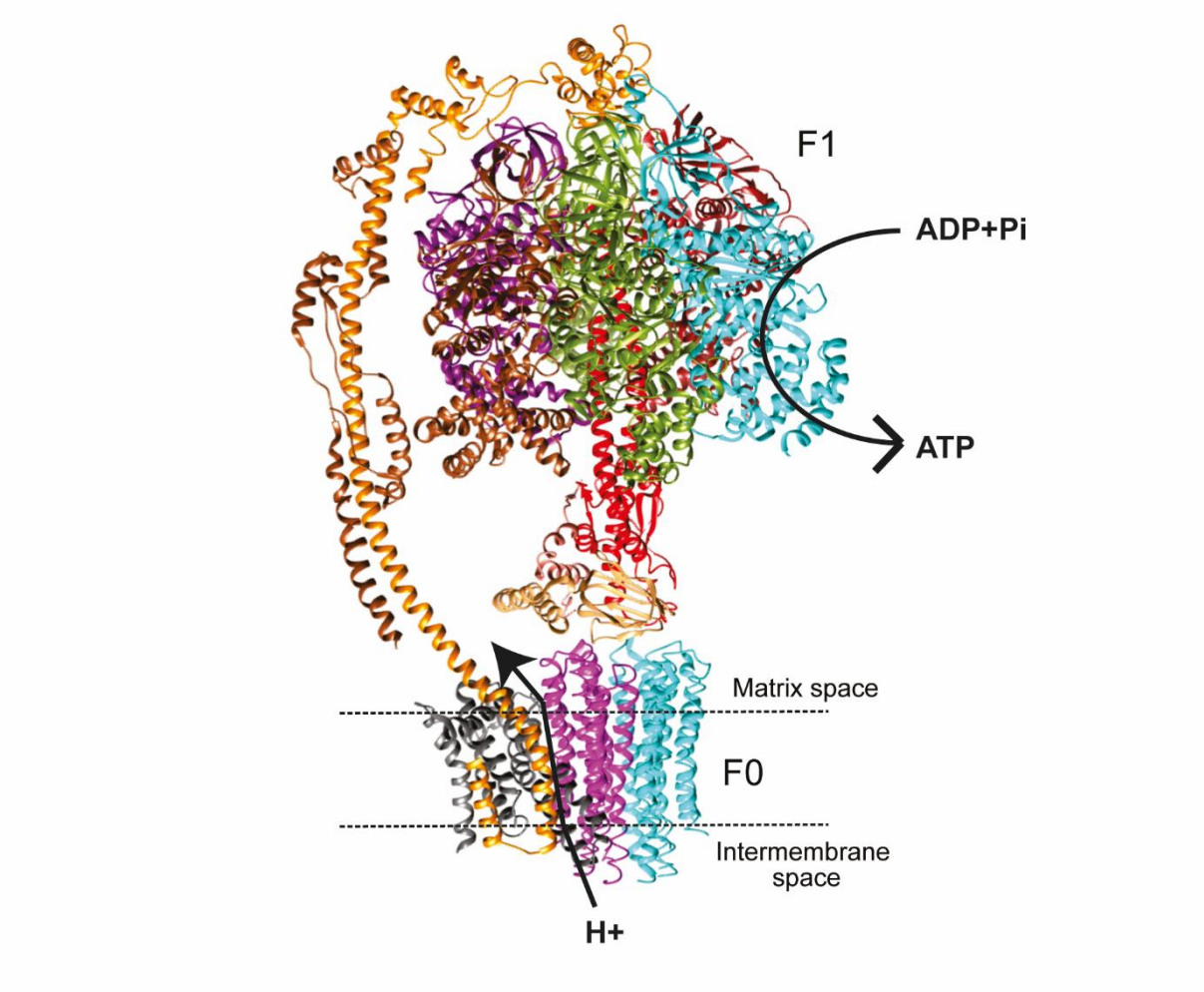

Figure 4.7 Annotated Cryo-EM structure of mitochondrial ATP synthase visualised using UCSF Chimera. ATP synthase contains two subunits, including the membrane subunit F0.

To do so, we examined the predicted binding affinity of efavirenz and rilpivirine to the mitochondrial complex I (Figure 4.8, Table 4.1 and Table 4.2) and ATP synthase preliminarily by *in silico* molecular docking (Figure 4.9 and Table 4.3).

4.3.4.1 *In silico* predictions

The docking of mitochondrial complex I against efavirenz exhibited a favourable binding to the NADH-ubiquinone oxidoreductase chain 5 protein (ND5), as shown by the interaction's estimated Gibbs free energy (ΔG) score (-7.63 kcal mol^{-1}) and Full fitness score (-1330.74 kcal mol^{-1}) (Table 4.1). Although efavirenz has the ability to bind to NADH-ubiquinone oxidoreductase chain 4 protein (ND4), NADH-ubiquinone oxidoreductase chain 2 protein (ND2), NADH-ubiquinone oxidoreductase chain 4L protein (ND4L) plus NADH-ubiquinone oxidoreductase chain 6 protein (ND6) and NADH-ubiquinone oxidoreductase chain 3 protein

(ND3) plus NADH-ubiquinone oxidoreductase chain 1 protein (ND1), efavirenz exhibited a higher binding affinity to ND5 compared to other membrane subunits constituting complex I (Table 4.1).

Table 4.1 Full fitness and Gibbs free energy (ΔG) scores for docking of efavirenz to membrane subunits of mitochondrial complex I. The more negative the Gibbs Free energy (ΔG) value, the more exothermic the proposed interaction. Full fitness scores predicted by SwissDock indicate that lower values represent binding modes which are more favourable than higher scoring numbers. Efavirenz showed most favourable interaction with ND5 followed by ND2, ND4, ND4L+ND6, and ND3+ND1.

Subunit	Full fitness (kcal mol^{-1})	ΔG (kcal mol^{-1})
ND5	-1330.74	-7.63
ND4	-906.66	-6.92
ND2	-727.07	-7.00
ND4L+ND6	-715.95	-6.92
ND3+ND1	-815.96	-6.77

Interestingly, rilpivirine has a slightly lower binding affinity to ND5 compared to efavirenz, as reflected by its ΔG (-7.58 kcal mol^{-1}) (Table 4.2). Rilpivirine has a more negative ΔG to both ND2 and ND4L+ND6 subunits of mitochondrial complex I, suggesting a higher binding affinity to these subunits (Table 4.2).

Table 4.2 Full fitness and Gibbs free energy (ΔG) scores for docking of rilpivirine to membrane subunits of mitochondrial complex I. The more negative the Gibbs Free energy (ΔG) value, the more exothermic the proposed interaction. Full fitness scores predicted by SwissDock indicate that lower values represent binding modes which are more favourable than higher scoring numbers. Rilpivirine showed more exothermic interaction with ND2 followed by ND4L+ND6, ND5 and ND3+ND1.

Subunit	Full fitness (kcal mol^{-1})	ΔG (kcal mol^{-1})
ND5	-1585.83	-7.58
ND4	-1167.98	-7.51
ND2	-986.93	-7.69
ND4L+ND6	-987.44	-7.67
ND3+ND1	-1084.41	-7.52

There were 256 predicted binding poses for efavirenz docked in the ND5 subunit, arranged in 31 clusters. The most favourable binding pose of efavirenz (Figure 4.8, D) resides in the potential binding pocket of ND5 shown in Figure 4.8, B. There were 256 predicted binding poses for rilpivirine docked in the ND5 subunit, arranged in 38 clusters. The most favourable

binding pose of rilpivirine (Figure 4.8, E) resides in the potential binding pocket of ND5 shown in Figure 4.8, C.

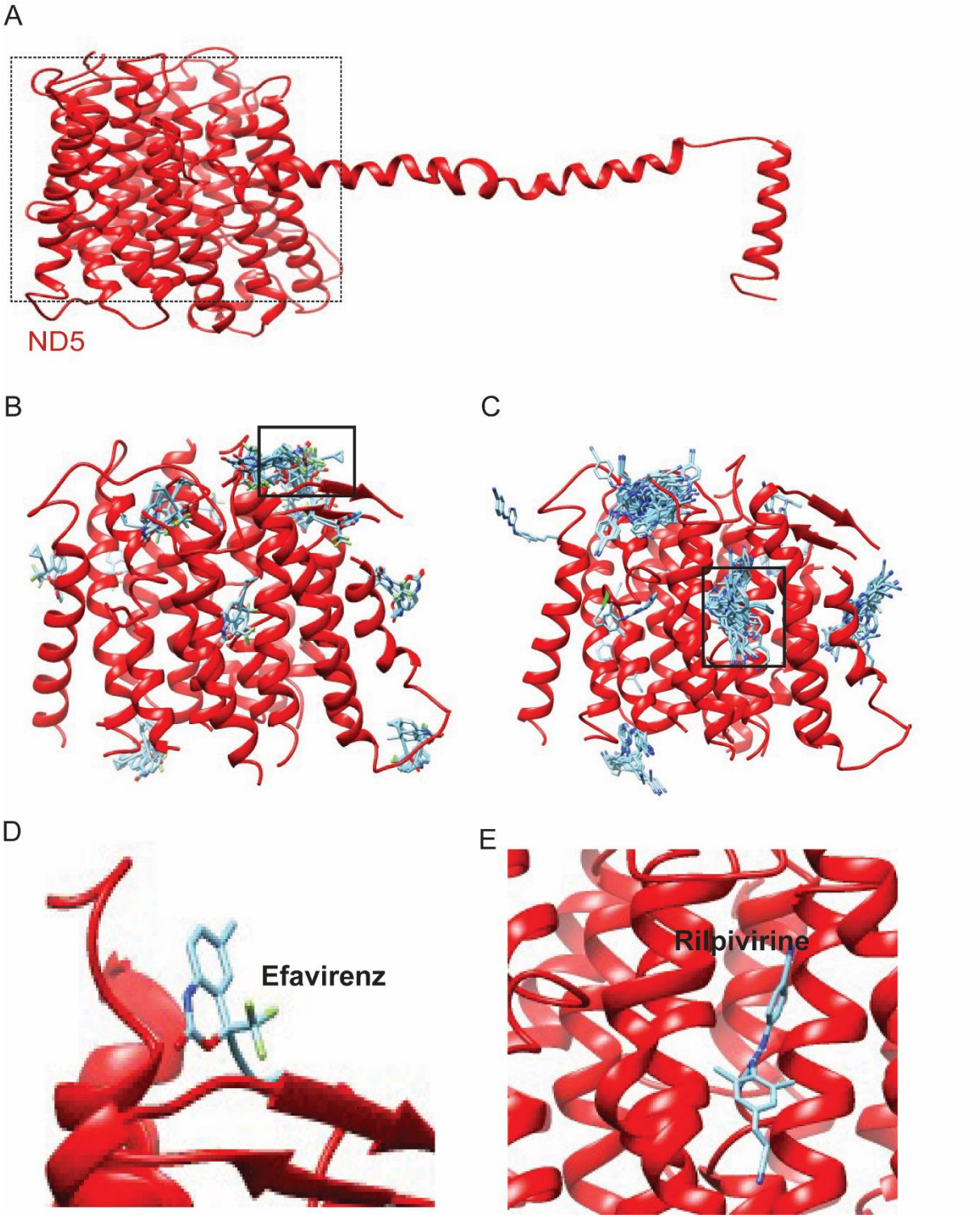

Figure 4.8 Efavirenz and rilpivirine are predicted to bind to different sites in the ND5 subunit of mitochondrial complex I. (A) View of the ND5 region. (B) Close-up view of ND5 and all binding poses of efavirenz to ND5 as predicted by SwissDock. (C) Close-up view of ND5 and all binding poses of rilpivirine to ND5 as predicted by SwissDock. (D) Close-up view of the favourable efavirenz binding site (ΔG = -7.63 kcal mol^{-1}) in the ND5 region

as predicted by SwissDock. (E) Close-up view of the favourable rilpivirine binding site (ΔG = -7.58 kcal mol^{-1}) in the ND5 region as predicted by SwissDock. Black square represents binding site pocket for the most favourable binding pose.

The docking of the mitochondrial ATP synthase against rilpivirine exhibited a favourable binding to the F_0 baseplate subunit, as shown by the estimated ΔG score (-8.54 kcal mol^{-1}) and Full fitness score (-2619.98 kcal mol^{-1}) (Table 4.3). The estimated ΔG score of the ATP synthase-rilpivirine complex is more negative than that of ATP synthase-efavirenz complex, suggesting a higher binding affinity of rilpivirine to the ATP synthase compared to efavirenz (Table 4.3).

Table 4.3 Full fitness and Gibbs free energy (ΔG) scores for docking of efavirenz and rilpivirine to the F_0 region of mitochondrial ATP synthase. The more negative the Gibbs Free energy (ΔG) value, the more exothermic the proposed interaction. Full fitness scores predicted by SwissDock indicate that lower values represent binding modes which are more favourable than higher scoring numbers. The docking of the mitochondrial ATP synthase against rilpivirine exhibited a favourable binding to the F0 region, as shown by the estimated Gibbs free energy (ΔG) score (-8.54 kcal.mol^{-1}). The estimated ΔG score of the ATP synthase (F0 region)-rilpivirine complex is more negative than that of ATP synthase (F0 region)- efavirenz complex, suggesting a higher binding affinity of rilpivirine to the ATP synthase compared to efavirenz.

Drug	Full fitness (kcal mol^{-1})	ΔG (kcal mol^{-1})
Efavirenz	-2348.71	-6.55
Rilpivirine	-2619.98	-8.54

We wanted to visualise the predicted binding sites of efavirenz and rilpivirine to the F0 region of the mitochondrial ATP synthase (Figure 4.9). There were 256 predicted binding poses for efavirenz docked in the F_0 region, arranged in 34 clusters (Figure 4.9, D). The most favourable binding pose (Figure 4.9, F) resides in the potential binding pocket in Figure 4.9, D, in the lower end of the central cavity of the F_0 region.

Rilpivirine has 256 predicted binding poses in the F0 region, arranged in 42 clusters (Figure 4.9, C) and has several different binding sites within the central cavity of the F_0 region. The most favourable binding pose of rilpivirine resides in the centre of the central cavity of the F_0 region of the ATP synthase (Figure 4.9, C and E).

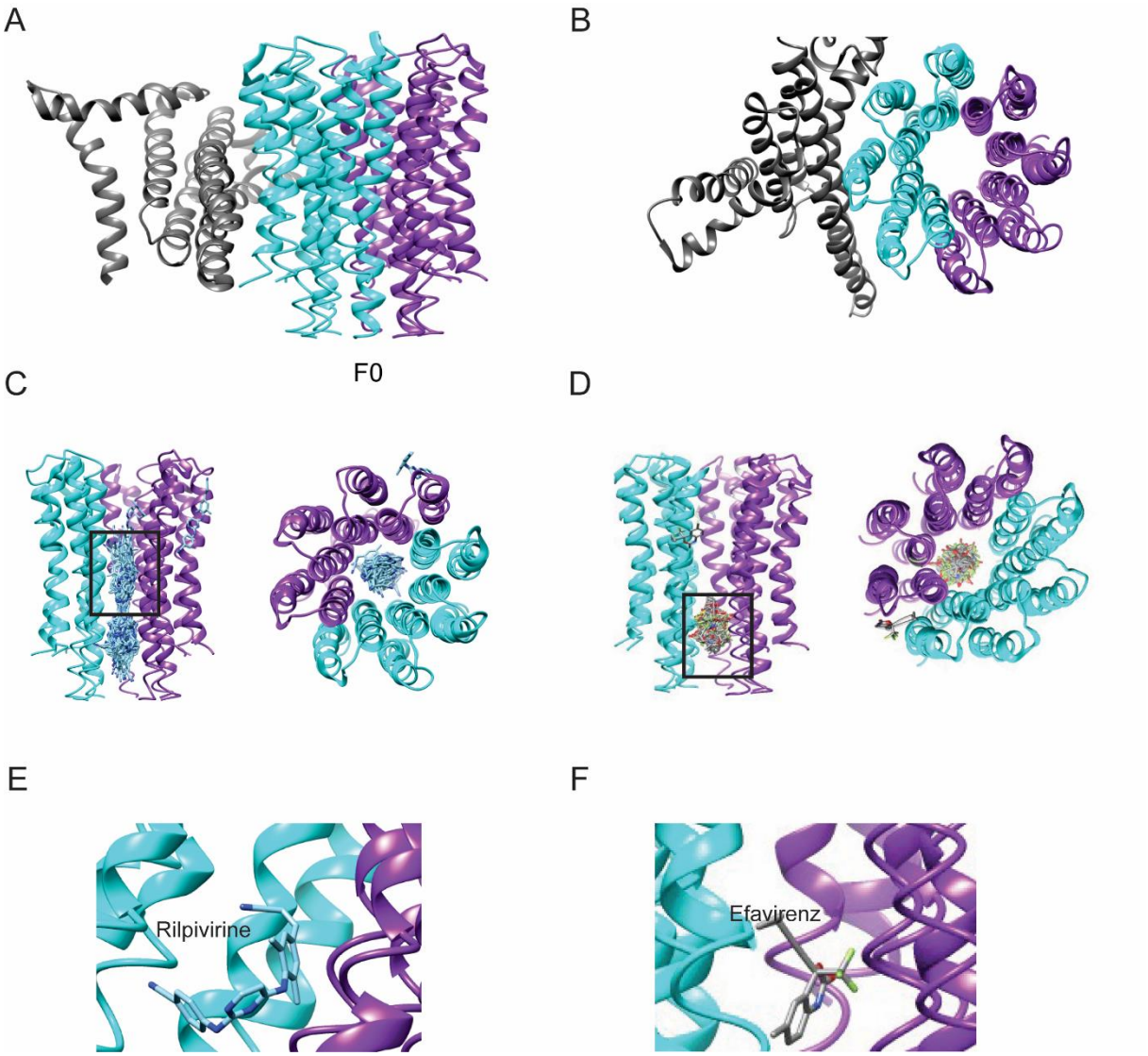

Figure 4.9 Binding predictions of efavirenz and rilpivirine to the mitochondrial ATP synthase. (A) Side-on view of the F0 region visualised using UCSF Chimera. (B) Top-down view of the F0 region visualised using UCSF Chimera. (C) Binding poses of rilpivirine in the central cavity of the F0 region from the side (left) and top-down (right) view as predicted by SwissDock. (D) Binding poses of efavirenz in the central cavity of the F0 region from the side (left) and top-down (right) view as predicted by SwissDock. (E) Close-up view of the predicted rilpivirine binding site (ΔG = -8.54 kcal mol^{-1}) in the F0 region as predicted by SwissDock. (F) Close-up view of the predicted efavirenz binding site (ΔG = -6.55 kcal mol^{-1}) in the F0 region as predicted by SwissDock. Rilpivirine has a stronger binding affinity to mitochondrial ATP synthase in comparison to efavirenz. Black square represents binding site pocket for most favourable binding pose.

4.3.4.2 Mitochondrial complex I activity measurements

To confirm the molecular docking predictions, we assessed the direct effects of efavirenz or rilpivirine on complex I activity in isolated mitochondria from INS-1E cells (Figure 4.10). To do so, isolated mitochondria were treated with efavirenz (20 µM) or rilpivirine (10 µM) before immediate analysis. Rilpivirine exhibited a slight increase in the activity of complex I, however, statistical significance was not reached in comparison to vehicle-treated control isolated mitochondria of INS-1E cells. In contrast, as predicted, we observed a statistically significant inhibition of complex I activity (~75%) following treatment with efavirenz in isolated mitochondria of INS-1E cells (Figure 4.10).

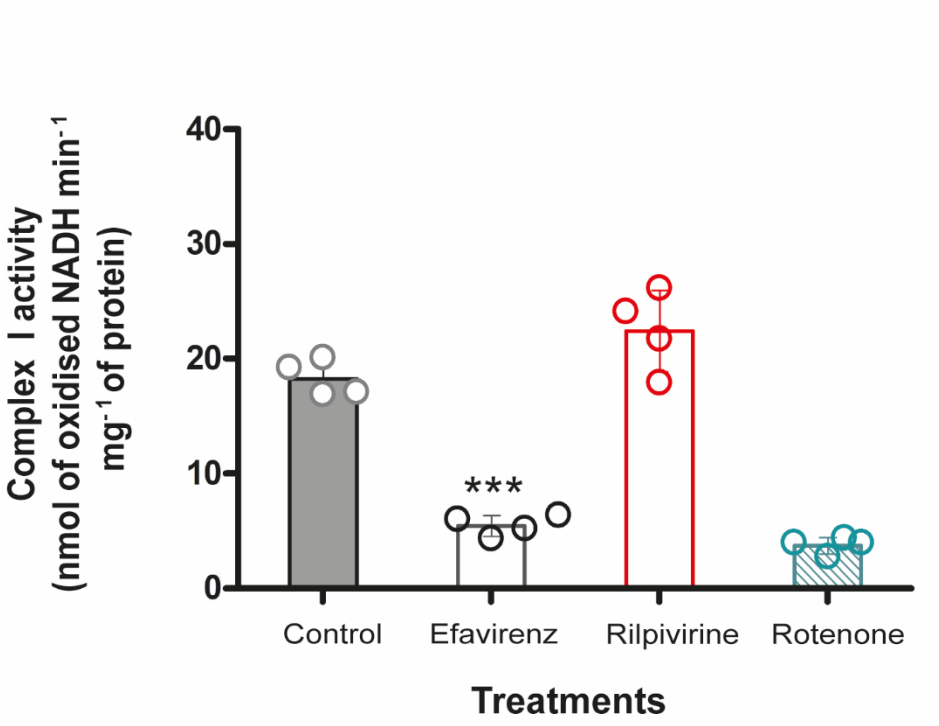

Figure 4.10 Efavirenz inhibits complex I activity in isolated mitochondria of INS-1E cells. Mitochondria were isolated from INS-1E cells and exposed to efavirenz (20 µM) or rilpivirine (10 µM) before immediate analysis by spectrophotometry to assess mitochondrial complex I activity. Rotenone (10 µM) served as a positive control. Dots represent individual data points from n = 4 independent experiments and the histograms represent mean ± SD. Statistically significant differences were determined using one-way ANOVA with Bonferroni's post hoc test where $p < 0.05$ was considered significant. *** $p < 0.001$, significantly different from vehicle-treated control groups.

4.3.5 Efavirenz, but not rilpivirine, upregulates the expression UCP2

UCP2, by virtue of its mitochondrial proton leak activity and consequent negative effect on ATP production, impairs GSIS in beta cells (Zhang *et al.*, 2001). We have previously shown that ATP production (Figure 4.5) and GSIS (**Chapter 3**) were hindered in INS-1E cells exposed

to efavirenz or rilpivirine for 24 hours. Therefore, we investigated whether UCP2 mediated, at least partially, the decreases in insulin secretion from INS-1E cells. To do so, we exposed INS-1E cells to efavirenz (20 µM) or rilpivirine (10 µM) for 24 hours before measuring mRNA and protein expression of UCP2.

Efavirenz significantly increased the mRNA expression of UCP2 by nearly two-fold (Figure 4.11, A). Fluorescent immunocytochemical analysis revealed that efavirenz increased UCP2 protein expression by nearly four-fold in INS-1E cells, as demonstrated by the increased fluorescence of UCP2 (Figure 4.11, B). There was an increasing trend in UCP2 mRNA expression in rilpivirine (10 µM)-treated cells, however, statistical significance was not reached ($p = 0.07$), and these effects were not seen in the context of protein expression.

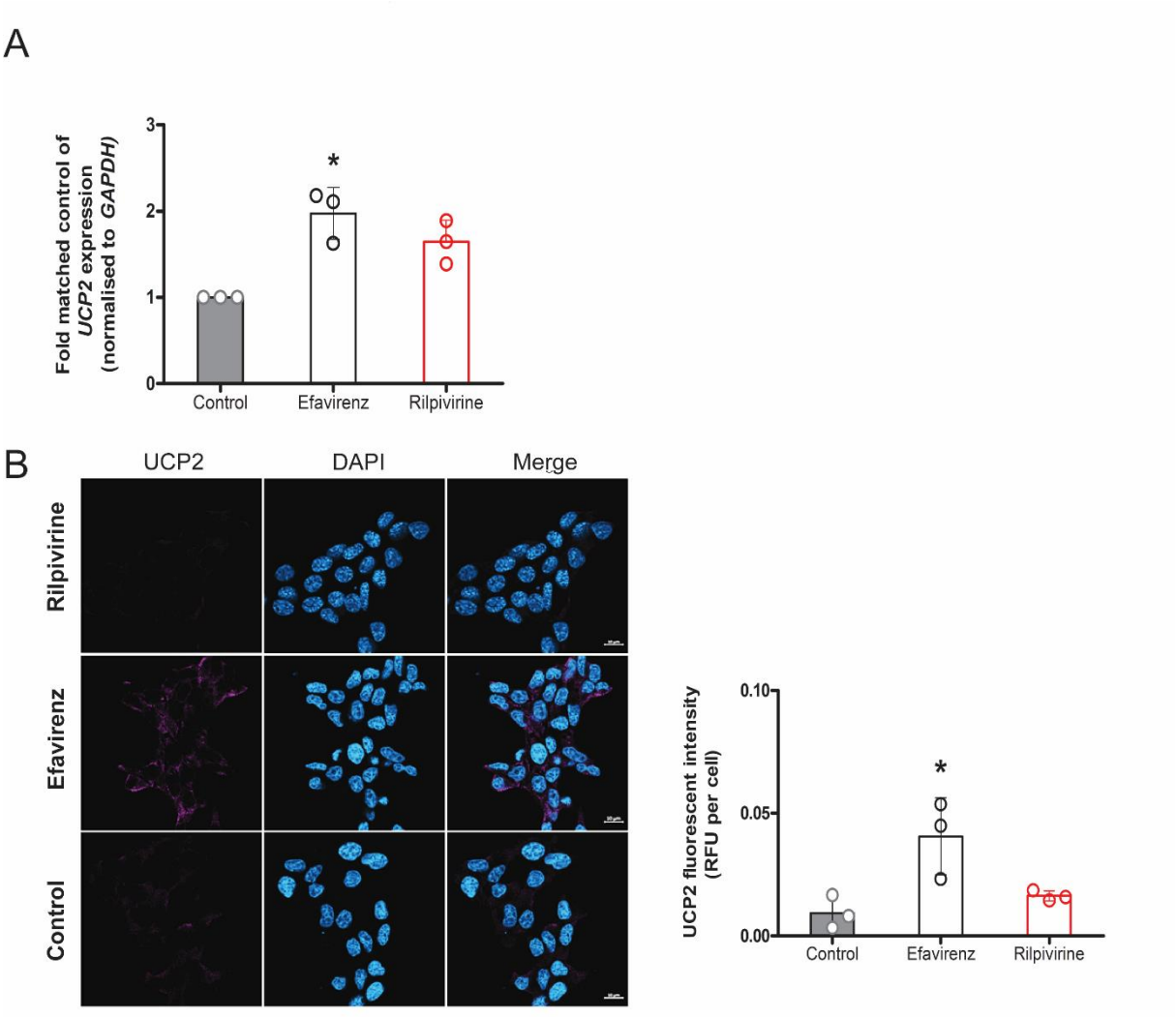

Figure 4.11 Efavirenz increases UCP2 mRNA and protein expression in INS-1E cells. INS-1E cells were exposed to efavirenz (20 µM) or rilpivirine (10 µM) for 24 hrs before quantifying UCP2 mRNA expression using RT-qPCR (A) and visualising (left) and quantifying (right) UCP2 expression in INS-1E cells by immunocytochemical analysis (B) (Scale bar, 10 µm). The fluorescence intensity of UCP2 protein expression (purple fluorescence) was measured using ImageJ and normalised to number of cells (DAPI positive nuclei) (blue fluorescence). Dots

represent individual data points from n = 3 independent experiments (3-5 technical replicates for ICC) and the histograms represent mean ± SD. Statistically significant differences were determined using Kruskal-Wallis with Dunn's post hoc test for mRNA expression or Student's t-test for protein levels where $p < 0.05$ was considered as significant. * $p < 0.05$, significantly different from vehicle-treated control groups.

4.4 Discussion

The mitochondrion, the 'powerhouse' of the cell, generates ATP predominately via OXPHOS complexes during which electrons are transported and a proton gradient is generated across the inner mitochondrial membrane to drive ATP synthesis (Sha *et al.*, 2020). Given the importance of this organelle, mitochondrial dysfunction is a central contributor to beta cell dysfunction and failure.

In light of our current observations of disruptions in Δψm, increases in mitochondrial superoxide production and a drop in ATP levels following exposure to efavirenz and rilpivirine point to a certain level of dysfunction within the respiratory chain that compromises the functioning of the mitochondria in INS-1E cells. Complex I is the major entry point for electrons of the ETC and is believed to play a central role in energy metabolism and superoxide ($O_2^{\bullet-}$) generation. Efavirenz was previously shown to directly inhibit complex I in isolated liver mitochondria (Blas-García *et al.*, 2010). Here, we show that this inhibition is extended to beta cells as efavirenz directly inhibited complex I activity by approximately 75% in isolated mitochondria of INS-1E cells. Furthermore, we show, for the first time the most likely binding site of efavirenz to complex I. Even though our molecular docking studies predicted that efavirenz may bind to several transmembrane subunits, efavirenz most likely binds to the ND5 membrane subunit of complex I as reflected by its higher binding affinity to ND5 compared to other subunits. Therefore, we postulate that efavirenz would almost certainly obstruct the flow of the H^+ proton to the intermembrane space through the ND5 subunit, hence inhibiting complex I activity.

Previous reports suggest that an inhibition of complex I may result in decreased Δψm and reduced proton-driven ATP synthesis (Kilbride *et al.*, 2021; Vial *et al.*, 2019). Our data show that efavirenz drastically reduced cellular ATP levels in INS-1E cells, likely to be a consequence of the inhibition of complex I and mitochondrial depolarisation induced by efavirenz following long-term (24-hour) exposure. It also seems fair to assume that a direct inhibition of complex I would result in a consistent reduction in Δψm throughout a 24-hour time period since several reports stated that the later effect accompanies the former (Li *et al.*,

2003). Although this is true following long-term exposure to efavirenz, as efavirenz caused mitochondrial depolarisation (*i.e.*, reduced Δψm) in INS-1E cells treated for 24 hours, exposure to efavirenz for 2, 4 and 6 hours resulted in mitochondrial hyperpolarisation (*i.e.*, increased Δψm). A possible explanation requires the in-depth familiarisation with the effects of complex I inhibition on Δψm. Rotenone, at low concentrations, was shown not only to inhibit complex I by approximately ~75% but also consistently hyperpolarise the mitochondria following a 4-hour incubation period in the 143B human cell line (Barrientos & Moraes, 1999). Mitochondrial depolarisation was only achieved when 143B cells were exposed to low concentrations of rotenone for 48 hours (Barrientos & Moraes, 1999). These findings are consistent with our findings, since efavirenz inhibited mitochondrial complex I activity by approximately 75% and caused mitochondrial hyperpolarisation in INS-1E incubated with efavirenz for up to 6 hours. Mechanistically, as a result of inhibited complex I activity and subsequent decreased electron transport, the rate of H^+ ion delivery to the intermembrane space should be decreased. However, alterations in ionic homeostasis may produce an increase in that rate or a decrease in the removal of the H^+ ions from the intermembrane space, inducing the observed efavirenz-mediated hyperpolarisation. When cells lose ion homeostasis, this scenario could be reversed, producing a drop in the $\Delta\psi_m$ (Barrientos & Moraes, 1999). This could explain the drop in Δψm in INS-1E cells treated with efavirenz for 24 hours. Another possible aggravator for the loss of Δψm observed in INS-1E cells exposed to efavirenz for 24 hours involves UCP2. We show, for the first time, that the mRNA and protein expression of UCP2 was upregulated in INS-1E cells exposed to efavirenz for 24 hours. Previous findings report that the glucose (20 mM)-stimulated mitochondrial membrane hyperpolarization was reduced in beta cells overexpressing UCP2, providing a potential mechanism explaining the drop in Δψm observed after long-term exposure to efavirenz (Chan *et al.*, 2001b). Additionally, UCP2 overexpression was shown to reduce ATP production in beta cells (Chan *et al.*, 2001b). In relation to our data, UCP2 overexpression could have worsened the depletion in ATP observed in INS-1E cells exposed to efavirenz.

Our results also demonstrate that mitochondrial superoxide formation is increased in INS-1E cells exposed to efavirenz and rilpivirine. Complex I is considered as the main site of mitochondrial superoxide formation where electrons leaks and single electrons react with oxygen, generating superoxide anions. Inhibition of complex I can result in increased mitochondrial superoxide formation by increasing the formation of ubisemquinone, the primary electron donor in mitochondrial superoxide generation (Heinz *et al.*, 2017; Li *et al.*, 2003). Efavirenz increased mitochondrial superoxide generation during mitochondrial

hyperpolarisation, as well as depolarisation in INS-1E cells. As previously described, oxidative stress caused by ROS can cause mitochondrial depolarisation and subsequent impairment of OXPHOS (Park *et al.*, 2011). Mitochondrial complex I activity is readily restricted by oxidative damage as shown both in *in vivo* and *in vitro* models (Nicholls, 2002). This would suggest that the efavirenz-mediated increase in mitochondrial superoxide formation in INS-1E cells was probably responsible for the mitochondrial depolarisation observed at 24 hours, giving insight into a vicious cycle starting with a direct inhibition of complex I which further compromises the mitochondrial and cellular function, which may surpass cellular antioxidant and beta cell survival capacity. This would only lead to further aggravation of cellular function and threatening the cellular capacity of beta cells.

On the other hand, previous findings have observed that the high magnitude of Δψm also raises the possibility of increased formation of superoxide and H_2O_2 in mitochondria of beta cells (Gerencser, 2018). Indeed, increased Δψm leads to increased ROS production from mitochondrial complex III, the cell's chief superoxide (O^2)-generating source (Bleier & Dröse, 2013). This is consistent with our data indicating that rilpivirine-mediated mitochondrial hyperpolarization may be upstream of superoxide formation, and hence the cause of increased oxidative stress in INS-1E cells. Our results indicate that rilpivirine increased mitochondrial superoxide production in INS-1E following a 24-hour time course experiment suggesting that rilpivirine increases mitochondrial ROS generation in as little as 2 hours, consistently keeping the levels of mitochondrial ROS drastically high. This coincides with the significant increases in Δψm observed following incubation with rilpivirine for 2, 4, 6 and 24 hours in INS-1E cells. In summary, increased mitochondrial ROS production may be a result of, rather than causal to, increased Δψm, and may link rilpivirine's toxicity in beta cells to its ability to enhance Δψm. Although *in silico* studies have predicted that rilpivirine may bind to complex I, we show that, unlike efavirenz, rilpivirine did not directly affect complex I activity. However, we postulate that rilpivirine may potentially bind to and inhibit another component of the ETC.

We determined that rilpivirine markedly increased Δψm in INS-1E following short- and long-term exposure. In theory, the increased supply of reducing equivalents is expected to increase the rate of electron transport, which should increase proton efflux and hyperpolarise the mitochondria. Previous findings associated the pharmacological inhibition of the mitochondrial ATP synthase with oligomycin, a potent inhibitor of ATP synthase, to increased Δψm in pancreatic beta cells (Duchen *et al.*, 1993; Haythorne *et al.*, 2019). Our molecular docking

supports this hypothesis as rilpivirine was predicted to bind to the central cavity of the F0 region, which would almost certainly prevent proton flux into mitochondrial matrix and subsequent rotation of the circular rotor, hence inhibiting the function of mitochondrial ATP synthase. In theory, the inhibition of ATP synthase would prevent dissipation of mitochondrial inner membrane by aborting H^+ flux through the ATP synthase (Haythorne *et al.*, 2019). The inhibition of ATP synthase directly inhibits cellular ATP synthesis, an effect we observed with rilpivirine following a 24-hour exposure in INS-1E cells. Although efavirenz may bind to the mitochondrial ATP synthase, it has a much lower binding affinity to this enzyme in comparison to rilpivirine. However, *in vitro* experiments measuring the activity of ATP synthase should be conducted to confirm these predictions. It should be noted that, while *in silico* molecular modelling can be helpful in predicting binding affinities to target proteins, it is necessary to perform *in vitro* experiments to confirm any effects, as demonstrated in the case of rilpivirine and complex I. Although rilpivirine was predicted to bind to complex I, we show that rilpivirine had no direct effect on the activity of complex I *in vitro*.

ROS can affect the activity and expression of UCP2. We show that a 24-hour exposure to efavirenz simultaneously increased mitochondrial superoxide generation and upregulated the mRNA and protein expression of UCP2 in INS-1E cells. Upregulation of UCP2 has been observed following increased ROS levels in beta cells (Chan *et al.*, 2004). In pancreatic beta cells, UCP2-mediated proton leak decreases the yield of ATP from glucose, hence negatively regulating GSIS (Chan *et al.*, 2004; Jitrapakdee *et al.*, 2010; Zhang *et al.*, 2001). Indeed, previous findings suggest that upregulation of UCP2 hinders GSIS and lowers cellular ATP in pancreatic rat islets and clonal beta cells (Chan *et al.*, 2001a). Therefore, efavirenz-mediated increases in superoxide formation can negatively regulate insulin secretion through the activation of UCP2, hence reducing $\Delta\psi m$ and, subsequently reducing ATP content, a major signal for GSIS. Our results indicate that efavirenz reduces insulin secretion from INS-1E cells (**Chapter 3**), further strengthening the potential role of UCP2 in efavirenz-induced beta cell dysfunction. In addition, mitochondrial superoxide formation was shown to enhance the activity of UCP2-mediated proton leak, hence lowering ATP levels and impairing GSIS in pancreatic beta cells (Affourtit & Brand, 2008; Krauss *et al.*, 2003; Zhang *et al.*, 2001). Nonetheless, the mechanism underlying the activation of UCP2 by ROS and the precise effects of UCP2 on insulin secretion remain unclear (Sha *et al.*, 2020).

When mitochondrial electron transport is inhibited, either at the complex I or ATP synthase level by efavirenz or rilpivirine, respectively, cells are depleted of ATP, mitochondrial ROS production is enhanced and $\Delta\psi m$ is disrupted. These mitochondrial alterations are the starting point of a cascade of events promoting apoptosis and reducing insulin secretion from beta cells. As described in **Chapter 3**, efavirenz and rilpivirine both reduced insulin secretion from INS-1E cells and rat islets of Langerhans and increased apoptosis in INS-1E cells. In response to mitochondrial impairment, a calcium efflux from mitochondria probably occurs, which could contribute to perpetuate a vicious cycle of mitochondrial permeability transition and ROS production, resulting in further complex I and ATP synthase inhibition, disruption of calcium homeostasis, beta cell dysfunction and cell death. However, it is still possible that both efavirenz and rilpivirine affect other components of the ETC, such as complex IV in the case of efavirenz as it has been previously shown to inhibit complex IV activity in mouse brain regions (Streck *et al.*, 2011).

4.5 Conclusions

In conclusion, both NNRTIs efavirenz and rilpivirine impair beta cell function and worsen beta cell survival likely through differential and direct effects on the mitochondria. Disturbances in $\Delta\psi m$, increases in mitochondrial superoxide production and a drop in cellular ATP levels following exposure to efavirenz and rilpivirine point to a certain level of dysfunction within the respiratory chain that compromises the functioning of the mitochondria in beta cells. This dysfunction is likely mediated by the inhibition of mitochondrial complex I activity in the case of efavirenz coupled with UCP2 upregulation. On the other hand, rilpivirine has no effect on UCP2 expression and may cause mitochondrial hyperpolarisation by directly inhibiting the mitochondrial ATP synthase. However, this should be confirmed by *in vitro* measurements of ATP synthase activity.

So far, rilpivirine piqued our interest in terms of its mechanisms mediating beta cell dysfunction and death. Therefore, the next chapter will focus on rilpivirine, investigating if this agent directly inhibits a key channel for beta cell function: the pancreatic beta cell ATP-sensitive potassium (K_{ATP}) channel.

5. Beyond the ROS hypothesis: modulation of pancreatic beta cell ATP-sensitive potassium (K_{ATP}) channels by rilpivirine

5.1 Introduction

The physiological importance of pancreatic beta cell ATP-sensitive potassium (K_{ATP}) channels in insulin secretion was established 38 years ago by Ashcroft *et al.* (1984). These ion channels play a critical role in glucose homeostasis by linking glucose metabolism to electrical excitability and insulin release from beta cells. Under physiological conditions, K_{ATP} channel activity is determined by the balance between the intracellular nucleotides ATP, which blocks the channel, and magnesium ADP, which reverses ATP-induced channel inhibition (Ashcroft & Rorsman, 2004; Hattersley & Ashcroft, 2005). At substimulatory glucose concentrations, potassium (K^+) efflux through open K_{ATP} channels maintains the beta cell membrane at a hyperpolarized potential of around −70 mV, which keeps voltage-gated calcium (Ca^{2+}) channels closed (Ashcroft *et al.*, 1984). Elevation of blood glucose concentrations increases glucose uptake and metabolism by the beta cell, producing changes in intracellular nucleotide concentrations (*i.e.*, increase in ATP levels) that result in K_{ATP} channel closure. This leads to a membrane depolarization that opens voltage-gated Ca^{2+} channels, allowing the influx of Ca^{2+} and the subsequent exocytosis of insulin granules and secretion (Gribble *et al.*, 1998; Hattersley & Ashcroft, 2005).

The K_{ATP} channel is an octameric complex of sulfonlyurea receptors (SURs) and the pore-forming inwardly rectifying potassium channel (Kir), mainly found embedded in the cellular plasma membrane. SUR subunit varies, with SUR1 being present in pancreatic beta cells, while Kir6.2 is found in pancreatic beta cells as well as cardiac and smooth muscle cells (Proks *et al.*, 2004). The pancreatic beta cell K_{ATP} channel contains equal numbers of Kir6.2 and SUR1 subunits (Figure 5.1, B and C). Four Kir6.2 form the channel pore and each Kir6.2 subunit is linked to SUR1 that is involved in the regulation of channel gating. The Kir6.2 subunit serves to allow K^+ ions to pass into the cell while the SUR1 is the regulatory subunit of the ion channel, through its nature as an ATP-binding cassette (Enkvetchakul & Nichols, 2003).

Pancreatic beta cell K_{ATP} channels are also the target for sulfonylurea drugs, which are widely used to manage type 2 diabetes (T2D). Direct pharmacological inhibition of pancreatic beta cell K_{ATP} channels by potent blockers such as sulfonylureas has provided an important therapeutic

avenue that proved to be effective in the management of T2D. Gliclazide, a second-generation sulfonylurea is commonly used for the treatment of T2D as dual therapy in addition to metformin, or as an alternative first-line treatment if metformin is contraindicated or not tolerated (National Institute for Health and Care Excellence, 2022). Gliclazide stimulates insulin secretion primarily by binding to SUR1 and subsequently close K_{ATP} channels in pancreatic beta cells. By closing the pancreatic beta cell K_{ATP} channels, intracellular K^+ ions are increased, leading to membrane depolarisation and activation of voltage-dependent Ca^{2+} channels. Subsequently, insulin is secreted from beta cells, thus reducing plasma glucose.

In **Chapter 3**, we report that rilpivirine reduced insulin release from beta cells and isolated rat islets of Langerhans. The pancreatic beta cell K_{ATP} channel is very unique to beta cells, therefore, if rilpivirine activates this ion channel, this could explain the lack of rilpivirine-mediated cellular toxicity in other cell types such as hepatocytes, which do not possess Kir6.2/SUR1 channels (Malhi *et al.*, 2000; Sola *et al.*, 2015; Szeto *et al.*, 2018). In addition to potentially impairing insulin release via oxidative stress and mitochondrial toxicity (**Chapter 3**), we hypothesise that rilpivirine may also reduce insulin secretion by directly activating pancreatic beta cell K_{ATP} channels (Figure 5.1, A). To follow up, we suggest that co-treating beta cells with a potent K_{ATP} channel inhibitor such as gliclazide could attenuate the rilpivirine-mediated damaging effects.

Therefore, the aim of this study was to investigate the direct effects of rilpivirine on the activity of pancreatic beta cell K_{ATP} channels (Kir6.2/SUR1) by electrophysiology and the effects of gliclazide on rilpivirine-mediated beta cell dysfunction and death.

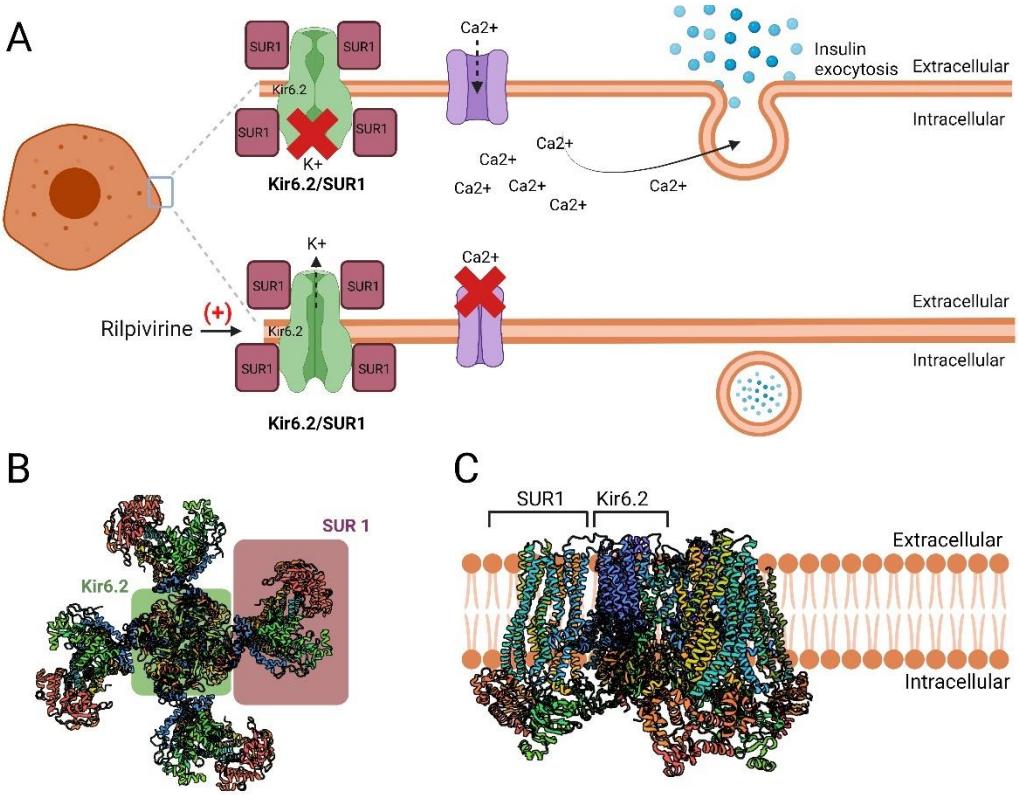

Figure 5.1 Rilpivirine may directly activate pancreatic beta cell K_{ATP} channels (Kir6.2/SUR1). (A) Proposed modulation of the pancreatic beta cell Kir6.2/SUR1 channel by rilpivirine. By activating Kir6.2/SUR1 channels, K^+ efflux increases and consequently causes a hyperpolarisation of beta cells. Subsequently, voltage-gated Ca^{2+} channels remain closed and subsequent insulin exocytosis and release is suppressed. (B) Top-down view of the Kir6.2 (green)/ SUR1 (purple) pancreatic beta cell channel. (C) Side-view of the Kir6.2/SUR1 channel. **(+)** sign indicates activation.

5.2 Materials and Methods

5.2.1 Materials

Xenopus oocyte ovaries were purchased from the European Xenopus Resource Centre (University of Portsmouth, UK). Subcloning Efficiency™ DH5α Competent Cells and S.O.C medium were obtained from Invitrogen (Thermo Fisher Scientific, USA). The ZymoPURE II Plasmid Midi Prep kit was obtained from Zymo Research (USA). Female *Xenopus laevis* lobes containing *Xenopus* oocytes were purchased from the European Xenopus Resource Centre (University of Portsmouth, UK). Liberase TM was obtained from Roche (Mannheim, Germany). The StuI Restriction Enzyme and CutSmart Buffer® from New England Biolabs (UK). The mMESSAGE mMACHINE T7 promoter kit was obtained from (Invitrogen, Thermo Fisher Scientific, USA). Mineral oil was obtained from Sigma-Aldrich (UK). Gliclazide was obtained from Thermo Fisher (USA). All other materials were obtained as described in Materials, **Chapter 2** (see 2.1).

5.2.1.1 Buffers

96 mM K^+ solution

96 mM KCl

2mM NaCl

1 mM $MgCl_2$

1.8 mM $CaCl_2$

5 mM HEPES

Buffer was adjusted to pH 7.4 with KOH

Sterile Barth's Saline (MBS) solution

96 mM NaCl

2 mM KCl

5 mM $MgCl_2$

0.5 mM $CaCl_2$

5 mM HEPES

10 mM KH_2PO_4

Buffer was adjusted to pH 7.6 with KOH.

Tris acetate EDTA (TAE) buffer

40 mM Tris

20 mM acetic acid

1 mM EDTA

Buffer was adjusted to pH 7.6

5.2.1.2 Luria Broth medium and agar plates

Luria Broth (LB) medium

Bacto-tryptone 10 g

Yeast Extract 5 g

NaCl 10 g

Components were dissolved in 800 mL of deionised water and the pH adjusted to 7.5 using NaOH before adjusting the volume to 1 L with deionised water. LB was autoclaved before cooling to 50°C and adding the antibiotic ampicillin (50 µg/mL). LB was stored at 4°C for no longer than 3 months.

Luria Broth (LB) agar plates

Agar 15 g

Bacto-tryptone 10 g

Yeast extract 5 g

NaCl 10 g

Components were dissolved in 800 mL of deionised water and the pH adjusted to 7.5 using NaOH before adjusting the volume to 1 L. LB agar was autoclaved before cooling to 50°C and adding the antibiotic ampicillin (50 µg/mL). Plates were poured into petri dishes under a Bunsen flame in a designated sterile area washed with virkon (500 mg/mL) and 70% ethanol prior to use. Plates were then left to set under a constant flame before being stored at 4°C for no longer than 3 months.

5.2.2 Methods

5.2.2.1 *In silico* molecular docking

Chemical structures were plotted using Jmol, an open-source Java viewer for chemical structures in 3D. For docking, the cryo-EM structure of Kir6.2/SUR1 (PDB: 5TWV) was prepared for docking with UCSF Chimera (Martin *et al.*, 2017b; Pettersen *et al.*, 2004). Due to their large size, both proteins were truncated as to obtain intracellular or intermembrane domains for docking. Unguided docking of efavirenz and rilpivirine to predict binding sites was performed using SwissDock with CHARMM forcefield (Grosdidier *et al.*, 2011).

5.2.2.2 Molecular biology

5.2.2.2.1 Bacterial transformation of Kir6.2 and SUR1 plasmids in DH5-alpha chemically competent *Escherichia coli*

Bacterial transformation is performed as a step in molecular cloning in order to produce multiple copies of recombinant DNA molecules of interest. Here, we perform bacterial transformation of Kir6.2 and SUR1 plasmids in a pcDNA3.1-C-(k) DYK mammalian expression vector. The pcDNA3.1-C-(k) DYK expression vector ensures stable transcribed RNA and high-level expression in *Xenopus* oocytes (Huez *et al.*, 1974).

Human Kir6.2 and SUR1 genes in the pcDNA3.1-C-(k) DYK ampicillin-resistance mammalian expression vector were obtained from GeneScript (USA) and reconstituted to a final concentration of 4 μg by adding 20 μL nuclease-free water, heating to 50°C for 10 mins, and mixing vigorously using a vortex for 1 min.

The resuspended Kir6.2 and SUR1 constructs were transformed using DH5-α chemically competent *Escherichia coli (E. coli)* cells and the heat shock method. Snap-top polypropylene tubes were placed on ice for 15 mins prior to starting the transformation procedure. Next, 50 μL of DH5-α cells were added to each tube. 1 μL of the reconstituted Kir6.2 or SUR1 plasmids were then added to the 50 μL DH5-α cells and gently mixed with a micropipette tip before being incubated on ice for 20 mins.

After 20 mins, the polypropylene tubes containing the competent cells and recombinant plasmids were transferred to a water bath at 42^{o}C for 45 secs before being returned to ice for 2 mins. The polypropylene tubes were then removed from the ice and 900 μL of Super Optimal broth with Catabolite repression (S.O.C) medium was added to each tube before being incubated at 37^{o}C for 1 hr at 150 rpm in a Incu-Shake Mini incubator (SciQuip, USA). Following incubation, the plasmid containing DH5-α bacterial cell /S.O.C medium suspension was diluted 1:10 to a final volume of 100 μL onto separate LB agar plates containing the selection antibiotic ampicillin (50 μg/mL) (prepared as described above, see 5.2.1) and spread with a sterile spreader. The LB ampicillin agar plates were then incubated at 37^{o}C in a stationary incubator for 14-16 hrs. As pcDNA3.1-C-(k) DYK contains an ampicillin-resistance gene, only colonies formed on the LB ampicillin agar plates that possess the recombinant plasmids containing Kir6.2 or SUR1.

Single colonies were then picked (one per polypropylene tube) using a sterile 10 µL tip and dropped into a polypropylene tub containing 3 mL of LB medium (see 5.2.1) and incubated at 37^{o}C and 250 rpm for 16 hrs.

Active growth was monitored throughout the culture process by assessing optical density (OD), an indicator of bacterial cell growth.

5.2.2.2.2 Plasmid midi prep purification

The OD at 600 nm was measured using a spectrophotometer (BioTek Synergy HT Microplate Reader, USA). OD was used to gauge the bacterial culture growth stage. OD measures the degree of light scattering caused by the bacteria within a culture; the more bacteria there are, the more the light is scattered. This ensures that bacterial growth took place. After ensuring that bacterial growth took place, we commenced the plasmid isolation process.

Isolation of ultra-pure plasmid DNA from DH5-α competent cells was performed using the ZymoPURE II Plasmid Midi Prep kit (Cat#: D4201, Zymo Research, USA), according to manufacturer's instructions. Briefly, bacterial cells were resuspended in ZymoPURE P1 solution by vortexing vigorously. Then, ZymoPURE P2 was added for 2 mins to lyse bacterial cells. Then, ZymoPURE P3 was added to neutralise the lysis process. The neutralised lysate was then loaded into a syringe filter and clarified into a conical tube. Binding buffer was added to the cleared lysate and was mixed thoroughly by inverting the capped conical tube 8 times. The entire sample was passed through a spin column by centrifuging the spin column assembly at 500 x g for 2 mins. Then, the column assembly was washed twice by adding the wash buffer and centrifuging at 500 x g for 2 mins. The spin column was then transferred to a collection tube in order to remove any residual wash buffer by centrifuging at 10,000 x g for 1 min in a microcentrifuge. Then, the spin column was transferred into a clean microcentrifuge tube before adding the elution buffer provided directly to the column matrix. After waiting for 2 mins, the spin column in the microcentrifuge tube was centrifuged at 10,000 x g for 1 min. These are eluates containing isolated Kir6.2 and SUR1 DNA plasmids. Finally, the concentration of DNA and the A260/280 ratio were measured to assess the amount and purity of the isolated DNA plasmids using a Nanodrop® Lite spectrophotometer (Thermo Fisher, USA), with nuclease-free water as zero absorbance reference (Table 5.1).

Values close to 1.8 are generally accepted as 'pure' DNA. Once the purity was deemed acceptable, the plasmid midi prep stocks were stored at -20^{o}C prior to linearisation.

Table 5.1 Concentration and A260/280 ratio of Kir6.2 and SUR1 DNA plasmids

DNA plasmid	Concentration of DNA (ng/µL)	A260/280
Kir6.2	1672	1.76
SUR1	1205	1.83

5.2.2.2.3 Linearisation of plasmids

The eluates of DNA plasmids for Kir6.2 and SUR1 were thawed on ice prior to the linearisation process. Linearised DNA plasmids are more accessible to reverse transcriptase compared to unlinearised, uncut DNA plasmids. The linearisation process involves cleaving a circular DNA plasmid with the restriction enzyme StuI. Linearisation was performed using the StuI Restriction Enzyme (Cat#: R0187, New England Biolabs, UK) in CutSmart Buffer® (Cat#: R0187, New England Biolabs, UK) according to manufacturer's instructions. Briefly, a 25 µL reaction was prepared by adding the components stated in Table 5.2 together and mixing gently by pipetting up and down. The mixture was incubated for 20 mins at 37°C to perform the linearisation process.

The exact amounts of components to be added to the reaction were determined for 10 µg of plasmid (Table 5.2). For instance, 10 µg of DNA plasmid for Kir6.2 corresponds to the following equation:

$$\frac{10\ \mu g\ (amount\ required)\ X\ 1\ \mu L}{1.672\ \mu g} = 6\ \mu L$$

Table 5.2 Components for the linearisation of Kir6.2 and SUR1 plasmids

	Kir 6.2				**SUR1**			
	Restricting enzyme	Buffer	Plasmid (10 µg)	H_2O	Enzyme	Buffer	Plasmid (10 µg)	H_2O
Volume (in µL)	**1***	**3***	**6**	**20**	**1***	**3***	**8**	**18**

*Set volumes as per manufacturer's instructions

Finally, linearised DNA concentrations and A260/280 ratios of purity were measured using a Nanodrop® Lite spectrophotometer, with nuclease-free water as zero absorbance reference (Thermo Fisher, USA). This would allow to monitor the purity of the isolated linearised DNA, as well as measure concentrations of linearised DNA that would serve for RNA transcription as detailed below.

Table 5.3 shows the measurements for concentrations of unlinearised Kir6.2 and SUR1 DNA.

Table 5.3 Concentration and A260/280 ratio of Kir6.2 and SUR1 linearised DNA

Plasmid	Concentration of linearised DNA (ng/mL)	A260/280
Kir6.2	406.7	1.78
SUR1	373.4	1.77

However, it is necessary to ensure that the DNA plasmids have been linearised prior to transcription into RNA. Therefore, we performed an agarose gel electrophoresis of our unlinearised DNA samples.

5.2.2.2.4 Agarose gel electrophoresis

Agarose gel electrophoresis was performed on the linearised DNA plasmids to ensure the successful linearisation had occurred. Briefly, a 0.8% agarose gel was prepared by dissolving 0.4 g of agarose in 50 mL of TAE buffer (see Materials, 5.2.1). The agarose slurry was melted until full dissolution and 3 µL of SYBR safe DNA gel stain was added in order to visualise the DNA using blue light image capture (BioRad Gel Doc EZ system) post run. The gel tank was filled with 1x TAE buffer, and the wells filled with 5 µL of 10 Kb DNA marker, 40 µL of linearised Kir6.2 and SUR1, and unlinearised plasmids of the same constructs as a negative control (Figure 5.2). The negatively charged DNA or RNA is attracted to the positive electrode and moves through the gel, with larger fragments moving slower than smaller fragments, allowing for the separation of different DNA or RNA fragments based on size. Uncropped gel electrophoresis image can be found in Figure 21, Appendix II.

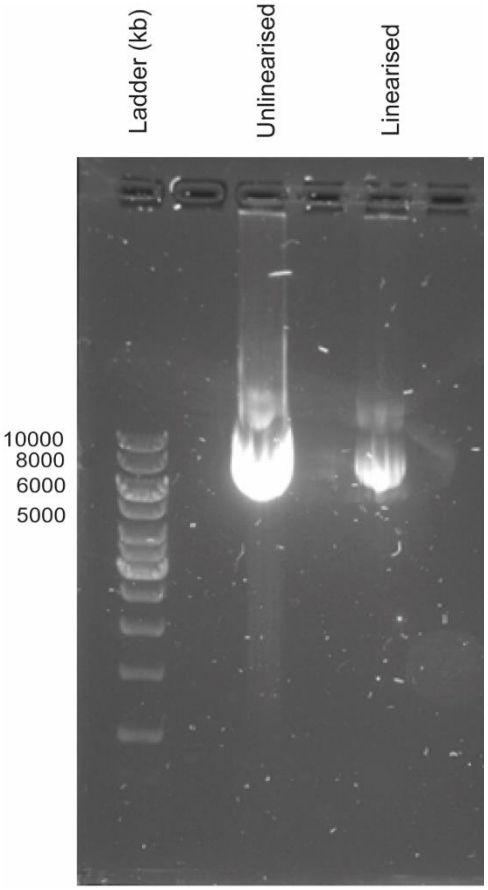

Figure 5.2 Unlinearised and linearised SUR1 DNA run in agarose gel electrophoresis. Unlinearised SUR1 plasmid is visibly bigger than the linearised SUR1 plasmid.

After confirming that DNA is in fact linearised, we proceeded to transcribe the linearised DNA to RNA.

5.2.2.2.5 *In vitro* transcription

cRNA synthesised *in vitro* is widely used to for heterologous expression of ion channels in *Xenopus* oocytes. cRNA was prepared from linearised Kir6.2 or SUR1 pcDNA3.1 constructs using the mMESSAGE mMACHINE T7 promoter kit, according to manufacturer's instructions (Invitrogen, Thermo Fisher; Cat #: AM1344). The T7 promoter system is a commonly used sequence of DNA base pairs that is recognised by the T7 RNA polymerase which in turn enables transcription of linearised DNA to RNA.

Briefly, a 20 μL reaction was prepared by adding the components outlined in Table 5.4 and mixing thoroughly by pipetting the mixture up and down gently. Then, the reaction was incubated for 2 hrs at 37ºC. TURBO DNase (1 μL) was added to remove the template DNA and the mixture was incubated again for 15 mins at 37ºC. To stop the reaction and precipitate

RNA, nuclease-free water (25 µL) and lithium chloride (25 µL) were added. The mixture was then mixed by pipetting up and down before chilling for at least 30 mins at -20°C. After chilling, the mixture was centrifuged at 4°C for 15 mins at maximum speed to pellet the RNA. The supernatant was then carefully removed, and the pellet was washed once with 1 mL of 70% ethanol and re-centrifuged. This is to maximise that removal of unincorporated nucleotides. After centrifugation, the 70% ethanol was carefully removed, and the RNA was resuspended in nuclease-free water (20 µL).

According to the linearised DNA concentrations of Kir6.2 and SUR1 (Table 5.3), we calculated the amount of template linearised DNA corresponding to 1 µg. For instance, 1 µg of linearised DNA for Kir6.2 corresponds to the following equation:

$$\frac{1\ \mu g\ (amount\ required)\ X\ 1\ \mu L}{0.4067\ \mu g} = 2.5\ \mu L.$$

Table 5.4 summarises the components for the *in vitro* RNA transcription of the Kir6.2 and SUR1 linearised DNA.

Table 5.4 Components of cRNA transcription of Kir6.2 and SUR1 linearised plasmids

	Kir6.2					**SUR1**				
	2xNTP	10x reaction buffer	Linearised plasmid (1 µg)	Enzyme mix	Nuclease-free H_2O	2xNTP	10x reaction buffer	Linearised plasmid (1 µg)	Enzyme mix	Nuclease-free H_2O
Volume (in µL)	**10***	**2***	**2.5**	**2**	**3.5**	**10***	**2***	**2.7**	**2**	**3.3**
Total volume of reaction (in µL)	**20**					**20**				

The reactions were prepared by mixing the components mentioned in Table 5.4 using a vortex. The reactions were then incubated for 2 hrs at 37°C. Following incubation, 1 µL of DNase was added to the reaction. Then, the reaction was stopped with 25 µL of lithium chloride before adding 25 µL of H_2O to elute the RNA. The concentration and purity (*i.e.*, A260/280) of RNA were determined using a Nanodrop® Lite spectrophotometer (Thermo Fisher, USA), with nuclease-free water as zero absorbance reference. Values close to 2 are generally accepted as 'pure' RNA. Once the purity was deemed acceptable, and the amount of cRNA was determined, then reverse transcription was carried out (Table 5.5). The cRNA in eluate was stored at -20°C.

Table 5.5 Concentration and A260/280 ratio of transcribed Kir6.2 and SUR1 cRNA

Plasmid	Concentration of RNA (ng/µL)	A260/280
Kir6.2	1273.2	1.98
SUR1	1489.9	1.87

Then, cRNA quality was assessed by agarose gel electrophoresis (see 5.2.2.2.4). Two distinct bands and an absent smear below the second band signifies that the cRNA is of good quality. An example is shown below (Figure 5.3). Uncropped gel electrophoresis image can be found in Figure 22, Appendix II.

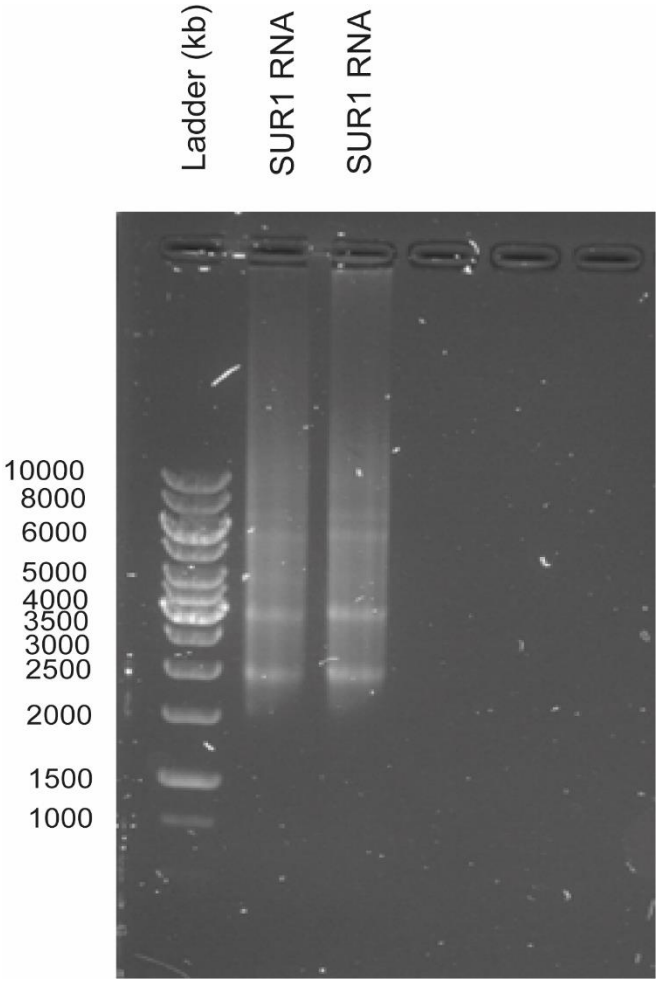

Figure 5.3 Agarose gel electrophoresis for SUR1 RNA. Two distinct bands and an absent smear below the second band can be visualised (two technical replicates).

5.2.2.2.6 cRNA dilution

Kir6.2 cRNA samples were diluted to a final concentration of 2 ng per 23 nL which equates to 0.087 ng/nL. Example: Concentration of RNA for Kir6.2 is 1273.2 ng/µL, which equates to 1.2732 ng/nL (Table 5.5). So 1.2732/0.087 = factor of 14.6. Hence dilute 1 µL of RNA in 14.6 µL of RNase-free water to get a concentration of 0.087 ng/nL. So when 23 nL is injected it will in fact be 2 ng of Kir6.2 RNA. SUR1 cRNA samples were diluted to a final concentration of 5 ng per 23 nL which equates to 0.217 ng/nL. The calculations were performed as explained in the example given above.

Figure 5.4 summarises the process implemented in order to generate cRNA from Kir6.2 and SUR1 plasmids.

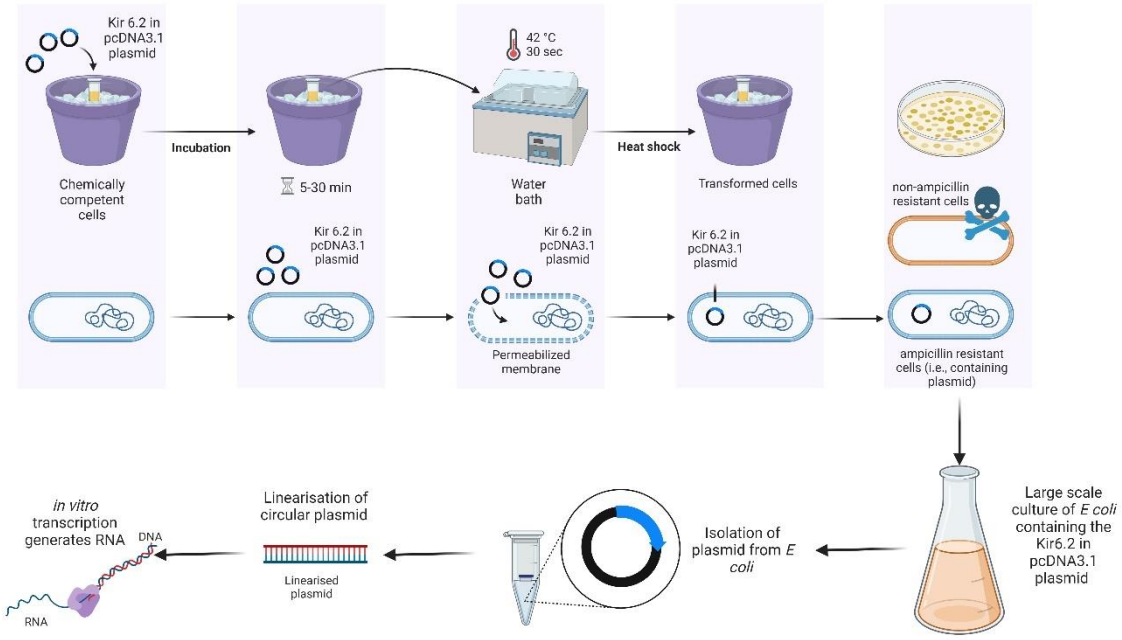

Figure 5.4 Schematic summary of transformation, isolation and linearisation of plasmids and *in vitro* transcription used in this study. Figure created with BioRender.com.

5.2.2.3 *Xenopus* oocyte preparation

Female *Xenopus laevis* ovaries were purchased from the European Xenopus Resource Centre (University of Portsmouth, UK). First, the ovaries were dissected into small clumps containing 15-20 oocytes and washed in sterile Barth's Saline (MBS) supplemented with penicillin (100 µg/mL) and streptomycin (100 µg/mL). The cells were then transferred to 15 mL of MBS containing 250 µL of liberase enzyme (Thermo Fisher UK) and rotated at 10 rpm at room temperature (~25^{o}C) for 30-45 mins or until the follicular cell layer was visibly digested. The defolliculated oocytes were then washed 10 times with MBS. After washing, only healthy-looking *Xenopus* oocytes (*i.e.*, perfectly spherical and with intact pigmentation) were transferred using a Pasteur pipette to a 60 mm diameter, 15 mm depth Petri dish filled with MBS solution (~ 100 oocytes per dish). Stage V and VI oocytes were then selected ready for cRNA injection.

5.2.2.4 cRNA injection

5.2.2.4.1 Electrode and injection pipette fabrication

Glass injection pipettes were pulled using a two-stage Narishige PP-83 pipette puller (Narishige Scientific Instrument Laboratory, Japan). For injection, pipettes were pulled at a stage one pull of 64.8°C, stage two pull of 48.8°C, with two large and one small weight attached.

Glass recording electrodes were manufactured from thin-walled borosilicate glass capillaries (1.0 mm OD, 0.78 mm ID, 75 mm L). Pipettes were pulled at a stage one pull of 65.1°C, stage two pull of 44.9°C, with two large and one small weight attached.

5.2.2.4.2 Injection procedure

The injection pipette was backfilled with mineral oil using a 10 mL syringe. Then, the microinjection pipette was mounted onto an automatic microinjection apparatus (Nanoinject III, Drummond Scientific, USA) as shown in Figure 5.5. Pre-back-filled needles were filled with cRNA by dispensing a 1 µL volume of Kir6.2 and SUR1 cRNA working solution (see 5.2.2.2.6) each and mixing using a pipette tip onto a piece of para-film tightly stretched over a fabricated stage. Then, the mixed cRNA working solution was taken up into the back-filled needle ready for injection into oocytes. Selected *Xenopus* oocytes were strategically placed onto

a grid placed in a 35 mm diameter petri dish filled with MBS using a Pasteur pipette. A programme was set and ran to ensure oocytes were injected with 23 nL of Kir6.2 and SUR1 to inject individual oocytes as described previously (see 5.2.2.2.6). The injection pipette was carefully inserted into the centre of the vegetal pole of the *Xenopus* oocyte and the cRNA was injected at a flow rate of 10 nL/second. Following injection with cRNA, the injected *Xenopus* oocytes were transferred to a new 35 mm petri dish filled with MBS (Figure 5.5). *Xenopus* oocytes were maintained at 16^{o}C for 5 days to express the Kir6.2/SUR1 channels while changing MBS solution twice daily, prior to electrophysiological measurements.

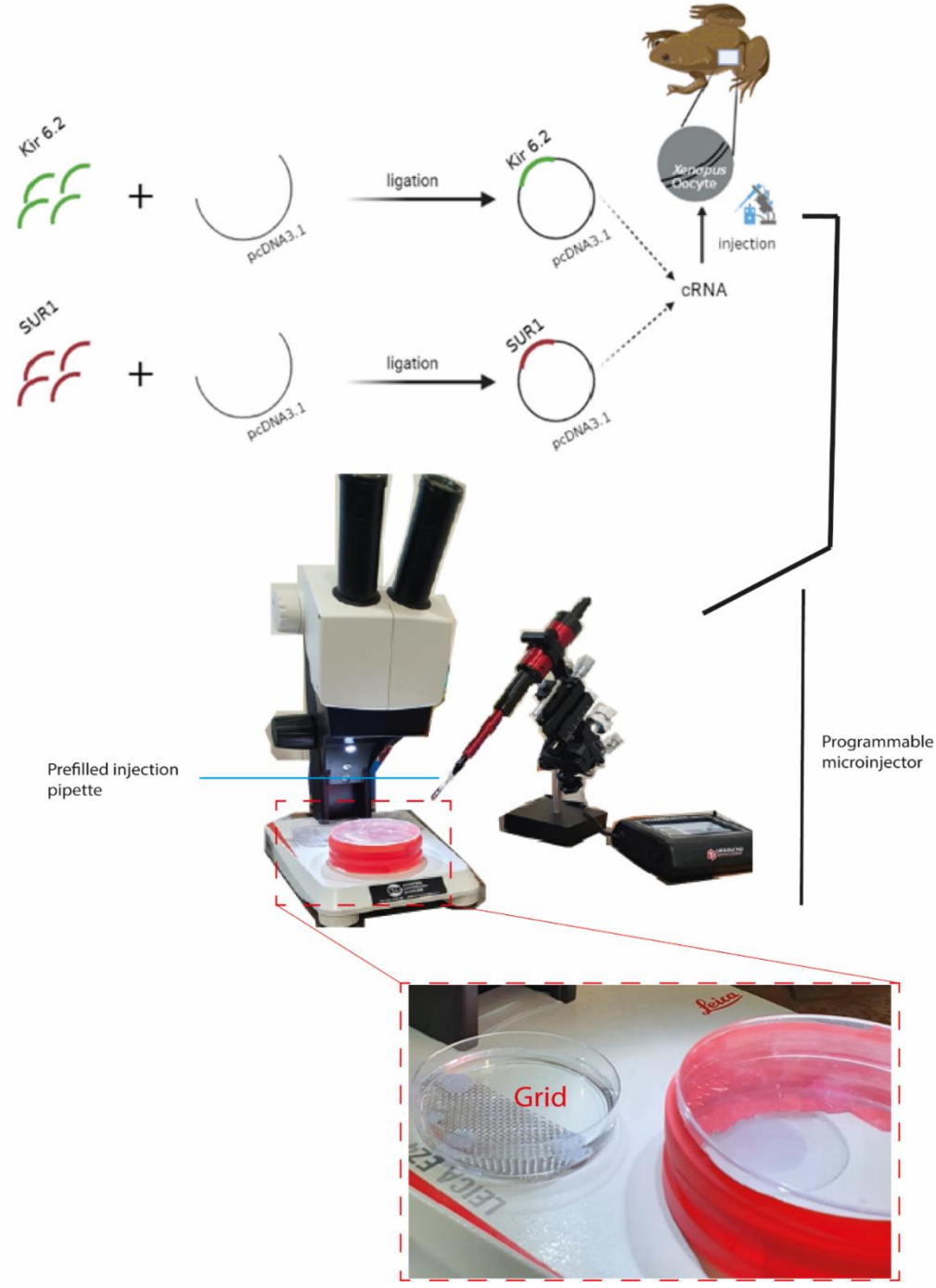

Figure 5.5 Summarised cRNA injection protocol and injection system setup for electrophysiological analysis of Kir6.2/SUR1. cRNA prepared from bacterially transformed Kir6.2 and SUR1 DNA was injected into individual *Xenopus* oocytes using a programmable microinjector unit.

5.2.2.5 Two-electrode voltage clamp (TEVC) electrophysiology

TEVC is a method of measuring ion current through membrane of excitable cells, while holding the membrane voltage at a set level. The method measures membrane potential and changes the membrane voltage to a desired value by adding the necessary current, effectively clamping the

cell membrane at a constant voltage desired by the experimenter and allowing the voltage clamp to record what currents are delivered. Oocytes are positioned into a bath which is mounted under a microscope and connected to a gravity perfusion system. The oocyte is impaled by two microelectrodes through manual manipulation with microelectrode holders. The microelectrodes are connected to an amplifier which controls the holding potential of the membrane by clamping it at a pre-set command voltage. The amplifier is connected to an analogue to digital converter, which is in-turn connected to a PC.

Following 5-days post-injection, the injected *Xenopus* oocytes were subject to the TEVC method. All the following procedures were conducted at room temperature (~25^{o}C).

5.2.2.5.1 Recording from oocytes

The recording rig was prepared by checking the gravity perfusion and aspiration system before loading all the solutions (Table 5.6) required in the perfusion system (Figure 5.6, A). A fairly large oocyte with well-defined animal and vegetal poles was chosen. The oocyte was transferred to the mesh in a bath filled with 96 mM K^+ solution. The mesh in the bath restricts the movement of the oocyte.

A recording (V) and a current (I) electrode were backfilled halfway with 3 M KCl and slotted on electrode holders containing chloride-silver wires. The recording electrode senses change in voltage relative to the ground electrode, while the current electrode injects current into the cell. These microelectrodes then compare the membrane potential against the set command voltage and use negative feedback to maintain the cell at this set voltage. Both electrodes are connected to an amplifier, which measures the membrane potential and sends this signal into a feedback amplifier that subtracts the membrane potential from the command potential and sends an output to the current electrode. If the cell deviates from the command potential the amplifier will then generate an error signal, which is the difference between the command potential and the actual voltage of the cell. This results in the feedback circuit passing current into the cell to reduce this error signal to zero. Prior to recording both microelectrodes were compensated for by manually adjusting the offset using controls available for both voltage and the current electrodes. Tip resistances were measured by placing the electrodes into the bath solution and adjusting the offset to 0 mV.

Oocytes were recorded using an Oocyte Clamp O0-725C amplifier (Warner Instruments, Harvard Apparatus) and Digidata 1550 digitizer (Molecular Devices) while running pCLAMP

10.4 software (Molecular Devices, LLC. Sunnyvale, CA) on Windows 10 operating system. The micromanipulators were used to get the electrodes close to the oocyte. Then, the fine dials were used to poke the oocyte slowly and gently with the electrode all the while observing under the scope and watching the read out from the electrodes. An indent on the oocyte membrane, which reformed once the electrode pierced through should be observed. When the electrode enters the oocyte, the electrode will display the resting potential of the oocyte. For a healthy oocyte, the resting potential should be around –50 mV. The clamp was adjusted to fast, and the gain turned to maximum before the voltage protocol was applied. Recordings were made using the following voltage-step protocol. Recordings were conducted by maintaining a holding potential of 0 mV by 100 ms voltage steps in 10 mV increments from – 120 to +50 mV (Fig. 5.6, B).

5.2.2.5.2 Treatment protocol

A stock solution (25 mM) of rilpivirine was prepared as per Table 1, **Appendix I**. To prepare a 100 µM rilpivirine working solution, 400 µL of rilpivirine stock solution (25 mM) was diluted in 100 mL of 96 mM K^+ solution.

Control (DMSO) and rilpivirine solutions were applied by gravity perfusion (Figure 5.6, A). A recording of the control *Xenopus* oocyte (*i.e.*, oocyte in 96 mM K^+ solution with DMSO only) was performed. Once the recording for the control was performed, the 96 mM K^+ solution with DMSO was exchanged with 100 µM rilpivirine 96 mM K^+ solution using the perfusion and aspiration system. After a 3-minute exposure to rilpivirine 100 µM, the recording was performed from the oocyte. Following the recording, the oocyte was discarded using a Pasteur pipette. Then, the water bath was thoroughly washed with 96 mM K^+ solution using the aspiration and perfusion system. This was repeated again with another healthy oocyte.

The solutions are used in the order stated in Table 5.6.

Table 5.6 Treatment protocol for TEVC analysis of Kir6.2/SUR1 channels

Steps in order	Solution	Purpose
START – Place oocyte in bath filled with 96 mM K^+ solution		
1	96 mM K^+ solution	Control
2	Rilpivirine (100 µM) diluted in K^+ solution	Agent under investigation
END – Dispose of the oocyte and wash the bath by perfusion and aspiration. Load another oocyte and repeat process.		

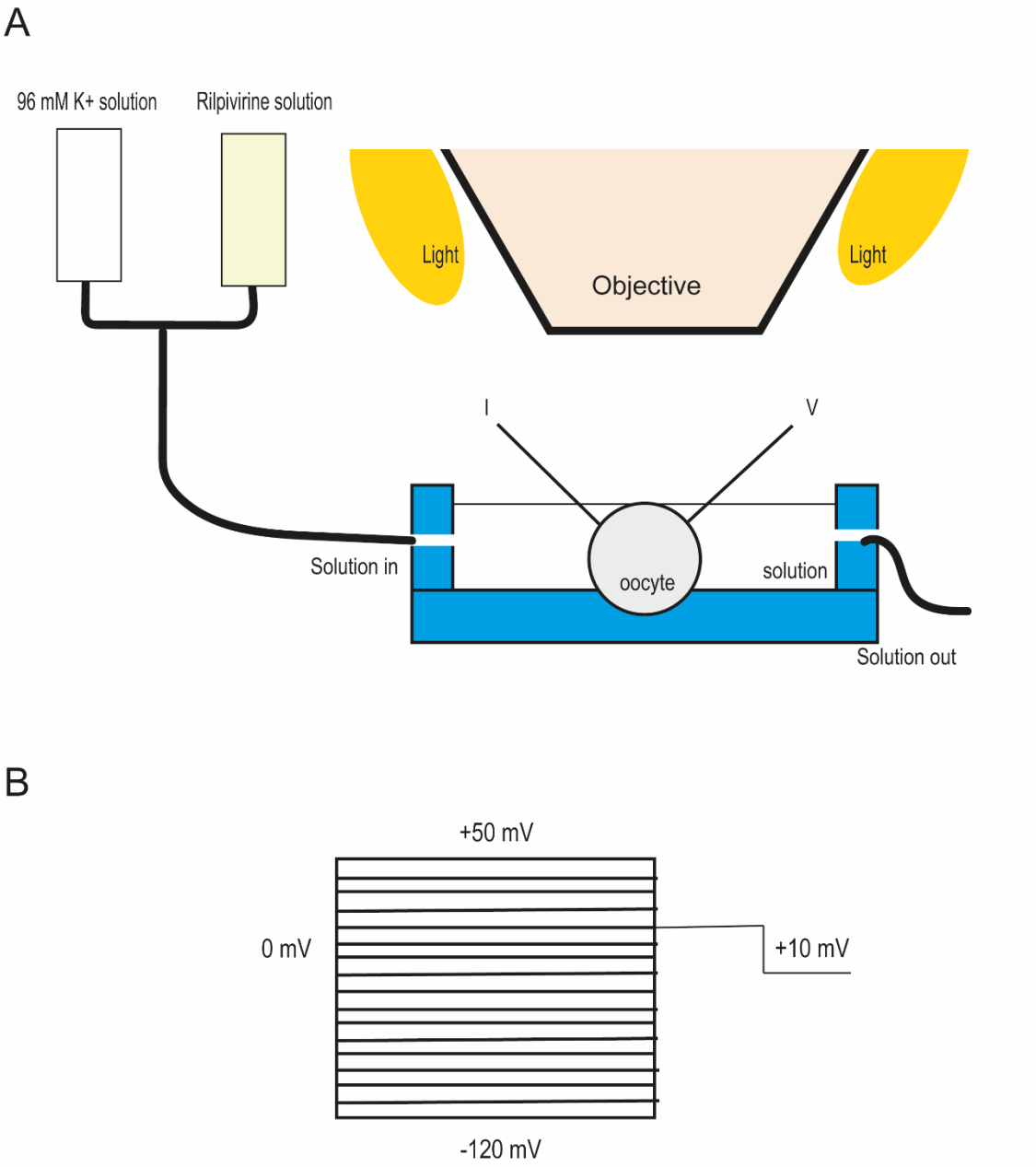

Figure 5.6 Schematic summarising the oocyte set-up as part of a TEVC recording. (A) Oocyte in a bath chamber with a 96 mM K^+ or rilpivirine solution for perfusion. Inserted are the current (i) and voltage (v) electrodes under an objective, with light sources directed either side. (B) Diagram of the voltage protocol used for this study. Currents evoked at 10 mV were measured. -120 to +50 mV are the highest and lowest voltages of the step protocol, 0 mV is the holding potential. n.b. size not to scale.

5.2.2.6 Treatment protocol for experiments in INS-1E cells

After cell growth as described in **Chapter 2** (see 2.2.1), INS-1E cells were exposed to rilpivirine (3 or 10 µM) or gliclazide (0.1, 0.3 or 1 µM) alone or to rilpivirine (3 or 10 µM) plus gliclazide (0.1, 0.3 or 1 µM) for 24 hrs.

Gliclazide (MW = 323.412 g/mol) stock solution (5 mM) was prepared by adding 1.62 mg of gliclazide to 1 mL of DMSO. Then, solutions of different concentrations (0.1, 0.3, and 1 μM) of gliclazide were prepared by diluting the stock solution in 5 mL RPMI-1640 media supplemented with 3% heat-inactivated FCS, 50 μM 2-mercaptoethanol and 1% penicillin-streptomycin (Table 2 and Table 4, Appendix I). Vehicle (DMSO) controls were included in each experiment.

Following treatment protocol, glucose-stimulated insulin secretion (GSIS) (see 2.2.3.1), cell viability (see 2.2.5), apoptosis levels (see 2.2.6.2), intracellular ROS generation (see 2.2.7.1) and mitochondrial membrane potential (Δψm) (see 2.2.8) were assessed as described in **Chapter 2.**

5.2.2.7 Data analysis

For TEVC, data analysis was performed using the Clampfit 10.2 software (Molecular Devices, LLC. Sunnyvale, USA). Traces were analysed by placing markers at identical positions on every recorded trace where the steady-state current was observed. I-V relationship curves were plotted using Clampfit 10.2 software, and the data transferred into an excel spreadsheet to calculate the mean I-V relationship for all oocytes in the experiment. Each oocyte represents one independent experiment. Exemplar traces were transposed from Clampfit 10.2 results table (Properties, hide, voltage steps, edit, transfer traces) into GraphPad Prism 8 (GraphPad Software, San Diego, USA) to create graphs.

For *in vitro* experiments in INS-1E cells, data and statistical analysis were performed as described in **Chapter 2** (see 2.2.15).

5.3 Results

5.3.1 Rilpivirine is predicted to bind to the pancreatic K_{ATP} channel (Kir6.2/SUR1)

The pancreatic beta cell K_{ATP} channel is a crucial component of the insulin-secreting machinery. Therefore, we investigated if rilpivirine binds to and activates the pancreatic beta cell K_{ATP} channel. After confirming the expression of Kir6.2 and SUR1 in INS-1E cells (Figure 2, **Appendix I**), we attempted to predict the binding probabilities of rilpivirine to the Cryo-EM structure of the pancreatic beta cell Kir6.2 (PDB: 5TWV)/SUR1 (PDB: 6PZI) channel.

Even though rilpivirine has the ability to bind to Kir6.2 (transmembrane domains) and SUR1 (intracellular domains), rilpivirine exhibited the most favourable binding free energy to SUR1 (transmembrane domains), as shown by the estimated Gibbs free energy (ΔG) score (-8.71 kcal mol^{-1}) (Table 5.7). Therefore, we focused on this domain for further molecular docking analysis.

Table 5.7 Full fitness and Gibbs free energy (ΔG) scores for docking of rilpivirine to subunits of Kir6.2/SUR1. The more negative the ΔG value, the more exothermic the proposed interaction. Full fitness scores predicted by SwissDock indicate that lower values represent binding modes which are more favourable than higher scoring numbers. Rilpivirine showed most favourable interaction with SUR1 (transmembrane domains).

Subunit	ΔG (kcal mol^{-1})	Full fitness (kcal mol^{-1})
Kir6.2 (transmembrane domains)	-7.31	-1619.46
Kir6.2 (intracellular domains)	-7.57	-5143.14
SUR1 (transmembrane domains)	-8.71	-3157.47
SUR1 (intracellular domains)	-7.54	-3972.60

We show that rilpivirine has several potential binding configurations to the SUR1 transmembrane domains (Figure 5.7, C). There were 256 predicted binding poses for rilpivirine docked in the SUR1 transmembrane unit, arranged in 39 clusters. We show the most favourable binding pose of rilpivirine to SUR1 (between transmembrane domain 0 and 2), exhibiting the highest estimated ΔG (-8.71 kcal mol^{-1}) in comparison to other configuration poses (Figure 5.7, E and F). Interestingly, we also found that several rilpivirine binding poses were predicted to bind to the sulfonylurea binding site (between transmembrane domain 1 and 2), exhibiting a ΔG of -7.8 kcal mol^{-1} and full fitness score of -3145.943 kcal mol^{-1} (Figure 5.7, C, D and F). The sulfonylurea binding site was previously proposed by Martin *et al.* (2017a) and Walczewska-Szewc and Nowak (2021). We also performed molecular docking for gliclazide docked in the SUR1 transmembrane unit. We confirmed that gliclazide binds to this established sulfonylurea binding site (Figure 3, **Appendix I**).

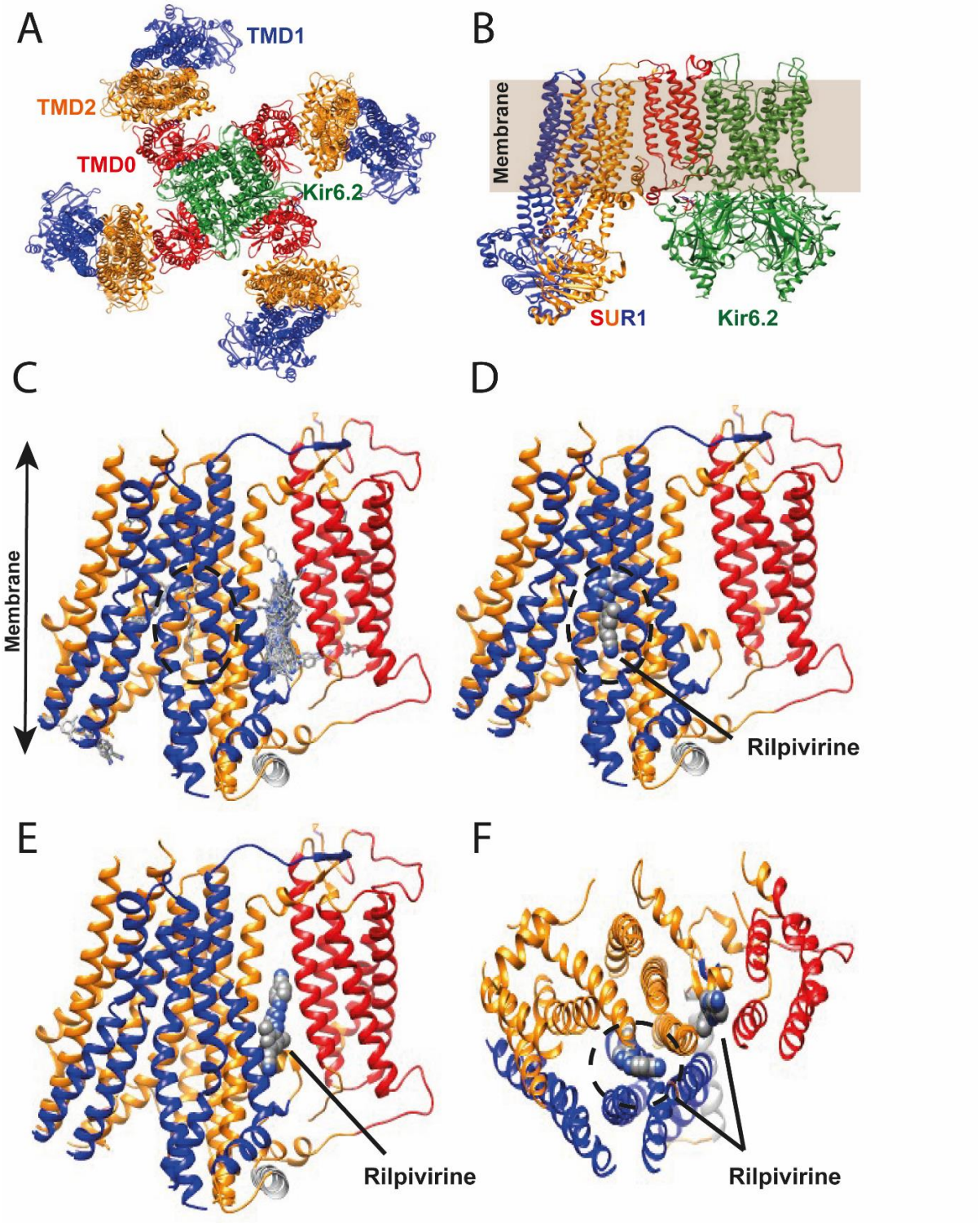

Figure 5.7 Rilpivirine is predicted to strongly bind to the transmembrane domains of SUR1 of the pancreatic beta cell K_{ATP} channel. (A) Top-down view of the Cryo-EM structure of the pancreatic beta cell K_{ATP} channel (Kir6.2/SUR1). TMD0, TMD1 and TMD2 stand for the SUR transmembrane domain 0, 1 and 2, respectively. (B) Side view of transmembrane (grey) and intracellular domains of Kir6.2 and SUR1. (C) All the binding configurations of rilpivirine to the transmembrane domains of SUR1. The established binding site of sulfonylureas is shown as a black dashed oval. (D) Rilpivirine is predicted to bind to the sulfonylurea binding site (ΔG = -7.8 kcal mol^{-1}). The binding site of sulfonylureas is shown as a black dashed oval. Atoms are represented as spheres. (E) Most favourable pose of rilpivirine to the transmembrane domain of SUR1 based on (ΔG = -8.71 kcal mol^{-1}). Atoms are represented as spheres. (F) Top-down view of two relevant poses of rilpivirine to the SUR1

transmembrane protein. The binding site of sulfonylureas is shown as a black dashed oval. Atoms are represented as spheres.

5.3.2 Rilpivirine activates the pancreatic beta cell K_{ATP} channel (Kir6.2/SUR1)

We showed that rilpivirine is predicted to bind to the pancreatic beta K_{ATP} channel, however, its effect on this channel is not clear yet. Therefore, we attempted to understand the effects of rilpivirine on the activity of the pancreatic beta cell K_{ATP} channel (Kir6.2/SUR1) in *Xenopus* oocytes using TEVC. Whole pancreatic beta cell K_{ATP} channels (Kir6.2/SUR1) were stimulated by rilpivirine as shown by the I-V relationship curve and current density measurements (Figure 5.8). Rilpivirine increased Kir6.2/SUR1 channel currents within the -120 mV to -60 mV voltage range in comparison to control (Figure 5.8, C). The K_{ATP} channel current density in control oocytes was approximately -0.14 μA (Figure 5.8, D). When rilpivirine (100 μM) was added, K_{ATP} channel current density was significantly increased to approximately -0.36 μA (–120 mV) (Figure 5.8, D). On the other hand, no statistically significant stimulation was observed in the inward-rectifier K^+ channel subunit Kir6.2 following exposure to rilpivirine (Figure 5.8, B).

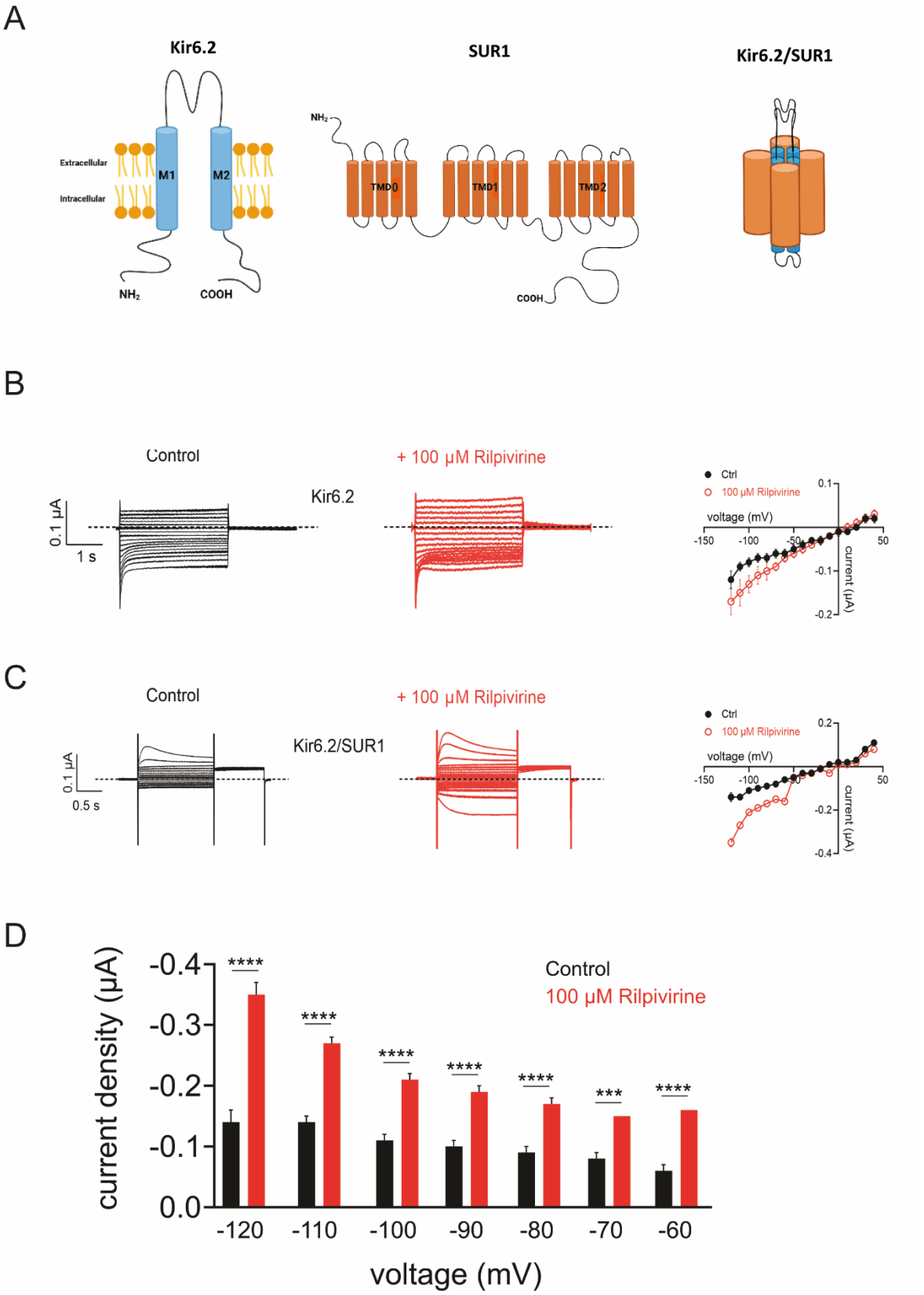

Figure 5.8 Rilpivirine directly activates pancreatic beta cell K_{ATP} (Kir6.2/SUR1) channels but not the inward-rectifier K^+ channel subunit Kir6.2. (A) The cartoon topology of Kir6.2 (blue) (left), SUR1 (orange) (middle) and Kir6.2/SUR1 (right). The SUR1 receptor contains two transmembrane domains (TMD1 and TMD2). SUR1 has an additional set of five N-terminal transmembrane helices (TMD0) that is connected to TMD1. Representative channel currents (left panel) and the mean I–V relationships (right) of Kir6.2 (B) and

Kir6.2/SUR1 (C) channels before and after application of control (vehicle) or rilpivirine 100 µM measured by TEVC in *Xenopus* oocytes. (D) Current density of Kir6.2/SUR1 channels in *Xenopus* oocytes exposed to vehicle control or rilpivirine 100 µM. The K_{ATP} channel (Kir6.2/SUR1) potassium current density was significantly increased in oocytes exposed to rilpivirine in comparison to control. Data are expressed as mean ± SEM from *n* = 7-11 independent experiments. Statistical analysis was carried out using Student's t-test where $p < 0.05$ was considered significant; *** $p < 0.0002$, **** $p < 0.0001$ vs. vehicle-treated control groups.

5.3.3 Gliclazide partially improves rilpivirine-mediated GSIS impairment

Following the observation that rilpivirine activates the pancreatic beta cell K_{ATP} channel, we investigated whether a potent pharmacological inhibitor of the pancreatic beta cell K_{ATP} channel (*i.e.*, gliclazide) offers protection against rilpivirine-mediated GSIS impairment in INS-1E cells. We previously show that rilpivirine, at a concentration of 10 µM, significantly reduced GSIS from INS-1E cells (**Chapter 3**). Gliclazide (1 µM) improved GSIS from approximately 25% in rilpivirine (10 µM)-alone treated cells to 56% in combination treatments with gliclazide (1 µM) ($p < 0.05$ vs. rilpivirine alone treated cells). As expected gliclazide (0.1, 0.3 and 1 µM) drastically increased GSIS from INS-1E cells. It is worth noting that insulin secreted from INS-1E cells exposed to gliclazide alone exceeds that of gliclazide plus rilpivirine treatments by approximately 6-fold (Figure 5.9).

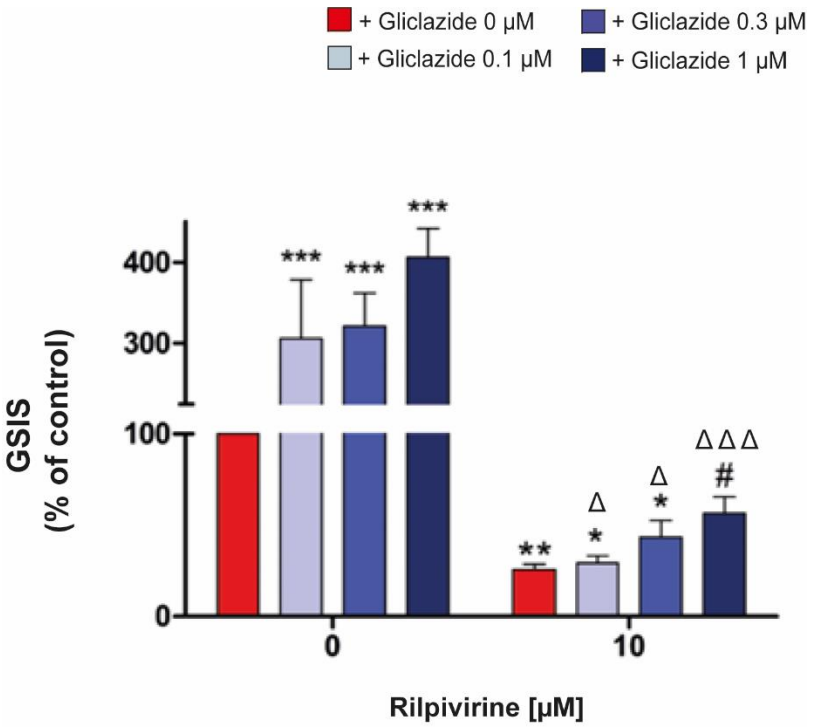

Figure 5.9 Gliclazide partially improves GSIS from rilpivirine-treated INS-1E cells. INS-1E cells were exposed to rilpivirine (10 µM) alone or in combination with gliclazide (0.1, 0.3 or 1 µM) for 24 hrs before assessing GSIS. Data are expressed as mean ± SEM from *n* = 3 independent experiments. Statistical analysis was carried out using

Friedman's test where $p < 0.05$ was considered significant; * $p < 0.05$, ** $p < 0.01$, *** $p < 0.001$ vs. vehicle-treated control cells, # $p < 0.05$ vs. rilpivirine alone treated cells, Δ $p < 0.05$ vs. gliclazide alone treated cells, ΔΔΔ $p < 0.001$ vs. gliclazide alone treated cells.

5.3.4 Gliclazide protects INS-1E cells from rilpivirine-induced early apoptosis

Although we did not observe much protection in the context of GSIS, we investigated whether gliclazide can attenuate the increase in early cell apoptosis in rilpivirine-treated INS-1E cells (Figure 5.10). To assess INS-1E cell early apoptosis, we exposed INS-1E cells to rilpivirine 10 µM, a concentration shown to increase early apoptotic cell rates in INS-1E cells (**Chapter 3**). Gliclazide (0.3 and 1 µM) significantly reduced apoptotic cells levels from approximately 15% (rilpivirine alone), to 9% (gliclazide plus rilpivirine treatments) ($p < 0.05$ vs. rilpivirine alone treated cells).

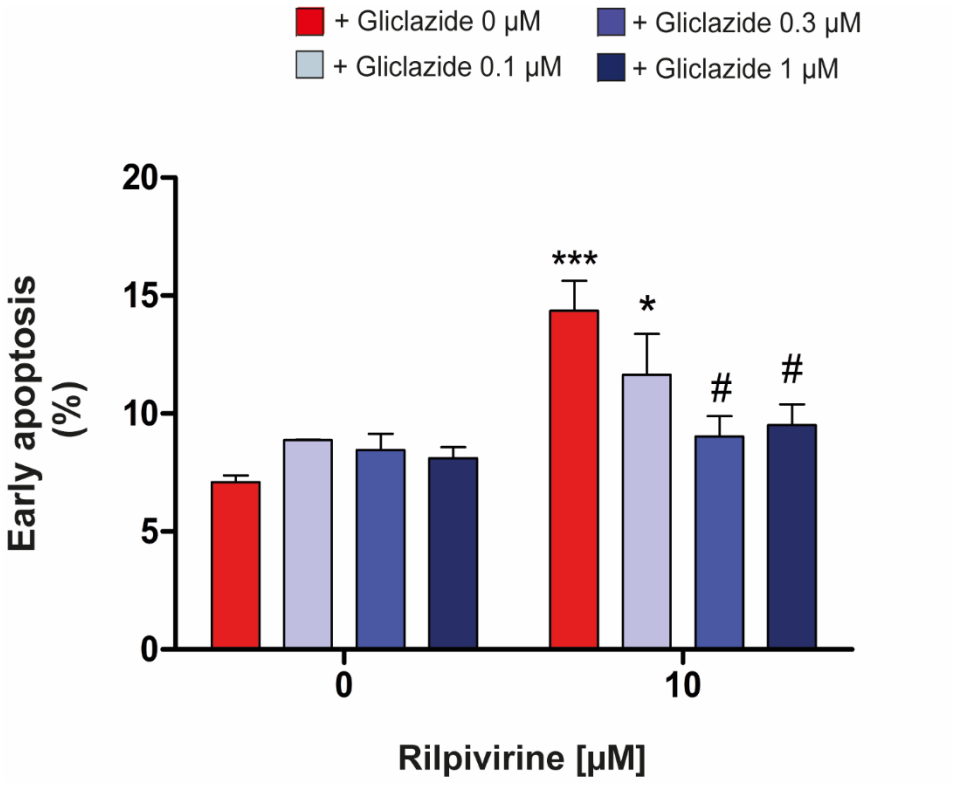

Figure 5.10 Gliclazide attenuates rilpivirine-mediated early apoptosis in INS-1E cells. INS-1E cells were treated with rilpivirine (10 µM) alone or in combination with gliclazide (0.1, 0.3 or 1 µM) for 24 hrs before measuring early apoptosis following staining with Annexin V-FITC and flow cytometric analysis of 10,000 cells per treatment. Data are expressed as mean ± SEM from *n* = 5 independent experiments. Statistical analysis was carried out using two-way ANOVA and Bonferroni post-hoc test where $p < 0.05$ was considered significant; * $p < 0.05$, *** $p < 0.001$ vs. vehicle-treated cells, # $p < 0.05$ vs. rilpivirine alone treated cells.

5.3.5 Gliclazide attenuates rilpivirine-mediated increases in Δψm

We wanted to further clarify if the gliclazide-mediated protection against rilpivirine-induced INS-1E cell apoptosis involved ROS generation and mitochondrial function (Figure 5.11 and Figure 5.12). Therefore, we evaluated whether gliclazide attenuates the rilpivirine-mediated increases in Δψm and intracellular ROS generation observed in INS-1E cells (**Chapter 3**). To do so, we exposed cells to rilpivirine (3 or 10 µM), two concentrations that were shown to increase Δψm and intracellular ROS generation in INS-1E cells (**Chapter 3**). Although rilpivirine (3 µM) exposure caused a profound increase in Δψm, exposure to gliclazide (0.3 and 1 µM) attenuated the rilpivirine (3 µM)-mediated increase in Δψm ($p < 0.05$ vs. rilpivirine alone) (Figure 5.11). Gliclazide (1 µM) significantly reduced Δψm from approximately 170% (rilpivirine 10 µM) to approximately 120% (gliclazide 1 µM plus rilpivirine 10 µM) ($p < 0.05$ vs. rilpivirine alone treated cells) (Figure 5.11).

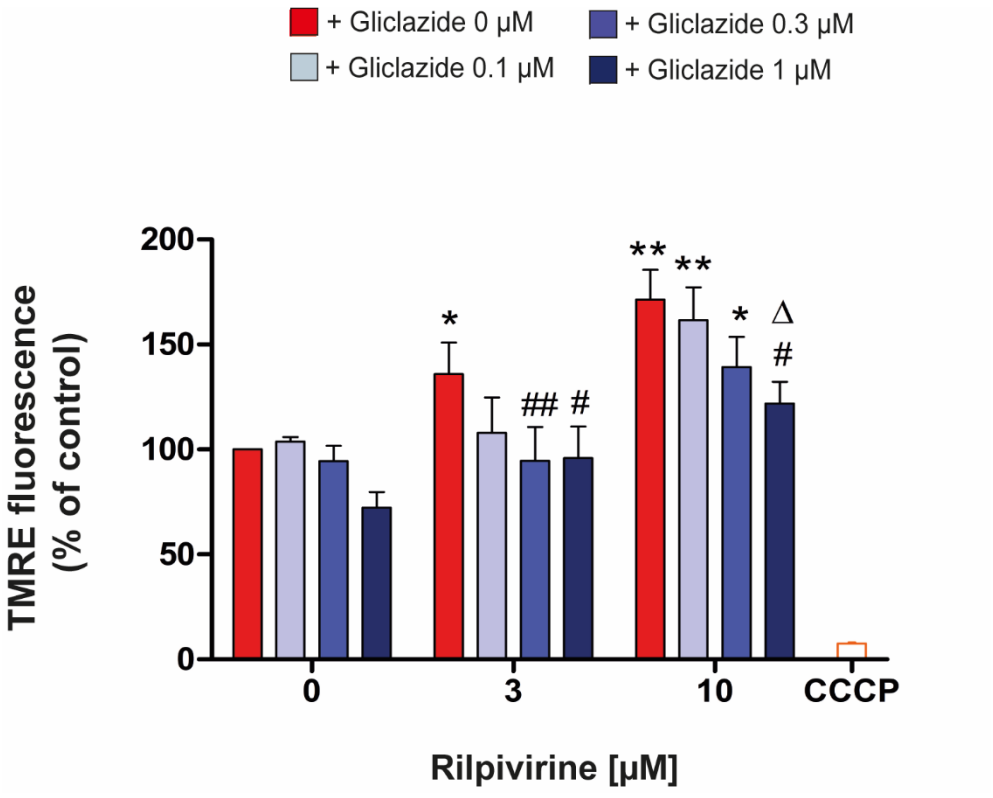

Figure 5.11 Gliclazide attenuates rilpivirine-mediated increases in Δψm in INS-1E cells. INS-1E cells were treated with rilpivirine (10 µM) alone or in combination with gliclazide (0.1, 0.3 or 1 µM) for 24 hrs before assessing changes in Δψm following TMRE staining. TMRE fluorescence is proportional to Δψm. Data are expressed as mean ± SEM from *n* = 5 independent experiments. Statistical analysis was carried out using Freidman's test where $p < 0.05$ was considered significant. * $p < 0.05$, ** $p < 0.01$ vs. vehicle-treated cells, # $p < 0.05$, ## $p < 0.01$ vs. rilpivirine alone treated cells, Δ $p < 0.05$ vs. gliclazide alone treated cells.

5.3.6 Gliclazide protects against rilpivirine-induced intracellular ROS generation

Then, we sought to investigate whether gliclazide reduces intracellular ROS production in INS-1E cells exposed to rilpivirine (3 or 10 µM). Gliclazide (0.1, 0.3 or 1 µM) significantly reduced intracellular ROS generation from nearly 3 RFU (rilpivirine 10 µM) to approximately 0.5 RFU (gliclazide plus rilpivirine treatments) ($p < 0.001$ vs. rilpivirine alone treated cells) (Figure 5.12).

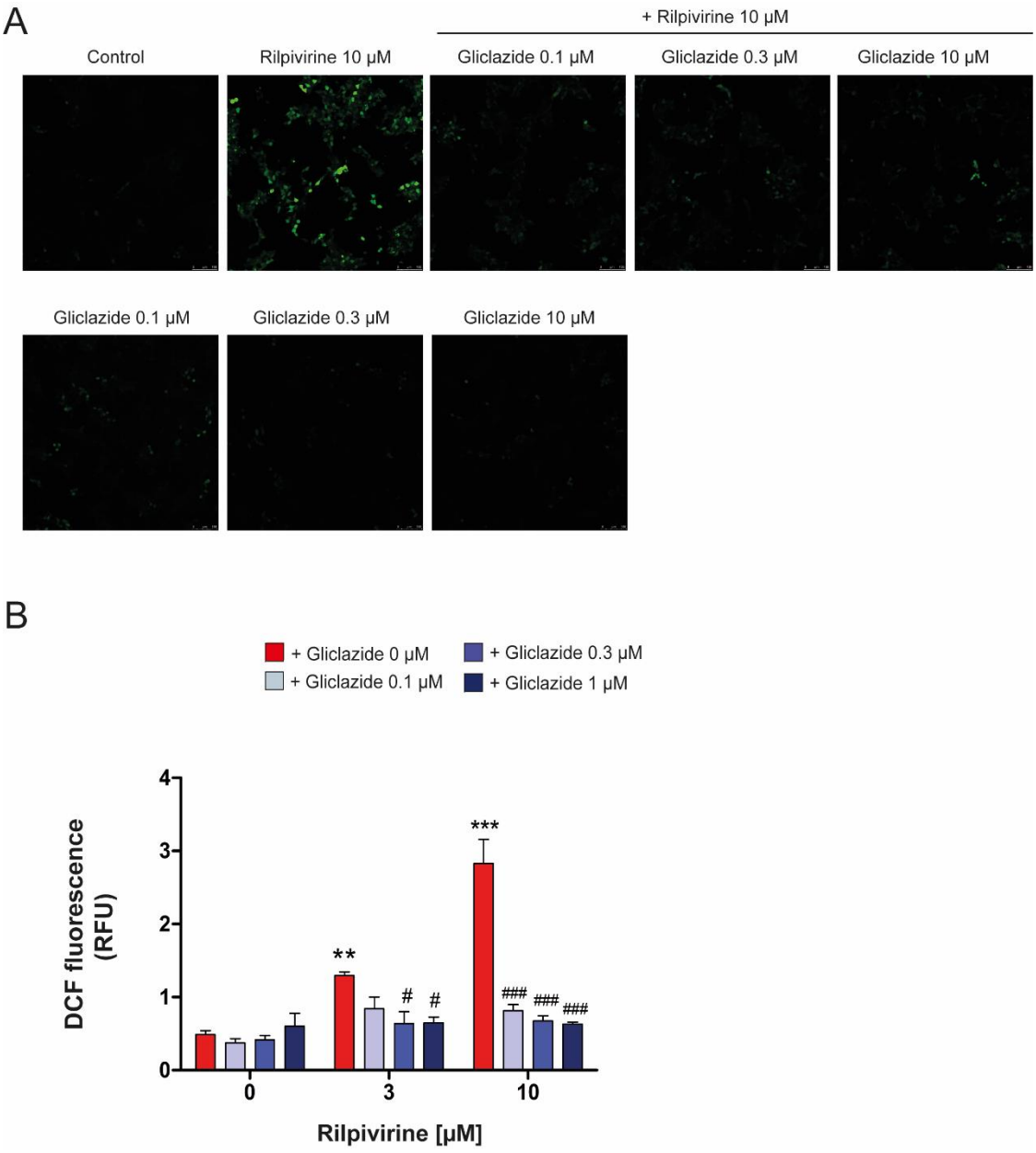

Figure 5.12 Gliclazide protects INS-1E cells from rilpivirine-mediated increases in intracellular ROS generation. INS-1E cells were treated with rilpivirine (10 µM) alone or in combination with gliclazide (0.1, 0.3 or 1 µM) for 24 hrs before measuring intracellular ROS levels with the DCFH-DA assay. (A) Confocal images and (B) quantification graphs of DCFH-DA assay. The fluorescence intensity, expressed as relative fluorescence intensity

(RFU), is proportional to the levels of intracellular ROS. Data are expressed as mean ± SEM from *n* = 3 independent experiments. Statistical analysis was carried out using two-way ANOVA and Bonferroni post hoc test where $p < 0.05$ was considered significant. ** $p < 0.01$, *** $p < 0.001$ vs. vehicle-treated cells, # $p < 0.05$, ### $p < 0.001$ vs. rilpivirine alone treated cells.

5.4 Discussion

We have previously established that the second-generation NNRTI rilpivirine impairs beta cell function and increases beta cell apoptosis (**Chapter 3**). These deleterious effects may, at least partially, be due to increased oxidative stress and mitochondrial dysfunction. Identifying a suitable protective agent can further elucidate the mechanisms by which rilpivirine inhibits insulin release from beta cells and provide a potential therapeutic candidate against rilpivirine-mediated beta cell dysfunction and death. Therefore, we determined the effects of rilpivirine on pancreatic beta cell K_{ATP} channel activity using the TEVC technique while identifying potential binding sites by *in silico* molecular docking. We also studied the effects gliclazide, a potent pancreatic beta cell K_{ATP} channel inhibitor, on the rilpivirine-induced secretory dysfunction and apoptosis in INS-1E cells.

Sulfonylureas such as gliclazide increase insulin release from beta cells mainly through direct, allosteric inhibition of the pancreatic beta cell K_{ATP} channel, a crucial component of the insulin secretory machinery. On the contrary, it has been previously established that the activation of K_{ATP} channels reduces insulin secretion from beta cells. Due to our current, as well as our previous observations (**Chapter 3**), we hypothesise that rilpivirine may directly activate the pancreatic beta cell K_{ATP} channel, resulting in downstream effects leading to reductions in insulin secretion from beta cells.

We show for the first time that rilpivirine activates the pancreatic beta cell K_{ATP} channel (Kir6.2/SUR1) as shown by our TEVC studies in *Xenopus* oocytes. Our *in silico* docking studies predict that rilpivirine highly binds to the SUR1 subunit of the pancreatic beta cell K_{ATP} channel. We confirm these results, as our TEVC studies showed that rilpivirine had no effect on the inward-rectifier K^+ channel subunit Kir6.2. alone, however, rilpivirine activated the whole pancreatic beta cell K_{ATP} channel and needed the presence of SUR1 in order to have a stimulatory effect. Activation of pancreatic beta cell K_{ATP} channels opens the pore allowing K^+ efflux to produce a hyperpolarisation of beta cells, as illustrated previously by using the selective Kir6.2/SUR1 potassium channel activator diazoxide (Shyng *et al.*, 1997). Consequently, L-type $Ca2^+$ channels display low activity or remain closed and insulin release

is reduced. Before conducting our TEVC experiments, we ensured that the pharmacological and biophysical properties of pancreatic K_{ATP} channels in INS-1E cells share the same characteristics with those in pancreatic beta cells (Yang *et al.*, 2005). This would allow us to link our insulin secretion results observed in **Chapter 3** and this current study, with our TEVC data. Our previous findings and current findings demonstrate that rilpivirine alone inhibited insulin secretion from INS-1E cells. Additionally, even at stimulatory glucose concentrations (20 mM) that would induce insulin secretion, GSIS levels remained low in rilpivirine alone treated INS-1E cells. This suggests rilpivirine prevents the closure of pancreatic K_{ATP} channels, preventing cell depolarisation and subsequent insulin secretion from INS-1E cells. In addition to the earlier proposed mechanisms (*i.e.*, oxidative stress and mitochondrial toxicity) related to the rilpivirine-potentiated decrease in insulin secretion, we hypothesise that rilpivirine may also inhibit insulin secretion from beta cells by directly and prolongedly activating pancreatic beta cell K_{ATP} channels.

Furthermore, we predict that rilpivirine may bind to the sulfonylurea binding site in SUR1, as per our *in silico* molecular docking studies. To strengthen this hypothesis, our observations in INS-1E cells treated with both gliclazide and rilpivirine revealed that GSIS from INS-1E cells treated with gliclazide plus rilpivirine was significantly lower in comparison to GSIS seen in gliclazide alone treated cells. This may signify that rilpivirine is affecting the pharmacodynamic activity of gliclazide at the sulfonylurea binding site level in SUR1. It is therefore tempting to speculate that rilpivirine may modulate K_{ATP} channels through competitive binding with gliclazide to the sulfonylurea binding site in SUR1. Rilpivirine may be a potential SUR1 receptor agonist at the sulfonylurea binding site level, leading to the activation of pancreatic K_{ATP} channels as well as the interference with gliclazide's (SUR1 antagonist) binding to SUR1 and the subsequent inhibition of the K_{ATP} channel. Due to its highly potent nature, gliclazide has a high affinity for SUR1, and thus occupies a significant proportion of SUR1, even at low concentrations. To reiterate, we show that rilpivirine prevents any functional protection in INS-1E cells co-treated with gliclazide. However, it is worth noting that INS-1E cells were exposed to a high concentration (10 µM) of rilpivirine compared to lower concentrations (0.1 - 1 µM) of gliclazide. Although it is well established that gliclazide has a high affinity and potency to bind to the SUR1 receptor, we can still assume that rilpivirine has an equally high affinity to SUR1 receptors but probably not the same potency.

We cannot eliminate the possibility that rilpivirine binds to a different site in SUR1, as per our other *in silico* docking predictions. By binding to the other predicted site, between the TMD0

and TMD2 domains of SUR1, rilpivirine may affect the role of these proteins. TMD0 is a crucial modulator of gating and increases the channel open probability (Aittoniemi *et al.*, 2009). We can only hypothesise, that by binding to the site between TMD0 and TMD2 of SUR1, rilpivirine may stimulate the function of TMD0 of increasing the K_{ATP} channel open probability, hence resulting in beta cell hyperpolarisation and subsequent reductions in insulin secretion. Therefore, the binding site of rilpivirine is not fully established, however, it is clear that rilpivirine activates the pancreatic beta cell K_{ATP} channels, a possible mechanism explaining the reductions in GSIS observed in beta cells. Therefore, the activation of pancreatic K_{ATP} channels plays a major role in the beta cell secretory dysfunction mediated by rilpivirine.

However, we show that gliclazide did not offer much functional protection against rilpivirine-mediated impairment of GSIS. Indeed, INS-1E cells treated with both gliclazide and rilpivirine had an improved GSIS in comparison to rilpivirine alone treated cells. However, secreted insulin levels from INS-1E cells treated with gliclazide plus rilpivirine were nowhere near the secreted insulin levels seen in cell treated with gliclazide alone. We also demonstrate that gliclazide restores mitochondrial function and abolishes increased intracellular ROS generation in INS-1E cells exposed to rilpivirine. Therefore, gliclazide may have a minor protective effect against rilpivirine-mediated GSIS impairment which could be due to gliclazide protecting against the increased oxidative stress and mitochondrial dysfunction. This also signifies that rilpivirine is causing GSIS impairment in beta cells through multiple mechanisms, including via its activating effect in pancreatic beta cell K_{ATP} channels.

On the other hand, we demonstrate that gliclazide protected INS-1E cells from rilpivirine-mediated increases in apoptosis, hence may protect against the loss of beta cell mass. The protective effects of gliclazide against rilpivirine-induced beta cell apoptosis are likely mediated by the attenuation of oxidative stress, as we demonstrate that the attenuation of rilpivirine-induced increases in intracellular ROS generation correlates with reductions in INS-1E cell apoptosis. Previous work found that gliclazide prevents pancreatic beta cells from apoptosis, likely through its free radical scavenging properties (Kimoto *et al.*, 2003). Kimoto *et al.* (2003) found that gliclazide protected MIN6 cells from ROS-induced cell apoptosis, potentially due to its antioxidant capacity. Interestingly, these protective effects were not observed with glibenclamide, another sulfonylurea. Similarly, Del Guerra *et al.* (2007) determined that gliclazide, but not glibenclamide, profoundly reduced apoptosis, mitochondrial alterations, and the levels of nitrotyrosine, an oxidative stress marker. Altogether, our findings suggest that gliclazide protects against rilpivirine-induced beta cell apoptosis possibly through

its established antioxidant properties. Sliwinska *et al.* (2012) found that gliclazide protects against ROS-induced apoptotic cell death likely through the inhibition of ROS production due to its antioxidant properties.

We also suggest that by attenuating Δψm, gliclazide can protect against the rilpivirine-mediated increases in Δψm and subsequent apoptosis. Although the effects of gliclazide on Δψm in beta cells have not been investigated previously, gliclazide was shown to decrease Δψm in other cell types (Sliwinska *et al.*, 2012). The pharmacology of the mitochondrial K_{ATP} channel is believed to be similar to that of the plasma membrane K_{ATP} channels, including inhibition by sulfonylureas (Paucek *et al.*, 1992). Here, we show that gliclazide attenuates the rilpivirine-mediated increases in Δψm. We can only speculate that rilpivirine may activate mitochondrial K_{ATP} channels, explaining the increases in Δψm seen in INS-1E cells (**Chapter 3** and **4**). However, gliclazide may protect mitochondrial function of INS-1E cells by inhibiting the mitochondrial K_{ATP} channel in beta cells, causing a slight loss of Δψm (*i.e.*, mitochondrial depolarisation). If this is the case, the rilpivirine-mediated increase in Δψm could be counteracted with the decrease in Δψm that may be caused by gliclazide. However, these are only speculations and further work is warranted to confirm this. Moreover, although the presence of K_{ATP} channels have been found in the mitochondria of cardiomyocytes, neurones and skeletal muscle cells, mitochondrial K_{ATP} channels have not been confirmed in pancreatic beta cells (Paucek *et al.*, 1992). However, some researchers believe that these channels, can in fact, be found in the mitochondria of beta cells. This is still a controversial topic as some researchers failed to detect any immunoreactivity of K_{ATP} channel subunits Kir6.2 and SUR1 in the mitochondria of mouse islets and MIN6 cells (Varadi *et al.*, 2006). Nevertheless, the restoration of mitochondrial function by gliclazide may also explain its protective effects against rilpivirine-mediated apoptosis. Indeed, mitochondria also play a critical role in controlling beta cell mass. Thus, changes in Δψm, such as an increase, lead to mitochondria-mediated apoptosis (Diane *et al.*, 2022; Scarlett *et al.*, 2000). When mitochondrial hyperpolarisation dissipates, the voltage-sensitive permeability transition pore (PTP) will open and release pro-apoptotic agents such as cytochrome *c* into the cytoplasm and drive apoptotic cell death (Scarlett *et al.*, 2000). Therefore, by decreasing Δψm, gliclazide may reduce cytochrome *c* release and subsequent apoptosis observed in rilpivirine-treated INS-1E cells. Sliwinska *et al.* (2012) found that gliclazide restored Δψm and diminished intracellular calcium levels evoked by H_2O_2. Therefore, mitochondrial toxicity and oxidative seem to play an

important role in rilpivirine-mediated beta cell apoptosis by activating key pathways such as the mitochondria-dependent apoptotic pathway.

5.5 Conclusions

In conclusion, the present study sheds light into novel perspectives in the rilpivirine-induced insulin-secretory dysfunction in pancreatic beta cells. We uncover, for the first time, an important and novel mechanism for rilpivirine-mediated secretory dysfunction in pancreatic beta cells. Rilpivirine directly activates the pancreatic beta cell K_{ATP} channel, partly explaining its negative impact on insulin secretion. The binding site is yet to be uncovered, however, there is a strong possibility that rilpivirine binds to the sulfonylurea binding site, hence directly affecting gliclazide's mode of action: inhibiting insulin secretion. On the other hand, gliclazide protected beta cells from rilpivirine-induced beta cell apoptosis, hence contributing to the preservation of beta cell mass, likely through its antioxidant properties and partial mitochondrial preservation. These findings may provide a crucial insight into an effective management of T2D in HIV-infected individuals on rilpivirine-based ART regimens.

The following chapter will investigate the effects of the NNRTIs efavirenz and rilpivirine in a pathophysiologically relevant diabetic milieu.

6. Synergistic effects of efavirenz or rilpivirine and the saturated free fatty acid palmitate in promoting beta cell dysfunction and death

6.1 Introduction

The worldwide prevalence of type 2 diabetes (T2D) is rapidly increasing, partially due to the growing obesity epidemic, with obesity considered as an important risk factor for the development of T2D (Cnop *et al.*, 2005; Cunha *et al.*, 2008).

T2D is characterised by a loss of insulin sensitivity and impaired insulin secretion followed by a progressive loss of beta cell mass, all of which may be influenced by changes in lipid availability (Diakogiannaki *et al.*, 2007; Newsholme *et al.*, 2007). Obesity is associated with alterations in the circulating free fatty acid (FFA) profile of affected individuals (Diakogiannaki *et al.*, 2007; Kahn *et al.*, 2006b; Rhodes, 2005). Circulating FFAs are albumin-bound lipid molecules mainly derived from adipose tissue lipolysis.

Over the last decades, the central role of pancreatic beta cell dysfunction and loss of beta cell mass in the pathogenesis of T2D has become increasingly appreciated. Although the main cause(s) of this deterioration are unknown, several hypotheses have been suggested following extensive scientific research. Amongst them, lipotoxicity has been postulated to contribute to the worsening of beta cell function and loss of beta cell mass over time, taking part of a vicious cycle involving impairment of insulin secretion which further aggravates metabolic disruptions and so forth, and may contribute to the increased incidence of T2D (Oh *et al.*, 2018; Poitout *et al.*, 2010b). 'Lipotoxicity' is an umbrella term for the damaging effects of fat accumulation in non-adipose tissues, ensuing chronic elevated plasma FFAs and concomitant overwhelming of adipocytes due to limited lipid storage capacity (Engin, 2017; Sobczak *et al.*, 2019). Both stimulatory and deleterious effects of saturated FFAs on pancreatic beta cell function have long been established, linking acute exposure to a substantial increase in insulin secretion, whereas a prolonged exposure leads to a desensitisation and suppression of insulin secretion (Ciregia *et al.*, 2017; Haber *et al.*, 2006; Poitout & Robertson, 2008) Indeed, prolonged exposure (≥ 24 hours) of pancreatic beta cells to high concentrations of certain saturated FFAs has been shown to have detrimental effects, falling under the lipotoxicity phenomenon in which the cells display secretory dysfunction, loss of cell viability and increased rates of apoptosis (Ciregia *et al.*, 2017;

Dhayal *et al.*, 2019). The lipotoxic effects of FFAs seem to depend mainly on the degree of their saturation and duration of exposure. Prolonged exposure to long-chain saturated FFAs such as palmitate (C16:0), one of the most abundant saturated FFAs in the human plasma, induced secretory dysfunction and apoptosis in pancreatic beta cells, whereas longer chain unsaturated FFAs (e.g., oleate (C18:1n-9) and palmitoleate (C16:1n-7)) potentiated glucose-stimulated insulin secretion (GSIS) and exerted a cytoprotective effect in beta cells (Keane *et al.*, 2010; Morgan *et al.*, 2008; Welters *et al.*, 2006). The mechanisms surrounding lipotoxicity in pancreatic beta cells remain unclear, however, it has been suggested that oxidative stress, impairment of mitochondrial function and activation of endoplasmic reticulum (ER) stress may be involved in impairing insulin secretion and triggering apoptosis in beta cells (Ciregia *et al.*, 2017; Cnop *et al.*, 2005; Dhayal *et al.*, 2019; Sargsyan & Bergsten, 2011). Furthermore, as previously demonstrated in **Chapter 3**, both the first- and second-generation NNRTIs efavirenz and rilpivirine impaired beta cell function and worsened beta cell survival, possibly through oxidative stress, mitochondrial dysfunction, and ER stress.

Here, we hypothesise that efavirenz or rilpivirine can synergise with palmitate to potentiate damaging effects on beta cell function and survival. Therefore, our aim was to investigate the potential synergistic effects of efavirenz or rilpivirine and palmitate by exposing INS-1E cells to concentrations of efavirenz and rilpivirine that were shown to have no effect on beta cell function and survival, in addition to physiological concentrations of palmitate.

6.2 Materials and methods

6.2.1 Materials

All materials were obtained as described in Materials, **Chapter 2** (see 2.1).

6.2.2 Preparation of palmitate solutions

Serum palmitate concentrations range between 10 μM under physiological conditions to 300 μM in diabetes (Clore *et al.*, 2002; Wu *et al.*, 2021). We consider the concentration range (3 – 100 μM) of palmitate as physiologically relevant: although total plasma fatty acids can be as high as 1 mM or even higher under some physiological and pathological conditions (obesity and T2D), the concentration of palmitate under most conditions is generally much lower (Belfort *et al.*, 2005; Kien *et al.*, 2013; Patková *et al.*, 2014).

Here, we investigate the potential synergistic effects of efavirenz or rilpivirine and palmitate on INS-1E cells, as per the following definition. A combination of drugs is synergistic when the combined effect is larger than the additive effect of each individual drug (García-Fuente *et al.*, 2018).

Palmitate solutions were freshly prepared before each experiment. A palmitate (sodium salt) stock solution (10 mM) was prepared by dissolving 27.8 mg of sodium palmitate in 5 mL of distilled water, 200 µL of sodium hydroxide (NaOH) and 200 µL of 100% absolute ethanol, by continuously stirring at 98.5 °C in a preheated water bath. When the palmitate (sodium salt) was visibly dissolved, 1 mL of the stock palmitate solution was conjugated with 1 mL of 6 mM FFA-free BSA solution in a 3:1 molar ratio for 1 hr at 37°C (Beeharry *et al.*, 2003). The conjugated palmitate was then diluted in RPMI-1640 medium supplemented with 3% heat-inactivated FCS to a final concentration of 3, 10, 30 and 100 µM of palmitate (Table 6, **Appendix I**).

6.2.3 Preparation of working solutions

Efavirenz (1, 3 or 10 µM) or rilpivirine (0.3, 1 or 3 µM) were added to palmitate 3, 10, 30 or 100 µM solutions as to prepare eight combination treatments (Table 6, **Appendix I**). Additionally, efavirenz (1, 3 or 10 µM) and rilpivirine (0.3, 1 or 3 µM) solutions were prepared according to Table 6, **Appendix I**. Vehicle (BSA, NaOH and ethanol) controls were included in each experiment and exerted no effect in INS-1E cells.

6.2.4 Treatment protocol

Following cell growth as described in **Chapter 2** (**see** 2.2.1), the cells were exposed to efavirenz (1, 3 or 10 µM), rilpivirine (0.3, 1 or 3 µM) or palmitate (3, 10, 30 or 100 µM) alone, or to the combination treatments described above. Treated cells were incubated at 37°C in a humidified atmosphere of 95% air and 5% CO_2 for 24 hrs.

Then, GSIS (see 2.2.3.1), cell viability (see 2.2.5), apoptosis and necrosis levels (see 2.2.2.6), intracellular ROS generation (see 2.2.8.1), mitochondrial membrane potential ($\Delta\psi m$) (see 2.2.2.9) and expression of CHOP protein (see 2.2.12) were assessed as described in **Chapter 2.**

6.3 Results

6.3.1 Efavirenz or rilpivirine plus palmitate trigger a synergistic loss of cell viability

Previous findings have reported that exposure to palmitate (≥ 250 µM) caused a loss of cell viability in cultured primary and clonal insulin-secreting beta cells (Diakogiannaki *et al.*, 2007; Morgan & Dhayal, 2010; Welters *et al.*, 2004). We previously found that the NNRTIs efavirenz (≥ 20 µM) and rilpivirine (≥ 10 µM) caused a loss in cell viability in INS-1E cells (**Chapter 3**). Here, we investigate the effects of efavirenz or rilpivirine plus palmitate on INS-1E cell viability (Table 6.1 and 6.2).

As expected, a 24-hour exposure to increasing concentrations of palmitate or efavirenz alone had no effect on INS-1E cell viability (Table 6.1). On the other hand, a significant reduction in cell viability was observed in INS-1E cells exposed to palmitate plus efavirenz. For example, efavirenz (10 µM) and palmitate (10 µM) alone had no effect on INS-1E cell viability, however, combination treatment with efavirenz (10 µM) plus palmitate (10 µM) caused a synergistic reduction (31%) in cell viability ($p < 0.01$ vs. efavirenz or palmitate alone) (Table 6.1).

Table 6.1 The effects of a 24-hour exposure to efavirenz plus palmitate on INS-1E cell viability. INS-1E cells were exposed to BSA, NaOH plus ethanol (0 µM), 1 µM (A), 3 µM (B) or 10 µM (C) of efavirenz alone, palmitate (3, 10, 30 and 100 µM) alone, or efavirenz plus palmitate before assessing cell viability. Exposure to efavirenz or palmitate alone had no effects on INS-1E cell viability while exposure to efavirenz plus palmitate combination treatments significantly reduced cell viability. Data are expressed as mean ± SEM from n = 5 independent experiments. Statistical analysis was carried out using carried out using Friedman's test where $p < 0.05$ was considered significant; * $p < 0.05$, ** $p < 0.01$ vs. vehicle-treated control cells. # $p < 0.05$, ## $p < 0.01$ vs. efavirenz alone treated cells. Δ $p < 0.05$, ΔΔ $p < 0.01$ vs. palmitate alone treated cells. n.b. Cell viability and SEM were rounded up to nearest one decimal place.

Efavirenz (µM)	Palmitate (µM)				
	0	3	10	30	100
0	100.0±0%	101.2±1%	100.9±1%	103.4±3%	95.7±2%
1	98.1±10%	100.7±1%	100.4±1%	101.4±1%	91.6±2%
3	97.2±7%	92.9±2%	96.2±1%	96.5±1%	86.4±2%*#
10	95.4±8%	81.1±4%*#ΔΔ	69.1±2%**##ΔΔ	78.5±4%**##ΔΔ	70.1±6%**##Δ

As expected, a 24-hour exposure to increasing concentrations of palmitate or rilpivirine alone had no effect on INS-1E cell viability (Table 6.2). On the other hand, a significant reduction in cell viability was observed in INS-1E cells exposed to palmitate plus rilpivirine. For example,

rilpivirine (3 µM) and palmitate (30 µM) alone had no effect on INS-1E cell viability, however, combination treatment with rilpivirine (3 µM) plus palmitate (30 µM) caused a synergistic reduction (13%) in cell viability ($p < 0.05$ vs. rilpivirine or palmitate alone) (Table 6.2).

Table 6.2 The effects of a 24-hour exposure to rilpivirine plus palmitate on INS-1E cell viability. INS-1E cells were exposed to BSA, NaOH plus ethanol (0 µM), 0.3 µM (A), 1 µM (B) or 3 µM (C) of rilpivirine alone, palmitate (3, 10, 30 and 100 µM) alone, or rilpivirine plus palmitate before assessing cell viability using an MTT assay. Exposure to rilpivirine or palmitate alone had no effects on INS-1E cell viability while exposure to rilpivirine plus palmitate combination treatments significantly reduced cell viability. Data are expressed as mean ± SEM from *n* = 3 - 4 independent experiments. Statistical analysis was carried out using using Friedman's test where $p < 0.05$ was considered significant; * $p < 0.05$, ** $p < 0.01$ vs. vehicle-treated control cells. # $p < 0.05$, ## $p < 0.01$ vs. rilpivirine alone treated cells, Δ $p < 0.05$ vs. palmitate alone treated cells. n.b. Cell viability and SEM were rounded up to nearest one decimal place.

Rilpivirine (µM)	Palmitate (µM)				
	0	3	10	30	100
0	100.0±0%	96.3±6%	99.2±5%	104.6±4%	96.9±4%
0.3	97.2±3%	93.0±1%	93.6±1%	94.5±2%	90.8±1%
1	94.9±5%	86.2±1%	90.7±11%	86.5±7%*	84.5±1%*#
3	97.4±3%	74.4±10%***##	76.2±8%**#	86.6±5%*#Δ	82.5±7%**##Δ

These initial preliminary studies established the suitable combination treatments to investigate further. Therefore, we focused on the synergistic effects of efavirenz (3 or 10 µM) or rilpivirine (0.3 or 1 µM) in combination with palmitate (10 or 30 µM) on GSIS and cell death in INS-1E cells.

6.3.2 Efavirenz or rilpivirine plus palmitate trigger a synergistic impairment of glucose-stimulated insulin secretion (GSIS)

In view with the previous results, we measured GSIS in INS-1E cells exposed to efavirenz (3 or 10 µM) or rilpivirine (0.3 or 1 µM) alone or in combination with palmitate (10 or 30 µM) for 24 hours (Figure 6.1). Palmitate was previously shown to reduce GSIS from INS-1E cells following 24-hour exposure to high concentrations (40 mM) of palmitate (Barlow & Affourtit, 2013; Barlow *et al.*, 2016). We previously found that the NNRTIs efavirenz (≥ 20 µM) and rilpivirine (≥ 3 µM) cause a reduction in GSIS from INS-1E cells (**Chapter 3**).

As expected, a 24-hour exposure to palmitate or efavirenz alone had no effect on GSIS from INS-1E cells (Figure 6.1, A). On the other hand, a significant reduction in GSIS from INS-1E cells exposed to palmitate (10 or 30 µM) plus efavirenz (3 or 10 µM) was observed. For

example, efavirenz (10 µM) and palmitate (10 µM) alone had no effect on INS-1E cell viability, however, combination treatment with efavirenz (10 µM) plus palmitate (10 µM) caused a synergistic reduction (50%) in GSIS from INS-1E cells ($p < 0.05$ vs. efavirenz or palmitate alone) (Figure 6.1, A).

Similarly, a 24-hour exposure to palmitate or rilpivirine alone had no effect on GSIS from INS-1E cells (Figure 6.1, B). On the other hand, a significant reduction in GSIS from INS-1E cells exposed to palmitate (10 or 30 µM) plus rilpivirine (0.3 or 1 µM) was observed. For example, rilpivirine (1 µM) and palmitate (10 µM) alone had no effect on INS-1E cell viability, however, combination treatment with rilpivirine (1 µM) plus palmitate (10 µM) caused a synergistic reduction (75%) in GSIS form INS-1E cells ($p < 0.01$ vs. rilpivirine or palmitate alone) (Figure 6.1, A).

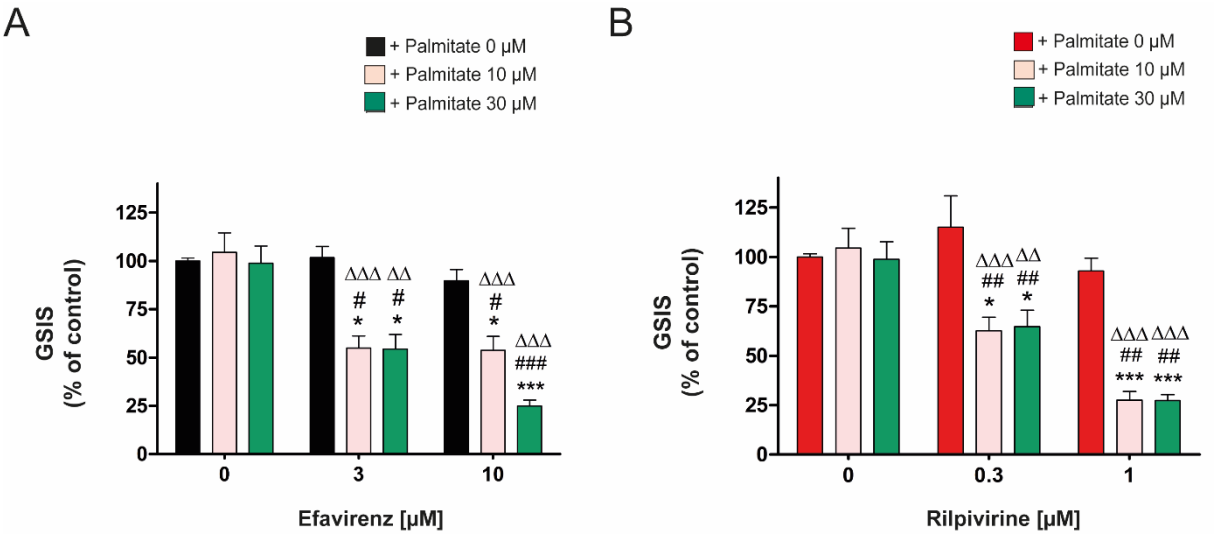

Figure 6.1 Efavirenz or rilpivirine plus palmitate exert synergistic reductions in GSIS from INS-1E cells. INS-1E cells were exposed to BSA, NaOH plus ethanol (0 µM), efavirenz (3 or 10 µM) (A), rilpivirine (0.3 or 1 µM) (B) or palmitate (10 or 30 µM) alone or in combination with palmitate (10 or 30 µM) before assessing insulin concentrations. Data are expressed as mean ± SEM from *n* = 4 independent experiments. Statistical analysis was carried out using Friedman's test where $p < 0.05$ was considered significant; * $p < 0.05$, *** $p < 0.001$ vs. vehicle-treated control cells, # $p < 0.05$, ## $p < 0.01$, ### $p < 0.001$ vs. efavirenz or rilpivirine alone treated cells, ΔΔ $p < 0.01$, ΔΔΔ $p < 0.001$ vs. palmitate alone treated cells.

6.3.3 Efavirenz or rilpivirine plus palmitate synergistically increase early apoptosis

We next sought to assess the levels of apoptosis and necrosis in INS-1E cells following a 24-hour exposure to efavirenz (Figure 6.2) or rilpivirine (Figure 6.3) alone, or in combination with palmitate. Previous findings suggest that beta cell apoptosis can be initiated by exposure (24

and 48 hours) to high levels of palmitate (500 µM or higher) in INS-1E cells (Sargsyan & Bergsten, 2011).

As expected, a 24-hour exposure to palmitate or efavirenz alone had no effect on early apoptosis and late apoptosis/primary necrosis from INS-1E cells (Figure 6.2). On the other hand, a significant increase in early apoptosis in INS-1E cells exposed to palmitate (10 or 30 µM) plus efavirenz (10 µM) was observed. For example, efavirenz (10 µM) and palmitate (10 µM) alone had no effect on early apoptosis, however, combination treatment with efavirenz (10 µM) plus palmitate (10 µM) synergistically doubled early apoptotic cell levels in INS-1E cells (Figure 6.2, B) cells as demonstrated by the representative plots that show an increase in the number of INS-1E cells in the early apoptotic quadrant (Annexin V+/PI-) ($p < 0.05$ vs. efavirenz or palmitate alone) (Figure 6.2, A).

Efavirenz in combination with palmitate had no effect on late apoptosis/primary necrosis in INS-1E cells (Figure 6.2, C).

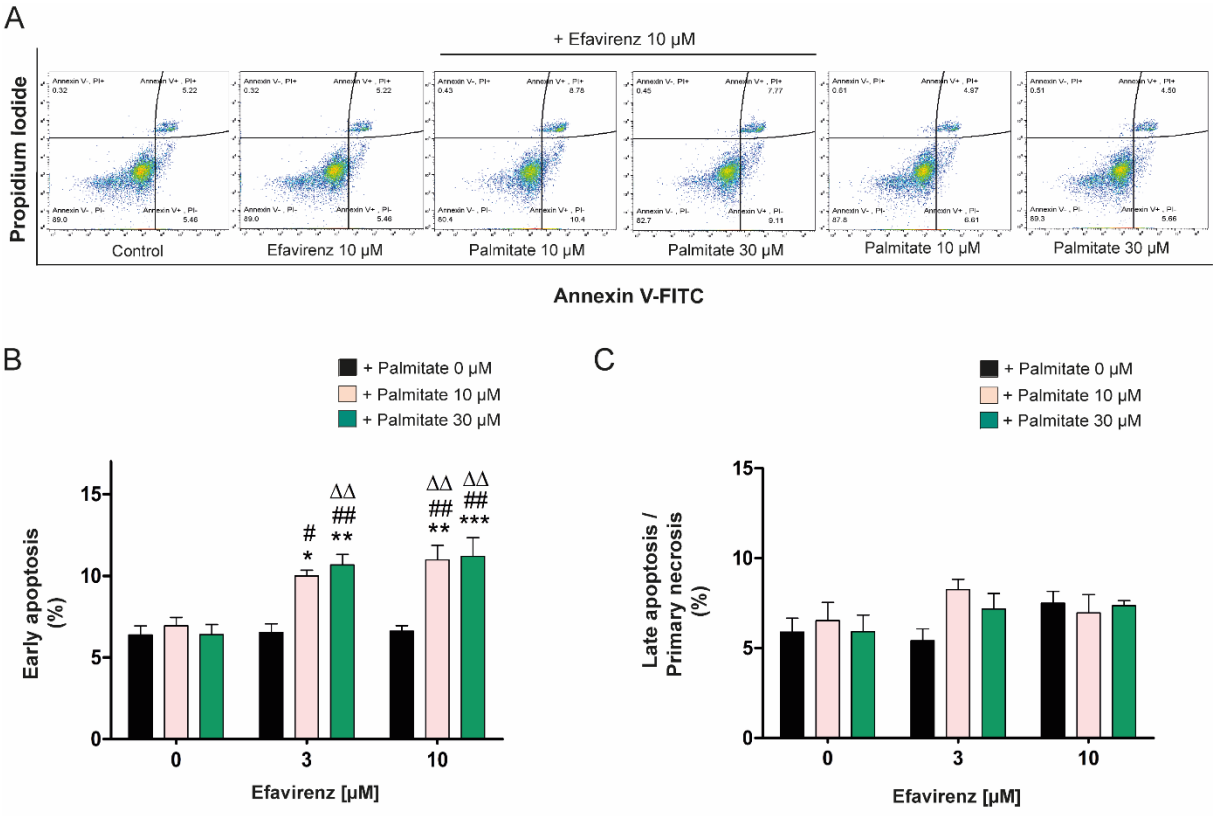

Figure 6.2 Efavirenz plus palmitate cause a synergistic increase in early apoptosis in INS-1E cells. INS-1E cells were exposed to BSA, NaOH plus ethanol (0 µM), efavirenz (3 or 10 µM) alone or in combination with palmitate (10 or 30 µM) for 24 hrs before assessing apoptosis and necrosis by flow cytometry following staining with Annexin V and PI. Data are expressed as mean ± SEM from $n = 4$ independent experiments. Statistical analysis was carried out using two-way ANOVA and Bonferroni correction where $p < 0.05$ was considered significant; * $p < 0.05$, ** $p < 0.01$, *** $p < 0.001$ vs. vehicle-treated cells, # $p < 0.05$, ## $p < 0.01$ vs. efavirenz alone treated cells, ΔΔ $p < 0.01$ vs. palmitate alone treated cells.

As expected, a 24-hour exposure to palmitate or rilpivirine alone had no effect on early apoptosis and late apoptosis/primary necrosis from INS-1E cells (Figure 6.3). On the other hand, palmitate (30 µM) plus rilpivirine (1 µM) caused a synergistic increase (50%) in early apoptosis in INS-1E (Figure 6.3, B) cells as demonstrated by the representative plots that show an increase in the number of INS-1E cells in the early apoptotic quadrant (Annexin V+/PI-) ($p < 0.05$ vs. rilpivirine alone) (Figure 6.3, A).

Rilpivirine in combination with palmitate had no effect on late apoptosis/primary necrosis in INS-1E cells (Figure 6.3, C).

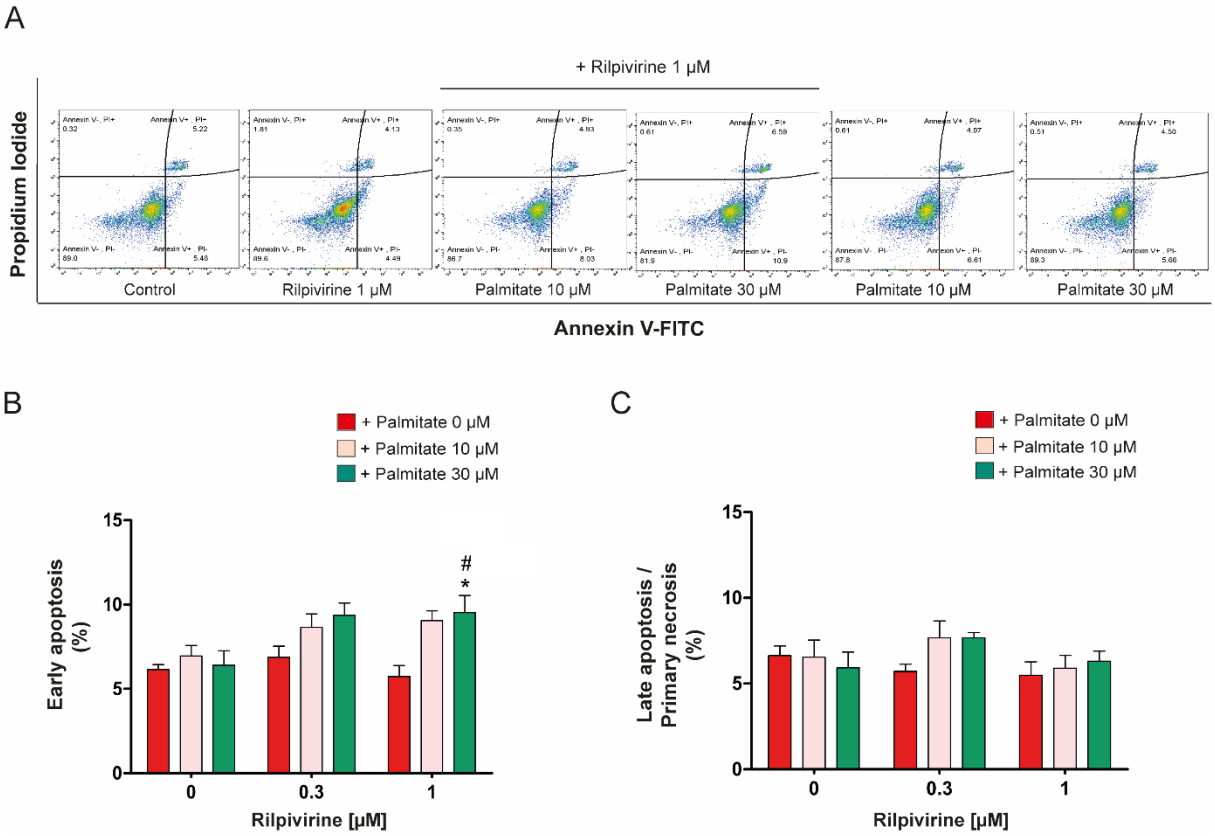

Figure 6.3 Rilpivirine plus palmitate cause a synergistic increase in early apoptosis rates in INS-1E cells. INS-1E cells were exposed to BSA, NaOH plus ethanol (0 µM), rilpivirine (0.3 or 1 µM) alone or in combination with palmitate (10 or 30 µM) for 24 hrs before assessing cell death by flow cytometry following staining with Annexin V and PI. Data are expressed as mean ± SEM from *n* = 4 independent experiments. Statistical analysis was carried out using two-way ANOVA and Bonferroni correction where $p < 0.05$ was considered significant; * $p < 0.05$ vs. vehicle-treated cells, # $p < 0.05$ vs. rilpivirine alone treated cells.

6.3.4 Potential cellular mechanisms

After observing the synergistic damaging effects of palmitate plus efavirenz or rilpivirine on INS-1E cells, we focused on identifying possible mechanisms by which efavirenz or rilpivirine plus palmitate synergise to cause secretory dysfunction and death in INS-1E cells.

6.3.4.1 Synergistic increase in intracellular ROS generation by palmitate plus efavirenz or rilpivirine

Previous reports have shown that exposure (24 hours) to higher concentrations of palmitate (≥ 250 μM) induce intracellular ROS generation in a variety of primary and clonal beta cells (Nemecz *et al.*, 2019). We also found that exposure to higher concentrations of efavirenz (≥ 20 μM) and rilpivirine (≥ 3 μM) was shown to induce intracellular ROS generation in INS-1E cells (**Chapter 3**). Therefore, we investigated whether exposure to combination treatments of efavirenz (Figure 6.4) or rilpivirine (Figure 6.5) plus palmitate induce a synergistic increase in intracellular ROS generation.

A profound increase in intracellular ROS generation was observed in INS-1E cells exposed to efavirenz or rilpivirine plus palmitate compared to control (Figure 6.4 and Figure 6.5).

Although a 24-hour exposure to efavirenz or palmitate alone had no effects on intracellular ROS generation in INS-1E cells, cells exposed to palmitate plus efavirenz increased intracellular ROS generation by nearly 10-fold (efavirenz 10 μM plus palmitate 10 μM) ($p < 0.01$ vs. palmitate or efavirenz alone), suggesting that efavirenz and palmitate synergistically induced intracellular ROS generation in INS-1E cells (Figure 6.4, B).

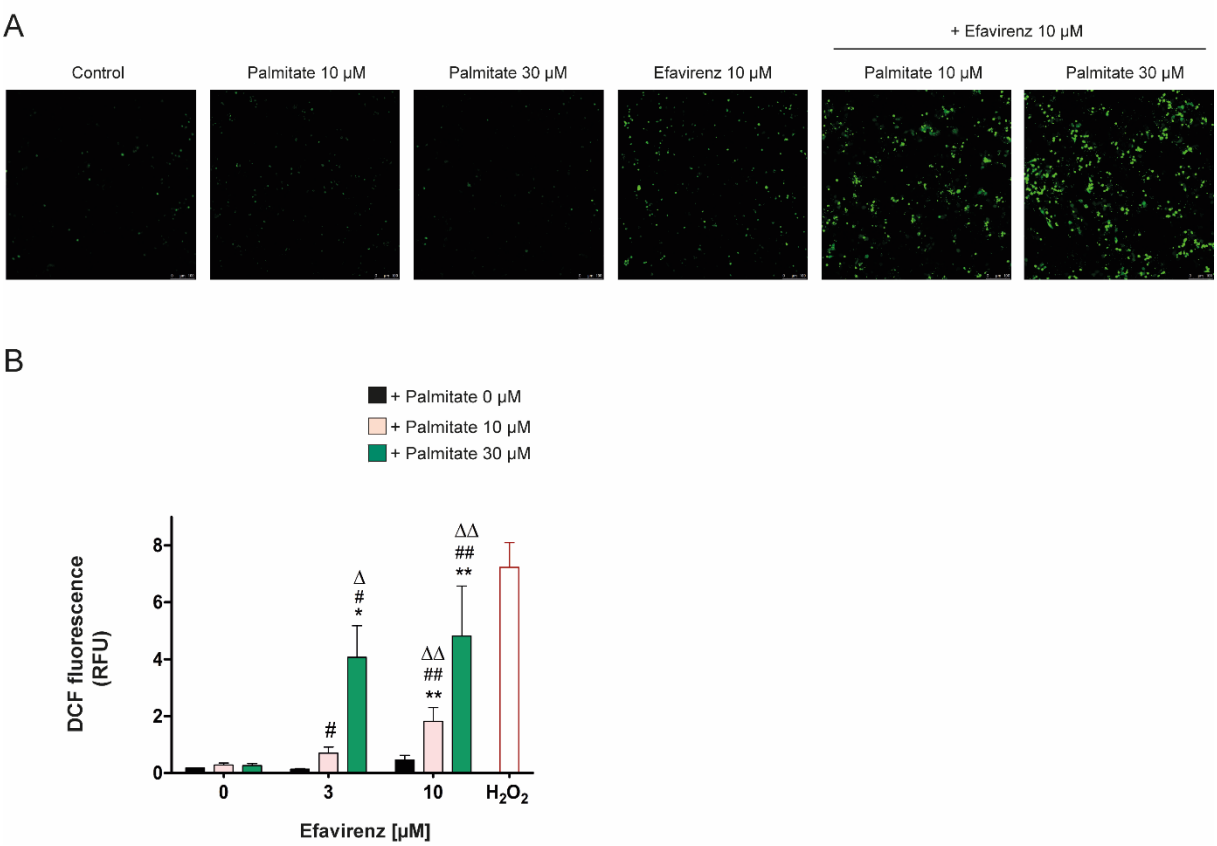

Figure 6.4 Efavirenz plus palmitate cause a synergistic increase in intracellular ROS generation in INS-1E cells. INS-1E cells were exposed to BSA, NaOH plus ethanol (0 µM), efavirenz (3 or 10 µM) alone or in combination with palmitate (10 or 30 µM) for 24 hrs before assessing intracellular ROS generation by confocal microscopy. INS-1E cells were incubated with 100 µM H_2O_2 for 1 hr to induce ROS generation. (A) Confocal images of INS-1E exposed to efavirenz or palmitate alone, and combination treatments of efavirenz plus palmitate. The green fluorescence represents DCF which was oxidised from DCFH. (Scale bar, 100 µm). (B) Quantification graphs of intracellular ROS levels in INS-1E cells exposed to efavirenz or palmitate alone, and combination treatments of efavirenz plus palmitate determined by DCF mean fluorescence intensity using the image processing software Image J. DCF fluorescence intensity expressed as relative fluorescence intensity (RFU) is proportional to the levels of intracellular ROS. Data are expressed as mean ± SEM from *n* = 4 independent experiments. Statistical analysis was carried out using two-way ANOVA and Bonferroni post hoc test where $p < 0.05$ was considered significant; * $p < 0.05$, ** $p < 0.01$ vs. vehicle-treated control cells, # $p < 0.05$, ## $p < 0.01$ vs. efavirenz alone treated cells, Δ $p < 0.05$, ΔΔ $p < 0.01$ vs. palmitate alone treated cells.

Although a 24-hour exposure to rilpivirine or palmitate alone had no to negligible effects on intracellular ROS generation in INS-1E cells, cells exposed to palmitate plus rilpivirine increased intracellular ROS generation by 12-fold (rilpivirine 1 µM plus palmitate 10 µM) ($p < 0.01$ vs. palmitate or rilpivirine alone), suggesting that rilpivirine and palmitate synergistically induced intracellular ROS generation in INS-1E cells (Figure 6.5, B).

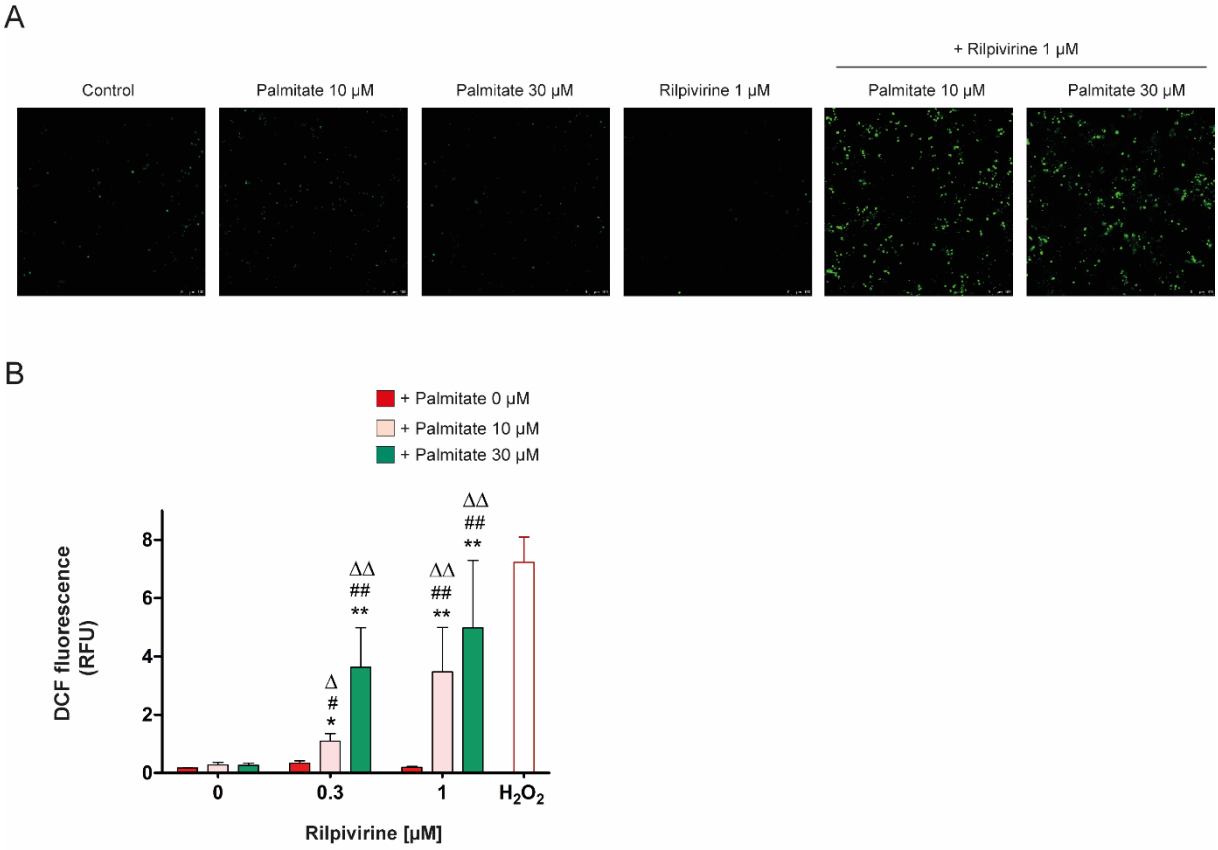

Figure 6.5 Rilpivirine plus palmitate cause a synergistic increase in intracellular ROS generation in INS-1E cells. INS-1E cells were exposed to BSA, NaOH plus ethanol (0 µM), rilpivirine (0.3 or 1 µM) alone or in combination with palmitate (10 or 30 µM) for 24 hrs before assessing intracellular ROS generation by confocal microscopy. INS-1E cells were incubated with 100 µM H_2O_2 as a positive control. (A) Confocal images of INS-1E exposed to rilpivirine or palmitate alone, and combination treatments of rilpivirine plus palmitate. The green fluorescence represents DCF which was oxidised from DCFH. (Scale bar, 100 µm). (B) Quantification graphs of intracellular ROS levels in INS-1E cells exposed to rilpivirine or palmitate alone, and combination treatments of rilpivirine plus palmitate determined by DCF mean fluorescence intensity. DCF fluorescence intensity expressed as relative fluorescence intensity (RFU) is proportional to the levels of intracellular ROS. Data are expressed as mean ± SEM from *n* = 4 independent experiments. Statistical analysis was carried out using two-way ANOVA and Bonferroni post hoc test where $p < 0.05$ was considered significant; ** $p < 0.01$ vs. vehicle-treated control cells, # $p < 0.05$, ## $p < 0.01$ vs. rilpivirine alone treated cells, Δ $p < 0.05$, ΔΔ $p < 0.01$ vs. palmitate alone treated cells.

6.3.4.2 Efavirenz or rilpivirine plus palmitate trigger synergistic disruptions in mitochondrial membrane potential (Δψm)

Exposure to high concentrations of palmitate was shown to decrease Δψm in beta cells (Song *et al.*, 2014). We also found that exposure to higher concentrations of efavirenz (≥ 20 µM) and rilpivirine (≥ 3 µM) was shown to decrease Δψm, in the case of efavirenz, or increase in Δψm in INS-1E cells (**Chapter 3**). Therefore, we investigated the effects of palmitate (10 or 30 µM), efavirenz (3 or 10 µM) or rilpivirine (0.3 or 1 µM) alone or in combination with palmitate on Δψm (Figure 6.6).

Although a 24-hour exposure to efavirenz or palmitate alone had no effects on Δψm, INS-1E cells exposed to palmitate (10 µM) plus efavirenz (10 µM) decreased Δψm by nearly 50% ($p < 0.05$ vs. palmitate or efavirenz alone), suggesting that efavirenz and palmitate synergistically decreased Δψm in INS-1E cells (Figure 6.6, A).

Although a 24-hour exposure to rilpivirine or palmitate alone had no to negligible effects on Δψm in INS-1E cells, INS-1E cells exposed to palmitate (10 µM) plus rilpivirine (1 µM) increased Δψm by nearly 2-fold ($p < 0.01$ vs. palmitate or rilpivirine alone), suggesting that rilpivirine and palmitate synergistically increase Δψm in INS-1E cells (Figure 6.6, B).

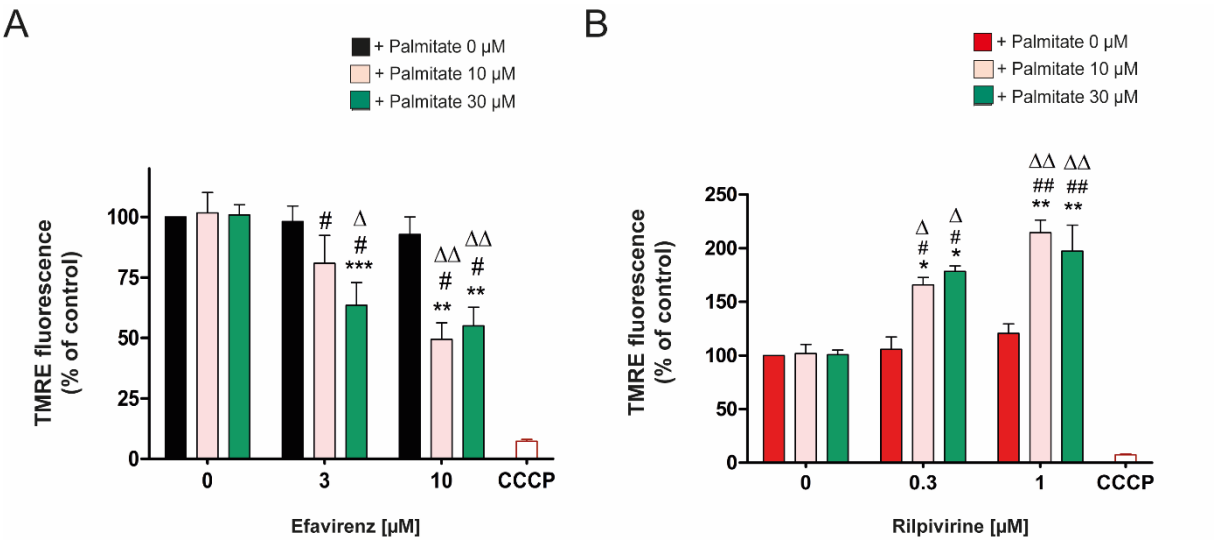

Figure 6.6 Efavirenz or rilpivirine in combination with palmitate disrupt Δψm in INS-1E cells. INS-1E cells were exposed to BSA, NaOH plus ethanol (0 µM), efavirenz (3 and 10 µM) (A), rilpivirine (0.3 and 1 µM) (B), or palmitate (10 or 30 µM) only or efavirenz or rilpivirine plus palmitate for 24 h before assessing Δψm. TMRE fluorescence is proportional to Δψm. A positive control of INS-1E cells treated with 50 µM carbonyl cyanide m-chlorophenyl hydrazine (CCCP) was used to dissipate Δψm. Data are expressed as mean ± SEM from $n = 4$ independent experiments. Statistical analysis was carried out using Friedman's test where $p < 0.05$ was considered significant; ** $p < 0.01$ vs. vehicle-treated control cells, # $p < 0.05$, ## $p < 0.01$ vs. efavirenz or rilpivirine alone treated cells, Δ $p < 0.05$, ΔΔ $p < 0.01$ vs. palmitate alone treated cells.

6.3.4.3 Efavirenz or rilpivirine plus palmitate do not induce ER stress

ER stress has been previously shown to contribute to the pathogenesis of diabetes by inducing pancreatic beta cell loss via apoptosis (Eizirik *et al.*, 2006). ER stress is particularly relevant in palmitate-mediated apoptosis, as previous work reported increased expression of a key ER stress marker, CHOP, was observed in INS-1E cells exposed to higher concentrations of palmitate (500 µM) (Cunha *et al.*, 2008). Additionally, our results show that exposure to efavirenz and rilpivirine at higher concentrations (20 and 10 µM, respectively) induce the

mRNA and protein expression of CHOP (**Chapter 3**). However, the mRNA and protein expression of ER stress chaperones (*i.e.*, GRP78) was not altered in INS-1E cells exposed to palmitate for 24 hours (Sommerweiss *et al.*, 2013). Hence, we examined whether palmitate plus efavirenz or rilpivirine synergistically induce CHOP expression in INS-1E cells. Therefore, we measured the protein expression of CHOP by Western blot following a 24-hour exposure to efavirenz or rilpivirine plus palmitate in INS-1E cells (Figure 6.7). A 24-hour exposure to palmitate plus efavirenz or rilpivirine did not increase the expression of CHOP in INS-1E cells (Figure 6.7).

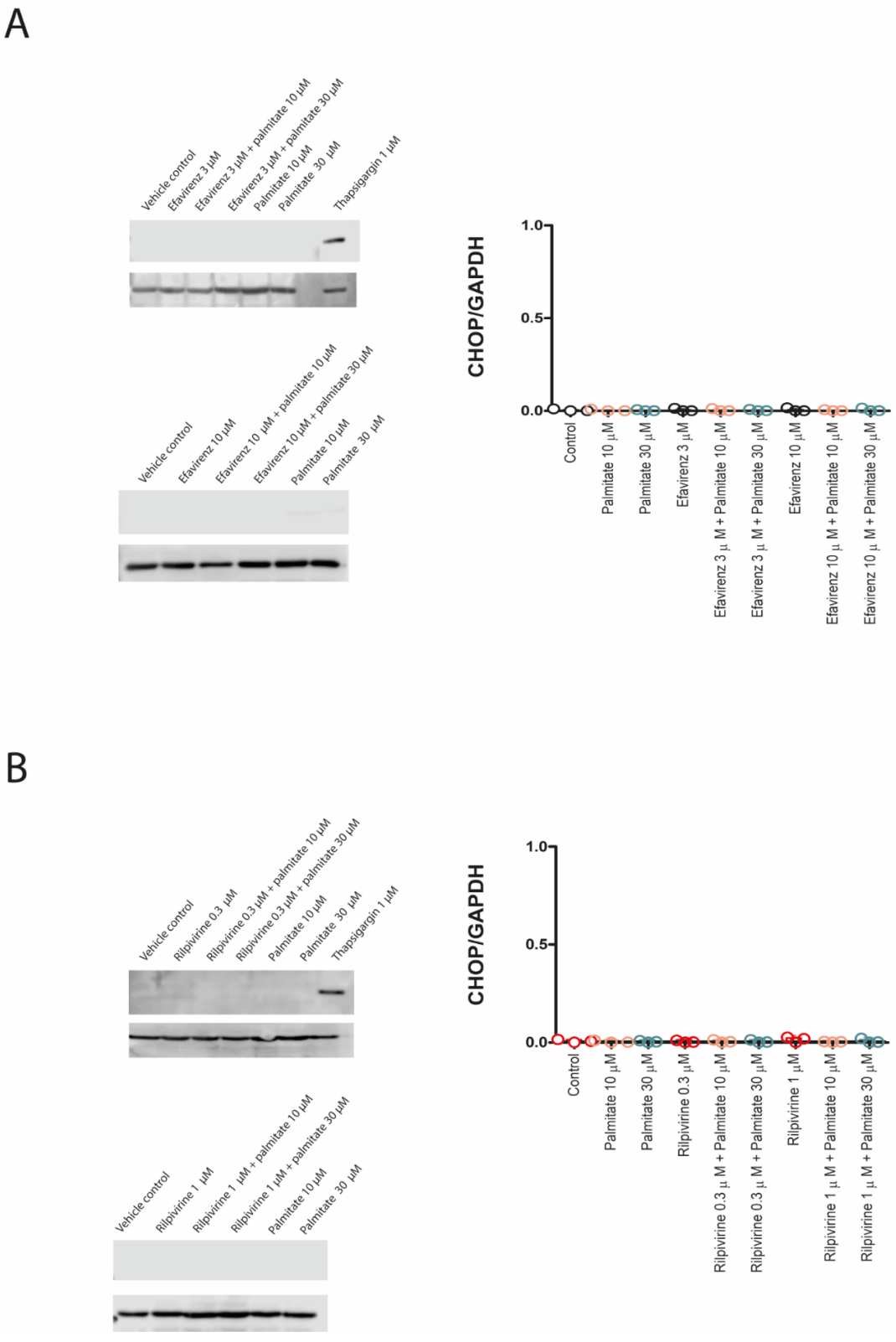

Figure 6.7. A 24-hour exposure to efavirenz and rilpivirine plus palmitate does not induce CHOP protein expression in INS-1E cell. (A) Representative Western blot of CHOP protein expression from one independent experiment (left panel) following a 24-hour exposure to BSA, NaOH plus ethanol (0 µM), efavirenz (3 or 10 µM), palmitate (10 or 30 µM) alone or combination treatments of efavirenz plus palmitate. (B) Representative Western blot of CHOP protein expression from one independent experiment (left panel) following a 24-hour exposure to rilpivirine (0.3 or 1 µM), palmitate (10 or 30 µM) alone or combination treatments of rilpivirine plus palmitate. Results are expressed as CHOP protein normalised to GAPDH protein. Dots represent individual data points from

n = 3 independent experiments and the histograms represent mean ± SD. Statistically significant differences were determined using two-way ANOVA and Bonferroni post hoc where $p < 0.05$ was considered significant.

6.4 Discussion

Lipotoxicity is a common pathological process seen in obesity and T2D, through its negative effects on pancreatic beta cells. Exposure to high concentrations of saturated FFAs such as palmitate, has been linked to pancreatic beta cell dysfunction and subsequent loss of beta cell mass (Cunha *et al.*, 2008). Here, we investigate the potential synergistic effects of palmitate in combination with efavirenz or rilpivirine on beta cell function and survival. Our data show that the NNRTIs efavirenz or rilpivirine act in synergy to impair the secretory function of beta cells, induce loss of beta cell viability and trigger beta cell apoptosis.

We show that although palmitate (10 and 30 μM), efavirenz (3 and 10 μM) and rilpivirine (0.3 and 1 μM) alone had no effect on GSIS, palmitate in combination with efavirenz or rilpivirine synergistically reduced GSIS from INS-1E cells. Palmitate, in acute conditions, exerts a stimulatory effect (Lytrivi et al., 2020). However, a substantial body of evidence suggest that long-term (24 - 72 hours) exposure to high concentrations (≥ 500 μM) of palmitate inhibited GSIS from a variety of clonal beta cell lines (including INS-1E cells), and from human and rodent pancreatic islets (Barlow *et al.*, 2016; Hoppa *et al.*, 2009; Maedler *et al.*, 2001; Watson *et al.*, 2011; Zhou & Grill, 1994). These deleterious effects on the secretory-insulin function of beta cells and survival may be explained by the increased oxidative stress and mitochondrial dysfunction.

We also report that although palmitate (10 and 30 μM), efavirenz (3 and 10 μM) and rilpivirine (0.3 and 1 μM) alone had no effect on INS-1E cell viability and death, palmitate in combination with efavirenz or rilpivirine synergistically induced apoptosis and reduced cell viability in INS-1E cells. Previous findings demonstrate that palmitate induces apoptosis and reduces beta cell viability in rat and human islets and a variety of clonal beta cell lines, including INS-1 cells (Karaskov *et al.*, 2006; Lai *et al.*, 2008; Maedler *et al.*, 2001; Martino *et al.*, 2012; Sommerweiss *et al.*, 2013).

Prolonged exposure to palmitate has been shown to have destructive effects, leading to decreased secretory function of beta cells and cell death potentially through increased ROS, mitochondrial dysfunction, and activation of ER stress (Ciregia *et al.*, 2017; Cnop *et al.*, 2005; Sargsyan & Bergsten, 2011). Our data shows that a reduced GSIS correlated with increased intracellular ROS generation in INS-1E cells treated with efavirenz or rilpivirine plus palmitate,

suggesting that increased oxidative stress may, at least partially, be responsible for the impairment of GSIS. Oxidative stress has been implicated in the pathogenesis of FFA-induced beta cell dysfunction (Koshkin *et al.*, 2003; Yuan *et al.*, 2010). We show that exposure to physiological concentrations of palmitate in combination with efavirenz or rilpivirine synergistically induced intracellular ROS generation in INS-1E cells. ROS are essential signalling molecules that regulate physiological cell functions. However, the overproduction of ROS coupled with intrinsically low antioxidant capacity in beta cells has detrimental consequences, causing organellar stress, injury, and cell death. Many studies have established that palmitate is a potent inducer of intracellular and mitochondrial ROS in murine and human beta cells, as well as in pancreatic islets (Carlsson *et al.*, 1999b; Lin *et al.*, 2012; Nemecz *et al.*, 2019). Mitochondrial fatty acid oxidation has been proposed as the main process leading to ROS generation in palmitate-mediated lipotoxicity (Ly *et al.*, 2017). FFAs are used as a metabolic fuel by the mitochondrial via β-oxidation, priming the TCA cycle to produce more NADH and $FADH_2$ which may subsequently lead to raised superoxide ($O_2^{\bullet-}$) production. Palmitate can also induce oxidative stress in beta cells through peroxisomal β-oxidation and activation of NADPH oxidase (NOX). NOX is an essential source of $O_2^{\bullet-}$ which can be stimulated by saturated FFAs, resulting in increased ROS production (Newsholme *et al.*, 2009). As a sequel of palmitate-induced oxidative stress, mitochondrial function can be impaired (Lytrivi *et al.*, 2020).

We also demonstrate that exposure to palmitate plus efavirenz or rilpivirine altered Δψm in beta cells. Interestingly, efavirenz alone did not disturb Δψm, however, in addition to physiological concentrations of palmitate, efavirenz caused a drastic decrease in Δψm in INS-1E cells. Palmitate has been shown to rapidly inhibit mitochondrial complex I activity. Indeed, palmitate (0 - 2 µmol/mg of protein) acted as a specific inhibitor of complex I of the respiratory chain (Loskovich *et al.*, 2005). We also show that efavirenz directly inhibited complex I activity in isolated mitochondria of INS-1E cells (**Chapter 4**). Therefore, we suggest that palmitate and efavirenz synergistically inhibit complex I activity in beta cells, contributing to increased ROS generation and mitochondrial dysfunction in INS-1E cells. Consequently, mitochondrial function is impaired (*i.e.*, loss of Δψm) with subsequent impairment of GSIS and worsening of INS-1E cell survival. It was reported that palmitate induced mitochondrial depolarisation, decreased ATP production, and consequently reduced insulin secretion in several beta cell lines and isolated islets, indicating the involvement of mitochondrial dysfunction in palmitate-induced GSIS defects (Barlow & Affourtit, 2013; Carlsson *et al.*, 1999b; Elsner *et al.*, 2010;

Koshkin *et al.*, 2003). Moreover, according to Brun *et al.* (1997), prolonged exposure of INS-1 cells to palmitate markedly suppressed GSIS through overexpression of the mitochondrial uncoupling protein 2 (UCP2) (Chan *et al.*, 2001a). We also previously show that efavirenz induced the expression of UCP2, suggesting that efavirenz in combination with palmitate may also impair beta cell function through a synergistic increase in the expression of UCP2 in beta cells.

We also show that rilpivirine (0.3 and 1 μM) had no effect on Δψm, however, in addition to physiological concentrations of palmitate, we observed a drastic increase in Δψm in INS-1E cells. On the contrary, previous findings report that palmitate causes mitochondrial depolarisation in several clonal beta cell lines and isolated islets (Carlsson *et al.*, 1999b; Newsholme *et al.*, 2019). These findings are not in line with our observations, prompting speculations on the mechanism(s) underlying the synergistic hyperpolarisation of the mitochondria by palmitate and rilpivirine.

Palmitate may also act on non-mitochondrial processes relevant to GSIS such as ATP-sensitive K+ (K_{ATP}) channel activity, Ca^{2+} and insulin exocytosis (Hoppa *et al.*, 2009; Larsson *et al.*, 1996; Zhao *et al.*, 2007). Circulating palmitate is transported into cells and converted to palmitoyl-CoA, a substrate for palmitoylation. Palmitoyl-CoA, but not palmitate, was shown to activate the K_{ATP} channel through the palmitoylation of Kir6.2, but not SUR1 (Yang *et al.*, 2020). We found that rilpivirine directly activates the Kir6.2/SUR1 channel as described in **Chapter 5**. Therefore, we suggest that palmitate and rilpivirine may synergistically activate K_{ATP} channels in pancreatic beta cells, contributing to the impairment of insulin release.

Palmitate-induced apoptosis of beta cells has been attributed to both the apoptotic mitochondrial pathway and ER stress. Previous work reported that ER stress signalling pathways were activated in pancreatic beta cells exposed to FFAs and that palmitate 500 μM upregulated the expression of *CHOP* in INS-1E cells (Cunha *et al.*, 2008). However, our data suggest that efavirenz or rilpivirine in combination with palmitate did not synergistically increase the protein expression of CHOP. We also found that palmitate plus efavirenz or rilpivirine triggered INS-1E cell apoptosis, suggesting an ER stress-independent apoptotic pathway. Although palmitate can initiate a proapoptotic pathway in the ER, it can also initiate one in the mitochondrion (Šrámek *et al.*, 2021). The pro-survival Akt (PI3K (phosphoinositide 3-kinase)-PDK1 (phosphoinositide-dependent protein kinase 1)-Akt) pathway is inhibited by saturated fatty acids in beta cells. This leads to the activation of FoxO1 (most abundant isoform in pancreatic beta cells) its translocation into the nucleus and the upregulation and activation of

proapoptotic members of the Bcl-2 family and Bax proteins (Wrede *et al.*, 2002). Subsequently, the mitochondrial pathway of apoptosis is activated. Additionally, the inhibition of Akt may also induce the activation of proapoptotic JNK and p38 MAPK (Šrámek *et al.*, 2021). Cunha *et al.* (2012) demonstrated that palmitate induced beta cell death through the mitochondrial/intrinsic pathway of apoptosis. Indeed, palmitate induced cytochrome *c* release from the mitochondria, Bax translocation form the cytosol to the mitochondria and caspase 3 and 9 activation, which activate the downstream executioner caspases (Cunha *et al.*, 2012; Maedler *et al.*, 2003). If rilpivirine also induces cytochrome *c* release from the mitochondria, this would explain the synergistic effects of rilpivirine and palmitate on increasing $\Delta\psi m$. Indeed, an increased cytochrome *c* release has been shown to induce mitochondrial hyperpolarisation (*i.e.*, increase in $\Delta\psi m$) (Scarlett *et al.*, 2000).

However, it is still possible for efavirenz or rilpivirine in combination with palmitate to impair beta cell function and mass through a synergistic proinflammatory effect, dysregulation of autophagy and increase in ceramide formation, other mechanisms associated with palmitate-mediated beta cell dysfunction (Ciregia *et al.*, 2017; Cnop *et al.*, 2005; Sargsyan & Bergsten, 2011; Šrámek *et al.*, 2021).

A great body of evidence shows that certain FFAs and their toxic metabolites (*i.e.*, ceramides, fatty acyl-CoA and diacylglycerol) are important mediators of insulin secretion and apoptosis in pancreatic beta cells (Boden, 1999; Sobczak *et al.*, 2019). Indeed, increased ceramide production has been suggested to play a key role in beta cell lipotoxicity, through its modulation of several beta cell signalling pathways and processes implicated in beta cell diabetic disease such as cytokine secretion, insulin gene expression and apoptosis (Boslem *et al.*, 2012; Lupi *et al.*, 2002).

6.5 Conclusions

Taking into account our findings, we demonstrated that palmitate plus efavirenz or rilpivirine cause synergistic destructive effects in INS-1E cells, likely through their synergistic increase in oxidative stress and impairment of mitochondrial function. Lipotoxicity is suggested to occur hand-in-hand with glucotoxicity, hence the phenomenon of glucolipotoxicity. Glucolipotoxicity is likely to occur in T2D. Therefore, we also hypothesise that glucose and palmitate will most likely work in synergy in combination with efavirenz or rilpivirine to cause

the same or even enhanced damaging effects on beta cells as the ones observed with lipotoxic conditions.

7. The effects of NRTIs on beta cell function and survival

7.1 Introduction

Advances in modern medicine have transformed HIV from a terminal disease to a chronic but manageable condition through the development of antiretroviral therapy (ART). Undoubtedly, many clinical trials and clinical care settings have shown that ART, when adhered to, profoundly improved clinical outcomes in HIV patients by reducing HIV progression to AIDS and AIDS-related death rates (Kitahata *et al.*, 2009; Mannheimer *et al.*, 2006; Mocroft *et al.*, 1998). Zidovudine, the first antiretroviral drug licensed in 1987, paved the way to triple combination ART, also known as combination antiretroviral therapy (cART) or simply ART. Inhibition of the HIV reverse transcriptase is highly effective in impairing HIV viral replication, prompting guidelines surrounding standardised regimens for HIV treatment and prophylaxis to include the first line use of reverse transcriptase inhibitors. Reverse transcriptase inhibitors are divided into two classes: the nucleoside/tide reverse transcriptase inhibitors (NRTIs) and the non-nucleoside reverse transcriptase inhibitors (NNRTIs). The NRTI class is a key drug class used in the management and prophylaxis of HIV infection. Amongst all NRTIs, the 'newer' NRTIs tenofovir disoproxil fumarate (DF), emtricitabine and lamivudine are commonly used as part of standardised regimens for the management and pre- (PreP) and post-exposure (PeP) prophylaxis of HIV infection (Grant *et al.*, 2010; Thigpen *et al.*, 2012). NRTIs act by competitively inhibiting HIV reverse transcriptase via DNA chain termination after incorporation of their respective nucleoside analogue into viral DNA, halting viral replication.

Tenofovir DF, an analogue of adenosine, is widely prescribed and is an integral part of national and international standardised regimens for treatment of HIV-1 and HIV-2 in antiretroviral-naive adults and adolescents (Reeves *et al.*, 2021; Waters *et al.*, 2016). Approved in 2001 by the Food and Drug Administration (FDA), tenofovir DF is now used as a gold-standard NRTI in combination with emtricitabine or lamivudine as an NRTI backbone and can be found in fixed-dose combination tablets such as Truvada® (tenofovir DF/emtricitabine), Atripla® (tenofovir DF/emtricitabine/efavirenz) and Eviplera® (tenofovir DF/emtricitabine/rilpivirine). The popularity of tenofovir DF has largely been attributed to its convenient dosing schedule as part of combination single pill tablets, antiviral efficacy, and a relatively favourable side-effect profile, making it one of the most widely prescribed antiretroviral drugs for the management of HIV-1 and HIV-2 (Reeves *et al.*, 2021; Waters *et al.*, 2016). Tenofovir DF is an acyclic

nucleotide analogue of adenosine monophosphate. It is polar and ionised, making it hard to be absorbed. However, its water-soluble ester prodrug tenofovir disoproxil, is easily absorbed and converted to the active tenofovir (Morse, 2015). Figure 7.1 depicts the 2D and 3D structures of tenofovir DF.

Lamivudine is an analogue of cytidine approved by the FDA in 2001. Lamivudine undergoes intracellular phosphorylation to the putative active metabolite, lamivudine triphosphate. Encouraging preliminary data suggest that lamivudine is poised to become an important component of HIV combination regimens, in combination with other NRTIs, NNRTIs and protease inhibitors. Figure 7.1 depicts the 2D and 3D structures of lamivudine.

In 2003, emtricitabine, a fluorinated derivative of lamivudine, was approved by the FDA and is currently recommended as first-line treatment of HIV, along with tenofovir DF (Waters et al., 2016). Studies show that emtricitabine, in combination with other antiretroviral agents, is efficacious in treating HIV in treatment-naïve and experienced patients (Benson *et al.*, 2004; Masho *et al.*, 2007; Molina *et al.*, 2000; Molina *et al.*, 2005; Saag *et al.*, 2004). The tenofovir DF and emtricitabine combination is a very popular combination regimen for the management and pre- and post-exposure prophylaxis of HIV infection in developed countries as well as in resource-limited settings, following efforts to phase out the more toxic older NRTIs (*i.e.*, stavudine, didanosine and zalcitabine). Figure 7.1 depicts the 2D and 3D structures of emtricitabine.

NRTIs are an important component of regimens used for the prophylaxis and management of HIV, alone or in combination with other antiretroviral classes such as NNRTIs, protease inhibitors and integrase inhibitors. However, NRTIs are associated with several adverse events. Mitochondrial toxicity due to the use of NRTIs can manifest as one of the following: nephrotoxicity, myopathy, lipoatrophy, neuropathy, dyslipidaemia and lactic acidosis (Dalakas, 2001). These adverse events are usually drug specific and are mainly associated with 'older' NRTIs.

Several NRTIs were attributed with increased incidence of type 2 diabetes (T2D) in HIV-positive individuals. Cumulative exposure to NRTIs (tenofovir DF, didanosine, stavudine and lamivudine) was associated with increased risk of incident diabetes in HIV-infected individuals (Ledergerber *et al.*, 2007; Tien *et al.*, 2007). Additionally, the NRTIs lamivudine, emtricitabine and tenofovir DF been associated with an increased risk of developing insulin resistance, which is a driving factor in the development of T2D (Brown *et al.*, 2005b; Dirajlal-Fargo *et al.*, 2016).

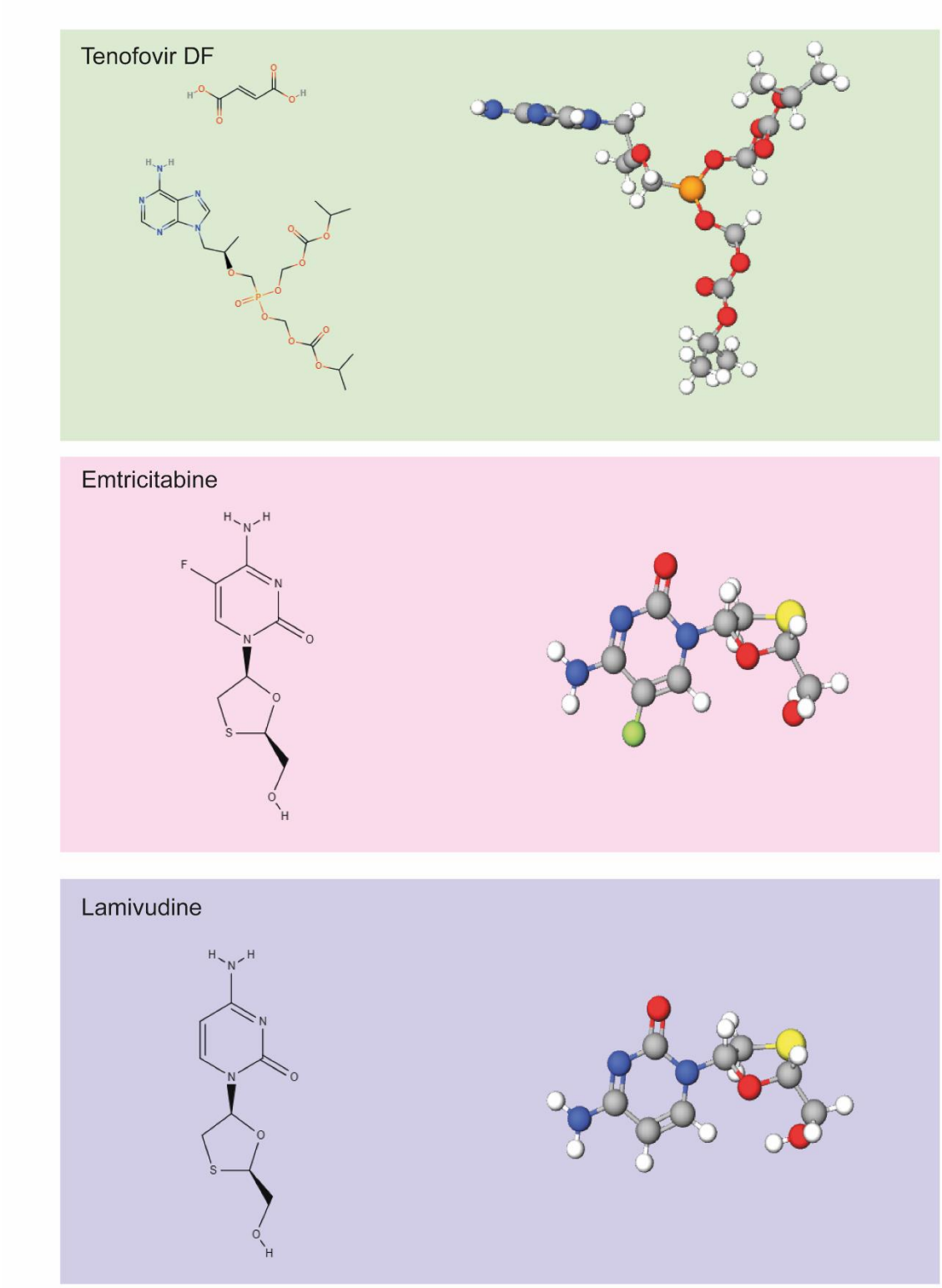

Figure 7.1 2D and 3D chemical structures of the NRTIs tenofovir DF, emtricitabine and lamivudine visualised by Molview. Tenofovir DF is chemically described as [[(2*R*)-1-(6-aminopurin-9-yl) propan-2-yl] oxymethyl-(propan-2-yloxycarbonyloxymethoxy) phosphoryl] oxymethyl propan-2-yl carbonate;but-2-enedioic acid. Emtricitabine is chemically described as 5-fluoro-1-(2R,5S)- [2- (hydroxymethyl)-1,3-oxathiolan-5-yl] cytosine. It has a fluorine in the 5-position, which differentiates emtricitabine from other cytidine analogues (FDA, 2006). As for lamivudine, it is chemically described as 4-amino-1-[(2*R*,5*S*)-2-(hydroxymethyl)-1,3-oxathiolan-5-yl] pyrimidin-2-one.

Direct damaging effects on beta cell function and survival by NRTIs may predispose individuals to impaired glycaemic control and loss of beta cell mass, increasing the risk of diabetic complications and insulin dependency. Due to their classification as 'newer' NRTIs, we hypothesise that tenofovir DF, emtricitabine and lamivudine have no effect on beta cell function and survival. Therefore, the aim of this study was to investigate the direct effects of the NRTIs tenofovir DF, emtricitabine and lamivudine on beta cell function and survival.

7.2 Materials and Methods

7.2.1 Materials

All materials were obtained as described in Materials, **Chapter 2** (see 2.1).

7.2.2 Treatment protocol

After cell growth as described in **Chapter 2** (see 2.2.1), INS-1E cells were exposed to DMSO (vehicle) or increasing concentrations (3, 10, 20 or 30 μM) of the NRTIs tenofovir DF, emtricitabine or lamivudine for 24 hrs at 37°C in a humidified atmosphere of 95% air and 5% CO_2.

A 25 mM stock solution for each drug was prepared by dissolving each NRTI in DMSO (Table 1, Appendix I). Then, solutions of different concentrations (3, 10, 20 and 30 μM) of tenofovir DF, emtricitabine and lamivudine were prepared by diluting the stock solution in RPMI-1640 media supplemented with 3% heat-inactivated FCS, 50 μM 2-mercaptoethanol and 1% penicillin-streptomycin according to Table 2, Appendix I. After treatment protocol, glucose-stimulated insulin secretion (GSIS) (see 2.2.3.1), cell viability (see 2.2.5) and apoptosis and necrosis (see 2.2.6.2) were assessed as described in **Chapter 2**. Cellular mechanisms were investigated by measuring intracellular ROS generation (2.2.8.1), antioxidant capacity (2.2.8.3) and mitochondrial membrane potential ($\Delta\psi m$) changes (see 2.2.9) as described in **Chapter 2.**

7.3 Results

7.3.1 Effects of NRTIs on glucose-stimulated insulin secretion (GSIS) from INS-1E cells

The primary function of pancreatic beta cells, GSIS was evaluated in INS-1E cells treated with NRTIs for 24 hours (Figure 7.2). The NRTIs tenofovir DF, emtricitabine and lamivudine had no effect on GSIS from INS-1E cells (Figure 7.2).

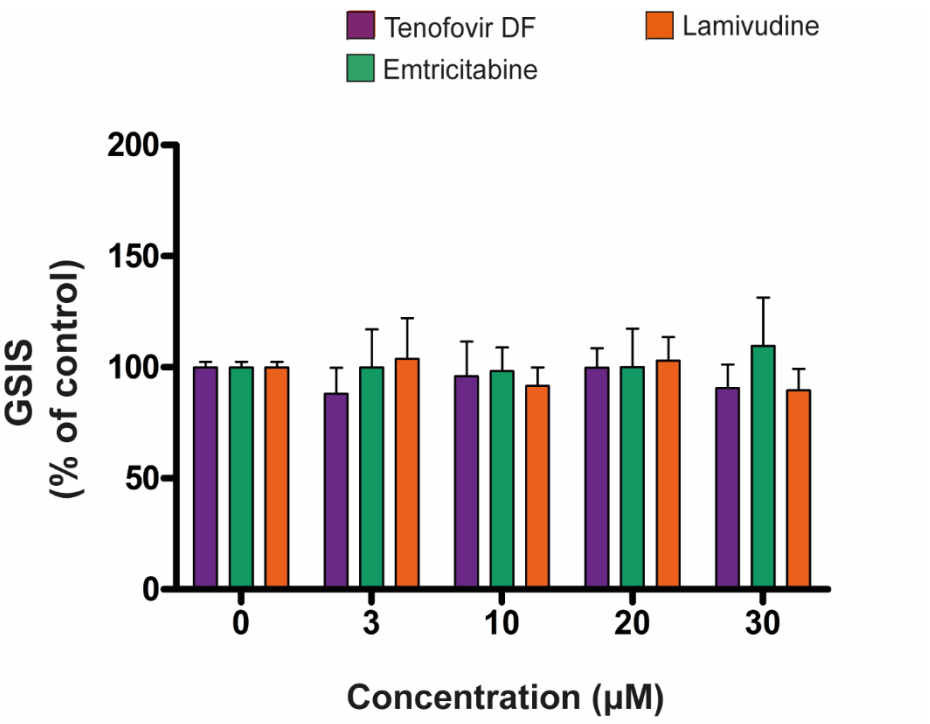

Figure 7.2 Effects of a 24-hour exposure to NRTIs on GSIS from INS-1E cells. Tenofovir DF, emtricitabine and lamivudine had no effect on GSIS from INS-1E cells. Data are expressed as mean ± SEM from $n = 3$ independent experiments with 3 technical replicates per treatment. Statistically significant differences were determined using Kruskal-Wallis with Dunn's post hoc test where $p < 0.05$ was considered as significant.

7.3.2 Effects of NRTIs on INS-1E cell viability

Next, we investigated the viability of INS-1E cells treated with NRTIs to determine whether the absence of GSIS impairment was reciprocated in the context of cell viability (Figure 7.3). Indeed, tenofovir DF, emtricitabine and lamivudine had no effect on cell viability in INS-1E cells (Figure 7.3).

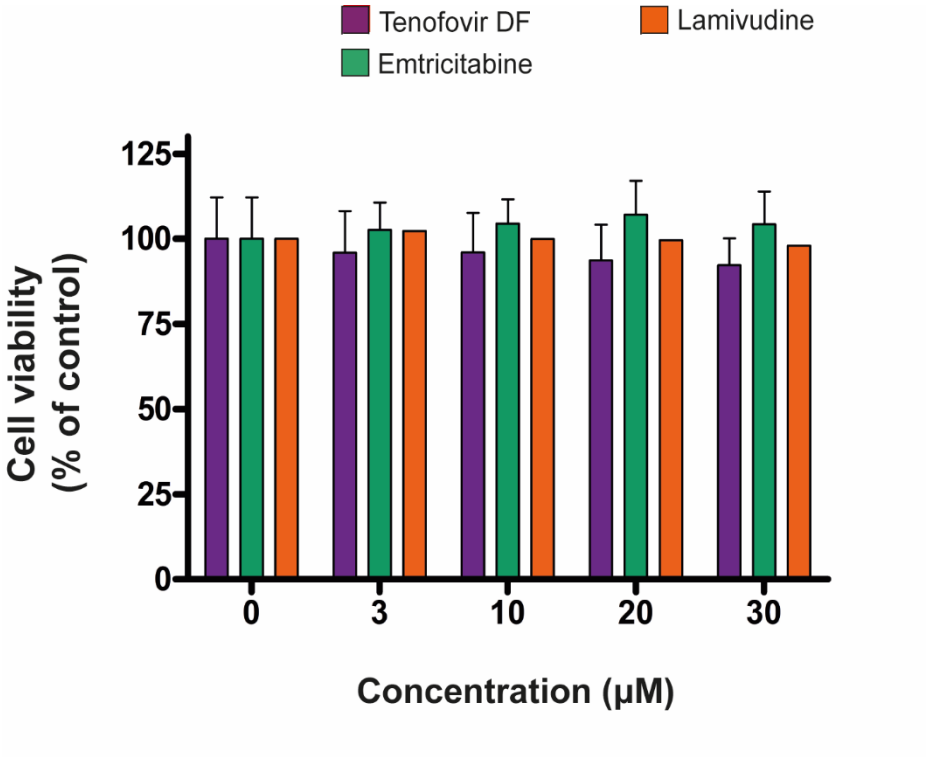

Figure 7.3 Effects of a 24-hour exposure to NRTIs on INS-1E cell viability. Tenofovir DF, emtricitabine and lamivudine had no effect on cell viability in INS-1E cells. Data are expressed as mean ± SEM from $n = 5$ independent experiments with 6 technical replicates per treatment. Statistically significant differences were determined using one-way ANOVA with Bonferroni post hoc test where $p < 0.05$ was considered as significant.

7.3.3 Effects of NRTIs on INS-1E cell death

We next sought to determine INS-1E cell survival by measuring the levels of apoptosis and necrosis in INS-1E cells exposed to tenofovir DF, emtricitabine and lamivudine for 24 hours by flow cytometry (Figure 7.4). Tenofovir DF, emtricitabine and lamivudine had no effect on early apoptotic (Figure 7.4, A) and late apoptotic/primary necrotic (Figure 7.4, B) cell levels in INS-1E cells.

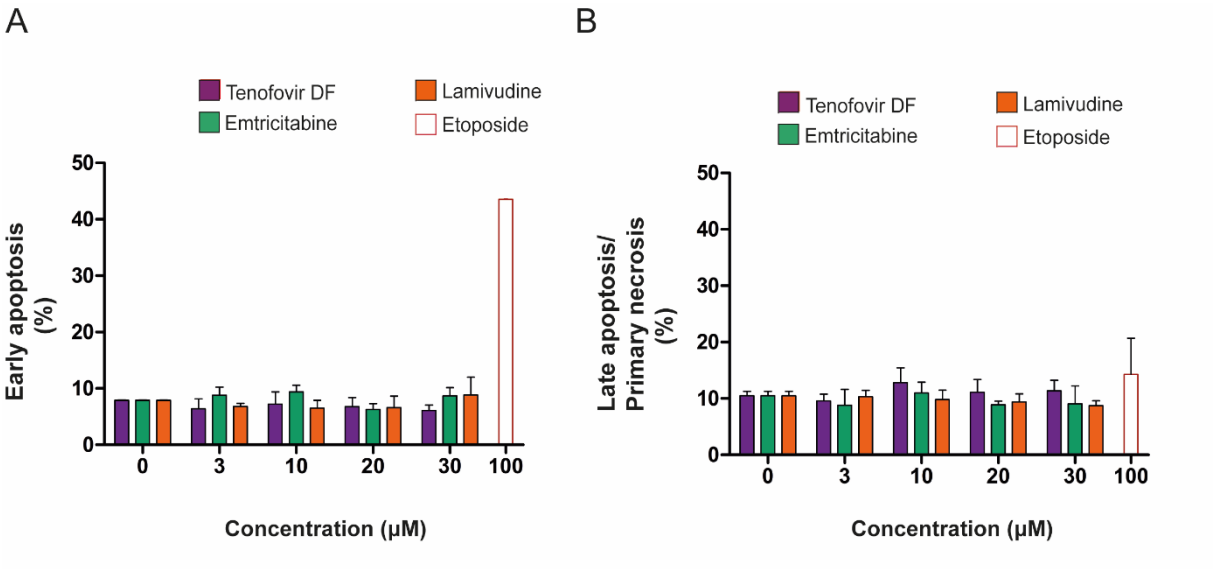

Figure 7.4 Effects of a 24-hour exposure to NRTIs on INS-1E cell apoptosis and necrosis. Quantitative representation of early apoptosis in INS-1E cells treated with tenofovir DF, emtricitabine and lamivudine (A) and late apoptosis/primary necrosis in INS-1E cells treated with tenofovir DF, emtricitabine and lamivudine (B). Tenofovir DF, emtricitabine and lamivudine had no effect on apoptosis and necrosis in INS-1E cells. Data are expressed as mean ± SEM from $n = 3$ independent experiments. Statistically significant differences were determined using one-way ANOVA with Bonferroni post hoc test where $p < 0.05$ was considered as significant.

7.3.4 Potential cellular mechanisms

After observing the lack of direct damaging effects of NRTIs on INS-1E cell function and survival, we focused on ruling out possible mechanisms related to beta cell dysfunction and death.

7.3.4.1 Oxidative Stress

We attempted to confirm the absence of oxidative stress in INS-1E cells exposed to the NRTIs tenofovir DF, emtricitabine and lamivudine by measuring intracellular ROS generation (Figure 7.5) and antioxidant capacity (Figure 7.6). Unsurprisingly, tenofovir DF, emtricitabine and lamivudine had no effect on intracellular ROS levels in INS-1E cells (Figure 7.5).

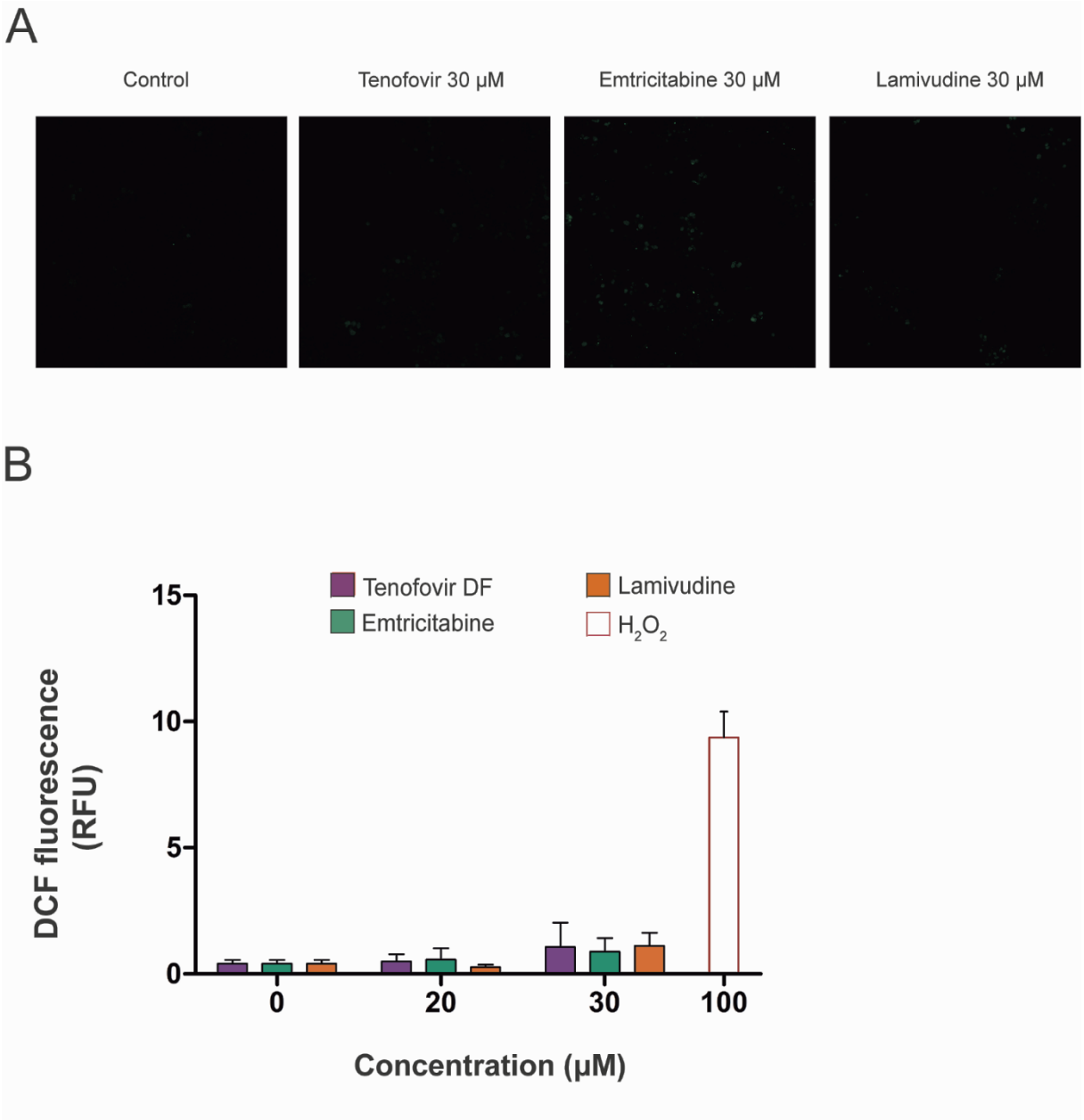

Figure 7.5 A 24-hour exposure to tenofovir DF, emtricitabine and lamivudine had no effect on intracellular ROS formation in INS-1E cells. DCF mean fluorescence intensity was determined using the image processing software Image J. (A) Confocal images of DCFH-DA assay and (B) quantification graphs. (Scale bar, 100 µM). DCF fluorescence intensity expressed as relative fluorescence intensity (RFU) is proportional to the levels of intracellular ROS. INS-1E cells were incubated with 100 µM hydrogen peroxide (H_2O_2) for 1 hr as a positive control. Data are expressed as mean ± SEM from $n = 3$ independent experiments. Statistically significant differences were determined using one-way ANOVA with Bonferroni post hoc where $p < 0.05$ was considered as significant.

7.3.4.1.2 Antioxidant capacity

Then, we measured antioxidant capacity in INS-1E cells exposed to NRTIs. Unsurprisingly, tenofovir DF, emtricitabine and lamivudine had no effect on antioxidant capacity in INS-1E cells (Figure 7.6).

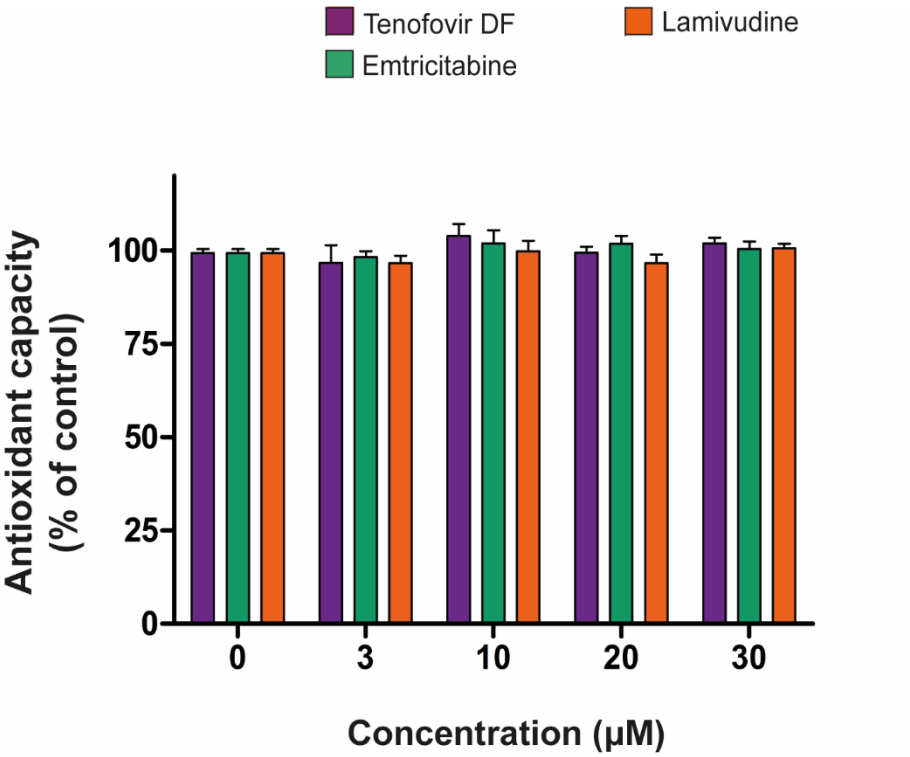

Figure 7.6 A 24-hour exposure to tenofovir DF, emtricitabine and lamivudine had no affect on antioxidant capacity in INS-1E cells. Data are expressed as mean ± SEM from $n = 3$ independent experiments with 3 technical replicates per treatment. Statistically significant differences were determined using Kruskal-Wallis with Dunn's post hoc test where $p < 0.05$ was considered as significant.

7.3.4.2 Mitochondrial membrane potential (Δψm) changes

As well as not inducing oxidative stress, we sought to further confirm the absence of mitochondrial toxicity since the mitochondrion is both the main source of ROS and a major target of oxidative stress (Marchi *et al.*, 2012). Therefore, we assessed mitochondrial function by measuring changes in Δψm in INS-1E cells treated with NRTIs for 24 hours (Figure 7.7). As expected, the NRTIs tenofovir DF, emtricitabine and lamivudine did not affect Δψm in INS-1E cells (Figure 7.7).

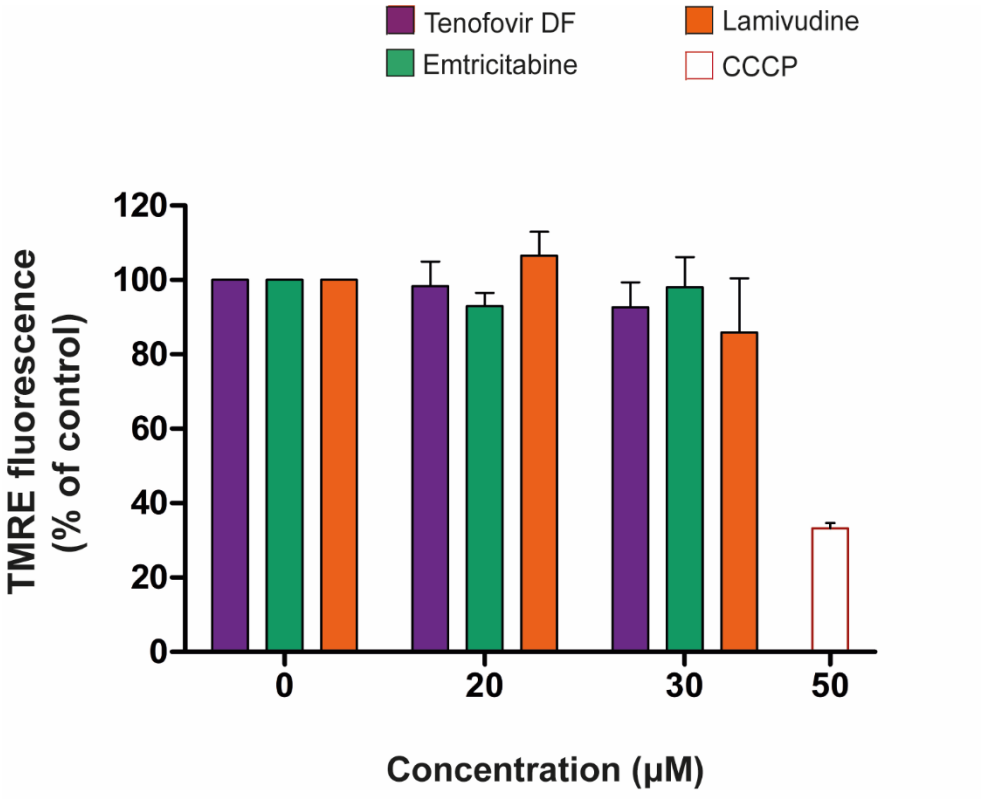

Figure 7.7 A 24-hour exposure to tenofovir DF, emtricitabine and lamivudine had no effect on Δψm in INS-1E cells. INS-1E cells were exposed to tenofovir DF, emtricitabine and lamivudine for 24 hrs. TMRE fluorescence intensity is proportional to Δψm. A positive control, carbonyl cyanide m-chlorophenyl hydrazine (CCCP) 50 μM was used to dissipate Δψm. Tenofovir DF, emtricitabine and lamivudine had no to negligible effect on Δψm in INS-1E cells. Data are expressed as mean ± SEM from n = 3 independent experiments. Statistically significant differences were determined using Kruskal-Wallis with Dunn's post hoc test where $p < 0.05$ was considered as significant.

7.4 Discussion

Although the use of NRTIs improves clinical outcomes in people living with HIV, there is growing concern about the alarming increase in T2D and insulin resistance in the HIV population on NRTI-based ART. To the best of our knowledge, this is the first study to demonstrate the effects of the NRTIs tenofovir DF, emtricitabine and lamivudine on beta cell function and survival.

We demonstrate that the NRTIs tenofovir DF, emtricitabine and lamivudine had no direct damaging effects on the secretory function of beta cells, as well as beta cell survival. In this study, we show that the NRTIs tenofovir DF, emtricitabine and lamivudine had no effect on GSIS, cell viability and apoptosis and necrosis levels in INS-1E cells, indicating the lack of NRTI-induced dysfunction and toxicity in beta cells. We also show that tenofovir DF, emtricitabine and lamivudine did not disrupt $\Delta\psi m$ and did not affect intracellular ROS formation and antioxidant capacity in INS-1E cells, indicating the lack of mitochondrial stress and oxidative stress in beta cells.

Older NRTIs such as stavudine, zalcitabine and didanosine can interfere with mitochondrial DNA (mtDNA) synthesis and can subsequently cause ROS generation as per the 'polymerase-γ (poly- γ) hypothesis' (Apostolova *et al.*, 2011a). Owing to their mechanism of action, NRTIs mimic the nucleoside bases, adenosine and cytidine, that are needed during the formation of viral DNA. The nucleoside/tide analogues compete with natural nucleosides and when the reverse transcriptase attempts to incorporate them into the growing viral DNA chain, the elongation process is halted (Morse, 2015). NRTIs also act as substrates for pol-γ and are able to interfere with mtDNA synthesis and may subsequently cause mitochondrial ROS generation as per the 'poly-γ hypothesis'. However, it is widely accepted that older NRTI compounds induce more mitochondrial manifestations compared to newer NRTI compounds (*i.e.*, tenofovir DF, emtricitabine and lamivudine) which is related to their capacity to inhibit poly-γ and inhibit mtDNA (Apostolova *et al.*, 2011a; Venhoff *et al.*, 2007). Unlike older NRTIs, newer NRTIs are weak inhibitors of the mtDNA replication enzyme, which may explain the lack of mitochondrial toxicity and ROS generation in beta cells. Tenofovir DF and emtricitabine were shown to have no effect on cell viability, cell death and intracellular oxidative stress in endothelial cells (Faltz *et al.*, 2017). Additionally, tenofovir DF and lamivudine produced no significant effects on mtDNA levels in human hepatocytes, skeletal muscle and renal proximal tubular endothelial cells, as opposed to the 'older' NRTIs stavudine and didanosine (Birkus *et*

al., 2002). However, conflicting data regarding the effects of tenofovir DF on proximal tubule epithelium exists to date. Contradictory to Birkus *et al.* (2002), Ramamoorthy *et al.* (2019) showed an increase in apoptosis in tubular and glomerular cells in kidneys in tenofovir DF-treated rats (Ramamoorthy *et al.*, 2019). Rats administrated with tenofovir DF had increased ROS and reactive nitrogen species (RNS) production, depleted antioxidants and increased mitochondrial damage in their kidneys (Ramamoorthy *et al.*, 2019). Tenofovir DF was also shown to induce apoptosis in Human Kidney 2 cell line (Lu *et al.*, 2019; Murphy *et al.*, 2017; Zhao *et al.*, 2017). In summary, tenofovir DF may potentially cause mitochondrial toxicity in rat proximal tubular cells and human kidney cells. However, we show that this mitochondrial toxicity seen in kidney cells is not extended to beta cells.

7.5 Conclusion

Based on the data presented here, we conclude that exposure to NRTIs does not affect beta cell function and survival. This may be explained by the lack of mitochondrial toxicity and oxidative stress.

8. General Discussion

Antiretroviral therapy has undoubtedly saved millions of lives during the past decades. This life-saving therapy has transformed the management of HIV by preventing its progression to life-threatening AIDS. Due to its chronic nature, the management of HIV infection requires a lifetime use of ART which eventually precipitates further complications to the management of HIV infection. A commonly reported complication of ART includes an increased incidence of type 2 diabetes (T2D), often seen in cohort studies in HIV-infected individuals. ART is also becoming increasingly popular as a preventative strategy for HIV infection and is taken as both pre-exposure prophylaxis (PreP) and post-exposure prophylaxis (PeP) in people at risk of contracting the virus. The use of ART is indispensable for the prevention and management of HIV infection and hence warrants the need to understand the toxicological effects of common antiretroviral agents on the function and survival of beta cells to further elucidate the implications of these agents in the progression of T2D in PLWH and individuals at risk of contracting HIV.

Altogether, this study painted a picture of the nature of HIV reverse transcriptase in the context of beta cell function and survival, revealing that HIV reverse transcriptase inhibitors have divergent effects.

The first part of our study revealed that within the NNRTI class, we found intraclass contrasting effects in relation to their cellular and molecular effects in beta cells. The second part of our study then revealed further differences in the effects of NNRTIs in regard to their respective mechanistic modulation of mitochondrial function. The third part of this study revealed that rilpivirine activates the pancreatic beta cell K_{ATP} channel, another potential mechanism mediating the rilpivirine-potentiated insulin-secretory dysfunction. It also revealed that gliclazide, a sulfonylurea, protected against rilpivirine-mediated apoptotic beta cell death. The fourth part of this study found that non-toxic concentrations of efavirenz and rilpivirine act in synergy in combination with physiological amounts of palmitate to potentiate cellular dysfunction and death in beta cells. Finally, the fifth part of this study found that the NRTIs had no effect on beta cell function and survival.

8.1 The effects of NRTIs on beta cell function and survival

The first approved antiretroviral agent for the management of HIV/AIDS was the NRTI zidovudine that inhibited the very crucial step of viral reverse transcription via its nucleoside-

like structure. This discovery in the late 1980s, paved the way to newer NRTIs and classes approved in hopes of maximising ART efficacy and safety. As of today, zidovudine, amongst other NRTIs, are classified as 'older' NRTIs and are being slowly discontinued due to the approval of 'newer' NRTIs with better efficacy and safety profiles. Only recently, newer NRTIs have gained in popularity as a preventative approach as PreP and PeP, and as a gold-standard backbone as part of combination ART.

Several older NRTIs have been shown to cause mitochondrial toxicity in a variety of cell types secondary to their ability to inhibit mitochondrial DNA (mtDNA) synthesis. In our study, we tested three newer NRTIs: tenofovir DF, emtricitabine and lamivudine. We found that these newer NRTIs had no effect on the secretory function of beta cells and beta cell death. Unlike older NRTIs, newer NRTIs are weak inhibitors of the mtDNA replication enzyme, which may explain the lack of mitochondrial toxicity and ROS generation in beta cell.

8.2 First-generation NNRTI (efavirenz)-mediated beta cell dysfunction and death: the predictable

Following the approval of NRTIs, the search for novel ART classes continued. In the late 1990s, the first NNRTI nevirapine was approved giving way to a novel approach to inhibiting the viral replication, via binding to a hydrophobic pocket found in the viral reverse transcriptase. Today, the NNRTIs are classified into first-generation, second-generation and 'novel' subclasses depending on their dates of approval. The novel NNRTI doravirine is believed to have a better efficacy and safety profile than its predecessors, the second-generation NNRTIs (*i.e.*, rilpivirine) and so on. This signifies that first-generation NNRTIs, such as efavirenz, have a suboptimal safety profile in comparison to second-generation and novel NNRTIs. Indeed, efavirenz has been shown to have more adverse events when compared to newer NNRTIs. Previous findings demonstrated that efavirenz causes cellular toxicity in a variety of cell types including hepatocytes, adipocytes and neurones.

Unsurprisingly, we found that efavirenz also causes beta cell dysfunction and triggers beta cell apoptosis, which mirrors the above-mentioned previous findings. By inducing oxidative and mitochondrial dysfunction, efavirenz may potentiate cellular dysfunction and induces cell death. We suggest that these deleterious effects are likely mediated by oxidative stress (*i.e.*, increased generation of mitochondrial superoxide and intracellular ROS and reduced antioxidant capacity), secondary to the direct inhibition of the activity of mitochondrial

complex I of the electron transport chain (ETC), a mechanism previously established in isolated mitochondria of the liver (Blas-García *et al.*, 2010). The efavirenz-mediated increases in oxidative stress may have caused mitochondrial dysfunction, characterised by a loss of Δψm and depletion of cellular ATP levels (Figure 8.1). As opposed to rilpivirine, efavirenz also increased the expression of UCP2, a phenomenon likely induced by ROS. Overall, the mitochondrial dysfunction and oxidative stress caused by efavirenz may have damaging repercussions on the function of beta cells, as demonstrated by the reductions in insulin secretion from pancreatic beta cells, as well as the activation of the mitochondria-dependent apoptotic pathway (Figure 8.1). This pathway can contribute to the increased apoptotic cell rates in beta cells exposed to efavirenz, however, we believe that ER stress is also an important mediator of efavirenz-induced apoptosis due to the efavirenz-induced increases in ER stress that can trigger the unfolded protein response (UPR)-mediated apoptotic pathway (Figure 8.1).

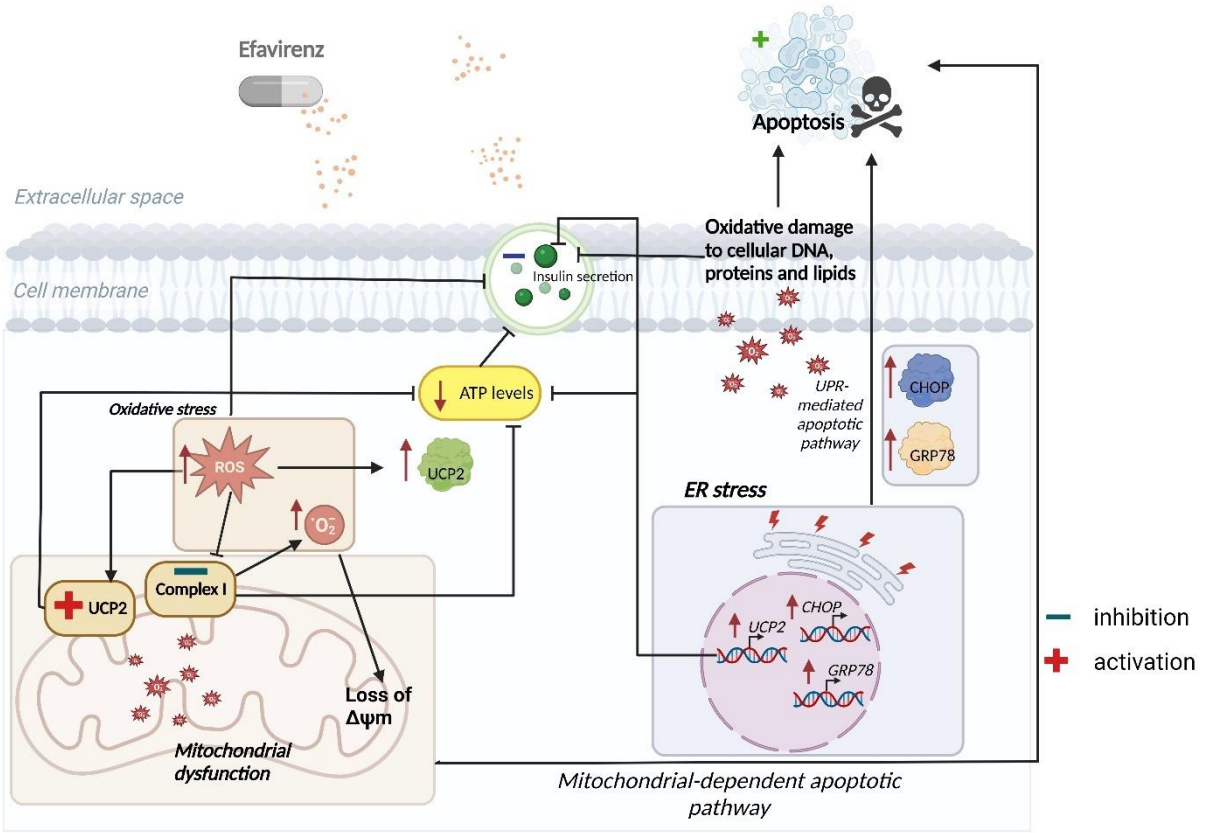

Figure 8.1 A schematic representation of the proposed mechanisms for efavirenz-mediated beta cell dysfunction and death in our study. Figure created with BioRender.com.

When combined with palmitate, efavirenz exerts a synergistic impairment of the insulin-secretory function of beta cells and increase in apoptotic cell death (Figure 8.2). Due to its established effect as a specific inhibitor of complex I, palmitate may potentiate the inhibition

of the activity of this mitochondrial enzyme by efavirenz, explaining the synergistic impairment of mitochondrial function and increase in oxidative stress (Figure 8.2). Although efavirenz and palmitate do not upregulate the expression of CHOP, it is apparent that the mitochondria-dependent pathway of apoptosis plays an important role in mediating efavirenz and palmitate synergistic beta cell apoptosis (Figure 8.2).

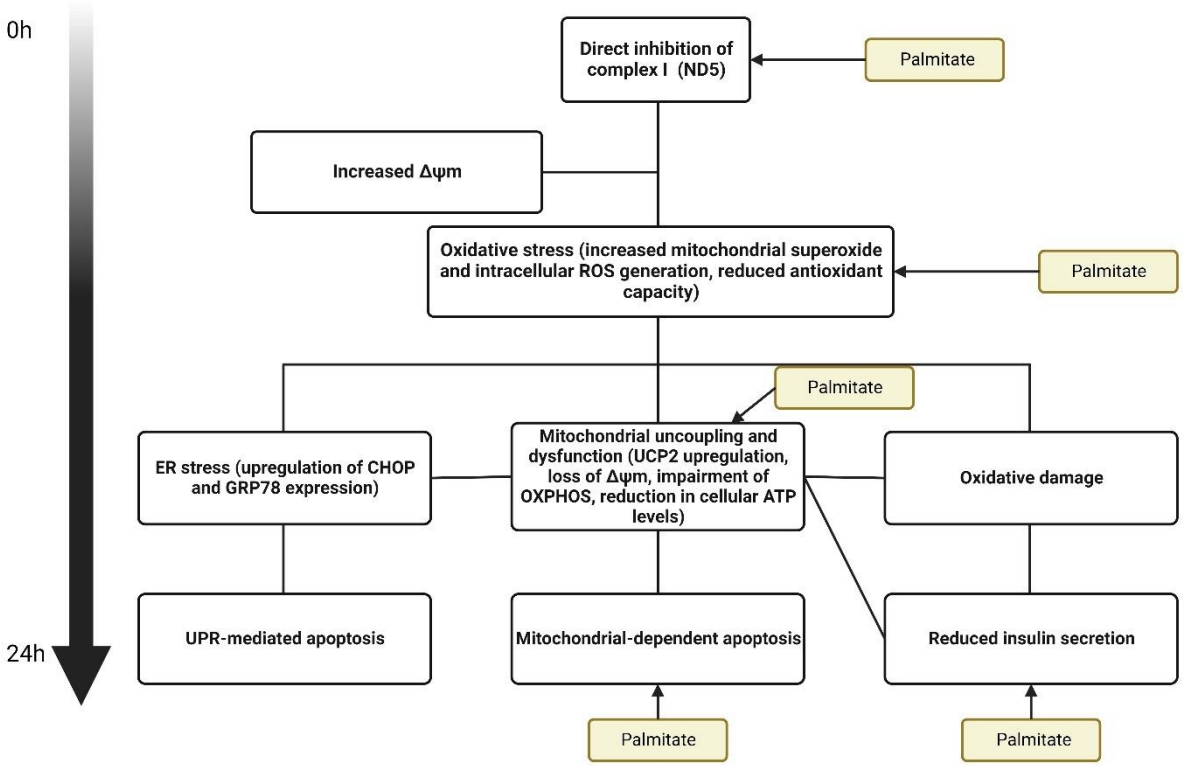

Figure 8.2 Proposed effects of efavirenz-mediated beta cell dysfunction and death and role of palmitate. Figure created with BioRender.com.

8.3 Second-generation NNRTI (rilpivirine)-mediated beta cell dysfunction and death: the unpredictable

Due to its status as a second-generation NNRTI, we predicted that rilpivirine would have no effect on beta cell function and survival, as opposed to the first-generation NNRTI efavirenz. To our surprise, despite being a second-generation NNRTI approved in hopes of ameliorating first-generation NNRTI safety profiles, we show, for the first time, that rilpivirine has damaging cellular effects.

We show in our present study that rilpivirine impaired the insulin-secretory function of beta cells (Figure 8.3). This prompted the investigation into the potential occurrence of oxidative

stress and mitochondrial dysfunction, key players of diabetic beta cell dysfunction. Rilpivirine had no effect on mitochondrial complex I activity as opposed to efavirenz; however, another crucial mitochondrial enzyme could be involved. We suggest that by directly inhibiting the activity of mitochondrial ATP synthase, rilpivirine increases $\Delta\psi m$, causing the mitochondria to increase its production of ROS. Due to the physiological nature of beta cells containing intrinsically low levels of antioxidant activity, coupled with a rilpivirine-mediated reduction in antioxidant capacity, oxidative stress may play a central role in inhibiting insulin release from beta cells. Indeed, rilpivirine-induced oxidative stress and subsequent oxidative damage may have deleterious effects at the mitochondrion level, as demonstrated by reductions in cellular ATP levels (Figure 8.3).

We also investigated the direct effects of rilpivirine on a crucial component of the insulin secretory machinery: the pancreatic beta cell K_{ATP} channel. Due to the important and central nature of this ion channel in beta cells, we postulate that rilpivirine may have an effect on this channel, which could explain the absence of cellular toxicity in other cell types. In our present study, we found, for the first time, that rilpivirine directly activates the pancreatic beta cell K_{ATP} channel (Kir6.2/SUR1) (Figure 8.3). This may undeniably have a major impact on insulin secretion from beta cells, suggesting that rilpivirine has multiple mechanisms responsible for the reductions in insulin secretion. Further, despite attenuating mitochondrial dysfunction and completely abolishing increases in intracellular ROS generation, gliclazide failed to fully protect against the rilpivirine-mediated reductions in GSIS, suggesting that rilpivirine-mediated overactivation of the pancreatic beta cell K_{ATP} channel plays an important role in beta cell insulin-secretory dysfunction.

On the other hand, gliclazide fully protected beta cells against rilpivirine-mediated apoptosis while abolishing the increases in ROS generation and attenuating mitochondrial dysfunction. To explain this, gliclazide may have prevented oxidative stress and subsequent oxidative damage due to its antioxidant properties, suggesting that the mitochondria-dependent apoptotic pathway is an important regulator of apoptosis in beta cells exposed to rilpivirine. As to its direct effects on the mitochondria, we also postulate that mitochondrial K_{ATP} channels may be activated by rilpivirine due to the strong pharmacological similarities between the plasma and mitochondrial K_{ATP} channels, however, this hypothesis is yet to be confirmed due to the lack of strong evidence of K_{ATP} channels in the mitochondria of beta cells. However, we believe that ER stress is also an important mediator of rilpivirine-induced apoptosis due to the rilpivirine-

induced increases in ER stress that can trigger the UPR-mediated apoptotic pathway (Figure 8.3).

Altogether, we postulate that rilpivirine inhibits insulin secretion likely through a direct prolonged activation of pancreatic beta cell K_{ATP} channels and that the increased mitochondrial metabolism (*i.e.*, increased $\Delta\psi m$ and elevated generation of mitochondrial superoxide and intracellular ROS) may be a compensatory response to counteract the secretory defect of beta cells. This compensatory response may further impair the insulin-secretory function of beta cells as well as trigger beta cell apoptosis.

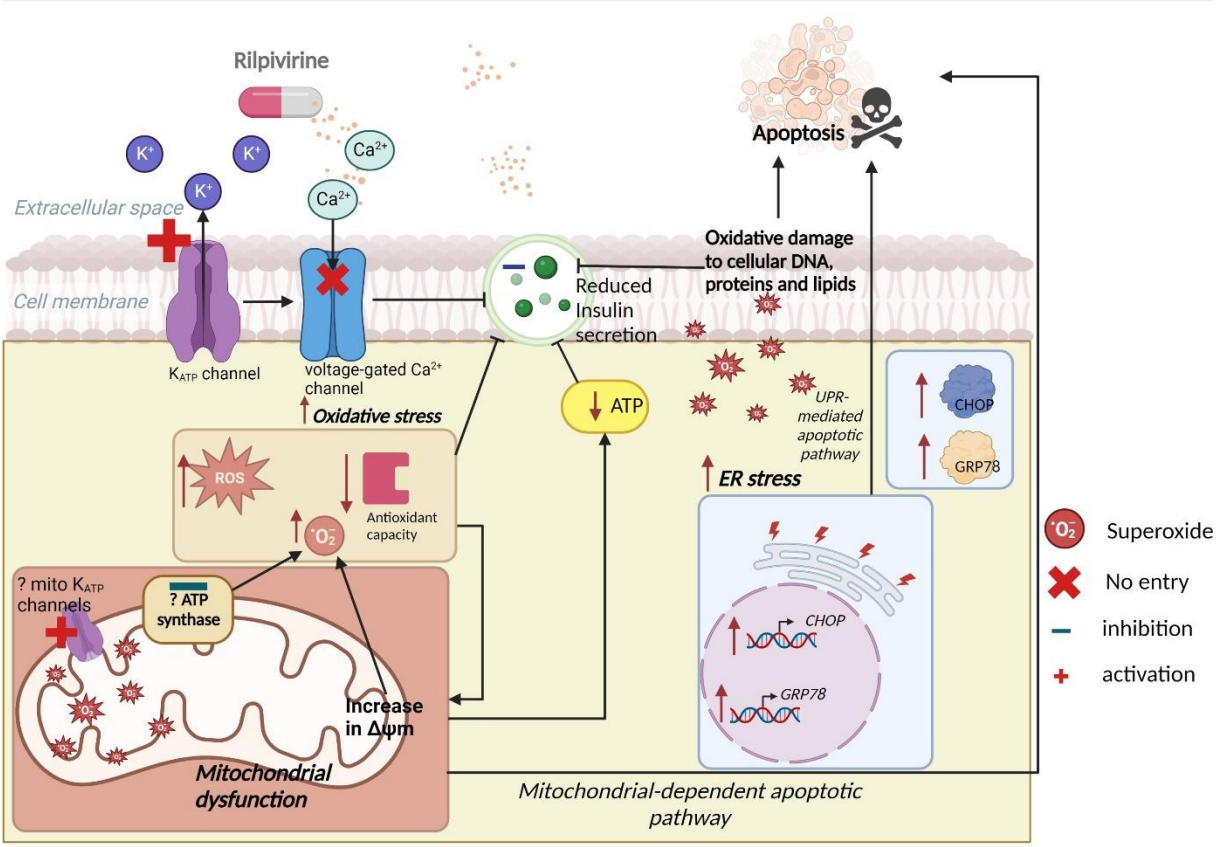

Figure 8.3 A schematic representation of the proposed mechanisms for rilpivirine-mediated beta cell dysfunction and death in our study. Figure created with BioRender.com.

Rilpivirine in combination with palmitate synergistically induced apoptotic cell levels while potentiating mitochondrial dysfunction and ROS generation. It is worth noting that since a synergistic increase in $\Delta\psi m$ was observed in beta cells exposed to rilpivirine and palmitate, we hypothesise that the synergistic activation of mitochondrial K_{ATP} channels by both of these agents could have resulted in potentiated mitochondrial hyperpolarisation (Figure 8.4). Another possible reason for mitochondrial hyperpolarisation is the release of cytochrome *c* by both palmitate and rilpivirine. However, this hypothesis should be confirmed experimentally.

Rilpivirine in combination with palmitate synergistically impaired insulin secretion from beta cells while potentiating mitochondrial dysfunction and ROS generation. The resulting oxidative stress and mitochondrial impairment may play a role in reducing insulin release from beta cells. However, since we also observe that rilpivirine activates the pancreatic beta cell K_{ATP} channel, we postulate that through its established effect (*i.e.*, palmitoylation of Kir6.2) on pancreatic K_{ATP} channels, palmitate may act in synergy with rilpivirine to activate this ion channel, explaining the amplified decreases in insulin secretion observed in beta cells (Figure 8.4).

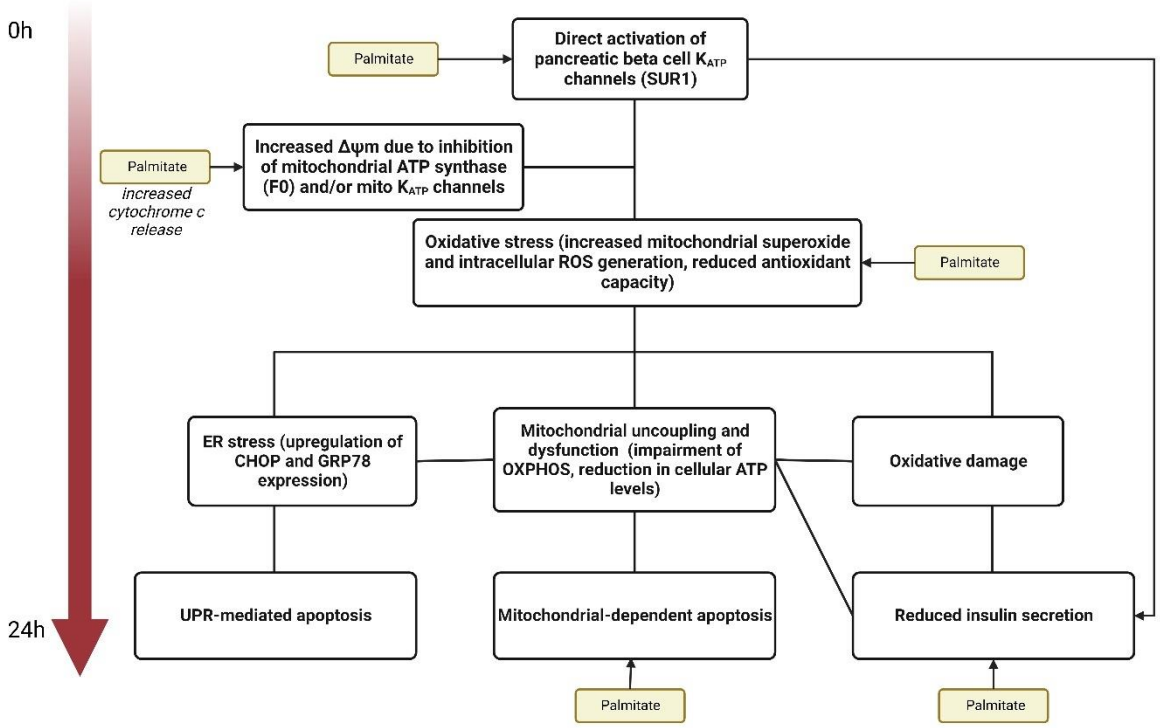

Figure 8.4 Proposed effects of rilpivirine-mediated beta cell dysfunction and death and role of palmitate. Figure created with BioRender.com.

Although the mechanism of action for the therapeutic purpose of the management of HIV is the same, the NNRTI-mediated effects seen in pancreatic beta cells are distinct. Therefore, we ask the question: why do these NNRTIs have different off-target activities? We can only speculate that the different drug structures could account for the different off-target effects and subsequent different mitochondrial effects between efavirenz and rilpivirine.

8.4 Interplay of these mechanisms in beta cell dysfunction and death: a vicious cycle

Oxidative stress induced by efavirenz and rilpivirine could cause further mitochondrial dysfunction and ER stress, further aggravating ROS production in beta cells. For example, mitochondrial dysfunction is generally associated with increased mitochondrial ROS production by the organelle itself, which acts to potentiate oxidative stress. Mitochondrial ROS production may also further aggravate oxidative stress through contributing to ER stress. ER stress has been established as a crucial player of apoptotic cell death seen in the context of T2D, leading to a loss of beta cell mass. Although not confirmed, we can only speculate that both efavirenz and rilpivirine can induce oxidative damage to other essential mitochondrial and cellular proteins, lipids and DNA that may be involved in the insulin-secretory machinery and programmed cell death. Damage to cellular proteins by ROS can in fact trigger an ER stress response followed by the UPR-mediated apoptotic pathway (Figure 8.1 and Figure 8.3). We can only confirm that PDX-1 expression is not involved in the efavirenz- and rilpivirine-associated beta cell dysfunction and death.

ER stress is also a potent ROS producer and contributes to cellular dysfunction mainly by increasing its oxidative protein folding of proinsulin and mitochondrial dysfunction (Eguchi *et al.*, 2021; Kaufman *et al.*, 2010). ER stress causes a Ca^{2+} leakage, resulting in a disruption of calcium homeostasis in the mitochondria and increased mitochondrial ROS production (Back & Kaufman, 2012). Altogether, these bidirectional interactions clarify the potential sequels of oxidative stress, mitochondrial dysfunction and ER stress caused by the NNRTIs efavirenz and rilpivirine in beta cells.

8.5 Potential clinical implications

People living with HIV (PLWH) are at increased risk of developing T2D due to several factors including exposure to ART. Although it is crucial to treat HIV, it is also important to optimise cART regimens to ensure a healthy ageing HIV population. Identifying common antiretroviral agents that are capable of causing cellular dysfunction is of extreme importance due to its potential clinical implications. In our case, investigating the effects of common antiretroviral agents on beta cell function and survival is of extreme importance to predict clinical outcomes and help guide therapeutic regimens, mainly in the context of T2D. Treatment of beta cells with tenofovir DF, emtricitabine and lamivudine, at concentrations that exceed those concentrations

achieved at therapeutically relevant levels in plasma (maximum plasma concentrations: 1.03, 7.28 and 15 μM, respectively), were not associated with beta cell dysfunction and worsening of beta cell survival (Gallant & Moore, 2009; Molina *et al.*, 2004). Altogether, our data and previous data support the hypothesis that newer NRTIs have a better toxicological profile than their predecessors. From a clinical perspective, the use of the NRTIs tenofovir DF, emtricitabine and lamivudine is potentially safe in the context of T2D in HIV.

The damaging effects of efavirenz seen in this study are at concentrations comparable to those seen clinically where the Cmax of efavirenz was reported as 12.4 ± 3.7 μM, with studies showing that efavirenz concentrations display a major interindividual variability, reaching 50 μM in many individuals (Apostolova *et al.*, 2017; Marzolini *et al.*, 2001). Although the damaging effects of rilpivirine were observed at concentrations higher than the reported Cmax (approximately 1 μM), the interindividual variability in HIV patients is yet to be fully elucidated (Lamorde *et al.*, 2015). However, as HIV-infected individuals on ART now have a normal lifespan, their pancreatic beta cells may be exposed to drugs like efavirenz and rilpivirine for decades. Therefore, we cannot rule out that the beta cell damaging effects induced by efavirenz and rilpivirine seen in our study may occur ensuing long-term exposure to therapeutic concentrations.

From a clinical perspective, the first- and second-generation NNRTIs efavirenz and rilpivirine may contribute to poor glycaemic control and insulin dependency in type 2 diabetics who are also HIV positive or at risk of contracting HIV infection. The use of rilpivirine may need to be reconsidered as HIV prophylaxis or treatment in type 2 diabetic HIV-infected patients and individuals at risk of contracting HIV infection due to its deleterious effects on beta cell function and survival. Further, rilpivirine may affect the sensitivity of K_{ATP} channels to gliclazide and/or may disturb the primary mode of action of gliclazide, hence potentially reducing its therapeutic efficacy. The potential development of rilpivine formulations for PreP may pose challenges in people with T2D, potentially impairing their glycaemic control, complicating effective management, and possibly increasing their likelihood of becoming insulin dependent.

Gliclazide was shown to protect against rilpivirine-mediated beta cell death, and this effect was observed at the lower end of its therapeutic range. The reported Cmax of gliclazide was up to 24.7 μM for oral administration of gliclazide 40 to 120 mg (Palmer & Brogden, 1993). However, gliclazide does not confer functional protection in beta cells. Despite its ability to

potentially protect beta cell mass, the interaction between gliclazide and rilpivirine on beta cell function may impair the therapeutic effectiveness of gliclazide, impairing glycaemic control with the likelihood of an increased risk of hyperglycaemia-mediated complications. This might be extended to other sulfonylureas due to the nature of its pharmacological effects on pancreatic beta cell K_{ATP} channels. Individuals with T2D with a good management of their HIV infection on rilpivirine-based ART regimens should potentially avoid gliclazide and an alternative antidiabetic agent should be considered. Care should be taken when this combination is prescribed for the clinical benefit of diabetic patients. However, further basic and clinical research is warranted to confirm this.

From a T2D pathophysiological point of view, clinically relevant concentrations of efavirenz or rilpivirine act in synergy with palmitate to induce beta cell dysfunction and trigger apoptosis. From a clinical perspective, this could mean that HIV positive type 2 diabetics who are also obese and on efavirenz or rilpivirine-based ART regimens, are potentially more prone to poor glycaemic control, complicating effective management, and possibly increasing their likelihood of insulin dependency. Moreover, previous findings show that the HIV population is affected by the obesity epidemic through risk factors including exposure to ART, further contributing to this lipotoxic environment, that further aggravates the damaging effects of these drugs in our study (Crum-Cianflone *et al.*, 2008; Obry-Roguet *et al.*, 2018; Tate *et al.*, 2012).

The novel NNRTI doravirine increased basal insulin release and GSIS at supraphysiological concentrations as the reported Cmax of doravirine is approximately 3 μM (Yee Ka *et al.*, 2017). Nevertheless, from a clinical perspective, doravirine may be considered as an NNRTI of choice in the context of T2D in the HIV population. Therefore, the novel NNRTI doravirine and the NRTIs tenofovir DF, emtricitabine and lamivudine may be safe to use for the prophylaxis or management of HIV infection as backbone agents in the case of NRTIs and as an additional agent in the case of doravirine as part of a triple therapy cART regimen in individuals at risk of developing metabolic diseases and T2D.

8.6 Limitations of this study and future work

One limitation of our study is the lack of confirmation in *in vivo* animal models, which could have been useful in confirming these effects in a more relevant and reliable model.

We conducted very few experiments to confirm the effects observed in rat INS-1E cells in the human 1.4E7 beta cell line. We show that efavirenz and rilpivirine significantly reduced cell

viability in 1.4E7 cells (Figure 4, **Appendix I**). There was an increasing trend in intracellular ROS generation following exposure to efavirenz and rilpivirine, but not doravirine, in human 1.4E7 cells, as observed in rat INS-1E cells (Figure 5, **Appendix I**). However, due to the lack of biological replicates, we can only predict that the damaging effects seen in rat beta cells are mirrored in a human beta cell line. It is worth mentioning that such human beta cell lines have yielded inconsistent results in the past (Leslie, 2019).

The interpretation and clinical implications of our results, including the mitochondrial targets involved, is a complex issue that demands further evaluation. *In silico* molecular modelling is a helpful tool in determining binding affinities and finding potential targets, however, the effects of efavirenz and rilpivirine on the activity of mitochondrial ATP synthase should be investigated *in vitro* in order to confirm our speculations.

Future work includes confirming these effects in *in vivo* animal models and in *in vitro* pancreatic human islets as to further strengthen our hypothesis of the clinical implications of our study. Finally, conducting clinical studies in HIV-infected and type 2 diabetic patients (ideally on gliclazide or other sulfonylureas) on rilpivirine-based cART regimens is necessary to confirm the clinical implications of our study.

Appendices

Appendix I

Table 1. NNRTIs and NRTIs and their respective stock solution concentration. NNRTIs and NRTIs were added to 1 mL of DMSO to make up 25 mM stock solutions.

	Antiretroviral Agent	Weight of the drug (in mg)	Concentration of stock solution (in mM)
NNRTIs	Efavirenz	7.0	25
	Rilpivirine	9.1	25
	Doravirine	8.4	25
NRTIs	Tenofovir DF	10.9	25
	Emtricitabine	5.8	25
	Lamivudine	5.7	25

DF, Disoproxil fumarate; NNRTIs, non-nucleoside reverse transcriptase inhibitors; NRTIs, nucleoside/tide reverse transcriptase inhibitors

Table 2 Volumes required to produce solutions of increasing concentrations of NNRTIs. NNRTIs (25 mM stock solution) were diluted in 5 mL of 3% heat-inactivated FCS RPMI-1640 media.

	NNRTIs		
Concentration (in µM)	Efavirenz (in µL)	Rilpivirine (in µL)	Doravirine (in µL)
1	0.2	0.2	0.2
3	0.6	0.6	0.6
10	2	2	2
20	4	4	4
30	6	6	6

Table 3 Ct method for RT-qPCR with example

Treatment	Ct values						
	CHOP – Efavirenz 20 µM	CHOP - control	GAPDH – Efavirenz 20 µM	GAPDH - control			
Technical replicate (1)	21.13	22.81	19.2	19.45			
Technical replicate (2)	21.26	22.85	20.19	19.92			
Technical replicate (3)	21.45	22.44	20.01	19.52	ΔCtExp	ΔCtC	ΔΔcT
Average	**21.28**	**22.7**	**19.8**	**19.63**	[1]**1.48**	[2]**3.07**	[3]**-1.59**

[1] ΔCtExp = (CHOP – Efavirenz 20 µM) – (GAPDH – Efavirenz 20 µM) = 21.28 - 19.8 = 1.48

[2] ΔCtC = (CHOP-control) – (CHOP-control) = 22.7 - 19.63 = 3.07

[3] ΔCtExp – ΔCtC = 1.48 - 3.07 = -1.59

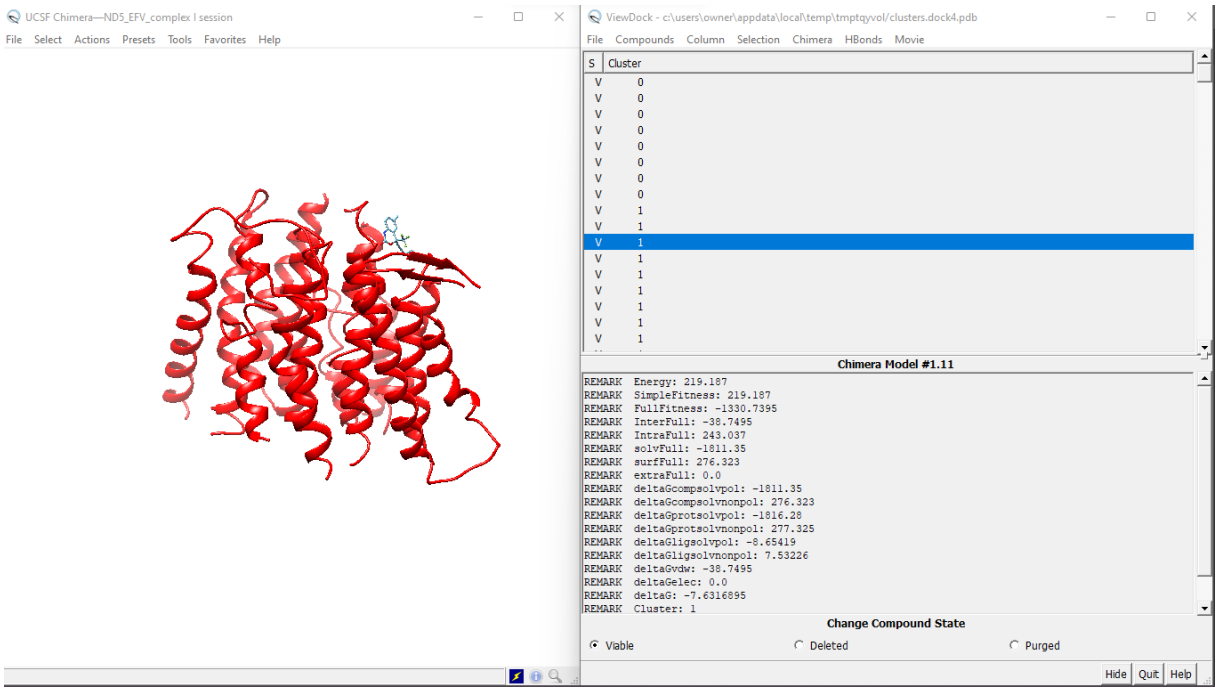

Figure 1 Sample SwissDock predictions output file for efavirenz docked in the ND5 subunit of mitochondrial complex I visualised in Chimera UCSF

Table 4 Volumes required to produce solutions of increasing concentrations of gliclazide. A 5 mM stock solution of gliclazide was diluted in 5 mL of 3% heat-inactivated FCS RPMI-1640 media

Concentration (in µM)	Gliclazide (in µL)	Stock solution (in mM)
0.1	1	0.5 (1:10 dilution of 5 mM stock solution)
0.3	3	0.5 (1:10 dilution of 5 mM stock solution)
1	1	5

Table 5 Acquisition settings for confocal microscopy

Setting	Optimised setting
Laser power	0.1-10%
Gain	2-6%

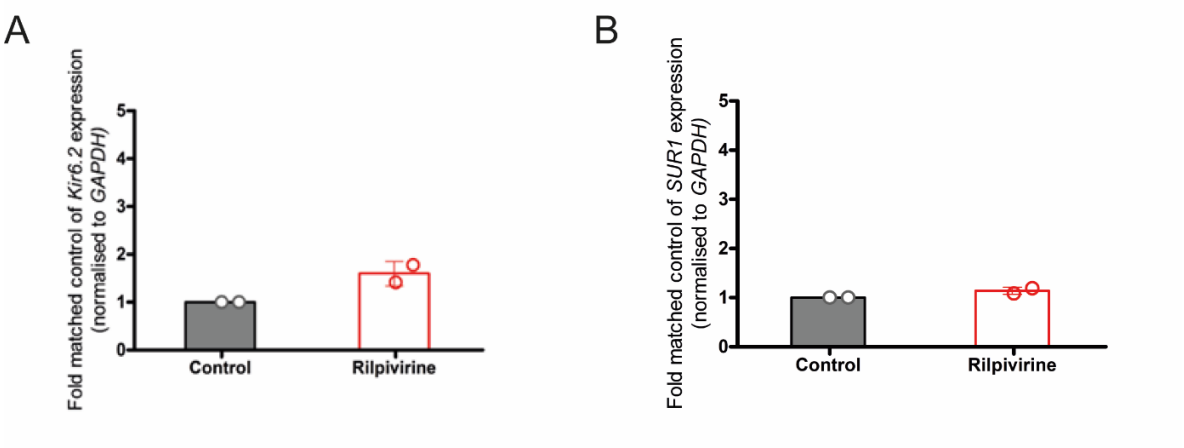

Figure 2 Confirmed expression of Kir6.2 (A) and SUR1(B) in INS-1E cells. mRNA expression was assessed in INS-1E cells exposed to vehicle (DMSO)-treated cells (control) or 10 μM rilpivirine for 24 hrs by RT-qPCR.

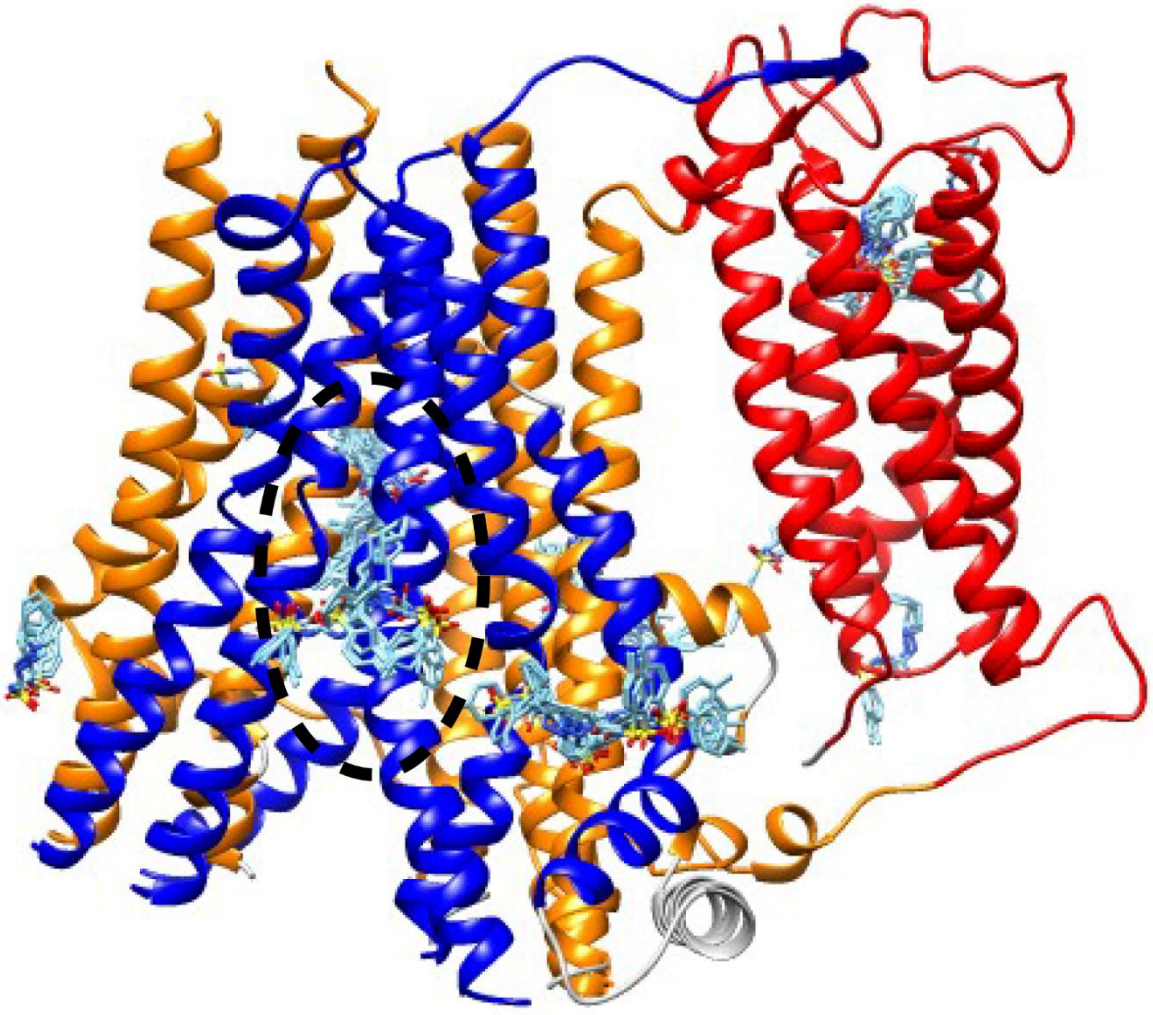

Figure 3 Gliclazide binds to the intermembrane site of sulfonylurea receptor 1. The established binding site of sulfonylureas is shown as a black dashed oval.

Table 6 Volumes required to produce palmitate combination treatments. Increasing concentrations of palmitate 3, 10, 30 and 100 µM were prepared by diluting palmitate stock solution in 50 mL of 3% heat-inactivated FCS supplemented RPMI-1640. Stock solutions of efavirenz, rilpivirine and doravirine were used to make working solutions in 10 mL of palmitate solutions.

Combination treatment	Efavirenz stock solution (µL)	Rilpivirine stock solution (µL)	Palmitate stock solution (µL)
Efavirenz 3 µM plus Palmitate 10 µM	1.2	0	50
Efavirenz 3 µM plus Palmitate 30 µM	1.2	0	150
Efavirenz 10 µM plus Palmitate 10 µM	4	0	50
Efavirenz 10 µM plus Palmitate 30 µM	4	0	150
Rilpivirine 0.3 µM plus Palmitate 10 µM	0	0.12	50
Rilpivirine 0.3 µM plus Palmitate 30 µM	0	0.12	150
Rilpivirine 1 µM plus Palmitate 10 µM	0	0.4	50
Rilpivirine 1 µM plus Palmitate 30 µM	0	0.4	150

Table 7 Volumes required to produce solutions of increasing concentrations of NRTIs to treat INS-1E cells. NRTIs (25 mM stock solution) were diluted in 5 mL of 3% heat-inactivated FCS RPMI-1640 media.

NRTIs			
Concentration (in µM)	Tenofovir DF (in µL)	Emtricitabine (in µL)	Lamivudine (in µL)
1	0.2	0.2	0.2
3	0.6	0.6	0.6
10	2	2	2
20	4	4	4
30	6	6	6

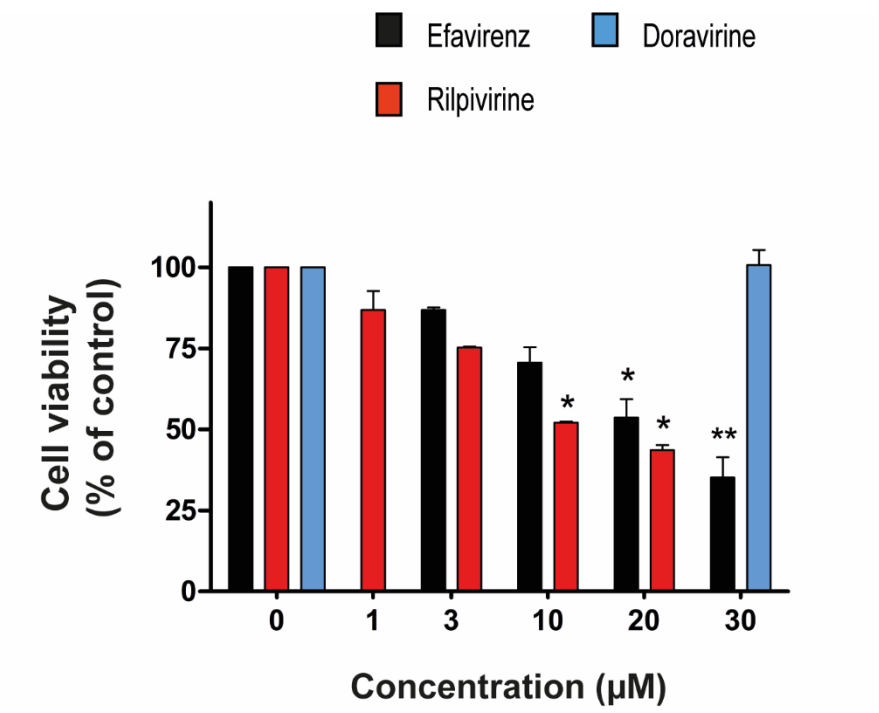

Figure 4 Effects of NNRTIs on cell viability in human 1.4E7 cells. 1.4E7 cells were cultured for 24 hrs (see 2.2.1) before exposing cells to increasing concentrations of efavirenz, rilpivirine or doravirine for 24 hrs before measuring cell viability using an MTT assay. Efavirenz and rilpivirine, but not doravirine, reduced cell viability

in 1.4E7 cells. Data are expressed as mean ± SEM from *n* = 3 independent experiments. Statistically significant differences were determined using Kruskal-Wallis with Dunn's post hoc test. * $p < 0.05$, ** $p < 0.01$ significantly different from vehicle-treated control cells.

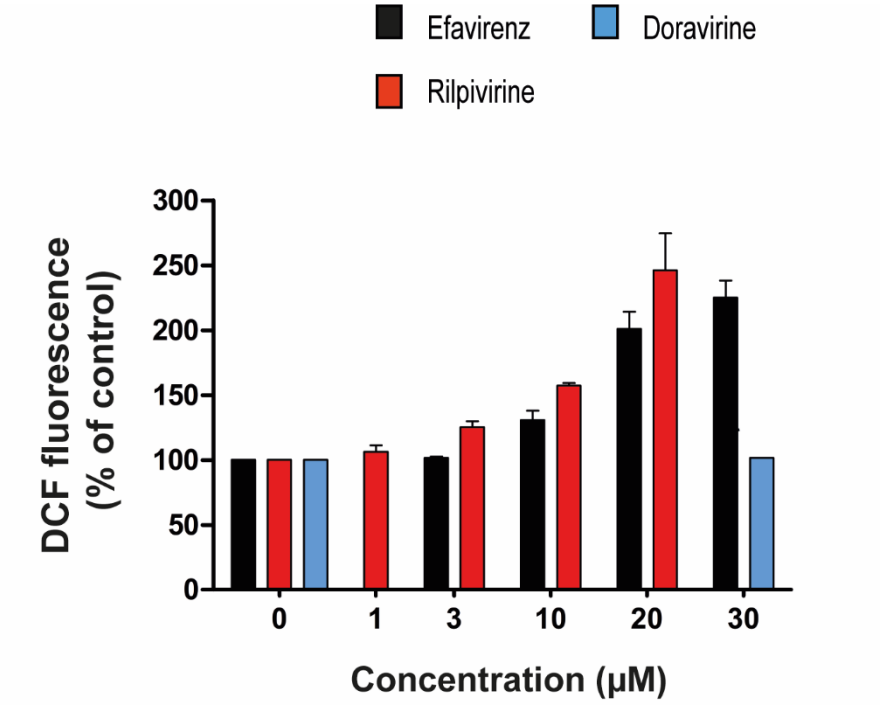

Figure 5 Effects of NNRTIs on intracellular ROS generation in human 1.4E7 cells. 1.4E7 cells were cultured for 24 hrs (see 2.2.1) before exposing cells to increasing concentrations of efavirenz, rilpivirine or doravirine for 24 h before measuring intracellular using a DCF assay. DCF fluorescence is proportional to the levels of intracellular ROS. Intracellular ROS generation is determined by DCF fluorescence normalised to cell proliferation by Crystal Violet assay. There was an increasing trend in increased intracellular ROS generation following efavirenz and rilpivirine, but not doravirine exposure. Data are expressed as mean ± SEM from *n* = 2 independent experiments. No statistical analysis was performed due to the limited number of independent experiments.

Appendix II

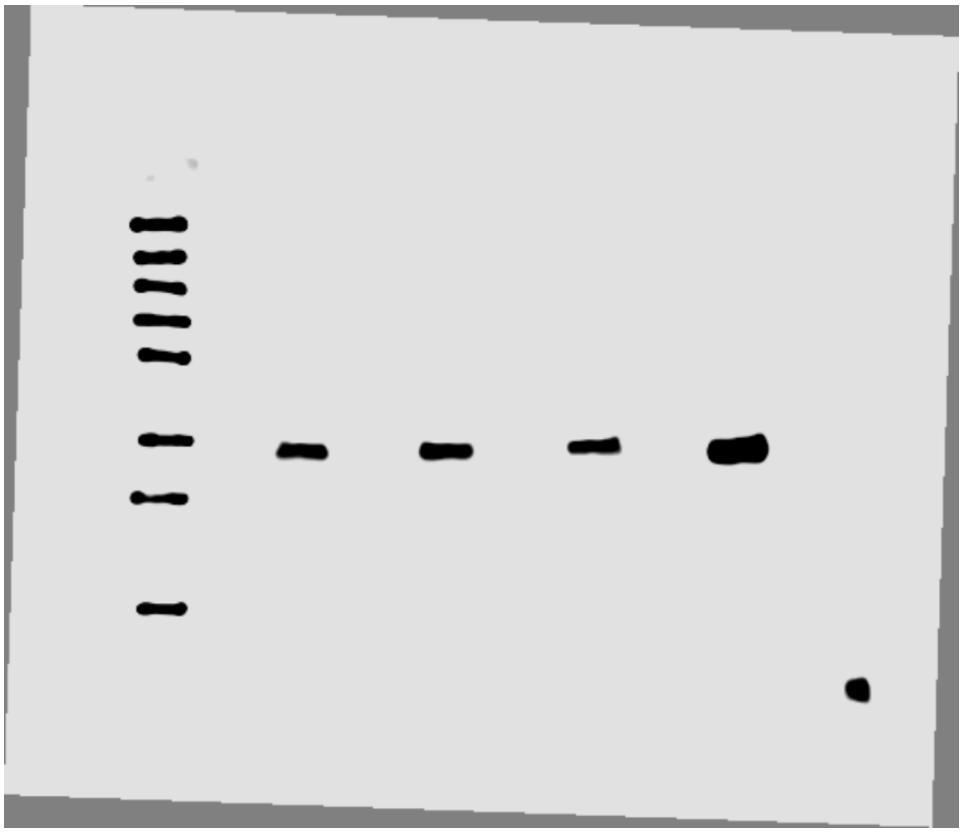

Figure 1 Uncropped blot image for CHOP expression in INS-1E cells treated with efavirenz 20 µM (n = 1, n = 2, n = 3) or thapsigargin 1 µM (positive control) for 24 hrs. Details below:

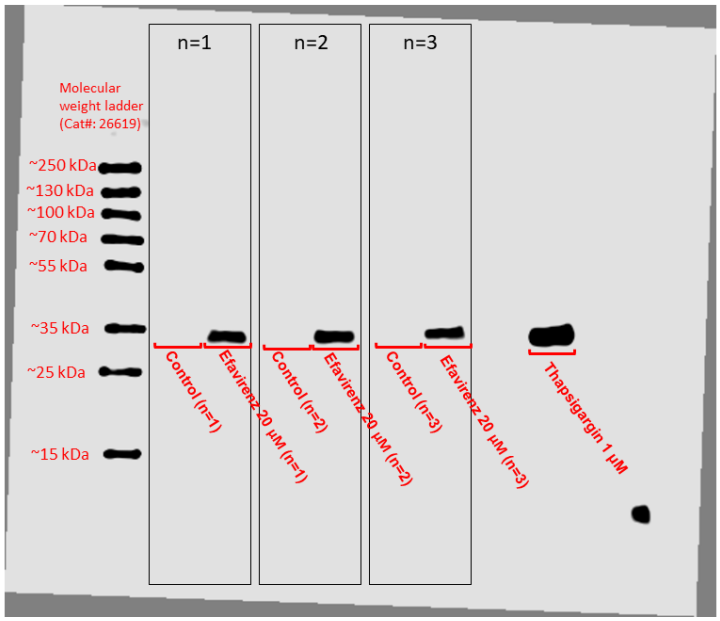

Figure 2 Uncropped stripped blot image in INS-1E cells treated with efavirenz 20 μM (n = 1, n = 2, n = 3) or thapsigargin 1 μM (positive control) for 24 hrs.

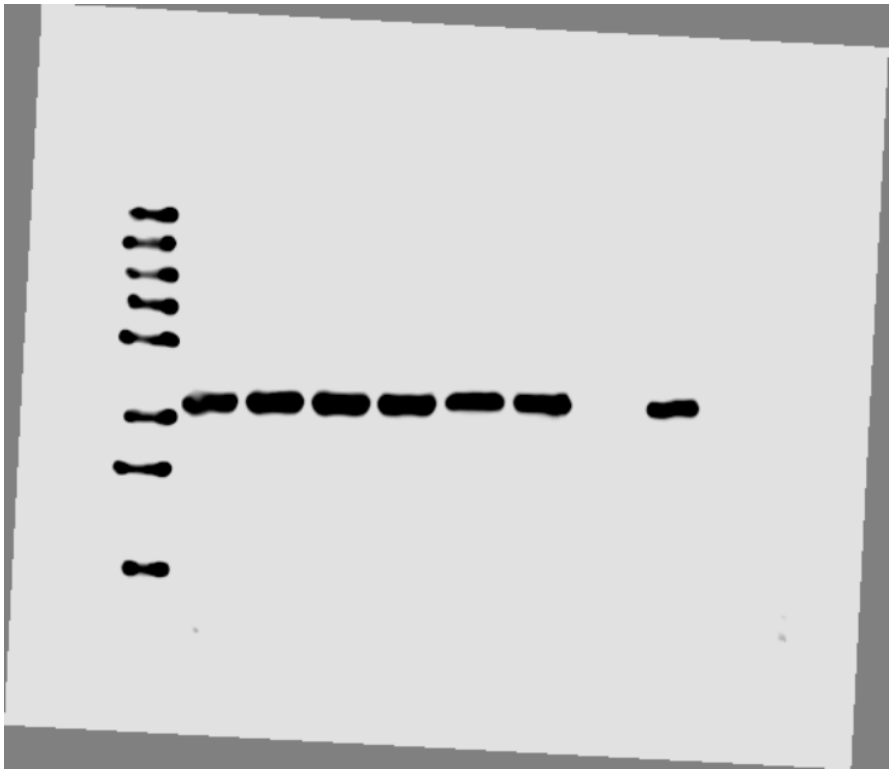

Figure 3 Uncropped blot image for GAPDH expression in INS-1E cells treated with efavirenz 20 μM (n = 1, n = 2, n = 3) or thapsigargin 1 μM (positive control) for 24 hrs. Details below:

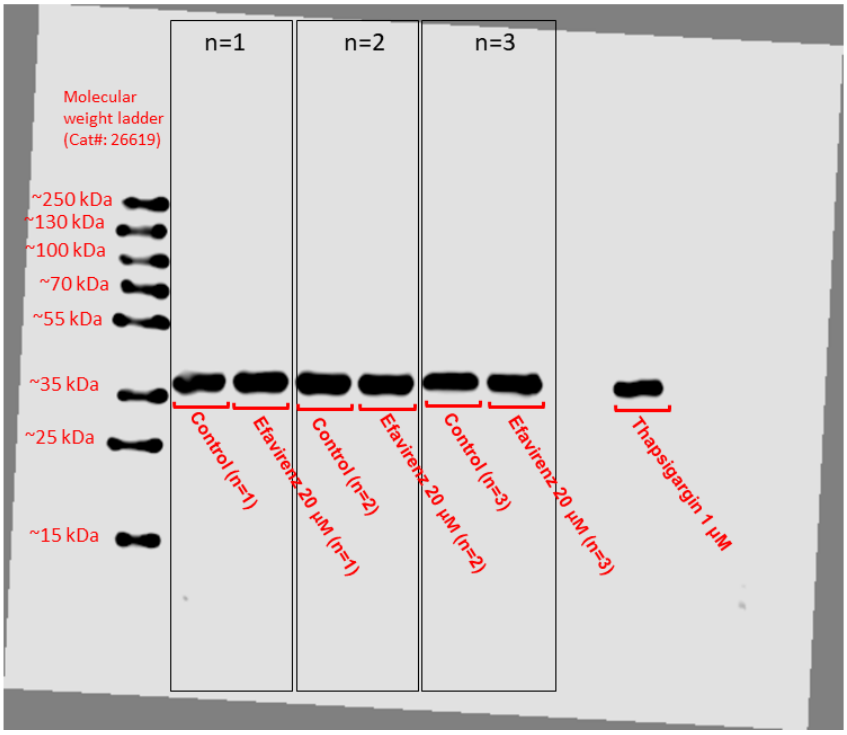

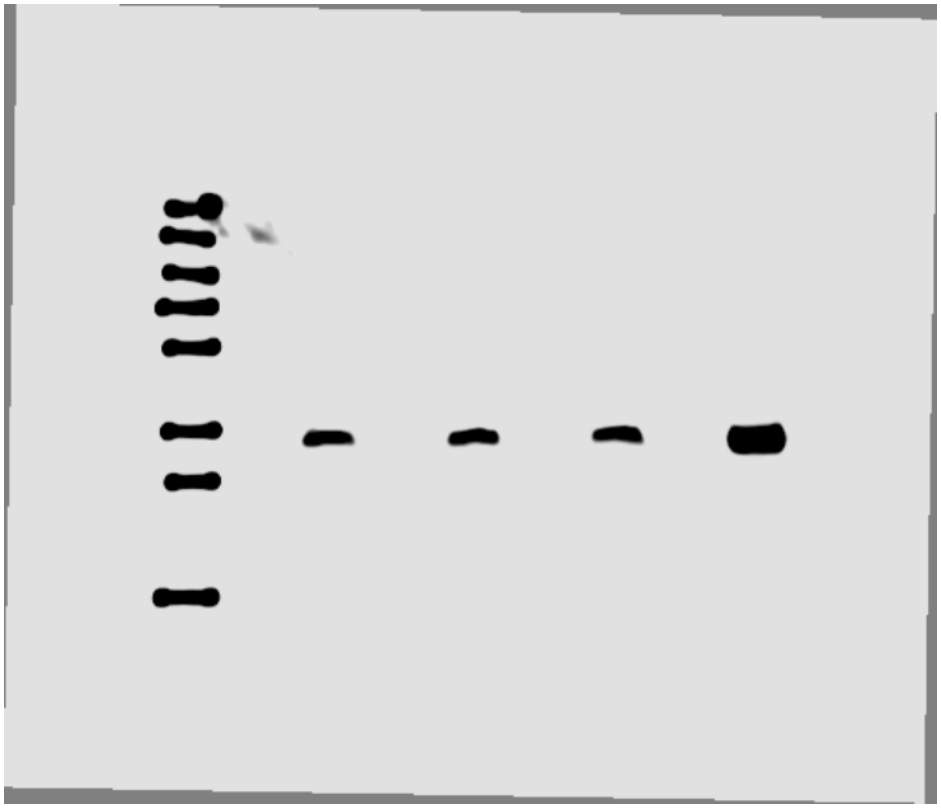

Figure 4 Uncropped blot image for CHOP expression in INS-1E cells treated with rilpivirine 10 µM (n = 1, n = 2, n = 3) or thapsigargin 1 µM (positive control) for 24 hrs. Details below:

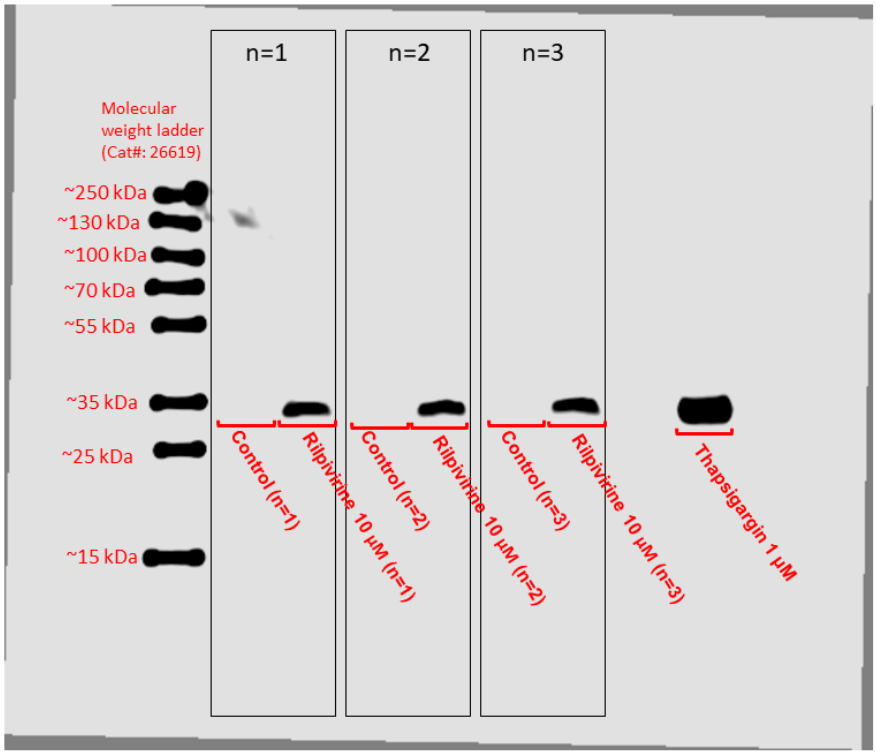

Figure 5 Uncropped stripped blot image in INS-1E cells treated with rilpivirine 10 µM (n = 1, n = 2, n = 3) or thapsigargin 1 µM (positive control) for 24 hrs.

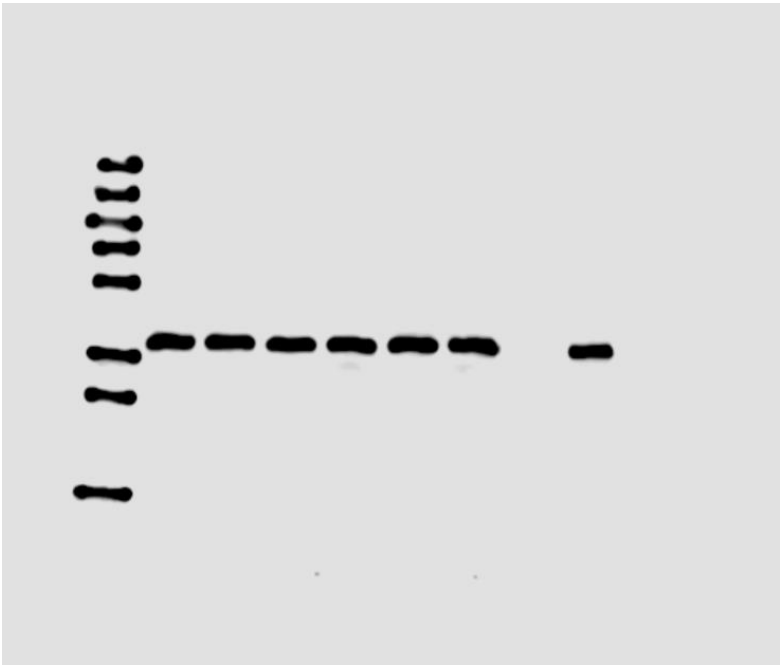

Figure 6 Uncropped blot image for GAPDH expression in INS-1E cells treated with rilpivirine 10 µM (n = 1, n = 2, n = 3) or thapsigargin 1 µM (positive control) for 24 hrs. Details below:

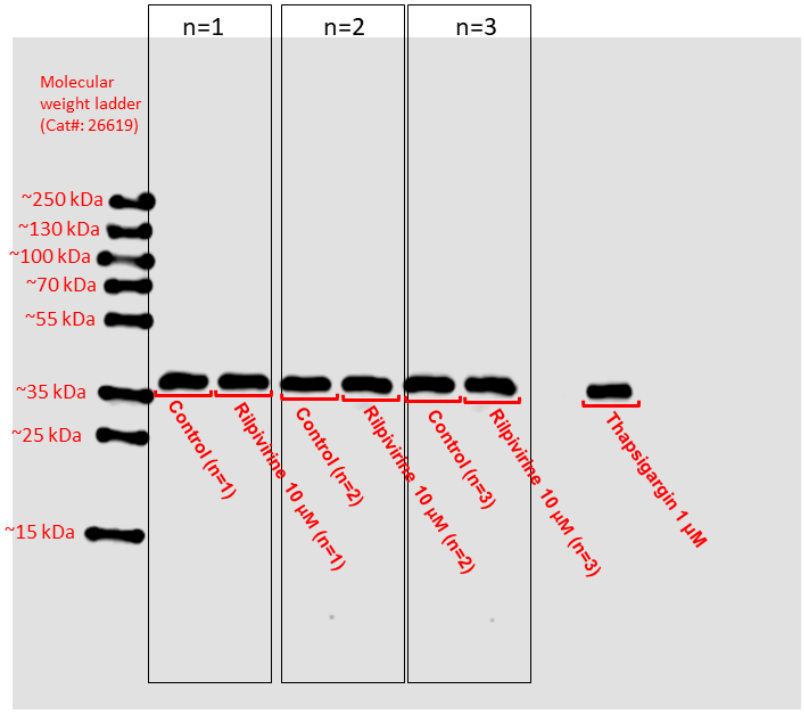

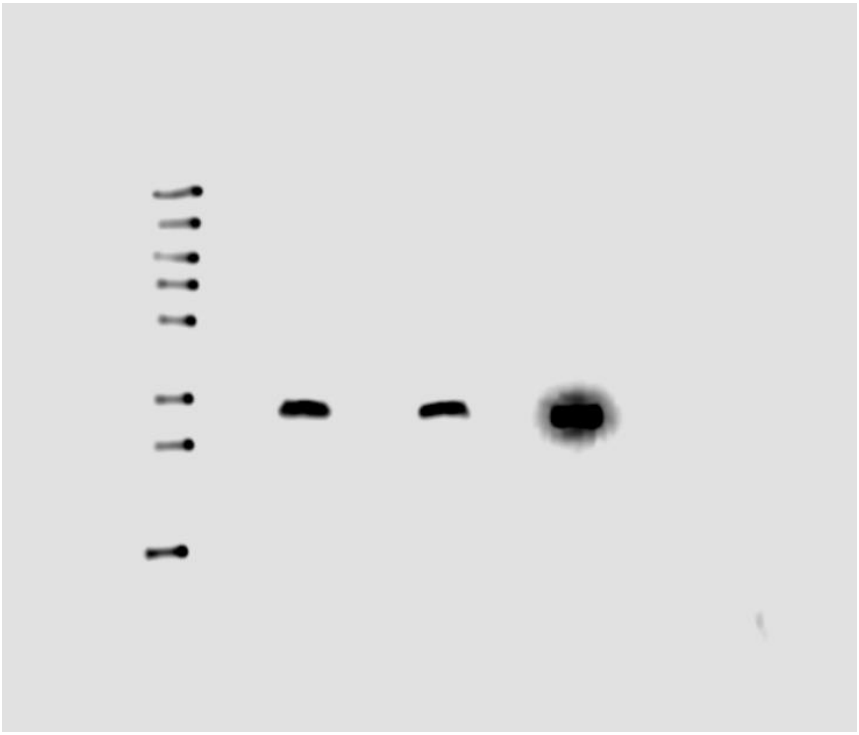

Figure 7 Uncropped blot image for CHOP expression in INS-1E cells treated with efavirenz 20 µM (n = 4 and n = 5) or thapsigargin 1 µM (positive control) for 24 hrs. Details below:

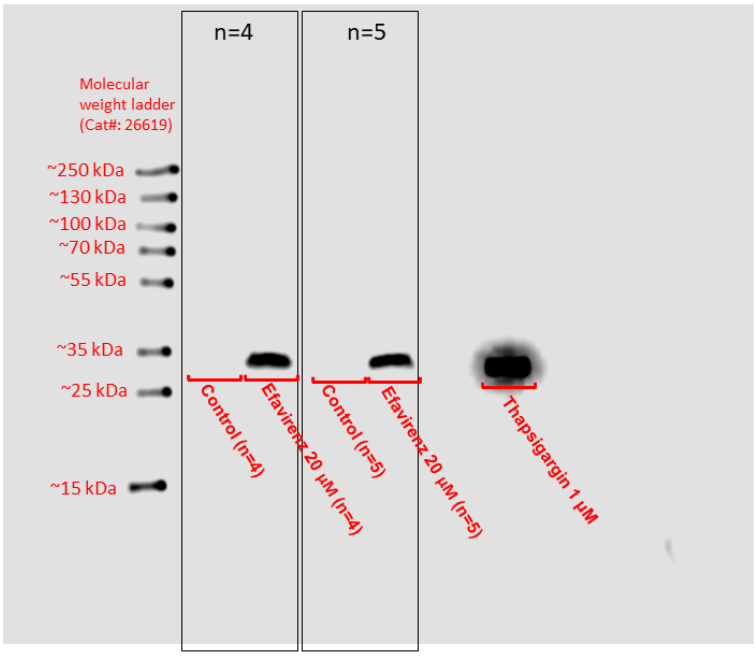

Figure 8 Uncropped stripped blot image in INS-1E cells treated with efavirenz 20 μM (n = 4 and n = 5) or thapsigargin 1 μM (positive control) for 24 hrs.

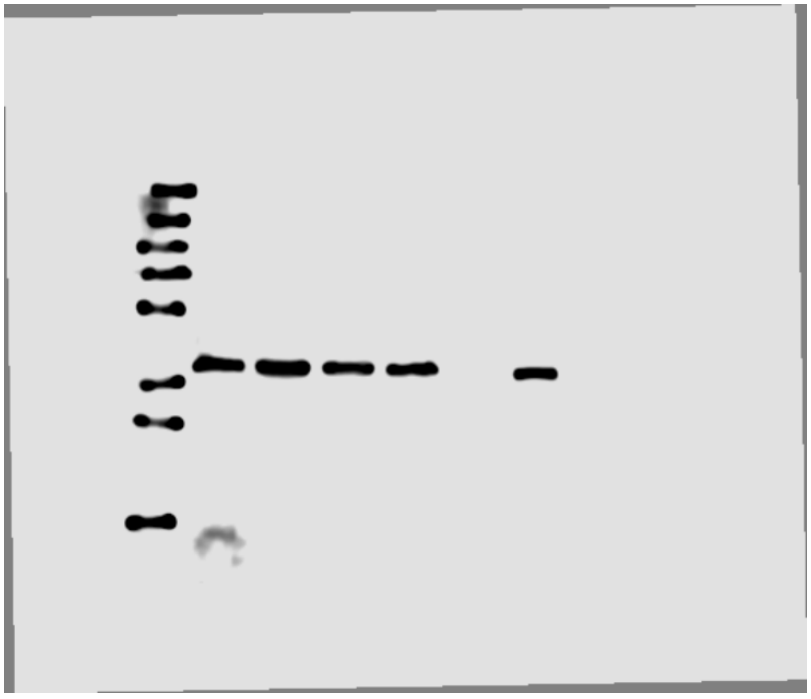

Figure 9 Uncropped blot image for GAPDH expression in INS-1E cells treated with efavirenz 20 μM (n = 4 and n = 5) or thapsigargin 1 μM (positive control) for 24 hrs. Details below:

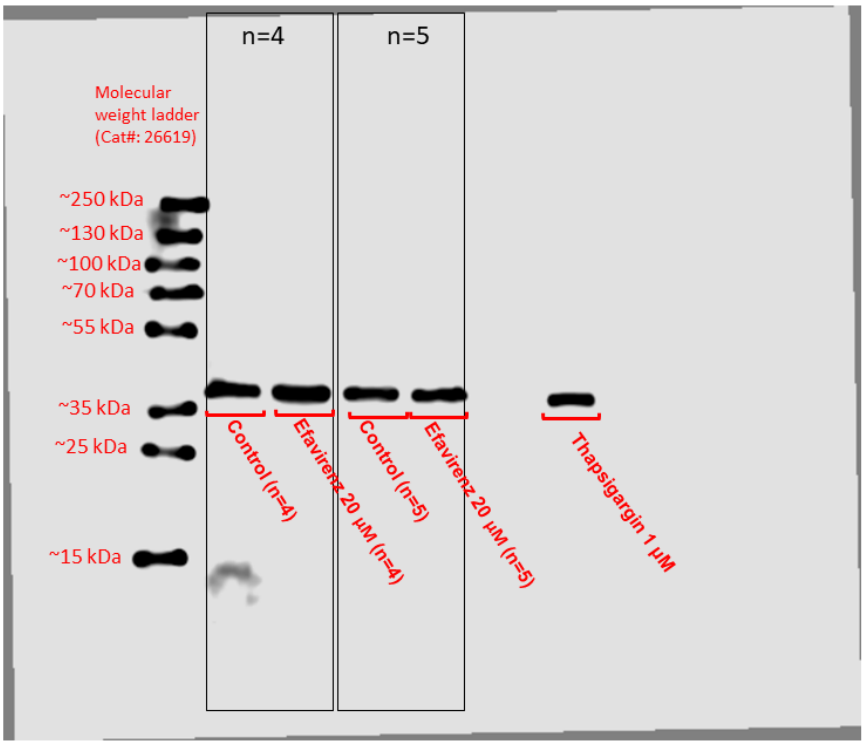

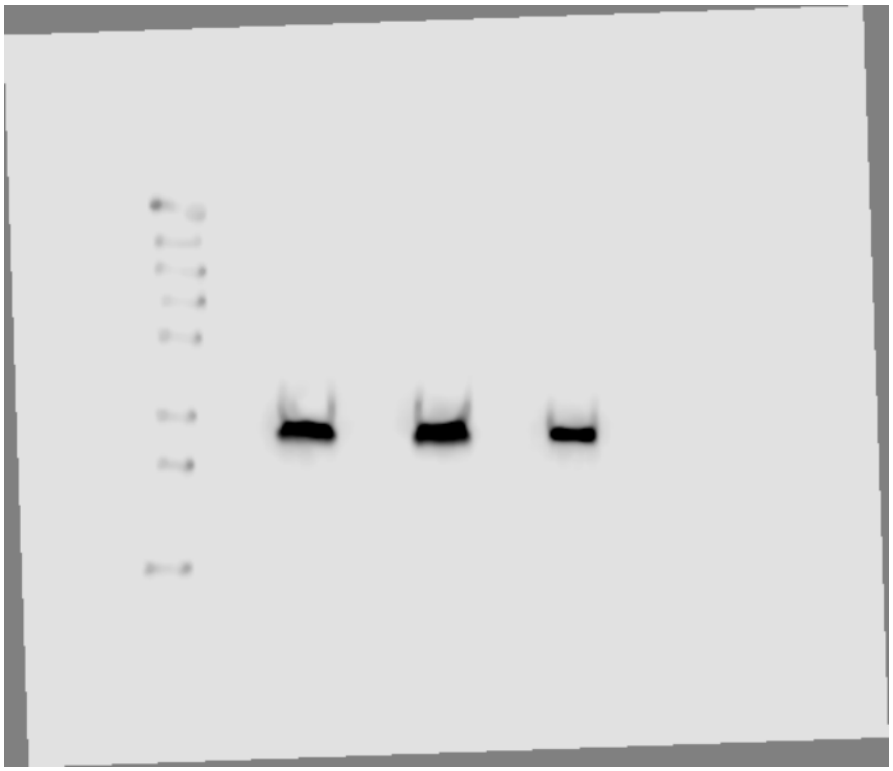

Figure 10 Uncropped blot image for CHOP expression in INS-1E cells treated with rilpivirine 10 µM (n = 4 and n = 5) or thapsigargin 1 µM (positive control) for 24 hrs. Details below:

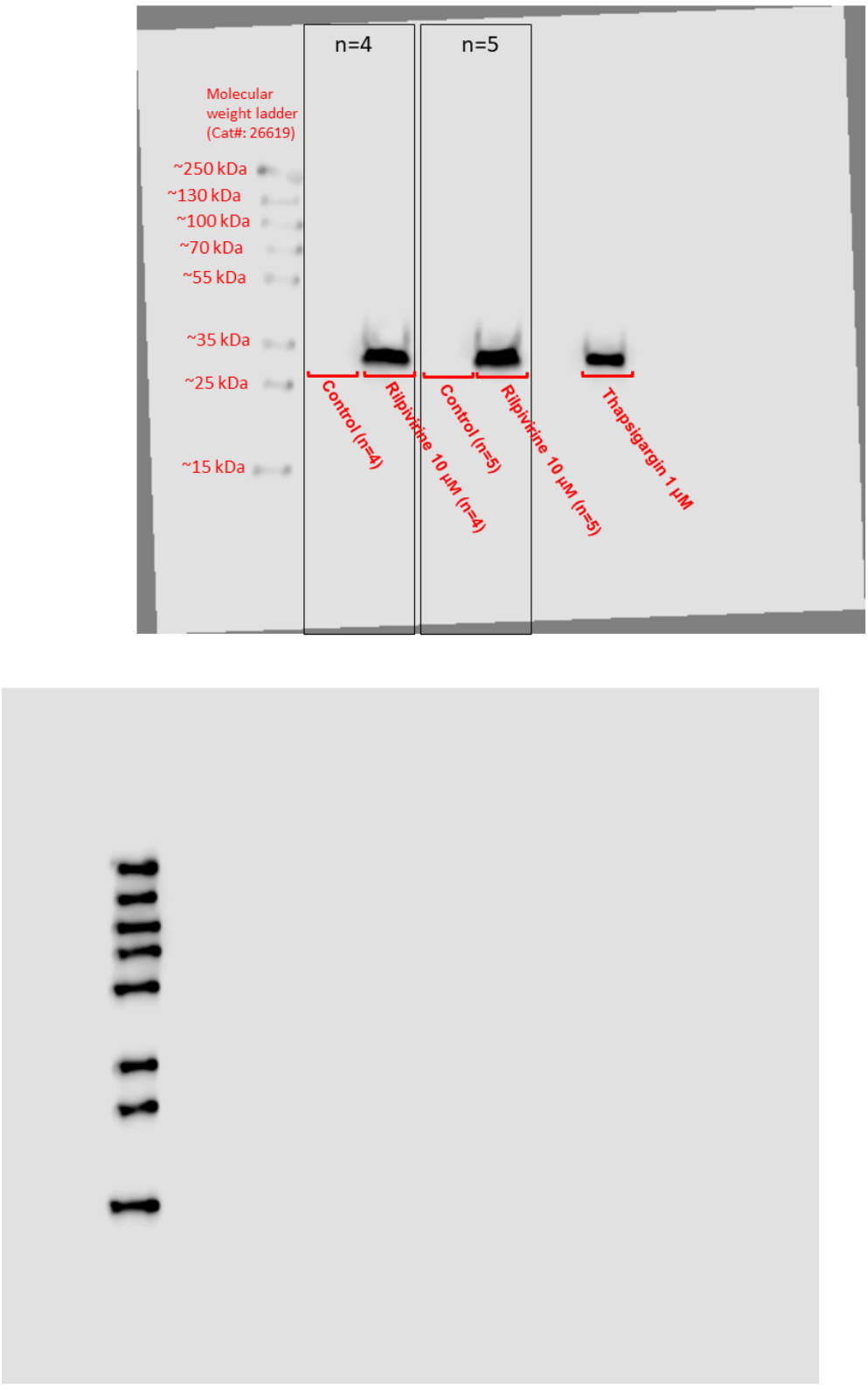

Figure 11 Uncropped stripped blot image in INS-1E cells treated with rilpivirine 10 µM (n = 4 and n = 5) or thapsigargin 1 µM (positive control) for 24 hrs

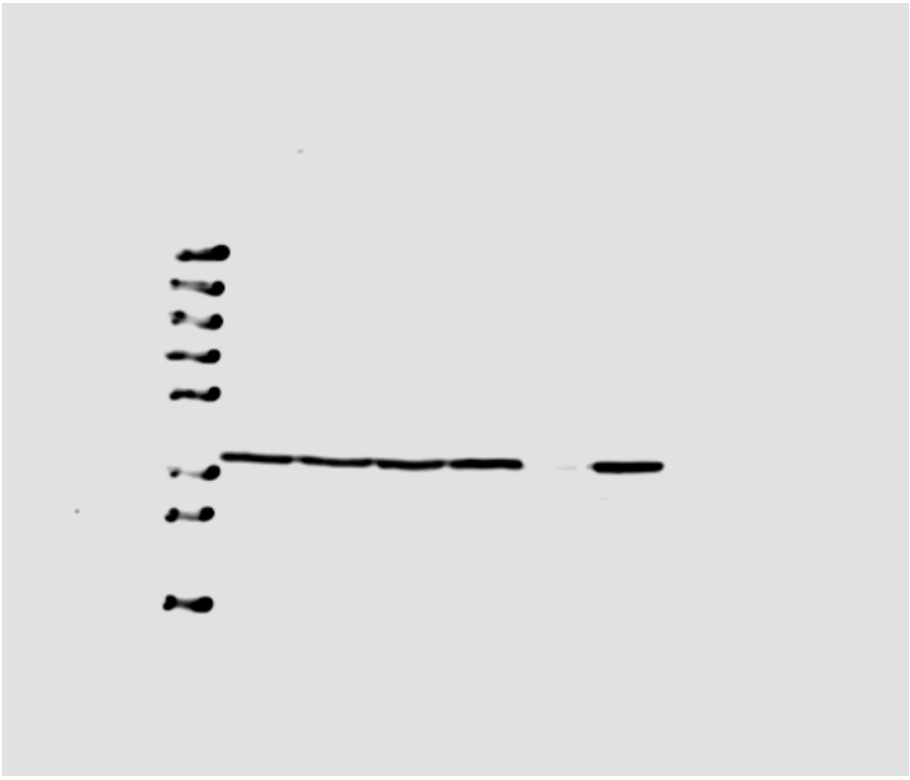

Figure 12 Uncropped blot image for GAPDH expression in INS-1E cells treated with rilpivirine 10 µM (n=4 and n=5) or thapsigargin 1 µM (positive control) for 24 hrs. Details below:

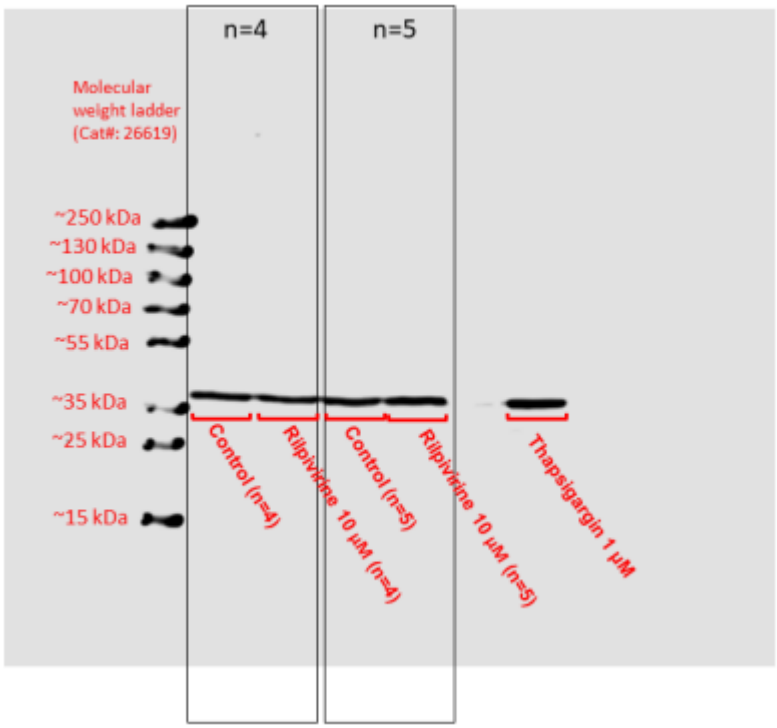

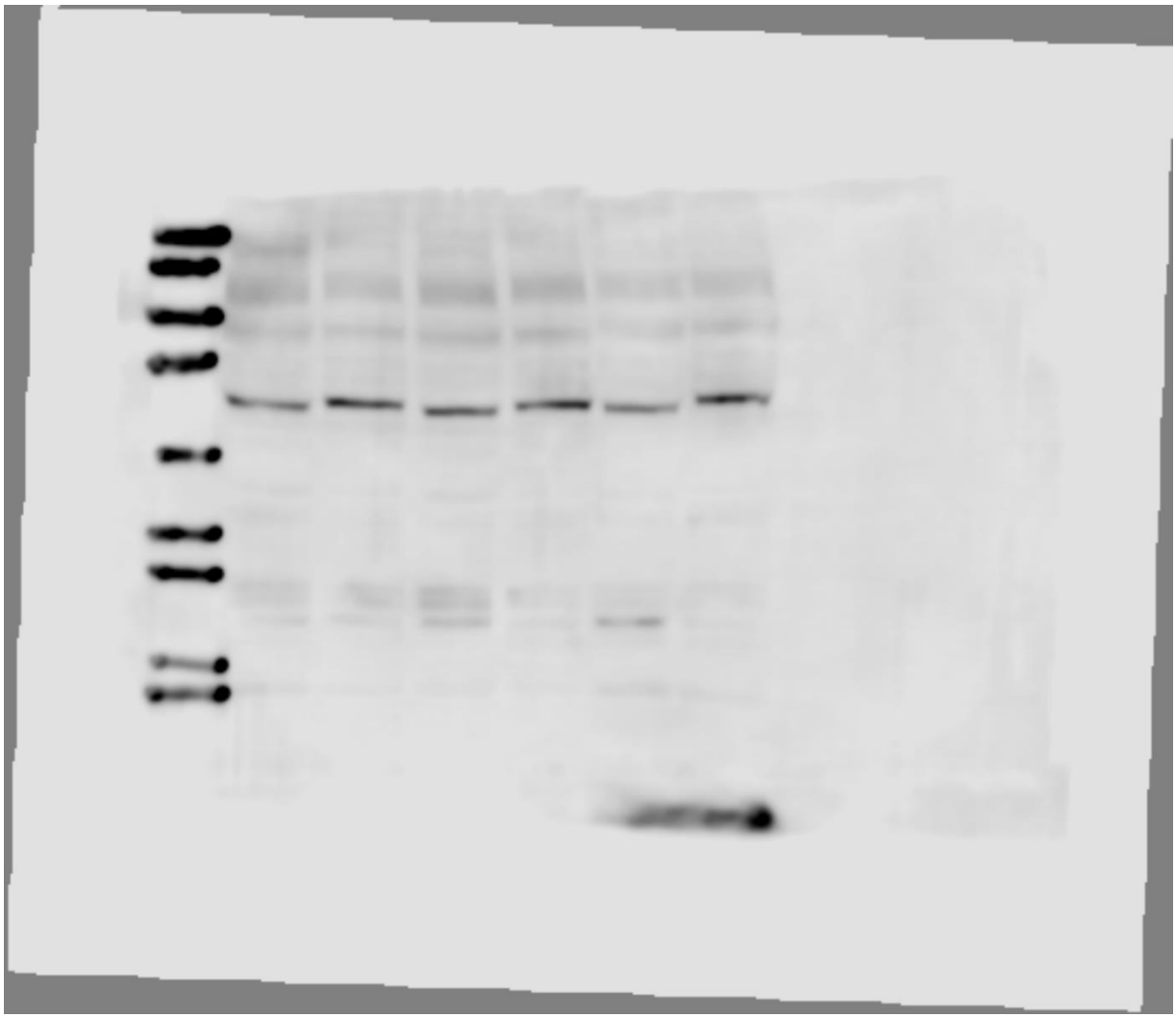

Figure 13 Uncropped blot image for GRP78 expression in INS-1E cells treated with rilpivirine 10 µM (n=1, n = 2 and n = 3) for 24 hrs. Details below:

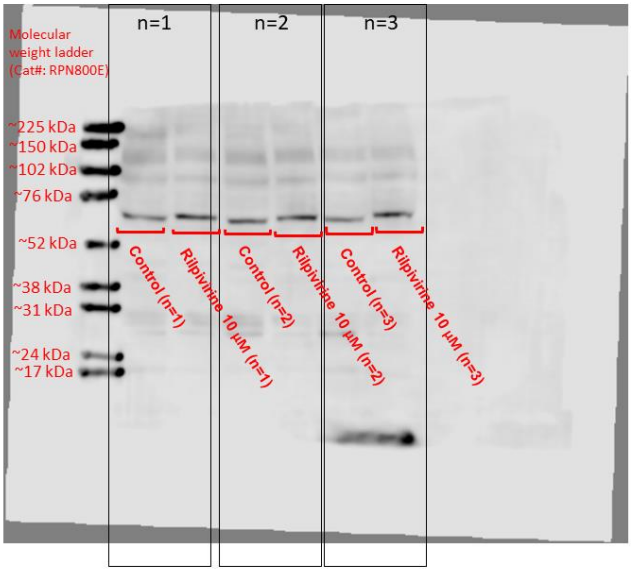

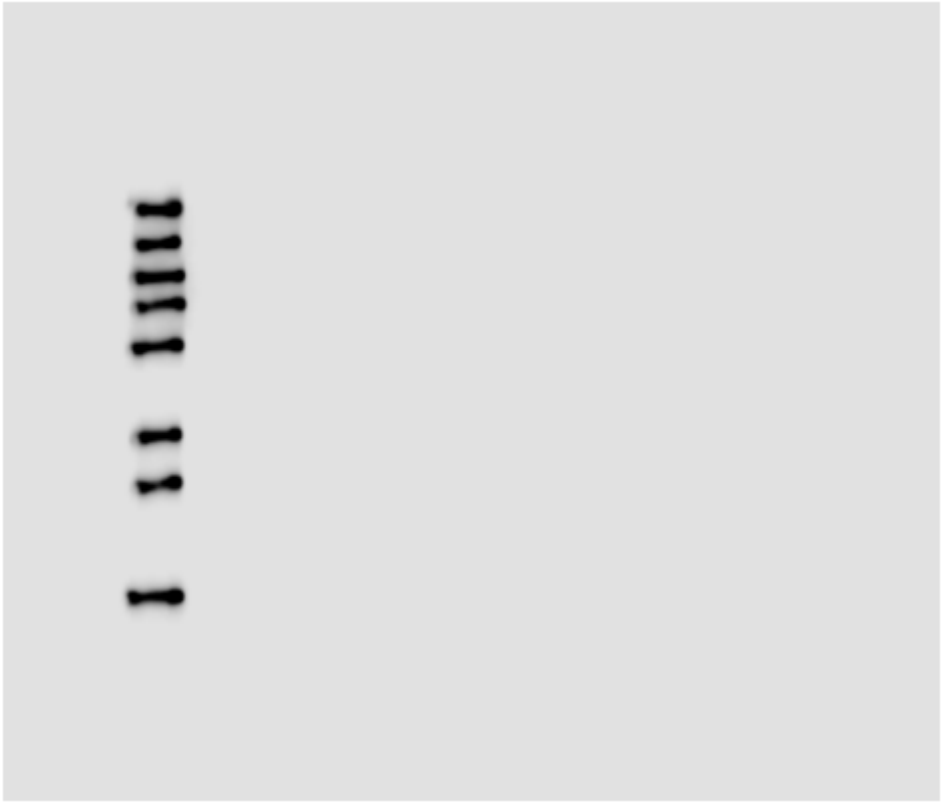

Figure 14 Uncropped stripped blot image in INS-1E cells treated with rilpivirine 10 µM (n = 1, n = 2 and n = 3) for 24 hrs (GRP78 expression)

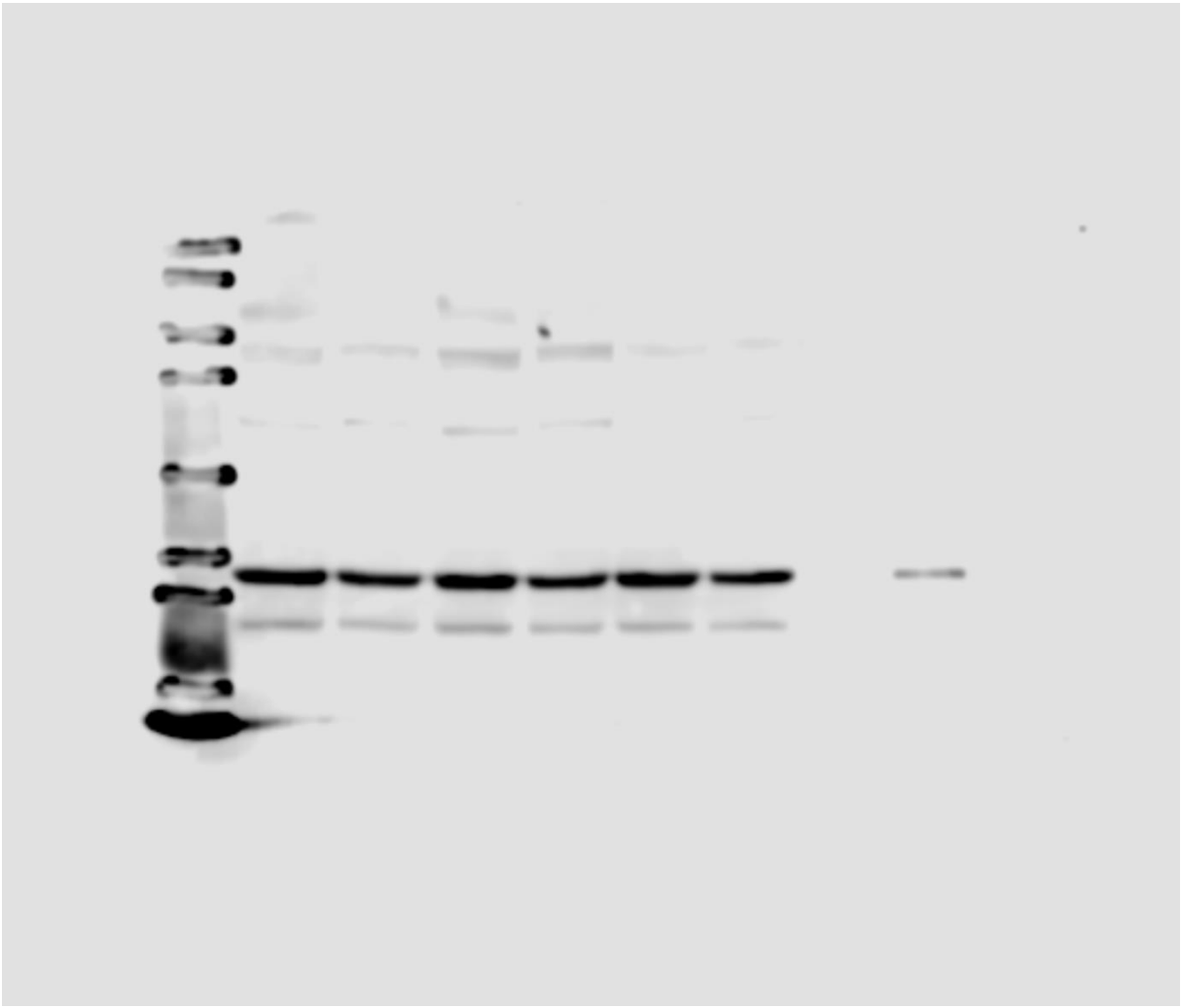

Figure 15 Uncropped blot image for GAPDH expression in INS-1E cells treated with rilpivirine 10 µM (n = 1, n = 2 and n = 3) or thapsigargin 1 µM (positive control) for 24 hrs. Details below:

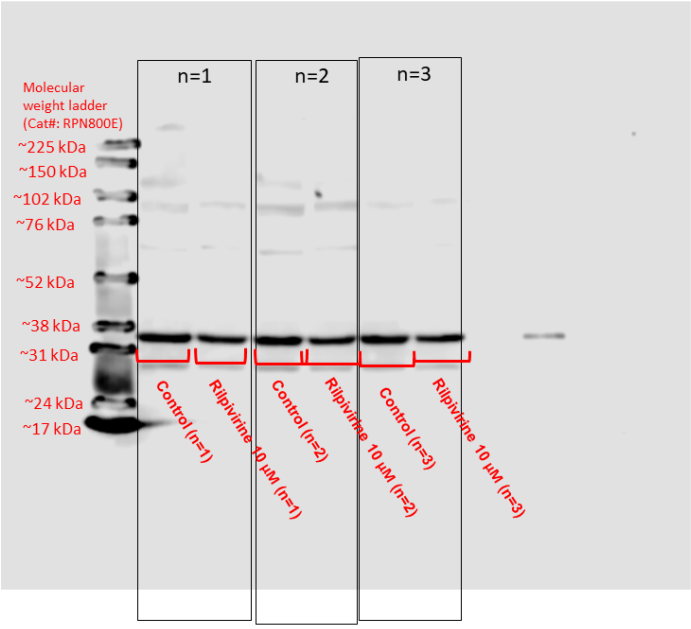

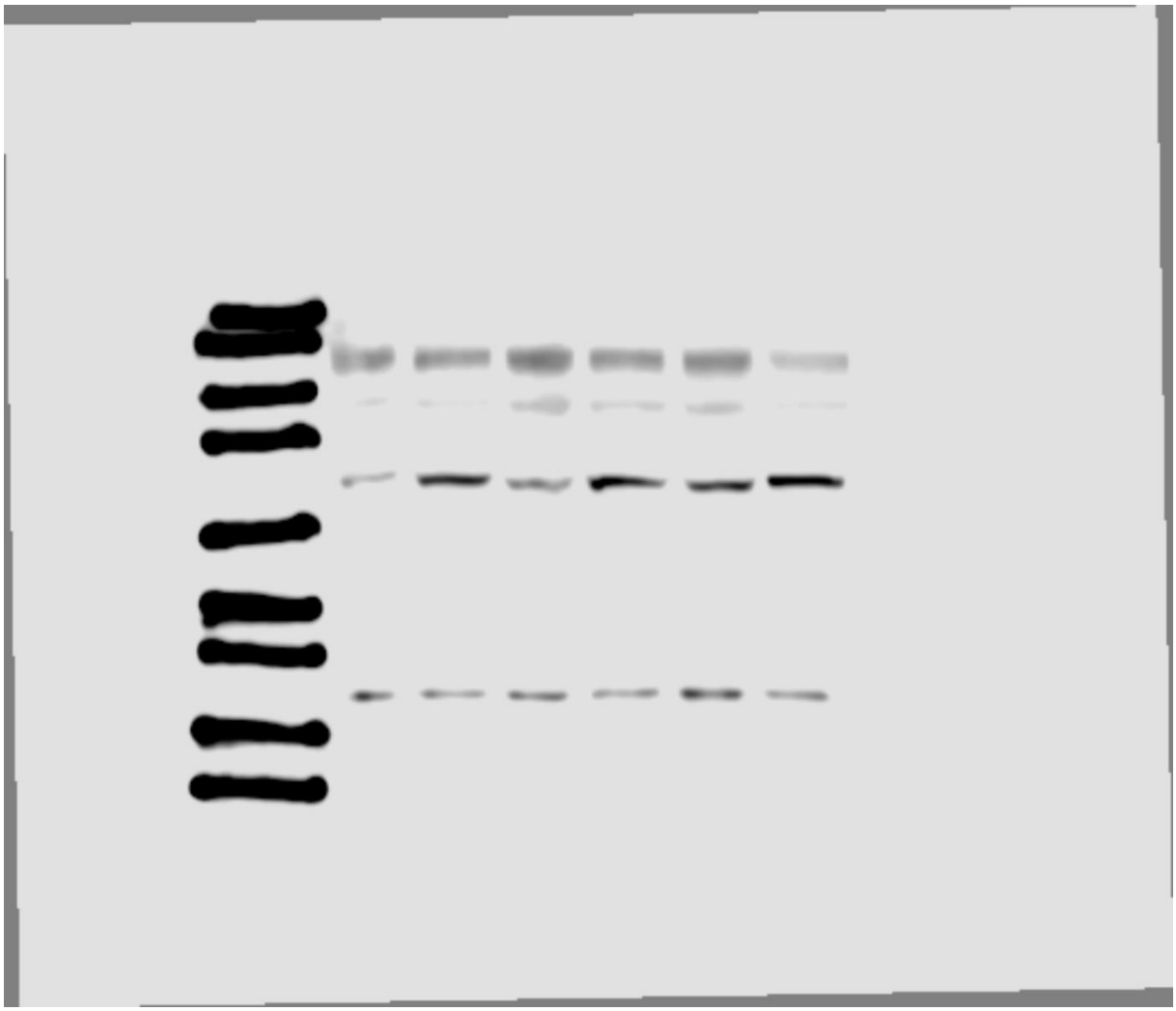

Figure 16 Uncropped blot image for GRP78 expression in INS-1E cells treated with efavirenz 20 µM (n = 1, n = 2 and n = 3) for 24 hrs. Details below:

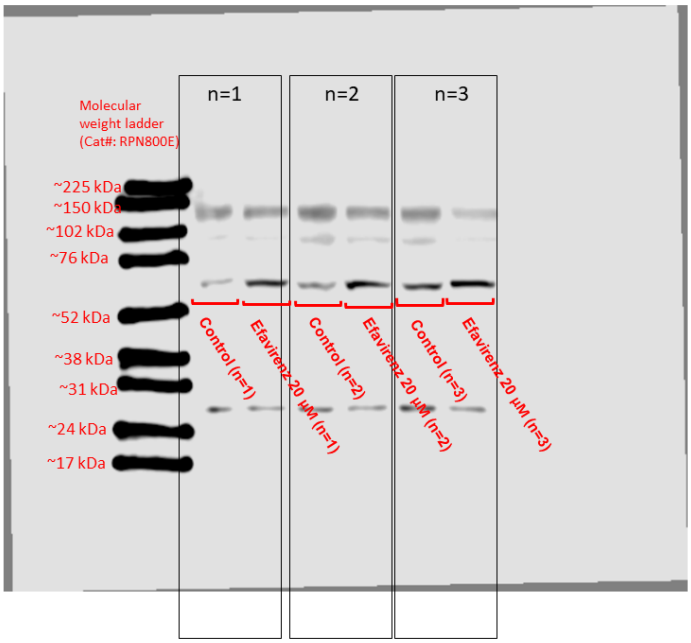

Figure 17 Uncropped stripped blot image in INS-1E cells treated with efavirenz 20 µM (n = 1, n = 2 and n =3) for 24 hrs (GRP78 expression)

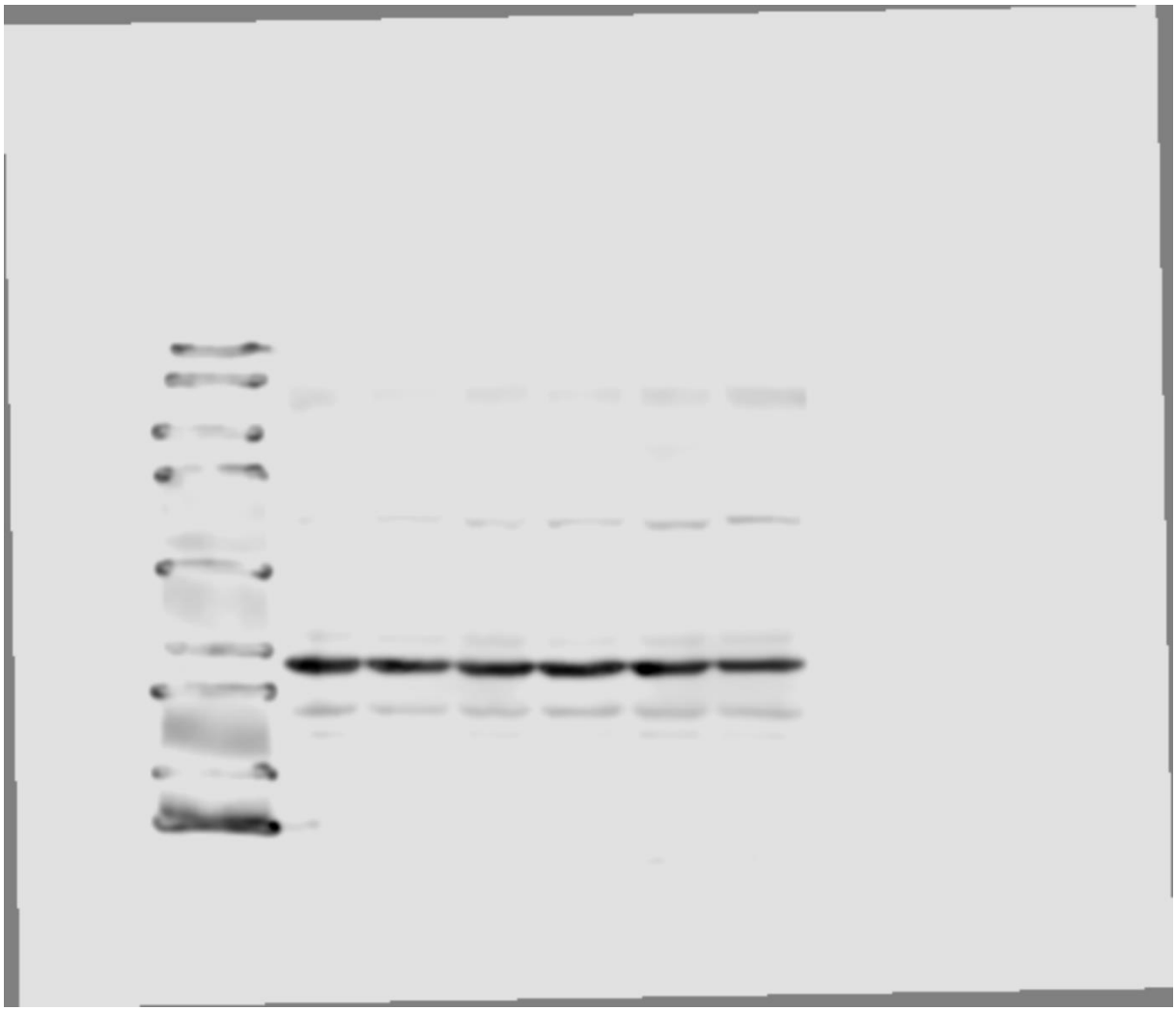

Figure 18 Uncropped blot image for GAPDH expression in INS-1E cells treated with efavirenz 20 µM (n = 1, n = 2 and n = 3) for 24 hrs. Details below:

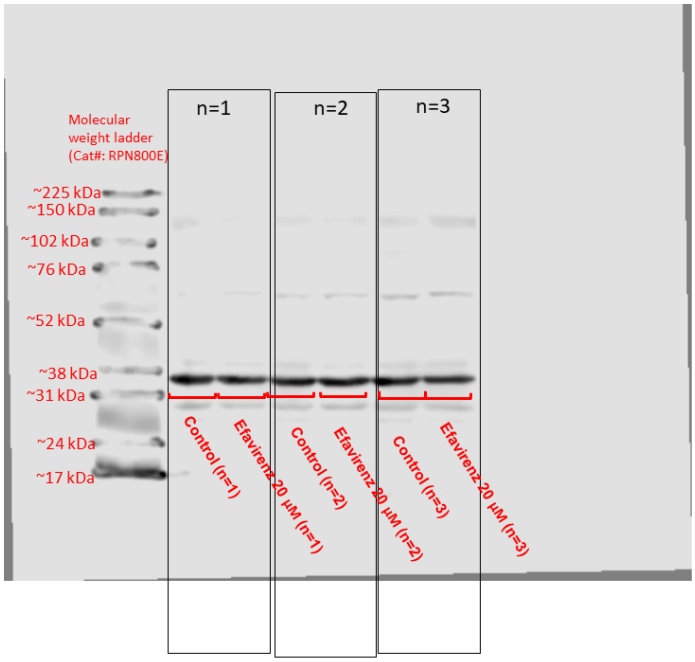

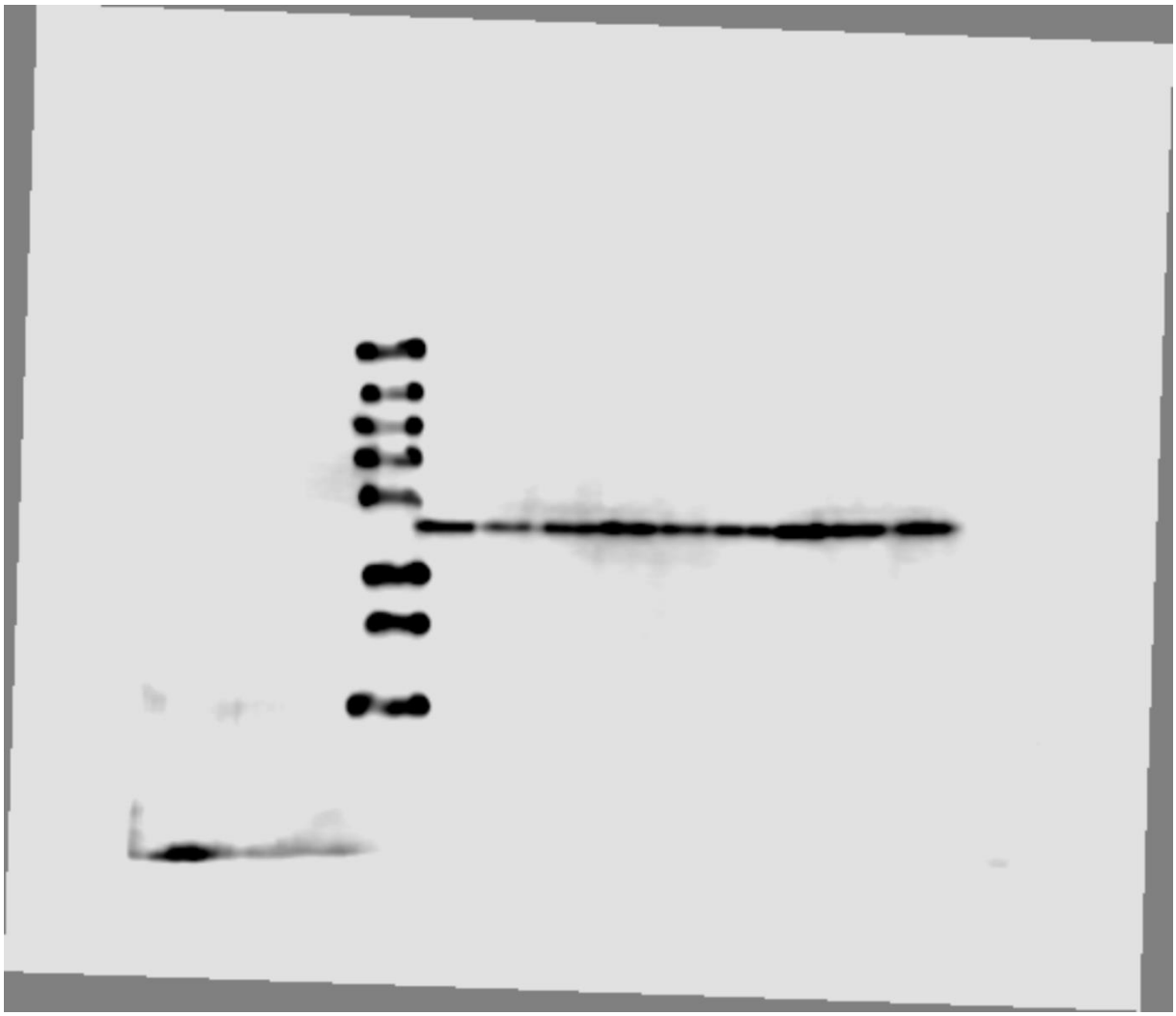

Figure 19 Uncropped blot image for PDX-1 expression in INS-1E cells treated with efavirenz (20 μM) or rilpivirine 10 μM (n = 1, n = 2 and n = 3) for 24 hrs. Details below:

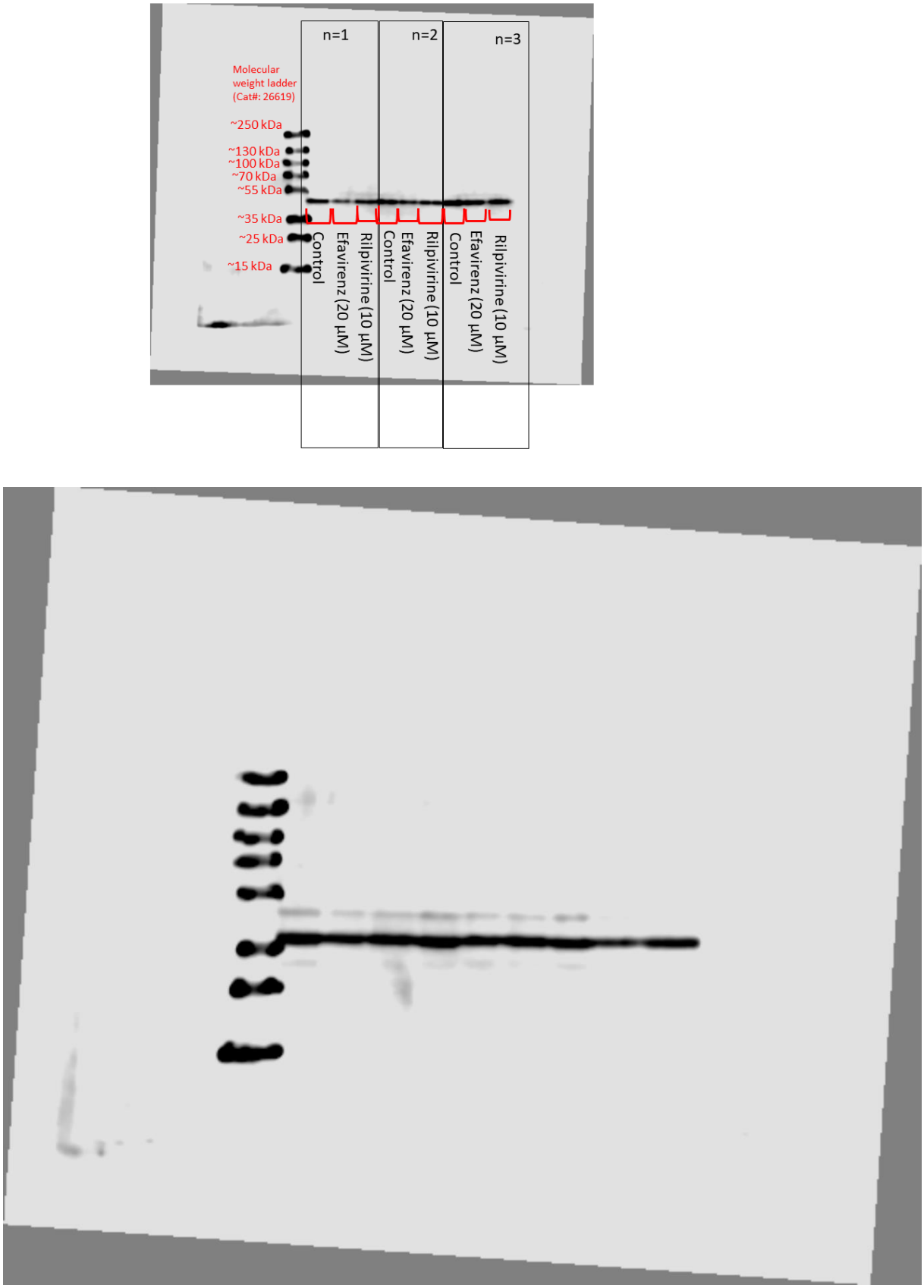

Figure 20 Uncropped blot image for GAPDH in INS-1E cells treated with efavirenz (20 µM) or rilpivirine 10 µM (n = 1, n = 2 and n = 3) for 24 hrs. Details below:

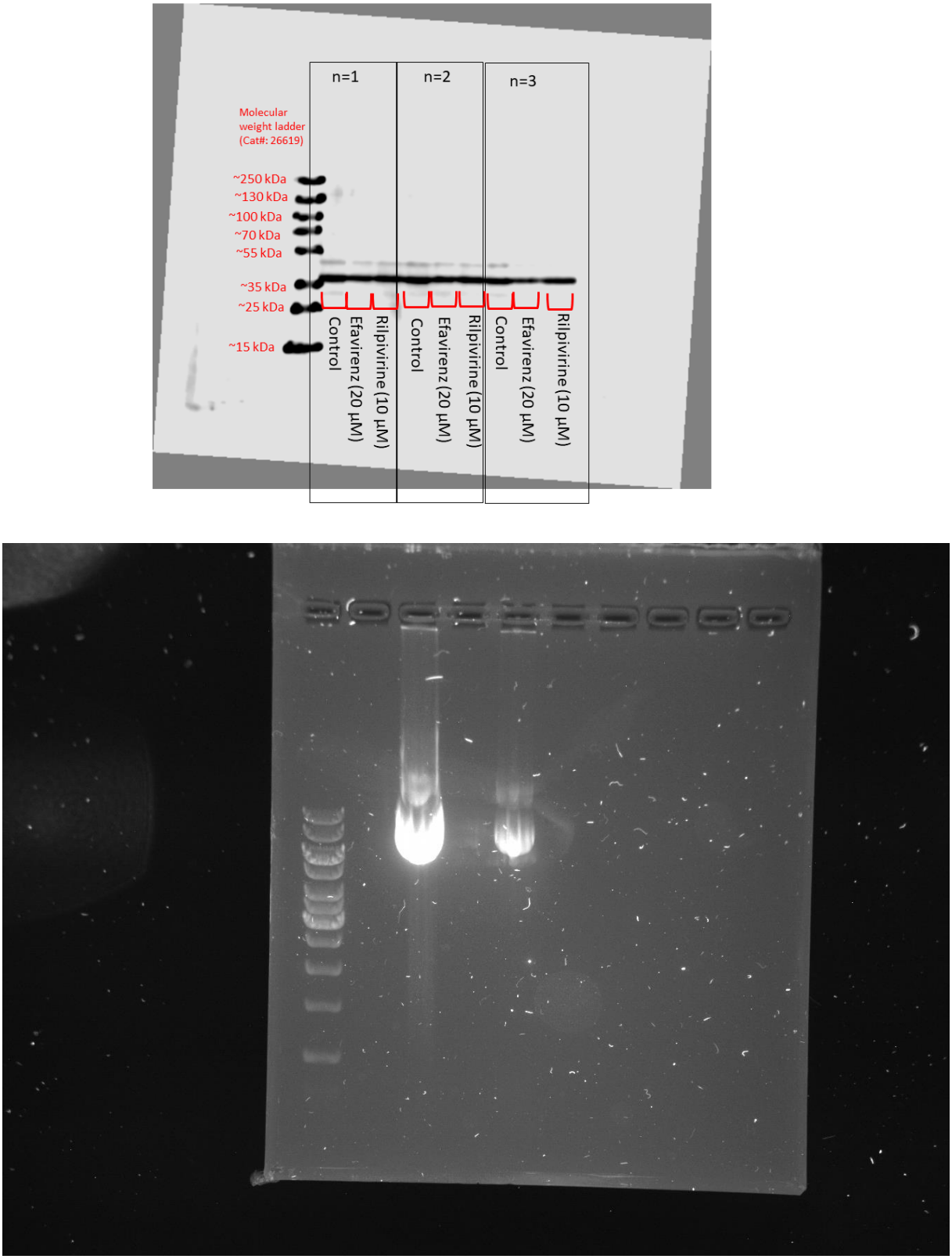

Figure 21 Uncropped agarose gel electrophoresis for analysis of unlinearised and linearised SUR1 DNA

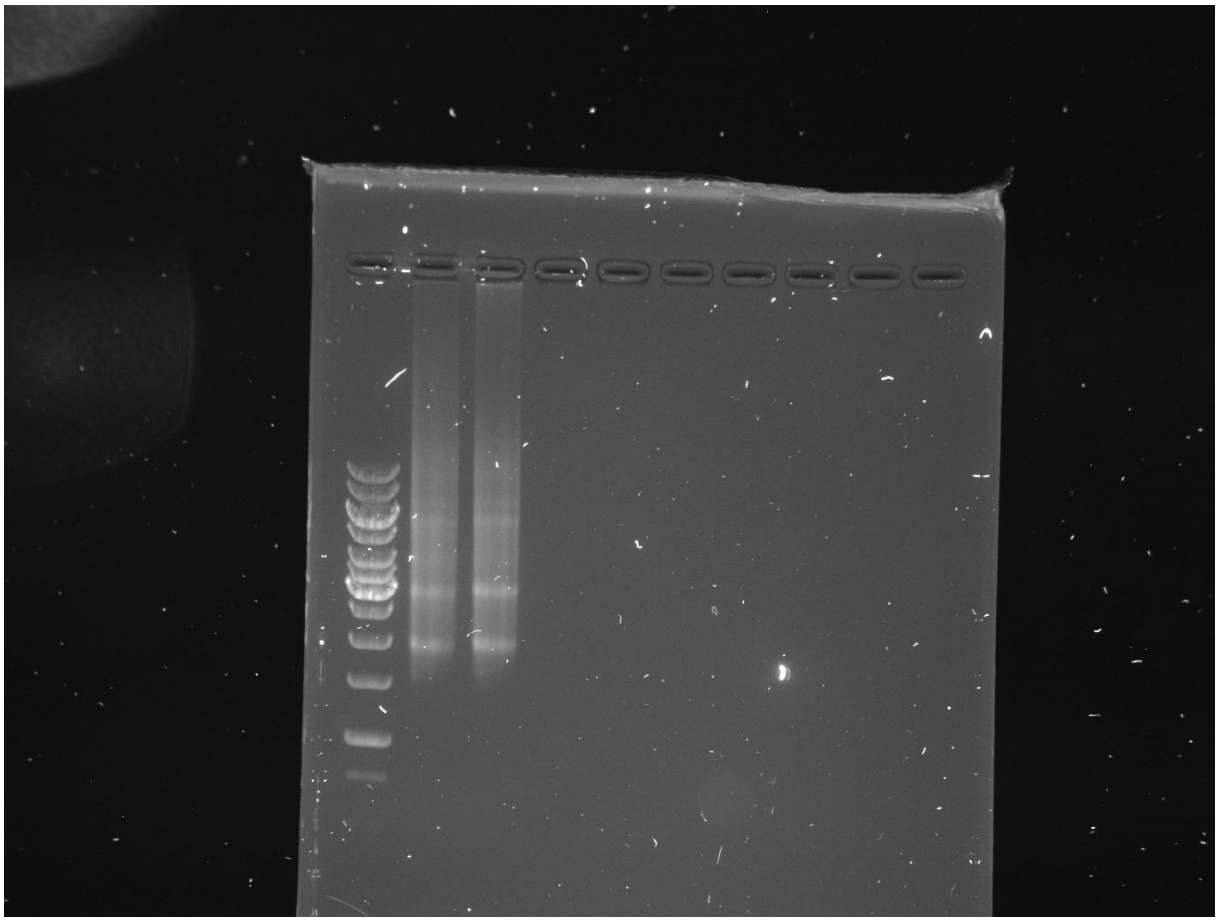

Figure 22 Uncropped DNA electrophoresis of RNA elutes for Kir6.2 and SUR1

Appendix III

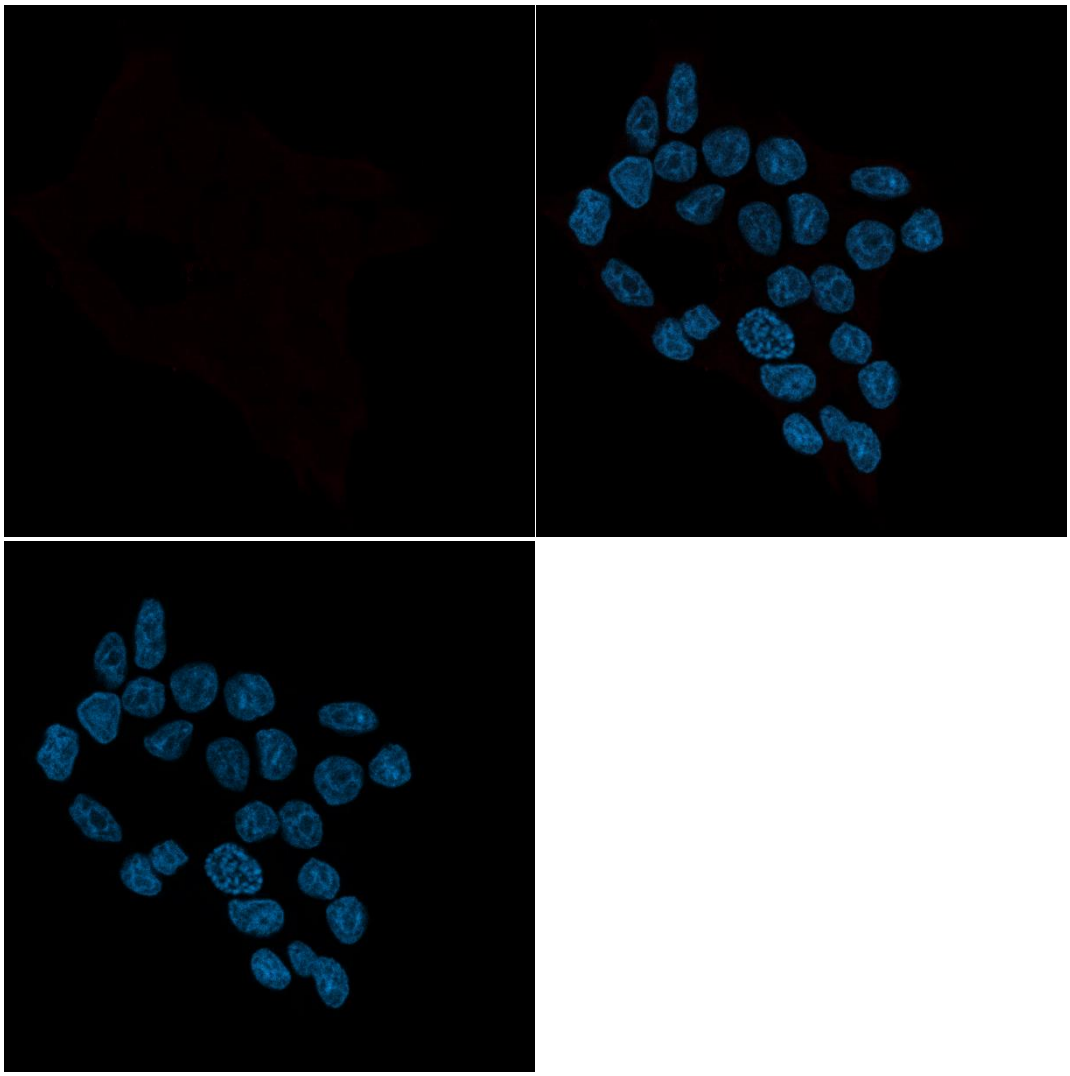

Figure 1 Uncropped cleaved caspase-3 ICC images (control). INS-1E cells were exposed to vehicle (DMSO) for 24 hrs before analysing cleaved caspase-3 by ICC. Red fluorescence represents cleaved caspase-3. Blue fluorescence (DAPI) represents nuclei.

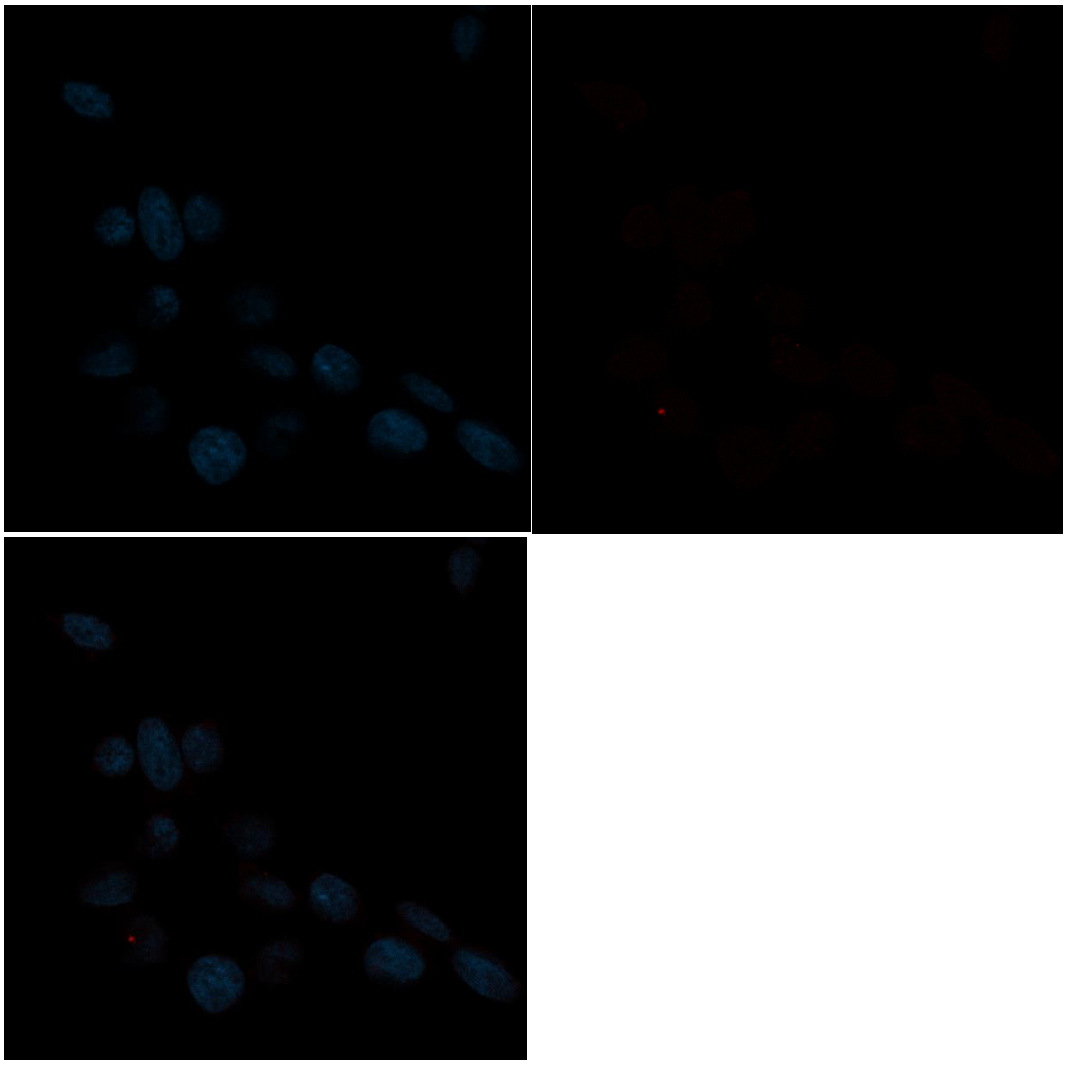

Figure 2 Uncropped cleaved caspase-3 ICC images (efavirenz). INS-1E cells were exposed to efavirenz 20 µM for 24 hrs before analysing cleaved caspase-3 by ICC. Red fluorescence represents cleaved caspase-3. Blue fluorescence (DAPI) represents nuclei.

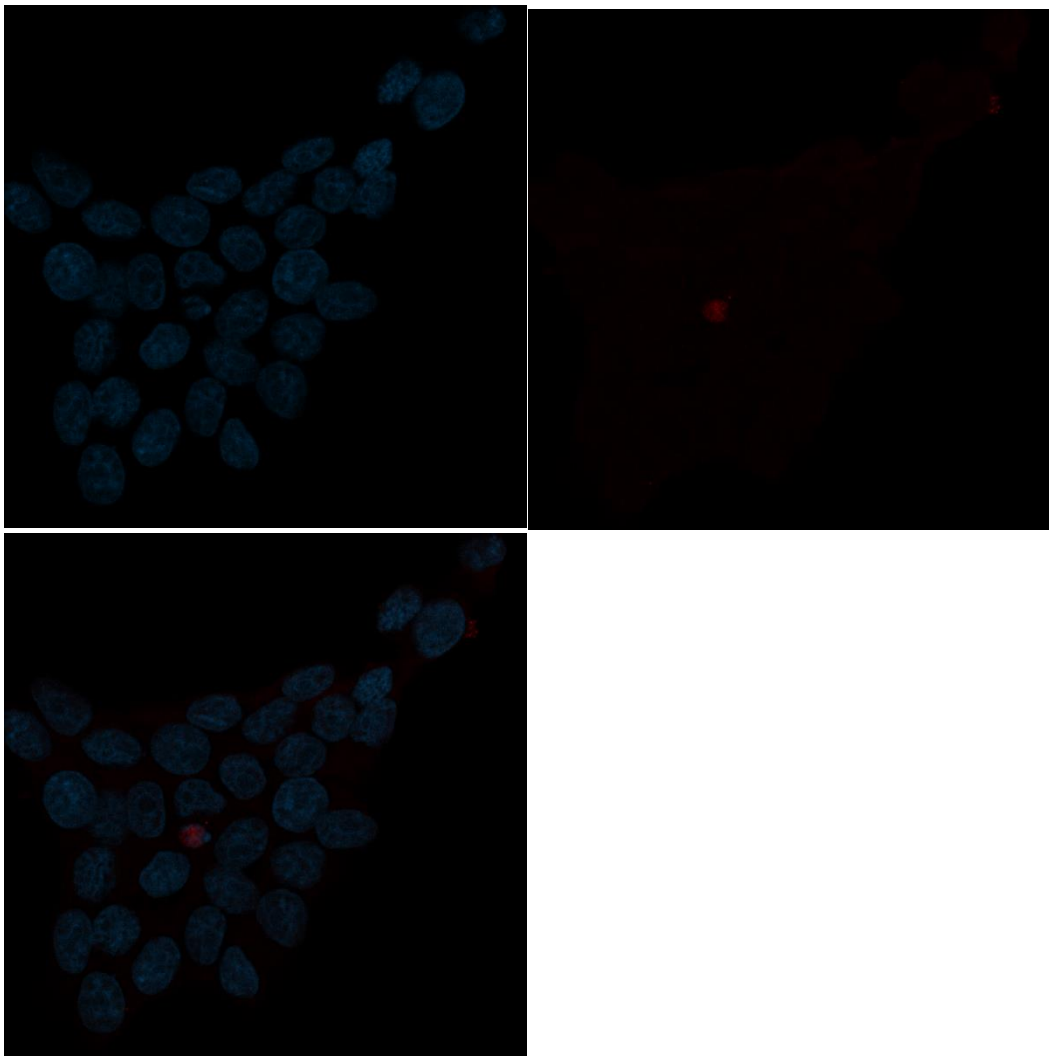

Figure 3 Uncropped cleaved caspase-3 ICC images (rilpivirine). INS-1E cells were exposed to rilpivirine 10 µM for 24 hrs before analysing cleaved caspase-3 by ICC. Red fluorescence represents cleaved caspase-3. Blue fluorescence (DAPI) represents nuclei.

References

Affourtit, C., & Brand, M. D. (2008). On the role of uncoupling protein-2 in pancreatic beta cells. *Biochimica et Biophysica Acta (BBA) - Bioenergetics, 1777*(7), 973-979. doi:https://doi.org/10.1016/j.bbabio.2008.03.022

Affourtit, C., Jastroch, M., & Brand, M. D. (2011). Uncoupling protein-2 attenuates glucose-stimulated insulin secretion in INS-1E insulinoma cells by lowering mitochondrial reactive oxygen species. *Free Radical Biology and Medicine, 50*(5), 609-616. doi:https://doi.org/10.1016/j.freeradbiomed.2010.12.020

Aittoniemi, J., Fotinou, C., Craig, T. J., de Wet, H., Proks, P., & Ashcroft, F. M. (2009). Review. SUR1: a unique ATP-binding cassette protein that functions as an ion channel regulator. *Philosophical transactions of the Royal Society of London. Series B, Biological sciences, 364*(1514), 257-267. doi:10.1098/rstb.2008.0142

Alnahdi, A., John, A., & Raza, H. (2019). N-acetyl cysteine attenuates oxidative stress and glutathione-dependent redox imbalance caused by high glucose/high palmitic acid treatment in pancreatic Rin-5F cells. *PLoS ONE, 14*(12), e0226696. doi:10.1371/journal.pone.0226696

Anello, M., Lupi, R., Spampinato, D., Piro, S., Masini, M., Boggi, U., Del Prato, S., Rabuazzo, A. M., Purrello, F., & Marchetti, P. (2005). Functional and morphological alterations of mitochondria in pancreatic beta cells from type 2 diabetic patients. *DIABETOLOGIA, 48*(2), 282-289. doi:10.1007/s00125-004-1627-9

Antiretroviral Therapy Cohort Collaboration. (2010). Causes of death in HIV-1—infected patients treated with antiretroviral therapy, 1996–2006: collaborative analysis of 13 HIV cohort studies. *Clinical Infectious Diseases, 50*(10), 1387-1396.

Apostolova, N., Blas-García, A., & Esplugues, J. V. (2011a). Mitochondrial interference by anti-HIV drugs: mechanisms beyond Pol-γ; inhibition. *Trends in Pharmacological Sciences, 32*(12), 715-725. doi:10.1016/j.tips.2011.07.007

Apostolova, N., Blas-Garcia, A., Galindo, M. J., & Esplugues, J. V. (2017). Efavirenz: What is known about the cellular mechanisms responsible for its adverse effects. *European Journal of Pharmacology, 812*, 163-173. doi:https://doi.org/10.1016/j.ejphar.2017.07.016

Apostolova, N., Funes, H. A., Blas-Garcia, A., Galindo, M. J., Alvarez, A., & Esplugues, J. V. (2015). Efavirenz and the CNS: what we already know and questions that need to be answered. *Journal of Antimicrobial Chemotherapy, 70*(10), 2693-2708. doi:10.1093/jac/dkv183

Apostolova, N., Gomez-Sucerquia, L. J., Alegre, F., Funes, H. A., Victor, V. M., Barrachina, M. D., Blas-Garcia, A., & Esplugues, J. V. (2013). ER stress in human hepatic cells treated with Efavirenz: Mitochondria again. *Journal of Hepatology, 59*(4), 780-789. doi:10.1016/j.jhep.2013.06.005

Apostolova, N., Gomez-Sucerquia, L. J., Gortat, A., Blas-Garcia, A., & Esplugues, J. V. (2011b). Compromising mitochondrial function with the antiretroviral drug efavirenz induces cell survival-promoting autophagy. *Hepatology, 54*(3), 1009-1019. doi:https://doi.org/10.1002/hep.24459

Apostolova, N., Gomez-Sucerquia, L. J., Moran, A., Alvarez, A., Blas-Garcia, A., & Esplugues, J. V. (2010). Enhanced oxidative stress and increased mitochondrial mass during Efavirenz-induced apoptosis in human hepatic cells. *British Journal of Pharmacology, 160*(8), 2069-2084. doi:10.1111/j.1476-5381.2010.00866.x

Araki, E., Oyadomari, S., & Mori, M. (2003). Impact of endoplasmic reticulum stress pathway on pancreatic beta-cells and diabetes mellitus. *Experimental Biology and Medicine (Maywood), 228*(10), 1213-1217. doi:10.1177/153537020322801018

Armstrong, R. A., & Hilton, A. C. (2010). Nonparametric Analysis of Variance. In *Statistical Analysis in Microbiology: Statnotes* (pp. 123-126).

Arrington, A. K. a. R., Taylor S. . (2022). Endocrine Pancreas In C. Townsend (Ed.), *Textbook of Surgery* (Vol. 1, pp. 941-963).

Arunagiri, A., Haataja, L., Cunningham, C. N., Shrestha, N., Tsai, B., Qi, L., Liu, M., & Arvan, P. (2018). Misfolded proinsulin in the endoplasmic reticulum during development of beta cell failure in diabetes. *Annals of the New York Academy of Sciences, 1418*(1), 5-19. doi:10.1111/nyas.13531

Ashcroft, F., & Rorsman, P. (2004). Type 2 diabetes mellitus: not quite exciting enough? *Hum Mol Genet, 13 Spec No 1*, R21-31. doi:10.1093/hmg/ddh066

Ashcroft, F. M., Harrison, D. E., & Ashcroft, S. J. (1984). Glucose induces closure of single potassium channels in isolated rat pancreatic beta-cells. *Nature, 312*(5993), 446-448. doi:10.1038/312446a0

Atta, M. G., De Seigneux, S., & Lucas, G. M. (2019). Clinical Pharmacology in HIV Therapy. *Clinical Journal of the American Society of Nephrology, 14*(3), 435. doi:10.2215/CJN.02240218

Avert. (2018). Origin of HIV & AIDS. Retrieved from https://www.avert.org/professionals/history-hiv-aids/origin

Azijn, H., Tirry, I., Vingerhoets, J., de Béthune, M. P., Kraus, G., Boven, K., Jochmans, D., Van Craenenbroeck, E., Picchio, G., & Rimsky, L. T. (2010). TMC278, a next-generation nonnucleoside reverse transcriptase inhibitor (NNRTI), active against wild-type and NNRTI-resistant HIV-1. *Antimicrobial agents and chemotherapy*, *54*(2), 718-727. doi:10.1128/aac.00986-09

Azzu, V., Affourtit, C., Breen, E., Parker, N., & Brand, M. (2008). Dynamic regulation of uncoupling protein 2 content in INS-1E insulinoma cells. *Biochimica et biophysica acta, 1777*, 1378-1383. doi:10.1016/j.bbabio.2008.07.001

Back, S. H., & Kaufman, R. J. (2012). Endoplasmic reticulum stress and type 2 diabetes. *Annual Review of Biochemistry, 81*, 767-793. doi:10.1146/annurev-biochem-072909-095555

Bagella, P., De Socio, G. V., Ricci, E., Menzaghi, B., Martinelli, C., Squillace, N., Maggi, P., Orofino, G., Calza, L., Carenzi, L., Celesia, B. M., Penco, G., Di Biagio, A., Valsecchi, L., Vichi, F., Colombo, V., Parruti, G., Dentone, C., Falasca, K., Bonfanti, P., Madeddu, G., & C.I.S.A.I. Study Group, I. (2018). Durability, safety, and efficacy of rilpivirine in clinical practice: results from the SCOLTA Project. *Infection and drug resistance, 11*, 615-623. doi:10.2147/IDR.S152090

Bain, L. E., Nkoke, C., & Noubiap, J. J. N. (2017). UNAIDS 90–90–90 targets to end the AIDS epidemic by 2020 are not realistic: comment on “Can the UNAIDS 90–90–90 target be achieved? A systematic analysis of national HIV treatment cascades”. *BMJ Global Health, 2*(2), e000227. doi:10.1136/bmjgh-2016-000227

Baker, J. V., Sharma, S., Achhra, A. C., Bernardino, J. I., Bogner, J. R., Duprez, D., Emery, S., Gazzard, B., Gordin, J., Grandits, G., Phillips, A. N., Schwarze, S., Soliman, E. Z., Spector, S. A., Tambussi, G., & Lundgren, J. (2017). Changes in Cardiovascular Disease Risk Factors With Immediate Versus Deferred Antiretroviral Therapy Initiation Among HIV‐Positive Participants in the START (Strategic Timing of Antiretroviral Treatment) Trial. *Journal of the American Heart Association, 6*(5), e004987. doi:doi:10.1161/JAHA.116.004987

Barlow, J., & Affourtit, C. (2013). Novel insights into pancreatic β-cell glucolipotoxicity from real-time functional analysis of mitochondrial energy metabolism in INS-1E insulinoma cells. *Biochemical Journal, 456*(3), 417-426. doi:10.1042/BJ20131002

Barlow, J., Jensen, Verena H., Jastroch, M., & Affourtit, C. (2016). Palmitate-induced impairment of glucose-stimulated insulin secretion precedes mitochondrial dysfunction in mouse pancreatic islets. *Biochemical Journal, 473*(4), 487-496. doi:10.1042/BJ20151080

Barrientos, A., & Moraes, C. T. (1999). Titrating the Effects of Mitochondrial Complex I Impairment in the Cell Physiology. *Journal of Biological Chemistry, 274*(23), 16188-16197. doi:10.1074/jbc.274.23.16188

Baumel-Alterzon, S., & Scott, D. K. (2022). Regulation of Pdx1 by oxidative stress and Nrf2 in pancreatic beta-cells. *Frontiers in Endocrinology (Lausanne), 13*, 1011187. doi:10.3389/fendo.2022.1011187

Beeharry, N., Lowe, J. E., Hernandez, A. R., Chambers, J. A., Fucassi, F., Cragg, P. J., Green, M. H. L., & Green, I. C. (2003). Linoleic acid and antioxidants protect against DNA damage and apoptosis induced by palmitic acid. *Mutation Research/Fundamental and Molecular Mechanisms of Mutagenesis, 530*(1), 27-33. doi:https://doi.org/10.1016/S0027-5107(03)00134-9

Behl, S., Adem, A., Hussain, A., & Singh, J. (2019). Effects of rilpivirine, 17β-estradiol and β-naphthoflavone on the inflammatory status of release of adipocytokines in 3T3-L1 adipocytes in vitro. *Molecular biology reports*.

Behrens, G., Dejam, A., Schmidt, H., Balks, H.-J., Brabant, G., Körner, T., Stoll, M., & Schmidt, R. E. (1999). Impaired glucose tolerance, beta cell function and lipid metabolism in HIV patients under treatment with protease inhibitors. *AIDS, 13*(10), F63-F70. doi:10.1097/00002030-199907090-00001

Bekker, L. G., Li, S., Pathak, S., Tolley, E. E., Marzinke, M. A., Justman, J. E., Mgodi, N. M., Chirenje, M., Swaminathan, S., Adeyeye, A., Farrior, J., Hendrix, C. W., Piwowar-Manning, E., Richardson, P., Eshelman, S. H., Redinger, H., Williams, P., & Sista, N. D. (2020). Safety and tolerability of injectable Rilpivirine LA in HPTN 076: A phase 2 HIV pre-exposure prophylaxis study in women. *EClinicalMedicine, 21*. doi:10.1016/j.eclinm.2020.100303

Belfort, R., Mandarino, L., Kashyap, S., Wirfel, K., Pratipanawatr, T., Berria, R., DeFronzo, R. A., & Cusi, K. (2005). Dose-Response Effect of Elevated Plasma Free Fatty Acid on Insulin Signaling. *Diabetes, 54*(6), 1640-1648. doi:10.2337/diabetes.54.6.1640

Ben-Romano, R., Rudich, A., Török, D., Vanounou, S., Riesenberg, K., Schlaeffer, F., Klip, A., & Bashan, N. (2003). Agent and cell-type specificity in the induction of insulin resistance by HIV protease inhibitors. *AIDS, 17*(1), 23-32. doi:10.1097/00002030-200301030-00005

Benson, C. A., van der Horst, C., Lamarca, A., Haas, D. W., McDonald, C. K., Steinhart, C. R., Rublein, J., Quinn, J. B., Mondou, E., & Rousseau, F. (2004). A randomized study of emtricitabine and lamivudine in stably suppressed patients with HIV. *AIDS, 18*(17), 2269-2276. doi:10.1097/00002030-200411190-00007

Bertrand, L., Velichkovska, M., & Toborek, M. (2019). Cerebral Vascular Toxicity of Antiretroviral Therapy. *Journal of Neuroimmune Pharmacology*. doi:10.1007/s11481-019-09858-x

Bhattarai, K. R., Riaz, T. A., Kim, H.-R., & Chae, H.-J. (2021). The aftermath of the interplay between the endoplasmic reticulum stress response and redox signaling. *Experimental & Molecular Medicine, 53*(2), 151-167. doi:10.1038/s12276-021-00560-8

Birkus, G., Hitchcock, M. J. M., & Cihlar, T. (2002). Assessment of mitochondrial toxicity in human cells treated with tenofovir: comparison with other nucleoside reverse transcriptase inhibitors. *Antimicrobial agents and chemotherapy, 46*(3), 716-723. doi:10.1128/aac.46.3.716-723.2002

Blas-García, A., Polo, M., Alegre, F., Funes, H. A., Martínez, E., Apostolova, N., & Esplugues, J. V. (2014). Lack of mitochondrial toxicity of darunavir, raltegravir and rilpivirine in neurons and hepatocytes: a comparison with efavirenz. *Journal of Antimicrobial Chemotherapy, 69*(11), 2995-3000. doi:10.1093/jac/dku262

Blas-García, A., Apostolova, N., Ballesteros, D., Monleón, D., Morales, J. M., Rocha, M., Victor, V. M., & Esplugues, J. V. (2010). Inhibition of mitochondrial function by efavirenz increases lipid content in hepatic cells. *Hepatology, 52*(1), 115-125.

Bleier, L., & Dröse, S. (2013). Superoxide generation by complex III: from mechanistic rationales to functional consequences. *Biochimica et biophysica acta, 1827*(11-12), 1320-1331. doi:10.1016/j.bbabio.2012.12.002

Boden, G. (1999). Free Fatty Acids, Insulin Resistance, and Type 2 Diabetes Mellitus. *Proceedings of the Association of American Physicians, 111*(3), 241-248. doi:https://doi.org/10.1046/j.1525-1381.1999.99220.x

Bonfanti, P., Ricci, E., Landonio, S., Valsecchi, L., Timillero, L., Faggion, I., Quirino, T., grp, C. s., Infection, C. s. g. I. C. f. t. S. o. H., & Allergies. (2001). Predictors of protease inhibitor-associated adverse events. *Biomedicine & Pharmacotherapy, 55*(6), 321-323. doi:10.1016/S0753-3322(01)00070-1

Boothby, M., McGee, K. C., Tomlinson, J. W., Gathercole, L. L., McTernan, P. G., Shojaee-Moradie, F., Umpleby, A. M., Nightingale, P., & Shahmanesh, M. (2009). Adipocyte differentiation, mitochondrial gene expression and fat distribution: differences between zidovudine and tenofovir after 6 months. *Antiviral Therapy, 14*(8), 1089-1100.

Boslem, E., Meikle, P. J., & Biden, T. J. (2012). Roles of ceramide and sphingolipids in pancreatic β-cell function and dysfunction. *Islets, 4*(3), 177-187. doi:10.4161/isl.20102

Brauchle, E., Thude, S., Brucker, S. Y., & Schenke-Layland, K. (2014). Cell death stages in single apoptotic and necrotic cells monitored by Raman microspectroscopy. *Scientific Reports, 4*(1), 4698. doi:10.1038/srep04698

Brissova, M., Shiota, M., Nicholson, W. E., Gannon, M., Knobel, S. M., Piston, D. W., Wright, C. V., & Powers, A. C. (2002). Reduction in pancreatic transcription factor PDX-1 impairs glucose-stimulated insulin secretion. *Journal of Biological Chemistry, 277*(13), 11225-11232.

Brown, L. A. M., Jin, J., Ferrell, D., Sadic, E., Obregon, D., Smith, A. J., Tan, J., & Giunta, B. (2014). Efavirenz Promotes β-Secretase Expression and Increased Aβ1-40,42 via Oxidative Stress and Reduced Microglial Phagocytosis: Implications for HIV Associated Neurocognitive Disorders (HAND). *PLoS ONE, 9*(4), e95500. doi:10.1371/journal.pone.0095500

Brown, T. T., Cole, S. R., Li, X., Kingsley, L. A., Palella, F. J., Riddler, S. A., Visscher, B. R., Margolick, J. B., & Dobs, A. S. (2005a). Antiretroviral Therapy and the Prevalence and Incidence of Diabetes Mellitus in the Multicenter AIDS Cohort Study. *JAMA Internal Medicine, 165*(10), 1179-1184. doi:10.1001/archinte.165.10.1179

Brown, T. T., Li, X., Cole, S. R., Kingsley, L. A., Palella, F. J., Riddler, S. A., Chmiel, J. S., Visscher, B. R., Margolick, J. B., & Dobs, A. S. (2005b). Cumulative exposure to nucleoside analogue reverse transcriptase inhibitors is associated with insulin resistance markers in the Multicenter AIDS Cohort Study. *AIDS, 19*(13), 1375-1383. doi:10.1097/01.aids.0000181011.62385.91

Brown, T. T., & Qaqish, R. B. (2006). Antiretroviral therapy and the prevalence of osteopenia and osteoporosis: A meta-analytic review. *AIDS, 20*(17), 2165-2174. doi:10.1097/QAD.0b013e32801022eb

Brun, T., Assimacopoulos-Jeannet, F., Corkey, B. E., & Prentki, M. (1997). Long-Chain Fatty Acids Inhibit Acetyl-CoA Carboxylase Gene Expression in the Pancreatic β-Cell Line INS-1. *Diabetes, 46*(3), 393-400. doi:10.2337/diab.46.3.393

Buettner, C., & Camacho, R. C. (2008). Hypothalamic Control of Hepatic Glucose Production and Its Potential Role in Insulin Resistance. *Endocrinology and Metabolism Clinics of North America, 37*(4), 825-840. doi:10.1016/j.ecl.2008.09.001

Burcelin, R., Dolci, W., & Thorens, B. (2000). Glucose sensing by the hepatoportal sensor is GLUT2-dependent: in vivo analysis in GLUT2-null mice. *Diabetes, 49*(10), 1643-1648. doi:10.2337/diabetes.49.10.1643

Butler, A. E., Janson, J., Bonner-Weir, S., Ritzel, R., Rizza, R. A., & Butler, P. C. (2003). Beta-cell deficit and increased beta-cell apoptosis in humans with type 2 diabetes. *Diabetes, 52*(1), 102-110. doi:10.2337/diabetes.52.1.102

Butt, A. A., Chang, C.-C., Kuller, L., Goetz, M. B., Leaf, D., Rimland, D., Gibert, C. L., Oursler, K. K., Rodriguez-Barradas, M. C., Lim, J., Kazis, L. E., Gottlieb, S., Justice, A. C., & Freiberg, M. S. (2011). Risk of heart failure with human immunodeficiency virus in the absence of prior diagnosis of coronary heart disease. *Archives of internal medicine, 171*(8), 737-743. doi:10.1001/archinternmed.2011.151

Butt, A. A., McGinnis, K., Rodriguez-Barradas, M. C., Crystal, S., Simberkoff, M., Goetz, M. B., Leaf, D., Justice, A. C., & Veterans Aging Cohort, S. (2009). HIV infection and the risk of diabetes mellitus. *AIDS, 23*(10), 1227-1234. doi:10.1097/QAD.0b013e32832bd7af

Cadenas, E., & Davies, K. J. A. (2000). Mitochondrial free radical generation, oxidative stress, and aging11This article is dedicated to the memory of our dear friend, colleague, and mentor Lars Ernster (1920–1998), in gratitude for all he gave to us. *Free Radical Biology and Medicine, 29*(3), 222-230. doi:https://doi.org/10.1016/S0891-5849(00)00317-8

Capeau, J., Bouteloup, V., Katlama, C., Bastard, J.-P., Guiyedi, V., Salmon-Ceron, D., Protopopescu, C., Leport, C., Raffi, F., Chêne, G., Cohort, A. C. A.-C., & Group, A. C. A.-C. C. S. (2012). Ten-year diabetes incidence in 1046 HIV-infected patients started on a combination antiretroviral treatment. *AIDS, 26*(3), 303-314. doi:10.1097/QAD.0b013e32834e8776

Cardozo, A. K., Heimberg, H., Heremans, Y., Leeman, R., Kutlu, B., Kruhøffer, M., Ørntoft, T., & Eizirik, D. L. (2001). A comprehensive analysis of cytokine-induced and nuclear factor-kappa B-dependent genes in primary rat pancreatic beta-cells. *Journal of Biological Chemistry, 276*(52), 48879-48886. doi:10.1074/jbc.M108658200

Carlsson, C., Borg, L. A., & Welsh, N. (1999a). Sodium palmitate induces partial mitochondrial uncoupling and reactive oxygen species in rat pancreatic islets in vitro. *Endocrinology, 140*(8), 3422-3428. doi:10.1210/endo.140.8.6908

Carlsson, C., Håkan Borg, L. A., & Welsh, N. (1999b). Sodium Palmitate Induces Partial Mitochondrial Uncoupling and Reactive Oxygen Species in Rat Pancreatic Islets in Vitro*. *Endocrinology, 140*(8), 3422-3428. doi:10.1210/endo.140.8.6908

Carr, A., Samaras, K., Thorisdottir, A., Kaufmann, G. R., Chisholm, D. J., & Cooper, D. A. (1999). Diagnosis, prediction, and natural course of HIV-1 protease-inhibitor-associated lipodystrophy, hyperlipidaemia, and diabetes mellitus: acohort study. *The Lancet, 353*(9170), 2093-2099. doi:10.1016/S0140-6736(98)08468-2

Casado, J. L. (2013). Liver toxicity in HIV-infected patients receiving novel second-generation nonnucleoside reverse transcriptase inhibitors etravirine and rilpivirine. *AIDS Reviews, 15*(3), 139-145.

Cento, V., & Perno, C. F. (2020). Two-drug regimens with dolutegravir plus rilpivirine or lamivudine in HIV-1 treatment-naïve, virologically-suppressed patients: Latest evidence from the literature on their efficacy and safety. *Journal of Global Antimicrobial Resistance, 20*, 228-237. doi:https://doi.org/10.1016/j.jgar.2019.08.010

Cernea, S., & Dobreanu, M. (2013). Diabetes and beta cell function: from mechanisms to evaluation and clinical implications. *Biochemia Medica (Zagreb), 23*(3), 266-280. doi:10.11613/bm.2013.033

Chan, C. B., De Leo, D., Joseph, J. W., McQuaid, T. S., Ha, X. F., Xu, F., Tsushima, R. G., Pennefather, P. S., Salapatek, A. M., & Wheeler, M. B. (2001a). Increased uncoupling protein-2 levels in beta-cells are associated with impaired glucose-stimulated insulin secretion: mechanism of action. *Diabetes, 50*(6), 1302-1310. doi:10.2337/diabetes.50.6.1302

Chan, C. B., De Leo, D., Joseph, J. W., McQuaid, T. S., Ha, X. F., Xu, F., Tsushima, R. G., Pennefather, P. S., Salapatek, A. M. F., & Wheeler, M. B. (2001b). Increased Uncoupling Protein-2 Levels in β-cells Are Associated With Impaired Glucose-Stimulated Insulin Secretion: Mechanism of Action. *Diabetes, 50*(6), 1302-1310. doi:10.2337/diabetes.50.6.1302

Chan, C. B., & Harper, M. E. (2006). Uncoupling proteins: role in insulin resistance and insulin insufficiency. *Current Diabetes Reviews, 2*(3), 271-283. doi:10.2174/157339906777950660

Chan, C. B., Saleh, M. C., Koshkin, V., & Wheeler, M. B. (2004). Uncoupling Protein 2 and Islet Function. *Diabetes, 53*(suppl_1), S136-S142. doi:10.2337/diabetes.53.2007.S136

Chan, F. K., Moriwaki, K., & De Rosa, M. J. (2013). Detection of necrosis by release of lactate dehydrogenase activity. *Methods in Molecular Biology, 979*, 65-70. doi:10.1007/978-1-62703-290-2_7

Chandra, S., Mondal, D., & Agrawal, K. C. (2009). HIV-1 protease inhibitor induced oxidative stress suppresses glucose stimulated insulin release: protection with thymoquinone. *Experimental Biology and Medicine (Maywood), 234*(4), 442-453. doi:10.3181/0811-rm-317

Chatterjee, M., & Scobie, I. (2002). The pathogenesis of type 2 diabetes mellitus. *Practical Diabetes International, 19*(8), 255-257. doi:https://doi.org/10.1002/pdi.385

Chatterjee, S., Khunti, K., & Davies, M. J. (2017). Type 2 diabetes. *The Lancet, 389*(10085), 2239-2251. doi:https://doi.org/10.1016/S0140-6736(17)30058-2

Chen, C.-H., Vazquez-Padua, M., & Cheng, Y.-C. (1991). Effect of anti-human immunodeficiency virus nucleoside analogs on mitochondrial DNA and its implication for delayed toxicity. *Molecular Pharmacology, 39*(5), 625-628.

Chen, X., Cui, Z., Wei, S., Hou, J., Xie, Z., Peng, X., Li, J., Cai, T., Hang, H., & Yang, F. (2013). Chronic high glucose induced INS-1β cell mitochondrial dysfunction: a comparative mitochondrial proteome with SILAC. *Proteomics, 13*(20), 3030-3039. doi:10.1002/pmic.201200448

Ciregia, F., Bugliani, M., Ronci, M., Giusti, L., Boldrini, C., Mazzoni, M. R., Mossuto, S., Grano, F., Cnop, M., Marselli, L., Giannaccini, G., Urbani, A., Lucacchini, A., & Marchetti, P. (2017). Palmitate-induced lipotoxicity alters acetylation of multiple proteins in clonal β cells and human pancreatic islets. *Scientific Reports, 7*(1), 13445. doi:10.1038/s41598-017-13908-w

Clore, J. N., Allred, J., White, D., Li, J., & Stillman, J. (2002). The role of plasma fatty acid composition in endogenous glucose production in patients with type 2 diabetes mellitus. *Metabolism - Clinical and Experimental, 51*(11), 1471-1477. doi:10.1053/meta.2002.35202

Cnop, M., Abdulkarim, B., Bottu, G., Cunha, D. A., Igoillo-Esteve, M., Masini, M., Turatsinze, J. V., Griebel, T., Villate, O., Santin, I., Bugliani, M., Ladriere, L., Marselli, L., McCarthy, M. I., Marchetti, P., Sammeth, M., & Eizirik, D. L. (2014). RNA sequencing identifies dysregulation of the human pancreatic islet transcriptome by the saturated fatty acid palmitate. *Diabetes, 63*(6), 1978-1993. doi:10.2337/db13-1383

Cnop, M., Toivonen, S., Igoillo-Esteve, M., & Salpea, P. (2017). Endoplasmic reticulum stress and eIF2α phosphorylation: The Achilles heel of pancreatic β cells. *Molecular Metabolism, 6*(9), 1024-1039. doi:10.1016/j.molmet.2017.06.001

Cnop, M., Welsh, N., Jonas, J.-C., Jörns, A., Lenzen, S., & Eizirik, D. L. (2005). Mechanisms of Pancreatic β-Cell Death in Type 1 and Type 2 Diabetes. *Many Differences, Few Similarities, 54*(suppl 2), S97-S107. doi:10.2337/diabetes.54.suppl_2.S97

Côté, H. C. F., Brumme, Z. L., Craib, K. J. P., Alexander, C. S., Wynhoven, B., Ting, L., Wong, H., Harris, M., Harrigan, P. R., O'Shaughnessy, M. V., & Montaner, J. S. G. (2002). Changes in Mitochondrial DNA as a Marker of Nucleoside Toxicity in HIV-Infected Patients. *New England Journal of Medicine, 346*(11), 811-820. doi:10.1056/NEJMoa012035

Cottet-Rousselle, C., Ronot, X., Leverve, X., & Mayol, J. F. (2011). Cytometric assessment of mitochondria using fluorescent probes. *Cytometry Part A, 79*(6), 405-425. doi:10.1002/cyto.a.21061

Crum-Cianflone, N., Tejidor, R., Medina, S., Barahona, I., & Ganesan, A. (2008). Obesity among patients with HIV: the latest epidemic. *AIDS patient care and STDs, 22*(12), 925-930. doi:10.1089/apc.2008.0082

Cunha, D. A., Hekerman, P., Ladrière, L., Bazarra-Castro, A., Ortis, F., Wakeham, M. C., Moore, F., Rasschaert, J., Cardozo, A. K., Bellomo, E., Overbergh, L., Mathieu, C., Lupi, R., Hai, T., Herchuelz, A., Marchetti, P., Rutter, G. A., Eizirik, D. L., & Cnop, M. (2008). Initiation and execution of lipotoxic ER stress in pancreatic β-cells. *Journal of Cell Science, 121*(14), 2308-2318. doi:10.1242/jcs.026062

Cunha, D. A., Igoillo-Esteve, M., Gurzov, E. N., Germano, C. M., Naamane, N., Marhfour, I., Fukaya, M., Vanderwinden, J.-M., Gysemans, C., Mathieu, C., Marselli, L., Marchetti, P., Harding, H. P., Ron, D., Eizirik, D. L., & Cnop, M. (2012). Death Protein 5 and p53-Upregulated Modulator of Apoptosis Mediate the Endoplasmic Reticulum Stress–Mitochondrial Dialog Triggering Lipotoxic Rodent and Human β-Cell Apoptosis. *Diabetes, 61*(11), 2763-2775. doi:10.2337/db12-0123

Curtis, M. J., Alexander, S., Cirino, G., Docherty, J. R., George, C. H., Giembycz, M. A., Hoyer, D., Insel, P. A., Izzo, A. A., Ji, Y., MacEwan, D. J., Sobey, C. G., Stanford, S. C., Teixeira, M. M., Wonnacott, S., & Ahluwalia, A. (2018). Experimental design and analysis and their reporting II: updated and simplified guidance for authors and peer reviewers. *British Journal of Pharmacology, 175*(7), 987-993. doi:https://doi.org/10.1111/bph.14153

Dai, C., Kayton, N. S., Shostak, A., Poffenberger, G., Cyphert, H. A., Aramandla, R., Thompson, C., Papagiannis, I. G., Emfinger, C., Shiota, M., Stafford, J. M., Greiner, D. L., Herrera, P. L., Shultz, L. D., Stein, R., & Powers, A. C. (2016a). Stress-impaired transcription factor expression and insulin secretion in transplanted human islets. *Journal of Clinical Investigation, 126*(5), 1857-1870. doi:10.1172/jci83657

Dalakas, M. C. (2001). Peripheral neuropathy and antiretroviral drugs. *Journal of the Peripheral Nervous System, 6*(1), 14-20. doi:10.1046/j.1529-8027.2001.006001014.x

Daniel, W. W., & Cross, C. L. (2019). *Biostatistics: A Foundation for Analysis in the Health Sciences* (10th ed.): John Wiley & Sons.

Das, K., Bauman, J. D., Clark, A. D., Jr, Frenkel, Y. V., Lewi, P. J., Shatkin, A. J., Hughes, S. H., & Arnold, E. (2008). High-resolution structures of HIV-1 reverse transcriptase/TMC278 complexes: strategic flexibility explains potency against resistance mutations. *Proceedings of the National Academy of Sciences of the United States of America, 105*(5), 1466–1471. https://doi.org/10.1073/pnas.0711209105

De Francesco, D., Wit, F. W., Cole, J. H., Kootstra, N. A., Winston, A., Sabin, C. A., Underwood, J., van Zoest, R. A., Schouten, J., Kooij, K. W., Prins, M., Guaraldi, G., Caan, M. W. A., Burger, D., Franceschi, C., Libert, C., Bürkle, A., & Reiss, P. (2018). The 'COmorBidity in Relation to AIDS' (COBRA) cohort: Design, methods and participant characteristics. *PLoS ONE, 13*(3), e0191791. doi:10.1371/journal.pone.0191791

De Vos, A., Heimberg, H., Quartier, E., Huypens, P., Bouwens, L., Pipeleers, D., & Schuit, F. (1995). Human and rat beta cells differ in glucose transporter but not in glucokinase gene expression. *Journal of Clinical Investigation, 96*(5), 2489-2495. doi:10.1172/jci118308

Deeks, S. G., Overbaugh, J., Phillips, A., & Buchbinder, S. (2015). HIV infection. *Nat Reviews Disease Primers, 1*, 15035. doi:10.1038/nrdp.2015.35

DeFronzo, R. A., Ferrannini, E., Zimmet, P., & Alberti, G. (2015). *International textbook of diabetes mellitus*: John Wiley & Sons.

Del Guerra, S., Grupillo, M., Masini, M., Lupi, R., Bugliani, M., Torri, S., Boggi, U., Del Chiaro, M., Vistoli, F., Mosca, F., Del Prato, S., & Marchetti, P. (2007). Gliclazide protects human islet beta-cells from apoptosis induced by intermittent high glucose. *Diabetes/Metabolism Research and Reviews, 23*(3), 234-238. doi:10.1002/dmrr.680

Deng, S., Vatamaniuk, M., Huang, X., Doliba, N., Lian, M. M., Frank, A., Velidedeoglu, E., Desai, N. M., Koeberlein, B., Wolf, B., Barker, C. F., Naji, A., Matschinsky, F. M., & Markmann, J. F. (2004). Structural and functional abnormalities in the islets isolated from type 2 diabetic subjects. *Diabetes, 53*(3), 624-632. doi:10.2337/diabetes.53.3.624

Desai, M., Joyce, V., Bendavid, E., Olshen, R. A., Hlatky, M., Chow, A., Holodniy, M., Barnett, P., & Owens, D. K. (2015). Risk of cardiovascular events associated with current exposure to HIV antiretroviral therapies in a US veteran population. *Clinical infectious diseases : an official publication of the Infectious Diseases Society of America, 61*(3), 445-452. doi:10.1093/cid/civ316

Dhayal, S., Zummo, F., Anderson, M., Thomas, P., Welters, H., Arden, C., & Morgan, N. (2019). Differential effects of saturated and unsaturated fatty acids on autophagy in pancreatic β-cells. *Journal of Molecular Endocrinology, 63*. doi:10.1530/JME-19-0096

Diabetes UK. (2018). Us, diabetes and a lot of facts and stats.

Diakogiannaki, E., Dhayal, S., Childs, C. E., Calder, P. C., Welters, H. J., & Morgan, N. G. (2007). Mechanisms involved in the cytotoxic and cytoprotective actions of saturated versus monounsaturated long-chain fatty acids in pancreatic β-cells. *Journal of Endocrinology, 194*(2), 283-291. doi:10.1677/JOE-07-0082

Diane, A., Al-Shukri, N. A., Bin Abdul Mu-u-min, R., & Al-Siddiqi, H. H. (2022). β-cell mitochondria in diabetes mellitus: a missing puzzle piece in the generation of hPSC-derived pancreatic β-cells? *Journal of Translational Medicine, 20*(1), 163. doi:10.1186/s12967-022-03327-5

Díaz-Delfín, J., del Mar Gutiérrez, M., Gallego-Escuredo, J. M., Domingo, J. C., Mateo, M. G., Villarroya, F., Domingo, P., & Giralt, M. (2011). Effects of nevirapine and efavirenz on human adipocyte differentiation, gene expression, and release of adipokines and cytokines. *Antiviral Research, 91*(2), 112-119.

Díaz-Delfín, J., Domingo, P., Mateo, M. G., Gutierrez, M. D. M., Domingo, J. C., Giralt, M., & Villarroya, F. (2012). Effects of rilpivirine on human adipocyte differentiation, gene expression, and release of adipokines and cytokines. *Antimicrobial agents and chemotherapy, 56*(6), 3369-3375. doi:10.1128/AAC.00104-12

Dirajlal-Fargo, S., Moser, C., Brown, T. T., Kelesidis, T., Dube, M. P., Stein, J. H., Currier, J., & McComsey, G. A. (2016). Changes in Insulin Resistance After Initiation of Raltegravir or Protease Inhibitors With Tenofovir-Emtricitabine: AIDS Clinical Trials Group A5260s. *Open Forum Infectious Diseases, 3*(3). doi:10.1093/ofid/ofw174

Dobson, E. L. and Luque, A. E. (2013). Rilpivirine. Retrieved from http://www.antimicrobe.org/d99.asp#R6

Donath, M. Y., & Halban, P. A. (2004). Decreased beta-cell mass in diabetes: significance, mechanisms and therapeutic implications. *DIABETOLOGIA, 47*(3), 581-589. doi:10.1007/s00125-004-1336-4

Drews, G., Krippeit-Drews, P., & Düfer, M. (2010). Oxidative stress and beta-cell dysfunction. *Pflügers Archiv - European Journal of Physiology, 460*(4), 703-718. doi:10.1007/s00424-010-0862-9

Dubé, M. P., Parker, R. A., Tebas, P., Grinspoon, S. K., Zackin, R. A., Robbins, G. K., Roubenoff, R., Shafer, R. W., Wininger, D. A., Meyer Iii, W. A., Snyder, S. W., & Mulligan, K. (2005). Glucose metabolism, lipid, and body fat changes in antiretroviral-naive subjects randomized to nelfinavir or efavirenz plus dual nucleosides. *AIDS, 19*(16), 1807-1818. doi:10.1097/01.aids.0000183629.20041.bb

Duchen, M. R., Smith, P. A., & Ashcroft, F. M. (1993). Substrate-dependent changes in mitochondrial function, intracellular free calcium concentration and membrane channels in pancreatic β-cells. *Biochemical Journal, 294*(1), 35-42. doi:10.1042/bj2940035

Duncan, A. D., Goff, L. M., & Peters, B. S. (2018). Type 2 diabetes prevalence and its risk factors in HIV: A cross-sectional study. *PLoS ONE, 13*(3), e0194199-e0194199. doi:10.1371/journal.pone.0194199

Eguchi, K., Manabe, I., Oishi-Tanaka, Y., Ohsugi, M., Kono, N., Ogata, F., Yagi, N., Ohto, U., Kimoto, M., Miyake, K., Tobe, K., Arai, H., Kadowaki, T., & Nagai, R. (2012). Saturated fatty acid and TLR signaling link β cell dysfunction and islet inflammation. *Cell Metabolism, 15*(4), 518-533. doi:10.1016/j.cmet.2012.01.023

Eguchi, N., Vaziri, N. D., Dafoe, D. C., & Ichii, H. (2021). The Role of Oxidative Stress in Pancreatic β Cell Dysfunction in Diabetes. *International Journal of Molecular Sciences, 22*(4). doi:10.3390/ijms22041509

Ehrenberg, B., Montana, V., Wei, M. D., Wuskell, J. P., & Loew, L. M. (1988). Membrane potential can be determined in individual cells from the nernstian distribution of cationic dyes. *Biophysical Journal, 53*(5), 785-794. doi:https://doi.org/10.1016/S0006-3495(88)83158-8

Eizirik, D. c. L., Cardozo, A. K., & Cnop, M. (2008). The Role for Endoplasmic Reticulum Stress in Diabetes Mellitus. *Endocrine Reviews, 29*(1), 42-61. doi:10.1210/er.2007-0015

El Hadri, K., Glorian, M., Monsempes, C., Dieudonné, M.-N., Pecquery, R., Giudicelli, Y., Andreani, M., Dugail, I., & Fève, B. (2004). In vitro suppression of the lipogenic pathway by the nonnucleoside reverse transcriptase inhibitor efavirenz in 3T3 and human preadipocytes or adipocytes. *Journal of Biological Chemistry, 279*(15), 15130-15141.

Electronic Medicines Compendium. (2018a). Atripla 600 mg/200 mg/245 mg film coated tablets. Retrieved from https://www.medicines.org.uk/emc/product/6173/smpc

Electronic Medicines Compendium. (2018b). Eviplera 200 mg/25 mg/245 mg film coated tablets SPC. Retrieved from https://www.medicines.org.uk/emc/product/2764/smpc

Electronic Medicines Compendium. (2018c). Kivexa film-coated tablets. Retrieved from https://www.medicines.org.uk/emc/product/3881/smpc

Electronic Medicines Compendium. (2019). Truvada film-coated tablets. Retrieved from https://www.medicines.org.uk/emc/product/3890/smpc

Elsner, M., Gehrmann, W., & Lenzen, S. (2010). Peroxisome-Generated Hydrogen Peroxide as Important Mediator of Lipotoxicity in Insulin-Producing Cells. *Diabetes, 60*(1), 200-208. doi:10.2337/db09-1401

Ena, J., Amador Concepcion and Benito Concepcion. (2003). Risk and determinants of developing severe liver toxicity during therapy with nevirapine-and efavirenz-containing regimens in HIV-infected patients. *International Journal of STD & AIDS, 14*(11), 776-781. doi:10.1258/09564620360719840

Engin, A. (2017). The Definition and Prevalence of Obesity and Metabolic Syndrome. In A. B. Engin & A. Engin (Eds.), *Obesity and Lipotoxicity* (pp. 1-17). Cham: Springer International Publishing.

Enkvetchakul, D., & Nichols, C. G. (2003). Gating mechanism of KATP channels: function fits form. *Journal of General Physiology, 122*(5), 471-480. doi:10.1085/jgp.200308878

Erel, O. (2004). A novel automated direct measurement method for total antioxidant capacity using a new generation, more stable ABTS radical cation. *Clin Biochem, 37*(4), 277-285. doi:10.1016/j.clinbiochem.2003.11.015

Eruslanov, E., & Kusmartsev, S. (2010). Identification of ROS using oxidized DCFDA and flow-cytometry. *Methods in Molecular Biology, 594*, 57-72. doi:10.1007/978-1-60761-411-1_4

Faltz, M., Bergin, H., Pilavachi, E., Grimwade, G., & Mabley, J. G. (2017). Effect of the Anti-retroviral Drugs Efavirenz, Tenofovir and Emtricitabine on Endothelial Cell Function: Role of PARP. *Cardiovascular Toxicology, 17*(4), 393-404. doi:10.1007/s12012-016-9397-4

Fazakerley, D. J., Chaudhuri, R., Yang, P., Maghzal, G. J., Thomas, K. C., Krycer, J. R., Humphrey, S. J., Parker, B. L., Fisher-Wellman, K. H., Meoli, C. C., Hoffman, N. J., Diskin, C., Burchfield, J. G., Cowley, M. J., Kaplan, W., Modrusan, Z., Kolumam, G., Yang, J. Y. H., Chen, D. L., Samocha-Bonet, D., Greenfield, J. R., Hoehn, K. L., Stocker, R., & James, D. E. (2018). Mitochondrial CoQ deficiency is a common driver of mitochondrial oxidants and insulin resistance. *eLife, 7*. doi:10.7554/eLife.32111

Feng, M., Sachs Nancy, A., Xu, M., Grobler, J., Blair, W., Hazuda Daria, J., Miller Michael, D., & Lai, M.-T. (2016). Doravirine Suppresses Common Nonnucleoside Reverse Transcriptase Inhibitor-Associated Mutants at Clinically Relevant Concentrations. *Antimicrobial agents and chemotherapy, 60*(4), 2241-2247. doi:10.1128/AAC.02650-15

Fernandez-Alvarez, J., Conget, I., Rasschaert, J., Sener, A., Gomis, R., & Malaisse, W. J. (1994). Enzymatic, metabolic and secretory patterns in human islets of type 2 (non-insulin-dependent) diabetic patients. *DIABETOLOGIA, 37*(2), 177-181. doi:10.1007/s001250050090

Fernandez, C., & van Halsema, C. L. (2019). Evaluating cabotegravir/rilpivirine long-acting, injectable in the treatment of HIV infection: emerging data and therapeutic potential. *HIV/AIDS (Auckland, N.Z.), 11*, 179-192. doi:10.2147/HIV.S184642. (Accession No. 31447590)

Fex, M., Nicholas, L. M., Vishnu, N., Medina, A., Sharoyko, V. V., Nicholls, D. G., Spégel, P., & Mulder, H. (2018). The pathogenetic role of β-cell mitochondria in type 2 diabetes. *Journal of Endocrinology, 236*(3), R145-R159. doi:10.1530/JOE-17-0367

Fiala, M. M. D., Murphy, T., Macdougall, J., Yang, W., Luque, A., Iruela-arispe, L., Cashman, J., Buga, G., Byrns, R. E., Barbaro, G., & Arthos, J. (2004). HAART drugs induce mitochondrial damage and intercellular gaps and gp 120 causes apoptosis. *Cardiovascular Toxicology, 4*(4), 327-337. doi:http://dx.doi.org/10.1385/CT:4:4:327

Fleischman, A., Johnsen, S., Systrom, D. M., Hrovat, M., Farrar, C. T., Frontera, W., Fitch, K., Thomas, B. J., Torriani, M., Côté, H. C., & Grinspoon, S. K. (2007). Effects of a nucleoside reverse transcriptase inhibitor, stavudine, on glucose disposal and mitochondrial function in muscle of healthy adults. *American journal of physiology-Endocrinology and metabolism, 292*(6), E1666-1673. doi:10.1152/ajpendo.00550.2006

Fong, P. S., Flynn, D. M., Evans, C. D., & Korthuis, P. T. (2017). Integrase strand transfer inhibitor-associated diabetes mellitus: A case report. *Int J STD AIDS, 28*(6), 626-628. doi:10.1177/0956462416675107

Food and Drug Administration. (2006). ATRIPLA™ (efavirenz 600 mg/emtricitabine 200 mg/tenofovir disoproxil fumarate 300 mg).

Formentini, L., Sánchez-Aragó, M., Sánchez-Cenizo, L., & Cuezva, José M. (2012). The Mitochondrial ATPase Inhibitory Factor 1 Triggers a ROS-Mediated Retrograde Prosurvival and Proliferative Response. *Molecular Cell, 45*(6), 731-742. doi:https://doi.org/10.1016/j.molcel.2012.01.008

Fortgang, L. S., Belitsos, P. C., Chaisson, R. E., & Moore, R. D. (1995). Hepatomegaly and Steatosis in HIV--Infected Patients Receiving Nucleoside Analog Antiretroviral Therapy. *American Journal of Gastroenterology (Springer Nature), 90*(9).

Freiberg, M. S., Chang, C.-C. H., Kuller, L. H., Skanderson, M., Lowy, E., Kraemer, K. L., Butt, A. A., Bidwell Goetz, M., Leaf, D., Oursler, K. A., Rimland, D., Rodriguez Barradas, M., Brown, S., Gibert, C., McGinnis, K., Crothers, K., Sico, J., Crane, H., Warner, A., Gottlieb, S., Gottdiener, J., Tracy, R. P., Budoff, M., Watson, C., Armah, K. A., Doebler, D., Bryant, K., & Justice, A. C. (2013). HIV Infection and the Risk of Acute Myocardial Infarction. *JAMA Internal Medicine, 173*(8), 614-622. doi:10.1001/jamainternmed.2013.3728

Frezza, C., Cipolat, S. & Scorrano, L. (2007) Organelle isolation: functional mitochondria from mouse liver, muscle and cultured filroblasts. *Nature Protocols* 2, 287–295. https://doi.org/10.1038/nprot.2006.478

Galic, S., Oakhill, J. S., & Steinberg, G. R. (2010). Adipose tissue as an endocrine organ. *Molecular and Cellular Endocrinology, 316*(2), 129-139. doi:10.1016/j.mce.2009.08.018

Gallant, J. E., & Moore, R. D. (2009). Renal function with use of a tenofovir-containing initial antiretroviral regimen. *AIDS (London, England), 23*(15), 1971-1975. doi:10.1097/QAD.0b013e32832c96e9

Ganta, K. K., Mandal, A., & Chaubey, B. (2017). Depolarization of mitochondrial membrane potential is the initial event in non-nucleoside reverse transcriptase inhibitor efavirenz induced cytotoxicity. *Cell Biology and Toxicology, 33*(1), 69-82. doi:10.1007/s10565-016-9362-9

García-Aguilar, A., & Cuezva, J. M. (2018). A Review of the Inhibition of the Mitochondrial ATP Synthase by IF1 in vivo: Reprogramming Energy Metabolism and Inducing Mitohormesis. *Frontiers in Physiology, 9*(1322). doi:10.3389/fphys.2018.01322

García-Fuente, A., Vázquez, F., Viéitez, J. M., García Alonso, F. J., Martín, J. I., & Ferrer, J. (2018). CISNE: An accurate description of dose-effect and synergism in combination therapies. *Scientific Reports, 8*(1), 4964. doi:10.1038/s41598-018-23321-6

Garvey, W. T. (1992). Glucose Transport and NIDDM. *Diabetes Care, 15*(3), 396-417. doi:10.2337/diacare.15.3.396

Gatechompol, S., Avihingsanon, A., Apornpong, T., Han, W. M., Kerr, S. J., & Ruxrungtham, K. (2019). Efficacy and improvement of lipid profile after switching to rilpivirine in resource limited setting: real life clinical practice. *AIDS Research and Therapy, 16*(1), 7. doi:10.1186/s12981-019-0222-6

Gerber. (2017). The Role of Oxidative Stress and Hypoxia in Pancreatic Beta-Cell Dysfunction in Diabetes Mellitus. *Antioxidants & Redox Signaling, 26*(10), 501-518. doi:10.1089/ars.2016.6755

Gerber, P. A., & Rutter, G. A. (2016). The Role of Oxidative Stress and Hypoxia in Pancreatic Beta-Cell Dysfunction in Diabetes Mellitus. *Antioxidants & Redox Signaling, 26*(10), 501-518. doi:10.1089/ars.2016.6755

Gerencser, A. A. (2018). Metabolic activation-driven mitochondrial hyperpolarization predicts insulin secretion in human pancreatic beta-cells. *Biochim Biophys Acta Bioenerg, 1859*(9), 817-828. doi:10.1016/j.bbabio.2018.06.006

Getahun, Z., Azage, M., Abuhay, T., & Abebe, F. (2020). Comorbidity of HIV, hypertension, and diabetes and associated factors among people receiving antiretroviral therapy in Bahir Dar city, Ethiopia. *Journal of Comorbidity, 10*, 2235042X19899319. doi:10.1177/2235042X19899319

Glavas, M. M., Hui, Q., Tudurí, E., Erener, S., Kasteel, N. L., Johnson, J. D., & Kieffer, T. J. (2019). Early overnutrition reduces Pdx1 expression and induces β cell failure in Swiss Webster mice. *Scientific Reports, 9*(1), 3619. doi:10.1038/s41598-019-39177-3

Gomes, A., Fernandes, E., & Lima, J. L. F. C. (2005). Fluorescence probes used for detection of reactive oxygen species. *Journal of Biochemical and Biophysical Methods, 65*(2), 45-80. doi:https://doi.org/10.1016/j.jbbm.2005.10.003

Gorwood, J., Bourgeois, C., Pourcher, V., Pourcher, G., Charlotte, F., Mantecon, M., Rose, C., Morichon, R., Atlan, M., Le Grand, R., Desjardins, D., Katlama, C., Fève, B., Lambotte, O., Capeau, J., Béréziat, V., & Lagathu, C. (2020). The Integrase Inhibitors Dolutegravir and Raltegravir Exert Proadipogenic and Profibrotic Effects and Induce Insulin Resistance in Human/Simian Adipose Tissue and Human Adipocytes. *Clinical infectious diseases : an official publication of the Infectious Diseases Society of America, 71*(10), e549-e560. doi:10.1093/cid/ciaa259

Grant, R. M., Lama, J. R., Anderson, P. L., McMahan, V., Liu, A. Y., Vargas, L., Goicochea, P., Casapía, M., Guanira-Carranza, J. V., Ramirez-Cardich, M. E., Montoya-Herrera, O., Fernández, T., Veloso, V. G., Buchbinder, S. P., Chariyalertsak, S., Schechter, M., Bekker, L.-G., Mayer, K. H., Kallás, E. G., Amico, K. R., Mulligan, K., Bushman, L. R., Hance, R. J., Ganoza, C., Defechereux, P., Postle, B., Wang, F., McConnell, J. J., Zheng, J.-H., Lee, J., Rooney, J. F., Jaffe, H. S., Martinez, A. I., Burns, D. N., Glidden, D. V., & iPrEx Study, T. (2010). Preexposure chemoprophylaxis for HIV prevention in men who have sex with men. *The New England Journal of Medicine, 363*(27), 2587-2599. doi:10.1056/NEJMoa1011205

Gray, J. P., & Heart, E. (2010). Usurping the mitochondrial supremacy: extramitochondrial sources of reactive oxygen intermediates and their role in beta cell metabolism and insulin secretion. *Toxicol Mechanisms and Methods, 20*(4), 167-174. doi:10.3109/15376511003695181

Gribble, F. M., Tucker, S. J., Seino, S., & Ashcroft, F. M. (1998). Tissue specificity of sulfonylureas: studies on cloned cardiac and beta-cell K(ATP) channels. *Diabetes, 47*(9), 1412-1418. doi:10.2337/diabetes.47.9.1412

Grigem, S., Fischer-Posovszky, P., Debatin, K. M., Loizon, E., Vidal, H., & Wabitsch, M. (2005). The Effect of the HIV Protease Inhibitor Ritonavir on Proliferation, Differentiation, Lipogenesis, Gene Expression and Apoptosis of Human Preadipocytes and Adipocytes. *Hormone and Metabolic Research, 37*(10), 602-609. doi:10.1055/s-2005-870526

Grosdidier, A., Zoete, V., & Michielin, O. (2011). SwissDock, a protein-small molecule docking web service based on EADock DSS. *Nucleic Acids Research, 39*, W270-277. doi:10.1093/nar/gkr366

Group, T. I. S. S. (2015). Initiation of Antiretroviral Therapy in Early Asymptomatic HIV Infection. *New England Journal of Medicine, 373*(9), 795-807. doi:10.1056/NEJMoa1506816

Guaraldi, G., Orlando, G., Zona, S., Menozzi, M., Carli, F., Garlassi, E., Berti, A., Rossi, E., Roverato, A., & Palella, F. (2011). Premature Age-Related Comorbidities Among HIV-Infected Persons Compared With the General Population. *Clinical Infectious Diseases, 53*(11), 1120-1126. doi:10.1093/cid/cir627

Gurgul-Convey, E., Mehmeti, I., Plötz, T., Jörns, A., & Lenzen, S. (2016). Sensitivity profile of the human EndoC-βH1 beta cell line to proinflammatory cytokines. *DIABETOLOGIA, 59*(10), 2125-2133. doi:10.1007/s00125-016-4060-y

Haber, E. P., Procópio, J., Carvalho, C. R. O., Carpinelli, A. R., Newsholme, P., & Curi, R. (2006). New Insights into Fatty Acid Modulation of Pancreatic β-Cell Function. In *International Review of Cytology* (Vol. 248, pp. 1-41): Academic Press.

Hadigan, C., Borgonha, S., Rabe, J., Young, V., & Grinspoon, S. (2002). Increased rates of lipolysis among human immunodeficiency virus-infected men receiving highly active antiretroviral therapy. *Metabolism, 51*(9), 1143-1147. doi:10.1053/meta.2002.34704

Han, W. M., Jiamsakul, A., Kiertiburanakul, S., Ng, O. T., Sim, B. L., Sun, L. P., Van Nguyen, K., Choi, J. Y., Lee, M. P., Wong, W. W., Kamarulzaman, A., Kumarasamy, N., Zhang, F., Tanuma, J., Do, C. D., Chaiwarith, R., Merati, T. P., Yunihastuti, E., Pujari, S., Ditangco, R., Khusuwan, S., Ross, J., Avihingsanon, A., & Asia-Pacific, I. (2019). Diabetes mellitus burden among

people living with HIV from the Asia-Pacific region. *Journal of the International AIDS Society, 22*(1), e25236. doi:10.1002/jia2.25236

Hattersley, A. T., & Ashcroft, F. M. (2005). Activating Mutations in Kir6.2 and Neonatal Diabetes : New Clinical Syndromes, New Scientific Insights, and New Therapy. *Diabetes, 54*(9), 2503-2513. doi:10.2337/diabetes.54.9.2503

Haythorne, E., Rohm, M., van de Bunt, M., Brereton, M. F., Tarasov, A. I., Blacker, T. S., Sachse, G., Silva dos Santos, M., Terron Exposito, R., Davis, S., Baba, O., Fischer, R., Duchen, M. R., Rorsman, P., MacRae, J. I., & Ashcroft, F. M. (2019). Diabetes causes marked inhibition of mitochondrial metabolism in pancreatic β-cells. *Nature Communications, 10*(1), 2474. doi:10.1038/s41467-019-10189-x

Hebert, V. Y., Crenshaw, B. L., Romanoff, R. L., Ekshyyan, V. P., & Dugas, T. R. (2004). Effects of HIV drug combinations on endothelin-1 and vascular cell proliferation. *Cardiovascular Toxicology, 4*(2), 117-131. doi:http://dx.doi.org/10.1385/CT:4:2:117

Heinz, S., Freyberger, A., Lawrenz, B., Schladt, L., Schmuck, G., & Ellinger-Ziegelbauer, H. (2017). Mechanistic Investigations of the Mitochondrial Complex I Inhibitor Rotenone in the Context of Pharmacological and Safety Evaluation. *Scientific Reports, 7*(1), 45465. doi:10.1038/srep45465

Henquin, J. C., Kahn, C. R., Weir, G., Jacobson, A., & Moses, A. (2005). Joslin's diabetes mellitus. In: Philadelphia, Lippincott, Wilkins Wa, editors.

Hernandez, L. V., Gilson, I., Jacobson, J., Affi, A., Puetz, T. R., & Dindzans, V. J. (2001). Antiretroviral hepatotoxicity in human immunodeficiency virus-infected patients. *Alimentary Pharmacology & Therapeutics, 15*(10), 1627-1632. doi:10.1046/j.1365-2036.2001.01086.x

Hetherington, S. V., Lenhard, J. M., & Powell, G. S. (2001). Abacavir and diabetes. *New England Journal of Medicine, 344*(2), 143-144.

Hoppa, M. B., Collins, S., Ramracheya, R., Hodson, L., Amisten, S., Zhang, Q., Johnson, P., Ashcroft, F. M., & Rorsman, P. (2009). Chronic palmitate exposure inhibits insulin secretion by dissociation of Ca(2+) channels from secretory granules. *Cell Metabolism, 10*(6), 455-465. doi:10.1016/j.cmet.2009.09.011

Hou, N., Torii, S., Saito, N., Hosaka, M., & Takeuchi, T. (2008). Reactive Oxygen Species-Mediated Pancreatic β-Cell Death Is Regulated by Interactions between Stress-Activated Protein Kinases, p38 and c-Jun N-Terminal Kinase, and Mitogen-Activated Protein Kinase Phosphatases. *Endocrinology, 149*(4), 1654-1665. doi:10.1210/en.2007-0988

Howell, S. L., & Taylor, K. W. (1968). Potassium ions and the secretion of insulin by islets of Langerhans incubated in vitro. *Biochem J, 108* (1), 17-24. doi:10.1042/bj1080017

Hruz, P. W. (2010). Molecular mechanisms for insulin resistance in treated HIV-infection. *Best Practice & Research: Clinical Endocrinology & Metabolism, 25*(3), 459-468. doi:10.1016/j.beem.2010.10.017

Hsue, P. Y., & Waters, D. D. (2018). Time to Recognize HIV Infection as a Major Cardiovascular Risk Factor. *Circulation, 138*(11), 1113-1115. doi:10.1161/circulationaha.118.036211

Huez, G., Marbaix, G., Hubert, E., Leclercq, M., Nudel, U., Soreq, H., Salomon, R., Lebleu, B., Revel, M., & Littauer, U. Z. (1974). Proceedings: Role of the polyadenylic segment in the translation of globin messenger RNA. *Hoppe-Seylers Zeitschrift fur Physiologische Chemie, 355*(10), 1211.

Hull, M. W., & Montaner, J. S. (2011). Ritonavir-boosted protease inhibitors in HIV therapy. *Ann Med, 43*(5), 375-388. doi:10.3109/07853890.2011.572905

Ighodaro, O. M., & Akinloye, O. A. (2018). First line defence antioxidants-superoxide dismutase (SOD), catalase (CAT) and glutathione peroxidase (GPX): Their fundamental role in the entire

antioxidant defence grid. *Alexandria Journal of Medicine, 54*(4), 287-293. doi:https://doi.org/10.1016/j.ajme.2017.09.001

Ijuin, T., Hatano, N., Hosooka, T., & Takenawa, T. (2015). Regulation of insulin signaling in skeletal muscle by PIP3 phosphatase, SKIP, and endoplasmic reticulum molecular chaperone glucose-regulated protein 78. *BBA - Molecular Cell Research, 1853*(12), 3192-3201. doi:10.1016/j.bbamcr.2015.09.009

Jain, R. G., Furfine, E. S., Pedneault, L., White, A. J., & Lenhard, J. M. (2001). Metabolic complications associated with antiretroviral therapy. *Antiviral Research, 51*(3), 151-177. doi:https://doi.org/10.1016/S0166-3542(01)00148-6

Jamaluddin, M. S., Lin, P. H., Yao, Q., & Chen, C. (2010). Non-nucleoside reverse transcriptase inhibitor efavirenz increases monolayer permeability of human coronary artery endothelial cells. *Atherosclerosis, 208*(1), 104-111. doi:10.1016/j.atherosclerosis.2009.07.029

Janssen, P. A. J., Lewi, P. J., Arnold, E., Daeyaert, F., de Jonge, M., Heeres, J., Koymans, L., Vinkers, M., Guillemont, J., Pasquier, E., Kukla, M., Ludovici, D., Andries, K., de Béthune, M.-P., Pauwels, R., Das, K., Clark, A. D., Frenkel, Y. V., Hughes, S. H., Medaer, B., De Knaep, F., Bohets, H., De Clerck, F., Lampo, A., Williams, P., & Stoffels, P. (2005). In Search of a Novel Anti-HIV Drug: Multidisciplinary Coordination in the Discovery of 4-[[4-[[4-[(1E)-2-Cyanoethenyl]-2,6-dimethylphenyl]amino]-2- pyrimidinyl]amino]benzonitrile (R278474, Rilpivirine). *Journal of Medicinal Chemistry, 48*(6), 1901-1909. doi:10.1021/jm040840e

Ježek, P., Dlasková, A., & Plecitá-Hlavatá, L. (2012). Redox homeostasis in pancreatic β cells. *Oxidative medicine and cellular longevity, 2012*, 932838-932838. doi:10.1155/2012/932838

Ježek, P., Jabu˚rek, M., & Plecita´ -Hlavata, L. (2019). Contribution of Oxidative Stress and Impaired Biogenesis of Pancreatic β-Cells to Type 2 Diabetes. *Antioxidants & Redox Signaling, 31* (10), 722-751. doi:10.1089/ars.2018.7656

Jin, J., Grimmig, B., Izzo, J., Brown, L. A., Hudson, C., Smith, A. J., Tan, J., Bickford, P. C., & Giunta, B. (2016). HIV non-nucleoside reverse transcriptase inhibitor efavirenz reduces neural stem cell proliferation in vitro and in vivo. *Cell transplantation, 25*(11), 1967-1977.

Jitrapakdee, S., Wutthisathapornchai, A., Wallace, J. C., & MacDonald, M. J. (2010). Regulation of insulin secretion: role of mitochondrial signalling. *DIABETOLOGIA, 53*(6), 1019-1032. doi:10.1007/s00125-010-1685-0

Johnson, J. D., Ahmed, N. T., Luciani, D. S., Han, Z., Tran, H., Fujita, J., Misler, S., Edlund, H., & Polonsky, K. S. (2003). Increased islet apoptosis in Pdx1+/– mice. *The Journal of Clinical Investigation, 111*(8), 1147-1160. doi:10.1172/JCI16537

Joint United Nations Programme on HIV/AIDS. (2016). The importance of HIV care and support services [Press release]. Retrieved from https://www.unaids.org/en/resources/presscentre/featurestories/2016/december/20161202_HIV-care

Joint United Nations Programme on HIV/AIDS. (2017). UNAIDS Data 2017. Retrieved from https://www.unaids.org/sites/default/files/media_asset/20170720_Data_book_2017_en.pdf

Jones, S. P., Janneh, O., Back, D. J., & Pirmohamed, M. (2005a). Altered adipokine response in murine 3T3-F442A adipocytes treated with protease inhibitors and nucleoside reverse transcriptase inhibitors. *Antiviral Therapy, 10* (2), 207-213.

Jones, S. P., Qazi, N., Morelese, J., Lebrecht, D., Sutinen, J., Yki-Jărvinen, H., Back, D. J., Pirmohamed, M., Gazzard, B. G., Walker, U. A., & Moyle, G. J. (2005b). Assessment of adipokine expression and mitochondrial toxicity in HIV patients with lipoatrophy on stavudine-and zidovudine-containing regimens. *Journal of Acquired Immune Deficiency Syndromes, 40*(5), 565-572. doi:10.1097/01.qai.0000187443.30838.3e

Jonsson, J., Carlsson, L., Edlund, T., & Edlund, H. (1994). Insulin-promoter-factor 1 is required for pancreas development in mice. *Nature, 371*(6498), 606-609. doi:10.1038/371606a0

Joslin, E. P., & Kahn, C. R. (2005). *Joslin's Diabetes Mellitus: Edited by C. Ronald Kahn.* Lippincott Williams & Wilkins.

Justman, J. E., Benning, L., Danoff, A., Minkoff, H., Levine, A., Greenblatt, R. M., Weber, K., Piessens, E., Robison, E., & Anastos, K. (2003). Protease Inhibitor Use and the Incidence of Diabetes Mellitus in a Large Cohort of HIV-Infected Women. *JAIDS Journal of Acquired Immune Deficiency Syndromes, 32*(3), 298-302. doi:10.1097/00126334-200303010-00009

Kahn, S. E., Haffner, S. M., Heise, M. A., Herman, W. H., Holman, R. R., Jones, N. P., Kravitz, B. G., Lachin, J. M., O'Neill, M. C., Zinman, B., & Viberti, G. (2006a). Glycemic Durability of Rosiglitazone, Metformin, or Glyburide Monotherapy. *New England Journal of Medicine, 355*(23), 2427-2443. doi:10.1056/NEJMoa066224

Kahn, S. E., Hull, R. L., & Utzschneider, K. M. (2006b). Mechanisms linking obesity to insulin resistance and type 2 diabetes. *Nature, 444*(7121), 840-846. doi:10.1038/nature05482

Kajimoto, Y., & Kaneto, H. (2004). Role of Oxidative Stress in Pancreatic β-Cell Dysfunction. *Annals of the New York Academy of Sciences, 1011*(1), 168-176. doi:10.1196/annals.1293.017

Kakuda, T. N. (2000). Pharmacology of nucleoside and nucleotide reverse transcriptase inhibitor-induced mitochondrial toxicity. *Clinical Therapeutics, 22*(6), 685-708. doi:https://doi.org/10.1016/S0149-2918(00)90004-3

Kalra, S., Kalra, B., Agrawal, N., & Unnikrishnan, A. G. (2011). Understanding diabetes in patients with HIV/AIDS. *Diabetology & Metabolic Syndrome, 3*(1), 2. doi:10.1186/1758-5996-3-2

Kaneto, H., Matsuoka, T. A., Nakatani, Y., Kawamori, D., Miyatsuka, T., Matsuhisa, M., & Yamasaki, Y. (2005). Oxidative stress, ER stress, and the JNK pathway in type 2 diabetes. *Journal of Molecular Medicine (Berl), 83*(6), 429-439. doi:10.1007/s00109-005-0640-x

Karamchand, S., Leisegang, R., Schomaker, M., Maartens, G., Walters, L., Hislop, M., Dave, J. A., Levitt, N. S., & Cohen, K. (2016). Risk factors for incident diabetes in a cohort taking first-line nonnucleoside reverse transcriptase inhibitor-based antiretroviral therapy. *Medicine (United States), 95*(9), e2844. doi:10.1097/MD.0000000000002844

Karaskov, E., Scott, C., Zhang, L., Teodoro, T., Ravazzola, M., & Volchuk, A. (2006). Chronic Palmitate But Not Oleate Exposure Induces Endoplasmic Reticulum Stress, Which May Contribute to INS-1 Pancreatic β-Cell Apoptosis. *Endocrinology, 147*(7), 3398-3407. doi:10.1210/en.2005-1494

Kaufman, B. A., Li, C., & Soleimanpour, S. A. (2015). Mitochondrial regulation of β-cell function: maintaining the momentum for insulin release. *Molecular aspects of medicine, 42*, 91-104. doi:10.1016/j.mam.2015.01.004

Kaufman, R. J., Back, S. H., Song, B., Han, J., & Hassler, J. (2010). The unfolded protein response is required to maintain the integrity of the endoplasmic reticulum, prevent oxidative stress and preserve differentiation in β-cells. *Diabetes, Obesity and Metabolism, 12*(s2), 99-107. doi:https://doi.org/10.1111/j.1463-1326.2010.01281.x

Kawamori, D., Kajimoto, Y., Kaneto, H., Umayahara, Y., Fujitani, Y., Miyatsuka, T., Watada, H., Leibiger, I. B., Yamasaki, Y., & Hori, M. (2003). Oxidative stress induces nucleo-cytoplasmic translocation of pancreatic transcription factor PDX-1 through activation of c-Jun NH(2)-terminal kinase. *Diabetes, 52*(12), 2896-2904. doi:10.2337/diabetes.52.12.2896

Keane, Deirdre C., Takahashi, Hilton K., Dhayal, S., Morgan, Noel G., Curi, R., & Newsholme, P. (2010). Arachidonic acid actions on functional integrity and attenuation of the negative effects of palmitic acid in a clonal pancreatic β-cell line. *Clinical Science, 120*(5), 195-206. doi:10.1042/CS20100282

Kendall, C. E., Wong, J., Taljaard, M., Glazier, R. H., Hogg, W., Younger, J., & Manuel, D. G. (2014). A cross-sectional, population-based study measuring comorbidity among people living with HIV in Ontario. *BMC Public Health, 14*(1), 161. doi:10.1186/1471-2458-14-161

Kharroubi, I., Ladrière, L., Cardozo, A. K., Dogusan, Z., Cnop, M., & Eizirik, D. c. L. (2004). Free Fatty Acids and Cytokines Induce Pancreatic β-Cell Apoptosis by Different Mechanisms: Role of Nuclear Factor-κB and Endoplasmic Reticulum Stress. *Endocrinology, 145*(11), 5087-5096. doi:10.1210/en.2004-0478

Kien, C. L., Bunn, J. Y., Poynter, M. E., Stevens, R., Bain, J., Ikayeva, O., Fukagawa, N. K., Champagne, C. M., Crain, K. I., Koves, T. R., & Muoio, D. M. (2013). A Lipidomics Analysis of the Relationship Between Dietary Fatty Acid Composition and Insulin Sensitivity in Young Adults. *Diabetes, 62*(4), 1054-1063. doi:10.2337/db12-0363

Kilbride, S. M., Telford, J. E., & Davey, G. P. (2021). Complex I Controls Mitochondrial and Plasma Membrane Potentials in Nerve Terminals. *Neurochemical Research, 46*(1), 100-107. doi:10.1007/s11064-020-02990-8

Kimoto, K., Suzuki, K., Kizaki, T., Hitomi, Y., Ishida, H., Katsuta, H., Itoh, E., Ookawara, T., Suzuki, K., Honke, K., & Ohno, H. (2003). Gliclazide protects pancreatic β-cells from damage by hydrogen peroxide. *Biochemical and Biophysical Research Communications, 303*(1), 112-119. doi:https://doi.org/10.1016/S0006-291X(03)00310-3

Kitahata, M. M., Gange, S. J., Abraham, A. G., Merriman, B., Saag, M. S., Justice, A. C., Hogg, R. S., Deeks, S. G., Eron, J. J., Brooks, J. T., Rourke, S. B., Gill, M. J., Bosch, R. J., Martin, J. N., Klein, M. B., Jacobson, L. P., Rodriguez, B., Sterling, T. R., Kirk, G. D., Napravnik, S., Rachlis, A. R., Calzavara, L. M., Horberg, M. A., Silverberg, M. J., Gebo, K. A., Goedert, J. J., Benson, C. A., Collier, A. C., Van Rompaey, S. E., Crane, H. M., McKaig, R. G., Lau, B., Freeman, A. M., & Moore, R. D. (2009). Effect of early versus deferred antiretroviral therapy for HIV on survival. *The New England Journal of Medicine, 360*(18), 1815-1826. doi:10.1056/NEJMoa0807252

Koshkin, V., Wang, X., Scherer, P. E., Chan, C. B., & Wheeler, M. B. (2003). Mitochondrial Functional State in Clonal Pancreatic β-Cells Exposed to Free Fatty Acids. *Journal of Biological Chemistry, 278*(22), 19709-19715. doi:10.1074/jbc.M209709200

Koster, J. C., Remedi, M. S., Qiu, H., Nichols, C. G., & Hruz, P. W. (2003). HIV Protease Inhibitors Acutely Impair Glucose-Stimulated Insulin Release. *Diabetes, 52*(7), 1695-1700. doi:10.2337/diabetes.52.7.1695

Kramer, A. A., Manas; Krickeberg, Klaus. (2010). Principles of Infectious Disease Epidemiology In M. K. Alexander Kramer, Klaus Krickeberg (Ed.), *Modern Infectious Disease Epidemiology: Concepts, Methods, Mathematical Models, and Public Health* (pp. 88): Springer Science & Business Media.

Krauss, S., Zhang, C.-Y., Scorrano, L., Dalgaard, L. T., St-Pierre, J., Grey, S. T., & Lowell, B. B. (2003). Superoxide-mediated activation of uncoupling protein 2 causes pancreatic β cell dysfunction. *The Journal of Clinical Investigation, 112*(12), 1831-1842. doi:10.1172/JCI19774

Lagathu, C., Eustace, B., Prot, M., Frantz, D., Gu, Y., Bastard, J.-P., Maachi, M., Azoulay, S., Briggs, M., Caron, M., & Capeau, J. (2007). Some HIV antiretrovirals increase oxidative stress and alter chemokine, cytokine or adiponectin production in human adipocytes and macrophages. *Antiviral Therapy, 12*(4), 489-500.

Lagathu, C., Kim, M., Maachi, M., Vigouroux, C., Cervera, P., Capeau, J., Caron, M., & Bastard, J.-P. (2005). HIV antiretroviral treatment alters adipokine expression and insulin sensitivity of adipose tissue in vitro and in vivo. *Biochimie, 87*(1), 65-71. doi:https://doi.org/10.1016/j.biochi.2004.12.007

Lai, E., Bikopoulos, G., Wheeler, M. B., Rozakis-Adcock, M., & Volchuk, A. (2008). Differential activation of ER stress and apoptosis in response to chronically elevated free fatty acids in pancreatic β-cells. *American Journal of Physiology-Endocrinology and Metabolism, 294*(3), E540-E550. doi:10.1152/ajpendo.00478.2007

Lamorde, M., Walimbwa, S., Byakika-Kibwika, P., Katwere, M., Mukisa, L., Sempa, J. B., Else, L., Back, D. J., Khoo, S. H., & Merry, C. (2015). Steady-state pharmacokinetics of rilpivirine under different meal conditions in HIV-1-infected Ugandan adults. *Journal of Antimicrobial Chemotherapy, 70*(5), 1482-1486. doi:10.1093/jac/dku575

Larson, R., Capili, B., Eckert-Norton, M., Colagreco, J. P., & Anastasi, J. K. (2006). Disorders of glucose metabolism in the context of human immunodeficiency virus infection. *Journal of the American Academy of Nurse Practitioners, 18*(3), 92-103. doi:10.1111/j.1745-7599.2006.00109.x

Larsson, O., Deeney, J. T., Bränström, R., Berggren, P.-O., & Corkey, B. E. (1996). **Activation of the** ATP-sensitive K+ channel by long chain acyl-CoA. A role in modulation of pancreatic beta-cell glucose sensitivity. *Journal of Biological Chemistry, 271*(18), 10623-10626. doi:10.1074/jbc.271.18.10623

Ledergerber, B., Furrer, H., Rickenbach, M., Lehmann, R., Elzi, L., Hirschel, B., Cavassini, M., Bernasconi, E., Schmid, P., Egger, M., & Weber, R. (2007). Factors associated with the incidence of type 2 diabetes mellitus in HIV-infected participants in the Swiss HIV Cohort Study. *Clinical infectious diseases : an official publication of the Infectious Diseases Society of America, 45*(1), 111-119. doi:10.1086/518619

Lemoine, M., Serfaty, L., & Capeau, J. (2012). From nonalcoholic fatty liver to nonalcoholic steatohepatitis and cirrhosis in HIV-infected patients: diagnosis and management. *Current opinion in infectious diseases, 25*(1), 10-16.

Leslie, K. A. (2019). *Signal transducer and activator of transcription 6 (STAT6) as a regulator of pancreatic beta cell death.* (Doctor of Philosophy). University of Exeter, Retrieved from https://ore.exeter.ac.uk/repository/bitstream/handle/10871/37361/Afi%20LeslieK.pdf?sequence=1&isAllowed=y

Li, N., Brun, T., Cnop, M., Cunha, D. A., Eizirik, D. L., & Maechler, P. (2009). Transient oxidative stress damages mitochondrial machinery inducing persistent beta-cell dysfunction. *The Journal of biological chemistry, 284*(35), 23602-23612. doi:10.1074/jbc.M109.024323

Li, N., Ragheb, K., Lawler, G., Sturgis, J., Rajwa, B., Melendez, J. A., & Robinson, J. P. (2003). Mitochondrial Complex I Inhibitor Rotenone Induces Apoptosis through Enhancing Mitochondrial Reactive Oxygen Species Production. *Journal of Biological Chemistry, 278*(10), 8516-8525. doi:10.1074/jbc.M210432200

Lifson, J. D., & Engleman, E. G. (1989). Role of CD4 in normal immunity and HIV infection. *Immunol Rev, 109*, 93-117. doi:10.1111/j.1600-065x.1989.tb00021.x

Lihn, A. S., Pedersen, S. B., & Richelsen, B. (2005). Adiponectin: action, regulation and association to insulin sensitivity. *Obesity Reviews, 6*(1), 13-21. doi:10.1111/j.1467-789X.2005.00159.x

Lin, N., Chen, H., Zhang, H., Wan, X., & Su, Q. (2012). Mitochondrial reactive oxygen species (ROS) inhibition ameliorates palmitate-induced INS-1 beta cell death. *Endocrine, 42*(1), 107-117. doi:10.1007/s12020-012-9633-z

Lin, S. P., Wu, C.-Y., Wang, C.-B., Li, T.-C., Ko, N.-Y., & Shi, Z.-Y. (2018). Risk of diabetes mellitus in HIV-infected patients receiving highly active antiretroviral therapy: A nationwide population-based study. *Medicine, 97*(36), e12268-e12268. doi:10.1097/MD.0000000000012268

Liu, C., Wan, X., Ye, T., Fang, F., Chen, X., Chen, Y., & Dong, Y. (2014). Matrix metalloproteinase 2 contributes to pancreatic Beta cell injury induced by oxidative stress. *PLoS ONE, 9*(10), e110227. doi:10.1371/journal.pone.0110227

Lo, Y.-C., Chen, M.-Y., Sheng, W.-H., Hsieh, S.-M., Sun, H.-Y., Liu, W.-C., Wu, P.-Y., Wu, C.-H., Hung, C.-C., & Chang, S.-C. (2009). Risk factors for incident diabetes mellitus among HIV-infected patients receiving combination antiretroviral therapy in Taiwan: a case–control study. *HIV Medicine, 10*(5), 302-309. doi:10.1111/j.1468-1293.2008.00687.x

Loskovich, M. V., Grivennikova, V. G., Cecchini, G., & Vinogradov, A. D. (2005). Inhibitory effect of palmitate on the mitochondrial NADH:ubiquinone oxidoreductase (complex I) as related to the active-de-active enzyme transition. *Biochemical Journal, 387*(Pt 3), 677-683. doi:10.1042/bj20041703

Lu, M., Dong, H., Bao, D., Liu, H., & Liu, B. (2019). Tenofovir disoproxil fumarate induces pheochromocytoma cells apoptosis. *European Journal of Pharmacology, 844*, 139-144. doi:10.1016/j.ejphar.2018.12.006

Lundgren, J. D., Babiker, A. G., Gordin, F., Emery, S., Grund, B., Sharma, S., Avihingsanon, A., Cooper, D. A., Fätkenheuer, G., Llibre, J. M., Molina, J.-M., Munderi, P., Schechter, M., Wood, R., Klingman, K. L., Collins, S., Clifford Lane, H., Phillips, A. N., Neaton, J. D., The, I. S. S. G., & Group, I. S. S. (2015). *Initiation of Antiretroviral Therapy in Early Asymptomatic HIV Infection.* (373). Massachusetts Medical Society, WALTHAM.

Lupi, R., Dotta, F., Marselli, L., Del Guerra, S., Masini, M., Santangelo, C., Patané, G., Boggi, U., Piro, S., Anello, M., Bergamini, E., Mosca, F., Di Mario, U., Del Prato, S., & Marchetti, P. (2002). Prolonged Exposure to Free Fatty Acids Has Cytostatic and Pro-Apoptotic Effects on Human Pancreatic Islets: Evidence that β-Cell Death Is Caspase Mediated, Partially Dependent on Ceramide Pathway, and Bcl-2 Regulated. *Diabetes, 51*(5), 1437-1442. doi:10.2337/diabetes.51.5.1437

Ly, L. D., Xu, S., Choi, S.-K., Ha, C.-M., Thoudam, T., Cha, S.-K., Wiederkehr, A., Wollheim, C. B., Lee, I.-K., & Park, K.-S. (2017). Oxidative stress and calcium dysregulation by palmitate in type 2 diabetes. *Experimental & Molecular Medicine, 49*(2), e291-e291. doi:10.1038/emm.2016.157

Lytrivi, M., Castell, A.-L., Poitout, V., & Cnop, M. (2020). Recent Insights Into Mechanisms of β-Cell Lipo- and Glucolipotoxicity in Type 2 Diabetes. *Journal of Molecular Biology, 432*(5), 1514-1534. doi:https://doi.org/10.1016/j.jmb.2019.09.016

MacDonald, M. J., Longacre, M. J., Langberg, E. C., Tibell, A., Kendrick, M. A., Fukao, T., & Ostenson, C. G. (2009). Decreased levels of metabolic enzymes in pancreatic islets of patients with type 2 diabetes. *DIABETOLOGIA, 52*(6), 1087-1091. doi:10.1007/s00125-009-1319-6

Maedler, K., & Ardestani, A. (2017). mTORC in β cells: more Than Only Recognizing Comestibles. *Journal of Cell Biology, 216*(7), 1883-1885. doi:10.1083/jcb.201704179

Maedler, K., Oberholzer, J., Bucher, P., Spinas, G. A., & Donath, M. Y. (2003). Monounsaturated Fatty Acids Prevent the Deleterious Effects of Palmitate and High Glucose on Human Pancreatic β-Cell Turnover and Function. *Diabetes, 52*(3), 726-733. doi:10.2337/diabetes.52.3.726

Maedler, K., Spinas, G. A., Dyntar, D., Moritz, W., Kaiser, N., & Donath, M. Y. (2001). Distinct Effects of Saturated and Monounsaturated Fatty Acids on β-Cell Turnover and Function. *Diabetes, 50*(1), 69-76. doi:10.2337/diabetes.50.1.69

Malhi, H., Irani, A. N., Rajvanshi, P., Suadicani, S. O., Spray, D. C., McDonald, T. V., & Gupta, S. (2000). KATP channels regulate mitogenically induced proliferation in primary rat hepatocytes and human liver cell lines. Implications for liver growth control and potential therapeutic targeting. *The Journal of biological chemistry, 275*(34), 26050-26057. doi:10.1074/jbc.M001576200

Malmgren, S., Nicholls, D. G., Taneera, J., Bacos, K., Koeck, T., Tamaddon, A., Wibom, R., Groop, L., Ling, C., Mulder, H., & Sharoyko, V. V. (2009). Tight coupling between glucose and mitochondrial metabolism in clonal beta-cells is required for robust insulin secretion. *The Journal of biological chemistry, 284*(47), 32395-32404. doi:10.1074/jbc.M109.026708

Mannheimer, S. B., Morse, E., Matts, J. P., Andrews, L., Child, C., Schmetter, B., Friedland, G. H., Terry Beirn Community Programs, C., & Terry Beirn Community Programs for Clinical Research on, A. (2006). Sustained Benefit From a Long-Term Antiretroviral Adherence Intervention: Results of a Large Randomized Clinical Trial. *JAIDS Journal of Acquired Immune Deficiency Syndromes, 43 Suppl 1*(1), S41-S47. doi:10.1097/01.qai.0000245887.58886.ac

Mantzoros, C. N., D; Mulder, J (2018). Insulin resistance: Definition and clinical spectrum.

Marchetti, P., Bugliani, M., De Tata, V., Suleiman, M., & Marselli, L. (2017). Pancreatic Beta Cell Identity in Humans and the Role of Type 2 Diabetes. *Frontiers in Cell and Development Biology, 5*, 55. doi:10.3389/fcell.2017.00055

Marchi, S., Giorgi, C., Suski, J. M., Agnoletto, C., Bononi, A., Bonora, M., De Marchi, E., Missiroli, S., Patergnani, S., Poletti, F., Rimessi, A., Duszynski, J., Wieckowski, M. R., & Pinton, P. (2012). Mitochondria-ros crosstalk in the control of cell death and aging. *Journal of signal transduction, 2012*, 329635-329635. doi:10.1155/2012/329635

Margolis, A. M., Heverling, H., Pham, P. A., & Stolbach, A. (2014). A Review of the Toxicity of HIV Medications. *Journal of Medical Toxicology, 10*(1), 26-39. doi:10.1007/s13181-013-0325-8

Martin, E. A., Lai, M. T., Ngo, W., Feng, M., Graham, D., Hazuda, D. J., Kumar, S., Hwang, C., Sklar, P., & Asante-Appiah, E. (2020). Review of Doravirine Resistance Patterns Identified in Participants During Clinical Development. *Journal of Acquired Immune Deficiency Syndromes, 85*(5), 635-642. doi:10.1097/qai.0000000000002496

Martin, G. M., Kandasamy, B., DiMaio, F., Yoshioka, C., & Shyng, S.-L. (2017a). Anti-diabetic drug binding site in a mammalian KATP channel revealed by Cryo-EM. *eLife, 6*, e31054. doi:10.7554/eLife.31054

Martin, G. M., Yoshioka, C., Rex, E. A., Fay, J. F., Xie, Q., Whorton, M. R., Chen, J. Z., & Shyng, S. L. (2017b). Cryo-EM structure of the ATP-sensitive potassium channel illuminates mechanisms of assembly and gating. *eLife, 6*. doi:10.7554/eLife.24149

Martino, L., Masini, M., Novelli, M., Beffy, P., Bugliani, M., Marselli, L., Masiello, P., Marchetti, P., & De Tata, V. (2012). Palmitate Activates Autophagy in INS-1E β-Cells and in Isolated Rat and Human Pancreatic Islets. *PLoS ONE, 7*(5), e36188. doi:10.1371/journal.pone.0036188

Marzolini, C., Telenti, A., Decosterd, L. A., Greub, G., Biollaz, J., & Buclin, T. (2001). Efavirenz plasma levels can predict treatment failure and central nervous system side effects in HIV-1-infected patients. *AIDS, 15*(1), 71-75. doi:10.1097/00002030-200101050-00011

Masho, S. W., Wang, C.-L., & Nixon, D. E. (2007). Review of tenofovir-emtricitabine. *Therapeutics and clinical risk management, 3*(6), 1097-1104.

McGowan, I., Dezzutti, C. S., Siegel, A., Engstrom, J., Nikiforov, A., Duffill, K., Shetler, C., Richardson-Harman, N., Abebe, K., Back, D., Else, L., Egan, D., Khoo, S., Egan, J. E., Stall, R., Williams, P. E., Rehman, K. K., Adler, A., Brand, R. M., Chen, B., Achilles, S., & Cranston, R. D. (2016). Long-acting rilpivirine as potential pre-exposure prophylaxis for HIV-1 prevention (the MWRI-01 study): an open-label, phase 1, compartmental, pharmacokinetic and pharmacodynamic assessment. *Lancet HIV, 3*(12), e569-e578. doi:10.1016/s2352-3018(16)30113-8

Merglen, A., Theander, S., Rubi, B., Chaffard, G., Wollheim, C. B., & Maechler, P. (2004). Glucose sensitivity and metabolism-secretion coupling studied during two-year continuous culture in INS-1E insulinoma cells. *Endocrinology, 145*(2), 667-678. doi:10.1210/en.2003-1099

Meshkani, R., & Adeli, K. (2009). Hepatic insulin resistance, metabolic syndrome and cardiovascular disease. *Clin Biochem, 42*(13-14), 1331-1346. doi:10.1016/j.clinbiochem.2009.05.018

Misler, S. (2010). The isolated pancreatic islet as a micro-organ and its transplantation to cure diabetes. *Islets, 2*(4), 210-224. doi:10.4161/isl.2.4.12156

Mocroft, A., Vella, S., Benfield, T. L., Chiesi, A., Miller, V., Gargalianos, P., d'Arminio Monforte, A., Yust, I., Bruun, J. N., Phillips, A. N., & Lundgren, J. D. (1998). Changing patterns of mortality across Europe in patients infected with HIV-1. EuroSIDA Study Group. *Lancet, 352*(9142), 1725-1730. doi:10.1016/s0140-6736(98)03201-2

Molina, J.-M., Ferchal, F., Rancinan, C., Raffi, F., Rozenbaum, W., Sereni, D., Morlat, P., Journot, V., Decazes, J.-M., Chêne, G., & Group, f. t. M. S. (2000). Once-Daily Combination Therapy with Emtricitabine, Didanosine, and Efavirenz in Human Immunodeficiency Virus—Infected Patients. *The Journal of Infectious Diseases, 182*(2), 599-602. doi:10.1086/315711

Molina, J. M., Journot, V., Morand-Joubert, L., Yéni, P., Rozenbaum, W., Rancinan, C., Fournier, S., Morlat, P., Palmer, P., Dupont, B., Goujard, C., Dellamonica, P., Collin, F., Poizot-Martin, I., & Team, A. S. (2005). Simplification Therapy with Once-Daily Emtricitabine, Didanosine, and Efavirenz in HIV-1–Infected Adults with Viral Suppression Receiving a Protease Inhibitor–Based Regimen: A Randomized Trial. *The Journal of Infectious Diseases, 191*(6), 830-839. doi:10.1086/428091

Molina, J. M., Peytavin, G., Perusat, S., Lascoux-Combes, C., Sereni, D., Rozenbaum, W., & Chene, G. (2004). Pharmacokinetics of emtricitabine, didanosine and efavirenz administered once-daily for the treatment of HIV-infected adults (pharmacokinetic substudy of the ANRS 091 trial). *HIV Med, 5*(2), 99-104. doi:10.1111/j.1468-1293.2004.00194.x

Monsalve, M., Borniquel, S., Valle, I., & Lamas, S. (2007). Mitochondrial dysfunction in human pathologies. *Front Biosci, 12*, 1131-1153. doi:10.2741/2132

Morgan, D., Oliveira-Emilio, H. R., Keane, D., Hirata, A. E., Santos da Rocha, M., Bordin, S., Curi, R., Newsholme, P., & Carpinelli, A. R. (2007). Glucose, palmitate and pro-inflammatory cytokines modulate production and activity of a phagocyte-like NADPH oxidase in rat pancreatic islets and a clonal beta cell line. *DIABETOLOGIA, 50*(2), 359-369. doi:10.1007/s00125-006-0462-6

Morgan, N. G., & Dhayal, S. (2010). Unsaturated fatty acids as cytoprotective agents in the pancreatic beta-cell. *Prostaglandins, leukotrienes, and essential fatty acids, 82 4-6*, 231-236.

Morgan, N. G., Dhayal, S., Diakogiannaki, E., & Welters, Hannah J. (2008). The cytoprotective actions of long-chain mono-unsaturated fatty acids in pancreatic β-cells. *Biochemical Society Transactions, 36*(5), 905-908. doi:10.1042/BST0360905

Morse, G. D. a. N., Sarah. (2015). *Frontiers in HIV Research* (Vol. 1): Bentham E-books.

Moure, R., Domingo, P., Gallego-Escuredo, J. M., Villarroya, J., Gutierrez Mdel, M., Mateo, M. G., Domingo, J. C., Giralt, M., & Villarroya, F. (2016). Impact of elvitegravir on human adipocytes: Alterations in differentiation, gene expression and release of adipokines and cytokines. *Antiviral Research, 132*, 59-65. doi:10.1016/j.antiviral.2016.05.013

Moyo, D., Tanthuma, G., Mushisha, O., Kwadiba, G., Chikuse, F., Cary, M. S., Steenhoff, A. P., & Reid, M. J. (2013). Diabetes mellitus in HIV-infected patients receiving antiretroviral therapy. *South African Medical Journal, 104*(1), 37-39. doi:10.7196/samj.6792

Mueckler, M. (2001). Insulin resistance and the disruption of Glut4 trafficking in skeletal muscle. *The Journal of Clinical Investigation, 107*(10), 1211-1213. doi:10.1172/JCI13020

Murata, H., Hruz, P. W., & Mueckler, M. (2000). The Mechanism of Insulin Resistance Caused by HIV Protease Inhibitor Therapy. *Journal of Biological Chemistry, 275*(27), 20251-20254. doi:10.1074/jbc.C000228200

Murata, H., Hruz, P. W., & Mueckler, M. (2002). Indinavir inhibits the glucose transporter isoform Glut4 at physiologic concentrations. *AIDS, 16*(6), 859-863. doi:10.1097/00002030-200204120-00005

Murphy, R. A., Stafford, R. M., Petrasovits, B. A., Boone, M. A., & Valentovic, M. A. (2017). Establishment of HK-2 cells as a relevant model to study tenofovir-induced cytotoxicity. *International Journal of Molecular Sciences, 18*(3), 531. doi:10.3390/ijms18030531

Nakatsu, D., Horiuchi, Y., Kano, F., Noguchi, Y., Sugawara, T., Takamoto, I., Kubota, N., Kadowaki, T., & Murata, M. (2015). L-cysteine reversibly inhibits glucose-induced biphasic insulin secretion and ATP production by inactivating PKM2. *Proceedings of the National Academy of Sciences of the United States of America, 112*(10), E1067-1076. doi:10.1073/pnas.1417197112

National Institute for Health and Care Excellence. (2018). Scenario: Post-exposure prophylaxis for HIV. Retrieved from https://cks.nice.org.uk/hiv-infection-and-aids#!scenario:3

National Institute for Health and Care Excellence. (2022). Scenario: Management - adults. Retrieved from https://cks.nice.org.uk/topics/diabetes-type-2/management/management-adults/

Nemecz, M., Constantin, A., Dumitrescu, M., Alexandru, N., Filippi, A., Tanko, G., & Georgescu, A. (2019). The Distinct Effects of Palmitic and Oleic Acid on Pancreatic Beta Cell Function: The Elucidation of Associated Mechanisms and Effector Molecules. *Frontiers in Pharmacology, 9*. doi:10.3389/fphar.2018.01554

Newsholme, P., Cruzat, V. F., Keane, K. N., Carlessi, R., & de Bittencourt, P. I. H., Jr. (2016). Molecular mechanisms of ROS production and oxidative stress in diabetes. *Biochemical Journal, 473*(24), 4527-4550. doi:10.1042/BCJ20160503C

Newsholme, P., Keane, D., Welters, H. J., & Morgan, N. G. (2007). Life and death decisions of the pancreatic beta-cell: the role of fatty acids. *Clinical Science (Lond), 112*(1), 27-42. doi:10.1042/cs20060115

Newsholme, P., Keane, K. N., Carlessi, R., & Cruzat, V. (2019). Oxidative stress pathways in pancreatic β-cells and insulin-sensitive cells and tissues: importance to cell metabolism, function, and dysfunction. *American Journal of Physiology-Cell Physiology, 317*(3), C420-C433. doi:10.1152/ajpcell.00141.2019

Newsholme, P., Morgan, D., Rebelato, E., Oliveira-Emilio, H. C., Procopio, J., Curi, R., & Carpinelli, A. (2009). Insights into the critical role of NADPH oxidase(s) in the normal and dysregulated pancreatic beta cell. *DIABETOLOGIA, 52*(12), 2489-2498. doi:10.1007/s00125-009-1536-z

Newsholme, P., Rebelato, E., Abdulkader, F., Krause, M., Carpinelli, A., & Curi, R. (2012). Reactive oxygen and nitrogen species generation, antioxidant defenses, and β-cell function: a critical role for amino acids. *The Journal of endocrinology, 214*(1), 11-20. doi:10.1530/joe-12-0072

Nicholls, D. G. (2002). Mitochondrial function and dysfunction in the cell: its relevance to aging and aging-related disease. *The International Journal of Biochemistry & Cell Biology, 34*(11), 1372-1381. doi:https://doi.org/10.1016/S1357-2725(02)00077-8

Nolan, D., Hammond, E., Martin, A., Taylor, L., Herrmann, S., McKinnon, E., Metcalf, C., Latham, B., & Mallal, S. (2003). Mitochondrial DNA depletion and morphologic changes in adipocytes associated with nucleoside reverse transcriptase inhibitor therapy. *AIDS, 17*(9), 1329-1338.

Nolte, L. A., Yarasheski, K. E., Kawanaka, K., Fisher, J., Le, N., & Holloszy, J. O. (2001). The HIV Protease Inhibitor Indinavir Decreases Insulin- and Contraction-Stimulated Glucose Transport in Skeletal Muscle. *Diabetes, 50*(6), 1397-1401. doi:10.2337/diabetes.50.6.1397

Noor, M. A., Flint, O. P., Maa, J.-F., & Parker, R. A. (2006). Effects of atazanavir/ritonavir and lopinavir/ritonavir on glucose uptake and insulin sensitivity: Demonstrable differences in vitro and clinically. *AIDS, 20*(14), 1813-1821. doi:10.1097/01.aids.0000244200.11006.55

Obry-Roguet, V., Brégigeon, S., Cano, C. E., Lions, C., Zaegel-Faucher, O., Laroche, H., Galie, S., De Lamarlière, P. G., Orticoni, M., Soavi, M.-J., Saout, A., & Poizot-Martin, I. (2018). Risk factors

associated with overweight and obesity in HIV-infected people: Aging, behavioral factors but not cART in a cross-sectional study. *Medicine, 97*(23), e10956-e10956. doi:10.1097/MD.0000000000010956

Oh, Y. S., Bae, G. D., Baek, D. J., Park, E.-Y., & Jun, H.-S. (2018). Fatty Acid-Induced Lipotoxicity in Pancreatic Beta-Cells During Development of Type 2 Diabetes. *Frontiers in Endocrinology, 9*. Retrieved from https://www.frontiersin.org/articles/10.3389/fendo.2018.00384

Orkin, C., Squires, K., Molina, J.-M., Sax, P., Wong, W., Sussmann, O., Lin, G., Kumar, S., Hanna, G., Hwang, C., Martin, E., & Teppler, H. (2018). LB1. Doravirine/Lamivudine/Tenofovir DF Continues to Be NonInferior to Efavirenz/Emtricitabine/Tenofovir DF in Treatment-Naïve Adults With HIV-1 Infection: Week 96 Results of the DRIVE-AHEAD Trial. *Open Forum Infectious Diseases, 5*(suppl_1), S759-S759. doi:10.1093/ofid/ofy229.2175

Paengsai, N., Jourdain, G., Salvadori, N., Tantraworasin, A., Mary, J. Y., Cressey, T. R., Chaiwarith, R., Bowonwatanuwong, C., Bhakeecheep, S., & Kosachunhanun, N. (2019). Recommended First-Line Antiretroviral Therapy Regimens and Risk of Diabetes Mellitus in HIV-Infected Adults in Resource-Limited Settings. *Open Forum Infectious Diseases, 6*(10), ofz298-ofz298. doi:10.1093/ofid/ofz298

Pakoskey, A. M., Lesher, E. C., & Scott, D. B. (1965). Hexokinase of Escherichia coli. Assay of enzyme activity and adaptation to growth in various media. *Journal of General Microbiology, 38*, 73-80. doi:10.1099/00221287-38-1-73

Palacios, R., Santos, J., Ruiz, J., González, M., & Márquez, M. (2003). Factors associated with the development of diabetes mellitus in HIV-infected patients on antiretroviral therapy: A case-control study [2]. *AIDS, 17*(6), 933-935. doi:10.1097/00002030-200304110-00025

Palmer, K. J., & Brogden, R. N. (1993). Gliclazide. An update of its pharmacological properties and therapeutic efficacy in non-insulin-dependent diabetes mellitus. *Drugs, 46*(1), 92-125. doi:10.2165/00003495-199346010-00007

Park, J., Lee, J., & Choi, C. (2011). Mitochondrial Network Determines Intracellular ROS Dynamics and Sensitivity to Oxidative Stress through Switching Inter-Mitochondrial Messengers. *PLoS ONE, 6*(8), e23211. doi:10.1371/journal.pone.0023211

Patková, J., Anděl, M., & Trnka, J. (2014). Palmitate-Induced Cell Death and Mitochondrial Respiratory Dysfunction in Myoblasts are Not Prevented by Mitochondria-Targeted Antioxidants. *Cellular Physiology and Biochemistry, 33*(5), 1439-1451. doi:10.1159/000358709

Paucek, P., Mironova, G., Mahdi, F., Beavis, A. D., Woldegiorgis, G., & Garlid, K. D. (1992). Reconstitution and partial purification of the glibenclamide-sensitive, ATP-dependent K+ channel from rat liver and beef heart mitochondria. *The Journal of biological chemistry, 267*(36), 26062-26069.

Pérez-Matute, P., Pérez-Martínez, L., Blanco, J. R., & Oteo, J. A. (2013). Role of Mitochondria in HIV Infection and Associated Metabolic Disorders: Focus on Nonalcoholic Fatty Liver Disease and Lipodystrophy Syndrome. *Oxidative medicine and cellular longevity, 2013*, 493413-493413. doi:10.1155/2013/493413

Peters, B., Post, F., Wierzbicki, A., Phillips, A., Power, L., Das, S., Johnson, M., Moyle, G., Hughes, L., Wilkins, E., McCloskey, E., Compston, J., & Di Angelantonio, E. (2013). Screening for chronic comorbid diseases in people with HIV: the need for a strategic approach. *HIV Medicine, 14*(S1), 1-11. doi:10.1111/j.1468-1293.2012.01055.x

Pettersen, E. F., Goddard, T. D., Huang, C. C., Couch, G. S., Greenblatt, D. M., Meng, E. C., & Ferrin, T. E. (2004). UCSF Chimera—A visualization system for exploratory research and analysis. *Journal of Computational Chemistry, 25*(13), 1605-1612. doi:https://doi.org/10.1002/jcc.20084

Pham-Huy, L. A., He, H., & Pham-Huy, C. (2008). Free radicals, antioxidants in disease and health. *International Journal of Biomedical Science, 4*(2), 89-96.

Phielix, E., & Mensink, M. (2008). Type 2 Diabetes Mellitus and Skeletal Muscle Metabolic Function. *Physiology & Behavior, 94*(2), 252-258. doi:10.1016/j.physbeh.2008.01.020

Pi, J., Bai, Y., Zhang, Q., Wong, V., Floering, L. M., Daniel, K., Reece, J. M., Deeney, J. T., Andersen, M. E., Corkey, B. E., & Collins, S. (2007a). Reactive Oxygen Species as a Signal in Glucose-Stimulated Insulin Secretion. *Diabetes, 56*(7), 1783-1791. doi:10.2337/db06-1601

Pi, J., Bai, Y., Zhang, Q., Wong, V., Floering, L. M., Daniel, K., Reece, J. M., Deeney, J. T., Andersen, M. E., Corkey, B. E., & Collins, S. (2007b). Reactive oxygen species as a signal in glucose-stimulated insulin secretion. *Diabetes, 56*(7), 1783-1791. doi:10.2337/db06-1601

Poitout, V., Amyot, J., Semache, M., Zarrouki, B., Hagman, D., & Fontés, G. (2010a). Glucolipotoxicity of the pancreatic beta cell. *Biochimica et biophysica acta, 1801*(3), 289-298. doi:10.1016/j.bbalip.2009.08.006

Poitout, V., Amyot, J., Semache, M., Zarrouki, B., Hagman, D., & Fontés, G. (2010b). Glucolipotoxicity of the pancreatic beta cell. *Biochimica et biophysica acta, 1801*(3), 289-298. doi:10.1016/j.bbalip.2009.08.006

Poitout, V., & Robertson, R. P. (2008). Glucolipotoxicity: Fuel Excess and β-Cell Dysfunction. *Endocrine Reviews, 29*(3), 351-366. doi:10.1210/er.2007-0023

Proks, P., Antcliff, J. F., Lippiat, J., Gloyn, A. L., Hattersley, A. T., & Ashcroft, F. M. (2004). Molecular basis of Kir6.2 mutations associated with neonatal diabetes or neonatal diabetes plus neurological features. *Proceedings of the National Academy of Sciences of the United States of America, 101*(50), 17539-17544. doi:10.1073/pnas.0404756101

Public Health England. (2019). *HIV in the United Kingdom: Towards Zero HIV transmissions by 2030* Retrieved from https://assets.publishing.service.gov.uk/government/uploads/system/uploads/attachment_data/file/858559/HIV_in_the_UK_2019_towards_zero_HIV_transmissions_by_2030.pdf

Ramamoorthy, H., Abraham, P., Isaac, B., & Selvakumar, D. (2019). Mitochondrial pathway of apoptosis and necrosis contribute to tenofovir disoproxil fumarate-induced renal damage in rats. *Human & Experimental Toxicology, 38*(3), 288-302. doi:10.1177/0960327118802619

Rebeiro, P. F., Jenkins, C. A., Bian, A., Lake, J. E., Bourgi, K., Moore, R. D., Horberg, M. A., Matthews, W. C., Silverberg, M. J., Thorne, J., Mayor, A. M., Lima, V. D., Palella, F. J., Saag, M. S., Althoff, K. N., Gill, M. J., Wong, C., Klein, M. B., Crane, H. M., Marconi, V. C., Shepherd, B. E., Sterling, T. R., & Koethe, J. R. (2021). Risk of Incident Diabetes Mellitus, Weight Gain, and Their Relationships With Integrase Inhibitor-Based Initial Antiretroviral Therapy Among Persons With Human Immunodeficiency Virus in the United States and Canada. *Clinical infectious diseases : an official publication of the Infectious Diseases Society of America, 73*(7), e2234-e2242. doi:10.1093/cid/ciaa1403

Re, R., Pellegrini, N., Proteggente, A., Pannala, A., Yang, M., & Rice-Evans, C. (1999). Antioxidant activity applying an improved ABTS radical cation decolorization assay. *Free radical biology & medicine, 26*(9-10), 1231–1237. https://doi.org/10.1016/s0891-5849(98)00315-3

Reeves, I., , B. C., , J. D., , R. D., , M. K., , C. T., , J., Thornhill, , M. T.-P., & , C. v. H. (2021). *British HIV Association guidelines for the management of HIV-2 2021*. Retrieved from https://www.bhiva.org/file/615ee3de98539/BHIVA-guidelines-for-the-management-of-HIV-2.pdf

Rhodes, C. J. (2005). Type 2 diabetes-a matter of beta-cell life and death? *Science, 307*(5708), 380-384. doi:10.1126/science.1104345

Richards, S. K., Parton, L. E., Leclerc, I., Rutter, G. A., & Smith, R. M. (2005). Over-expression of AMP-activated protein kinase impairs pancreatic β-cell function in vivo. *Journal of Endocrinology, 187*(2), 225-235. doi:10.1677/joe.1.06413

Ripamonti, D., Bombana, E., & Rizzi, M. (2014). Rilpivirine: drug profile of a second-generation non-nucleoside reverse transcriptase HIV-inhibitor. *Expert Review of Anti-Infective Therapy, 12*(1), 13-29. doi:http://dx.doi.org/10.1586/14787210.2014.863708

Roberts, H. (2016). Modelling hiv dynamics and evolution: prospects for viral control. Retrieved from https://ora.ox.ac.uk/objects/uuid:1e2c153f-bd52-4da2-a1d2-47008687fd09/download_file?file_format=application%2Fpdf&safe_filename=Hannah_Roberts_Thesis_toprint.pdf&type_of_work=Thesis

Robertson, R. P., Harmon, J., Tran, P. O. T., & Poitout, V. (2004). β-cell glucose toxicity, lipotoxicity, and chronic oxidative stress in type 2 diabetes. *Diabetes, 53*(suppl 1), S119-S124.

Robertson, R. P., & Harmon, J. S. (2007). Pancreatic islet β-cell and oxidative stress: The importance of glutathione peroxidase. *FEBS Letters, 581*(19), 3743-3748. doi:https://doi.org/10.1016/j.febslet.2007.03.087

Robinson, A. J., & Gazzard, B. G. (2005). Rising rates of HIV infection. *Bmj, 330*(7487), 320-321. doi:10.1136/bmj.330.7487.320

Robinson, H. L. (2018). HIV/AIDS Vaccines: 2018. *Clinical Pharmacology & Therapeutics, 104*(6), 1062-1073. doi:https://doi.org/10.1002/cpt.1208

Rock, A. E., Lerner, J., & Badowski, M. E. (2020). Doravirine and Its Potential in the Treatment of HIV: An Evidence-Based Review of the Emerging Data. *HIV/AIDS (Auckland, N.Z.), 12*, 201-210. doi:10.2147/hiv.S184018

Ross, D. A. (2010). Behavioural interventions to reduce HIV risk: what works? *AIDS, 24 Suppl 4*, S4-14. doi:10.1097/01.aids.0000390703.35642.89

Saag, M. S., Cahn, P., Raffi, F., Wolff, M., Pearce, D., Molina, J.-M., Powderly, W., Shaw, A. L., Mondou, E., Hinkle, J., Borroto-Esoda, K., Quinn, J. B., Barry, D. W., Rousseau, F., & Team, f. t. F.-A. S. (2004). Efficacy and Safety of Emtricitabine vs Stavudine in Combination Therapy in Antiretroviral-Naive PatientsA Randomized Trial. *JAMA, 292*(2), 180-189. doi:10.1001/jama.292.2.180

Sachdeva, M. M., Claiborn, K. C., Khoo, C., Yang, J., Groff, D. N., Mirmira, R. G., & Stoffers, D. A. (2009). Pdx1 (MODY4) regulates pancreatic beta cell susceptibility to ER stress. *Proceedings of the National Academy of Sciences, 106*(45), 19090-19095. doi:10.1073/pnas.0904849106

Sack M. N. (2006). Mitochondrial depolarization and the role of uncoupling proteins in ischemia tolerance. *Cardiovascular research, 72*(2), 210–219. https://doi.org/10.1016/j.cardiores.2006.07.010

Samaras, K. (2009). Prevalence and Pathogenesis of Diabetes Mellitus in HIV-1 Infection Treated With Combined Antiretroviral Therapy. *JAIDS Journal of Acquired Immune Deficiency Syndromes, 50*(5), 499-505. doi:10.1097/QAI.0b013e31819c291b

Sánchez-Cenizo, L., Formentini, L., Aldea, M., Ortega, Á. D., García-Huerta, P., Sánchez-Aragó, M., & Cuezva, J. M. (2010). Up-regulation of the ATPase inhibitory factor 1 (IF1) of the mitochondrial H+-ATP synthase in human tumors mediates the metabolic shift of cancer cells to a Warburg phenotype. *Journal of Biological Chemistry, 285*(33), 25308-25313. doi:10.1074/jbc.M110.146480

Sargsyan, E., & Bergsten, P. (2011). Lipotoxicity is glucose-dependent in INS-1E cells but not in human islets and MIN6 cells. *Lipids in Health and Disease, 10*(1), 115. doi:10.1186/1476-511X-10-115

Scarlett, J. L., Sheard, P. W., Hughes, G., Ledgerwood, E. C., Ku, H.-H., & Murphy, M. P. (2000). Changes in mitochondrial membrane potential during staurosporine-induced apoptosis in Jurkat cells. *FEBS Letters, 475*(3), 267-272. doi:https://doi.org/10.1016/S0014-5793(00)01681-1

Schütt, M., Meier, M., Meyer, M., Klein, J., Aries, S. P., & Klein, H. H. (2000). The HIV-1 protease inhibitor indinavir impairs insulin signalling in HepG2 hepatoma cells. *DIABETOLOGIA, 43*(9), 1145-1148. doi:10.1007/s001250051505

Schwarz, J.-M., Lee, G. A., Park, S., Noor, M. A., Lee, J., Wen, M., Lo, J. C., Mulligan, K., Schambelan, M., & Grunfeld, C. (2004). Indinavir increases glucose production in healthy HIV-negative men. *AIDS, 18*(13), 1852-1854. doi:10.1097/00002030-200409030-00017

Segerstolpe, Å., Palasantza, A., Eliasson, P., Andersson, E.-M., Andréasson, A.-C., Sun, X., Picelli, S., Sabirsh, A., Clausen, M., Bjursell, M. K., Smith, David M., Kasper, M., Ämmälä, C., & Sandberg, R. (2016). Single-Cell Transcriptome Profiling of Human Pancreatic Islets in Health and Type 2 Diabetes. *Cell Metabolism, 24*(4), 593-607. doi:10.1016/j.cmet.2016.08.020

Sension, M., & Deckx, H. (2015). Lipid metabolism and lipodystrophy in HIV-1-infected patients: the role played by nonnucleoside reverse transcriptase inhibitors. *AIDS Reviews, 17*(1), 21-36.

Sezgin, E., Van Natta, M. L., Thorne, J. E., Puhan, M. A., Jabs, D. A., & the Longitudinal Studies of the Ocular Complications of, A. R. G. (2018). Secular trends in opportunistic infections, cancers and mortality in patients with AIDS during the era of modern combination antiretroviral therapy. *HIV Medicine, 19*(6), 411-419. doi:https://doi.org/10.1111/hiv.12609

Sha, W., Hu, F., & Bu, S. (2020). Mitochondrial dysfunction and pancreatic islet β-cell failure (Review). *Experimental and Therapeutic Medicine, 20*(6), 266. doi:10.3892/etm.2020.9396

Sharma, A., Zangen, D. H., Reitz, P., Taneja, M., Lissauer, M. E., Miller, C. P., Weir, G. C., Habener, J. F., & Bonner-Weir, S. (1999). The homeodomain protein IDX-1 increases after an early burst of proliferation during pancreatic regeneration. *Diabetes, 48*(3), 507-513. doi:10.2337/diabetes.48.3.507

Sharma, M., & Saravolatz, L. D. (2012). Rilpivirine: a new non-nucleoside reverse transcriptase inhibitor. *Journal of Antimicrobial Chemotherapy, 68*(2), 250-256. doi:10.1093/jac/dks404

Sharp, P. M., & Hahn, B. H. (2011). Origins of HIV and the AIDS pandemic. *Cold Spring Harb Perspect Med, 1*(1), a006841. doi:10.1101/cshperspect.a006841

Shubber, Z., Calmy, A., Andrieux-Meyer, I., Vitoria, M., Renaud-Thery, F., Shaffer, N., Hargreaves, S., Mills, E. J., & Ford, N. (2013). Adverse events associated with nevirapine and efavirenz-based first-line antiretroviral therapy: a systematic review and meta-analysis. *AIDS, 27*(9), 1403-1412. doi:10.1097/QAD.0b013e32835f1db0

Shyng, S., Ferrigni, T., & Nichols, C. G. (1997). Regulation of KATP channel activity by diazoxide and MgADP. Distinct functions of the two nucleotide binding folds of the sulfonylurea receptor. The *Journal of General Physiology, 110*(6), 643-654. doi:10.1085/jgp.110.6.643

Sico, J. J., Chang, C.-C. H., So-Armah, K., Justice, A. C., Hylek, E., Skanderson, M., McGinnis, K., Kuller, L. H., Kraemer, K. L., Rimland, D., Bidwell Goetz, M., Butt, A. A., Rodriguez-Barradas, M. C., Gibert, C., Leaf, D., Brown, S. T., Samet, J., Kazis, L., Bryant, K., & Freiberg, M. S. (2015). HIV status and the risk of ischemic stroke among men. *Neurology, 84*(19), 1933-1940. doi:10.1212/wnl.0000000000001560

Skelin Klemen, M., Dolenšek, J., Slak Rupnik, M., & Stožer, A. (2017). The triggering pathway to insulin secretion: Functional similarities and differences between the human and the mouse β cells and their translational relevance. *Islets, 9*(6), 109-139. doi:10.1080/19382014.2017.1342022

Skuratovskaia, D., Komar, A., Vulf, M., & Litvinova, L. (2020). Mitochondrial destiny in type 2 diabetes: the effects of oxidative stress on the dynamics and biogenesis of mitochondria. *PeerJ, 8*, e9741. doi:10.7717/peerj.9741

Sliwinska, A., Rogalska, A., Szwed, M., Kasznicki, J., Jozwiak, Z., & Drzewoski, J. (2012). Gliclazide may have an antiapoptotic effect related to its antioxidant properties in human normal and cancer cells. *Molecular Biology Reports, 39*(5), 5253-5267. doi:10.1007/s11033-011-1323-z

Sobczak, A., Blindauer, C., & Stewart, A. (2019). Changes in Plasma Free Fatty Acids Associated with Type-2 Diabetes. *Nutrients, 11*(9), 2022. doi:10.3390/nu11092022

Sola, D., Rossi, L., Schianca, G. P., Maffioli, P., Bigliocca, M., Mella, R., Corlianò, F., Fra, G. P., Bartoli, E., & Derosa, G. (2015). Sulfonylureas and their use in clinical practice. *Arch Med Sci, 11*(4), 840-848. doi:10.5114/aoms.2015.53304

Sommerweiss, D., Gorski, T., Richter, S., Garten, A., & Kiess, W. (2013). Oleate rescues INS-1E β-cells from palmitate-induced apoptosis by preventing activation of the unfolded protein response. *Biochemical and Biophysical Research Communications, 441*(4), 770-776. doi:https://doi.org/10.1016/j.bbrc.2013.10.130

Song, H., Wohltmann, M., Tan, M., Ladenson, J., & Turk, J. (2014). Group VIA Phospholipase A2 Mitigates Palmitate-Induced Beta Cell Mitochondrial Injury and Apoptosis. *The Journal of biological chemistry, 289*. doi:10.1074/jbc.M114.561910

Spinazzi, M., Casarin, A., Pertegato, V., Salviati, L., & Angelini, C. (2012). Assessment of mitochondrial respiratory chain enzymatic activities on tissues and cultured cells. *Nature Protocols, 7*(6), 1235-1246. doi:10.1038/nprot.2012.058

Šrámek, J., Němcová-Fürstová, V., & Kovář, J. (2021). Molecular Mechanisms of Apoptosis Induction and Its Regulation by Fatty Acids in Pancreatic β-Cells. *International Journal of Molecular Sciences, 22*(8). doi:10.3390/ijms22084285

Stauch, K. L., Emanuel, K., Lamberty, B. G., Morsey, B., & Fox, H. S. (2017). Central nervous system-penetrating antiretrovirals impair energetic reserve in striatal nerve terminals. *Journal of neurovirology, 23*(6), 795-807. doi:10.1007/s13365-017-0573-5

Streck, E. L., Ferreira, G. K., Scaini, G., Rezin, G. T., Gonçalves, C. L., Jeremias, I. C., Zugno, A. I., Ferreira, G. C., Moreira, J., & Fochesato, C. M. (2011). Non-nucleoside reverse transcriptase inhibitors efavirenz and nevirapine inhibit cytochrome C oxidase in mouse brain regions. *Neurochemical research, 36*(6), 962-966.

Sulkowski, M. S. (2004). Drug-Induced Liver Injury Associated with Antiretroviral Therapy that Includes HIV-1 Protease Inhibitors. *Clinical Infectious Diseases, 38*(Supplement_2), S90-S97. doi:10.1086/381444

Summers, S. A., Whiteman, E. L., & Birnbaum, M. J. (2000). Insulin signaling in the adipocyte. *International Journal of Obesity, 24*(S4), S67-S70. doi:10.1038/sj.ijo.0801509

Sun, J., Cui, J., He, Q., Chen, Z., Arvan, P., & Liu, M. (2015). Proinsulin misfolding and endoplasmic reticulum stress during the development and progression of diabetes☆. *Molecular aspects of medicine, 42*, 105-118. doi:https://doi.org/10.1016/j.mam.2015.01.001

Szabadkai, G., & Duchen, M. R. (2009). Mitochondria mediated cell death in diabetes. *Apoptosis, 14*(12), 1405-1423. doi:10.1007/s10495-009-0363-5

Szeto, V., Chen, N.-h., Sun, H.-s., & Feng, Z.-p. (2018). The role of KATP channels in cerebral ischemic stroke and diabetes. *Acta Pharmacologica Sinica, 39*(5), 683-694. doi:10.1038/aps.2018.10

Tate, T., Willig, A. L., Willig, J. H., Raper, J. L., Moneyham, L., Kempf, M.-C., Saag, M. S., & Mugavero, M. J. (2012). HIV infection and obesity: where did all the wasting go? *Antiviral Therapy, 17*(7), 1281-1289. doi:10.3851/IMP2348

Tebas, P. (2008). Insulin Resistance and Diabetes Mellitus Associated With Antiretroviral Use in HIV-Infected Patients: Pathogenesis, Prevention, and Treatment Options. *JAIDS Journal of Acquired Immune Deficiency Syndromes, 49 Suppl 2, HIV and Cardiometabolic Abnormalities: New Perspectives and Treatment Update*(Supplement 2), S86-S92. doi:10.1097/QAI.0b013e31818651e6

Terelius, Y., Figler, R. A., Marukian, S., Collado, M. S., Lawson, M. J., Mackey, A. J., Manka, D., Qualls, C. W., Blackman, B. R., Wamhoff, B. R., & Dash, A. (2016). Transcriptional profiling

suggests that Nevirapine and Ritonavir cause drug induced liver injury through distinct mechanisms in primary human hepatocytes. *Chemico-Biological Interactions, 255*, 31-44. doi:https://doi.org/10.1016/j.cbi.2015.11.023

Thamrongwonglert, P., Chetchotisakd, P., Anunnatsiri, S., & Mootsikapun, P. (2016). Improvement of lipid profiles when switching from efavirenz to rilpivirine in HIV-infected patients with dyslipidemia. *HIV Clinical Trials, 17*(1), 12-16. doi:10.1080/15284336.2015.1112480

Thigpen, M. C., Kebaabetswe, P. M., Paxton, L. A., Smith, D. K., Rose, C. E., Segolodi, T. M., Henderson, F. L., Pathak, S. R., Soud, F. A., Chillag, K. L., Mutanhaurwa, R., Chirwa, L. I., Kasonde, M., Abebe, D., Buliva, E., Gvetadze, R. J., Johnson, S., Sukalac, T., Thomas, V. T., Hart, C., Johnson, J. A., Malotte, C. K., Hendrix, C. W., & Brooks, J. T. (2012). Antiretroviral preexposure prophylaxis for heterosexual HIV transmission in Botswana. *The New England Journal of Medicine, 367*(5), 423-434. doi:10.1056/NEJMoa1110711

Thomas L. (1971). Notes of a biology-watcher. The lives of a cell. *The New England journal of medicine*, *284*(19), 1082–1083.

Tien, P. C., Schneider, M. F., Cole, S. R., Levine, A. M., Cohen, M., DeHovitz, J., Young, M., & Justman, J. E. (2007). Antiretroviral therapy exposure and incidence of diabetes mellitus in the Women's Interagency HIV Study. *AIDS, 21*(13). Retrieved from https://journals.lww.com/aidsonline/Fulltext/2007/08200/Antiretroviral_therapy_exposure_and_incidence_of.9.aspx

Tripathi, A., Liese, A. D., Jerrell, J. M., Zhang, J., Rizvi, A. A., Albrecht, H., & Duffus, W. A. (2014). Incidence of diabetes mellitus in a population-based cohort of HIV-infected and non-HIV-infected persons: the impact of clinical and therapeutic factors over time. *Diabetic Medicine, 31*(10), 1185-1193. doi:10.1111/dme.12455

Turpin, J., Frumence, E., El Safadi, D., Meilhac, O., Krejbich-Trotot, P., & Viranaïcken, W. (2020). Improvement of immunodetection of the transcription factor C/EBP homologous protein by western blot. *Analytical biochemistry, 601*, 113775. doi:https://doi.org/10.1016/j.ab.2020.113775

U.K Prospective Diabetes Study Group. (1995). U.K. Prospective Diabetes Study 16: Overview of 6 Years' Therapy of Type II Diabetes: A Progressive Disease. *Diabetes, 44*(11), 1249. doi:10.2337/diab.44.11.1249

Urbano, F., Filippello, A., Di Pino, A., Barbagallo, D., Di Mauro, S., Pappalardo, A., Rabuazzo, A. M., Purrello, M., Purrello, F., & Piro, S. (2016). Altered expression of uncoupling protein 2 in GLP-1-producing cells after chronic high glucose exposure: implications for the pathogenesis of diabetes mellitus. *American Journal of Physiology-Cell Physiology, 310*(7), C558-C567. doi:10.1152/ajpcell.00148.2015

Usach, I., Melis, V., & José-Esteban, P. (2013). Non-nucleoside reverse transcriptase inhibitors: a review on pharmacokinetics, pharmacodynamics, safety and tolerability. *Journal of the International AIDS Society, 16*(1).

van Leth, F., Phanuphak, P., Ruxrungtham, K., Baraldi, E., Miller, S., Gazzard, B., Cahn, P., Lalloo, U. G., van der Westhuizen, I. P., Malan, D. R., Johnson, M. A., Santos, B. R., Mulcahy, F., Wood, R., Levi, G. C., Reboredo, G., Squires, K., Cassetti, I., Petit, D., Raffi, F., Katlama, C., Murphy, R. L., Horban, A., Dam, J. P., Hassink, E., van Leeuwen, R., Robinson, P., Wit, F. W., & Lange, J. M. A. (2004). Comparison of first-line antiretroviral therapy with regimens including nevirapine, efavirenz, or both drugs, plus stavudine and lamivudine: a randomised open-label trial, the 2NN Study. *The Lancet, 363*(9417), 1253-1263. doi:https://doi.org/10.1016/S0140-6736(04)15997-7

Varadi, A., Grant, A., McCormack, M., Nicolson, T., Magistri, M., Mitchell, K. J., Halestrap, A. P., Yuan, H., Schwappach, B., & Rutter, G. A. (2006). Intracellular ATP-sensitive K+ channels in mouse pancreatic beta cells: against a role in organelle cation homeostasis. *Diabetologia, 49*(7), 1567-1577. doi:10.1007/s00125-006-0257-9

Vella, S., Schwartländer, B., Sow, S. P., Eholie, S. P., & Murphy, R. L. (2012). The history of antiretroviral therapy and of its implementation in resource-limited areas of the world. *AIDS, 26*(10), 1231-1241. doi:10.1097/QAD.0b013e32835521a3

Venhoff, N., Setzer, B., Melkaoui, K., & Walker, U. A. (2007). Mitochondrial toxicity of tenofovir, emtricitabine and abacavir alone and in combination with additional nucleoside reverse transcriptase inhibitors. *Antiviral Therapy, 12*(7), 1075-1085.

Vial, G., Detaille, D., & Guigas, B. (2019). Role of Mitochondria in the Mechanism(s) of Action of Metformin. *Frontiers in Endocrinology, 10*. doi:10.3389/fendo.2019.00294

Vigouroux, C., Gharakhanian, S., Salhi, Y., Nguyên, T. H., Adda, N., Rozenbaum, W., & Capeau, J. (1999). Adverse metabolic disorders during highly active antiretroviral treatments (HAART) of HIV disease. *Diabetes and Metabolism, 25*(5), 383-392.

Virág, L., Robaszkiewicz, A., Rodriguez-Vargas, J. M., & Oliver, F. J. (2013). Poly(ADP-ribose) signaling in cell death. *Molecular aspects of medicine, 34*(6), 1153-1167. doi:https://doi.org/10.1016/j.mam.2013.01.007

Volpe, C. M. O., Villar-Delfino, P. H., Dos Anjos, P. M. F., & Nogueira-Machado, J. A. (2018). Cellular death, reactive oxygen species (ROS) and diabetic complications. *Cell Death & Disease, 9*(2), 119. doi:10.1038/s41419-017-0135-z

Waki, H., & Tontonoz, P. (2007). Endocrine functions of adipose tissue. *Annual review of pathology, 2*, 31–56. https://doi.org/10.1146/annurev.pathol.2.010506.091859

Walczewska-Szewc, K., & Nowak, W. (2021). Photo-Switchable Sulfonylureas Binding to ATP-Sensitive Potassium Channel Reveal the Mechanism of Light-Controlled Insulin Release. *The Journal of Physical Chemistry B, 125*(48), 13111-13121. doi:10.1021/acs.jpcb.1c07292

Wang, J., & Wang, H. (2017). Oxidative Stress in Pancreatic Beta Cell Regeneration. *Oxidative medicine and cellular longevity, 2017*, 1930261-1930261. doi:10.1155/2017/1930261

Watada, H., Kajimoto, Y., Umayahara, Y., Matsuoka, T.-a., Kaneto, H., Fujitani, Y., Kamada, T., Kawamori, R., & Yamasaki, Y. (1996). The Human Glucokinase Gene β-Cell-Type Promoter: An Essential Role of Insulin Promoter Factor 1/PDX-1 in Its Activation in HIT-T15 Cells. *Diabetes, 45*(11), 1478-1488. doi:10.2337/diab.45.11.1478

Waters, L., N Ahmed, B. A., M Boffito, M Bower, D Churchill, D Dunn, S Edwards, C Emerson, S Fidler, M Fisher, R, Horne, S. K., C Leen, N Mackie, N Marshall, F Monteiro, M Nelson, C Orkin, A Palfreeman, S Pett, A Phillips,, & F Post, A. P., I Reeves, C Sabin, R Trevelion, J Walsh, E Wilkins, I Williams, A Winston. (2016). *BHIVA guidelines for the treatment of HIV-1-positive adults with ART 2015 (2016 interim update)*. Retrieved from

Watson, M. L., Macrae, K., Marley, A. E., & Hundal, H. S. (2011). Chronic Effects of Palmitate Overload on Nutrient-Induced Insulin Secretion and Autocrine Signalling in Pancreatic MIN6 Beta Cells. *PLoS ONE, 6*(10), e25975. doi:10.1371/journal.pone.0025975

Weber, R., & Sabin, C. (2006). Friis-M0ller N, et al. Liver-related deaths in persons infected with the human immunodeficiency virus: The D: A: D study. *Archives of internal medicine, 166*(15), 1632-1641.

Weiß, M., Kost, B., Renner-Müller, I., Wolf, E., Mylonas, I., & Brüning, A. (2016a). Efavirenz Causes Oxidative Stress, Endoplasmic Reticulum Stress, and Autophagy in Endothelial Cells. *Cardiovascular Toxicology, 16*(1), 90-99. doi:10.1007/s12012-015-9314-2

Weiß, M., Kost, B., Renner-Müller, I., Wolf, E., Mylonas, I., & Brüning, A. (2016b). Efavirenz causes oxidative stress, endoplasmic reticulum stress, and autophagy in endothelial cells. *Cardiovascular Toxicology, 16*(1), 90-99.

Welters, H. J., Diakogiannaki, E., Mordue, J. M., Tadayyon, M., Smith, S. A., & Morgan, N. G. (2006). Differential protective effects of palmitoleic acid and cAMP on caspase activation and cell viability in pancreatic beta-cells exposed to palmitate. *Apoptosis, 11*(7), 1231-1238. doi:10.1007/s10495-006-7450-7

Welters, H. J., Tadayyon, M., Scarpello, J. H. B., Smith, S. A., & Morgan, N. G. (2004). Mono-unsaturated fatty acids protect against β-cell apoptosis induced by saturated fatty acids, serum withdrawal or cytokine exposure. *FEBS Letters, 560*(1), 103-108. doi:https://doi.org/10.1016/S0014-5793(04)00079-1

Wise, J. (2014). HIV pandemic originated in Kinshasa around 1920, say scientists. *BMJ : British Medical Journal, 349*, g5967. doi:10.1136/bmj.g5967

Wit, S. D., Sabin, C. A., Weber, R., Worm, S. W., Reiss, P., Cazanave, C., El-Sadr, W., Monforte, A. d. A., Fontas, E., Law, M. G., Friis-Møller, N., & Phillips, A. (2008). Incidence and Risk Factors for New-Onset Diabetes in HIV-Infected Patients. *Diabetes Care, 31*(6), 1224-1229. doi:10.2337/dc07-2013

Woerle, H. J., Mariuz, P. R., Meyer, C., Reichman, R. C., Popa, E. M., Dostou, J. M., Welle, S. L., & Gerich, J. E. (2003). Mechanisms for the Deterioration in Glucose Tolerance Associated With HIV Protease Inhibitor Regimens. *Diabetes, 52*(4), 918-925. doi:10.2337/diabetes.52.4.918

World Health Organization. (2016). *Global Report on Diabetes*. Retrieved from

World Health Organization. (2020). HIV/AIDS. Retrieved from https://www.who.int/news-room/fact-sheets/detail/hiv-aids

World Health Organization. (2021a). *Consolidated guidelines on HIV prevention, testing, treatment, service delivery and monitoring: recommendations for a public health approach*. Retrieved from file:///C:/Users/Owner/Downloads/9789240031593-eng%20(1).pdf

World Health Organization. (2021b). Obesity and overweight. Retrieved from https://www.who.int/news-room/fact-sheets/detail/obesity-and-overweight

World Health Organization. (2022). HIV. Retrieved from https://www.who.int/news-room/fact-sheets/detail/hiv-aids

Wrede, C. E., Dickson, L. M., Lingohr, M. K., Briaud, I., & Rhodes, C. J. (2002). Protein Kinase B/Akt Prevents Fatty Acid-induced Apoptosis in Pancreatic β-Cells (INS-1). *Journal of Biological Chemistry, 277*(51), 49676-49684. doi:10.1074/jbc.M208756200

Wu, Z. S., Huang, S. M., & Wang, Y. C. (2021). Palmitate Enhances the Efficacy of Cisplatin and Doxorubicin against Human Endometrial Carcinoma Cells. *International Journal of Molecular Science, 23*(1). doi:10.3390/ijms23010080

Xue, S. Y., Hebert, V. Y., Hayes, D. M., Robinson, C. N., Glover, M., & Dugas, T. R. (2013). Nucleoside reverse transcriptase inhibitors induce a mitophagy-associated endothelial cytotoxicity that is reversed by coenzyme Q10 cotreatment. *Toxicological sciences : an official journal of the Society of Toxicology, 134*(2), 323-334. doi:10.1093/toxsci/kft105

Yan, Q., & Hruz, P. W. (2005). Direct Comparison of the Acute In Vivo Effects of HIV Protease Inhibitors on Peripheral Glucose Disposal. *JAIDS Journal of Acquired Immune Deficiency Syndromes, 40*(4), 398-403. doi:10.1097/01.qai.0000176654.97392.c7

Yang, H.-Q., Martinez-Ortiz, W., Hwang, J., Fan, X., Cardozo, T. J., & Coetzee, W. A. (2020). Palmitoylation of the KATP channel Kir6.2 subunit promotes channel opening by regulating PIP2 sensitivity. *Proceedings of the National Academy of Sciences, 117*(19), 10593-10602. doi:10.1073/pnas.1918088117

Yang, W., Yang, G., Jia, X., Wu, L., & Wang, R. (2005). Activation of KATP channels by H2S in rat insulin-secreting cells and the underlying mechanisms. *The Journal of Physiology, 569*(2), 519-531. doi:https://doi.org/10.1113/jphysiol.2005.097642

Yang, Y., Kang, D., Nguyen, L. A., Smithline, Z. B., Pannecouque, C., Zhan, P., Liu, X., & Steitz, T. A. (2018). Structural basis for potent and broad inhibition of HIV-1 RT by thiophene[3,2-d]pyrimidine non-nucleoside inhibitors. *eLife, 7*, e36340. doi:10.7554/eLife.36340

Yarasheski, K. E., Tebas, P., Sigmund, C., Dagogo-Jack, S., Bohrer, A., Turk, J., Halban, P. A., Cryer, P. E., & Powderly, W. G. (1999). Insulin resistance in HIV protease inhibitor-associated diabetes. *J Acquired Immune Deficiency Syndromes, 21*(3), 209-216. doi:10.1097/00126334-199907010-00005

Yee Ka, L., Sanchez Rosa, I., Auger, P., Liu, R., Fan, L., Triantafyllou, I., Lai, M.-T., Di Spirito, M., Iwamoto, M., & Khalilieh Sauzanne, G. (2017). Evaluation of Doravirine Pharmacokinetics When Switching from Efavirenz to Doravirine in Healthy Subjects. *Antimicrobial agents and chemotherapy, 61*(2), e01757-01716. doi:10.1128/AAC.01757-16

Yuan, H., Zhang, X., Huang, X., Lu, Y., Tang, W., Man, Y., Wang, S., Xi, J., & Li, J. (2010). NADPH Oxidase 2-Derived Reactive Oxygen Species Mediate FFAs-Induced Dysfunction and Apoptosis of β-Cells via JNK, p38 MAPK and p53 Pathways. *PLoS ONE, 5*(12), e15726. doi:10.1371/journal.pone.0015726

Zaccardi, F., Webb, D. R., Yates, T., & Davies, M. J. (2016). Pathophysiology of type 1 and type 2 diabetes mellitus: a 90-year perspective. *Postgraduate Medical Journal, 92*(1084), 63-69. doi:10.1136/postgradmedj-2015-133281

Zhang, C.-Y., Baffy, G., Perret, P., Krauss, S., Peroni, O., Grujic, D., Hagen, T., Vidal-Puig, A. J., Boss, O., Kim, Y.-B., Zheng, X. X., Wheeler, M. B., Shulman, G. I., Chan, C. B., & Lowell, B. B. (2001). Uncoupling protein-2 negatively regulates insulin secretion and is a major link between obesity, beta cell dysfunction, and type 2 diabetes. *Cell, 105*(6), 745-755. doi:10.1016/S0092-8674(01)00378-6

Zhang, S., Carper, M. J., Lei, X., Cade, W. T., Yarasheski, K. E., & Ramanadham, S. (2009). Protease inhibitors used in the treatment of HIV+ induce beta-cell apoptosis via the mitochondrial pathway and compromise insulin secretion. *American journal of physiology. Endocrinology and metabolism, 296*(4), E925-E935. doi:10.1152/ajpendo.90445.2008

Zhao, X., Sun, K., Lan, Z., Song, W., Cheng, L., Chi, W., Chen, J., Huo, Y., Xu, L., Liu, X., Deng, H., Siegenthaler, J. A., & Chen, L. (2017). Tenofovir and adefovir down-regulate mitochondrial chaperone TRAP1 and succinate dehydrogenase subunit B to metabolically reprogram glucose metabolism and induce nephrotoxicity. *Scientific Reports, 7*(1), 46344. doi:10.1038/srep46344

Zhao, Y., Sharp, G. W. G., & Straub, S. G. (2007). The inhibitors of protein acylation, cerulenin and tunicamycin, increase voltage-dependent Ca^{2+} currents in the insulin-secreting INS 832/13 cell. *Biochemical Pharmacology, 74*(2), 273-280. doi:https://doi.org/10.1016/j.bcp.2007.04.012

Zhou, A., Rohou, A., Schep, D. G., Bason, J. V., Montgomery, M. G., Walker, J. E., Grigorieff, N., & Rubinstein, J. L. (2015). Structure and conformational states of the bovine mitochondrial ATP synthase by cryo-EM. *eLife, 4*, e10180. doi:10.7554/eLife.10180

Zhou, M., He, H.-J., Tanaka, O., Sekiguchi, M., Kawahara, K., & Abe, H. (2011). Different Localization of ATP Sensitive K+ Channel Subunits in Rat Testis. *The Anatomical Record, 294*(4), 729-737. doi:https://doi.org/10.1002/ar.21348

Zhou, Y. P., & Grill, V. E. (1994). Long-term exposure of rat pancreatic islets to fatty acids inhibits glucose-induced insulin secretion and biosynthesis through a glucose fatty acid cycle. *The Journal of Clinical Investigation, 93*(2), 870-876. doi:10.1172/JCI117042

Zhu, J., Vinothkumar, K. R., & Hirst, J. (2016). Structure of mammalian respiratory complex I. *Nature, 536*(7616), 354-358. doi:10.1038/nature19095

Zorova, L. D., Popkov, V. A., Plotnikov, E. J., Silachev, D. N., Pevzner, I. B., Jankauskas, S. S., Zorov, S. D., Babenko, V. A., & Zorov, D. B. (2018). Functional Significance of the Mitochondrial Membrane Potential. *Biochemistry (Biokhimiya). Supplemental Series A, Membrane and Cell Biology, 12*(1), 20-26. doi:http://dx.doi.org/10.1134/S1990747818010129